Development ICP-MS isotope dilution preconcentration techniques for determination of platinum group elements in volcanic rocks

Woodland, Sarah Justine

University of Durham

Development of ICP-MS Isotope Dilution Preconcentration Techniques for Determination of Platinum Group Elements in Volcanic Rocks

By

Sarah Justine Woodland

A thesis submitted in partial fulfillment of
the requirements for the degree of Doctor of Philosophy

Department of Geological Sciences
University of Durham
July 1999

Declaration

I declare that this thesis, which I submit for the degree of Doctor of Philosophy at the University of Durham, is my own work and not substantially the same as any which has previously been submitted at this or another university.

Sarah Justine Woodland

S. J. Woodland.

University of Durham
July 1999

ABSTRACT

Understanding PGE geochemistry in low abundance (i.e. sub ppb level) geological samples has been hampered by the absence of an accurate, low blank, preconcentration technique. Ni-S fire assay, the traditional preconcentration method, has been critically assessed and combined with isotope dilution to enable reproducible analysis of standards in the 1–10ppb concentration range. In addition, a new anion exchange chromatography, low blank, isotope dilution method has been developed that allows analysis of Re, Os, Ir, Ru, Pt and Pd, at pg levels, from the same sample aliquot by ICP-MS. This method enables PGE abundances and Os isotopic ratios to be determined on the same sample dissolution, permitting geochronological studies. Samples are digested in Carius tubes and total procedural blanks are routinely less than 10pg/g for all elements, except Pt (25pg/g). Reproducibility is sufficient at the 10ppt level to confidently identify inter-element PGE fractionations.

Using this anion exchange preconcentration technique, PGEs have been characterised in a suite of plume-generated picrites from West Greenland, and a suite of subduction-related lavas, including fractionation series from Grenada (Lesser Antilles arc) and from Izu-Bonin. PGE concentrations are higher within the picrites of West Greenland, than in the picrites of Grenada, or boninites of Izu-Bonin. This is attributed to higher degrees of melting and less fractionation during West Greenland magma genesis. There is similarity in the PGE-patterns between all environments suggesting that relative PGE behaviour is not greatly altered during mantle melting in a subduction zone vs a plume.

Subtle differences occur in inter-PGE ratios between the different environments and within the fractionation suites. Os and Ir do not behave in an analogous manner during fractionation indicating "compatibility" with different crystallising phases. The PGEs are associated with olivine fractionation in all of the primitive rock types, but, may also be compatible with other phases (e.g. magnetite/chromite/amphibole) during high-level fractionation in arc magma chambers. The PGE signatures in the evolved arc rocks are controlled by multi-stage fractionation. PGE concentrations decrease as fractionation progresses, except for Re and Ru. PGE compatibility during arc-lava fractionation decreases in the order Os>Ir>Pt>Pd>Ru>Re. There is not a strong sulfide control on PGE fractionation in any of the rock suites analysed, probably because the primary melts were generally S-undersaturated. This places important constraints on the nature of the mantle in the different tectonic environments. Os-isotopic studies indicate the presence of a radiogenic component in both the West Greenland picrite plume source region (recycled crust or outer core material) and the Grenada picrite source region (slab-derived fluids).

Acknowledgements

Supervision:

I would like to thank my supervisors Graham Pearson and Julian Pearce; particularly Graham without whose endless optimism and help this project would not have been possible.

Thanks for Provision of Samples are due to:

Matthew Thirlwall for Grenada Samples, the ODP core store in Lamont for sediment samples, Lotte Larsen for the GGU West Greenland picrite samples, Julian Pearce for the boninite samples from ODP Leg 125 and Ian McDonald for providing copious amounts of the standard WITS-1.

Thanks for Technical Help are due to:

Graham Pearson and Gordon Irvine who both ran Os-samples (by N-TIMS) on my behalf at the Dept. of Terrestrial Magnetism, Carnegie Institution of Washington. Chris Ottley an "unofficial supervisor" for all of his help in the laboratory and with running the ICP-MS. Ron Hardy for XRF analysis of my samples and Julie Southern for preparing my rock thin sections.

Thanks for Additional help in Preparing this Thesis are due to:

The Seismic Research Unit in Trinidad and Peter Martin-Kaye for their help in obtaining geological maps of the Caribbean. Karen Atkinson for advice on drawings, Dave Stevenson for helping with computing matters, Gerry Dresser and Alan Carr for help with photography and finally Caroll and Claire for secretarial help.

Personal Thanks:

Are reserved for all my friends who've helped keep me sane over the past three years particularly Caroline, Gordon, Matt, Toby and Andy (the geologists) and also Jo and Charlotte.

Special thanks are due to all of my family, especially my parents for their support and encouragement through all stages of my academic career.

Finally, most sincere thanks are saved for Phil for his endless help, patience and love over the past four years.

This project was funded by a NERC grant (No: GT 4/95/71 E).

List of Abbreviations Used

ICP-MS: Inductively coupled plasma mass spectrometer

N-TIMS: Negative thermal ionisation mass spectrometer

INAA: Instrumental neutron activation analysis

x-flow: Cross flow (Meinhard) nebuliser

DIN: Direct injection nebuliser — MCN: Micro-concentric nebuliser

I.D.:Isotope dilution — CPS: Counts per second

MBCF: Mass bias correction factor — AMU: Atomic mass units

RSD: Relative standard deviation — 2σ: 2 x RSD

MQ: Milli Q deionised, high-purity water

Conc: Concentrated — UpA: Ultra pure acid

200#: Mesh size of resin — SpA: Super pure acid

ORNL: Oakridge National Laboratory

DTM: Department of Terrestrial Magnetism (Carnegie Institution, Washington DC, USA)

PGE: Platinum group element — PGM: Platinum group mineral

IPGE: Ir-group of PGEs — PPGEs: Pd-group of PGEs

MSS: Mono-sulfide solution

HSE: Highly siderophile element — REE: Rare earth element

HFSE: High field strength element — LILE: Large ion lithophile element

fO_2 / fS_2: Oxygen / Sulfur fugacity — D: Bulk partition coefficient

Cpx/Opx: Clino- or, orthopyroxene — Amph: Amphibole

WGP: West Greenland picrite — MORB: Mid ocean ridge basalt

OIB: Ocean island basalt — CFB: Continental flood basalt

PUM: Primitive upper mantle

SCLM: Sub continental lithospheric mantle

ICB: Intermediate Ca boninite — HCB: High Ca boninite

ICBrzA: Intermediate Ca bronzite andesite

CONTENTS

1: AIMS OF PROJECT AND INTRODUCTION TO PGE GEOCHEMISTRY

2: ANALYTICAL TECHNIQUES COMMONLY USED IN DETERMINATION OF PGE CONCENTRATION IN GEOLOGICAL SAMPLES

3: EVALUATION OF NI-S FIRE ASSAY PRE-CONCENTRATION FOR ICP-MS ANALYSIS

4: DEVELOPMENT OF ICP-MS ISOTOPE RATIO MEASUREMENT ROUTINES AND PROCEDURES FOR OS EXTRACTION FROM GEOLOGICAL SAMPLES

5: DEVELOPMENT OF SOLVENT EXTRACTION/ANION EXCHANGE SEPARATION OF PGES FROM GEOLOGICAL SAMPLES

6: PLATINUM GROUP ELEMENT GEOCHEMISTRY OF WEST GREENLAND PICRITES

7: GEOCHEMISTRY OF GRENADA VOLCANIC ROCKS

9: CONCLUSIONS

1: Aims of Project and Introduction to PGE Geochemistry

1.1 Aims of Project

The platinum group elements (PGEs) are a coherent group of siderophile elements. They can be used to reveal information about the evolution of magma series that the lithophile elements do not. However, because of the difficulty in analysing PGE concentration levels in non-sulfide bearing rocks the data set is generally limited to Ir and Pd concentrations in mafic rocks (Barnes and Picard, 1993). The objectives of this project, have therefore been to:

- Develop a method suitable for analysing PGEs at low concentrations in rocks of greatly varying concentrations, that gives accurate and reproducible results. The method should also enable Re and Os analysis on the same sample aliquot. Thus, offering the potential of obtaining PGE and Os-isotope geochronological data on the same sample, by either N-TIMS or ICP-MS. No one technique to date is capable of providing such data.

- To expand on the existing PGE dataset for geological samples by characterising Os, Ir, Ru, Pt, Pd and Re abundances in a suite of subduction-related volcanics for the first time.

- To consider the behaviour and recycling of PGEs within a subduction zone environment.

- To assess whether intra-oceanic arc-systems may possess any economic potential with regard to PGE-mineralisation.

- To produce full PGE patterns for rocks evolved in a plume environment and to evaluate whether a core-mantle boundary signature can be seen within such rocks by study of the PGEs.

- To compare the PGE abundances and behaviour associated with these different tectonic systems and to see whether any systematic variations can be observed.

Samples used in this project consist of two suites of subduction-related volcanics, from Grenada in the Lesser Antilles Arc and from the Izu-Bonin Arc. In addition, a suite of plume derived picritic rocks from Greenland were also characterised. These provide a direct contrast to the picritic rocks from Grenada analysed. Analysis of these high MgO picritic samples should provide an insight into the PGE-characteristics of primitive magmas produced under different tectonic regimes.

The application of PGE geochemistry to addressing geological problems is relatively new and their behaviour is not particularly well constrained. A review of current literature on PGE-distribution and occurrence in geological samples has thus been undertaken. This will provide a framework within which the new data obtained during this study can be considered.

1.2 Review of PGE Behaviour and Occurrence

1.2.1 Introduction to PGE Geochemistry

The PGEs provide a unique tool for deducing the history of Earth accretion and subsequent geological processes. Furthermore, the existence of two geochronologically useful decay systems; i.e. $^{187}Re \rightarrow {}^{187}Os$ & $^{190}Pt \rightarrow {}^{186}Os$ within the series (Section 1.2.2), greatly enhance the value of this geochemical group to earth sciences.

The PGEs have traditionally been known as the Noble metals due to their chemical inertness. The PGEs can be divided into a light triad: ruthenium, rhodium and palladium, and a heavy triad: osmium, iridium and platinum. The light triad has only half the density of the heavy triad (Table 1.1). Despite this division, the PGEs tend to separate during geological processes into different groups, i.e. Os, Ir and Ru (the highest melting point PGEs) and Pd, Pt and Rh (lower melting temperatures). This division will be discussed in Section 1.3.2.

	Ru	Rh	Pd	Os	Ir	Pt
Atomic Number	44	45	46	76	77	78
Melting Point °C	2310	1966	1552	3045	2410	1722
Density	12.4	12.4	12.0	22.7	22.6	21.5

Table 1.1 Chemical properties of the PGEs (after Buchanan, 1988)

The PGEs are highly siderophile elements (HSEs) i.e. they tend to be preferentially partitioned into metallic iron. In the absence of metallic iron, however, the PGEs behave in a chalcophilic manner and concentrate in sulfides. Assuming that the Earth accreted from chondritic material, during core formation the separating metal and sulfide phases should have scavenged the HSEs, thus leaving the upper mantle depleted in PGEs relative to chondrite (Chou *et al.*, 1983, Morgan *et al.*, 1981, Morgan, 1986). However, the HSEs in mantle xenoliths originating from the Earth's upper mantle have a chondritic abundance pattern and their concentration is

higher than would be expected from core-mantle equilibrium. This has led to the proposal that a chondritic component was added to the earth following core formation during a stage of late meteorite bombardment (Chou *et al.*, 1983, Morgan *et al.*, 1981, Morgan, 1986). This is just one example of how the PGEs can be used to illuminate petrogenetic processes, explaining their usefulness in geology.

1.2.2 The Re-Os Method of Dating

Of the two decay schemes mentioned above, the Re-Os system is the more commonly used for dating of geological processes. Os has seven naturally occurring isotopes, all of which are stable. ^{187}Os however, is produced by the beta decay of ^{187}Re. The decay constant for ^{187}Re is 1.666×10^{-11} (Shirey and Walker, 1998 and references therein). Rocks composed of silicate minerals are greatly depleted in Re and Os compared to metallic meteorites (Faure, 1986; Table 1.2). This is because Re and Os are primarily siderophile elements and are thus probably located in the metallic core of the earth (Martin, 1990).

Material	Re, ppb	Os, ppb	Re/Os
Chondrite (Allende)	63.23	773.9	0.394
Iron meteorites	0.778-4816	8.8-65,740	0.353-0.940
Fertile Mantle	0.25-0.30	2.8-3.4	0.401
MORB	0.5-2	0.001-0.05	100-5000
Continental Crust	<1	<0.05	50

Table 1.2 Average concentrations of Re and Os in terrestrial and extraterrestrial materials (Shirey and Walker, 1998 and references therein).

Re during partial melting of the mantle is moderately incompatible, but Os is very compatible. As the crust is ultimately formed from such melts, almost all crustal rocks have very low Os concentrations and slightly higher Re concentrations relative to the mantle (Martin, 1990). Thus, in general, the Earth's crust has a much higher Re/Os ratio than the mantle. Consequently crustal Os is significantly enriched in radiogenic ^{187}Os compared to the mantle. In contrast, the mantle residue which remains after partial melting evolves with a Re/Os ratio less than that of the original

source and hence a $^{187}Os/^{188}Os$ ratio less than that of the bulk earth. The Re-Os system is thus a useful tracer of melt-crust interaction (Shirey and Walker, 1998).

The behaviour of the PGEs and Re during mantle processes remains poorly understood, primarily owing to difficulties in their routine analysis at the low concentrations in which they are encountered in non-mineralised rocks (Burnham, 1995). Re occurs almost entirely in minerals of other elements and is most strongly concentrated in molybdenite (MoS_2), whose Re concentrations vary from a few ppm up to percent levels. Molybdenites associated with copper sulfide minerals tend to have especially high Re concentrations (Faure, 1986). Os is considered to be somewhat heterogeneously distributed on a whole rock scale in the mantle (Martin, 1990). By analogy with other PGEs, it is thought to reside predominantly in solid solution in the intergranular base-metal sulfide phases present in the mantle (Mitchell and Keays, 1981).

During magmatic fractional crystallisation Re behaves incompatibly and does not partition into early crystallising phases. Re is only found in conjunction with cumulates when Fe-Ni sulfide phases are present. Os by contrast is highly compatible during fractional crystallisation and is often associated with olivine (Martin, 1990). The Os itself however, resides in discrete minerals such as osmiridium and laurite, solid PGE-bearing sulfides. These Os-rich sulfide phases are thought to be stable at high temperatures and probably precipitated from the magma at an early stage. Thus, by the time the melt reaches saturation with regard to Fe-Ni sulfides later in its crystallisation history, it is already depleted in Os relative to Re (Martin, 1990). Therefore, the study of Re-Os isotope systems can provide information about magma chamber, crust, and mantle evolution because of the contrasting geochemical behaviour of Re and Os during magmatic processes.

1.3 PGEs in the Upper Mantle and Upper Mantle Melts

1.3.1 Mantle Conditions affecting PGE distribution

The accessible present day upper mantle is moderately oxidizing and well above metal saturation (fertile upper mantle contains ~2000ppm Fe_2O_3). Relative fO_2 decreases with increase in pressure (and hence increasing depth) due to phase changes within the mantle minerals (Ballhaus, 1995). The high sulfide/silicate D values for the PGEs (Table 1.3) dictate that the bulk of the PGEs will be contained in the monosulfide solid solution of the upper mantle (~250ppm). The sulfide fraction will be chondritic with respect to relative PGE abundance (Ballhaus, 1995).

Estimates of S concentration in undepleted upper mantle are variable, but are generally <300ppm (Peach and Mathez, 1996). If sulfide is residual in the mantle after moderate degrees of partial melting, then chalcophile elements will remain primarily in the mantle and partial melts will contain only low concentrations. If all mantle sulfide is consumed by melting (~20-25% melting required to exhaust sulfide; Keays, 1995) then the relative PGE abundances of the melt should reflect those of the original mantle (Peach and Mathez, 1996). In lower degree mantle melts the PGEs can be variably fractionated from one another and relative to primitive mantle. The PGE pattern of primitive mantle melts will thus reflect the relative stability of PGE-bearing phases in the residue, and PGE species dissolved in the partial melt (Ballhaus, 1995).

1.3.2 Fractionation Behaviour of the PGEs related to their Partition Coefficients

The PGEs are commonly divided into two subgroups on the basis of their behaviour during melting and fractionation (Barnes *et al.*, 1985):

- The Ir Group, or **IPGEs,** consist of Os, Ir and Ru and tend to be compatible during mantle melting and fractional crystallisation.
- The Pd Group, or **PPGEs,** consist of Rh, Pt and Pd and tend to be more incompatible during mantle melting and fractional crystallisation.

The subgroups can thus become fractionated from one another. For example, during low degrees of mantle partial melting the PPGEs may enter the melt, while the IPGEs are retained within residual mantle phases. Accordingly, in basic intrusions the IPGEs are typically found associated with early-formed phases (i.e. olivine/chromite). The PPGEs by contrast are usually associated with later crystallising phases such as base metal sulfides. Fractionation within the PGEs is thus principally governed by their differences in partitioning between solid and melt phases (Rollinson, 1993).

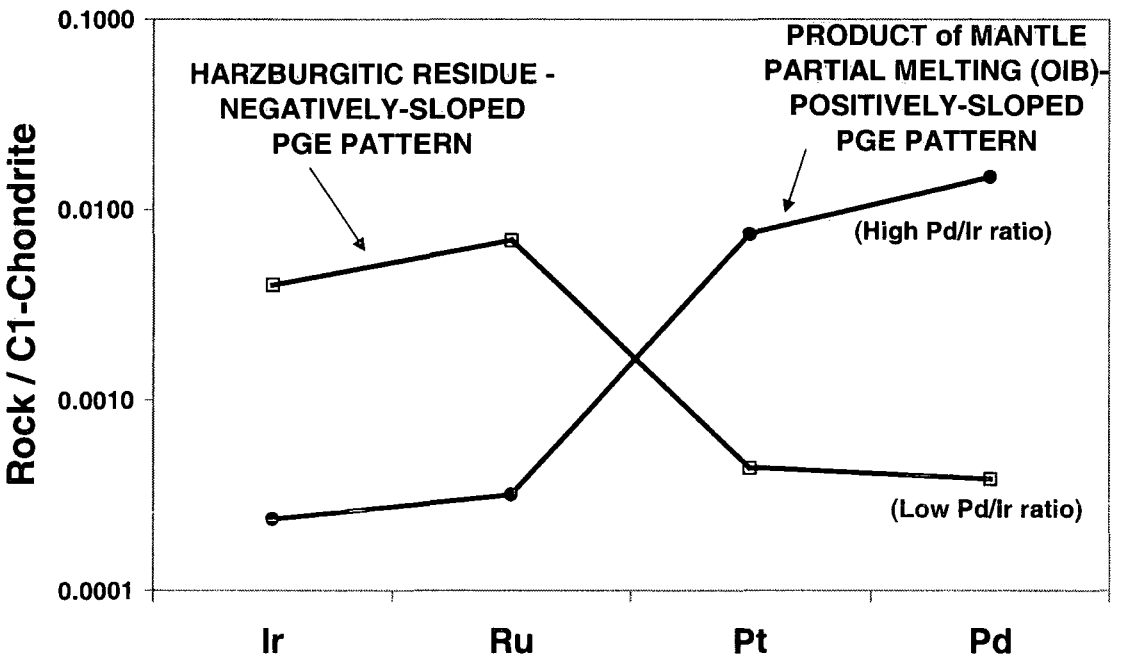

Fig 1.1 Differences in PGE patterns for mantle-melts vs mantle-residues to illustrate the difference in compatibility of the IPGEs and PPGEs

1.4 Experimental Determination of Partition Coefficients

1.4.1 Introduction

Partition coefficients (D) for the PGEs between solid and liquid phases in magmatic systems are poorly constrained, but are thought to be large when sulfide or metal are involved. Application of experimentally derived partition coefficients to nature is extremely difficult as there are many experimental problems leading to erratic partitioning behaviour for the PGEs. During laboratory experiments the PGEs behave as very different metals with their sulfide/silicate partitioning behaviour being highly dependent on the conditions used (Fleet *et al.*, 1996). Factors which affect PGE partitioning behaviour during experimental work include temperature, pressure, duration of experiment, fS_2, fO_2, concentration of the starting materials and composition of the starting materials. The affects of these variables will be examined in more detail below:

1.4.2 Concentration of the starting materials

Fleet *et al.* (1996) caution against the use of partition coefficients determined for 3 or 4 orders of magnitude beyond the concentration range in nature. This is because the D values increase as PGE concentration of the sulfides used increases. Likewise $D_{(PGE)}$ sulfide/silicate values determined at alloy saturation are about one order of magnitude higher than $D_{(PGE)}$ values for PGE concentrations approaching those in nature.

1.4.3 fO_2 and fS_2

Erratic behaviour of the PGEs on addition of silicate phases to experiments may occur because the oxygen-rich silicate phases alter the oxidation states of the PGE and hence affect their D values (Fleet *et al.*, 1996). Disagreement occurs as to whether raising fO_2 actually increases or decreases solubility of PGEs in a melt. Fleet *et al.* (1996) note that the solubilities of Os, Ir, Pt and Pd in basalt melt were markedly depressed in oxidizing conditions. Conversely, Bezmen *et al.* (1997) and

Borisov and Palme (1997) note that Pd solubility in silicate melt increases with increasing fO_2.

Variation in S content of the experimental set-up could account for much of the discrepancy between alloy/Fe-bearing silicate and sulfide/silicate partitioning coefficients. Even small amounts of S in the silicate melt could act to stabilise the PGEs in the melt as covalently bound PGE- species (Fleet *et al.*, 1996).

For experiments between sulfide liquids and mono-sulfide solution (MSS), the D values obtained are highly dependent on S-content of the run. Ir for example gives D (MSS/sulfide liquid) of 17 in S-saturated conditions and D (MSS/sulfide liquid) of 1 in S-undersaturated conditions (Barnes *et al.*, 1997). Several authors however (e.g. Peach *et al.*, 1994, Bezmen *et al.*, 1994), have noted that the partitioning of PGEs was generally insensitive to the range of fO_2 and fS_2 tested in their experiments.

1.4.4 Duration of run time

Sulfide/silicate partition coefficients generally increase with run time, in a manner consistent with either change in the chemical state of the metals in the silicate melt or passivation of alloy phases (Fleet *et al.*, 1996).

1.4.5 Composition of the starting materials

It has been suggested (Fleet *et al.*,1996), that the presence of both Ni and Fe in the experimental system may act to stabilise the PGEs in the silicate melt and thus have a significant effect on the sulfide/silicate partition coefficients (Fleet *et al.*, 1996). Major element composition also exerts marked control on partitioning of PGE between sulfide and silicate, and alloy and silicate. Erratic partitioning behaviour is associated with the introduction of a silicate melt phase to the system (Fleet *et al.*, 1996).

Calculated metal/silicate distribution coefficients from simple-system solubility experiments are often orders of magnitude higher than those reported from experiments in natural systems (O'Neill, 1997). For example, partitioning

experiments for the MORB system using MORB glass as a starting material vs a synthetic starting material, yielded D(Ir) values an order of magnitude apart. This is probably due to the presence of additional unidentified phases in natural systems that influence the solubility of Ir in the silicate melt (Peach and Mathez, 1996).

1.5 Application of Partition Coefficients to Natural Systems

Caution must be exercised in applying experimentally derived D values to natural systems as they are more complex and involve more components than can be simulated in a lab. Table 1.3 summarises the most recently determined partition coefficients for PGEs. The $DPGE_{sulfide/silicate}$ values calculated by Peach and Mathez (1996, i.e. 3.5×10^4 and 3.4×10^4 for D_{Ir} and D_{Pd} respectively) are preferred, as they have been calculated using experimental conditions appropriate for generation of mafic and ultramafic rocks.

These high values validate the assumption that sulfide melt dominates the geochemistry of the PGEs during igneous processes. The close similarity of D_{Ir} and D_{Pd} however, implies that the large fractionation of the IPGEs from the PPGEs observed in some intrusions, must be related to a process other than sulfide melt-silicate melt immiscibility (Peach and Mathez, 1996). The observed fractionation of Pd from Ir during mantle melting, therefore, poses the problem of identifying likely mantle phases other than sulfide which control the distribution of PGEs. Some of the possibilities are examined below.

Element	Partitioning	Between	D	Additional information	Author
Os	Olivine	Silicate melt	20 ± 5	Calculated from a picrite	1
Os	Sulfide	Silicate melt	2×10^6	Calculated from a lherzolite	
Os	Clinopyroxene	Silicate melt	1.5	Calculated from ankaramite	
Os	Os-Ni alloy Metal	Silicate melt Silicate	10^6-10^7	Weakly dependent on $f\ O_2$ at 1350°C	2
Ir			10^{12}		
Pt			10^{15}		
Pd			10^7		
Os	Very Ni-rich, Sulfide liquid	Basalt melt	10	1250°C – Ni-Fe composition of silicate melt affects partitioning of PGEs	3
Ir			51		
Ru			7		
Pt			16.5		
Pd			28		
Os	Os-Ir alloys	FeS	1400	11 GPa	4
Ir			160		
Ru			0.6		
Pt			32		
Pd			0.04		
Os	FePtOs alloy	Sulfide liquid	120	8.5 GPa	4
Ir			82		
Ru			5.0		
Pt			20		
Pd			0.1		
Os	(Fe)S (MSS)	Sulfide liquid	4.3	1 Bar (Crystallisation of sulfide liquid concentrates Os,Ir & Ru in MSS &Pd, Pt in residual liquids)	4
Ir			3.6		
Ru			4.2		
Pt			0.21		
Pd			0.21		
Ir	Sulfide	Silicate liquid	2.5-5.4×10^4	0.8Gpa,1450°C at O_2 and S_2 appropriate for mafic systems	5
Pd			1.2-7.8×10^4		
Ir	Sulfide	Silicate liquid	3.5×10^4	0.8Gpa, 1450°C at O_2 and S_2 appropriate for mafic systems	6
Pd			3.4×10^4		
Ir	MSS	Sulfide liquid	4.8	Calculated from Sudbury	7
Ir	Sulfide	Silicate liquid	1.2-1.6×10^4	Inferred from co-existing MORB sulfide-silicate	8
Pd			3.5×10^4		

Table 1.3 Summary of partition coefficients for the PGEs

[1] Hart & Ravizza, 1996; [2] Borisov & Palme, 1997; [3] Crocket *et al.*, 1997; [4] Fleet, 1997; [5] Mathez &Peach, 1997; [6] Peach *et al.*, 1994; [7] Naldrett, 1997; [8] Peach *et al.*, 1990; [9] Capobianco & Drake, 1990.

Element	Partitioning	Between	D	Additional information	Author
Ru	Spinel	Liquid	20	Fe-free system –Ru soluble	9
Pd			0.02	Pd insoluble in spinel	
Re	Garnet	Liquid	2.7	At mantle O_2 ~1300°C	10
Re	Magnetite	Melt	20-50	Sulfide-free system	11
Re			20-26	Sulfide-bearing system	
Re	Sulfide	Melt	2000		12
Ir	Mantle-residue	Mantle melt	6	Calculated from PGE comp.	13
Pt			0.6		
Pd			0.2		
Ir	MSS	Sulfide liquid	0.429 - 17	1 atm, 900 – 1100°C : S content of system is most important control	14
Pt			0.031 - 0.46		
Pd			0.005 – 0.435		
Ir	Sulfide melt	Silicate melt	6600	Merensky Reef studies	5
Pt			3900		
Pd			4000		
Ir	Sulfide melt	Silicate melt	174000	UG-2 studies	5
Pt			21000		
Pd			56000		
Os	Clinopyroxe	Liquid	0.08	1250°C, 1atm – Fe free-synthetic basalt	5
Re			0.04		
Ir	Olivine	Melt	~ 2	From komatiitic flows	15
Ru	Magnetite	Melt	> 1000	Fe-bearing synthetic system	16
Ir	Sulfide	Silicate melt	10700	1 Gpa, cooling from 1460°C in presence of Cr, Synthetic basalt + sulfide	17
Pd			37400		
Re			2300		
Ir	Chromite	Silicate melt	<1.1		16
Pd			<0.7		
Re			<2		
Ir	Alloy	Melt	10^5 to 10^9	Synthetic basalt melts at very high $f\ O_2$	
Pt			10^5 to 10^7		

Table 1.3 Summary of partition coefficients for the PGEs

[10] Righter & Hauri, 1998; [11] Righter *et al.*, 1998; [12] Jones & Drake, 1986; [13] Barnes & Picard, 1993; [14] Barnes *et al.*, 1997; [15] Brügmann *et al.*, 1987; [16] Capobianco & Drake, 1994; [17] Sattari *et al.*, 1998.

1.6 Phases Which Might Control PGE Fractionation During Mantle Melting

1.6.1 Fractionation by Silicates

In certain rock types (i.e. the Kambalda komatiites; Ross and Keays, 1979) olivine is significantly enriched in Ir compared to Pd. Thus, silicates such as olivine and spinel were proposed to be the refractory phases retaining the IPGEs within the mantle during partial melting (Ross and Keays, 1979). Peach and Mathez (1996) however, rule olivine out as a possible candidate for causing wholesale mantle fractionation of Ir from Pd, as the D $(Ir)_{olivine/melt}$ of ~2 is insufficient to explain the observed Pd-Ir fractionation in MORB.

Spinels and chromite-bearing spinels may also preferentially incorporate IPGEs, resulting in IPGE-PPGE fractionation. There is good correlation between Cr and Ir enrichment in cumulate piles of ophiolite complexes (e.g. Prichard and Lord, 1993) and Peach and Mathez (1996) state that the weight of geochemical evidence suggests that Ir is compatible in chromite. Capobianco *et al.* (1994) have found that Ru (and by inference Ir) partitions into spinel. Pd by contrast is insoluble in chromian-spinel. Thus, Cr-spinels are one phase capable of concentrating Ir over Pd (Capobianco and Drake, 1990).

Analyses of the silicate phases within a suite of mantle xenoliths however (i.e. olivine, spinel and garnet), reveal a general lack of Ir enrichment within silicate phases (Mitchell and Keays, 1981). Instead, the mantle xenoliths analysed indicated that 30% of the Ir was present within sulfides and the remainder was present as minute refractory metal particles. 70% of the Pd was present within sulfides, demonstrating the greater affinity of the PPGEs for sulfide phases (Mitchell and Keays, 1981).

1.6.2 Fractionation by Alloys

Closer inspection of many chromites has revealed that rather than partitioning into the chromite, the PGEs are present as microscopic inclusions of metal-alloys within the chromite (Peach and Mathez, 1996). Alloys may be formed by

precipitation from PGE-rich sulfide liquids (Peach *et al.*, 1994). Separation of a MSS from a sulfide liquid can cause fractionation of Ir and Pd under S-saturated conditions, as Ir is compatible with MSS but Pt and Pd are not (Barnes *et al.*, 1997).

Likewise, Fleet (1997) concludes from partitioning experiments between PGEs, sulfide, alloy and basalt melt, that separation of alloy from metal-rich sulfide liquid results in fractionation of IPGEs and PPGEs. Fractional crystallisation of sulfide liquid concentrates Os, Ir and Ru in MSS and Pt and Pd in the residual liquid. This is backed up by a recent estimate of $D(Ir)_{MSS/Sulfide\text{-}liquid}$ of 4.8 (Naldrett, 1997). Additionally, some PGEs (Ir, Os, Re and Pt) have been found to exist in magmatic liquids (both sulfide and silicate) as polymetallic clusters rather than as metal-S complexes (Ballhaus and Sylvester, 1997).

1.6.3 Fractionation by Fluids

Metal solubilities are strongly dependent on fO_2 and temperature, with solubilities generally decreasing with increasing fO_2 and temperature (Wood, 1987). As metal-oxides, only Pd exhibits any significant solubility in aqueous vapour under geologic conditions (Wood, 1987). PGE solubilities are only marginally enhanced by halogens and relatively low solubilities for PGE-chlorides are anticipated, except in extremely HCl-rich fluids. Where halogen-rich fluids are available, Fe, Ni and Cu are far more soluble and will thus decrease the amount of PGE dissolved in the fluid by competing for available chlorine (Wood, 1987). Redistribution of Pd (initially hosted by magmatic sulfide) by fluids however, may play an important role in modifying original Pd/Ir ratios (Peach *et al.*, 1994).

1.7 Effect of Mantle fO_2 on Mantle melting and PGE Fractionation

Ballhaus (1995) notes that fractionation of the PPGEs from the IPGEs decreases as depth of melting increases, such that in the deepest melts (e.g. kimberlites) the PGEs approach chondritic relative abundances. To explain this observation, it is suggested that fO_2 is the principle control on PGE fractionation between a mantle residue and a melt (Ballhaus, 1995). At the high fO_2 of the shallow mantle (i.e. MORB/OIB source), the PGEs probably reside in MSS rather than as alloys. Alloys are considered unstable at high fS_2 of the shallow mantle as PGE solubility in sulfide is too high to sustain a metal phase. MSS however, probably do not survive partial melting and would be dissolved in the silicate melt. This would instigate a fall in fS_2 and alloys may be stabilised (Ballhaus, 1995).

Fractionation patterns in low-pressure melts (e.g. MORB) indicate that with falling fS_2 and fO_2, metals precipitate in the order: Os, Ir, Ru ± Pt (at high fO_2), followed by Ni, Co and Fe (at lower fO_2). Pd and most of the Pt fractionate into the silicate melt, possibly because these elements form stable complexes with other elements (Fig 1.2). Thus, under the high fO_2 conditions of the shallow mantle, a residual alloy phase composed largely of the refractory PGEs (i.e. Os, Ir and Ru) may exist which is resistant to partial melting due to the high melting points of the pure metals (Ballhaus, 1995).

Deeper in the mantle, under lower fO_2 conditions alloys phases containing other metals (i.e. Fe, Ni, Co) may be stable (Fig 1.2). Due to low fO_2, alloys may become dominated by metallic Fe (and thus prone to partial melting) at around 300Km depth in the mantle. These base metals would decrease the thermal stability of the alloy. Thus, when partial melting occurs, the alloys may dissolve directly into the silicate melt with no IPGE segregation (Ballhaus, 1995). This would explain why deep-sourced (even low volume) melts such as kimberlites, exhibit a near chondritic relative PGE pattern, whereas, shallow mantle melts normally exhibit PPGE enrichment over the IPGEs (Ballhaus, 1995).

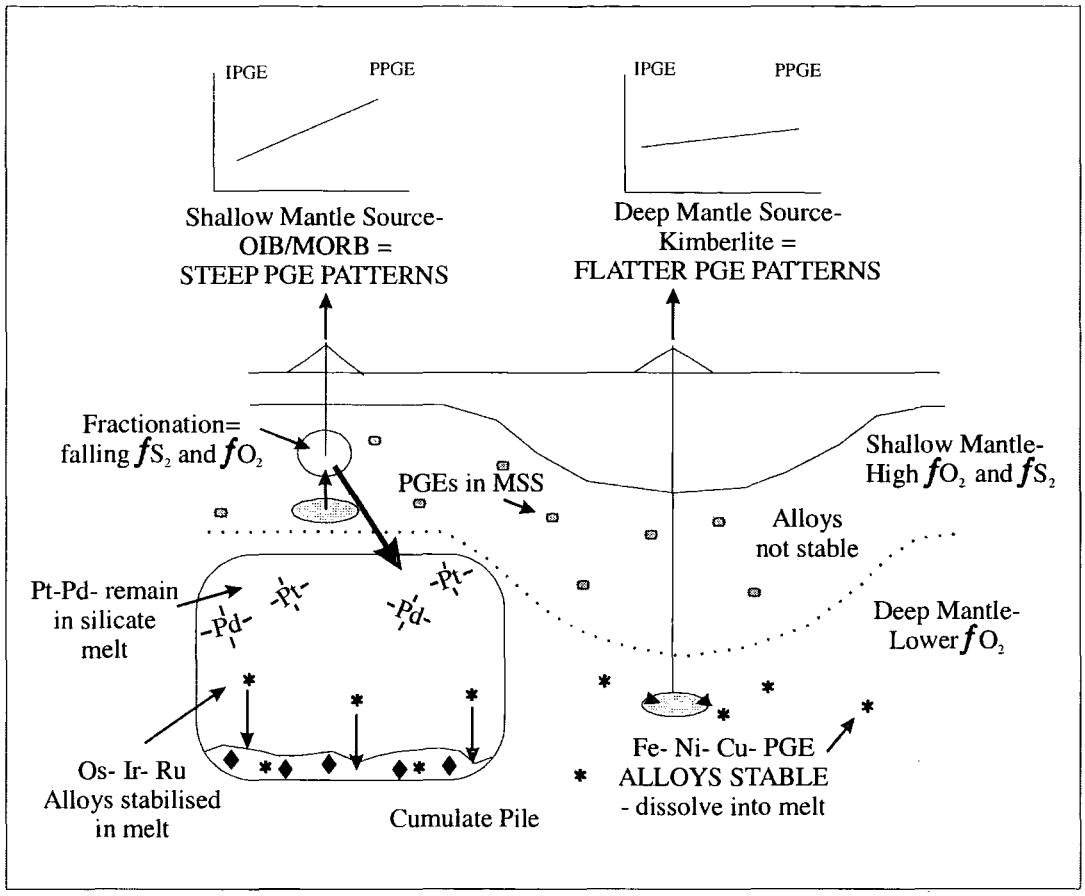

Fig 1.2 Schematic representation of PGE-pattern dependence on depth (fO_2 conditions) of magma source. Magmas generated at shallow depths, access PGEs in MSS phases. Fractionation of such a melt can lead to formation of residual IPGE-alloys, which separate from the melt during cumulate formation, so producing fractionated PGE patterns. Melts generated deeper, access PGEs in alloys, which are thermally destabilised because they incorporate base metals. Thus, all PGEs dissolve into melt; no residual IPGE phases are left in the mantle and magmas generated have non-fractionated PGE patterns (Ballhaus, 1995).

1.8 Crustal and Mantle Fractionation Processes Involved in the Concentration and Segregation of the PGEs: In More Detail

1.8.1 Introduction

There is still debate concerning the relative importance of different petrogenetic processes in generating PGE fractionation. IPGE/PPGE ratios are often quoted as a reflection of the amount of fractionation which has occurred. For example:

	Pd/Ir	
Chondritic (fertile mantle)	1.2	
Ophiolitic chromites	<1	(due to IPGE accumulation)
Layered Intrusion 'reefs'	1000	(PPGE "super-enrichment")

Table 1.4 Examples of extreme Pd/Ir ratios generated by PPGE/IPGE fractionation (data from Barnes *et al.*, 1985).

During petrogenesis there are three main stages where PGE-fractionation is likely to occur, these are:

- during initial partial melting of the mantle
- during crystal fractionation in the magma chamber, and
- during late-stage alteration

Each of these processes will be considered in turn with reference to specific case histories.

1.8.2 PGE Behaviour During Partial Melting

The initial concentrations of the PGEs in a magma are determined by the degree of partial melting of its mantle source. The IPGEs are presumed to be retained in a refractory mantle phase, while the PPGEs are contained within a phase that enters into the melt at an early stage (Naldrett *et al.*, 1979). Thus, lower degrees of partial melting generate more fractionated PGE patterns for both the melt and restite. For partial melting to play the dominant role in PGE fractionation, some minerals must retain the PGEs in the order Os>Ir>Ru>Rh>Pt>Pd. Olivine, sulfides and refractory metals have all been suggested (Barnes *et al.*, 1985).

1.8.3 Fractional Crystallisation

Following mantle melting, primary magmas generally undergo further PGE fractionation within higher-level magma chambers. Magmatic differentiation tends to concentrate Ir, Os and Ru within the early-crystallising cumulates. Rh, Pt and Pd by contrast, apparently behave as incompatible elements being progressively

concentrated in the liquid (Leblanc, 1991). The mineral phases with which the IPGEs are traditionally associated include the early formed silicates (i.e. olivine and pyroxene), chromite and sulfides. Rather than entering the cumulus silicates by solid (i.e. lattice) substitution, the PGEs often occur as discrete inclusions within the silicates (Fig 1.3).

Edwards (1990) reports that in the harzburgites of the Bay of Islands ophiolite complex, composite grains of PGM and Pt-Pd arsenides are present within both clino- and orthopyroxenes. The euhedral nature of the grains suggests that they are primary and were incorporated into the silicates as solid grains during silicate growth (Edwards, 1990). Magmatic PGM and PGE-sulfides are also found preserved within primary clinopyroxene in the Shetland ophiolite (Prichard *et al.*, 1994) and in boninites from Western Tasmania (Peck *et al.*, 1992). A conceptual model for the genesis and deposition of cumulus Os-Ir-Ru alloys from a boninitic magma is illustrated in Fig 1.3 (Peck *et al.*, 1992).

The highest PGE concentrations within the Shetland ophiolite are associated with chromite-rich rocks (Prichard *et al.*, 1994). Ru, Os, and Ir form discrete mineral phases (e.g. laurite RuS_2) prior to, or concurrently with, the chromite (Prichard *et al.*, 1994). Once laurite and the Os-Ir alloys have crystallised in a magma, chromite may nucleate around them (Barnes *et al.*, 1985). Settling of the chromite out of the magma will then leave a melt depleted in Ir-Os and Ru and a chromite cumulate rich in these elements (as in Fig 1.3).

The PPGE-bearing phases within the Shetland ophiolite post-date the formation of the chromite grains. Although often interstitial to the chromite grains, these phases are associated with base metal sulfides which have scavenged PPGEs from the silicate melt. Such mineralogical associations of the PGEs are similar for both layered intrusions and ophiolites (Prichard *et al.*, 1994) with Os-Ir and Ru content decreasing stratigraphically upward (Crocket, 1979).

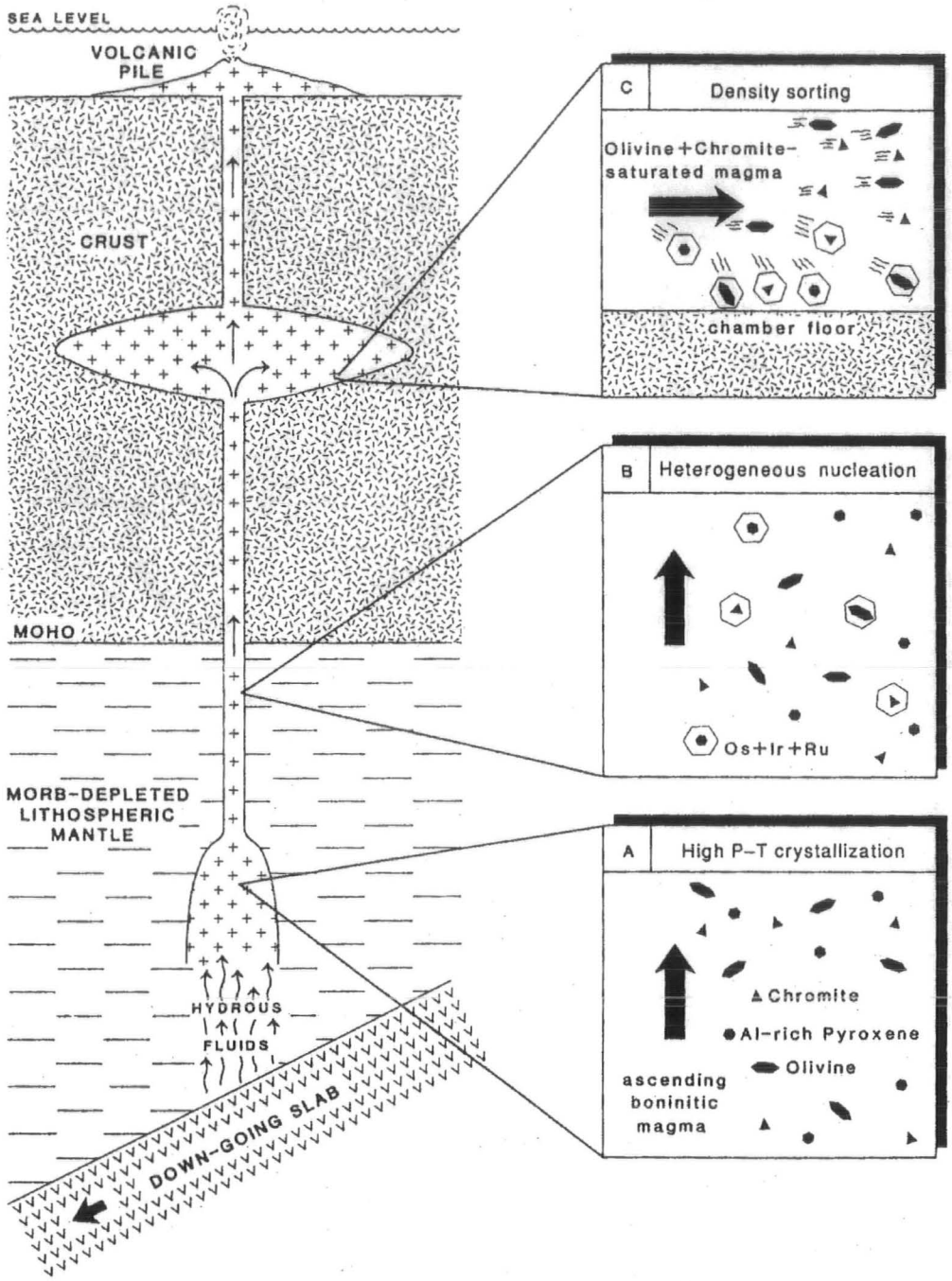

Fig 1.3 Schematic illustration of Os-Ir-Ru alloy formation – As magmas rise a meta-stable assemblage of olivine, chromite and pyroxene crystallises (A). As boninite continues to rise and crystallise, IPGEs become insoluble and nucleate around existing silicate phenocrysts (B). The Os-Ir-Ru alloys are carried into a crustal magma-chamber and due to their high density settle to the base of the chamber (C); from Peck *et al.*, 1992.

When a silicate melt becomes saturated with respect to sulfur an immiscible sulfide phase will form. Sulfide droplets in mafic and ultramafic magmas will act as collectors for PGE. If a sulfide liquid develops at an early stage it will be highly enriched in PGEs. If such metal-rich sulfide droplets become concentrated (e.g. by gravity settling) economically viable ore deposits may be formed. If, however, a sulfide phase does not separate until late in the crystallisation history of a magma, there will be insufficient time for scavenging and concentration of the PGEs. Thus, fractionation and concentration of PGEs in magmatic systems depends strongly on the relative timing of sulfide saturation and crystal fractionation (Leblanc, 1991).

If sulfide phases are absent, the PGEs will remain in the silicate magma, increasing in concentration as silicate crystallisation proceeds. Failure of a magma to become saturated in Fe-Ni-Cu-sulfides could lead to saturation of Os-Ir metal or laurite instead. This would result in the nucleation of very fine PGMs around which silicates may crystallise settling the PGMs out of the magma. Such a process could lead to fractionation within the PGE group, as the more soluble PPGEs would not exceed their saturation levels at this point and would thus continue to build up in the magma (Barnes *et al.*, 1985; Keays, 1995).

1.8.4 Solubility Differences between the IPGEs and the PPGEs

Inferred solubility for both Pt and Ir in silicate melt, decreases with increasing fO_2. At high fO_2 there is a very large drop in Ir solubility, however, the background solubility of Pt remains fairly high. This could lead to preferential precipitation of Ir (and other IPGEs) compared to the PPGEs (Amosse *et al.*, 1990). The fO_2 of a magma is thought to increase suddenly during cumulate crystallisation which could account for the association of IPGEs with early-crystallised silicates and chromite (Amosse *et al.*, 1990).

Increase in fS_2 of a melt also affects the PPGEs and IPGEs differently. Even with large increases of fS_2, Ir solubility shows no marked change. Pt solubility however, shows a strong increase (Amosse *et al.*, 1990). Thus, Pt becomes greatly enriched in melts at fS_2 in equilibrium with the base metal sulfides and will enter immiscible sulfide liquids formed (with the base metal sulfides), when the S-

saturation limit is reached. Precipitation of such sulfides produces the characteristic PPGE enriched Ni-Cu sulfide deposits (Amosse *et al.*, 1990).

1.8.5 Late Stage Alteration

The PPGEs are more mobile in late stage fluids than the IPGEs and this can contribute to fractionated PGE patterns (Barnes *et al.*, 1985). Solubility increases in the order: Ir < Os < Ru < Pd < Pt (Cousins, 1973). Although alteration is probably not the dominant process in PGE fractionation, certain geological formations have been recognised where alteration has generated IPGE/PPGE fractionation. For example, during metamorphism of the Kambalda komatiites Ir was unaffected and did not migrate from its original igneous sites. Pd conversely, underwent localised redistribution (Keays and Davison, 1976).

Different types of late-stage alteration do occur and thus the effects of the most geologically significant processes on PGE distribution and fractionation are considered in turn:

1.8.5.1 Serpentinisation

Keays and Davison (1976) remark that the PGEs are 'chemically inert' during serpentinization. Therefore, primary magmatic abundances of PGEs (i.e. in ophiolite; Leblanc, 1991) survive serpentinization (Edwards, 1990). The actual phases comprising the PGM assemblage however, can undergo some changes during alteration and serpentinisation (Prichard *et al.*, 1994). Edwards (1990) reports modification of PGM phases during serpentinization of the Springers Hill ophiolite due to addition of Cu, which is highly mobile during serpentinization.

1.8.5.2 Hydrothermal Alteration

It is widely accepted that Pt and Pd may be mobile as chloride, hydroxide or bisulfide complexes depending on pH, fO_2, temperature and ligand concentration (Mountain and Wood, 1987). Chloride complexing is considered most important under highly oxidising, acidic and saline conditions, whereas hydroxide complexing

predominates at neutral and basic pHs (Mountain and Wood, 1987). Bisulfide complexing is thought to be important in moderately reducing, low temperature hydrothermal solutions (Fleet and Wu, 1993). Pd is considered to have a greater solubility than Pt in most natural low temperature fluids (Parkinson *et al.*, 1992). Thus, Pd is most readily mobilised by hydrothermal alteration (Barnes *et al.*, 1985) and by weathering of sulfide ores (Plimer and Williams, 1987).

1.8.5.3 Ore Forming Processes

It is increasingly recognised that late stage hydrothermal alteration may be a key process in forming some of the world's most economically important PGE deposits (i.e. Bushveld and Stillwater; Boudreau and McCallum, 1992).

Fluids evolving in intercumulus melt or streaming off an underlying magma chamber, have the potential to selectively remobilize chalcophile and siderophile elements and concentrate them within restricted zones of fluid permeability (Fleet and Wu, 1993). At the Stillwater complex, Pd and Pt were probably re-mobilised by Cl-rich magmatic fluids which dissolved the minor magmatic sulfides and associated PGEs as they migrated upwards through solidifying cumulates (Boudreau and McCallum, 1992). Later concentration of such dispersed sulfides and alloys in zones of high permeability, is believed to be the key ore forming process in the production of concordant reef deposits within layered intrusions (Fleet and Wu, 1993).

1.8.5.4 Surface Processes

Low temperature processes which occur during weathering of PGE-bearing rocks can also produce some PGE fractionation. In the weathering environment, Os, Ir and Ru are relatively immobile and will remain in chromite grains, although these may become concentrated as placer deposits. Pt and Pd however, are much more mobile (Pd being the more mobile). Above mineralised PGE-chromite horizons on Shetland, Pd and Pt mobility is clearly demonstrated as the Pt/Pd ratio increases upwards through the soil profile, suggesting that whilst Pt is retained in the soil, Pd is transported away (Prichard and Lord, 1994).

Pt and Pd can be carried in solution by complexing with organic species such as humic acids, which have a high affinity for the PGEs. These organometallic compounds will be transported in solution until a change in conditions is encountered. The organic matter may then reduce the PGE complexes so that native PGE metal nuggets are precipitated. Such PGE nuggets can be distinguished from any magmatic PGM as they are typically two orders of magnitude larger than those in the silicate source rock, and do not show any signs of abrasive transport as would be expected of magmatically derived placer deposits (Bowles *et al.*, 1994).

1.9 DISTRIBUTION OF PGEs IN DIFFERENT ROCK TYPES

1.9.1 Introduction

The main PGE trend in geological samples is that there is a progressive decrease in average PGE content in sulfur-poor igneous silicate rocks, from ultrabasic, through basic to intermediate-acid compositions (Fig 1.4). Ore-deposits and ultrabasic rock suites and have been the most extensively studied, as they exhibit the highest PGE contents and are thus most easily analysed.

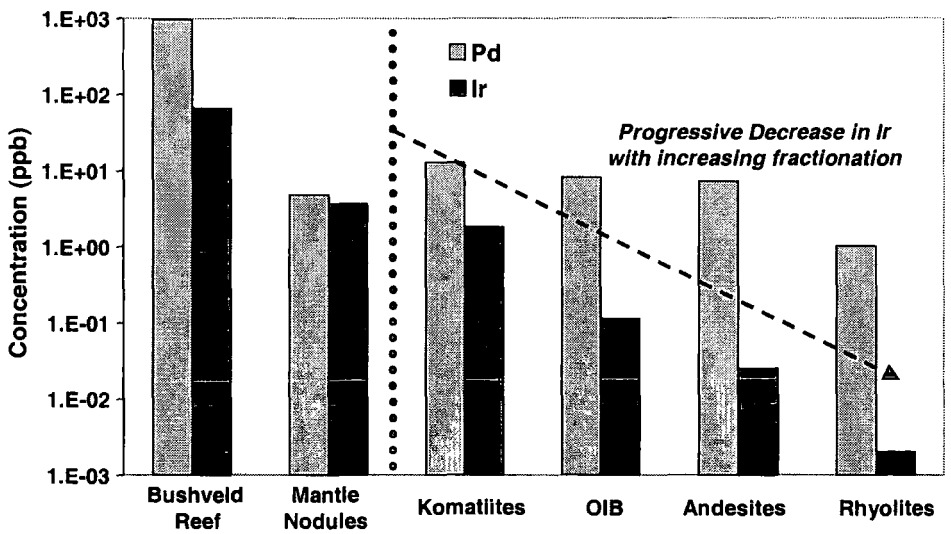

Fig 1.4 Variation in Pd and Ir concentrations in geological samples generated by increasing degrees of fractionation (Fleet and Wu, 1993; Morgan, 1986, Ross and Keays, 1979, Fryer and Greenough, 1992; Andesite & Rhyolite data – this project).

PGE data for geological samples are often restricted to Pd and Ir due to analytical difficulties involved in measuring the other PGEs. Data on the PGE contents of more silicic rocks are very restricted owing to the increasing analytical problems of sub ppb-level determination of PGE. Each of the major igneous rock groups has different overall PGE concentrations and Pd/Ir ratios related to degree of melting or fractionation (Table 1.6). Thus, comparison of PGE patterns for geological samples can indicate a great deal about their genesis. The PGE characteristics of the important igneous rock groups are summarised in Section 1.9.3 and 1.9.4. Firstly though, a brief review of PGE content and distribution in sedimentary rocks is presented. This has a bearing on this project, as one of the aims is to evaluate PGE-contribution to the mantle via sediment subduction.

1.9.2 PGE Occurrence in Sedimentary Rocks and the Marine Environment

Measurement of the PGEs in the marine environment is constrained by the detection limits of available analytical techniques. The distribution of Pd in the Pacific water column displays a nutrient-type surface depletion and deep enrichment (Lee, 1983). Pt and Pd concentrations in Pacific seawater are between 0.1-0.2 and 0.02-0.06ppt respectively (Parkinson *et al.*, 1992). Pt can occur up to levels of 0.1ppb in marine algae (Hodge *et al.*, 1986) and is believed to be scavenged down the water column, becoming depleted at depth (Jacinto and Van De Berg, 1989).

Ir has much lower concentrations in seawater than the other PGEs (~0.0009ppt), but can reach concentrations of 7.4ppb in manganese nodules (Hodge *et al.*, 1986). Pt may also be highly enriched within Mn-nodules (<1 ppm; Leblanc, 1991). This indicates how readily Ir and Pt are scavenged by ferromanganese phases in seawater. Iron-manganese oxyhydroxides however, are believed to only scavenge Ir under oxidising conditions, implying that anoxic environments are not a major sink for Ir (Anbar *et al.*, 1996).

There are four other main processes by which PGE can become concentrated in sediments:

1.9.2.1 By exhalation of PGE into the marine environment via black smokers.

Pd and Pt are easily mobilised by hydrothermal circulations (Falkner and Edmond, 1990). At sites of oceanic spreading, convective hydrothermal systems strongly leach the magmatic pile then precipitate massive sulfide deposits and metalliferous sediments on the ocean floor, which may display slight enrichments in Pt and Pd (Leblanc, 1991). Under certain conditions of PGE transport in saline solutions, Pd is less mobile than Pt (Mountain and Wood, 1987) as Pt forms more stable complexes with ligands such as bromide and chloride (Hodge *et al.,* 1986). Consequently, Pd is likely to be deposited closer to the hydrothermal conduit, whilst Pt is likely to be dispersed into seawater (Prichard and Lord, 1990; Falkner and Edmond, 1990) and may be enriched in Mn nodules (up to 1ppm) on the ocean floor (Leblanc, 1991).

1.9.2.2 By weathering of igneous rocks; either terrestrial or submarine.

Parkinson *et al.* (1992) report that vitric-rich clays (and thus the pore fluids interstitial to the clays) derived from the burial and diagenesis of volcanic arc rocks in the marine environment, are enriched in PGEs. Pt and Pd were probably mobilised and adsorbed onto the clay mineral surfaces during diagenesis of these arc-derived sediments. Later compaction of the sediments is thought to be responsible for desorption of the precious metals leading to elevated concentrations of PGE within the interstitial fluids. Clay-sized weathering products of Tahitian basalts show minor enrichment in Pd, with little if any change for Ir. As such, only slight differences in concentration of noble metals would be observed between source rocks and their derived sediments (Crocket *et al.,* 1973). Weathering and diagenesis of terrestrial igneous rocks such as cumulates can however lead to concentration of PGEs, either as placer deposits (derived by physical concentration of the heavy PGEs) or, the PPGEs can enter solution and be mobilised in groundwater and later precipitated as PGE nuggets (Bowles *et al.,* 1994).

1.9.2.3 By auto-oxidation and de-sulfurization of organic matter.

The Zechstein copper deposits of Poland provide a classic example of PGE concentration by this method. The Permian Zechstein deposits consist of white sandstones, overlain by dolomites and clay-bituminous, then Cu/Zn/Pb-bearing shales, overlain by further dolomites and limestones, which in turn are overlain by evaporite deposits. The transition elements and PGEs have been concentrated at the interface between oxidising (i.e. white sandstones) and reducing environments (i.e. organic-rich shales; Kucha, 1982). The transition metals acted to catalyse oxidation and desulfurization of the organic matter. This auto-oxidation process progressively concentrated U, Ni, Pt, Pd and Au, probably derived from brines of evaporitic origin as they percolated downwards across the redox-boundary. The source of the PGEs is suggested to be a fossil PGE placer deposit in the vicinity of the basement (Kucha, 1982).

1.9.2.4 By input of an anomalous PGE-rich material from an exotic source, (i.e. volcanic ash, or meteorite impact debris)

Possibly the most famous concentration of PGEs in sedimentary rocks is that known as the 'Ir layer' which is believed to mark the Cretaceous - Tertiary boundary. This PGE enriched-layer is thought to have been generated after the collision of a large bolide with the Earth's surface. The K-T boundary shales at Gubbio in Italy are 63 times more enriched in Ir than the background shales. At this site however, a stratigraphic thickness of 4m is enriched in Ir, with several subsidiary Ir peaks occurring above and below the boundary shale. This implies that the event which caused Ir enrichment lasted for at least 3 x 10^5yr. This time scale and the multiple peaks of Ir enrichment observed do not accord well with the impact theory. Thus, a cometary shower which lasted for over a million years is the only extraterrestrial origin which can explain the observed episodic Ir distribution (Crocket *et al.*, 1988).

An alternate explanation for the Ir anomaly in this particular case is that the multiple Ir peaks reflect a period of intense volcanic activity. Evidence for this is provided by shocked quartz and feldspar grains of the type associated with explosive volcanism which coincide with Ir maxima in samples from Gubbio (Crocket *et al.*, 1988). A study made during eruption of Kilauea identified Ir-rich airborne particulate

matter (Zoller *et al.*, 1983). Such observations show that Ir can be concentrated in the volatile components associated with basaltic volcanism (Crocket *et al.*, 1988).

1.9.3 PGE Occurrence in Ultramafic Rocks

Ultramafic rocks are of interest when studying PGEs as:

- They host most of the world's economic PGE deposits, and
- They can help in modelling the processes of magma generation within the mantle (Crocket, 1981).

Therefore, the important ultramafic rock groups with regard to the PGEs will now be considered in turn.

1.9.3.1 Komatiites

Barnes *et al.* (1985) state that average olivine spinifex textured komatiites from Australia and Canada have Pd/Ir ratios of approximately 10 and are therefore probably generated by 50% partial melting of the mantle. Komatiites frequently contain Ni-sulfide deposits which are presumed to be magmatic in origin and which have high PGE contents. In the Kambalda komatiites, Pd and Ir correlate strongly with the Ni-sulfide content of the rocks (Keays and Davison, 1976). The Ir content of the basal ore zone at Kambalda decreases stratigraphically upwards. This is attributed to Ir entering the early formed silicate phases such as olivine which, due to their density, gravitated along with immiscible sulfide droplets to the base of the ultramafic flow. The sulfide liquid is then perceived to have percolated downward through the crystal mush scavenging most of the Pd dissolved in the silicate melt. This explains the observed PGE depletion within the ultramafic host rock and the sulfide accumulations towards the base of the ultramafic flow (Keays and Davison, 1976).

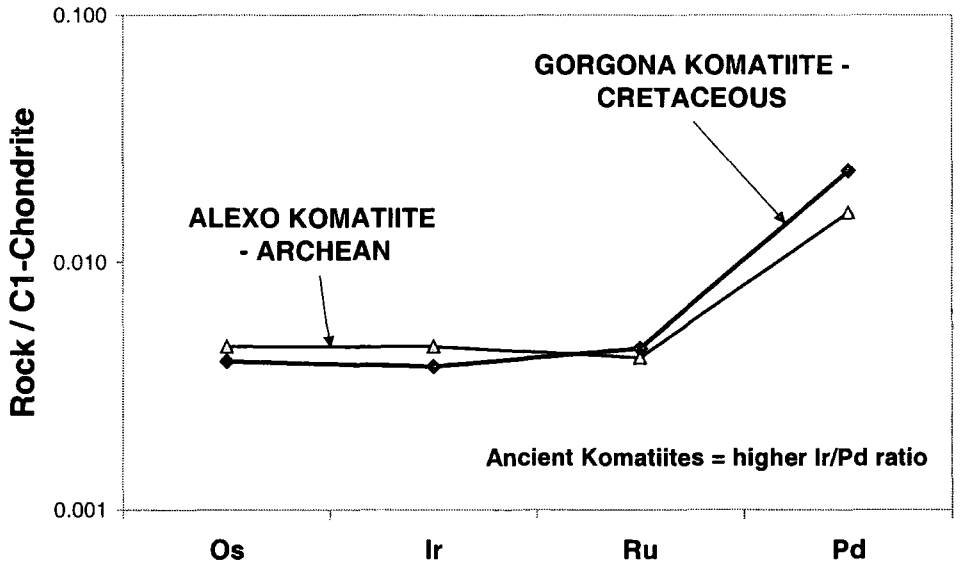

Fig 1.5 C1-normalised komatiite PGE patterns (data from Brügmann *et al.*, 1987)

1.9.3.2 Mantle Xenoliths

Kimberlites, the products of low-degree partial melting of a garnet-peridotite mantle source, commonly contain mantle xenoliths. The garnet-lherzolite nodules which they bear can provide information on the nature of PGE carriers in mantle rocks (Crocket, 1981). The majority of kimberlite-xenoliths from Siberia and South Africa have the characteristics of a residuum, i.e. flat PGE patterns which are due to relative enrichment in Ir and depletion in Pd (Crocket, 1981; Fig 1.6). This challenges the assumption that upper mantle rocks have chondritic PGE ratios (Morgan *et al.*, 1981).

A study of spinel lherzolites (Morgan *et al.*, 1981) suggests that abundances of the PGEs are very uniform within such mantle nodules (Table 1.4):

Os	**3.4 ± 1.2ppb**
Ir	**3.7 ± 1.1ppb**
Pd	**4.6 ± 2.0ppb**
Os/Ir Ratio (average)	***0.919***
Pd/Ir Ratio (average)	***1.243***

Table 1.4 Average PGE concentrations within spinel-lherzolite mantle nodules (Morgan *et al.*, 1981)

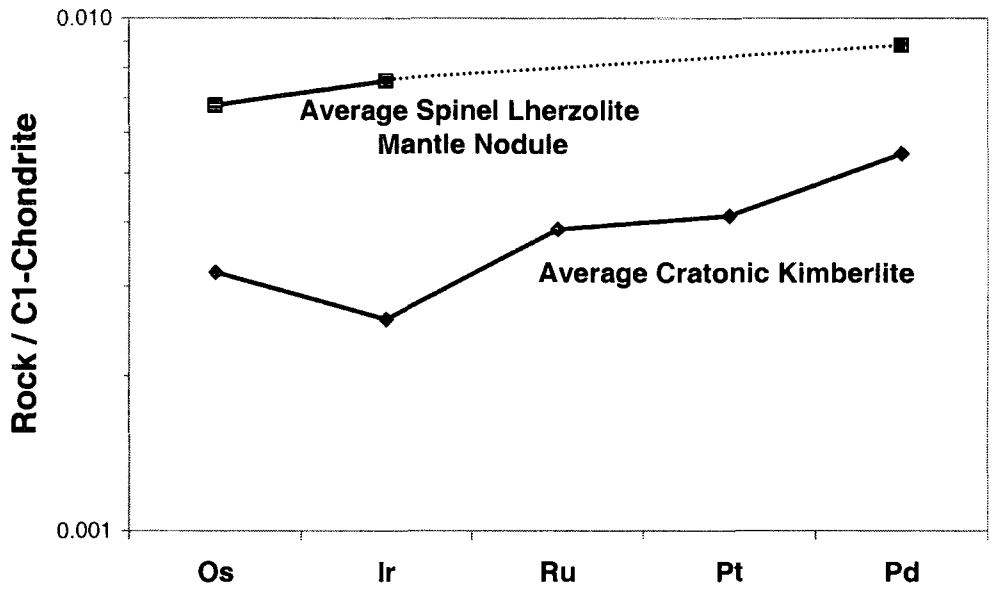

Fig 1.6 PGE patterns for a typical cratonic kimberlite (data from McDonald *et al.*, 1995) and for the spinel lherzolite mantle nodules which they contain (data from Morgan *et al.*, 1981)

PGE content in garnet lherzolite xenoliths, however, can be highly variable. This might be because the accessory phases which host the majority of the PGEs are volumetrically small in quantity and heterogeneously distributed (Crocket, 1981). This is termed the "nugget effect". Barnes *et al.* (1985) point out that mantle xenoliths are not necessarily a true representation of the mantle due to their unique mode of emplacement and their small size. Additionally, the PGE-geochemistry may have been altered through melt-rock interactions.

1.9.3.3 Ultramafic Rocks of Ophiolite Suites

The main ultramafic units of an ophiolite suite include a lower peridotite tectonite, represented by harzburgite with or without dunite, and upper cumulates consisting of dunites usually with chromitite, pyroxenites and layered gabbros (Crocket, 1981). Compared with other ultramafic rocks, ophiolites generally show no marked enrichment in PGE, except for a consistent enrichment of Ir within the chromitites which are cumulate in origin. The metamorphic peridotites and harzburgites of ophiolite sequences tend to show either slight Ir enrichment (consistent with either a residual or a cumulate origin), or else have relatively unfractionated PGE patterns (Crocket, 1981, Barnes *et al.*, 1985). A clear trend of

increasing Pd/Ir ratio occurs stratigraphically upward, from early formed dunite, to late formed gabbros and reflects a systematic decrease in Ir upwards through the cumulate pile (Table 1.5).

Chromitites :	Pd/Ir ratio =<0.1	Markedly enriched in Ir
Dunites :	Pd/Ir ratio= 9	Mildly Pd enriched
Pyroxenites :	Pd/Ir ratio =120	Very depleted in Ir

Table 1.5 Increase of Pd/Ir ratio stratigraphically upward through an ophiolite sequence (data from the Thetford ophiolite; Barnes *et al.*, 1985)

1.9.3.4 'Alpine' and 'Alaskan' Type Ultramafic Intrusions

Alpine complexes generally consist of harzburgitic and dunitic sequences and are now often regarded as dismembered parts of an ophiolite sequence. Thus, Alpine peridotites have the petrochemical characteristics of undepleted mantle (Crocket, 1981), and exhibit the same PGE patterns as ultramafic ophiolite sequences (see above).

Alaskan intrusions (e.g. the Urals) are dunitic plutons. These zoned, differentiated bodies are characterised by calcic clinopyroxene, lack of orthopyroxene, abundant hornblende, iron-rich chromitite and magnetite. They contain significantly higher PGE abundances than Alpine-type plutons and may be of economic interest. Marked enrichment of all PGE in chromite-rich schlieren and pods within the dunites are a feature of Alaskan-type intrusions (Crocket, 1979). Pd concentrations in the Urals reach 2220ppb, whilst Ir concentrations reach 205ppb (Crocket, 1981).

1.9.3.5 PGE in Ultramafic-Mafic Layered Complexes

Layered intrusions are hosts to several of the world's most important economic concentrations of PGE, for example, the Bushveld hosts 82% of the world's economic resources of PGEs (Buchanan, 1988). Both the Bushveld and Stillwater (the next most important PGE-bearing layered intrusion) are situated on stable Archaean cratons. They are the products of slow cooling of an extensive body

of magma in a non-orogenic environment. Slow cooling allows thorough fractionation to occur. Thus, texturally and compositionally distinctive layers can form, with the magma continually changing its composition until solidification is complete. Removal of the refractory phases, particularly in the presence of a sulfide phase, can result in sufficient enrichment of these minerals to form mineralised horizons within the intrusion. Mineralised horizons at the Bushveld are laterally continuous over tens of kilometres (Buchanan, 1988).

The reasons for mineralisation in layered intrusions are still poorly understood. Nevertheless, it is concluded that mineralisation of the Bushveld and Stillwater was not due to unusual PGE enrichment of a parental magma (Crocket, 1981). The parental magmas for such layered intrusions are thought to have been either of komatiitic or boninitic composition and were probably S-undersaturated at the time of emplacement into the crust (Keays, 1995)

The main ore-bearing horizons of the Bushveld are the Upper Group 2 (UG-2), (Pd/Ir = 14) and the Merensky Reef (Pd/Ir = 20). Both ore horizons show a similar PGE pattern, a steady increase from Ir to Pd. The parental magma at Stillwater is envisaged to have been much more Pd enriched (Pd/Ir of 220) than that of the Bushveld (Pd/Ir of 30; Barnes *et al.*, 1985). At Stillwater the regions in which PGE enrichment occurs, include horizons in the basal zone, chromites in the ultramafic unit and horizons of disseminated sulfide in the upper zone (Crocket, 1981). Pd/Ir ratios of 14 in the Stillwater chromites (as compared to the parental liquid ratio of Pd/Ir – 220) show that Ir has been concentrated in these chromites. In the Merensky reef of the Bushveld however, there is no evidence to suggest that chromite concentrates the PGEs (Barnes *et al.*, 1985).

The latest theories to explain the layered intrusion ore-deposits involve a multi-stage evolution. The PGEs are first thought to have been concentrated magmatically within chromites and sulfides, and later to have been remobilised and reconcentrated by hydrothermal processes (Fleet and Wu, 1993). This explains the extreme enrichments of the most mobile element Pd in some horizons (i.e. concentrations of 960ppb are recorded for Pd in the ultramafic zone at Stillwater; Crocket, 1981).

1.9.4 PGE Occurrence in Mafic Rocks

The mafic rocks not yet discussed are all volcanic in nature. While not economically important with regard to their PGE content, study of PGE signatures within mafic volcanics can be useful in understanding their genesis and constraining their source region. The mafic rocks (of basaltic composition) can be divided into subgroups according to the tectonic environment in which they were formed. The broad groups are: those basalts formed on the ocean floor by mid ocean ridge spreading, basalts generated at oceanic islands in intra-plate settings, and those basalts extruded onto the continents.

1.9.4.1 PGE Signature of Mid Ocean Ridge Basalts (MORB)

These basalts extruded on the ocean floor represent the Earth's greatest mass of mafic volcanic rocks. They can be distinguished from basalts erupted in any other setting as they have much lower contents of both Pd and Ir. An average Ir content of MORB is suggested as 0.02ppb, with average Pd content estimated at 1.1ppb (Ravizza and Pyle, 1997).

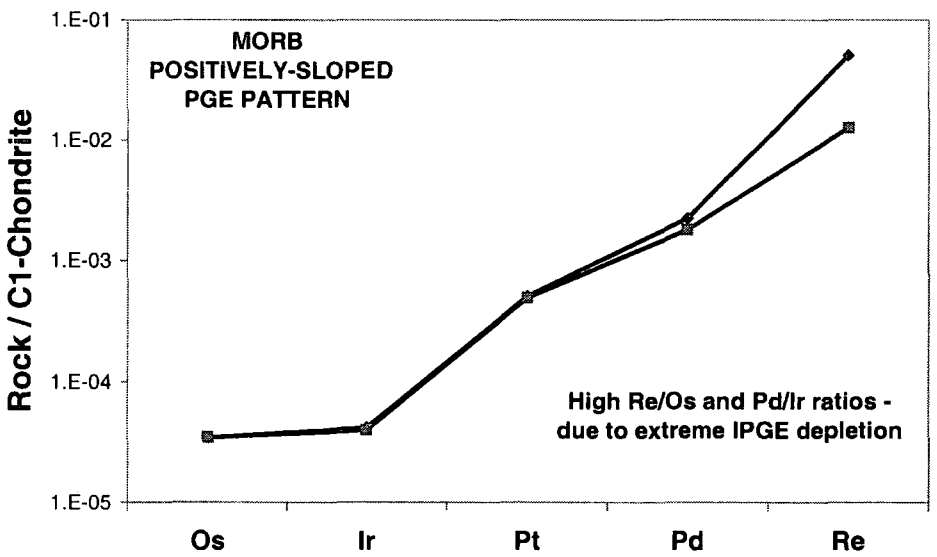

Fig 1.7 PGE Patterns for MORB, note high Pd/Ir ratios (data from Ravizza and Pyle, 1997)

Low PGE content in MORB is attributed to the fact that the MORB-source is S-saturated and thus during partial melting, the PGEs partition into residual sulfide liquids which remain in the mantle source (Hamlyn *et al.*, 1985). However, it is improbable that the huge depletion factors of Ir and Os in many ocean floor basalts relative to the mantle, are due solely to partitioning of these elements into the residue during partial melting. Instead, it is proposed that Ir and Os depletion in MORB is related to continuous fractionation of the magmas during ascent to the surface (Hertogen *et al.*, 1980). MORB has a pronounced chromium deficiency, indicating that chromite crystallised very early during fractionation. The Ir and Os depletion may therefore be attributed to their partitioning into early-formed chromite and thus removal from the melt (Hertogen *et al.*, 1980).

1.9.4.2 PGE Signature of Ocean Island Basalts (OIB)

Basalts formed in this setting are some 20 times higher in Ir and 2 to 3 times higher in Pd than MORB (Fig 1.8). An average Ir content of ~0.32ppb and average Pd content of ~1.6ppb have been proposed (Chou *et al.*, 1983). OIB Pd/Ir ratios are relatively low (~4.4). The increased PGE content of OIB as compared to MORB, is attributed to derivation of these magmas from a more primitive, fertile source region (Chou *et al.*, 1983).

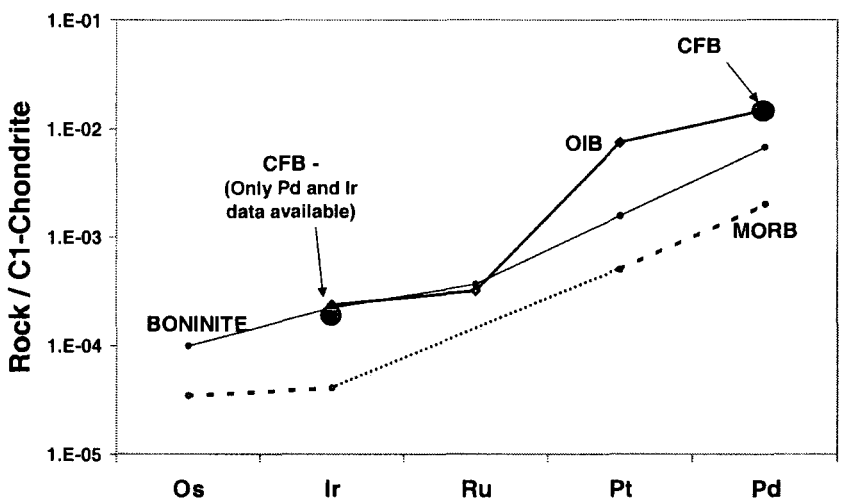

Fig 1.8 Comparison of PGE abundances and patterns between the major mafic rock groups; MORB (data: Ravizza and Pyle, 1997), OIB (data: Fryer and Greenough, 1992), boninites (data: this study) and CFB (data: Barnes *et al.*, 1985).

1.9.4.3 Continental Basalts

The continental plateau building flood basalts are characterised by high Pd/Ir averaging 90-100 (Crocket, 1981; Barnes *et al.,* 1985; Fig 1.8). There are however, great variations in Pd/Ir ratio between different provinces, perhaps suggesting significant differences in the Pd and Ir contents of the source regions (Crocket, 1981). The high Pd/Ir ratios demonstrate that these magmas are highly fractionated, probably due to a combination of processes, including crustal contamination and fractionation at the crust mantle boundary (Barnes *et al.,* 1985). Continental tholeiites are thought to be produced by 5-10% partial melting of fertile mantle (Barnes *et al.,* 1985), yet accepting this premise, they are found to contain much less Pd than would be expected. Thus, either Pd is not incompatible at these low degrees of partial melting or Pd is removed from the melt during magma ascent, possibly by sulfides (Barnes *et al.,* 1985). Overall, continental tholeiites compare more closely with oceanic intraplate basalts, than the sea-floor tholeiites in terms of average Pd and Ir contents (Crocket, 1979), suggesting derivation of both from a more fertile source region.

1.9.4.4 Volcanic Arc Basalts

Rocks evolved in these settings are low-Ti, magnesian basaltic andesites or boninites, and so are intermediate to mafic in composition. Few PGE analyses have been carried out on arc-rocks, but high (6.9-35ppb, mean 15ppb) Pd values have been reported for boninites of the Bonin forearc. By contrast, reported Ir contents are low (<0.01-1.9ppb, mean <0.23ppb; Hamlyn *et al.,* 1985). Compared to MORB these basalts contain higher Pd contents and slightly higher Ir contents (Fig 1.8). One explanation for these observed differences is that unlike MORB magmas which are generally sulfur saturated, boninites are exceptionally low in sulfur. Thus, PGE are not removed from boninites by immiscible sulfides during fractionation as they are in MORB (Leblanc, 1991).

PGE-rich boninitic magmas are produced by high degrees of partial melting of already depleted mantle in a water-rich subduction zone. This acts to remove all the refractory PGEs as well as Ni and Cr from the mantle, thus enriching them in the melt (Hamlyn *et al.,* 1985). If such boninitic magma resides in the crust, then thick

ultramafic units will be produced in which the PGEs are concentrated. Any magma subsequently erupted from this chamber will be depleted in Cr and PGEs, and have a composition typical of island arc tholeiites. The lavas erupted in this type of environment have the potential for huge variances in composition between the end members from MORB-like to boninite-type lavas. The composition of the erupted lavas is dictated by a combination of the following factors:

i) degree of partial melting which is in turn dependent on amount of water released from the down-going slab.

ii) residence time (if any) within a crustal magma chamber.

1.10 Overview of Previous Work

Some of the key points in PGE geochemistry which will be of importance when considering the new data obtained during this project are:

1) D values for sulfide liquid/ silicate melt of the order of 10^3 for PGEs support the hypothesis that PGEs within the mantle are hosted by sulfides/sulfide liquid.
2) Separation of an MSS from such a sulfide liquid may stabilise alloys, i.e. osmiridium/laurite (or polymetallic clusters) within the mantle which then become resistant to melting due to the high melting point of metallic PGEs.
3) The greater affinity of the IPGEs over the PPGEs for alloys during both melting and crystallisation, provides a mechanism for their fractionation.
4) Oxygen fugacity is probably of great importance to PGE fractionation, as at low mantle fO_2, siderophiles such as Fe, Ni and Co, become available as neutral species which dilute and destabilise residual Os-Ir-Ru alloys, which can then be removed from the mantle during partial melting.
5) Different tectonic environments produce very different PGE patterns and relative abundances (Table 1.6 and Fig 1.9). This is due to a complex combination of factors including initial mantle composition, degree of partial melting, degree of melt fractionation and extent of alteration. Thus, study of both PGE ratios and

PGE patterns are necessary to determine the extent of inter-PGE fractionation. This in turn can provide vital information about factors such as S-saturation status and which phases have crystallised from a magma.

	Ir (ppb)	Pd (ppb)	Pd/Ir
Deep sea sediments	0.3	4	13.3
Mn-nodules	8.5	4.5	0.5
Ophiolite (ultramafic)	6.7	3.8	0.6
Alaskan-type deposits (ultramafic)	9.6	32	3.3
Urals (ore deposit)	205	2220	10.8
Garnet-peridotite xenoliths	8.1	4.3	0.5
Spinel-lherzolite xenoliths	3.7	4.6	1.2
Boninites	0.23	15	65.2
MORB	0.02	1.1	55
OIB	0.114	8.11	71.1
CFB	0.092	8.3	90.2
Cratonic kimberlites	1.24	2.97	2.4

Table 1.6 Concentrations (ppb) and Pd/Ir ratios of common rock types (data from Crocket, 1981; Crocket, 1979; McDonald *et al.*, 1995; Brügmann *et al.*, 1987; Morgan *et al.*, 1981; Hamlyn *et al.*, 1985; Ravizza and Pyle, 1997 and Fryer and Greenough, 1992).

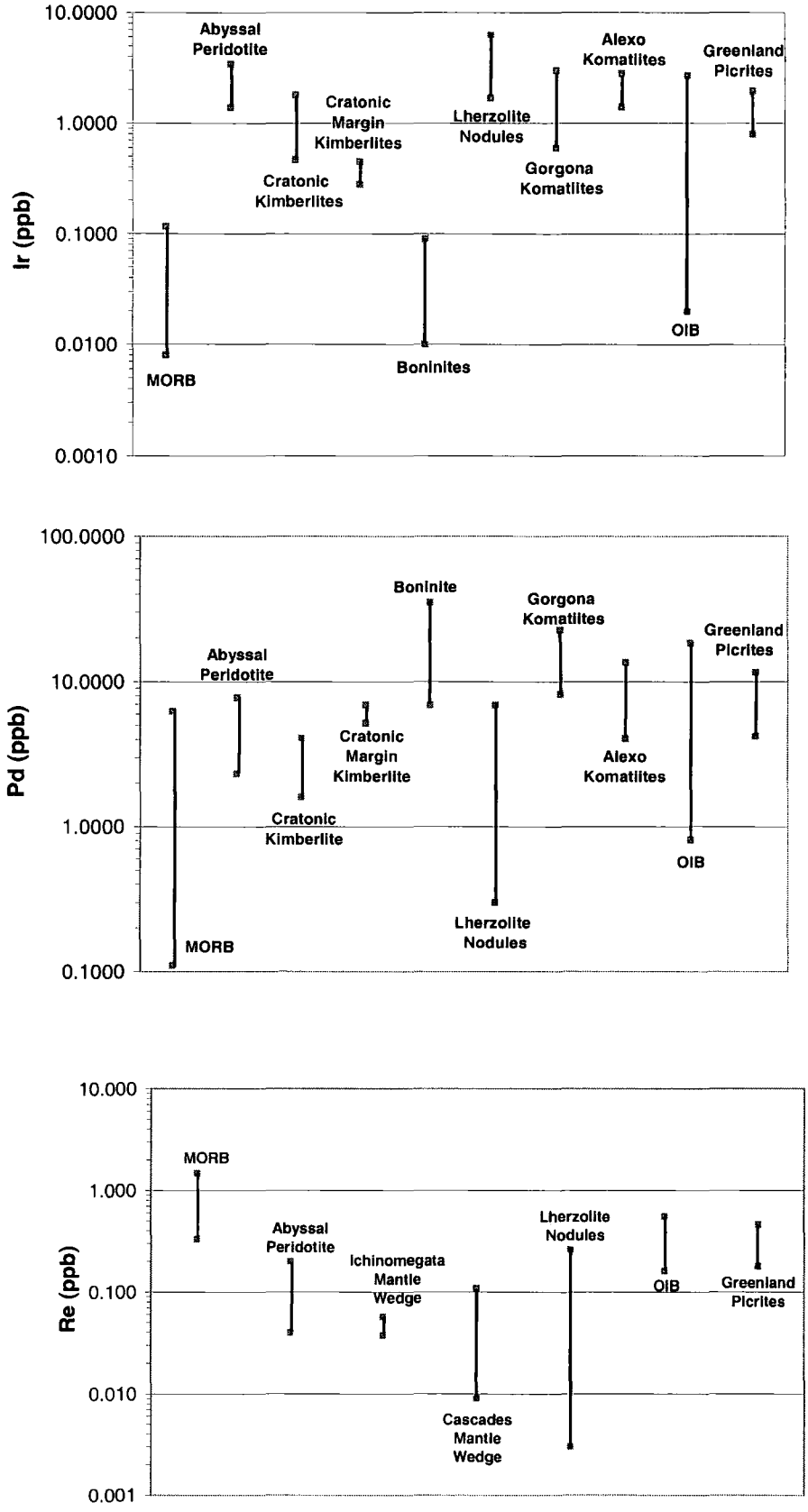

Fig 1.9 Summary range charts for Ir, Pd and Re within common rock types (data from Brügmann *et al.*, 1987; McDonald *et al.*, 1995; Brandon *et al.*, 1996, Pattou *et al.*, 1996 Fryer and Greenough, 1992 and Morgan *et al;* 1981).

2: Analytical Techniques Commonly Used in Determination of PGE Concentration in Geological Samples

2.1 Introduction

Many analytical techniques have been employed to determine PGE abundances in geological samples, accompanied by an equally varied spectrum of chemical separation and pre-concentration techniques. Some of the most commonly used procedures are summarised within this chapter and their applicability to this study are considered.

Different PGEs lend themselves with varying ease to chemical separation from geological matrices. Thus, the limiting factor in the application of instrumental techniques to geological samples is the ability to separate PGEs at the pg (10^{-12}g) level, while maintaining the low blank levels required to match instrumental detection limits. Appropriate analytical procedures for determination of PGE concentration in geological samples, generally have three steps: chemical decomposition of the sample, separation of the PGEs from the matrix (i.e. preconcentration) and finally elemental determination (Enzweiler *et al.*, 1995). Each of these steps will be considered, but firstly an additional stage of preparing and crushing the sample will be discussed.

2.2 Sample Preparation and Crushing

Special care has to be taken when crushing and preparing samples for PGE analysis, especially when only very low levels of PGE are present. This is due to the siderophilic nature of the PGEs which therefore have an affinity for contamination if crushed in iron or tungsten carbide.

McDonald *et al.* (1994) when determining PGE concentration in kimberlites, broke their samples into large fragments using a hammer, then crushed these fragments in a jaw crusher. The stainless steel jaw crusher is not thought to cause any sample contamination. Powdering was undertaken between agate rings in a swing mill. Barren quartz was crushed between the rings between each sample to eliminate

the possibility of Au, Pt or Pd contamination from the previous sample, as these PGEs are considered malleable enough to possibly smear onto the agate during crushing. Powders produced were then homogenised on a shaker prior to aliquots being removed for further analysis. This is to prevent fractionation occurring within the powders via settling of the heavier components (McDonald pers.comm.).

2.3 Chemical Decomposition

2.3.1 Acid Attack

Acid decompositions have the benefit of adding negligible contamination to the blank levels compared to fusions, provided suitably clean acids are used. Acid digestion techniques also have the advantage of rendering the sample in a form amenable to a variety of different pre-concentration procedures. However, poor recoveries of Pt and Pd via various acid digestion procedures (largely due to the occurrence of acid dissolution resistant discrete platinum group minerals within grains of the host matrix) have caused this method to be largely superseded by fire assay and fusion techniques (Hall and Pelchat, 1994).

Care also has to be taken during acid dissolutions to minimise Os and Ru loss from the solution. Thus, acid dissolutions are often conducted in Teflon bombs to prevent loss of Os following its oxidation to the volatile tetraoxide (OsO_4) by the acidic solutions. Solutions containing HF and HNO_3 particularly, cause Os oxidation and thus techniques (including addition of ethanol) to maintain reducing environments during dissolution have been developed (Martin, 1990). New problems however, arise from employing this technique as not all PGE bearing phases will dissolve in reducing environments.

2.3.2 Carius Tube Digestion

An oxidising acid digestion is utilised in Carius tube dissolutions. Although a very old technique this method has only recently become widely used in the

digestion of geological samples, specifically for Re-Os isotope work (Shirey and Walker, 1994).

This method involves digestion of relatively small samples in aqua regia within a Carius tube (a thick walled, sealed, Pyrex tube). The standard Carius tube attack for Re-Os isotope determination (Shirey and Walker, 1994) involves a high-temperature aqua-regia attack at between 220 and 240°C. Silicates are not completely digested by this method but its effectiveness in quantitatively extracting Os from silicate rocks has been well-documented (Cohen and Waters, 1996; Shirey and Walker, 1994). In addition, Rehkämper and Halliday (1997) have recently demonstrated the efficiency of Carius tube attack in quantifying Ru, Pt, Ir and Pt in geological samples.

The Carius tube digestion technique offers considerable versatility in being able to digest a wide range of materials including organic substances. The usual aqua-regia attack for Carius tube Re-Os analysis (Shirey and Walker, 1994) creates volatile Os tetraoxide but this is quantitatively retained by the impervious sealed glass vessel. As tubes are not re-used sample cross contamination, which can be a problem with oxidised Os solution in Teflon, is negligible. Furthermore, it is reported that Carius tube digestions liberate more Os from most matrices than Teflon vessel digestions (Shirey and Walker, 1995). The major attraction of Carius tube digestion for low-level PGE analysis is that it contributes very little blank to the procedure, providing that tubes are adequately cleaned. Thus, low detection limits can be routinely achieved which are largely controlled by acid blanks. Average Os blanks for the total Carius tube procedure are very low, typically < 5ppt (Shirey and Walker, 1995).

This technique requires that samples be very well ground before digestion so that the aqua-regia may effectively attack any PGE hosts included within silicates. Some samples may require re-grinding to ensure best results. One potential drawback of the Carius tube dissolution technique specific to noble metal determinations is that small sample aliquots are commonly used (c. <5g). Considering the likely heterogeneous distribution of PGEs in powdered rocks (commonly referred to as "the nugget effect") this may present problems with some rocks that are likely to be naturally heterogeneous with respect to their PGE contents (McDonald, 1998).

The main drawback with Carius tube digestions is their perceived danger, both in terms of sample loss and physical injury, but this aspect can be minimised with well annealed, well sealed tubes and some experience in being able to predict likely over-pressuring

2.3.3 Fusion Procedures (i.e. fusion with sodium peroxide)

The fusion of powdered samples with oxidising fluxes such as sodium peroxide, have the advantage that they are very effective in dissolving both refractory and sulfide mineral phases. However, such procedures must normally be restricted to small samples (< 1g) and thus are not suitable for any sample which may contain discrete PGE minerals (Enzweiler *et al.,* 1995). In such circumstances serious sampling errors are likely to occur (i.e. the nugget effect - small samples may not be truly representative of the bulk material, making reproducibility of results very difficult, McDonald *et al.,* 1994). An additional problem that arises when using such a small sample size is that a very high blank to sample ratio will be encountered, producing large errors within any data. Sodium peroxide fusions thus, although effective at dissolution of refractory phases such as chromite, induce a significant increase in blanks levels, either from the sodium peroxide or from the zirconium crucible in the case of Re-Os determinations (Morgan *et al.,* 1991) making work with very low Re level samples impossible.

Sodium peroxide fusions are carried out either in zirconium crucibles or in glassy carbon crucibles lined with a layer of sodium carbonate to protect the crucible from attack by the sodium peroxide flux during heating in a furnace (Enzweiler *et al.,* 1995). Use of such crucibles may in itself cause analytical problems as these crucibles are expensive and have to be repeatedly used for successive analyses. It is probable however, that the crucibles retain a 'memory effect' from the previous sample and this is potentially a very serious source of sample contamination.

A recent determination of PGE concentration in geological materials, combining ICP-MS with sodium peroxide fusion and Te coprecipitation, produced detection limits in the range of 0.3-2ppb for the elements Ru, Pd, Ir and Pt. In general, blanks for sodium peroxide fusions are generally > 50 pg g^{-1} and detection limits better than 50 ppt for Ir and 500 ppt for Pd, have not been reported (Yi and

Masuda, 1996). Although the method may work for some peridotites containing refractory chromites (Gueddari *et al.,* 1996) it is limited in its application to relatively high abundance samples as the average basalt or sediment may contain only 30 to 50 ppt Ir.

2.4 Preconcentration

2.4.1 Nickel Sulfide Fire Assay

For the past 2 decades, Ni-sulfide fire assay has been the favoured means of preconcentration of PGEs for numerous analytical techniques, in particular, instrumental neutron activation (INAA; Hoffman *et al.,* 1978; McDonald *et al.,* 1994). This technique or variants of it, also became popular for ICP-MS analysis (Hall and Pelchat, 1994; Jackson *et al.,* 1990; Patou *et al.,* 1996) and for Os isotope analysis by NTIMS (Hauri and Hart, 1997; Martin, 1990).

The Ni-S fire assay method offers the advantage of accepting large sample aliquots (~20-50g), thus minimising sampling errors (Enzweiler *et al.,* 1995) and producing low blank to sample ratios. Furthermore, the analyses are conducted within inexpensive clay crucibles, enabling a new crucible to be used for each analysis, so eliminating inter-sample contamination problems. Samples are combined with a flux and melted at 1100°C in a clay (or porcelain) crucible. At higher temperatures (i.e.1200°c) some of the nickel sulfide is found to remain distributed throughout the cooled slag (Robért *et al.,* 1971). During melting of this mixture, Ni-S is generated. The PGEs are quantitatively extracted from the silicate into the dense, immiscible sulfide phase as it descends through the melt and are present in the final assay button at the base of the crucible (McDonald *et al.,* 1994; Fig 2.1).

After fire-assay the buttons should be removed from the crucible, weighed and described, before being wrapped in a bag (to prevent contamination) and broken with a hammer. All of the sulfide chips are then emptied into a beaker, covered with concentrated HCl and allowed to dissolve, a procedure which takes 4 to 8 hours on a hotplate. The dissolution process generates H_2S gas. This maintains a reducing environment within the solution which should inhibit the dissolution of any PGE

sulfides. Thus the PGEs are etched out of the dissolving nickel sulfide forming a layer of tiny particles at the base of the beaker (McDonald *et al.*, 1994). When dissolution is complete, the beakers are quickly cooled with damp cloths and the solutions are filtered under vacuum through filter papers, trapping the PGE sulfide particles as a thin grey layer (McDonald *et al.*, 1994).

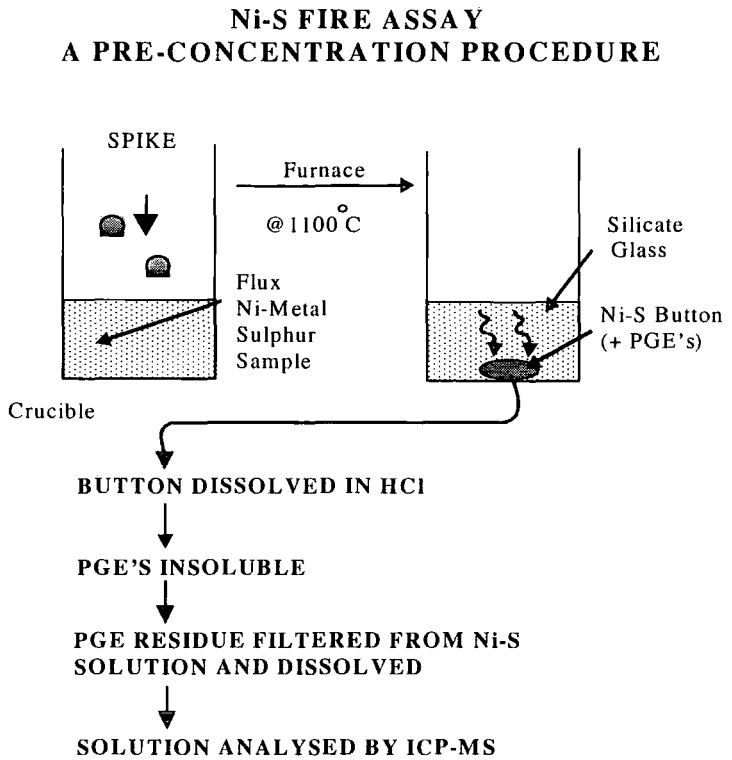

Fig 2.1 Ni-S fire assay procedure for ICP-MS analysis

To compensate for the possibility that geological samples can contain very low levels of PGEs, McDonald *et al.* (1994) designed a procedure whereby two assay buttons are combined during the dissolution and filtering, leading to double the normal amount of PGE residue on the filter paper prior to analysis. Other problems that can arise during PGE analysis by fire assay include, imperfect fusion of some rock types, namely rocks with high levels of carbonate and rocks which are low in silicate (i.e. peridotite, Mg-rich dunite). Samples with high CO_3 content do not form a stable melt: the highly basic mixture will attack the walls of the crucible, and any

button which forms is unstable, tending to disintegrate in air over a period of days. With peridotites a layer of forsteritic olivine can sometimes form above the nickel sulfide button. This then acts as a filter trapping some of the nickel sulfide (and thus potentially PGEs) within the silicate slag (McDonald *et al.*, 1994).

Alteration of flux compositions (for example by adding silica) can help in both of the above instances, however, the slag must always be carefully examined after firing to ensure that complete melting has occurred (McDonald *et al.*, 1994). Zereini *et al.* (1994) report 95% recovery of the whole PGE series into the initial Ni-S bead, however, they suggest that up to 10% of the Ir may remain in the slag. Thus, they use an additional step in which the slag of the first melt is crushed, mixed with half the amount of flux and collector, and re-melted under the same conditions as the first melt to try and improve recovery. The classical flux used is a mixture of sodium carbonate and sodium tetraborate. Experiments conducted into the use of lithium tetraborate as an alternative to sodium tetraborate however, led Zereini *et al.* (1994) to conclude that lithium tetraborate had a lower recovery rate than sodium tetraborate (except for chromites containing PGE abundances in the ppm-range). Thus, they decided that lithium tetraborate was not a useful alternative to sodium tetraborate.

A major consideration when using fire assay should be whether or not any PGE losses occur during dissolution. The most recent research (McDonald *et al.*, 1994) suggests that as long as dissolution is stopped and the solution filtered as soon as H_2S production ceases, then no significant losses occur. However, if the solutions are allowed to stand after H_2S production has stopped, losses of PGE (especially of Pd) rapidly increase (McDonald *et al.*, 1994). In order to overcome this problem isotope dilution can be employed (Section 2.6.). Assuming complete spike-sample equilibration at the fusion stage, any losses of PGE during dissolution will be mirrored by losses of the spike. Thus, the initial spike-sample ratio should remain unchanged, allowing calculation of original PGE content despite any losses which may occur during sample preparation. Although isotope dilution is the favoured approach for Os analysis by Ni-S fusion (Martin, 1990; Hauri and Hart, 1993) it has only recently been extended to other PGEs (Ravizza and Pyle, 1997).

A significant drawback of Ni-S fire assay is the difficulty in obtaining a regular supply of Ni metal of consistently adequate purity to allow determination of

all the PGEs at the 10s of ppt level necessary in many rocks leading to high and variable published analytical blanks. In addition, the method does not quantitatively separate Re for analysis. When fusions are spiked for isotope dilution, isotopic equilibrium between glass and bead is not achieved (Martin, 1990) and high Re blanks are endemic in the flux materials. Therefore, Re is usually determined on a separate sample aliquot, raising problems if the sample is heterogeneous.

Additional problems include: Os can only be isolated from the other PGEs for isotopic analysis (by either ICP-MS or N-TIMS) by taking an aliquot of the concentrate, usually the bead dissolution residue. This reduces overall sensitivity. Dissolution of the filter paper to dissolve the PGEs usually converts Os into the oxidised form. Oxidised forms of Os, particularly OsO_4, have enhanced ionisation compared to reduced forms (Gregoire, 1990) but also tend to produce much greater memory effects in ICP introduction systems. Furthermore, determination of Os in solution with Pt, where Pt is often at much higher concentrations, can cause significant interference of $^{190}Pt^{+}$ on $^{190}Os^{+}$ reducing precision (Ravizza and Pyle, 1997). Low level Ru analysis by Ni-S fire assay has proven troublesome in some instances (Ravizza and Pyle, 1997) due to carry over of Ni on the filter paper following bead dissolution, leading to a multitude of possible $^{x}Ni\text{-}^{y}Ar^{+}$ type interferences.

Ni-S fire assay has many advantages in dealing with large samples and is well suited to many applications in geochemistry (e.g. Ravizza and Pyle, 1997). However, it is not entirely suitable for projects requiring either accurate Re-Os geochronology or the routine analysis of PGEs in very low level (<<1ppb) materials solely by ICP-MS (Table 2.1).

2.4.2 Pb Fire Assay

This process is a reductive fusion and it is argued (Hall and Pelchat, 1994) that it provides the most reliable and cost effective means of preparation of rocks for PGE analysis. The main disadvantage of this technique however, is that it has a very high blank as it utilises metals such as Ag and Pb which are likely to naturally concentrate PGEs. Thus, it is only really suitable for analysis of high abundance, or

ore-grade samples. Detection limits currently reported for Pt and Pd are in the range, Pt: 3-15ppb and Pd: 1-5ppb (Hall and Pelchat, 1994).

The Pb-assay method consists of thoroughly mixing the finely divided sample with a flux, normally containing Ag as the PGE collector. During fusion, carbon powder is added to the mixture and reduces the PbO formed to Pb. The Pb sinks to the base of the crucible carrying the PGEs with it. The molten Pb and slag are poured into an Fe mould where the Pb button is separated for the second stage, cupellation. The Pb is removed by oxidation, vaporised and absorbed into the cupel thus leaving the Ag prill. This prill is then dissolved and the majority of the Ag is precipitated as AgCl upon addition of HCl. The resulting solution is then analysed for PGEs (Hall and Pelchat, 1994).

Pb fire assay is the classical method of analysis for Au and can be used to obtain quantitative recoveries of Pt, Pd and Rh. During cupellation (heating of the Pb-button in an open dish in an oxidising atmosphere) however, some Ir and Ru, and almost all Os are usually lost, unless specialised recovery procedures (i.e. cupellation must be replaced by dissolution of the Pb button and subsequent distillation) are implemented (Potts, 1987). In addition, the presence of AgCl creates a high dissoved solid content in the solution to be analysed, which can be problematical for ICP-MS analysis.

2.4.3 Techniques using Tellurium

2.4.3.1 Tellurium Sulfide Fire Assay

Shazali *et al.* (1987) investigated the possibility of using the chalcophile element Te as a collector of the PGEs via a fire assay procedure. Their results indicate that the temperature of fusion had to be tightly controlled to ensure total sample decomposition. Also, this method proved to be unsuitable for samples rich in chromium, as the Te-S button would not separate from the silicate slag. Comparison of the Ni-S and Te-S fire assay procedures led the above authors to conclude that Ni-S is a superior collector. The total recovery of Rh, Pd, Pt and Ir with Te-S, was 74,

81, 84 and 92% respectively of that by Ni-S fire assay. The results for Os and Ru were considered to be similar for both types of fire assay (Shazali *et al.*, 1987).

2.4.3.2 Te Coprecipitation

This step is useful as a "clean up stage", if the critical end stage of dissolution of the Ni-S bead, (i.e. cessation of H_2S production) is missed. Addition of Te (with tin chloride) removes any PGEs which may have entered solution, as a black precipitate which initially floats but then sinks to the bottom of the reaction vessel (McDonald *et al.*, 1994). However, if the end stage of dissolution is carefully observed and the beaker containing the acid (plus dissolved Ni-S) is removed from the heat and quickly cooled as soon as H_2S production ceases, Te precipitation is unnecessary (McDonald pers. comm.). Indeed, if possible, the Te precipitation step should be avoided as addition of Te, a natural concentrator of PGEs, will raise the blank level.

2.5 Chromatographic Separation of Ir, Pt, Pd, Ru & Re

2.5.1 Cation Chromatography

PGEs tend to form anionic complexes in most mineral acid solutions. Hence, in acid media such as hydrochloric acid, chloro-complexed PGE anionic complexes are not absorbed on to cation resin and pass straight through, whereas most other metals should be quantitatively adsorbed. PGE yields through cation columns may be very high (>95%) (Jarvis *et al.*, 1997[a]), especially if mixed organic-solvent/acid media are utilised (Korkisch and Klakl, 1968). Cation-exchange chromatography has recently been applied to PGE analyses of geological materials (Ely *et al.*, 1999; Jarvis *et al.*, 1997[a]; 1997[b]). One disadvantage with cation separations is that unless very small samples are used (Ely *et al.*, 1999) relatively large amounts of resin are necessary to adsorb the non-PGE metals and thus lengthy cleaning of the resin with large volumes of clean acid is required. In addition, quantitative elution of PGEs from the column requires relatively large amounts of eluant which tends to elute

other base metals (Jarvis *et al.*, 1997[b]). Zr and Hf particularly, may pass through a cation column in sufficient quantities to induce severe molecular interferences on certain PGEs (e.g. Pd, Ir & Pt). This has been noted by Ely *et al.* (1999) and is a major obstacle in accurately quantifying these elements using cation exchange methods.

There are two major drawbacks to cation chromatography as regards PGE analysis. Firstly, in schemes where Os is not separated from the other PGEs prior to loading of the sample onto the column, and Os is not in the +8 oxidation state, it can be strongly adsorbed on cation resin and hence be very difficult to elute. Even in procedures where Os is not volatilised during digestion, it cannot be easily or quantitatively eluted from a cation column. Secondly, the near simultaneous elution of PGEs from cation resin limits the opportunity for removal of potential interferences, thus, increasing the number of masses that must be measured within a single solution.

2.5.2 Anion Exchange Chromatography

For effective PGE analysis by ICP-MS it is desirable to have the option of being able to separate some of the PGEs into different solution fractions. This improves sensitivity, as fewer elements have to be analysed in the same solution. This allows analysis of smaller volumes of more concentrated solution. Ion-exchange chromatography is a very effective way of achieving these aims due to the differing behaviour of PGEs on anion resin (Korkisch, 1989; Korkisch and Klakl, 1968).

Anion exchange separation for PGE analysis by ICP-MS has been widely used to separate different combinations of PGEs from various geological materials (Colodner *et al.*, 1993; Crocket *et al.*, 1968; Morgan *et al.*, 1991; Yi and Masuda, 1996). Several combinations of elutants, some employing insitu-reduction to aid removal of Ir from the resin, are possible for the separation of Ir, Pt, Pd and Ru from other metals. Rehkämper and Halliday (1997) have presented a scheme for separation of PGEs and Re from anion resin for ICP-MS analysis using mixed acid elutions, but their method does not enable quantification of Os.

Stable PGE anionic chloro-complexes in mineral acid solutions are strongly retained by anion exchange resins (Crocket *et al.,* 1968; Korkisch, 1989; Korkisch and Klakl, 1968; Petrie and Morgan, 1982). The controlling factor for the adsorption of most elements appears to be valance state and ability to form stable ion pairs between the chloro-complexes and quaternary ammonium groups of the resin (Korkisch, 1989). In particular, reduction of strongly held $IrCl_6^{2-}$ to the weakly retained $IrCl_5^{2-}$ and $IrCl_4^-$ (or $IrCl_4[H_2O]_2^-$) species by the resin itself, is a problem that has necessitated the use of oxidants, co-loaded onto the column, to maintain the oxidation state (Crocket *et al.,* 1968; Yi and Masuda, 1996). A powerful oxidant is required to elevate Ir to the IV^+ oxidation state. The use of cerium ammonium nitrate for ICP-MS analysis is not favoured due to problems with isobaric interference of $^{140}Ce^{35}Cl^{16}O^+$ and $^{140}Ce^{37}Cl^{16}O^+$ on $^{191}Ir^+$ and $^{193}Ir^+$ respectively. Calcium hypochlorite ($CaOCl_2$) is preferred by some workers (Yi and Masuda, 1996). The disadvantage of this approach is that it may raise the blank through use of additional reagents.

Rehkämper and Halliday (1997) have used bromine-water as an oxidant. Colodner *et al.* (1993) bubbled the sample with chlorine gas prior to column loading to ensure complete conversion of Ir to the +4 oxidation state. Anbar *et al.* (1997) have also used Cl-oxidation of samples to ensure Ir retention on anion resin, followed by reductive elution using sulfurous acid. This method is attractive both in terms of minimising blanks to consistent levels and for its low cost.

Anion Exchange chromatography offers a potentially low-blank (<50ppt), technique for preconcentration and separation of the PGEs from their rock matrix, when used in conjunction with a suitable digestion technique (e.g. Carius tube digestion). This technique has the advantage that Re can be quantitatively obtained on the same sample as Os (via solvent extraction) and the other PGEs. In addition, each of the PGEs can be obtained within separate fractions, due to their differential adsorbtion characteristics on anion exchange resin. This alleviates problems of isobaric overlaps between the PGEs and also enhances sensitivity.

Technique	Advantages	Disadvantages
Acid Digestions	Low blank levels	1)Spike-sample equilibration can be a problem. 2)Precautions have to be taken to minimise Os and Ru loss through volatilisation. 3)Some residual PGE containing phases (i.e. chromite) may not dissolve.
Carius Tube Digestion	1)Very low blanks 2) Os not lost during dissolution as vessel sealed.	Can be dangerous if not handled properly.
Sodium Peroxide fusion	Very effective at dissolving resistant phases.	1)Uses very small sample size-may lead to nugget effect errors. 2)High blank to sample ratio. 3)Crucibles for fusion have to be reused introducing a contamination risk.
Lead Fire Assay	Relatively cheap method	1)Very high blank levels, make this method unsuitable for low-level PGE analysis. 2)Traditional Pb-assay methods result in the loss of all Os and some Ir and Ru.
Nickel Sulfide FireAssay	1)Uses a large sample aliquot, minimising sampling errors. 2)Low blank to sample ratio. 3)Fusions are done in disposable clay crucibles, preventing inter-sample contamination.	1)Silica-poor and carbonate -rich roc types may not fuse properly. 2)Care has to be taken to avoid PGE loss during sulfide bead dissolution (can be overcome by isotope dilution or Te precipitation). 3)Re cannot be quantitatively recovered precludes Re-Os geochronology.
Cation Chromatography	1)Can produce very high yields for PGEs (<95%). 2)Low associated blanks	1)Unless small samples used need a large volume of resin which is expensive and can raise blank. 2)Doesn't provide good separation between PGEs and Hf/Zr. 3)Os cannot be eluted from resin
Anion Chromatography	1)Allows precise separation of the PGEs from each other. 2)Low associated blanks	1)Unless small samples used need a large volume of resin which is expensive and can raise blank. 2)Care must be taken not to overload resin with matrix elements or PGEs will not be adsorbed.
Te Coprecipitation	Can be used to eliminate PGE losses during Ni-S bead dissolution.	1)Te concentrates PGEs and so will unnecessarily raise the blank levels. 2)Te can cause interferences if measuring PGE concentration via NAA.

Table 2.1 Summary table of the main disadvantages and advantages of techniques used in PGE analysis

2.6 Analytical Instrumentation

2.6.1 Instrumental Neutron Activation Analysis (INAA)

Neutron activation analysis is a sensitive method of rock analysis capable of determining a large number of elements simultaneously, without necessarily destroying the sample. INAA uses ~ 100mg of a powdered rock sample which are placed in a neutron flux within a nuclear reactor, together with the standards and irradiated for approximately 30 hours. The neutron flux gives rise to new, short-lived radioactive isotopes of the elements present which emit gamma radiations. Particular isotopes can be identified from the gamma radiations emitted and are counted by means of gamma ray spectrometry at set intervals after irradiation, with the intensity of the radiation being proportional to the amount of the isotope present (Rollinson, 1993).

Advantages of this technique include the simplicity of sample preparation. Rocks undergo no chemical treatment in the course of analysis, thus, provided care is taken in crushing and powdering samples they should be free from any contamination. Another advantage of this technique is that analyses are virtually free of matrix interference effects (Potts, 1987). The main disadvantage of this technique is that it requires specialised irradiation facilities and can be expensive in terms of sample irradiation (Potts, 1987).

INAA is of variable use in determining PGE concentrations. The sensitivity of this method with regard to the PGE series decreases in the order Ir> Au> Rh>> Pd> Pt> Os> Ru. Therefore, analyses are often limited to Ir, Au and Pd as the other elements are below the detection limit of this method (Rollinson, 1993). Detection limits can be raised for the PGEs by combining INAA with a preconcentration method such as Ni-S fire assay (McDonald *et al.*, 1994). Other reasons why data for the rest of the PGE series are not always presented include: Rh has a very short half-life (4.4min), thus, only laboratories that have counting facilities in the reactor building can analyse for Rh (Barnes *et al.*, 1985). A potential interference on Ru determination arises from Ru produced by uranium fission. This effectively precludes determination of Ru in basic and more silicic rocks (Crocket, 1979). INAA detection limits for Ir are between 2-500ppt.

2.6.2 Inductively Coupled Plasma Mass Spectrometer (ICP-MS)

The ICP-MS combines two analytical facilities to produce an instrument with powerful potential in the field of multi-element trace analysis. Samples must first be taken up into solution and are then aspirated into an argon plasma. This inductively coupled plasma is used as a source of ions which are then measured by the mass spectrometer. This technique thus combines a relative freedom from matrix interferences, characteristic of the inductively coupled plasma, with the favourable signal-to-background ratios obtainable by mass spectrometry (Potts, 1987). The main advantage of the ICP-MS is its ability to measure very low elemental concentrations (i.e. to sub ppb level).

Caution needs to be taken when analysing samples by ICP-MS, to ensure a complete washout between samples, so that samples do not become contaminated by memory effects within the machine (Hall and Pelchat, 1994). Os is particularly prone to causing memory effects, but this can be overcome by use of different nebulisation procedures (See Chapter 4 & Appendix 1).

When analysing material by ICP-MS account must be taken of some background mass interferences, which arise from five main sources

(i) The Ar plasma gas

(ii) The solvent in which the analysed species was dissolved

(iii) Air entrained in the plasma and impurity gases in the Ar itself

(iv) Material eroded off the aperture

(v) Reagent contamination

(Potts, 1987).

These effects can be observed by taking a background count of a blank solution which is subtracted from later sample analyses. Standard solutions of known elemental concentration are used for instrumental calibration and allow comparison of results obtained in different laboratories. In routine ICP-MS trace-element analysis, steps have to be taken to overcome instrumental drift with time which

occurs when a series of samples are analysed sequentially. Two methods exist by which instrumental drift can be overcome (Potts, 1987):

a) Internal Standardisation

This procedure involves addition of a solution of known concentration, to all samples and standard solutions. Analysed mass counts are then normalised with respect to the appropriate internal standard intensity. Internal standards should contain elements which have similar ionisation characteristics in the plasma as the elements to be determined (Potts, 1987).

b) Isotope Dilution

In addition to drift correction, measurement by isotope dilution can also be employed to compensate for losses of the analyte (Hall and Pelchat, 1994) during preparation and analysis. The principal behind isotope dilution is that many elements exist as two or more naturally occurring isotopes. For the specific element under analysis, an isotope dilution spike containing an enriched fraction of one of its isotopes is added at a known concentration to all solutions. The relative intensity of spike to natural isotope is measured. Quantification is then carried out using the isotopic abundance of the enriched spike, the measured isotope ratio, and the known natural isotopic ratio of the element (Potts, 1987). Any losses occurring during the pre-treatment of the sample (after spiking) will affect all the isotopes equally and leave the spiked isotope ratio unchanged (Van Heuzen *et al.*, 1989).

Addition of a single mixed spike to a sample is desirable to minimise weighing errors. Principles used to obtain optimal error propagation for isotope dilution measurements are outlined by Heumann (1988) and Van Heuzen *et al.* (1989). When measuring Os isotopes for tracing and geochronological purposes it is desirable to minimise the effects of the spike on the measured isotopic ratios, i.e., $^{187}Os/^{186}Os$, by not overspiking samples.

Limiting factors for the isotope dilution technique include the difficulty in finding two isotopes free of isobaric interferences and the need for some ability to predict likely sample concentrations, so as to optimise spiking (Heuzen *et al.*, 1989). Ravizza and Pyle (1997) have noted that Pt spikes enriched in ^{198}Pt can suffer from ^{198}Hg interferences and should be avoided. All of the PGEs except monoisotopic Rh

are amenable to isotope dilution. A potential difficulty with this technique is that equilibration between the spike and sample may not be achieved, as equilibration only occurs when there is total decomposition of the sample (Xie and Kerrich, 1995). A number of different authors however, have successfully used isotope dilution combined with one of the above digestion techniques for PGE determination in geological materials (Enzweiler *et al.*, 1995; Evans *et al.*, 1993; Gregoire, 1988; Ravizza and Pyle, 1997; Rehkämper and Halliday, 1997; Yi and Masuda, 1996).

Technique	Advantages	Disadvantages
Neutron Activation Analysis	1)Doesn't require any complex sample preparation. 2)Doesn't contribute to the blank	1)Requires specialised irradiation facilities. 2)Analyses are often limited to Au, Ir and Pd.
N-TIMS	Very precise isotopic measurements (i.e. for Re-Os geochronology)	Less rapid data collection than with ICP-MS.
Inductively Coupled Plasma Mass Spectrometry	1)Can measure the full range of PGEs. 2)High sensitivity, therefore can be used to analyse very low abundance samples.	1)Samples must be in the form of solutions for analysis, therefore care must be taken to ensure all residual phases have dissolved and to limit any contamination during preparation of the solutions. 2)Memory effects can occur within the machine.

Table 2.2 Summary table of the main disadvantages and advantages of analytical techniques used in PGE measurement

2.7 Detection Limit - Definition

Detection limit is generally defined as "that concentration equivalent to three times the standard deviation of a blank". For use with a fire assay procedure the blank should be taken through the procedures of decomposition, separation and analysis a number of times. Contamination by flux constituents and that introduced during the fire assay procedure itself, play a dominant role in deciding the detection limit (Hall and Pelchat, 1994). Further discussion of detection limits appropriate to this study are presented in Chapter 5.

3: Evaluation of Ni-S Fire Assay Pre-concentration for ICP-MS Analysis

3.1 Introduction

Following due consideration of all the methods available for measuring PGE content in geological samples (see Chapter 2), Ni-S Fire assay appeared the most promising method to pursue for PGE-measurement by ICP-MS. This is primarily because of the low blank to sample ratios associated with this method and the low dissolved solid content of the resulting solutions. In addition, the ability to process large sample quantities should permit analysis of samples with low PGE concentration and help to alleviate sample heterogeneity problems, providing sufficiently low blanks can be obtained. The experimental procedure employed in this technique and developments made therein are outlined below:

3.2 Methodology

3.2.1 Bead Preparation

(Amounts of reagents given are for a 15g sample, but can be scaled up or down, according to sample size used; based on the method of Jackson *et al.*, 1990).

1) Into a large glass vial are weighed:

15 g of sample

5g of Ni; (Carbonyl processed, Inco type 123) *collector*

3g of sublimed sulphur (BDH) *collector*

10g of anhydrous sodium carbonate (Hopkin & Williams) *flux*

20g of Analar borax (BDH) *flux*

3g of silica (BDH)

N.B. *i) Flux:sample ratio must be between 2:1 and 1:1,*

ii) 5g of silica are used if the sample is ultramafic.

iii) The reagents are all shaken within their bottles before weighing out to prevent any fractionation due to settling

2) The glass vial is sealed and shaken thoroughly for at least 5 minutes to ensure that the reagents are thoroughly mixed together.

3) The fusion mixture is placed in a porcelain/clay crucible, which is then placed in the furnace at a temperature of 950°C. If porcelain crucibles are being used the crucible containing the sample is placed within a second crucible to protect the furnace in the event of the fusion burning through the first crucible.

4) The furnace should then be turned up to a temperature of 1000°C, and the sample fused at this temperature for 1.25 hours.

5) After this time the crucibles should be carefully removed from the furnace and allowed to cool enough so that they can be handled with bare hands.

6) Break crucible and retrieve Ni-S bead from the base (checking that complete fusion has occurred, indicated by a homogenous black fusion glass and absence of any other disseminated Ni-S beads).

7) Beads are then weighed to determine the Ni-S collection efficiency and placed in a labelled, sealed bag.

3.2.2 Ni-S Bead Dissolution

1) After assay, the Ni-S button is cracked using a hammer (the bead is sealed inside a plastic bag to prevent any contamination).

2) The bead is then weighed again and the chips are transferred directly to a 500ml conical flask.

3) Into the conical flask is placed 350ml of 12N (36%) Analar HCl.

4) The flask is covered with a watch glass and boiled at a temperature of ~ 350°C.

5) Once dissolution is complete (and as soon as H_2S production ceases) the conical flask is cooled with a damp cloth.

6) The solution is then immediately filtered under vacuum (using a vacuum pump), through filter paper (pore size 0.45μm), trapping PGE sulfide particles.

7) When the filtration is complete and the vacuum flask has been washed down with MQ to remove any PGE particles which may have adhered to its surface, the filter paper is folded into a triangle and placed into a clean, sealed Teflon vial.

3.2.3 Filter Paper and PGE Residue Dissolution

1) 2ml of concentrated Romil grade double distilled HNO_3 is added to the Teflon vial containing the filter paper.

2) The vial is then sealed again and placed on a hotplate at 50°C for 10 minutes until the filter paper has dissolved.

3) Once the paper had dissolved, the vial is placed in the fridge to minimise volatile OsO_4 loss. 2ml of Romil grade concentrated HCl are then added to the Teflon vial and again the solution is heated at a temperature of 100°C in the sealed vial for 20 to 30 minutes, or until any visible precipitate dissolves.

4) Again cool the solution by placing in the fridge, then pour the solution into a 10ml volumetric flask. Wash the Teflon vial out with some MQ, also pour this into the volumetric flask. Finish by making the solution up to 10ml in the volumetric flask with MQ.

5) Pour the solution from the flask into a plastic vial, and analyse.

N.B. All glassware used is soaked for at least 24 hours in aqua regia and all Teflon vials used are cleaned overnight in Romil grade HNO_3 by refluxing on a hotplate at 100°C.

After initial work using the technique as outlined above, the composition of the fusion mixture was altered slightly to try and improve bead-recovery (after McDonald pers. comm.):

e.g. Reagents used for a 20g sample:

12g $NaCO_3$, 24g Borax, 5g Sulphur and 14g $NiCO_3$ (~8g Ni pwdr)

This mixture utilises a higher Ni:sample ratio than that of Jackson *et al.* (1990) and increases the bead recovery. It also varies from Jackson *et al.* (1990) in that no silica is added to the mixture for standard silicate rock analyses. Some points regarding the use of this method which became apparent during the project include:

a) Crucibles must be placed in the oven at the fusion temperature and must be removed from the furnace whilst hot. If the crucibles are allowed to either heat up/cool down slowly, the mixture does not fully equilibrate and the silicate slag becomes fractionated.

b) Bead recovery drops if the crucibles are not placed in the hottest part of the furnace.

c) During the bead dissolution stage the acid needs topping up periodically, this is best done by keeping a flask of spare acid on the hotplate, as cooling the dissolution solution in order to add more acid greatly increases the dissolution time.

d) Bead blanks made with silica are allowed to develop a white-coloured oxide coating prior to dissolution, as this seems to decrease dissolution time.

e) There is a very large scope for loss of PGEs during the Ni-S assay procedure. Notably during the dissolution stage, where it is essential to remove the solution from heat as soon as H_2S production ceases and also during the filtering procedure where residual grains (normally microscopic) may tend to adhere to the filtration equipment.

In order to overcome such problems people have tended to use the Te-coprecipitation method (see Chapter 2). However, it was decided to try and avoid using this method because of its large, inherent PGE blanks. Thus, to compensate for PGE losses which may occur during the Ni-S fusion and subsequent bead dissolution, isotope dilution was employed.

3.2.4 Isotope Dilution

Isotope dilution (I.D.) relies on achieving equilibrium between spike and sample during fusion, assuming this condition is met, subsequent processing losses can be tolerated. A mixed ^{191}Ir and ^{198}Pt spike was initially used. Optimum error

propagation is achieved using a $^{191}Ir/^{193}Ir$ ratio of the spike-sample mix, of ~2.5.

N.B. Natural Ir ratios = $^{191}Ir/^{193}Ir$ ~ 0.6

Spike Ir ratio = $^{191}Ir/^{193}Ir$ ~ 53.85

Natural Pt ratio = $^{198}Pt/^{195}Pt$ ~ 0.2

Spike Pt ratio = $^{198}Pt/^{195}Pt$ ~ 83.22

The spike was first calibrated using Ir and Pt standards made from stoichiometric Ir and Pt salts at DTM, Carnegie Institution, Washington D.C. and then rechecked by calibration with standards made from 1000ppm Ir and Pt stock solutions. The isotope ratios of the spike were ascertained by numerous trial runs on the ICP-MS.

3.2.5 Method for Combining Ni-S Fire Assay with Isotope Dilution

1) The dilute Ir spike is weighed into a clean Teflon vial which is then sealed.

2) If a large spike volume is required, the volume is reduced by gentle evaporation under purified air.

3) Using a Teflon spatula, a pit is excavated within the fusion mixture which has just been placed into the crucible

4) The spike is then transferred from the Teflon vial into the excavated pit in the crucible.

5) Wash the Teflon vial with a drop of MQ water to remove any residual spike, then pipette this into the crucible as well.

6) Cover the crucibles and leave for an hour to allow spike to dry into the powder.

7) When the spike is dry the sides of the crucible are gently tapped so that powder infills the excavated pit and covers over the spike.

8) Crucibles are then placed in the furnace (as before).

3.3 Results of Ni-S Fire Assay:- Blank Evaluation

3.3.1 Sources of the Blank

Ability to quantify and reduce the blank to an acceptable level is the limiting factor in analysing low PGE concentrations in geological samples, as technology now exists which has the capability to detect these elements at abundances of only 1ppt (i.e. the Elan 6000 ICP-MS). The blank associated with Ni-S fire assay is imparted to the sample from a number of sources, each of which have been addressed:

a) From the Ni used in the fusion

This appears to be the single largest contributor to the blank and every effort should be made to both quantify the exact PGE contents within Ni metal (or $NiCO_3$ powders) used, and to obtain a source of very 'clean' Ni powder with regard to the PGEs.

b) From the crucible during fusion

The crucibles initially used were made of clay and thus by the very nature of sediments may have heterogeneous and variable PGE contents. Any blank contribution from the clay crucible is likely to be very small. Comparisons of blank results obtained using both clay and porcelain crucibles are presented and suggest that porcelain crucibles may be more suitable for low abundance PGE measurement (Fig 3.2).

c) From the other fusion reagents

High-grade reagents should be used and thoroughly checked for possible blank contribution.

d) From acids used to dissolve filter paper and residual PGE grains

The PGE contents of ultrapure nitric and hydrochloric acids have been quantified by ROMIL by evaporating a number of 250ml samples to dryness and then dissolving in a small volume of 2% DsD acid (Table 3.1). This procedure is carried out in a clean laboratory.

	HNO_3	HCl
Ir	<5	<1
Os	<4	<6
Pd	<4	<3
Pt	<5	<2
Rh	<1	<7
Ru	<1	<2
Re	<1	<2
Au	<5	<1

Table 3.1 PGE contents of ROMIL ultrapure acids (values in ppt)

e) From unclean lab practices (i.e. dust/pipette contamination etc.)

Every attempt is made to prevent any contamination in this manner. For example, all working surfaces are covered with cling-film prior to use, gloves are worn at all times, all jewellery that may come into contact with the samples is removed, all glassware is soaked in aqua regia for at least 24 hours prior to use. Samples are dried down under clean air conditions.

3.3.2 Quantification of the Blank

Thirteen blank analyses were conducted with both blanks that were and were not spiked for isotope dilution (Table 3.2). The total PGE concentrations within each of the blank beads are presented in Table 3.3.

PGE concentrations within the non-I.D. blanks are extremely variable (Fig 3.1). By comparison, the PGE concentrations obtained by I.D. (Fig 3.2) are highly reproducible. This implies that during bead dissolution sporadic losses of the PGEs must be occurring. Use of I.D. compensates for these losses. The ability to generate reproducible blanks is extremely significant as it allows blank corrections to be confidently applied to both sample and standard data. It is considered however, that erratic distribution of PGEs may be an inherent problem with the fusion process if the PGEs are heterogeneously distributed as 'nuggets' within the Ni powders used.

Sample Name	Equivalent Sample Weight	Bead Recovery	Elements spiked for isotope dilution
Blank 1	15g	88%	
Blank 2	15g	79%	
Blank 4	15g	81%	
Clay Blank	5g	83%	Ir
Ceramic Blank	5g	80%	Ir
BL10	10g	90%	
BL50	50g	91%	
SBlankA	10g	89%	Ir, Pt, Os
SBlankB	10g	89%	Ir, Pt,
SCERB-1	5g	78%	Ir, Pt
SCERB-2	5g	90%	Ir,Pt
SBL10	10g	91%	Ir, Pt, Pd, Os
SBL50	50g	92%	Ir, Pt, Pd, Os

Table 3.2 Summary table of the blank samples run (N.B. Bead Recovery is a calculation of the bead weight, as a percentage of the weight of the Ni and S used for the fusion. Losses are probably due to volatilisation of S, however, the silicate glass must always be checked to ensure that no droplets of Ni-S bead (and hence PGEs) are disseminated within the glass.)

	Equivalent Sample Weight	Os	Ir	Ru	Pd	Pt
Blank 1	15g	1.899	0.076	13.271	3.242	0.989
Blank 2	15g	0.550	0.040	27.932	1.783	2.814
Blank 4	15g	0.462	0.035	30.136	0.899	0.648
Clay Blank	5g	0.117	0.200	1.048	8.159	150.716
Cer Blank	5g	0.064	0.046	0.507	1.603	501.218
BL10	10g	0.725	0.237	0.980	3.463	3.578
BL50	50g	0.767	0.207	11.469	7.594	3.609
SBlankA	10g	2.819	**0.148**	1.018	3.572	**3.511**
SBlankB	10g	3.969	**0.112**	1.184	3.793	**2.418**
SCERB-1	5g	**0.034**	**0.036**		**0.846**	**1.493**
SCERB-2	5g	**0.032**	**0.037**		**0.546**	**1.526**
SBL10	10g	**0.152**	**0.083**		**2.623**	**2.569**
SBL50	50g	**0.5325**	**1.395**		**9.748**	**8.744**

Table 3.3 Summary table of all blank data obtained in ppb (note different bead-weights) (N.B. prefix 'cer' denotes ceramic crucible used, prefix 'S' denotes blank spiked for I.D. Numbers given in bold print are those obtained by I.D.).

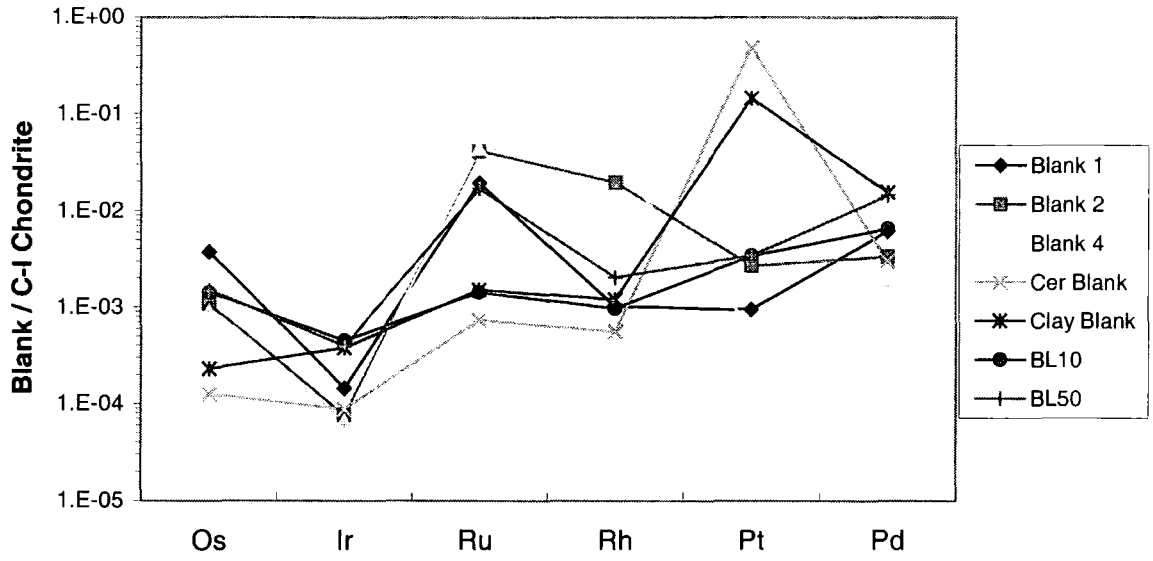

Fig 3.1 Chondrite-normalised log-plots of non-isotope dilution blanks

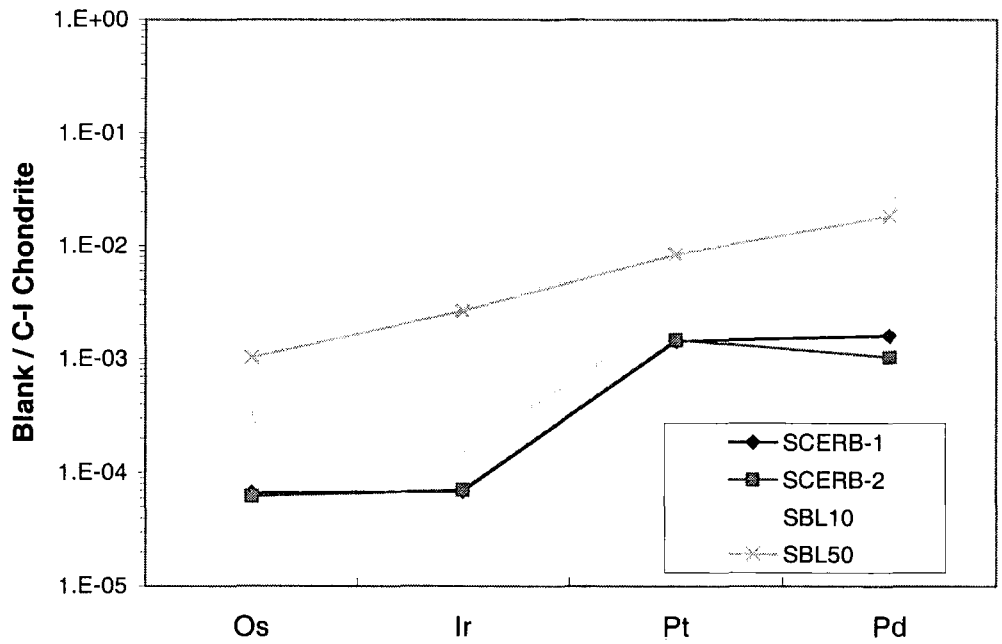

Fig 3.2 Chondrite-normalised plot of absolute PGE abundances in blanks obtained by isotope dilution; a comparison of the blanks associated with both clay and ceramic crucibles (SCERB = spiked blank using a ceramic crucible, SBl = spiked blank with clay crucible) N.B. For most of the PGEs the blank is considerably lower when using ceramic crucibles.

Initial results show that even using I.D. Ir and Pt concentrations in the blanks can differ widely (Table 3.4). This implies that the differences noted in blank data

are largely due to variable PGE content in the fusion reagents, rather than to variable loss of PGEs during dissolution and fusion. The average Pt and Ir abundances (Table 3.4) have been used to blank correct the later spiked standards by assuming that the blanks measured are representative of total Pt-Ir contribution from reagents used for a 10g sample.

Name of sample	SBLANK A	SBLANK B
Total Ir Measured (ng)	0.15	0.11
Total Pt Measured (ng)	3.51	2.42
Reproducibility of results for Ir	Values differ by 25 %	
Reproducibility of results for Pt	Values differ by 31%	
Average Ir in blank (ng)	0.13	
Average Pt in blank (ng)	2.97	

Table 3.4 Summary of results for calculation of Ir and Pt content of blank Ni-S beads, by isotope dilution.

The chondrite-normalised plots of the PGE abundances in the blanks (Fig 3.1 & 3.2) imply that none of the elements are significantly enriched relative to chondrite. Therefore, it can be assumed that the Ni-purification process does not lead to any significant fractionation effects within the PGE group. Care is always taken to thoroughly shake the Ni powder prior to use to prevent fractionation of the PGEs due to settling of the heavier elements (after McDonald pers. comm.).

3.3.3 Measurement of Blank Contribution from Ni

Blank contribution from the Ni powders are measured by dissolving 1g of Ni powder in nitric acid. Dissolution is easy for $NiCO_3$, with 1g of powder dissolving readily in 20ml of 10% double distilled HNO_3. 1ml of this solution is then generally diluted 11 fold (220-fold dilution in all) to produce a solution of suitable concentration for ICP-MS measurement. Dissolution of Ni metal is more problematical and requires heating of the solution (20ml of 10% HNO_3, to 1g Ni metal) in a sealed vial at 100°C for ~24 hours in order to generate a particulate-free Ni-metal solution. A wide variation in PGE content of Ni-powders occurs depending

on the manufacturer of the reagent (Table 3.5). Thus, Ni-reagents from new sources should always be thoroughly tested for blanks before use.

	Inco Ni	F.S. Ni	Specpure $NiCO_3$	Alfa $NiCO_3$	G.F.S Ni	ESPI Ni (3-nines)	ESPI Ni (5-nines)	Prolabo Ni
Ru	*3231*	*1845*	*1304*	*1182.5*	*3046*	*2991*	*1436.6*	*1943*
Pd	2.76	0.83	18.88	26.17	213.7	6.6	12.36	1.59
Os		1.99	2624.7	2260.5		295.7		
Ir	0.08	9.64	0.02	2.61	0.25	134.7	0.25	0.31
Pt	9.14	12.06	2.01	25.7	21.1	1186.8	1.53	5.58

Table 3.5 PGE content in ppb of various Ni-powders from different manufacturers (all values are based on at least two replicates of 1g of the same Ni-powder) N.B. Anomalous Ru concentrations due to Ni-Ar interferences

Things to note from these data include:

1) The Os values obtained for the Specpure and Alfa $NiCO_3$ should be discounted, as these huge values are artefacts of machine contamination from previously run Os-samples. This highlights the problem of memory effect in ICP-MS Os analysis.

2) Large standard deviations occurred between the replicate analyses, illustrating that there is a great deal of variability between separate dissolutions of the same Ni-powders, implying heterogeneous distribution of the PGE. This means that it is difficult to produce an accurate correction for the Ni-contribution to the blank.

3) The lowest blank levels are consistently recorded for Ir.

4) Minus concentration values are occasionally recorded for both Ir and Pd. This generally indicates that there are very low concentrations of the given element in the solution being measured (normally the case for Ir), or that an over-correction has been applied to the data to compensate for known interferences (sometimes the case with Pd). The data are routinely corrected online for direct interferences from elements with overlapping masses (see Chapter 4). It is attempted however, where possible, to measure isotopes of the PGE which do not experience any interferences.

3.3.4 Interferences on Ru

The spurious results obtained for Ru concentrations in the Ni-solutions (Table 3.5), show that Ru is the most problematical PGE to quantify by Ni-S fire assay and ICP-MS. The Ni-dissolution blanks give the impression that Ru is massively enriched. This is not an accurate representation of the Ru content however, as very different values are recorded for each of the three Ru isotopes routinely measured. In theory, the isotopes should have very similar values, but the measured abundances increase in the order $^{102}Ru > {}^{101}Ru > {}^{104}Ru$. This suggests that an interference is acting on some or all of the Ru isotopes. In order to try to determine the source of this interference, several different Ru standards made up in different matrices were analysed by ICP-MS (Table 3.6).

	^{101}Ru	^{102}Ru	^{104}Ru
Specpure $NiCO_3$	5337	8934	3877
0.5ppb Ru std (In HNO_3)	943	942	975
1ppb Ru std (In HNO_3)	1871	1830	1919
5ppb Ru std (In HNO_3)	11050	10838	11217
10ppb Ru std (In HNO_3)	18552	18302	18896
Ni Sol + 1ppb Ru std	6901	10962	5421
Ni Sol + 5ppb Ru std	12608	16423	11213
Ni Sol + 10ppb Ru std	19551	23354	18292
SP HCl	216	59	76
UP HCl	232	53	57

Table 3.6 Concentrations of the various Ru isotopes (ppt) as measured in different matrices

The results of these experiments indicate that the interference arises due to the presence of Ni in the system. When Ru standards made up in a matrix of HNO_3 are analysed, the different isotopes all show very similar values. However, when identical standards made up in matrix of $NiCO_3$ solution are analysed, very different concentrations are recorded for the different isotopes, again in the order $^{102}Ru > {}^{101}Ru > {}^{104}Ru$. The standards made in the $NiCO_3$ matrix typically record lower values of concentration than would be expected, with their concentration normally only between 75-95% of their separate $NiCO_3$ and Ru standard constituents. It is proposed

that the interferences encountered when using $NiCO_3$ as a matrix may be due to Ni-Argide interferences, i.e.

$$^{61}Ni + ^{40}Ar^{+} = ^{101}Ru$$

$$^{62}Ni + ^{40}Ar^{+} = ^{102}Ru$$

$$^{64}Ni + ^{40}Ar^{+} = ^{104}Ru$$

This would explain the very high values observed for ^{102}Ru, as ^{62}Ni is the most abundant of these three Ni isotopes, i.e. ^{61}Ni = 1.140%, ^{62}Ni = 3.364% and ^{64}Ni = 0.926%. The naturally occurring abundances of these isotopes are therefore: ^{62}Ni > ^{61}Ni > ^{64}Ni, which corresponds with the measured Ru abundances of ^{102}Ru > ^{101}Ru > ^{104}Ru (Fig 3.3). The situation is further complicated by addition of Ni to other Ar isotopes (i.e. ^{38}Ar) so that quantification is difficult. ^{101}Ru consistently has higher concentrations than the other isotopes when HCl matrices are analysed. This is probably due to Ni-Cl interference (i.e. $^{64}Ni + ^{37}Cl = ^{101}Ru$). The Ni, in this case, is thought to be contributed by the Ni-cones within the ICP-MS.

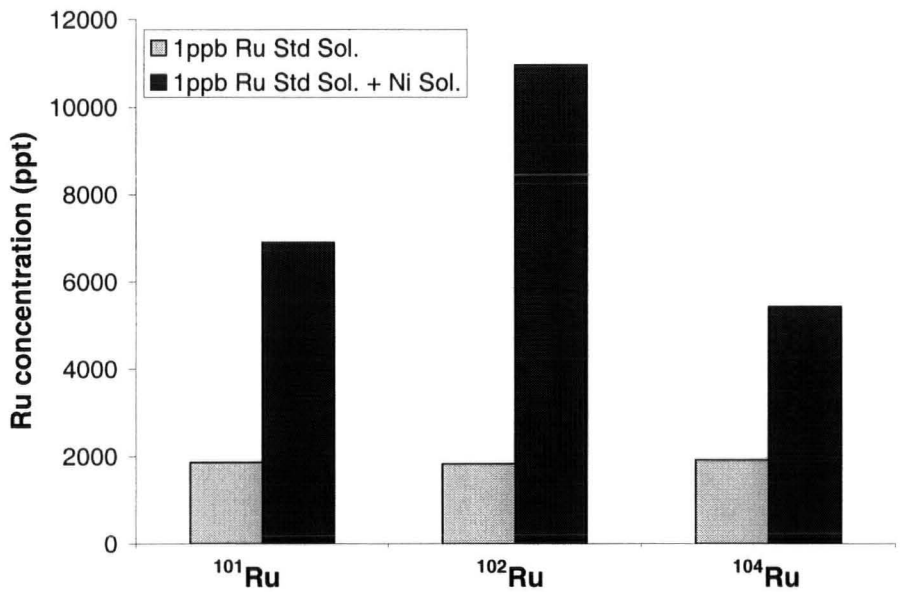

Fig 3.3 Enhancement of Ru-concentrations in standard solutions due to Ni-Ar interferences

3.4 Results of Fire Assay:- Evaluation of Ni-S Fire Assay via Standard Rock Analysis

3.4.1 Introduction

In order to evaluate how well the I.D. Ni-S fire assay was working, a number of standards well characterised for their PGE content were analysed. The standards chosen for this purpose were the international standard WPR-1, a peridotite and a proposed new PGE standard, WITS-1, a silicified komatiite sample. Accepted concentrations for these standards are shown in Table 3.7. WITS-1 has been analysed for PGEs by six different laboratories, using four different analytical techniques, thus, the PGE content is reasonably well constrained (except for Os; Tredoux & McDonald, 1996).

	WITS-1 (from McDonald *et al.*, 1996)	**WPR-1** (from Kane *et al.*, 1995)
Ru	5.1 ± 1.2	22.0 ± 4
Rh	1.3 ± 0.2	13.4 ± 0.9
Pd	7.9 ± 0.9	235.0 ± 9
Os	~ 1 – 1.5	No Value Reported
Ir	1.6 ± 0.2	13.5 ± 1.8
Pt	11 ± 2	285 ± 12

Table 3.7 Recommended PGE concentrations of WITS-1 and WPR-1

WITS-1, although not yet fully accepted as a certified reference material, was used in this study as it contains PGEs at levels appropriate to this study (i.e. 1-10 ppb). Also, the degree of inter-PGE fractionation in WITS-1 is small compared to many mineralised PGE standards (i.e. SARM-7). Thus, WITS-1 provides a closer comparison in noble metal concentrations between a standard and non-mineralised unknown samples, than many traditionally used standards. Finally, PGE distribution is more homogenous (although still nugget-controlled) in this fine-grained komatiite than in coarser-grained rocks, permitting the use of smaller sample sizes.

3.4.2 Results of Fire Assay Analyses of WITS-1 and WPR-1 (NON I. D.)

The values obtained for the first analyses of WITS-1 and WPR-1 are significantly lower than would be expected from the recommended values (Table 3.8). For WPR-1 the concentrations are about half of their recommended values, although the PGE patterns are very similar (Fig 3.4). For WITS-1 the values obtained are generally less than half of the recommended values (Fig 3.5), but again the overall PGE patterns remain very similar. This suggests that at some point during the formation and later dissolution of the Ni-S assay beads, wholesale losses of all the PGEs are occurring. Whether this is due to incomplete equilibration during fusion (seems unlikely as the silicate slag was black, homogeneous and did not contain any Ni-S blebs or un-melted rock powder) or due to later losses during bead dissolution, is uncertain.

	WITS-A	WITS-B		WPR-A	WPR-B	WPR-Sp
Ru	2.6	4.2		15.0	13.2	23.7
Pd	2.5	4.0		172.2	135.0	128.0
Os	1.8	1.6		30.7	18.7	30.6
Ir	0.4	0.5		7.8	6.6	
Pt	1.6	2.0		103.8	86.1	141.4

Table 3.8 Concentration of PGEs measured during first analyses of WITS-1 and WPR-1 (All concentrations in ppb). WITS-A & WITS-B etc. are replicate analysis. Prefix Sp= spiked.

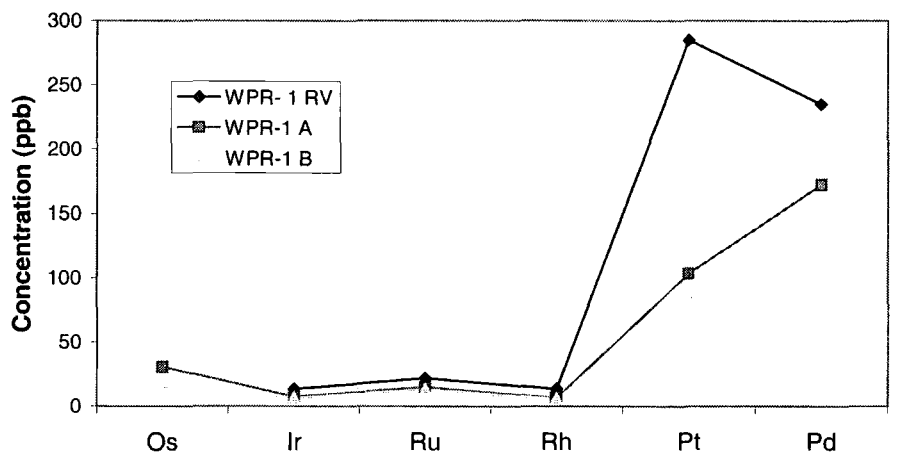

Fig 3.4 PGE concentrations in WPR-1 – Non I.D. (Prefix R.V. = recommended value)

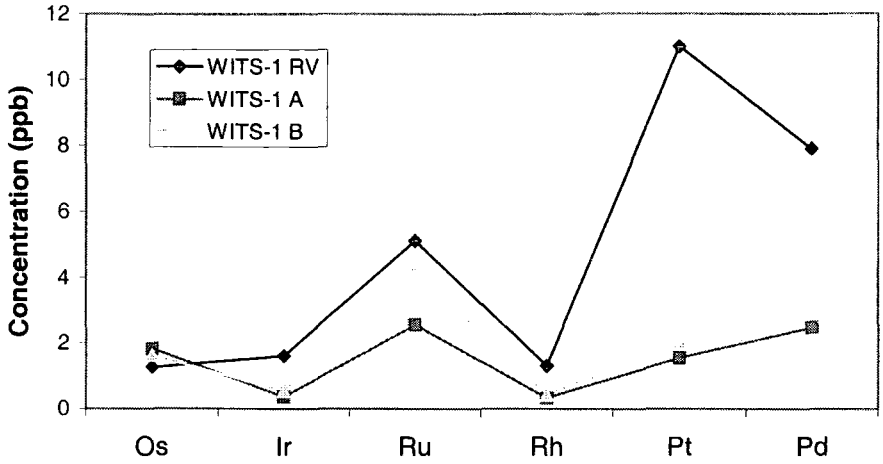

Fig 3.5 PGE concentrations in WITS-1 – Non I.D. (Prefix R.V. = recommended value)

3.4.3 Results of Fire Assay Analyses of WITS-1 and WPR-1 (USING I.D.)

The initial standard-rock analyses confirm that major losses of PGEs occur during the dissolution procedure. Thus, the potential of using I.D. in conjunction with the fire assay procedure for silicate rocks was investigated.

Standard	Sample Weight	Bead Recovery	Elements Spiked
WPR-1SP	5g	81%	Ir
WITS-1 SPA	20g	93%	Ir
WITS –1 SPB	20g	93%	Ir
SWPR-1 A	5g	82%	Ir, Pt, Os
SWPR-1 B	5g	86%	Ir, Pt
SWPR-1 C	5g	87%	Ir, Pt
SWITS-1 A	5g	83%	Ir, Pt, Os
SWITS-1 B	10g	88%	Ir, Pt, Os
SWITS-1 C	20g	90%	Ir, Pt
SWPR-1 D	5g	89.5%	Ir, Pt, Pd, Os
SWPR-1 E	5g	92%	Ir, Pt, Pd, Os
SWPR-1 F	5g	91%	Ir, Pt, Pd, Os
SWITS-1 D	5g	88.6%	Ir, Pt, Pd, Os
SWITS-1 E	10g	97%	Ir, Pt, Pd, Os
SWITS-1 F	20g	95%	Ir, Pt, Pd, Os

Table 3.9 Standards analysed in 1997 (S or SP in sample title indicates that sample was spiked, A, B etc. used to identify different replicate analysis)

PGE concentrations in both WITS-1 and WPR-1 were quantified and replicated using I.D. Initially the standards were spiked with Ir only. Ir was chosen as the most appropriate element to quantify because of its low blank. An Oakridge National Laboratory spike, enriched in ^{191}Ir was used (Ir isotopic composition of spike: $^{191}/^{193}$ = 54.573). The concentration of the spike was calculated by calibration with a DTM dilute Ir standard. The first standard spiked was WPR-1SP. This sample was spiked for Ir and produced the anomalously high value of 19ppb Ir (5.5ppb higher than the recommended value).

The next standards analysed were two replicates of WITS-1 (i.e. WITS-1 SPA/SPB, Table 3.10). Their preparation differed from WPR-1SP in having a higher Ni:sample ratio in the fusion mixture, which may account for the increased bead recoveries. WITS-1 SPA/B were analysed twice by ICP-MS using both a microconcentric and a Scott-type double pass nebulizer (which unless otherwise specified, is the nebulizer used for all other analyses). The microconcentric nebulizer has the advantage that it requires less sample solution and is made of Teflon; therefore, the aqua-regia solution used for dissolution of the filter paper and PGE residue could be analysed directly without dilution. Negation of the need to dilute the aqua regia effectively raises the detection limit (i.e. it would improve the relation between concentration and precision, Van Heuzen *et al.,* 1989). The potential for the use of this nebulizer will be further addressed in Chapter 4. In this set of analyses however, exactly the same solutions were run on both nebulizers and there was no appreciable difference between the results.

Comparison of the results obtained for both WITS SPA/SPB (Fig 3.6), show that there is still a lot of variability between the concentrations of these two identically prepared samples. They are still generally lower in concentration than the recommended concentrations for WITS-1. The exception to this statement is Ir, whose concentration has been calculated using I.D. The reproducibility between the Ir data is exceptional (0.7%, 1σ error) and calculated concentration is well within the range of the recommended WITS-1, Ir concentration, of 1.6 ± 0.2ppb.

WITS-1SPA = 1.44ppb (1.42ppb with Mass Bias Correction)

WITS-1SPB = 1.43ppb (1.41 ppb with Mass Bias Correction)

Further replicates of both WPR-1 and WITS-1 were prepared and spiked with Pt (and Os), as well as Ir. Like the above analyses of WITS-1, the results were very reproducible, although, the WITS-1 values tend to be lower than recommended (particularly for Pt; Table 3.11). The concentrations of both Ir and Pt obtained for all the WPR-1 spiked standards are slightly higher however, than the recommended values (Table 3.12).

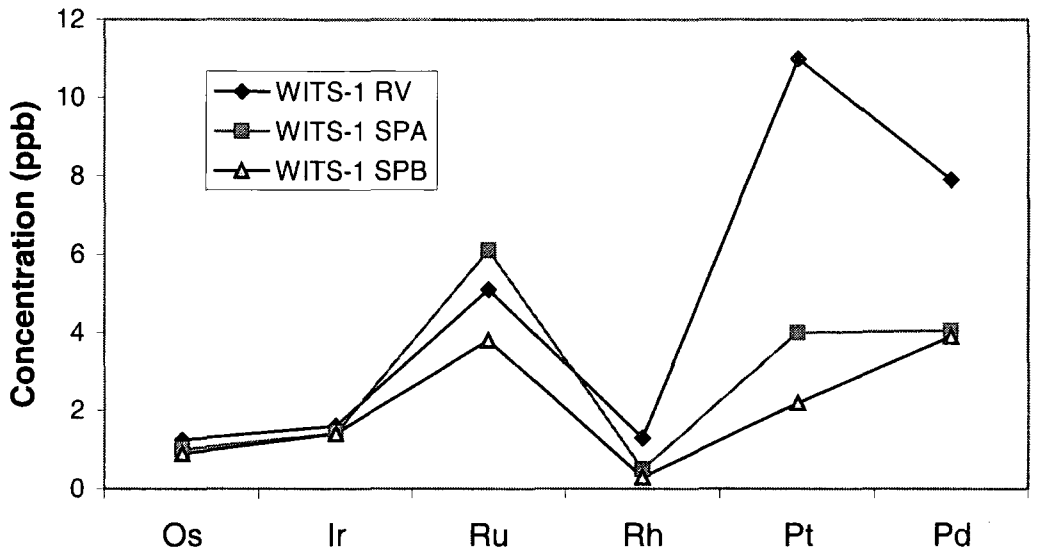

Fig 3.6 Comparison of the PGE concentrations in two WITS-1 samples, where Ir content was calculated by isotope dilution. Recommended PGE concentrations for WITS-1 = RV.

	SWITS-1 A	SWITS-1 B	SWITS-1 C
Ir Conc (ppb)	1.344	1.350	2.953
Average Ir	1.347		
Stdev (1σ)	0.004		
Reproducibilty (2σ %)	0.694 %		
	SWITS-1 A	**SWITS-1 B**	**SWITS-1 C**
Pt Conc (ppb)	8.175	6.207	9.455
Average Pt	7.946		
Stdev (1σ)	1.66		
Reproducibilty (2σ %)	41.18 %		

Table 3.11 Summary of results for WITS-1 spiked standards (Mass bias corrected). Anomalous values were recorded for SWITS-1C (Table 3.11). This sample has been omitted in calculating statistics for the WITS-1 samples. NB S in sample title indicates sample was spiked

	SWPR-1 A	SWPR -1 B	SWPR -1 C
Ir Conc (ppb)	17.35	17.069	16.951
Average Ir	17.123		
Stdev (1σ)	0.205		
Reproducibilty (2σ %)	2.394 %		
	WPR-1 A	**WPR -1 B**	**WPR -1 C**
Pt Conc (ppb)	322.544	333.220	321.319
Average Pt	325.694		
Stdev (1σ)	6.55		
Reproducibilty (2σ %)	4.02 %		

Table 3.12 Summary of results obtained for WPR-1 spiked standards (Mass bias corrected) N.B. S in sample tile indicates that sample was spiked

The quality of standard-rock data achieved for Ir and Pt was greatly improved by use of I.D. Thus, it was decided to utilise I.D. for analysis of all the PGEs (except Rh). Spikes were obtained in the form of pure metals and converted to a mixed spike solution (procedures outlined in Chapter 4). Three more replicates of both WITS-1 and WPR-1 were analysed using this mixed spike. The results of this study are presented in Table 3.13.

Sample	Ir	Os	^{194}Pt	^{198}Pt	Pd
WITS-1 RV	*1.6 ± 0.2*	*~ 1 – 1.5*	*11 ± 2*	*11 ±2*	*7.9 ± 0.9*
SWITS-1 D	1.84		7.03	6.69	4.97
SWITS-1 E	1.65	4.70	7.92	6.69	5.24
SWITS-1 F	1.45	2.0	7.82	8.51	5.34
AVERAGE	**1.65**	**3.35**	**7.59**	**7.30**	**5.18**
STDEV (1σ)	0.20	1.91	0.49	1.05	0.19
WPR-1 RV	*13.5 ± 1.8*		*285 ± 12*		*235 ± 9*
SWPR -1 D	18.77	21.70	357.71	323.74	251.44
SWPR -1 E	18.08	21.87	373.51	339.86	268.90
SWPR -1 F	18.83	20.97	360.12	328.44	264.79
AVERAGE	**18.56**	**21.51**	**363.78**	**330.68**	**261.71**
STDEV (1σ)	0.42	0.48	8.52	8.29	9.13

Table 3.13 Summary Table of I.D. data produced for the standards WPR-1 and WITS-1 using mixed PGE-spike (Mass bias corrected). RV = Recommended value

It was anticipated that the two spike-Pt isotope ratios would produce the same results, however, this was not the case (Table 3.13). Thus, the ^{198}Pt results have been used in preference to the ^{194}Pt results. This is largely because the isotope ratios achieved for this element were closer to the expected values. This discrepancy indicates that interferences are affecting on one or more of the Pt isotopes.

Excellent reproducibility was achieved for WPR-1 (Fig 3.7) where the separate analyses are barely distinguishable from one another. Particularly interesting are the Os results which have a reproducibility of 2.2% (1σ error). Thus, it appears that I.D. Ni-S fire assay may be a method capable of quantifying this problematical element.

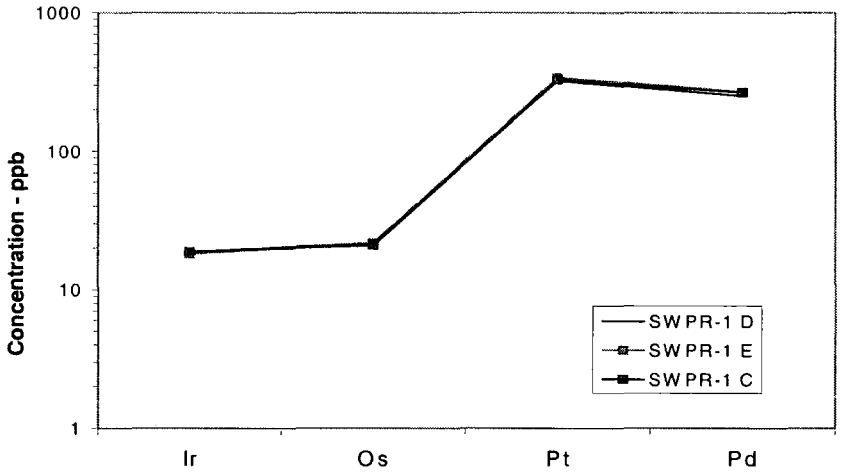

Fig 3.7 PGE pattern for WPR-1 replicates, using absolute abundances (error bars too small to be shown)

3.4.4 Compilation of PGE Analysis Results for WITS-1 and WPR-1, Compared with the Accepted Values

A full compilation of all data obtained for the standard WPR-1 by isotope dilution is shown in Table 3.14. The average PGE concentrations obtained for WPR-1 and the reproducibility between the separate results are also shown. The separate analyses are highly reproducibility (2 σ %), ranging from 9.4% for Ir, to 7.0% for Pd and 4.4% for Pt.

Sample	Ir	Os	Pt	Pd
WPR- 1 RV	*13.5 ± 1.8*		*285 ± 12*	*235 ± 9*
WPR-1 A	17.35		322.54	
WPR-1 B	17.07		333.22	
WPR-1 C	16.95		321.32	
SWPR-1 D	18.77	21.7	323.74	251.44
SWPR-1 E	18.08	21.87	339.86	268.90
SWPR-1 F	18.83	20.97	328.44	264.79
Average	**17.84**	**21.51**	**328.19**	**261.71**
Stdev (1σ)	**1.68**	**0.96**	**14.44**	**18.26**
Reproducibility (2σ%)	**9.44%**	**4.46%**	**4.40%**	**6.98%**

Table 3.14 Summary of PGE concentrations (ppb) produced by isotope dilution for WPR-1 (Mass bias corrected) RV = Recommended value. Prefix S in sample title indicates that sample was spiked

The average PGE concentrations obtained for WITS-1 by isotope dilution, and the reproducibility (2σ%) between samples is presented in Table 3.15. Like WPR-1, the reproducibility is reasonably good (Ir-24.6%, Pt-28.1% and Pd-7.3%), (Fig 3.8). The errors obtained are of a similar magnitude to those obtained on the recommended value (Fig 3.10). Unlike WPR-1 however, good reproducible results were not obtained for Os. This may be due to the lower concentration of Os initially within WITS-1 and because of the limited number of samples analysed for Os.

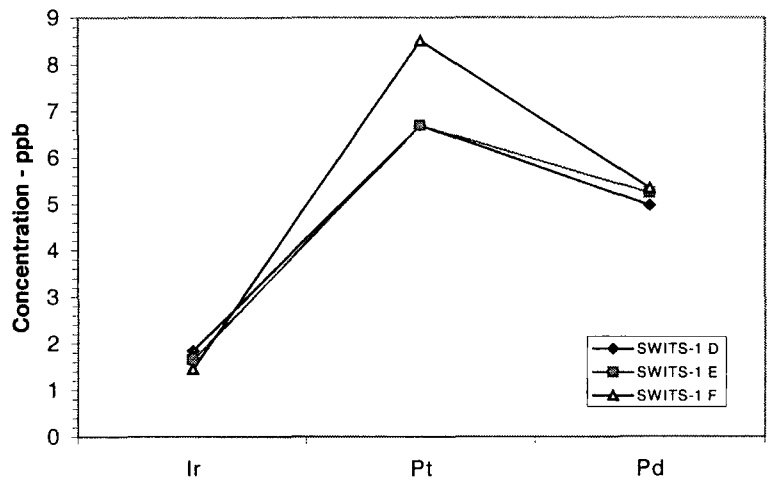

Fig 3.8 PGE pattern for WITS-1 replicates, using absolute abundances (error bars too small to be shown

Sample	Ir	Os	Pt	Pd
WITS-1 RV	*1.6 ± 0.2*	*~ 1 – 1.5*	*11 ± 2*	*7.9 ± 0.9*
WITS-1 SPA	1.42			
WITS-1 SPB	1.41			
WITS-1 A	1.34		8.18	
WITS-1 B	1.35		6.21	
SWITS-1 D	1.84		6.69	4.97
SWITS-1 E	1.65	4.70	6.69	5.24
SWITS-1 F	1.45	2.00	8.51	5.34
Average	1.50	3.35	7.26	5.18
Stdev (1σ)	0.37	3.83	2.04	0.38
Reproducibility (2σ%)	24.62%	114.1%	28.11%	7.34%

Table 3.15 Summary of standard concentrations (ppb) produced by isotope dilution for WITS-1 (Mass bias corrected). RV = Recommended value. Prefix S in sample title indicates that sample was spiked

The chondrite-normalised plots (Fig 3.9) illustrate the reproducibility of the I.D data. WITS-1 records lower values than the recommended, while WPR-1 generally produces higher values than those recommended. It may be that the accepted values for WPR-1 are too low (possibly an artefact of PGE losses in the original fire assays conducted without I.D.). The reason for the WITS-1 disagreement with recommended values is not clearly understood, but data from other labs (i.e. Ian McDonald pers. comm.) suggests that the recommended value may be slightly too high for some elements.

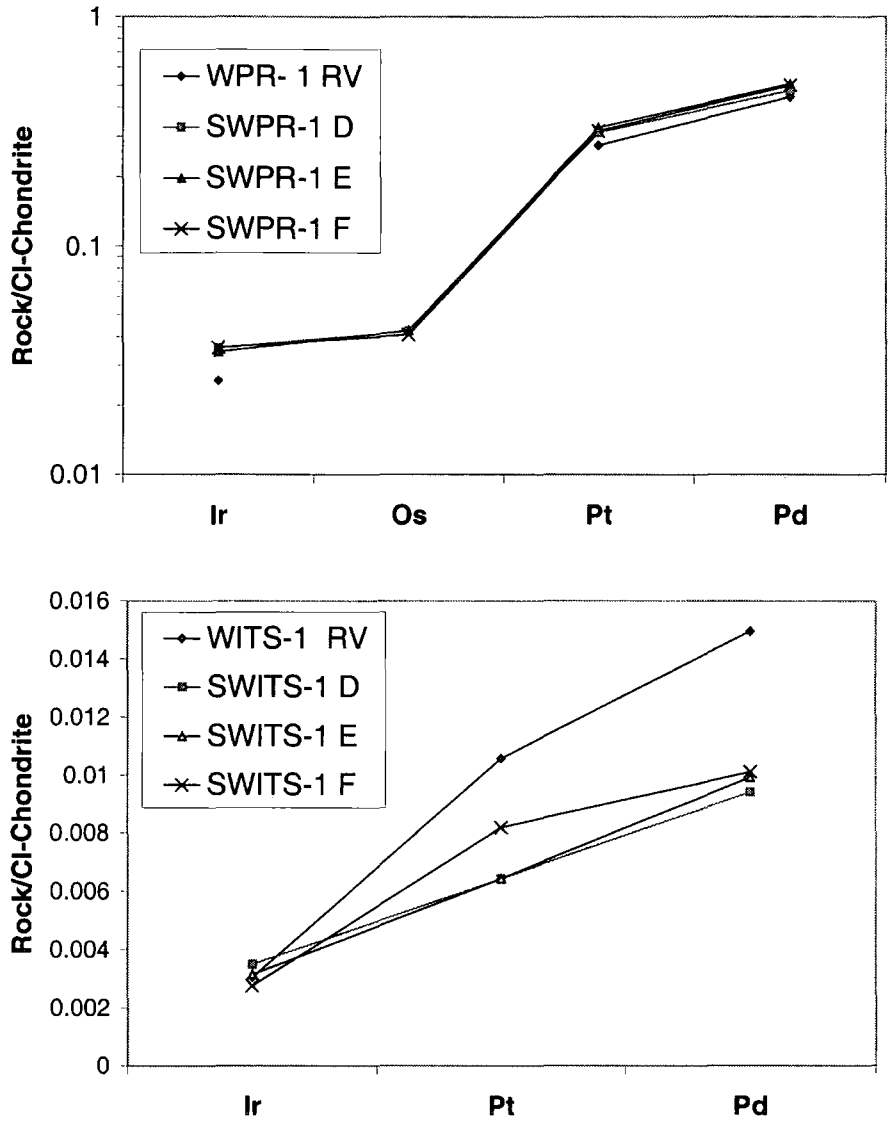

Fig 3.9 Chondrite normalised PGE patterns for WITS-1 and WPR-1 (N.B. R.V. = recommended value)

3.4.5 Errors Associated with Isotope Dilution Ni-S Fire Assay

The ability to reduce the errors on all data is one of the most important considerations when evaluating an analytical technique. On the whole for the WITS-1 data (Fig 3.10), the errors on the measurements made by isotope dilution are equal to, or less (especially for Pt), than those obtained on the recommended value by conventional fire assay techniques. This is also true for WPR-1 (Fig 3.11):

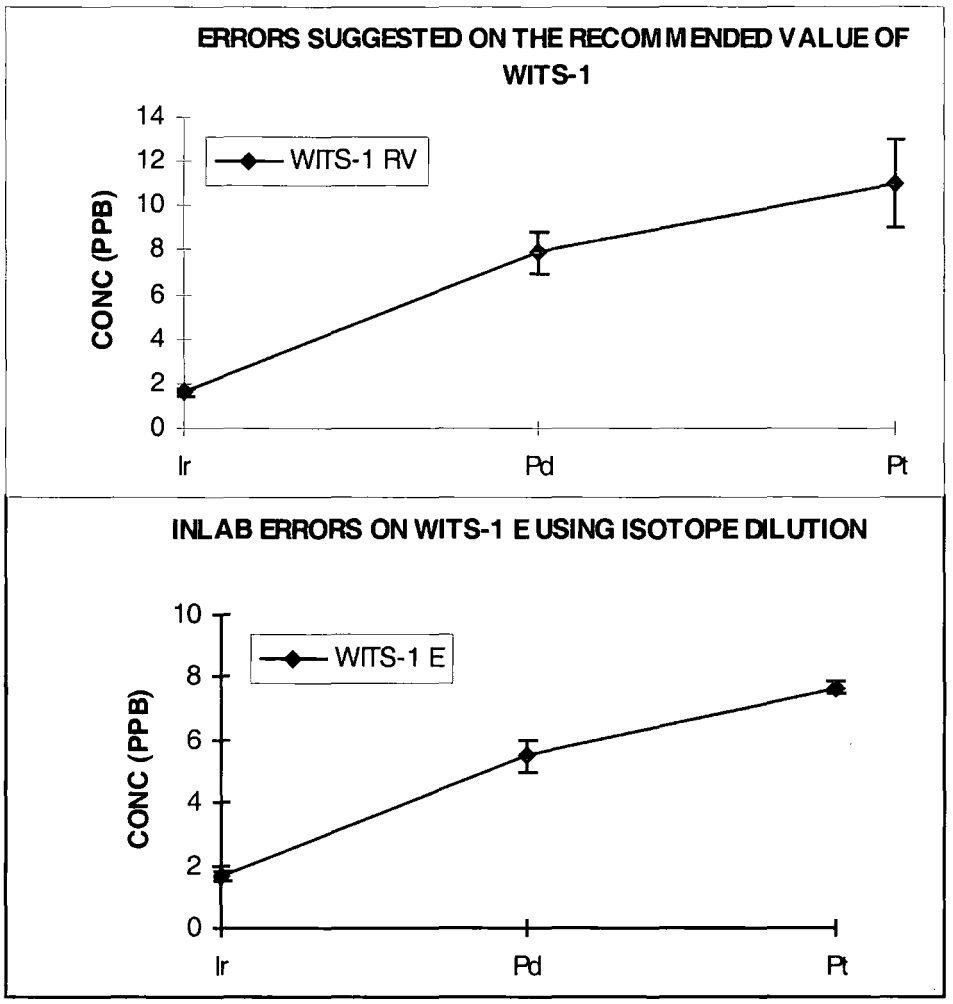

Fig 3.10 Comparison of recommended errors on WITS-1, with those obtained by isotope dilution (2σ error bars)

Whilst the WPR-1 results (Fig 3.11) show that Ir and Os values are almost equally reproducible by either method, the errors on Pt and Pd measurements are much higher when not using I.D. Further, Fig 10 illustrates clearly that much lower concentrations are recorded when not using I.D. This can be attributed to unavoidable losses of the PGE during processing of the Ni-S bead. Such evidence strongly supports the use of isotope dilution to compensate for losses of the PGEs during conventional Ni-S fire assay.

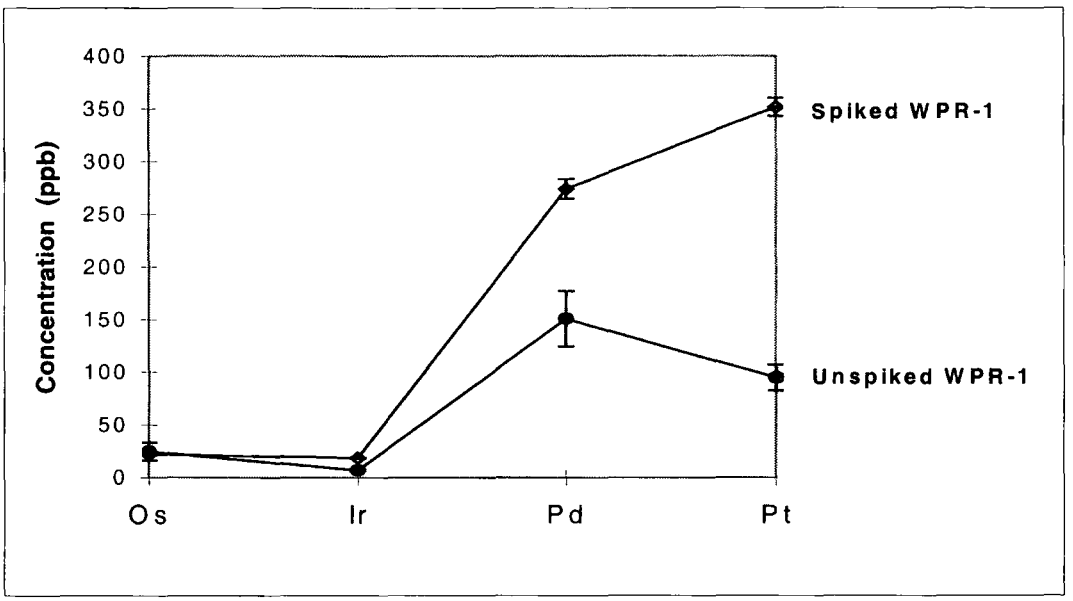

Fig 3.11 Comparison of errors on WPR-1, with and without using isotope dilution (2σ error bars)

3.5 Application of Ni-S Fire Assay to Elemental Ratio Measurement

Element ratios are frequently used when discussing geological processes, in preference to absolute abundances. For example, comparison of IPGE/PPGE ratios to chondritic ratios provides a very useful indicator of fractionation processes within the earth. The elemental ratios obtained for the standards in this study are presented in Table 3.16, with the recommended value given for comparison. The reproducibility of the values is exceptionally good, although they differ from the recommended values.

Plots of Ir vs Pt for both WITS-1 and WPR-1 (Fig 3.12) illustrate that the data form clusters. The non-linearity of these data suggests that heterogeneity between measurements is not due to the 'nugget effect' of PGE-grains (as nuggets would contain a similar ratio of Ir to Pt if they originate from the same rock) but instead, is perhaps more likely due to heterogeneity between crucibles used.

	Ir / Os	Ir / Pt	Ir / Pd	Pt / Pd
WITS-1 R.V.		0.15	0.20	1.39
SWITS-1 A		0.16		
SWITS-1 B		0.22		
SWITS-1 D	0.35	0.28	0.36	1.30
SWITS-1 E	0.73	0.23	0.31	1.33
SWITS-1 F		0.17	0.26	1.54
Reproducibility (1σ)	***0.26***	***0.05***	***0.05***	***0.13***
WPR-1 R.V.		0.05	0.06	1.21
SWPR-1 A		0.05		
SWPR-1 B		0.05		
SWPR-1 C		0.05		
SWPR-1 D	0.87	0.06	0.07	1.25
SWPR-1 E	0.83	0.05	0.07	1.22
SWPR-1 F	0.90	0.06	0.07	1.20
Reproducibility (1σ)	***0.04***	***0.003***	***0.004***	***0.02***

Table 3.16 Summary of isotope ratios for WITS-1 and WPR-1 standards analysed by I.D.

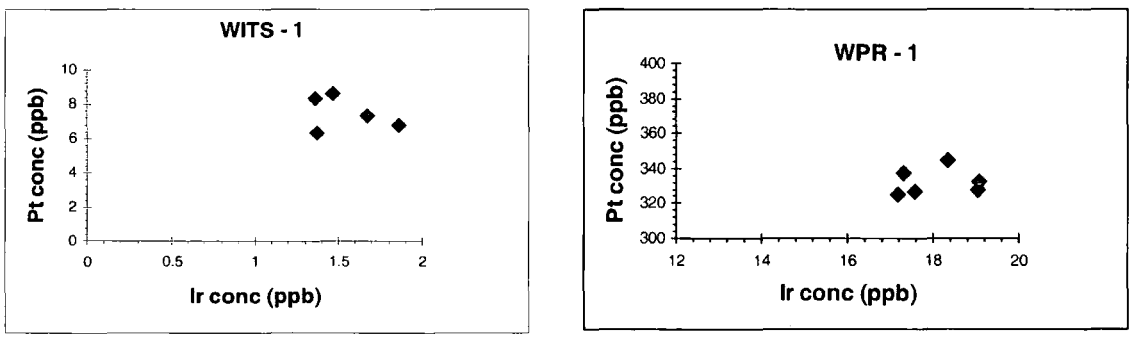

Fig 3.12 Ir - Pt ratios for WITS-1 and WPR-1 measured by I.D.

Once obtained, the PGE concentrations are frequently plotted on bivariate plots in order to show a scatter about the C1-chondrite line (e.g. Pattou *et al.*, 1996) (Fig 3.13). In the instance shown below, points that plot above the C1 line are enriched in Pd relative to Ir and as such are said to have been fractionated relative to chondrite, a process which causes enrichment of light PGE relative to heavy PGEs in the melt fraction.

Scatter around the C1 line is often used in interpretation of a rocks' petrogenesis, therefore it is essential to be confident about the precision of the data. Shown on Fig 3.13 are error bars for WITS-1 (2σ errors). When using I.D. the Pd error is significantly reduced. The large error bars obtained when not using I.D. clearly cover the scatter of points around the chondritic-ratio line. This suggests that

caution must be exercised in the interpretation of PGE inter-element ratios obtained using conventional non-I.D. fire-assay techniques.

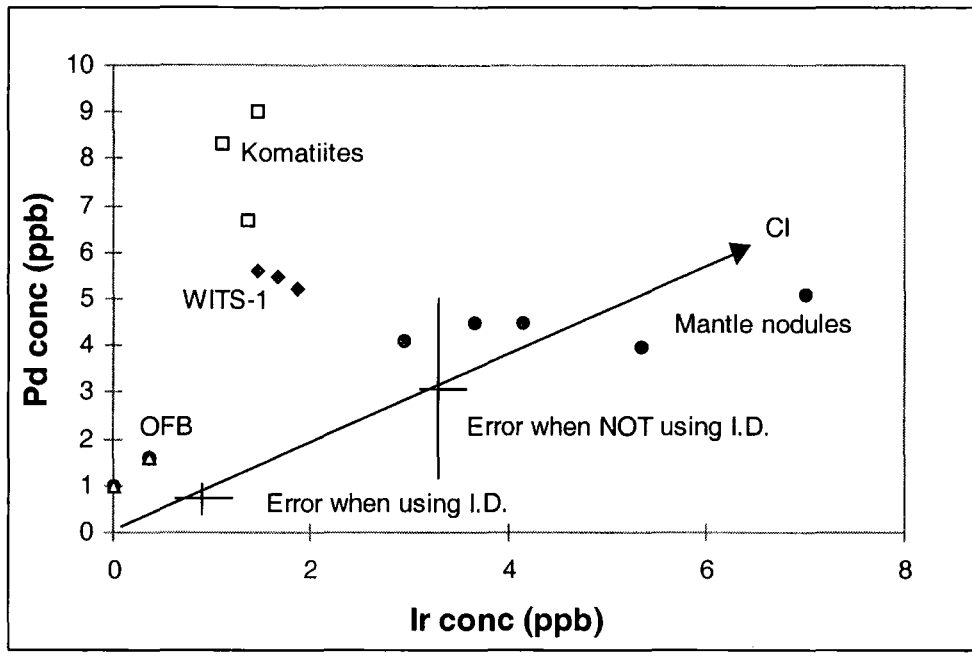

Fig 3.13 Plot of Ir versus Pd for WITS-1 showing how it compares to other rock types (WPR-1 could not be plotted due to its anomalous Pd enrichment). Mantle nodule data from Morgan *et al.*, 1981; OFB=ocean floor basalts, data from Fryer and Greenough, 1992; komatiite data from Brügmann *et al.*, 1987.

3.6 Importance of Error recognition and Correction

In a recent review of PGE data collection and interpretation, McDonald (1998) notes that in the past there has been a widespread failure to recognise and report the true uncertainties on PGE data. He points out that due to the nugget effect, there will always be a degree of uncertainty as to whether a selected sample aliquot is representative of the whole sample. This uncertainty should be assessed by appropriate replicate analyses of the unknown rock samples, as well as standard rocks, for a true measure of the precision of a technique. Standard practice should be for all PGE concentrations to be reported along with associated error. He concludes that this is essential in order to construct statistically justifiable arguments for small variations in PGE ratios. It was such proposals that prompted a rigorous approach to be adopted within this study, concerning evaluation of the blanks and

characterisation of PGE concentrations (and their reproducibility) in standard rock types.

3.7 Appraisal of Ni-S Fire Assay

The Ni-S fire assay technique although appearing to be one of the best methods of PGE preconcentration available at present, has some significant drawbacks, namely:

a) The technique is blank-dependent and relies entirely on the availability of Ni-metal with low PGE content.

b) Significant losses can occur at many stages during processing of the Ni-S bead, despite all reasonable precautions against this.

Consideration of the above factors has prompted the use of isotope dilution, which appears to:

i) Compensate for losses of PGEs during processing.

ii) Enable accurate measurement of Os as well as the other PGEs.

iii) Markedly increase reproducibility of results (significantly lowering the errors on all data).

iv) The best blanks obtained for Ir and Pt (using I.D.) were 0.13ppb and 2.96ppb respectively. The detection limits on these measurements (i.e. 3 x the standard deviation of the blank) were: Ir-0.080ppb, Pt-2.32ppb

It is concluded that the use of I.D. in conjunction with Ni-S fire assay will permit the acquisition of reliable data for relatively high abundance samples (>1ppb). However, due to the large inherent blanks connected with the Ni-S fire assay technique (which have not been possible to overcome in this lab), it appears unsuitable for use in measurement of rocks which contain sub-ppb levels of PGEs.

This effectively precludes the measurement of most sediments and acid volcanics by this technique, thus, explaining the lack of published PGE data on these rock types.

4: Development of ICP-MS Isotope Ratio Measurement Routines and Procedures for Os Extraction from Geological Samples

4.1 Introduction

This chapter is devoted to documenting some of the considerations and procedures which must be addressed and undertaken when measuring PGEs by ICP-MS. This includes discussion of the instrumentation used in this project and development of instrumental and analytical techniques for PGE analysis. Precautions to ensure high instrumental data quality are discussed, including mass bias correction, monitoring of isobaric interferences and elimination of instrument-contamination. In addition, methods for making and effective use of isotopically enriched spikes for I.D. analysis of PGEs are presented. Finally, special consideration is given to the analytical problems encountered in quantifying Ru abundance in geological samples.

4.2 Instrumentation

A Perkin Elmer Sciex, Elan 6000 quadrupole ICP-MS was used throughout this study. Most of the data were obtained using either a Scott-Type nebuliser (x-flow) or a Direct Injection Nebuliser (DIN). A third type, a Micro-Concentric nebuliser (MCN) was also given a brief trial (See Appendix I for descriptions of different nebulisers used). The typical ICP-MS (+ x-flow) operating conditions used during analysis of the PGEs are shown in Table 4.1:

R-F Power	1200 Watts
No. of Sweeps of mass range	25
No. of Replicates	25
Peak Dwell Time	20 ms
Auto Lens	ON
Rate of CeO production on Ce	< 3%

Table 4.1 ICP-MS operating conditions

4.2.1 Standard Analytical Procedure

Before sample analysis PGE standard solutions in the 0.1 to 10ppb range are analysed to establish mass-bias correction factors (Section 4.3.). Following this, Hf, Mo, Zr and Y solutions are analysed to monitor levels of oxide production for metal oxide species that may cause isobaric interferences on measured PGE isotopes. These correction factors are then updated in the software before running samples, so that isobaric interferences (Section 4.4) can be corrected on-line. Standard solutions are interspersed with samples during the day to monitor sensitivity and mass-bias drift which is usually negligible (Pearson and Woodland, 2000).

4.2.2 Nebulisation

A conventional x-flow nebuliser with a Scott-type double pass spray chamber was used for measurement of Re, Ru, Pt and Pd. This nebuliser has low memory for these elements. Detection limits using the x-flow nebuliser, are limited by the need to dilute samples to ~2mls for analysis (sample uptake rate is 1ml/min). However, the sensitivity achieved is adequate for PGE determination in sub-ppb geological samples when a suitable preconcentration technique is used. The washout procedure employed between samples consists of passing dilute HNO_3 through the ICP-MS for ~3mins. This is usually sufficient to reduce the PGE machine background to < 10 counts per second (cps) for Ir, Re and Ru, and < 20 cps for Pt and Pd. Machine background is always assessed prior to analysis of each sample. Oxide generation levels for elements that present isobaric interferences are on the order of 0.8 to c. 2.5% as metal-oxide to metal ratio (Table 4.5).

Os analysis with the Elan x-flow nebuliser is problematical due to irregular, often severe memory effects. Os (particularly in the oxidised form OsO_4) suffers from memory effects as it sticks to the walls of the peristaltic tubing used, to the spray chambers walls, and possibly even to Teflon where large surface areas are involved. Using the x-flow, samples containing partially oxidised Os at the 1ppb level or less introduced in fairly dilute HNO_3 (3.5%), washout to constant levels (on the order of 500 cps) in 10 to 15 minutes. However, in many cases this does not equate to all of the Os being washed out of the instrument. If hydrogen peroxide is subsequently introduced which is particularly effective at remobilising any adhered

Os in either the oxidised or reduced form, trapped Os is re-released (Pearson *et al.*, 1999).

To counteract these problems, a CETAC DIN was used for Os analysis. The all-Teflon nature of the sample uptake path and low dead volume results in negligible memory for samples in the concentration range measured in this study (Pearson and Woodland, 2000). Use of a DIN significantly reduces the washout time necessary between samples. There is a very sharp signal drop-off (to less than 10% of the former signal) within 5 seconds of commencing the washout and this decays to less than 1% of the original signal within 3 minutes (Pearson *et al.*, 1999).

The DIN is capable of very low volume analyses, thus improving on the sensitivity obtainable when using a x-flow nebuliser. The DIN however, has several major drawbacks with regard to PGE analysis. Firstly, oxide production is high (~6-12%), this can lead to substantial isobaric interferences. The DIN also has some memory effects for Pt, Pd and Re. Lastly, it was found that the DIN was difficult to optimise, resulting in drop in sensitivity and production of very erratic isotope data on standard solutions. Despite this, the DIN is considered the nebuliser of choice for analysis of Os.

Preliminary experiments with a desolvating CETAC MCN-6000 showed great promise for Ir, Pt, Pd, Re and Ru measurement because of its low sample uptake rates (c. 70 μl/min). This promotes greater sensitivity and gains in signal intensity of between 2 to 3 times for all PGEs, except Os, which is again prone to severe memory problems. For analysing Ir, Pt, Pd, Re and Ru, a desolvating nebuliser is clearly optimal in that it minimises oxide interferences (<0.03% oxide production). The desolvating action of the MCN-6000 also eliminates Ni-Ar interferences resulting from use of Ni-cones (Section 4.6). The relative pros and cons with regard to PGE analysis for each of the nebulisers tested are presented in Table 4.2.

	X-Flow	M.C.N	D.I.N
Advantages			
1	Can analyse all PGEs reasonably well.	Enhances signal intensity and sensitivity for all elements (except Os).	Can analyse Os with no memory effects.
2	Signal intensity very stable.	Ru reliably measured even with Ni-cones (minimal Ni-Ar).	Uses small volume of sample for analysis (<1ml).
3		Insignificant oxide production rates reduce isobaric interferences.	
Disadvantages			
1	Oxide production rate at ~2.5 % can be significant.	Instrumental Os-memory effects a problem.	Difficult to optimise sensitivity, signal intensity unstable.
2	Severe Os memory effects.		Oxide production at 11% causes significant isobaric interferences.
3	Measurement of Ru with Ni-cones can be problematical.		Isotope ratios (particularly Ru) can be erratic if nebuliser not properly optimised.
4	Samples need to be diluted to ~ 2mls for analysis, limiting sensitivity.		Has some memory affect for Re and Pt.

Table 4.2 Comparison of suitability of different nebuliser types for PGE analysis

4.2.3 Measurement Precision

Repeat isotopic analyses of the same solution using the x-flow, within the same analytical session, usually agree to better than 0.5% RSD producing minimal errors in the final ID concentration calculation. For samples with small signals (<1000 cps), repeat analyses of standard solutions agree to better than 5%, i.e. close to counting statistics. Reproducibility of individual measurements is usually at least a factor of 2 better than within-run precision.

4.3 Instrumental Mass Fractionation Effects

This is an instrumental transmission effect which tends to bias in favour of the heavier isotopes of an element. This consequently causes a shift in the isotope ratios measured for standard solutions away from the natural ratios. Fortunately however, the mass bias effect remains relatively constant (Fig 4.1) and can easily be corrected for. Typical mass bias correction factors (MBCF) for the PGEs are illustrated in Table 4.3. Although the correction factors are relatively small, all data is corrected to produce the best quality results possible.

The MBCF is calculated by dividing the expected isotopic ratio for a given element, by that measured. The data are then corrected with this factor to eliminate the effects of machine mass fractionation.

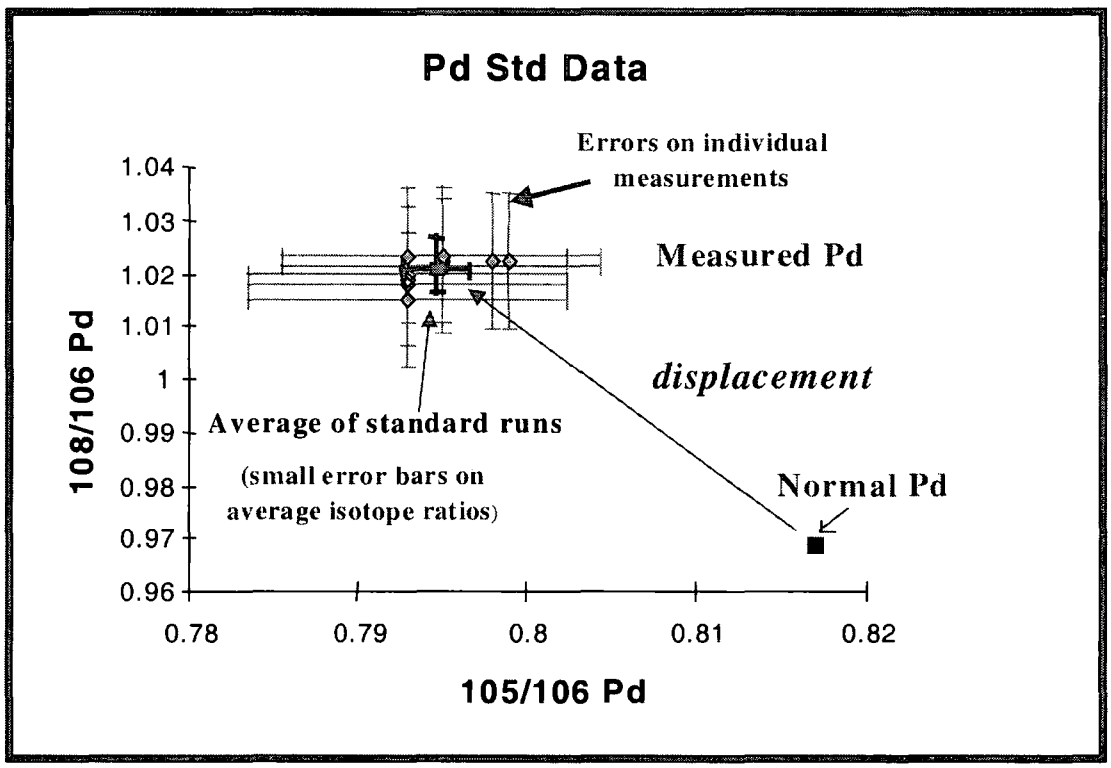

Fig 4.1 Effect of mass fractionation on standard solution isotope ratios

PGE Isotope Ratio Measured	**Ir 193/191**	**Os 192/190**	**Pt 195/194**	**Pd 105/106**	**Ru 101/99**	**Re 187/185**
Natural Ratio	1.681	1.553	1.027	0.817	1.346	1.674
Measured Ratio	1.721	1.598	1.031	0.795	1.412	1.689
M.B.C.F	0.983	0.978	0.987	1.029	0.963	0.982
2 σ error	0.833	0.226	1.338	0.495	0.399	1.084

Table 4.3 Typical mass bias correction factors for the PGEs (errors based on > 20 separate analyses). All data generated using X-flow nebuliser, except for Os, where DIN used.

Mass bias was estimated by analysis of standard solutions throughout each data collection session. 0.1 to 10ppb standard solutions were generally used, this concentration range being close to the sample concentrations and providing sufficient signal for accurate isotope ratio measurement. No significant differences in mass bias were found between standards of different concentration within this range. Within-run errors and overall reproducibility however, show a corresponding decline in quality for the smaller signals obtained from dilute solutions (Pearson and Woodland, 2000). Ravizza and Pyle (1997) have also documented independence of mass fractionation from the concentration of PGE standards analysed by ICP-MS.

According to convention, degree of mass bias is often expressed "per atomic mass unit" (AMU). This is calculated e.g. for Ir by: -

$$(1 - \text{MBCF}) \; / \; 2$$

(As two AMUs between the Ir isotopes ^{191}Ir and ^{193}Ir)

Mass bias effects for the PGE ratios measured are shown in Fig 4.2. As expected (e.g. see Ravizza and Pyle, 1997) lower atomic mass elements show the largest mass bias, those for Pd and Ru being on the order of 2.5% per atomic mass unit (AMU^{-1}). Although slight variation in MBCF occurs on a day to day basis, the mass bias within an individual session is extremely stable, with typical 2 sigma RSDs of 0.2 to 0.3 %. The variability in mass bias for Ru (2.44 ± 0.67 % AMU^{-1}) is twice that of Pd (2.47 ± 0.33 % AMU^{-1}, Fig 4.2). This is probably due to a combination of increased error from small signals (natural abundances of ^{101}Ru and ^{99}Ru are lower than for ^{105}Pd and ^{106}Pd) and the increased possibility of interferences

on Ru. Higher atomic masses show concomitantly lower mass bias with values for Re, Os, Ir and Pt all being less than 1.5% AMU^{-1} (Fig 4.2). Mass bias using the DIN is no different in magnitude to that obtained using the x-flow nebuliser (Pearson *et al.*, 1999). The mean value for Os (c.0.83 ± 0.22 % AMU^{-1}) using the DIN is similar to that for Ir (0.71 ± 0.26 % AMU^{-1}) using the x-flow nebuliser.

The mass bias of the heavier elements with similar mass (i.e. Ir and Re) can show slightly different degrees of mass bias on the ICP-MS, typically 0.65 to 0.93% AMU^{-1} for Ir, versus 0.72 to 1.38% AMU^{-1} for Re (Fig 4.2). The mean, long-term mass bias for Pt (1.08 ± 0.37 % AMU^{-1}) is slightly higher than for Re, Os or Ir. Although the variation is not large and within overall uncertainty, Ir and Re can show different behaviour between specific analytical sessions. For this reason Re standards are not used to mass bias correct Ir samples (or vice-versa) nor is internal spiking of samples with non-PGE elements of similar mass employed. Another reason for not using the internal spiking method for mass bias correction of PGEs, is that suitable PGE-free element solutions are lacking. Overall, the high level of reproducibility of mass bias, in a single analytical session, means that the error from this correction in the isotope dilution calculation scheme is trivial.

4.4 Isobaric Interferences

Isobaric interferences occur due to overlap in elemental or element-oxide masses. Most of the potentially important isobaric interferences on PGE masses measured in our procedures and those which are routinely corrected are shown in Table 4.4.

The isotope dilution scheme established for the PGEs during this project was designed so as to minimise direct isobaric interferences. Interference corrections for Hg on Pt isotopes, and Cd on Pd isotopes are routinely made online.

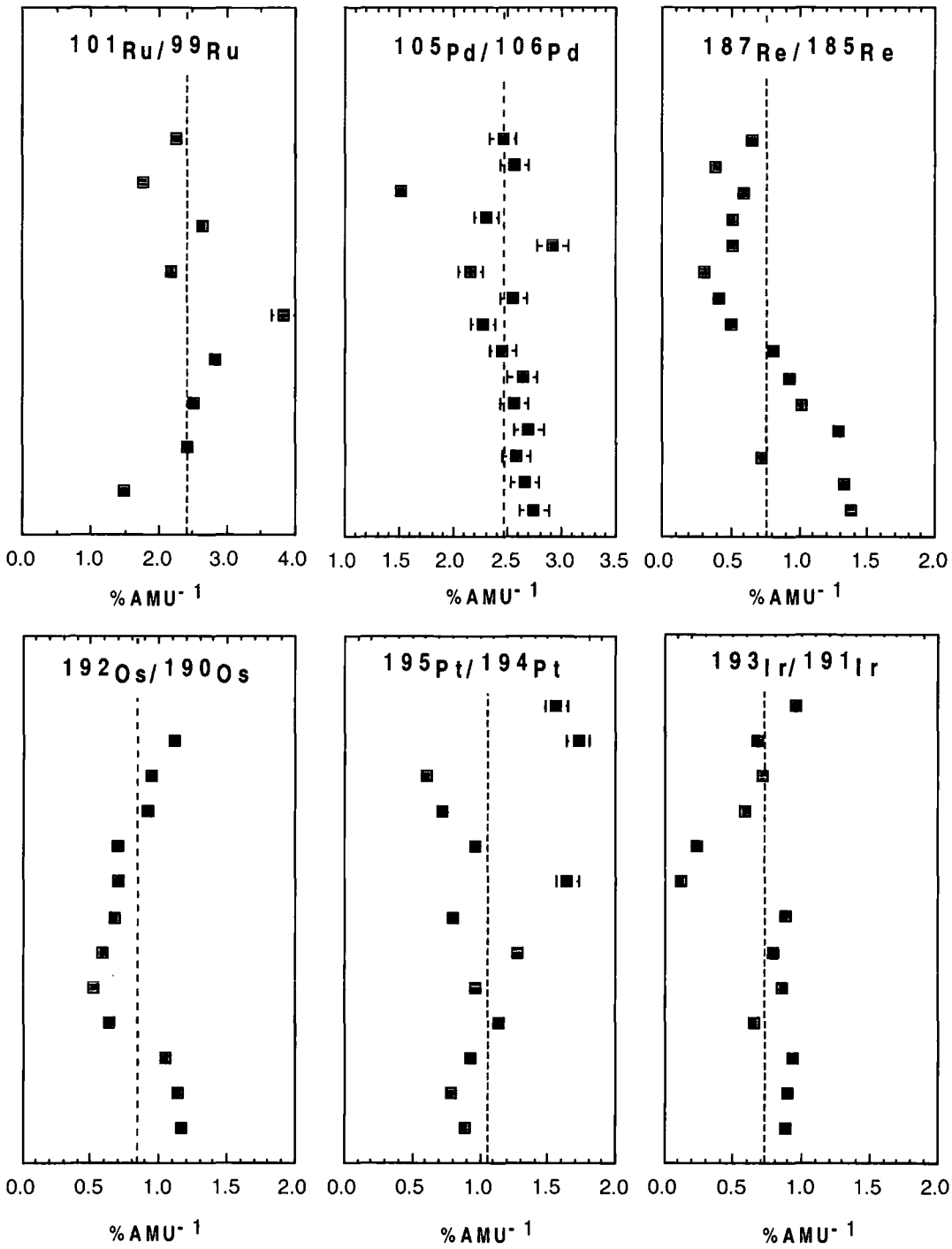

Fig 4.2 Mass bias per atomic mass unit for measured PGE isotope ratios.

Each data point represents between 5 and 12 separate analyses of standard solutions in the 0.1 to 10 ng/g concentration range. Error bars are 2 standard deviations of the mean standard value for each session. Dashed line indicates the overall mean for the plotted values (from Pearson and Woodland, 2000).

1) Oxides

Interference	Isotope Affected
RbO (^{85}Rb and ^{16}O)	^{101}Ru
RbO (^{87}Rb and ^{16}O)	^{103}Ru
YO (^{89}Y and ^{16}O)	^{105}Pd *
ZrO (^{90}Zr and ^{16}O)	^{106}Pd *
ZrO (^{92}Zr and ^{16}O)	^{108}Pd *
MoO (^{92}Mo and ^{16}O)	^{108}Pd *
YbO (^{171}Yb and ^{16}O)	^{187}Re
HfO (^{176}Hf and ^{16}O)	^{192}Os
YbO (^{176}Hf and ^{16}O)	^{192}Os
LuO (^{175}Lu and ^{16}O)	^{191}Ir
HfO (^{177}Hf and ^{16}O)	^{193}Ir *
HfO (^{178}Hf and ^{16}O)	^{194}Pt *
HfO (^{179}Hf and ^{16}O)	^{195}Pt *

2) Chlorides

Interference	Isotope Affected
CuCl (^{65}Cu and ^{35}Cl)	^{100}Ru
ZnCl (^{66}Zn and ^{35}Cl)	^{101}Ru
GaCl (^{71}Ga and ^{35}Cl)	^{106}Pd
GeCl (^{73}Ge and ^{35}Cl)	^{108}Pd
SmCl (^{150}Sm and ^{35}Cl)	^{185}Re
GdCl (^{156}Gd and ^{35}Cl)	^{191}Ir
TbCl (^{159}Tb and ^{35}Cl)	^{194}Pt

3) Argides

Interference	Isotope Affected
NiAr (^{60}Ni and ^{40}Ar)	^{100}Ru
NiAr (^{61}Ni and ^{40}Ar)	^{101}Ru
CuAr (^{65}Cu and ^{40}Ar)	^{105}Pd
ZnAr (^{66}Zn and ^{40}Ar)	^{106}Pd

4) Direct Interferences

Interference	Isotope Affected
^{100}Mo (9.63%)	^{100}Ru *
^{106}Cd (1.25%)	^{106}Pd *
^{108}Cd (0.89%)	^{108}Pd *
^{187}Os (1.6%)	^{187}Re *
^{190}Os (26.4%)	^{190}Pt *
^{192}Os (41.0%)	^{192}Pt *
^{196}Hg (0.15%)	^{196}Pt *

Table 4.4 Isobaric interferences on the PGEs (* = interferences corrected on-line)

Using the x-flow nebuliser, the most problematical isobaric interferences were due to metal-oxide species. The most significant being oxides of Zr, Hf, Y and Mo. Typical rates of isobaric oxide production for elements which interfere on the PGEs are shown in Table 4.5. Oxide generation levels for these elements, in standard solutions, are quite constant during a single analytical session but can vary on a longer-term basis. The stability of oxide generation levels allows oxides to be effectively corrected for in most solutions. This is demonstrated by comparison of data obtained for a picritic basalt sample, via both the x-flow nebuliser and a desolvating MCN, the latter having minimal levels of oxide generation (ca. 0.02%; Table 4.5). Using the x-flow nebuliser the $^{105}Pd/^{106}Pd$ ratio, when uncorrected for ^{90}Zr-^{16}O interference, is considerably higher than the value obtained when ZrO is corrected for. The oxide corrected x-flow value is within error of the $^{105}Pd/^{106}Pd$ value obtained for the same solution run with the MCN.

	$^{89}Y^{16}O/^{89}Y$	$^{90}Zr^{16}O/^{90}Zr$	$^{92}Mo^{16}O/^{92}Mo$	$^{177}Hf^{16}O/^{177}Hf$	$^{178}Hf^{16}O/^{178}Hf$
	0.933	1.66	0.13	1.95	2.08
	0.947	1.63	0.13	1.98	2.14
	0.946	1.60	0.16	2.00	2.10
	0.959	1.63	0.18	1.95	2.10
		1.65		1.99	2.05
		1.65		1.97	2.00
Mean	0.946	1.637	0.150	1.973	2.078
2 * Stdev	0.021	0.043	0.049	0.040	0.097

	^{90} Zr cps	$^{105}Pd/^{106}Pd$	(±)	Pd conc. ppb
GP-1: X-flow, no oxide correction	51,046	0.0768	0.002	6.98
GP-1: X-flow, oxide corrected		0.741	0.002	6.68
GP-1: MCN 6000 (0.02% oxides)	165,000	0.0747	0.0014	6.74

Table 4.5 Oxide production rates for elements, which generate isobaric interferences on the PGEs

The effectiveness of oxide corrections and the significance of interferences in general can be evaluated for Pt and Pd by use of spike-sample mixing line plots, of the type used by Ravizza and Pyle (1997). Spike-sample mixing plots necessitate the measurement of three different isotopes of any given element. Thus, this approach cannot be used for bi-isotopic elements such as Ir and Re. Essentially, all spiked samples should lie on a mixing line where end-members are defined by the spike and natural isotopic ratios. Failure of mass bias corrected data to plot on the spike-sample mixing line indicates the presence of interferences (Fig 4.3). Thus, plots of this nature are essential in order to check data quality. Additionally, the concentrations calculated by I.D. from different Pt and Pd isotope pairs should correspond if the data has not been compromised by interferences.

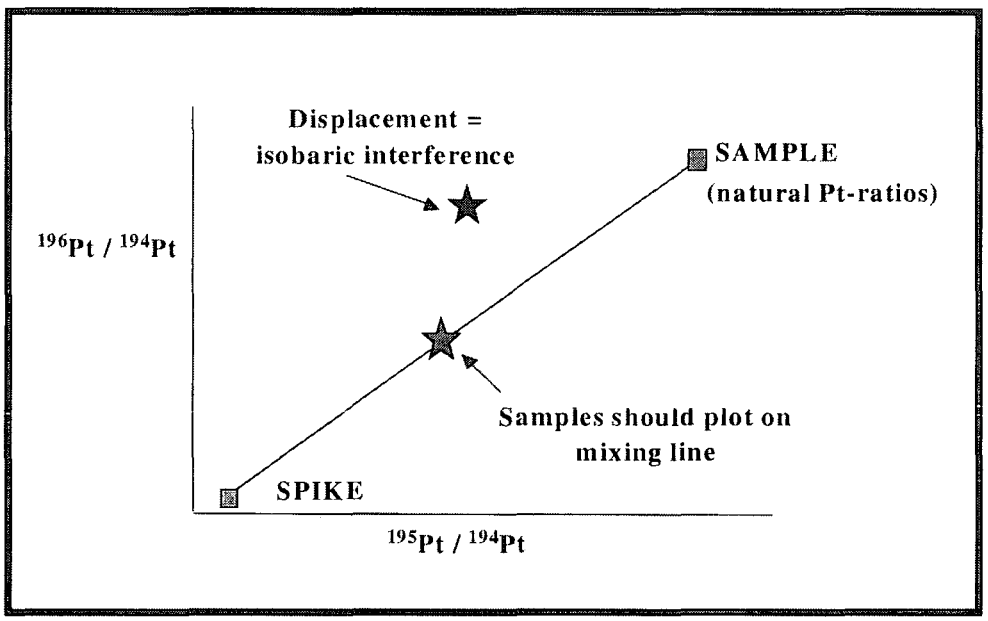

Fig 4.3 Effect of isobaric interferences on sample data (ratios are mass bias corrected).

4.5 PGE Spike Preparation

4.5.1 Introduction

In order to facilitate the use of I.D. a mixed, isotopically enriched PGE spike solution containing Pt, Pd, Ir, Ru, Os and Re is needed. The procedures used to make such a spike are outlined in this section. The PGE spikes were obtained in metallic form from ORNL (Table 4.6). Conversion of the metal-powders to a concentrated spike-solution involves a Carius tube digestion procedure for Pt, Pd and Os (after Shirey and Walker, 1995) and an alkali fusion procedure for Ru and Ir (after Enzweiler *et al.*, 1995).

Enriched Isotope	% Enrichment of Spike Isotope	Batch Number
^{190}Os	96.93	223701
^{191}Ir	98.23	188691
^{99}Ru	97.69	193491
^{194}Pt	95.54	186202
^{106}Pd	98.48	191391

Table 4.6 PGE isotopes used in the Durham mixed-PGE spike N.B. a pre-existing concentrated Re spike solution was utilised for making the more dilute mixed spikes.

4.5.2 Carius Tube Digestion (Pt, Pd, Os)

1) Clean Carius tubes (by boiling in aqua regia and then rinsing in MQ water) and small Teflon funnel used to transfer the spike into the Carius tube.

2) Chill Carius tubes in a water-ethanol mixture (-10°C) to prevent vigorous reactions occurring upon addition of acid to the PGE spikes. Os is particularly prone to losses at this stage if the mixture is not sufficiently chilled, due to volatilisation, upon addition of oxidising HNO_3.

3) Into the Carius tubes are placed:

a) The PGE spike (weighed precisely)

b) 2ml Romil UpA grade HCl (wash down into the Carius tube any spike powder stuck to funnel).

c) 70 µl of Romil UpA grade HNO_3.

4) Ensuring that the Carius tubes and their contents remain chilled, seal the Carius tubes (take care not to drop/knock tubes once sealed - a face shield should be used at all times when handling the sealed tubes).

5) Put Carius tubes in steel jackets and place in an oven at a temperature of 240°C, for approximately one week to ensure full digestion and equilibration between spike and acid.

6) After this time the Carius tubes should be removed from the oven and left to cool. Assuming complete digestion the following procedures should then be conducted. Note that a different procedure has to be assumed for Os compared to Pt and Pd. This is due to the problems involved in stabilising Os in the spike solution.

4.5.3 Procedure for Pt and Pd

1) Chill the Carius tubes to reduce internal pressure, then crack the neck of the tube, followed by the thicker walled body of the tube a few cms above the aqua regia mixture.

2) Using an acid-cleaned Pasteur pipette transfer the aqua regia mixture into a 15ml Teflon vial. Wash the Carius tube with 2mls of concentrated UpA HCl and then transfer this acid to the Teflon vial.

3) Under clean air, allow the solution to evaporate to ~1ml in volume (do not dry), then add 2ml of concentrated UpA HCl. Repeat twice to remove HNO_3 from the solution.

4) Transfer the remaining concentrated solution to a clean Teflon bottle and make up to the appropriate volume with 4N UpA HCl. Use some of this acid to rinse the Teflon vial 2 to 3 times to ensure complete transfer of all the spike into the Teflon bottle.

5) The concentrated spike stock-solution is now ready, but should be frequently shaken and allowed to equilibrate for 1 week before use.

4.5.4 Procedure for Os (Solvent Extraction)

1) After digestion, chill the Carius tube and then crack open at the neck.

2) Add 5mls of MQ water and 5mls of chloroform ($CHCl_3$) to the Carius tube and reseal.

3) Shake the Carius tube well and leave overnight.

4) After this time, again crack the tube open, initially at the neck and then a few cms above the liquid on the main body of the tube.

5) Take off the upper aqua regia fraction and place in a clean Teflon vial, to this add 5ml of $CHCl_3$, shake well and leave to stand overnight. This is a precaution to ensure that all the Os has been extracted from the aqua regia.

6) Transfer the $CHCl_3$ fraction from the Carius tube to a clean 30ml Teflon vial containing 5mls of UpA Romil HBr. Wash the Carius tube using a further 2mls of HBr and transfer these washings to the Teflon vial as well. Shake the Teflon vial well and leave overnight.

7) All of the Os should now have been reduced and back-extracted from the $CHCl_3$ into the HBr (i.e.$OsO_4 \rightarrow OsBr^{6-}$).

8) Pipette off the upper HBr fraction into a clean Teflon vial, screw lid down tightly and place vial in oven at 80°C overnight to 'fix' the Os into the HBr

9) Finalise the second extraction (step 5) by discarding the upper aqua regia fraction and adding 5ml of HBr to the remaining $CHCl_3$ fraction. After allowing this solution to stand overnight, transfer the upper HBr fraction to a clean Teflon vial and place in an oven at 80°C.

10) Following this step, both vials containing HBr-Os mixture should be placed under filtered air and allowed to evaporate to ~0.5ml.

11) Add 2mls of concentrated UpA HCl and gently evaporate to dryness to remove all traces of HBr, then take up in 2mls of concentrated UpA HCl, seal vial and place on warming plate (80°C) for 30 minutes.

12) This solution should now be cooled and then transferred to a clean Teflon bottle.

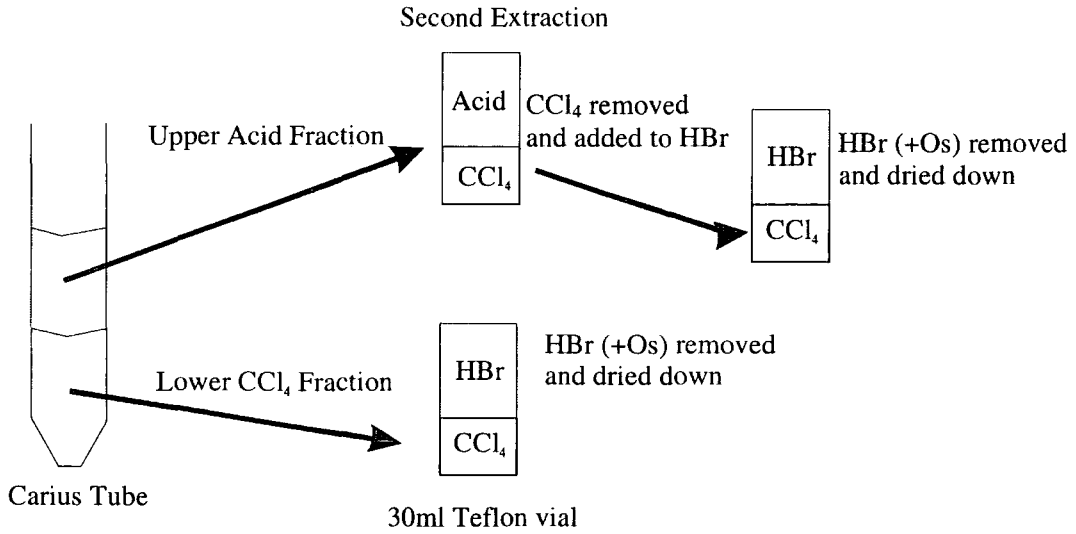

Fig 4.4 Solvent extraction of Os

13) Wash Teflon vials used for dry-downs with 5mls of 4N UpA HCl and transfer this acid to the Teflon bottle as well.

14) The spike stock solution can now be made up to the appropriate volume using 4N UpA HCl. Shake the bottle well for several days before using the stock solution.

N.B. Os spike solutions should be stored in the dark as Os is photochemically unstable.

4.5.5 Digestion by Sodium Peroxide Fusion - Procedure for Ir and Ru

An attempt was made to produce these spikes via a Carius tube digestion, however, Ir proved completely resistant to acid attack and the Ru spike was lost due to a Carius tube explosion. Thus, it was decided to digest the metallic spikes via an alternative procedure. The procedure chosen was a sodium peroxide fusion (after Yi and Masuda, 1996 and Enzweiler *et al.*, 1995).

1) Using new zirconium crucibles, weigh 1.5g of sodium peroxide onto base of crucible.

2) Tip spike onto sodium peroxide (~ 5mg of Ir + Ru spike used) and cover with a further 1g of sodium peroxide.

3) Place crucible + lid in a cold furnace and turn up to 200°C, leave at 200°C for 15 minutes, then turn furnace up to 490°C. After 15 minutes at this temperature give the crucibles a swirl and replace for a further 15 minutes. After this time, remove crucible and leave to cool.

4) Place ~40ml of MQ and the crucible in a fridge to cool. When chilled slowly add the water to the crucible to dissolve the sodium peroxide fusion cake. Beware as sodium peroxide is highly reactive in water. Ensure a larger Teflon beaker is standing by into which to pour the mixture when it starts to react.

5) Once fusion cake has been dissolved and transferred to the Teflon beaker, wash the crucible with a further 2ml of MQ, then with 6N HCl (use volume appropriate, so that when added to the rest of the spike + MQ, solution will have a concentration of approximately 1N HCl).

6) Filter solutions if they contain any undissolved material, then load onto a cation exchange column (~10cm^3 of ultra-clean cation resin) to remove most of the sodium and zirconium from the solution.

7) Immediately collect the eluant as it contains the Ir/Ru spike and make the spikes up to volume in Teflon bottles using 2N UpA HCl.

Analysis of the Ir/Ru spikes revealed that they were not as concentrated as anticipated. Assuming complete digestion of the 5mg of concentrated metallic spike, the spike solutions should have been:

$5x10^{-3}$ mg / 300ml = $1.667x10^{-5}$mg ml^{-1}, or 16.67ppm

However, the actual concentrations of the spike solutions were: Ir - 1.459ppm and Ru - 3.325ppm. This indicates that complete digestion did not occur. Although it is desirable to obtain the most concentrated solutions possible, in this particular case, the solutions obtained were still sufficiently concentrated to be usable.

4.5.6 PGE Spike Information

The spike stock solutions were made up to differing initial volumes with either 2N or 4N HCl. The volumes were partly based on the initial amount of metal spike used, but also calculated, so that the stock spikes solutions were suitably concentrated (Table 4.7).

PGE	Volume of Stock	Concentration of Stock
Ir	300	1.46
Pt	250	39.68
Os	500	25.44
Pd	100	16
Re	15	5.00
Ru	300	3.33

Table 4.7 Volume and concentration of the Durham PGE spike stock solutions

From the concentrated stock solutions a mixed spike solution of suitable concentration for analysing picrites was made by mixing together and diluting aliquots of each PGE-stock spike with 4N UpA HCl. The PGE concentrations within the mixed picrite-spike vary relative to each other (Table 4.8) to match the fractionated PGE pattern of the picrites (Fig 4.5).

PGE	Volume of stock added (ml)	Concentration (ppb) in picrite spike
Ir	2.32	13.5
Pt	0.686	108.9
Os	0.058	5.9
Pd	2.378	152.2
Re	0.282	5.6
Ru	0.517	6.9

Table 4.8 PGE concentrations within the Durham PGE picrite spike

Furthermore, the above spike concentrations have been calculated so that addition of just 0.1ml of spike to a typical picrite-type rock will give a correct spike to sample ratio (see Appendix II for calculations). Thus, the picrite spike is more concentrated than a picritic rock (Fig 4.5), but, the spike and rock have very similar PGE patterns (i.e. similar relative proportions of the PGEs).

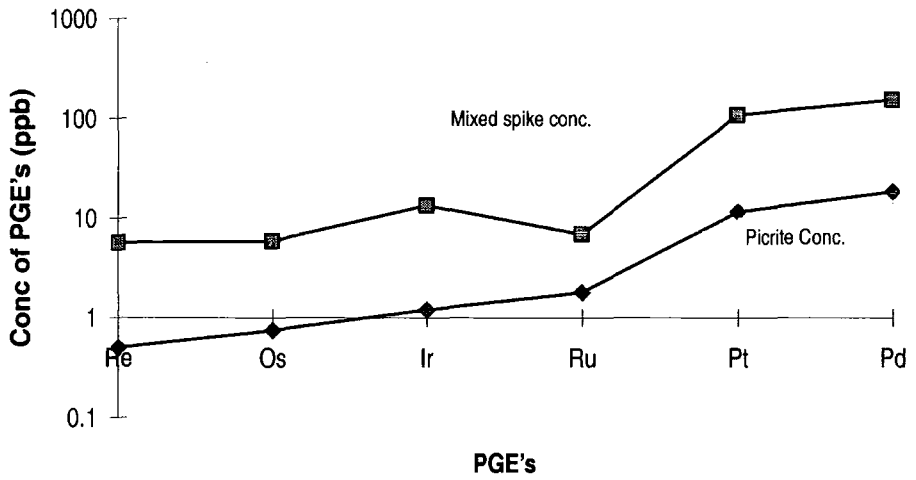

Fig 4.5 PGE patterns of a typical picrite rock (Ravizza and Pyle, 1997) and the mixed PGE spike used to analyse such rocks.

4.5.7 Calibration of Spikes – Introduction

The exact PGE concentrations of the spike solutions must be known in order to calculate the volume of spike which it is necessary to add to a rock sample to achieve the optimal spike/normal isotope ratios x 4 (Table 4.9). Thus, the spikes were calibrated using separate, dilute PGE standards made from new 1000ppm PGE standard solutions.

PGEs	Optimal Spike / Normal Isotope Ratio
Ir	191/193 x 4 = 2.38
Os	190/192 x 4 = 2.58
Pd	106/108 x 4 = 4.13
Pt	194/195 x 4 = 3.89
Ru	99/101 x 4 = 2.97
Re	185/187 x 4 = 2.4

Table 4.9 Optimal spike/normal isotope ratios for spiking of geological samples

4.5.8 Procedure for Spike Calibration - Re, Ru, Ir, Pt, Pd.

1) For each spike-standard calibration, note the weight of a clean 15ml Teflon vial.
2) Place the appropriate volume of spike is into the vial and record the new weight.
3) Place 1ml of standard into the vial, again noting the new weight.
4) Once both the spike and standard have been weighed into the vial, evaporate to dryness under clean air.
5) Take the spike/standard back into solution by adding 2ml of 3.5 % UpA HNO_3 then analyse.

4.5.9 Procedure for Spike Calibration - Os.

1) Weigh spike and standard into a vial as above, then transfer to a chilled Carius tube.
2) Wash the vial with 2ml HCl + 5ml HNO_3, then transfer to Carius tube, washing any drops of spike on the funnel into the Carius tube.
3) Seal the Carius tube and place in oven at 200°C overnight.
4) Remove the tube and chill. Os is then extracted via a triple solvent extraction procedure (See Chapter 5).
5) Once the HBr extract has dried down it is taken up in 2mls of 3.5% HNO_3 just before ICP-MS DIN analysis.

4.5.10 Calculation of amount of spike required

A simple calculation is required to work out the amount of spike needed for a spike-standard calibration, or amount of spike needed for a rock sample (See Appendix II). One drawback of this method however, is that the analyst must be able to estimate the abundances of PGE to be expected within the rock sample in order to calculate the amount of spike which must be added. The natural ratio of the spike: 'normal' isotope must also be known (Table 4.10).

	Spike Isotope Abundance	**Normal** Isotope Abundance
Ir	191 = 37.3%	193 = 62.7%
Pt	194 = 32.9%	195 = 33.8%
Os	190 = 26.4%	192 = 41.0%
Pd	106 = 27.33%	108 = 26.46%
Re	185 = 37.4%	187 = 62.6%
Ru	99 = 12.7%	101 = 17.1%

Table 4.10 Abundances of the spike and normal isotopes of the PGEs

4.5.11 Spike Instability

As a note of caution, it has been observed that Ru and Os spikes are prone to instability. It was discovered that the concentrations of these elements within their respective spike-stock solutions, decreased quite considerably over a period of many months (i.e. from ~3500ppb to ~1554 ppb in the case of the Ru). This was despite storage of the spikes in a dark cupboard to prevent any photochemical degradation. Thus, caution must be exercised in making up mixed spikes from stock spikes which have been stored for a while, as the concentration may not be as expected. It is recommended therefore, that the stock spikes should be recalibrated prior to their use in making up further spikes.

Ru within the more dilute mixed spike may also be unstable, particularly in the weeks immediately following preparation of the spike. Ru concentration within the picrite spike dropped from 4.21ppb to 3.29ppb, within two weeks of the spike preparation. A further spike calibration after another three weeks however, revealed a Ru concentration of 3.32ppb, indicating that the spike had stabilised at ~3.30ppb. The reason for this instability is unclear, but may be due to:

1) A long period was essential for equilibration

2) Presence of microscopic, particulate Ru in the spike

3) Stratification of Ru within the spike bottle.

In order to eliminate point 3) as a possibility, the spikes should be thoroughly shaken prior to use. It is also suggested, that a periodic recalibration of both Ru and

Os should be undertaken as part of the analytical routine when using I.D. to quantify PGEs.

4.6 Measurement of Ru by ICP-MS

Ru data for rocks in the geological literature is extremely scarce because of analytical difficulties in its measurement. Ru suffers badly from interferences during ICP-MS analysis. $Ni\text{-}Ar^{+}$ species are the worst culprits for causing interference problems because of the presence of high quantities of Ni in the system following Ni-S fire assay preconcentration. Ni can be eliminated from the analyte solution by utilising alternative digestion procedures to Ni-S fire assay. However, the Ni skimmer-cones used to direct the ion-beam in the ICP-MS can still cause some Ni-Ar interference problems, noticeably under "wet plasma" conditions.

The instrumental contribution to Ni-Ar interferences was assessed by analysing a series of Ru-standards (dilute HNO_3 matrix) using both Ni and Pt skimmer-cones. The $^{101}Ru/^{99}Ru$ ratio was measured (as this is the ratio used for I.D.) to see how close it would fall to the natural $^{101}Ru/^{99}Ru$ ratio of 1.346. Firstly, it is noted that the instrumental background ratio for $^{101}Ru/^{99}Ru$ is much closer to natural when using Pt cones (i.e. ~1.8). When using Ni cones, a large signal is generated on ^{101}Ru, probably due to the interference $^{61}Ni + {}^{40}Ar$. Thus, $^{101}Ru/^{99}Ru$ ratios are elevated to ~12. Due to the background noise encountered when using Ni cones, the $^{101}Ru/^{99}Ru$ ratio becomes progressively further from the expected ratio as concentration of the standard decreases (Fig 4.6). This is because at low concentrations the background interference of $^{61}Ni + {}^{40}Ar$ becomes an increasingly greater proportion of the total signal measured.

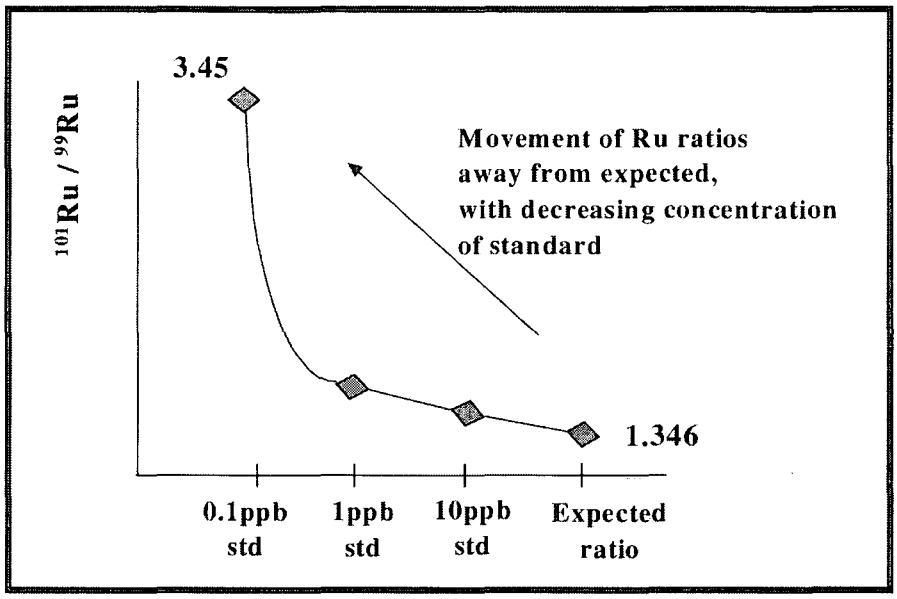

Fig 4.6 Illustration of the migration of ^{101}Ru / ^{99}Ru ratio away from expected with the decreasing concentration of standard (measured using Ni-cones in ICP-MS).

This Ni-Ar interference does appear to be wholly instrument generated and remains quite constant. Thus, background corrections can be performed to remove the Ni-Ar interference if Ni-cones have to be used. $^{101}Ru/^{99}Ru$ ratios obtained for 0.1ppb standards after blank correction, are within error of the natural ratio. The departure from the expected $^{101}Ru/^{99}Ru$ ratio of 1.346, can probably be attributed to mass fractionation which, by comparison with Pd, is known to be more significant for elements in the mass range of Ru.

The use of Pt-cones, instead of Ni-cones, within the ICP-MS is a viable option for quantification of all PGEs not just Ru, as the Pt background is <1ppt even when using Pt-cones. In addition, the $^{101}Ru/^{99}Ru$ ratio of low concentration standards is much closer to the natural ratio when using Pt-cones. Average $^{101}Ru/^{99}Ru$ ratios achieved for standards in the range 0.01ppb-1ppb using Pt-cones are 1.43 to 1.41 respectively. This implies that the Ni-cones were indeed the main source of the Ni-Ar interference. The Ru isotope measurements (and hence MBCF) are extremely stable when using the x-flow nebuliser in conjunction with Pt-cones (Table 4.11).

MBCF	STDEV between isotope ratio measurements	Number of isotope ratio measurements
0.9638	0.001	12
0.9613	0.021	8
0.9673	0.004	8
0.9621	0.013	12
0.9651	0.006	8
STDEV BETWEEN	**MBCFs = 0.0024**	

Table 4.11 Typical MBCFs for Ru using the x-flow nebuliser illustrating the stability of isotope ratio measurements. The different measurements were made over a period of several months, with the correction factor being based on a number of isotope ratio measurements (denoted by the number 'n') made on one day.

The results of the trials comparing Ni and Pt-cones led to the conclusion that Pt-cones are much more suited to Ru-analysis. Thus, Pt-cones are now routinely used within the Durham ICP-MS. The x-flow nebuliser is always used rather than the DIN for Ru-analysis, as the x-flow nebuliser enhances the stability of the Ru isotope ratios measured and produces an accordingly low background (i.e. <1ppt).

4.7 Carius Tube Digestion of Silicate Rocks for PGE Analysis

4.7.1 Introduction

Use of Carius tubes has already been discussed in this chapter in relation to making PGE spikes. Carius tubes however, are also effective for digestion of silicate rock samples and are used extensively for the work in Chapter 5. Such a method, coupled with solvent extraction of Os from its matrix, is described herein (after Shirey and Walker, 1994 and Cohen and Water, 1996).

4.7.2 Carius tube Digestion of Geological Samples

1) Clean Carius tubes by boiling in aqua regia.

2) Chill the Carius tube in a water-ethanol mixture (-10°C) and transfer weighed sample (1-2g) into the Carius tube via the funnel.

3) Add the pre-weighed spike (which should have been dried down to ~0.5ml, if using more than 0.1mls initially) from its clean Teflon vial.

4) Wash spike-vial with 2mls of conc. UpA HCl, then use to wash down any sample/spike which, may be stuck to the funnel.

5) Finally, add 5 ml of conc. UpA HNO_3 to the Carius tube.

6) Seal the Carius tube and allow to warm up to room temperature. Shake the tube well, to mix the sample and acid, and then place in an oven at 200 - 240°C for 2 to 3 days.

N.B. Take care not to heat the Carius tubes to >240°C, as pressure within the tubes increases exponentially with temperature (Gordon et al., 1944).

7) After this time, remove the tube from the oven, allow to cool, then place in a water-ethanol (or dry ice/ethanol) mixture to chill before opening.

4.7.3 Specialist Preparation of Rock samples prior to Carius Tube Digestion

Certain rock types e.g. sediments/carbonatites may need decarbonating prior to Carius tube digestion. This is an essential procedure for rocks which may produce volatiles on reaction with aqua regia, in order to prevent dangerous Carius tube explosions and loss of samples. The procedure adopted during this project to decarbonate sediments is described below (after Pearson pers. comm.):

1) Weigh sample into Teflon vial and add chilled 1N HCl drop-wise (~ 2mls/g of sample) until the sample has stopped reacting.

2) Dry sample down under clean air, to dry sample, add 6N HCl drop-wise (~2mls/g of sample) and again dry down.

3) Take up the dry sample in the appropriate volume of conc. UpA HCl (i.e. 2mls/g sample) and transfer the slurry into a chilled Carius tube. Use the HNO_3 for Carius digestion, to wash the Teflon vial and avoid any sample loss.

4.7.4 Solvent Extraction of Os following Carius Tube Digestion

1) Place a 50ml centrifuge tube in an ice bath.

2) Put 4ml of HBr in a 23ml Teflon vial (pre-cleaned by rinsing with a small amount of HBr) and place in an ice/water bath.

3) Now crack open the Carius tube (first at the neck and then just above the liquid). and pour the tube's contents into the chilled centrifuge tube.

4) Wash the Carius tube with a small amount of MQ and pour this liquid into the centrifuge tube.

5) Next, wash the cracked Carius tube with 4ml of CCl_4 and again pour the CCl_4 into the centrifuge tube.

6) Shake the centrifuge tube (containing the products of steps 4, 5 and 6) thoroughly to ensure mixing of the CCl_4 and aqua regia.

7) Stand the tube in the ice bath until the CCl_4 separates from the aqua regia/silicate phase.

8) Extract the CCl_4 from the base of the centrifuge tube and add to the vial containing HBr.

9) Add a further 4ml of CCl_4 to the centrifuge tube (+ aqua regia), seal and shake.

10) Step 8 is now repeated - this gives a **triple extraction** of Os from the aqua regia into the CCl_4.

11) After the final extraction as much of the CCl_4 as possible is removed from the centrifuge tube and no more is added. The aqua regia/silicate phase is set aside for further preconcentration of the other PGEs.

12) Remove the vial containing the CCl_4, HBr and Os, from the ice bath and shake thoroughly. Either heat gently or leave standing overnight, to ensure equilibration and extraction of Os into HBr.

13) Following this step, one of two methods can be adopted :

Either, a) Remove caps from Teflon vials and allow both CCl_4 and HBr to evaporate to dryness together. This tends to leave a red-brown residue.

Or, b) Separate the HBr (upper phase) from the CCl_4. Then allow the HBr to evaporate to dryness and discard the CCl_4. This is a much cleaner procedure and leaves much less residue.

14) The above steps enable Os measurement by ICP-MS, after addition of 2mls of dilute HNO_3 to the HBr dry-down.

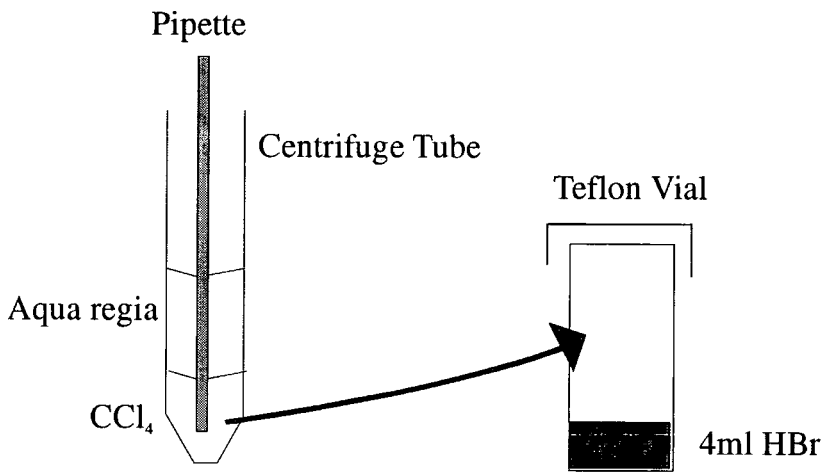

Fig 4.7 Separation of phases in Os extraction procedure.

4.7.5 Micro distillation of Os for N-TIMS analysis

If analysis of Os isotopes by N-TIMS is desired (rather than ICP-MS) further purification of the HBr-Os residue is required following Step 13b:

1) Take up the HBr dry-down in 20µl of chilled 9N H_2SO_4.

2) Transfer the dissolved HBr to the cap of a 7ml Teflon conical vial.

3) Onto the spot of H_2SO_4, pipette 5µl of 9N CrO_3 (up to 15µl of CrO_3 can be used if the dry-down is dirty) and ensure the two are gently mixed.

4) Pipette 20µl of 9N HBr into the BASE of the conical vial (which should have Teflon tape around the thread).

5) Once the H_2SO_4 and CrO_3 are thoroughly mixed, carefully invert the BASE of the rocket beaker (+ HBr) and screw down onto cap taking great care not to dislodge the drop of HBr from the tip of the rocket beaker base (Fig 4.8).

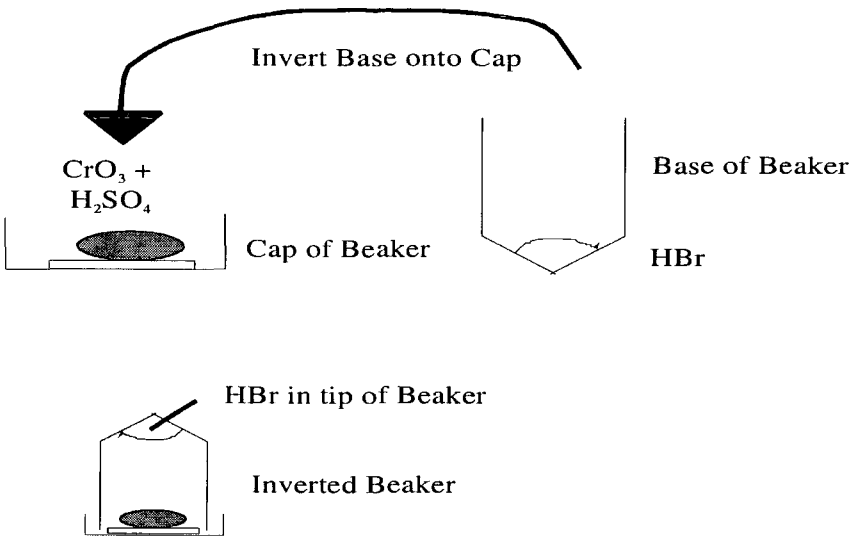

Fig 4.8 Micro-distillation of Os for Os-isotope analysis by N-TIMS (after Pearson pers. comm.)

6) Once the beaker has been successfully inverted, wrap in silver foil (leaving a small gap below the HBr to prevent it overheating).

7) Place beaker on hotplate at 80°C for ~2 hours. Oxidation of Os in the sample by the CrO_3, induces micro-distillation of the Os into the HBr. N.B. CrO_3 should retain its red colour after the distillation (if it has become green all the CrO_3 has been reduced and another micro-distillation may have to be carried out).

8) After 2 hours switch off the hotplate and carefully remove the foil from the beakers. Leave the beaker in the inverted position and unscrew the cap. Taking care not to knock the drop of HBr from its tip, turn the BASE of the beaker only, to the upright position.

9) Gently dry down the drop of HBr in beaker. Sample now ready for analysis of Os-isotopes by N-TIMS.

5: Development of Solvent Extraction/Anion Exchange Separation of PGEs from Geological Samples

5.1 Introduction

Progress on studies of PGE content in low abundance geological samples has been hampered by the limitation of methods for accurate and reproducible analysis, applicable to samples with extremely low PGE concentrations (Yi and Masuda, 1996). Experimentation with Ni-S fire assay (see Chapter 3) illustrated the limitation of this method to analysis of samples with PGE concentrations of >1-10ppb. The goal of the project therefore, was to develop a low-blank, routine chemical separation method for the high precision analysis of as many PGEs as possible by ICP-MS, with the possibility of Re-Os isotope analysis of the same sample aliquot by either ICP-MS or N-TIMS. A method employing Carius tube digestion, solvent extraction and anion-exchange chromatography to permit the analysis of Re, Os, Ir, Ru, Pt and Pd, at sub-ppb levels in geological samples was investigated and the results are presented in this chapter.

5.2 Choice of Methodology

A technique employing I.D. and digestion of the sample in a Carius tube was utilised as this technique has had considerable success in low abundance Re-Os analysis (Shirey and Walker, 1995). This digestion technique dissolves platinum group element minerals, metals and sulfides, and promotes complete chemical equilibration of sample with the spike (Shirey and Walker, 1995). The digestion is followed by organic extraction of the Os, then extraction of the other PGEs via an anion exchange column procedure.

The PGEs have a high affinity for strong base anion exchange resin. Thus, column chromatography is a natural method of separating the PGEs from their matrix. Application of this method to quantification of PGEs in geological samples, has been hampered by difficulty in obtaining quantitative elution of all elements from the resin (Jarvis *et al.*, 1997[a]). This can be overcome by the use of I.D. to

compensate for incomplete recoveries (Jarvis *et al.*, 1997[b]). The ion exchange column method is one of the most popular for preconcentration and separation of elements (e.g. Petrie and Morgan, 1982;Yi and Masuda 1996) as it offers high selectivity and is free from organic contamination compared to solvent extraction methods.

The PGEs form very stable anionic chloride complexes (Petrie and Morgan, 1982), with doubly charged complexes (MCl_6^{2-}) being more strongly sorbed onto the resin than triply charged complexes. Thus, steps are taken in the procedure to ensure that the elements are converted to their higher oxidation state. This can be done by one of two methods: either by addition of chlorinated lime to the sample in acidic media or by addition of chlorine gas (Yi and Masuda, 1996). The latter method has been chosen for this work in order to reduce the amount of matrix added to the column. Also, the blank associated with a gas should be substantially less than that associated with use of a salt.

5.3 Experimental Procedure for Carius Tube Digestion of Samples

(after Shirey and Walker, 1994)

1) Sample and spike are weighed into Carius tube and washed down with inverse aqua regia ~ 5ml HNO_3: 2ml HCl (Section 4.7.2).

2) After fusion of the mixture, the Os is extracted via the organic solvent method (Section 4.7.4).

3) The residual aqua regia containing all of the other PGEs is then prepared for the column chemistry:

i) The aqua regia + silicate sludge are dried down in a Teflon vial under clean air.

ii) Add 1ml conc. HNO_3 and dry down again (removes any residual CCl_4).

iii) Add 2mls conc. HF + 0.5ml conc. HNO_3, seal vial and warm on a hotplate, then dry down (dissolves residual silicate and then removes it as SiF_4 so reducing matrix loaded onto the column and releasing any PGEs which may be enclosed within silicate grains).

iv) Add 2mls of HNO_3 and dry down (remove any residual HF).

v) Add 2mls of conc. HCl and again dry down (converts all PGEs to chloride form necessary for column procedure).

vi) Take up in 10mls of 0.5M HCl.

vii) Centrifuge solution to remove any insoluble precipitates.

viii) Remaining liquid is chlorinated by bubbling Cl_2 gas through solution for several minutes. This solution is then left overnight to ensure full oxidation of the sample (i.e. conversion of Ir to Ir Cl_6^{2-}); (After Anbar *et al.*, 1997).

N.B. High quality acids ONLY are used for the above procedure.

It has been noted by Jarvis *et al.* (1997[a]) that certain acid digestions of the sample (i.e. $HClO_4$ based digests) adversely affect adsorption of the PGEs on the resin. They have demonstrated however, that HF- HNO_3-HCl digestions, such as that used above, maintain good retention of PGEs on the resin (i.e. Ir and Pt >99%, Pd >94% and Ru >90%).

The HF dissolution step although time consuming, is considered essential as experiments conducted without this step gave some spurious results. When the HF step was omitted samples frequently produced a green band on the column resin when reduced. This green band slowly moves down the column, eventually eluting with the PGE fractions. This green band is likely to represent metallic anionic complexes (such as Fe, Cu, Ni, Zn). When the sample is first digested with HF they pass straight through the column, but when the HF digest is omitted they stick to the anion resin. It is obviously not desirable to contaminate the PGE fractions with other metallic ions (Zn background on the ICP-MS was particularly problematical due to Zn-Cl interferences on Ru), therefore, the HF step is strongly recommended.

5.4 Anion Exchange Resin Preparation

5.4.1 Cleaning Anion Exchange Resin

The resin used in this study was Bio-Rad AG1 X8, 100-200 mesh resin (anion exchange). Initially a batch cleaning procedure was implemented *(N.B. SpA Acids Only Used):*

1) Place resin in a 1L bottle, half fill bottle with MQ water. Shake and allow resin to settle before decanting off the water. Repeat ~ 5 times; this should serve to remove any much finer resin which may have been in the bottle.

(N.B. Jarvis *et al.,* (1997[a]) have noted that commercially supplied resin contains a wider range of grain-sizes than that stated).

2) Half fill the bottle with 6N HCl and leave overnight on the shaker plate.

3) Decant off the HCl and wash the resin with MQ several times and decant off.

4) Half fill the bottle with ~ 2/3 MQ and 1/3 HNO_3, place bottle on shaker plate for a few hours (do not leave indefinitely as HNO_3 can attack the resin).

5) Decant off HNO_3, wash resin with MQ and decant off, then half fill bottle with MQ and whilst resin still in suspension pour into a tall column.

Once the resin is in the column and has settled, a reservoir is fitted to the top of the column to hold the acids used in the following sequence of washing (Table 5.1). N.B. Ensure resin has filled the column homogeneously and is not cracked in anyway. Also, ensure that the resin does not dry out at any point as this can produce cracks which can channel the acids and prevent thorough cleaning of all the resin.

Step	Volume	Acid
1	500ml	MQ H_2O
2	500ml	6N HCl
3	500ml	6N HCl
4	500ml	8N HNO_3
5	500ml	8N HNO_3

Table 5.1 Steps for column cleaning of anion exchange resin

Following the above steps, the resin is poured off the column into a clean container. The resin is then washed: twice with MQ, then with warm 12N HNO_3 (the resin is left on the shaker plate in the 12N HNO_3 for 15 minutes ONLY). Decant off the HNO_3 and rinse resin with MQ. The resin is now ready for the last wash in 6N HCl (this will reduce any residual Ir stuck to the resin, allowing it to be removed during the final resin wash on the micro columns). The HCl is decanted off and the resin is first thoroughly rinsed and then stored in MQ.

5.4.2 Resin Blank

In order to check the efficiency of the cleaning procedure several aliquots of cleaning acid were analysed for their PGE content. The later batch cleaning steps, using high strength acids, removed a considerable amount of PGEs. $1cm^3$ of resin was then loaded onto a micro-column in suspension with MQ and washed with different acids to assess the total blank contribution from the resin, which is ~2ppt or less for most PGEs.

Washing Procedure	Re (ppt	Pt (ppt)	Pd (ppt)	Ir (ppt)
Batch - 12N HNO_3	0.04	5.41	5.0	0.67
Batch - 6N HCl	8	36.76	37.38	0.78
Micro-col. 12N HNO_3	0.19	2.97	24.84	0.47
Micro-col. 12N HNO_3	0.07	2.05	4.4	0.47
Micro-col. 4N HNO_3	0.14	5.14	3.73	0.36
BACKGROUND	~0.2	2	2.5	~0.4
TOTAL BLANK	<1	~2.0	~2.5	<1

Table 5.2 Total blank contribution from resin.

5.4.3 Preconditioning of Resin before Use

Conditioning ion-exchange resin has two functions. One is to remove any species adsorbed onto the resin so preventing contamination of the analyte solution. Another important function is to establish the equilibrium conditions required for the desired separation (Jarvis *et al.*, 1997[b]). The procedure followed during this project, prior to loading samples onto the column, has been to prepare the resin in the following way:

i) Wash resin with ~30mls of warm 12N HNO_3 (to remove any residual contaminants) and then rinse thoroughly with MQ.

ii) Elute 30mls of 6N HCl from columns (converts the resin to the chloride form).

iii) Elute 30mls 0.5M HCl saturated with chlorine to create an oxidising environment in the resin (which is a natural reductant) and prevent reduction of Ir^{4+} to Ir^{3+} (after Anbar *et al.*, 1997).

5.5 Quantification of Blank associated with Column-Carius tube Procedure

The main source of blank contribution using the column-Carius tube procedure is from the resin, the acids used and the Carius tube itself. It has been demonstrated that the blank contribution from both the resin (<2pg for all elements), and from the ultra-high purity acids (<1pg for all PGEs) is negligible. The overall blank has been estimated by carrying out several complete blank-runs. The results for the optimum blank achievable are presented later.

5.5.1 Sources of Blank Contribution

5.5.1.1 Column Blank

Minor spike carry-over can sometimes be observed within the blanks, particularly for Pt and Pd. This is assumed to arise from re-use of the polypropylene columns to which Pt and Pd may be adsorbed, especially in highly oxidised states. Thus, to minimise cross contamination, the columns are thoroughly washed in warm 6N HCl between each use. In addition, columns are placed in an ultrasonic bath to ensure any particulate matter is removed from the column frits. Use of this cleaning procedure permits re-use of polypropylene columns (Table 5.3). This blank was quantified by filling both a new and an old column with $1cm^3$ of resin, then running 20mls of warm 12N HNO_3 through both for comparison. This acid was collected and analysed.

	^{191}Ir	^{193}Ir	^{185}Re	^{187}Re	^{99}Ru	^{101}Ru	^{194}Pt	^{195}Pt	^{196}Pt	^{105}Pd	^{106}Pd	^{108}Pd
Back Ground	4	4	2	5	12	9	6	10	10	11	11	7
New Col.	4	5	4	7	13	14	17	11	6	18	89	39
Used Col.	3	6	4	5	24	26	27	10	8	23	92	25

Table 5.3 The blanks associated with reuse of polypropylene columns (all values in cps)

The following conclusions can be drawn from the results in Table 5.3: Background = ~1ppt (or less) for Re, Ir, Ru, ~2ppt for Pt, Pd

∴ Total resin, column and HNO_3 blank below detection limit for Ir and Re. Blank at detection limit for Ru and Pt when using a new column, slightly increasing to ~2-3ppt when reusing a column (slight spike signature for ^{194}Pt).

For ^{105}Pd, blank ~3ppt when using new column, increasing to ~4ppt when using an old column.

For ^{106}Pd, apparent blank ~40-45ppt for old and new column. It is thought however that this may represent an ICP-MS analytical interference, as similar values are also observed when analysing reagents such as chlorinated water which have never come into contact with any ^{106}Pd spike.

It should be noted that the values above are the absolute maximum blank contribution from resin / column and in reality much of the above blank is eliminated from the column in the 12N HNO_3 wash prior to loading any sample on the column. Therefore, blank contribution will be significantly less than the values stated above.

5.5.1.2 Teflon Lab-ware Blank

Another possible source of contamination comes from reuse of Teflon vials, however, thorough cleaning of all Teflon vials used (i.e. by refluxing in conc. HCl, then conc. HNO_3, next boiling in 50:50, MQ:HNO_3, followed by boiling in 50:50, MQ:HCl and finally boiling in MQ) ensures that no cross-contamination occurs between vials.

5.5.1.3 Reagent Blank

Blanks in all reagents (esp. Cl-water and the H_2SO_3, incase of corrosion in the gas lines) should be periodically checked. In this study however, it was found that even highly corrosive Cl_2 which had been stood in the cylinder for >6 months, generated chlorine water with blanks of background, or less, for all elements except Pd (~4ppt).

5.5.1.4 Carius Tube Blank

The Carius tubes used are thick walled, pure borosilicate glass in the dimensions: Body - 20cm in length, 2cm in diameter, neck - 8cm in length, 8mm in diameter. Carius tubes were initially cleaned by washing with MQ then filling with aqua regia and allowing to stand for several days. Blank experiments however, revealed that after this cleaning procedure, a significant blank was imparted (particularly for Pt) from the Carius tube during sample digestion.

Such blank problems have also been reported by Rehkämper *et al.* (1998). In order to overcome this problem, they developed a modified Carius tube design incorporating a high purity quartz liner to prevent leaching of any PGEs from the Carius tube. This procedure appears to improve blanks (See Table 5.4), however, it is not without problems as the Carius tubes have to be cooled very slowly to avoid shattering of the quartz liner. The cost of the Carius tubes is also greatly increased by inclusion of a quartz liner.

(pg/g)	**Ru**	**Pd**	**Ir**	**Pt**
Without Quartz liner	≤ 6	≤ 6	≤ 3	204
With Quartz liner	≤ 6	≤ 6	≤ 3	≤ 15

Table 5.4 Procedural blank (pg/g), from Rehkämper *et al.* (1998)

In this study typical blanks derived from the Carius tubes when soaked in cold aqua regia are <2ppt for Ir, Re and Ru, but up to 25ppt for Pt and 30ppt for Pd (Table 5.5).

	Blank A (total procedural blank)	Blank B (total procedural blank)	Blank C (total procedural blank)	**Blank D (Carius tube blank ONLY)**
Ir		1.05	0.5	**<2**
Re	3	2.3	5.1	**<2**
Pt	19.5	25.5	30.3	**25**
Ru	< 6.6	< 5.4	5.9	**<2**
Pd	41.4	50	36	**30**

Table 5.5 Blanks when Carius tubes are cleaned by soaking in cold aqua regia (ppt)

The Pt blanks achieved are almost entirely derived from the Carius tube (Table 5.5). It seems however, that some of the Pd blank may be acquired during later processing of the sample. To try and lower the blanks even further, the Carius tubes are now cleaned by boiling in aqua regia. This lowers the Pd blank (Carius contribution) to <10ppt and the Ir, Re and Ru blank, to <1ppt. The Pd blank must be estimated from measurement of ^{105}Pd as the Carius tubes can sometimes have a high Zr content which produces false $^{108}Pd/^{106}Pd$ values. Despite boiling in aqua regia Pt blank (Carius contribution) remains at ~25 ppt.

5.5.2 Total Procedural Blanks Obtained

The optimal total procedural PGE blanks obtained within this study, as measured within respective column elution fractions, are generally very close to background (Table 5.6). By comparison with 10ppt standard solutions, these values equate to ~1pg or less, for Ir, Ru and Re. The total procedural blanks in (Table 5.6) are even below 10pg for Pt and Pd. The ability to reduce the blanks to these levels is somewhat dependent on the individual contributions from each batch of Carius tubes. Thus, it is considered necessary to frequently run total procedural blanks in conjunction with samples to correctly estimate the blank contribution.

	Re	Ru	Ir	Pt	Pd
Background	8	12	4	14	20
Blank 1 (Ir-cut)	4	5.2	5	18.39	39.5
(Pt-cut)	6.5	14.88	5.5	8.75	24.5
(Pd-cut)	9.5	16.74	4.5	11.89	27.5
(Ru-cut)	23	8.12	5	10.82	36.0
Blank2 (Ir-cut)	6	17.18	4.5	12.13	18
(Pt-cut)	7	17.59	4	11.36	20
(Pd-cut)	8	11.31	4	6.31	15
(Ru-cut)	25	18.11	6	6.6	19.5

Table 5.6 Optimal total procedural blank achieved (Values in cps)

The total procedural Os blanks are extremely consistent at less than 10pg (Table 5.7). The small blank which exists arises predominantly from the Carius tube (~5-7ppt), with a very minor contribution from the CCl_4 and HBr used in the solvent extraction.

	Counts / Second (^{190}Os)	Os Conc. in ppt
Background	6	
Blank A (Carius tube soaked in cold AqR)	61	7.8ppt
Blank B (Carius tube soaked in cold AqR)	68	9.14ppt
Blank C (Carius tube boiled in AqR)	15	2.1ppt

Table 5.7 Total procedural Os blank (following a triple solvent extraction procedure, based on volume of aqua regia used for a 1g sample). N.B. Note the extremely low background for Os due to using DIN in conjunction with the ICP-MS.

In conclusion, the typical blank corrections which are applied in I.D. calculations are listed in Table 5.8. If blanks such as those illustrated can be maintained, then the Carius-tube anion-exchange technique provides a good reliable method for analysing samples in the low pg range (i.e. sediments/acid rocks).

Ir	Re	Os	Ru	Pt	Pd
2ppt	2ppt	5ppt	5ppt	25ppt	10ppt

Table 5.8 Typical blank contribution to a 2g Sample from the Carius tube digestion, anion-exchange preconcentration procedure for PGE quantification (Elution Scheme 2).

5.6 Development of Column Elution Procedures

5.6.1 Initial Procedure Investigated

The initial column elution procedure (Elution Scheme 1) was adapted (in miniature) from that used by Petrie and Morgan (1982) and was designed so that each of the PGEs could be eluted from the column in separate fractions. The ability to collect each PGE in a separate fraction, enhances procedural detection limits and enables greater measurement precision by ICP-MS. This is because the PGE fractions do not have to be diluted to provide sufficient solution for a multi-element scan. Petrie and Morgan (1982) also describe a method whereby Pt and Pd can be eluted from the resin by use of a HCl-thiourea method. This method is considered inappropriate for this study however, as use of thiourea raises the blank and also necessitates dilution of samples for analysis by ICP-MS, due to high levels of total dissolved solids (Jarvis *et al.*, 1997[a]).

Elution Scheme 1 (after Petrie and Morgan, 1982):

Sample loaded on column (1cm^3 resin), in 0.5M HCl

0.5M HCl elution

0.1M H_2SO_3 elution (Reduces Ir + Pt)

2M HCl elution ----------> Ir

6M HCl elution ----------> Pt, Re, (Ru?)

MQ

0.2M $HClO_4$ elution ----------> Pd

5M HCl : 5M $HClO_4$ elution ----> Any residual PGEs (Ru?)

Each of the column cuts were collected and analysed in order to assess the efficiency of the procedure. Each cut was dried down under clean air and then taken up in 2mls of 3.5% HNO_3 prior to ICP-MS analysis. Preliminary results using Elution Scheme 1 (Table 5.9) indicate that the elements were eluted from the column in the right relative order using this method. However, there is poor separation between the elution peaks, with a significant amount of the Ir being present in the Pt fraction. Furthermore, it appears that 0.2M $HClO_4$ is not strong enough to elute Pd from the column as Pd was retained by the resin until the 5M HCl:5M $HClO_4$ cut. Almost all of the Ru and Re were also removed in this final elution. Another consideration is the relatively poor yields of the PGEs within their component cuts, e.g. Ir = 49%, Pt = 40%. However, 78% Re, 60% Ru and 77% Pd were present in the final cut.

		^{185}Re	^{101}Ru	^{191}Ir	^{190}Os	^{194}Pt	^{106}Pd
Sample A							
2M HCl cut	(Ir)	9	99	**701**	128	104	85
6M HCl cut	(Pt)	9	70	264	134	**500**	173
0.2M $HClO_4$ cut	(Pd)	155	43	129	102	70	**209**
5M HCl:5M $HClO_4$ cut	(Ru)	**600**	**320**	375	111	572	1603

Table 5.9 Analysis of column fractions from Elution Scheme 1 (all values in cps**) – BOLD values denote the fraction where the respective PGE, should have been eluted.**

$HClO_4$ is not ideal as an eluant because it is difficult to dry down, especially the higher molarity cut, and because the vapour is hazardous in nature. Thus, it was decided to substitute the final $HClO_4$ step used above for a step utilising warm 12N HNO_3 to remove the Pd, Re and Ru in a single cut. Warm 12N HNO_3 proved to be particularly efficient at stripping Pd, Re and Ru from the anion-exchange resin (Table 5.10). The yields of the respective PGEs within the final cut were greatly enhanced when using a 12N HNO_3 rather than a $HClO_4$ elution (Table 5.11). Thus, 12N HNO_3 was included in future elution schemes for elution of Pd, Ru and Re. Better separation of the Ir from the Pt peak (and higher Ir-Pt yield) however, is desirable and various methods of obtaining this such as using a longer column and finer mesh-size resin are later investigated.

		^{185}Re	^{101}Ru	^{191}Ir	^{194}Pt	^{106}Pd
Sample - WPR-1						
2M HCl cut	(Ir)		2279	**101915**	26379	199708
6M HCl cut	(Pt)	31	1786	105399	**415344**	54602
0.2M $HClO_4$ cut	(Pd)	4193	1445	4698	29791	33872
12N HNO_3 cut	(Ru-Re)	**35163**	**10259**	12320	151803	**393587**

Table 5.10 Analysis of column fractions from Elution Scheme 1, with final HNO_3 elution step (all values in cps) –BOLD values represent fraction where the respective PGE should have been eluted N.B. – Counts on ^{106}Pd could be enhanced by ZrO interference.

Ir – 2N HCl	45 %
Pt – 6N HCl	67 %
Pd - 12N HNO_3	58 %
Re - 12N HNO_3	89 %
Ru - 12N HNO_3	65 %
Pd (when using $HClO_4$)	*5 %*

Table 5.11 Yields of the PGEs in their respective fractions using modified Elution Scheme 1 (as in Table 5.9) N.B. Os yields are between 70 and 90 % (Cohen and Waters, 1996).

5.7 Investigation of Variation in Column Conditions and Elution Schemes on PGE Separation and Recovery Using Standard Rocks

5.7.1 Introduction

In order to investigate the column procedure further, 8 replicate samples of WPR-1 were prepared using I.D. Carius tube digestions. Although yields are low for certain PGE fractions, their isotope ratios should remain constant within different column fractions. Thus, enabling quantification of the PGE concentration of WPR-1. Therefore, in the following trials, isotope ratios were measured to enable concentration calculations and counts per second were measured to assess column yields. To maintain high data quality in I.D. calculations, mass bias and isobaric interference monitoring is essential. The isotope ratio data obtained for the WPR-1 replicates (Table 5.12) reveals the presence of previously undetected interferences.

5.7.2 Correction of Data

Unspiked WPR-1 isotope ratios differ from the natural isotope ratios due to mass fractionation. Thus, all data is corrected for mass bias. For the majority of the WPR-1 Pd-data this brings it much closer to the sample-spike mixing line (Fig 5.1). The exception to this observation is for the Pd-isotope ratios obtained in the initial 2N HCl elution (Ir-Cut). This indicates the presence of interfering ions in this initial column cut which particularly affect the $^{108}Pd/^{106}Pd$ ratio, but become less problematical during successive column elutions.

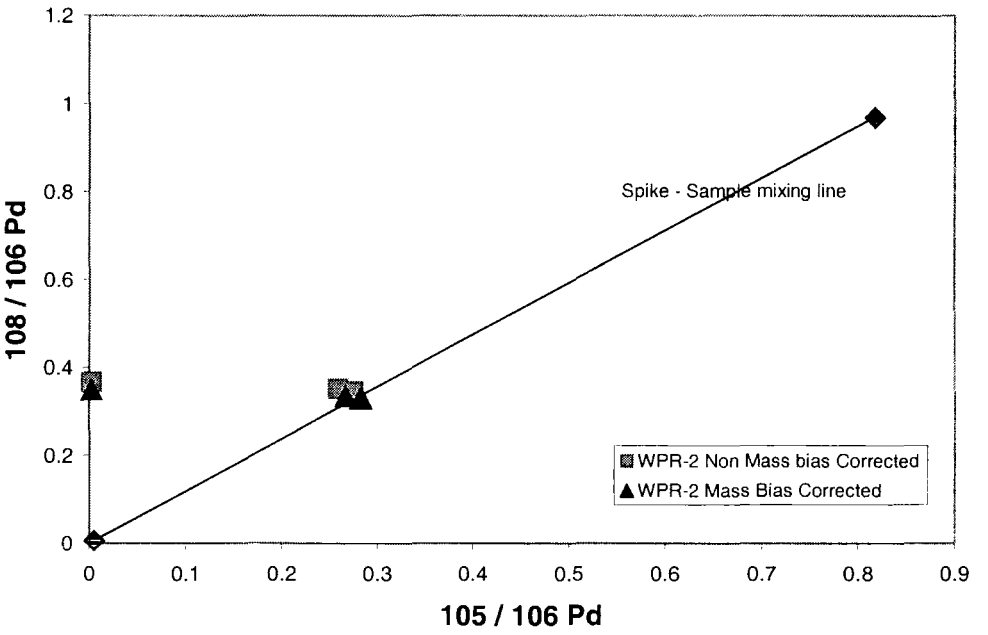

Fig 5.1 Spike sample mixing line for Pd-Isotopes in WPR-1 – Note mass bias correction brings data closer to mixing line, <u>except</u> for the data obtained in the initial 2N HCl Elution (Ir-cut), which is displaced due to isobaric interferences

Sample	Isotope Ratios				
	105/106Pd	108/106Pd	195/194Pt	196/194Pt	193/191Ir
EXPECTED VALUE	**0.81705**	**0.9686**	**1.0274**	**0.769**	**1.681**
10ppb Std	0.774	1.046	1.044	0.782	1.722
10ppb Std	0.761	1.019	1.046	0.775	1.721
AVERAGE	0.77	1.03	1.05	0.78	1.72
Values in spike :	0.0051		0.025		0.019
WPR-1 (2) Ir	0.002	0.367	0.421	0.47	0.385
WPR-1 (2) Pt	0.259	0.352	0.384	0.285	0.323
WPR-1 (2) Pd	0.275	0.346	0.392	0.287	0.328
WPR-1 (2) Ru	0.274	0.345	0.385	0.285	0.322
WPR-1 (4) Ir		0.366	0.51	0.795	0.365
WPR-1 (4) Pt	0.188	0.407	0.402	0.297	0.318
WPR-1 (4) Pd	0.274	0.344	0.399	0.299	0.322
WPR-1 (4) Ru	0.273	0.343	0.398	0.302	0.327
WPR-1 (7) Ir		0.373	0.483	0.674	0.335
WPR-1 (7) Pt	0.173	0.383	0.406	0.302	0.326
WPR-1 (7) Pd	0.334	0.366	0.404	0.299	0.325
WPR-1 (7) Ru	0.307	0.39	0.403	0.301	0.323
WPR-1 (8) Ir		0.374	0.536	0.939	0.358
WPR-1 (8) Pt	0.144	0.385	0.409	0.304	0.325
WPR-1 (8) Pd	2.3	0.906	0.412	0.303	0.327
WPR-1 (8) Ru	0.276	0.348	0.409	0.302	0.325
WPR-1 (5) Ir	0.001	0.369	0.413	0.369	0.353
WPR-1 (5) Pt	0.26	0.342	0.399	0.297	0.328
WPR-1 (5) Pd	0.273	0.34	0.397	0.299	0.323
WPR-1 (5) Ru	0.271	0.339	0.399	0.296	0.328
WPR (6)Ir		0.373	0.678	0.93	0.387
WPR (6)Pt	0.022	0.383	0.424	0.315	0.328
WPR (6)Pd	0.281	0.341	0.424	0.308	0.321
WPR (6) 12N HNO3	0.279	0.347	0.422	0.316	0.326
WPR (3) A-Ir	0.171	0.38	0.395	0.292	0.326
WPR (3) A-Pt	0.261	0.341	0.391	0.288	0.334
WPR (3) A-Pd/Ru	0.265	0.34	0.39	0.295	0.326
HF/HCL wash (x100)	0.021	0.37	0.521	0.114	1.499
WPR (3) B-Ir	0.002	0.366	0.406	0.386	0.356
WPR (3) B-Pt	0.055	0.362	0.387	0.295	0.364
WPR (3) B-Pd/Ru	0.208	0.347	0.396	0.297	0.394
EXPECTED VALUE	**0.81705**	**0.9686**	**1.0274**	**0.769**	**1.681**
WPR-1 Unspiked - Ir		0.366	0.662	1.1875	1.8645
"Pre-Ir MQ	0.079	0.358	0.531	0.535	2.294
" H2SO3 wash	0.015	0.359	0.761	0.834	1.754
" Pt	0.009	0.97	1.046	0.782	1.729
"Pre-Pt MQ wash	0.192	0.375	1.047	0.795	1.789
" Pd	0.681	0.915	1.039	0.785	1.744
" Ru	0.796	1.004	1.039	0.784	1.724

Table 5.12 Compilation of isotope ratio data measured for WPR-1 replicate standards (Raw data – not mass bias corrected). NOTE first column contains sample name + column cut identifier, e.g. WPR (1) –Ir: Ir denotes that this is the FIRST column elution (ie 2N HCl-Ir cut).

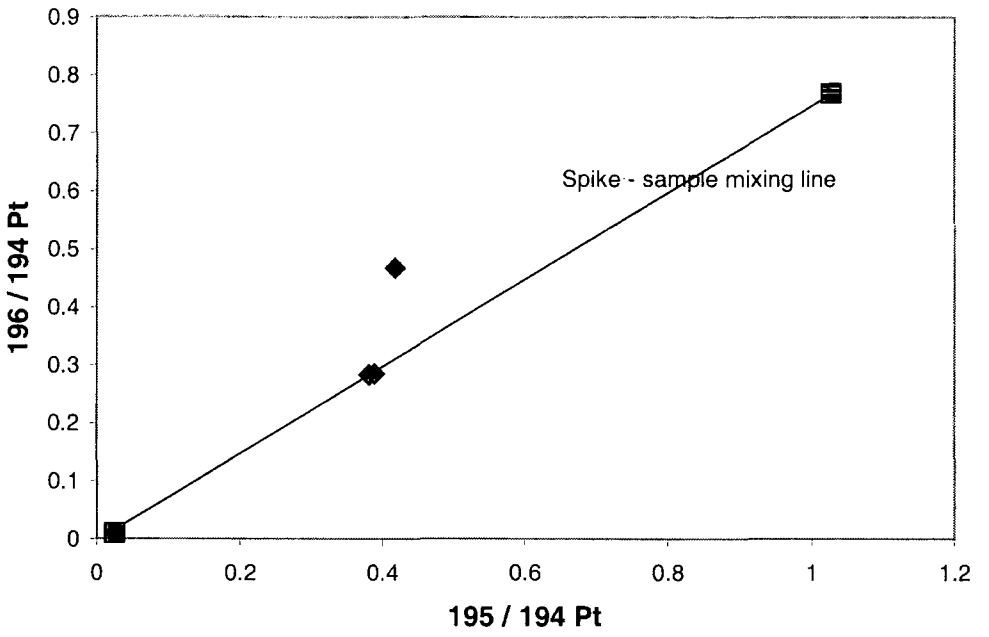

Fig 5.2 Replicates of Pt-data for WPR-1 (data mass bias corrected) - data obtained in the initial 2N HCl Elution (Ir-cut), is displaced above the mixing line due to isobaric interferences.

The presence of this same interference on Pd is also demonstrated by the unspiked sample (Table 5.12) whose isotope ratios only approach that expected, within the final column cut. Additional interferents which affect the Pt isotope ratios are also present (Fig 5.2). Displacement of both Pt and Pd data from the spike-sample mixing line is entirely due to isobaric interferences as the data has been mass-bias corrected. It could be argued that the presence of an interference affecting Pt and Pd isotope ratios in the Ir-Cut is unimportant, as most Pt and Pd (and hence most accurate isotope ratios) are eluted in later cuts not affected by the interference. It was however, considered important to try and identify the interferents, particularly those within the Ir-cut, incase Ir itself was being affected. In addition, it does sometimes become necessary to monitor isotope ratios in different column elutions due to accidental loss of a fraction or in very low abundance samples.

5.7.3 Identification of Interfering Elements

In order to determine the source of the isobaric interferences on the PGEs within the column elutions several different elements were measured during analysis of the WPR-1 column cuts (Table 5.13).

	Zr	Mo	Zn	Cu	Ni	Yb	Hf	W
Ir-Cut	52107	197698	88582	3419817	7650001	<104	3179784	447505
Pt-Cut	72692	14281	1770	3522	1449	<50	7689	6083
Ru/Re-Cut	1128	45344	5243	11811	1328	<23	262	6933

Table 5.13 Trace metal concentrations in column cuts for WPR-1 (6) (values in cps)

Isobaric interferences which might arise from the high concentrations of the above trace metals include: -

$^{66}Zn + {}^{40}Ar$ = mass 106 = Pd^{106}

$^{90}Zr + {}^{16}O$ = mass 106 = Pd^{106}

$^{92}Zr + {}^{16}O$ = mass 108 = Pd^{108}

$^{65}Cu + {}^{40}Ar$ = mass 105 = Pd^{105}

$^{61}Ni + {}^{40}Ar$ = mass 101 = Ru^{101}

$^{177}Hf + {}^{16}O$ = mass 193 = Ir^{193}

$^{180}Hf + {}^{16}O$ = mass 196 = Pt^{196}

Of these elements Zr and Hf seem the most likely as the main cause of the interference problem. High concentrations of both Zr and Hf were found to be co-eluting from the columns with the PGEs, sometimes creating severe oxide interferences on Pd and Pt-Ir respectively. The amount of Zr within column cuts in some instances was greater than that present in the original rock and probably originates from leaching of the borosilicate glass Carius tubes.

Zr and Hf may form stable anionic fluoro-complexes during the HF/HNO_3 de-silicification stage used after separation of Os. The formation of such complexes has been invoked to explain the similar behaviour of Hf to PGEs on cation resin (Ely *et al.*, 1999). However, experiments where the HF digestion step was eliminated, led to no significant reduction of Zr and Hf binding to the anion resin. These elements might therefore, form anionic chloro-complexes during chlorination rather than

fluoro-complexes. The desire to remove Zr and Hf from the eluted PGE fractions led to the development of elution scheme 2.

Another potential interference, although probably not of great significance, is that produced by $XeSO_2$. It has been noticed that Xe occurs as an impurity within the Ar gas used in the ICP-MS operation. The Xe content (although generally minor ~200 C.P.S.) can be variable and tends to increase towards the base of the gas tank due to fractional distillation. This could potentially couple with residual sulphurous acid compounds from the reductive column elution leading to interferences on Pt and Ir. Hence, in later samples extra caution was exercised in ensuring that all H_2SO_3 was washed off the column with excess MQ before eluting the PGEs.

The isobaric interference occurring in the PGE column cuts necessitated a more efficient procedure for eluting non-PGE anions (especially Hf and Zr). Thus, sample WPR-1 (3) was split in half and two different approaches were investigated:

1) WPR-1 (3) A, was chlorinated and loaded onto a column as normal. A new step was then inserted. This involved addition of 15mls of 1N HF/HCl (in order to elute the trace metals) prior to the H_2SO_3 step. A media of mixed HF/HCl is known to be efficient at elution of Zr, Hf and Ti from anion exchange resin (Barovich *et al.*, 1995). (N.B. the procedure used for WPR-1 (3) also included a 20ml MQ wash to remove any H_2SO_3 prior to collection of the Ir fraction)

2) WPR-1 (3) B, was NOT chlorinated, but was passed through a CATION exchange column containing $10cm^3$ of Bio-rad AG1 X50, 200-400# resin. The solution was immediately collected, along with a further 10ml of 0.1N HCl, which was used to wash the resin. This solution was dried down, taken up in 2mls of 0.1M HCl and then chlorinated prior to loading on the anion exchange column and eluting in the normal manner (no HF step).

The HF/HCl wash step proved to be particularly useful for removing the bulk of the Zr, Cu, Ni and Hf from the sample (Table 5.14). It however, removes only a relatively small percentage of the PGEs (Table 5.15). Thus, sensitivity of the procedure is not dramatically affected. Use of the cation column to remove the trace

metals was on the whole much less successful than the HF wash (Table 5.14). This may be because the Hf and Zr, and much of the Cu, Zn and Ni elute through as anions. The Ir and Pt cuts contain high abundances of Zr, Hf and Cu, following the cation column procedure when compared to the same cuts eluted after the HF/HCl wash (Table 5.14).

Sample		Zr	Mo	Zn	Cu	Ni	Hf	W
WPR-1, (3) A	HF/HCl Wash	6.25x 10^8	80700	87800	1.914x10^7	5224000	475900	150200
	Ir-Cut	16905		13786	44254	4120	1500	16920
	Pt-Cut	12409	2139	804	1564	172	897	2510
WPR-1 (3) B	Ir-Cut	3949300	22198	5891	161773	92039	268828	39698
	Pt-Cut	961938	3628	473	2873	1826	80147	7181
	Ru-Re - cut	413152	37405	623	2765	502	37685	7468

Table 5.14 Comparison of "clean-up" procedures in removing trace metals from samples. Where, WPR-1 (3)A, utilised an HF/HCl wash and WPR-1 (3)B was put through a cation-exchange column, prior to the normal anion exchange procedure.

^{191}Ir	^{105}Pd	^{195}Pt	^{101}Ru	^{185}Re
4.5%	5.6%	4.1%	24.8%	12.1%

Table 5.15 Percentage of PGEs lost within HF/HCl cut.

It is apparent that use of a 1N HCl/HF wash reduces interferences by looking at the isotope ratios for WPR-1 (3) A; (Table 5.12). In this sample there is far less variability between the isotope ratios in successive column cuts than in any of the other samples. When implementing the HF/HCl wash, the Pt data obtained in each of the column cuts (including the Ir fraction), all plot on the spike-sample mixing line. Furthermore, the points are practically indistinguishable from each other (Fig 5.3). Removal of Hf and Zr also reduces matrix suppression and should enhance signal. Thus, using this new technique in conjunction with applying a mass bias correction produces high quality, reproducible isotope ratio data for the PGEs.

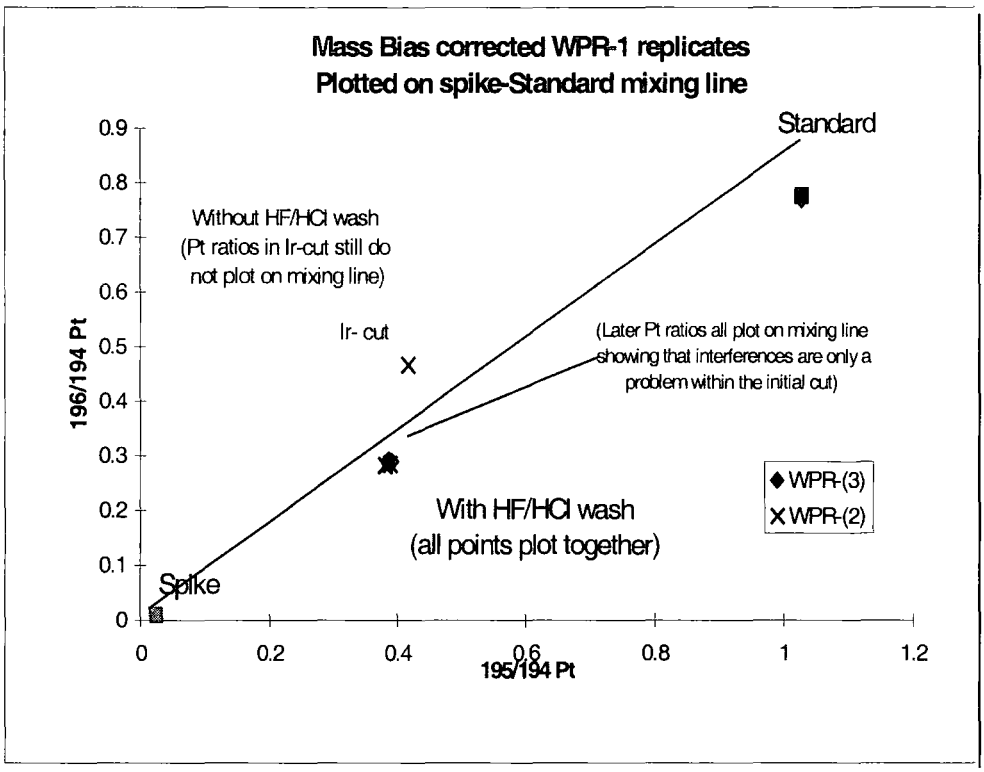

Fig 5.3 Comparison of Pt-ratios obtained with (WPR-(3) data), and without (WPR-(2) data), using HF-HCl elution step to remove interferents.

5.7.4 Online Corrections for Isobaric Interferences

Although the majority of the interfering elements are eluted from the column prior to elution of the PGEs, the following on-line corrections for isobaric interferences are still made to ensure high quality data:

^{89}Y on ^{105}Pd - $^{89}YO/^{89}Y$ = 0.92% ^{177}Hf on ^{193}Ir - $^{177}HfO/Hf$ = 1.37%

^{90}Zr on ^{106}Pd - $^{90}ZrO/^{90}Zr$ = 1.63% ^{179}Hf on ^{195}Pt - $^{179}HfO/Hf$ = 1.60%

^{92}Zr on ^{108}Pd - $^{92}ZrO/^{92}Zr$ = 1.68% ^{92}Mo on ^{108}Pd - $^{92}MoO/Mo$ = 0.60%

5.7.5 Preliminary Conclusions and Modifications of Column Experiments

Study of the replicate WPR-1 standard data (see Table 5.12 + Table 5.16), leads to the following conclusions:

1) Varying mesh size of the resin does not appreciably affect the yields.

2) The 0.2M $HClO_4$ elution is non-essential to the procedure and in fact decreases the yield of the Pd within the final cut. Thus, the procedure (i.e. the runs on WPR-1 3 A & B) has been modified to exclude this step.

3) Use of a longer column did not improve the peak separation between Ir and Pt.

4) Variance of the acid concentration (between 0.1 and 0.5N HCl) used for loading the sample does not appear to affect the yield. Use of 0.5N HCl has been adopted in future as this gives better dissolution of the silicate-chloride residue.

5) The problem of a low Ir-yield in the initial column cut has been effectively addressed by chlorinating the sample 12 hours before loading onto the column, thus, allowing sufficient time for complete oxidation of the sample. Low yields may have occurred initially as insufficiently oxidised Ir would wash straight off the column.

6) Washing the column with copious amounts of MQ prior to eluting Ir is advisable to eliminate any residual H_2SO_3 which may cause later interferences.

7) Use of a HF/HCl wash prior to eluting the PGEs decreases the concentration of trace metals in the system, thus minimising the potential for isobaric interferences.

8) The procedure used for collecting the WPR-1 (3) A data was the most effective in terms of overall yield and stability of isotope ratios. This method is outlined in detail below (Elution Scheme 2) and will be evaluated by analysis of lower abundance standards WGB-1 (Section 5.9) and WITS-1 (Section 5.10).

		Mesh Size of resin	YIELD %					
Sample (+ conc. of acid loaded in)	Eluants		^{191}Ir	^{195}Pt	^{106}Pd $HClO_4$	^{106}Pd HNO_3	^{185}Re	^{101}Ru
WPR-1 (2)		100 – 200 #	39.83	74.09	9.65	37.55	86.4	63.08
WPR-1 (3) A (0.5M HCl)	15mls of 1N HF/HCl, 22mls H_2SO_3, - reductant 20mls 2N HCl, - Ir 20mls 6N HCl, - Pt 20mls 12N HNO_3. - Ru,Re (Pd)	**100 - 200 #**	**70.17**	**61.86**		**50.19**	**99.57**	**63.13**
WPR-1 (3) B (0.1M HCl)	22mls H_2SO_3, 20mls 2N HCl, 20mls 6N HCl, 20mls 12N HNO_3.	100 - 200 #	71.11	60.01		27.73	99.51	9.40
WPR-1 (4) (0.5 M HCl)	12mls H_2SO_3, 20mls 2N HCl, 20mls 6N HCl, 20mls 0.2M $HClO_4$, - Pd, 20mls 12N HNO_3.	100 - 200 #	60.81	48.6	1.4	64.71	81.61	70.72
WPR-1 (5) (0.1 M HCl)	10mls H_2SO_3, 15mls 2N HCl, 15mls 6N HCl, 15mls 0.2M $HClO_4$, 20mls 12N HNO_3.	100 – 200 #	69.96	42.89	23.0	73.5	95.74	38.48
WPR-1 (6) (0.25 M HCl)	18mls H_2SO_3, 20mls 2N HCl, 20mls 6N HCl, 20mls 0.2M $HClO_4$, 20mls 12N HNO_3.	100 – 200 #	68.49	41.39	1.61	19.74	94.88	69.49
WPR-1 (7) (0.5 M HCl)	10mls H_2SO_3, 15mls 2N HCl, 15mls 6N HCl,15mls 0.2M $HClO_4$, 20mls 12N HNO_3.	200 - 400 #	68.19	46.54	0.97	79.92	51.41	38.08
WPR-1 (8) (0.5M HCl)	18mls H_2SO_3, 20mls 2N HCl, 18mls 6N HCl, 18mls 0.2M $HClO_4$, 20mls 12N HNO_3.	200 – 400 #	60.4	50.23	1.39	64.7	71.97	54.16
WPR-1 (Unspiked) LONG COLUMN (0.25 M HCl)	25mls H_2SO_3, 30mls 2N HCl, 25mls 6N HCl, 42mls 0.2M $HClO_4$, 20mls 12N HNO_3.	100 - 200 # (10cm of resin used)	55.8	26	0.5	99	78	61

Table 5.16 Compilation of yield data for varying column elution schemes, including use of different mesh size resin, and different length columns.

Elution Scheme 2:

1) Sample prepared as earlier method and diluted to 10mls with 0.5M HCl, then chlorinated ~12 hours before loading onto column.

2) Load $1cm^3$ of Bio-Rad AG1 X8, (100-200 # mesh size) resin onto column.

3) Resin cleaned with 20mls of warm 12N HNO_3, then 35mls of MQ.

Resin preconditioned with 30mls 6M HCl (to convert resin to chloride form), then 35mls of chlorinated 0.5M HCl (to ensure resin oxidised).

4) Sample loaded onto column, then 10mls of 1N HF/HCl + 5mls of chlorinated 0.8M HNO_3 are eluted to remove trace metals.

5) 20mls of 0.1M H_2SO_3 are eluted to reduce Ir.

6) 30mls of MQ are eluted to remove all traces of H_2SO_3.

7) 20mls of 2M HCl are eluted and collected (contains Ir-fraction).

8) 20mls of 6M HCl are eluted and collected (contains Pt-fraction).

9) 5mls of MQ are eluted to remove traces of HCl.

10) 20mls of 4N HNO_3 are eluted and collected (contains Re and Ru).

11) 20mls of warm 12N HNO_3 are eluted and collected (contains Pd fraction, + Re, Ru if step 10 not used).

N.B. Step 10 can be introduced to isolate Re and Ru in a separate fraction. The yield for Re in this fraction is <90%, with the Ru yield being approximately 68% (for WPR-1). This step is also advantageous as it will remove any strongly anionic trace metals still adhering to the resin prior to elution of Pd. This is desirable as Re and Ru do not suffer from interferences to the same extent as Pd. Step 10 can be removed, especially in the case of very low abundance samples, where it is better to have a greater Ru signal in one individual cut (i.e. the 12N HNO_3) rather than distributed across both the Ru and Pd fractions. Elution Scheme 2 (outlined in Fig 5.4) has been modified to include a 5ml 0.8N HNO_3 elution (Step 4) as this step is again particularly effective at removing Zr and Hf. This step was adopted (after

Rehkämper & Halliday, 1997) following experiments in Ru elution (see section 5.12.3).

5.8 Compilation of WPR-1 Data Obtained by Anion Exchange Chromatography

The WPR-1 replicates measured during the development of the anion exchange technique, have consistently higher concentrations than those officially published for WPR-1 (Table 5.17). The reason for this is unclear but may be due to: contamination, isobaric interferences or under-measurement of PGEs within the standard rocks to date.

	Ir	Pd	Pt
Official Value	13.5 ±1.8 ppb	235 ± 9 ppb	285 ± 12 ppb
WPR-2	17.85	264.12	312.23
WPR-3	18.10	265.3	319.05
WPR-4	17.88	264.14	333.30
WPR-5	18.30	268.22	331.52
WPR-6	18.10	281.90	368.06
WPR-7	18.00	319.96	340.77
WPR-8	18.22	268.88	346.30
Stdev 2 σ	0.34	40.62	36.85
Average (ppb)	18.06	276.07	335.89
Reproducibility %	1.86	14.71	10.97

Table 5.17 Compilation of PGE data obtained for WPR-1 by anion-exchange chromatography Note that only the Ir, Pt and Pd results are presented, as the other PGEs were not spiked for I.D. during these early studies.

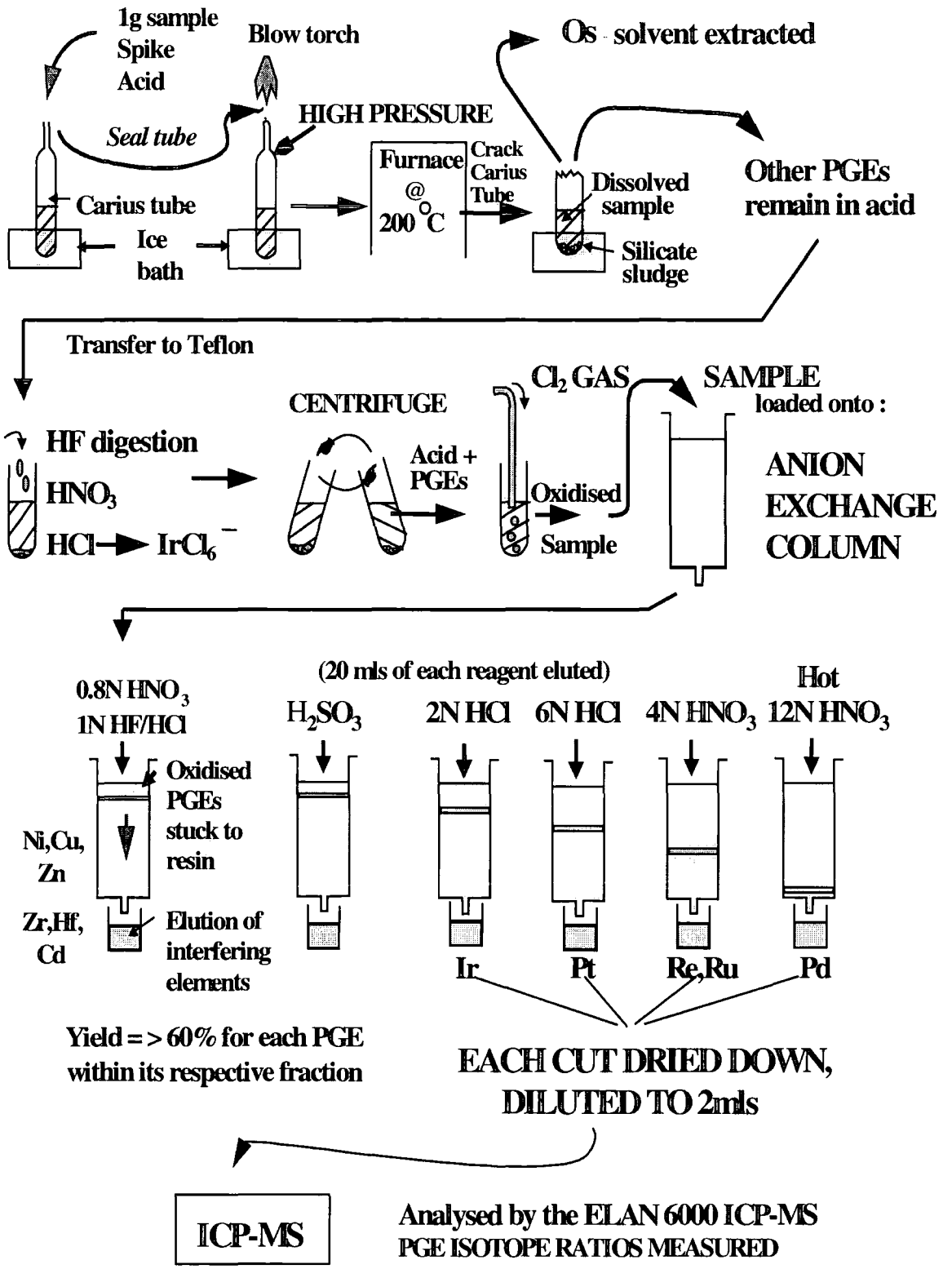

Fig 5.4 Carius tube - anion exchange chromatography preconcentration method

Separation of PGEs into 5 different fractions allows the number of masses measured in any fraction to be minimised, hence increasing sensitivity.

It is unlikely that contamination is responsible considering the reproducibility of the results (unless the standard powder used in this study has been contaminated wholesale by PGEs during the past). It is conceivable that an unidentified isobaric interference is affecting the results. It seems unlikely however, that interferences should be affecting PGEs across the mass range from 105-196 AMU. Also, a very high concentration of interferent would have to be present to affect a high abundance sample such as WPR-1. This is doubtful, especially in sample WPR-1 3, where the potential interference elements were largely removed from the column. One further point of consideration is that the values obtained are within error of the Ir, Pd and Pt data obtained for WPR-1 by I.D. Ni-S fire assay during this study (Table 5.18). It is suggested therefore, that the published standard values may be too low. This is an explanation also favoured by Jarvis *et al.* (1997[b]) to explain why their results for Pt and Pd in standards DZE-1 & 2 were approximately an order of magnitude higher than those expected.

		Average (ppb)		No. of Replicates
	Ir	**Pt**	**Pd**	
WPR-1 - Ni-S Fire Assay	18.56 ± 0.42	347.23 ± 8.40	261.71 ± 9.13	3
WPR-1 - Anion Exchange	18.06 ± 0.17	335.89 ± 18.42	276.07 ± 20.31	7

Table 5.18 Comparison of PGE concentrations obtained in WPR-1 by both Ni-S fire assay and anion exchange chromatography (errors are 1σ)

5.9 Evaluation of WGB-1 Standard Rock Type Using Column Elution Scheme

A trial of Elution Scheme 2 in analysis of a lower PGE-concentration standard rock was conducted by a triplicate analysis of WGB-1 (a gabbro). The data obtained (Table 5.19) is mass bias corrected and corrected online for the isobaric interferences listed in Section 5.7.4.

The replicate analyses of WGB-1 do not show particularly good reproducibility of PGE concentration, particularly for Os, Pt and Pd. Plots of the Pt isotopes, however (Fig 5.5), illustrate that the lack of reproducibility is not due to the

action of any isobaric interferences. Instead, it is suggested that the lack of reproducibility may be a function of inherent heterogeneity within the standard rock-types due to the nugget effect. The nugget effect is obviously exacerbated by the Carius tube digestion procedure which does not permit digestion of more than 2g of sample at a time.

	Os	Ir	Re	Ru	Pt	Pd
WGB 1	0.40	0.15	1.14	0.16	9.24	11.48
WGB 2	0.63	0.19	1.17	0.16	3.43	7.63
WGB 3	0.43	0.16	1.17	0.17	4.09	9.38
Average (ppb)	0.49	0.17	1.16	0.16	5.59	9.50
stdev	0.12	0.02	0.02	0.01	3.18	1.93
2 σ error as %	50.73	22.28	3.29	10.85	113.90	40.54

Table 5.19 Replicate analysis of WGB-1 by I.D. anion-exchange chromatography. Concentrations in ppb

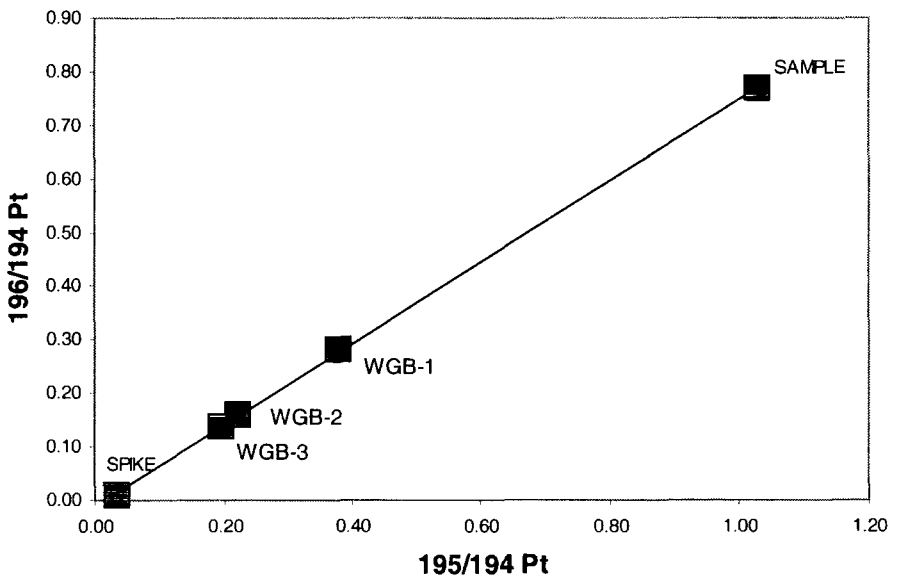

Fig 5.5 Spike sample mixing line for Pt-isotopes in WGB-1

Another possible explanation for the lack of reproducibility is that there was incomplete equilibration between spike and sample. This would also produce displacement of the isotope ratio data to different values along the spike-sample mixing line. This second explanation is treated with caution, as Carius tube digestions have been proven to promote equilibration between spike and sample, particularly for Os (Shirey and Walker, 1995). In this experiment however, Os is the least reproducible of all the PGEs. The inhomogeneity of WGB-1 has also been noted by Plessen and Erzinger (1997), following 30 separate analyses of this standard by 50g Ni-S fire assays. They note variations in average Pt content from 3.3ng/g in one container, to 6.4ng/g in another container, compared with the certified value of 6.1ng/g. They conclude from their results that it may be impossible to entirely homogenise samples with low PGE contents, including standards.

5.10 Evaluation of Suitability of Anion Exchange Chromatography for Analysis of Lower Abundance Samples – Replicate Analysis of Standard WITS-1

The Komatiite WITS-1, a standard rock recently characterised for PGEs (Tredoux and McDonald, 1996) was used to evaluate the anion-exchange technique. This standard was selected because its PGE abundance range is similar to that of un-mineralised magmatic rocks and to the samples to be analysed during this project. The data presented below (Table 5.20) are for 1g sample aliquots (sampling statistics affecting this sampling size can be estimated from Fig 5.10).

The analytical data for WITS-1 falls into 2 groups: elements that reproduce well, better than 15% (2 σ RSD), i.e. Ir, Os and Ru, and those that show worse reproducibilities, of around 20%, for Re, Pt and 42% for Pd (Table 5.20). Os and Ru reproduce exceptionally well for PGE analyses (7.5 and 8.8 % 2 σ RSD), being close to a factor of 2 within the scatter expected purely on the basis of sample heterogeneity (Fig 5.10). The mean Ru, Ir and Os concentrations are within error of the mean values suggested for WITS-1 by McDonald (1998). The value ascertained for Ru in this study is closer to the value of 5.1ppb originally suggested by Tredoux

and McDonald (1996). The values obtained for Os by DIN-ICP-MS agree very well with those obtained using the same chemical separation techniques and N-TIMS analysis (See Fig 5.6 and Table 5.20). Thus, the mean of both data sets (1.08 ± 0.05 ppb) is more likely to be the correct value of Os in WITS-1 and is used in preference to that given by Tredoux and McDonald (1996) and McDonald (1998) on the basis of preliminary data.

	Re	Os	Ir	Ru	Pt	Pd
Accepted Value (ppb)		1.4	1.5	5.5	11.8	7.6
Range of Values Obtained						4.1 - 7.6
Reproducibility (2 σ %)		11	26.4	25.4	30.4	23.6
This Study **ICP-MS**						
Mean Concentration (ppb)	0.063	1.08	1.44	5.29	6.26	5.59
Stdev 1 σ	0.007	0.04	0.09	0.23	0.61	1.18
Reproducibility (2 σ%)	20.8	7.5	13	8.8	19.5	42.1
Number of Replicates	17	10	18	11	11	19
This Study **N-TIMS**						
Mean Concentration (ppb)		1.07				
Stdev 1 σ		0.05				
Reproducibility (2 σ %)		9.72				
Number of Replicates		9				

Table 5.20 Compilation of standard data for WITS-1 – "Accepted" values from Tredoux and McDonald (1996) and McDonald (1998)

No Re data has previously been published for WITS-1 and the value determined during this study is proposed as an initial value, noting the relatively poor reproducibility. This variability in WITS-1, together with the fact that the $^{187}Os/^{188}Os$ ratio is unsupported by its Re concentration (Pearson pers. comm., unpublished) suggests the likelihood of post-crystallisation Re loss, possibly during the silicification and greenschist metamorphism identified by Tredoux and McDonald (1996).

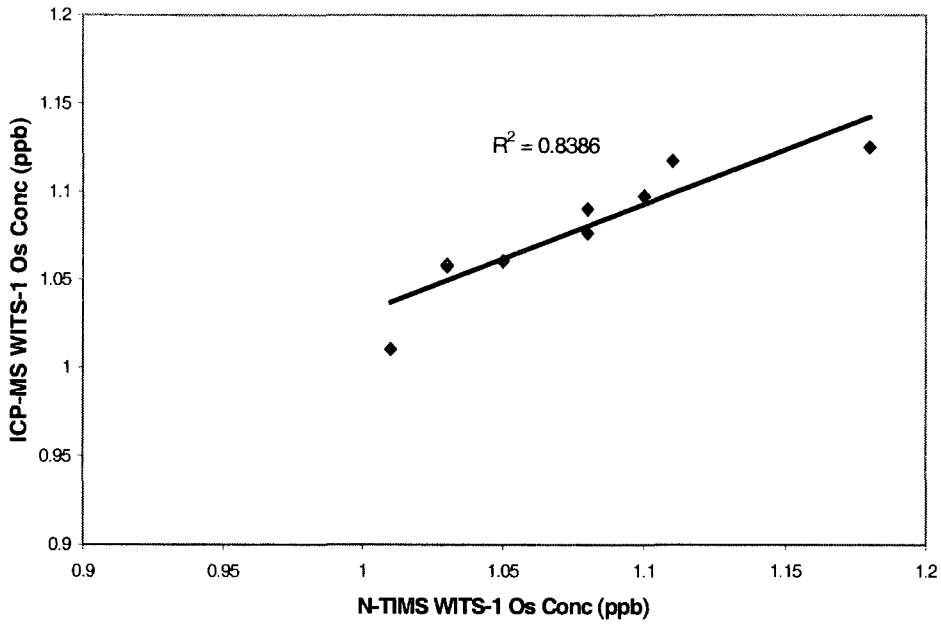

Fig 5.6 Comparison of Os concentrations determined for WITS-1 by both ICP-MS and N-TIMS, after I.D. Carius tube digestion and solvent extraction.

The mean values for Pt and Pd are both lower than those given by McDonald (1998). The mean value for Pd is within 2 σ error limits of the accepted value. It is noted that Tredoux and McDonald (1996) originally identified two populations of data in their initial characterisation of this rock, one with substantially lower Pd (4.2 ± 2.4ppb, 2σ) than the "preferred" value. This may suggest that WITS-1 is heterogeneous with respect to Pd and that the smaller sampling size used in the Carius tube digestion is much more sensitive to this than the fire-assay methods used by Tredoux and McDonald (1996). Alternatively, WITS-1 may contain mineral phases rich in Pd that the Carius tube digestion technique cannot consistently access. Similar reasoning and possibilities might be used to explain the discrepancy between the much lower mean value for Pt of 6.3 ±1.2ppb obtained in this study, and the value of 11.8 ± 3.6ppb given by McDonald (1998). The possibility for disturbance of some of the more mobile PGEs, enhancing heterogeneity, should be considered in the light of the above comments concerning Re.

Having noted the difference in mean concentration values for WITS-1, it is encouraging that the Pt/Pd and Ir/Os ratios calculated for both sets of mean values in

Table 5.20 (Table 5.21), obtained by very different techniques on quite different sampling aliquot sizes, agree within error.

	Re / Os	Ir / Os	Pt / Pd
Accepted (McDonald, 1998)		1.1	1.6
Measured (this study)	0.059	1.3	1.4
Stdev 1 σ	0.005	0.1	0.1
Reproducibility (2 σ %)	18.4	17.7	16.8

Table 5.21 Comparison of PGE ratios obtained for WITS-1

5.11 Application of Anion Exchange Chromatography to Geological Samples

The reproducibility of this method for Re and PGEs can be assessed by analysis of unknown samples. In addition, an indirect estimate of accuracy can be gained from scrutiny of the "smoothness" of the normalised PGE patterns, bearing in mind possible problems caused by inaccuracies in the characterisation of the chondritic meteorite reference data set (McDonald, 1998). A variety of volcanic rocks with widely ranging PGE concentrations were selected to evaluate reproducibility of the PGE as a function of concentration (Fig 5.7).

The first group of picrites (from Greenland) GP 5, 7 and 10 (Table 5.22) all have PGE concentrations above 1ppb and Re concentrations between 0.18 and 0.48ppb (see chapter 6 for more detail). Duplicate analyses show excellent reproducibility for all PGEs including Re, with 2 σ RSDs being better than 5% for all elements except Ru (8.4%). Reproducibilities of better than 6% are achieved for Re/Os and Pt/Pd ratios. Os/Ir shows excellent replication (1.6%). Replicate pairs are extremely coherent on chondrite-normalised PGE plots (Fig 5.7). Average reproducibility for this suite is within a factor of 2 of that expected for sampling of 1 g powder aliquots containing sparsely distributed PGE-rich nuggets (Fig 5.10). Sub-% replication of some elements in certain samples, probably indicates that these PGEs are more evenly distributed between mineral phases than the level assumed in the simple sampling theory calculations (Fig 5.10). The implication of this data is

that Carius tube digestions are highly effective at accessing PGEs contained with minerals in this type of volcanic rock in which the PGEs were presumably homogeneously distributed.

The second "unknown" sample group is a suite of 2 picrites and 2 andesites from the Lesser Antilles arc (sample pre-fix Gd; see Chapter 8 for full descriptions). They have Pt and Pd levels from 4 to <1ppb. Ru, Ir and Os are all substantially less than 1 ppb, with Ir in andesite GP17 being <5 ppt, i.e. close to detection limits. Even at such low Ir levels, the data reproduce very well compared to reproducibilities reported for similar rocks by Ravizza and Pyle (1997) and their chondrite-normalised PGE patterns are very similar. Even when both Os and Ir are at sub 20ppt levels, the sense of their relative Os/Ir fractionation shows good replication.

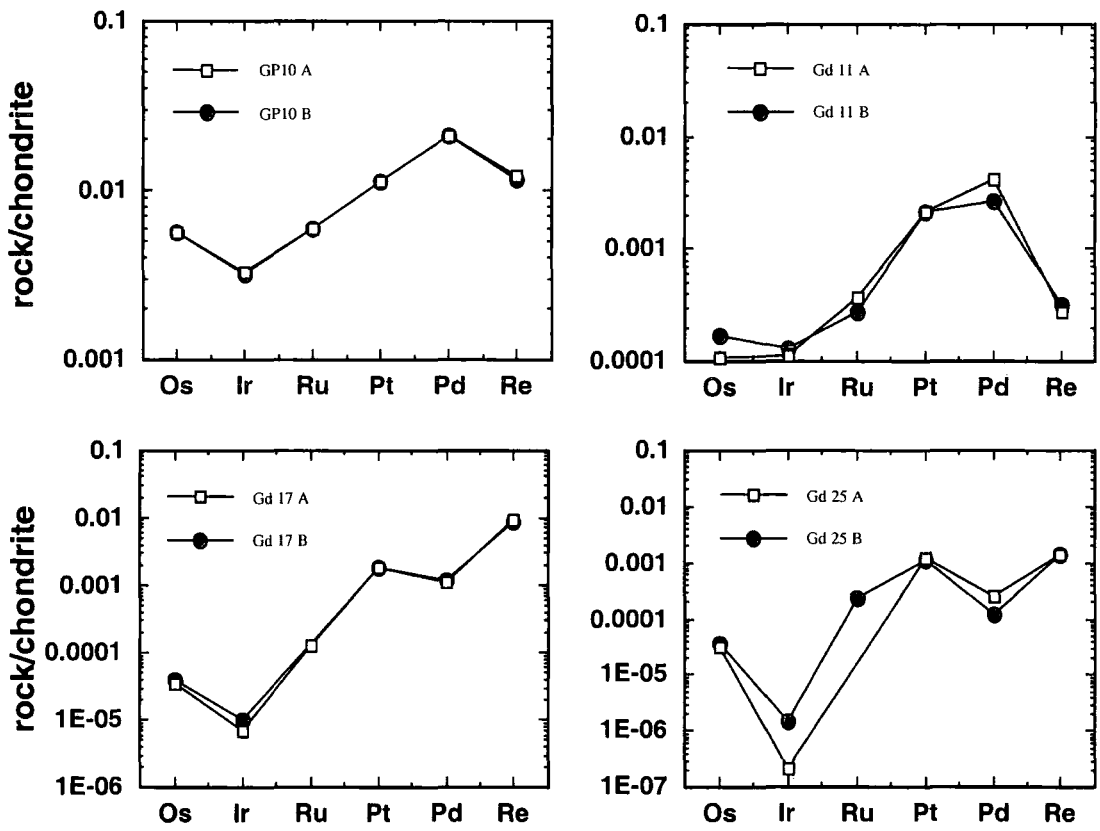

Fig 5.7 Chondrite-normalised plots of PGE abundances in replicate analyses of "unknowns" from Table 5.22. Normalising factors from McDonough and Sun (1995).

Reproducibility of PGE data is clearly not as good for the Lesser Antilles samples as for the GP picrite suite (Table 5.22), but the Lesser Antilles picrites still reproduce reasonably well. Extensive comparisons of this data with that for other samples of similar concentrations, analysed by other methods, are not possible because of a scarcity of published data at this concentration level and a common lack of documented analytical replicates (see McDonald, 1998, for more discussion of the latter point). The decrease in analytical precision for Re and PGEs compared to the GP picrite suite is attributable to lower concentrations. This effect of decreasing concentrations on analytical reproducibility is well illustrated by Re, which has a 2 σ RSD of under 2% for Gd17 (c. 0.35ppb Re), compared to a value of 20 % for Gd 11 (close to 10ppt Re).

In rocks with very low levels of PGEs (e.g. andesite Gd 25), precision for some elements shows a corresponding decline, with poor reproducibility for Ir, which is below likely detection limits (Table 5.22, Fig 5.7). Pd also shows relatively poor replication, however, even at these low levels, the general sense of inter-element PGE fractionations duplicate. Re in most of the unknowns replicates very well, even at the 10ppt level (Table 5.22, Fig 5.7) and in general better than in WITS-1. This lends credence to suspicions that alteration has accentuated heterogeneity for some elements in this rock.

The most problematical element to quantify in low abundance geological samples is Ru. This is because Ru yields can be erratic, between 30 and 60% in some samples. In most cases this is sufficient for a precise measurement as the I.D. procedure is relatively insensitive to yield. In very low abundance samples however, (e.g. andesites) insufficient signal is obtained within the relevant column fractions to permit an accurate measurement. Further discussion and attempts to overcome this problem are documented below.

Sample	Rock type	Os	Ir	Ru	Pt	Pd	Re
GP 5 A	Picrite	2.03	1.08	3.14	6.27	4.20	0.180
GP 5 B			1.11	2.95	6.01	4.48	0.179
RSD 2 σ			**3.72**	**8.82**	**5.99**	**9.12**	**0.79**
GP 7 A	Picrite	2.9	1.58	3.91	9.95	8.57	0.295
GP 7 B		2.72	1.49	3.66	9.9	8.74	0.286
RSD 2 σ		**9.06**	**8.29**	**9.34**	**0.71**	**2.78**	**4.38**
GP 10 A	Picrite	2.78	1.48	4.26	11.42	11.58	0.482
GP 10 B		2.79	1.46	4.48	11.44	11.5	0.461
RSD 2 σ		**0.51**	**1.92**	**7.12**	**0.25**	**0.98**	**6.30**
Mean RSD (2σ)		**4.8**	**4.6**	**8.4**	**2.3**	**4.3**	**3.8**
Gd 11 A	Picrite	0.0542	0.0517	0.266	2.20	2.28	0.0112
Gd 11 B		0.0834	0.0600	0.200	2.16	1.45	0.0129
RSD 2 σ		**60.0**	**21.02**	**40.1**	**2.59**	**62.9**	**20.0**
Gd 12 A	Picrite	0.0431	0.0977		3.970	2.85	0.033
Gd 12 B		0.0407	0.0819	0.154	3.48	2.82	0.032
RSD 2 σ		**8.10**	**24.9**		**18.6**	**1.50**	**4.35**
Gd 17 A	Andesite	0.0170	0.0032	0.092	1.91	0.638	0.362
Gd 17 B		0.0194	0.0047		1.88	0.673	0.357
RSD 2 σ		**18.6**	**53.7**		**2.24**	**7.55**	**1.97**
Mean RSD (2σ)		**28.9**	**33.2**	**40.1**	**7.81**	**24**	**8.75**
Gd 25 A	Andesite	0.0156	0.0001*		1.22	0.135	0.0562
Gd 25 B		0.0181	0.0007*	0.1726	1.10	0.0647	0.0554
RSD 2 σ		**0.02**	**0.0004**		**1.16**	**0.10**	**0.06**

Table 5.22 Replicate dissolutions of "unknown" samples.

GP series are Greenland picrites. Gd series are picrites and andesites from Grenada. Ir (*) in Gd 25 is below detection limits. Absence of data in a column means that no result was obtained for that fraction due to experimental error.

5.12 Problems with Ru Anion Exchange Chromatography in Geological samples

5.12.1 Introduction

Initial analyses of Ru in Grenada picrites and andesites revealed that the Ru was not eluted from the column with Re in the 4N HNO_3 fraction, as previously noted for WITS-1. Investigation of the other column cuts revealed that minor amounts of Ru had been slowly eluting from the column throughout the procedure (Fig 5.8), but, that generally no appreciable Ru was present within any of the PGE fractions. In the GP samples, gradual Ru-elution was sometimes punctuated by a peak in the 4N HNO_3 elution (Fig 5.8). The gradual decline observed implies that Ru was not effectively bound to the anion resin. The low overall Ru concentrations in the various column fractions suggest that significant losses of Ru have occurred. This could be due to removal of Ru within the HF wash, or by volatilisation of Ru during chlorination, or sample digestion following Os separation.

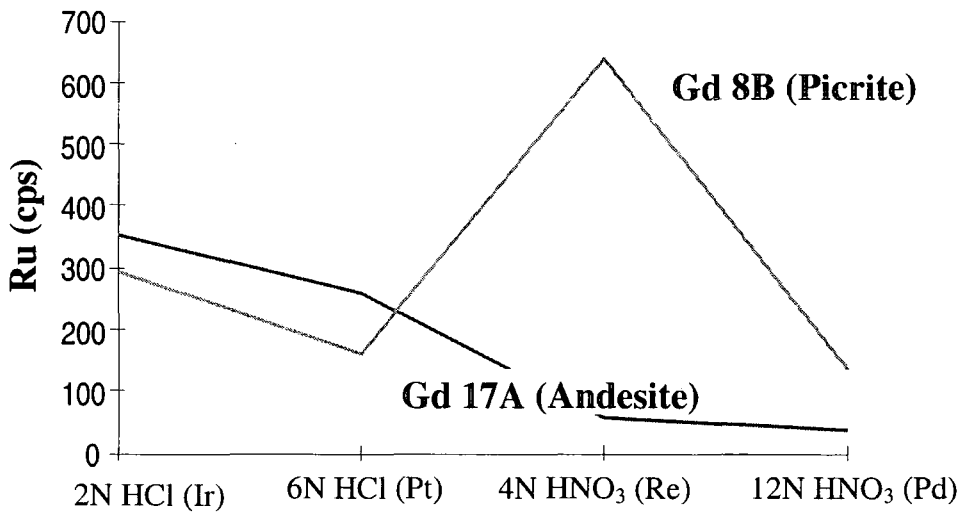

Fig 5.8 Graph illustrating elution of Ru from column in the different column cuts

5.12.2 Trials in Solvent Extraction of Ru

The above observations led to further experimentation into alternative methods of Ru separation from silicate rock matrices. The most common alternative methods being solvent extractions or distillations. Distillation of Ru is a complicated procedure, involving use of many different reagents which may contribute significantly to the blank (Gijbels & Zels, 1977). Thus, it was decided to investigate the use of a solvent extraction. It has been stated (Surasiti & Sandell, 1960) that the volatility and extractability of Ru-tetraoxide offers the best means of isolating and separating Ru from almost all other elements. Extraction by an immiscible organic solvent offers a convenient solution, as final volumes can be minimised and the Ru is obtained in an aqueous solution, free from acids and other contaminants.

It is documented in the literature that Ru may be quantitatively extracted from solution by CCl_4 (Meadows & Matlack, 1962; Surasiti & Sandell, 1960) in neutral or acidic solutions when in the RuO_4 state. Ru does not however, co-extract with Os in the CCl_4 extraction following Carius tube digestion of rock samples (Pearson pers. comm.). This is because Ru only exhibits a significant partition coefficient for CCl_4 when in the Ru^{8+} (i.e. RuO_4) state (Surasiti & Sandell, 1960) and it is assumed that Carius tube conditions are not sufficiently oxidising to convert Ru to its highest oxidation state. Addition of various highly oxidising compounds to Ru-containing solutions e.g. silver-oxide (Surasiti & Sandell, 1960) or sodium hydroxide and sodium hypochlorite (Meadows & Matlack, 1962) have been demonstrated to effectively oxidise Ru allowing extraction by CCl_4. Such compounds however, are considered unsuitable for this study due to their potential blank contribution and contribution of metal ions such as Na.

Consequently, it was attempted to convert the Ru to RuO_4 through chlorination with excess Cl_2 gas, then to extract it from solution with CCl_4 and finally to back-extract into HBr. However, both the HBr and CCl_4 contained disappointingly little Ru. It is therefore assumed that Cl_2 gas is not sufficiently oxidising to convert Ru to RuO_4. Difficulty in oxidising the Ru may be partly due to the stability of various tetrachloride and nitrous compounds which it forms (Meadows & Matlack, 1962). Thus, as solvent extraction without addition of highly oxidising metal salts proved unfeasible, solvent extraction of Ru was not pursued any

further. Instead, slightly altered column procedures were attempted to gain better Ru recovery.

5.12.3 Trials of Alternative Elution Procedures for Enhanced Ru Recovery

During the course of this project Rehkämper & Halliday (1997) have also been developing anion-exchange techniques for separation of the PGEs from geological samples. There are differences and similarities in sample preparation between this study and theirs (Table 5.23). In addition, they use an alternative elution scheme where Ru is eluted from the column prior to the other PGEs, either by 11M HCl or by 8N HNO_3, in order to enhance Ru-recovery.

	This study	Rehkämper & Halliday (1997)
Sample decomposition	Carius tube	Ni-S Fire assay
Sample weight	1-2g	5-10g
Anion resin volume used	1ml	1.25ml
PGEs recovered	Os, Ru, Re, Pt , Pd, Ir	Ru, Re, Pt, Pd, Ir
Sample oxidising agent	Chlorine gas	Bromine Water

Table 5.23 Similarities and differences in sample preparation between this study and Rehkämper & Halliday's method (1997)

As with this study, Rehkämper & Halliday's (1997) method relies on oxidising the PGEs in solution prior to loading on the anion column. In their method, once the sample is loaded onto a column bulk matrix elements are removed with weak HNO_3, followed by elution of Ru in 11N HCl, and then the other PGEs in stronger HNO_3 elutions. Care is taken during removal of the bulk matrix to retain oxidising conditions on the column and hence prevent premature elution of Ir. They document that elution of weakly reducing HCl in order to remove ~70% of the Ru does not cause elution of significant Ir. Thus, it was decided to investigate a hybrid method (Table 5.24) based on a combination of this study and that of Rehkämper & Halliday (1997) in order to achieve higher Ru yields. The trial method procedure is shown in Table 5.24.

Eluent	Volume (ml)	Eluted
Sample loaded in 0.5N HCl	~ 10	
0.8M HNO_3 (chlorinated)	8	Bulk matrix
1N HF/1N HCl	10	Bulk matrix
11M HCl	10	Ru ?
H_2SO_3	15	
MQ	30	H_2SO_3
2M HCl	20	Ir
6M HCl	20	Pt
MQ	10	
4N HNO_3	20	Re?
12N HNO_3 (warm)	20	Pd?

Table 5.24 Experimental elution procedure for better Ru separation, steps in BOLD from Rehkämper and Halliday (1997).

The conclusion of experiments into this trial procedure were that although Ru can be eluted from the anion resin by use of an initial 11M HCl step, less Ru is removed than suggested by Rehkämper & Halliday (1997); (i.e. ~27%, as opposed to 70%). In addition, the use of the 11M HCl step adversely affected retention of the other PGEs on the column, prematurely removing a significant quantity of Re and Ir (Fig 5.9). This does not occur in the study of Rehkämper & Halliday (1997). Thus, PGEs in this study may be binding less effectively to the resin than in their study. This could be because partition coefficients of the PGEs for the resin were adversely affected by digestion of the sample in inverse aqua regia in Carius tubes. This could convert the PGEs to stable nitrosyl complexes, inhibiting their later conversion to the anionic chloride complexes required for successful binding with the anion resin.

One advantage of the Rehkämper & Halliday (1997) method is the effective removal of matrix elements by the initial 0.8 M HNO_3 wash. This elution was more effective than the HF/HCl wash at removing Hf, Cd and Zr from the anion resin. The HF/HCl and HNO_3 washes are comparable at removal of Ta, whereas, the HF/HCl wash is more effective at removing Mo and Y from the anion resin. A combination of 1N HF/HCl and the 0.8N HNO_3 wash in small volumes should thus, effectively remove the bulk of potentially interfering matrix elements.

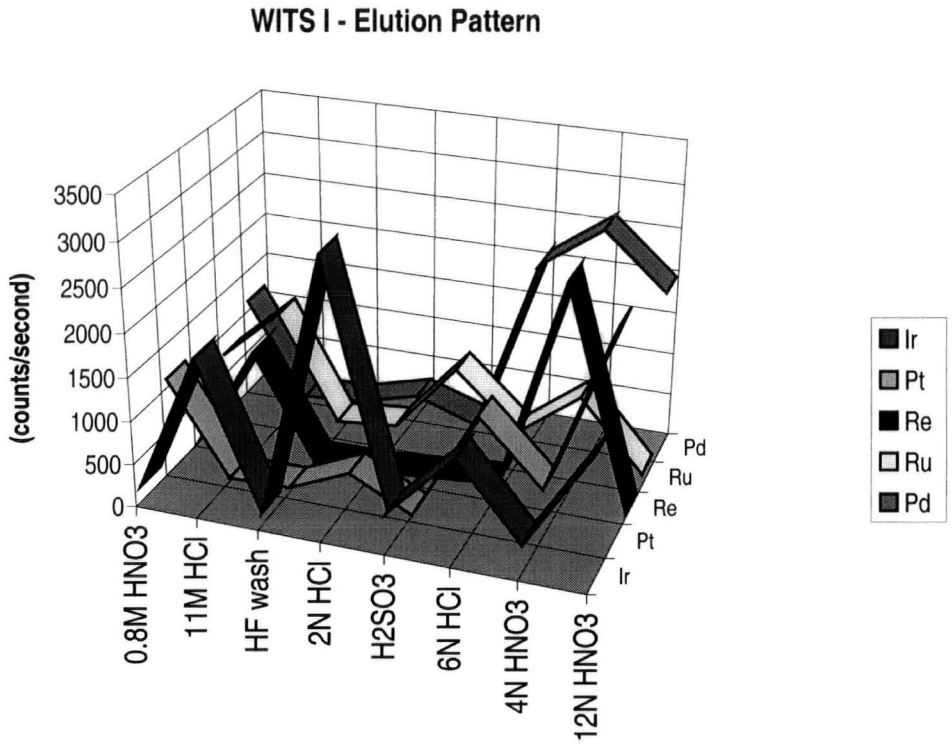

Fig 5.9 Elution patterns achieved using trial method (after Rehkämper & Halliday, 1997) – note significant quantities of Ir and Re, as well as Ru are removed in the 11M HCl

5.13 Evaluation of Anion Exchange Separation Techniques

5.13.1 Accuracy and Precision

When evaluating the accuracy and reproducibility of PGE analytical data and hence an analytical technique, several factors must be considered. McDonald (1998) has recently stressed the importance of performing replicate analyses of samples and standards in assessing PGE data, particularly the significance of inter-element fractionations. In terms of analytical standards, few suitable non-ore ICP-MS standards have been sufficiently characterised to effectively evaluate accuracy in the 1 to 5ppb range and below. Analysis of "established" ore and mineralised standards using existing (Jackson *et al.*,1990) and new PGE analytical techniques (Rehkämper

and Halliday, 1997; Yi and Masuda, 1996) show significant discrepancies between "accepted" values and those actually obtained.

In other studies where low abundance PGE standards have been analysed, relatively poor reproducibility of replicate analyses or lack of adequate documentation of reproducibility is often the norm. In many instances though, it is difficult to know whether the source of the discrepancy is a poorly constrained "accepted" value, a problem with the experimental technique, or with the homogeneity of the standard, or a combination of all three. As such, evaluation of a technique solely by comparison with "standard" rocks is not necessarily the optimal method of evaluating a given analytical technique.

Most published analytical methods for PGEs, quote reproducibility as 1 σ relative standard deviations (or coefficient of variation). For evaluation of data at higher confidence levels, the reproducibility of previously published data and that of the data obtained in this project, is expressed as 2 times the relative standard deviation (2*RSD). For most established PGE analytical techniques applied to common geological materials, reproducibility is on the order of between 20 to >100% 2*RSDs (McDonald, 1998), i.e. considerably worse than other element groups commonly analysed in geochemistry. Factors contributing to these problems have been discussed by McDonald (1998). For the purpose of this thesis, the issue of powder homogeneity, a particularly troublesome aspect of PGE analytical chemistry, will be concentrated on more specifically.

In rock powders where the elements of interest are largely contained within a few heterogeneously distributed grains (i.e. PGEs are contained predominantly in trace phases), sampling theory (Kleeman, 1967) can be used. This gives an estimate of the theoretical best possible reproducibility of element abundance measurements (Fig 5.10). Within silicate rocks PGEs are often concentrated within platinum-group minerals, or within Fe-Cu-Ni sulfides. The high concentrations of PGE in these phases compared to the silicate matrix, together with their scarcity, means that sampling of such "nuggets" becomes more difficult with decreasing size of sample aliquot (Loon and Barefoot, 1991; McDonald, 1998; Fig 5.10). For rock powders crushed to -120 mesh size, where PGEs are wholly contained in "nuggets" that are c. 0.05 vol. % abundant, it is unlikely that abundance measurements can be made that

are reproducible to better than 5-6% (2 σ RSD), for sampling at the 1 g level. Powders crushed to finer grain size (-200 mesh) are potentially more homogenous and 1g aliquots may give reproducibilities of the order of 2 to 3% (Fig 5.10), (Pearson and Woodland, 2000). Larger sample aliquots clearly give improved theoretical sampling statistics and this has been clearly demonstrated for diminishing standard aliquots analysed by Ni-S fire assay (McDonald, 1998).

Two caveats should be borne in mind when considering the simple theoretical approach summarised in Fig 5.10. One is that PGEs may be distributed between a variety of phases and this would improve sampling probabilities. On the other hand, it is unlikely that many rocks even approach being perfectly homogenised during preparation and this will act to make matters worse. So, the theoretical calculations appear to offer only a guide to likely best attainable results for given sample sizes.

5.13.2 Comparison of Anion Exchange Chromatography with Ni-S Fire Assay

To date, Ni-S fire assay has been the method of choice for determination of PGEs in most analytical laboratories. Serious limitations of fire assay are the dependence of the quality of results on the experience of the analyst and the difficulty involved in obtaining suitably low blanks to allow analysis of samples with low PGE concentrations. There is thus a pressing need to develop independent methods to validate and extend the data on PGEs in geological systems which has been based almost entirely on fire assay results to date (after Jarvis *et al.*, 1997[b]). It is suggested that the anion-exchange column procedure developed during this project provides a suitable new alternative to fire assay analysis of low PGE abundance geological samples.

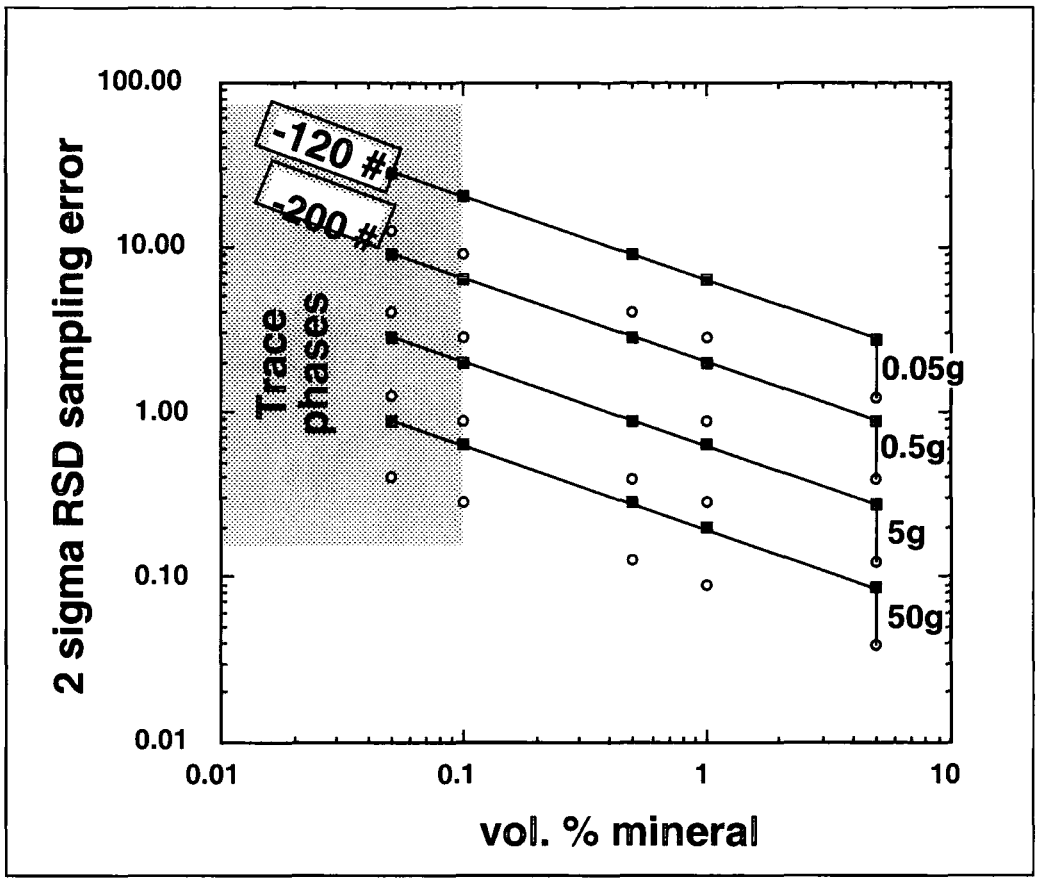

Fig 5.10 Sampling error for a single mineral phase (relative deviation at the 95% confidence level) in a powdered rock versus the abundance of the mineral in the rock (volume %) as a function of sample size.

Solid lines are for samples powdered to -120 mesh size, dashed lines are for samples powdered to -200 mesh size, assuming 1g of sample powdered to -120 mesh size (< 0.167 mm) contains 10^6 grains with density about 2.7 of a *uniform size*. For rocks/minerals of greater density a greater sample weight will be required to attain a given minimum sampling error. PGEs in silicate rocks are often hosted in mineral phases e.g., sulfides, that are less than 0.1 % abundant. If all the PGEs are contained within a single phase then the sampling error provides a theoretical best possible measurement error for those elements. See Kleeman (1967) for details of calculations (from Pearson and Woodland, 2000).

Anion-exchange chromatography does have some major advantages over Ni-S fire assay for measuring PGEs. Ravizza & Pyle (1997) noted that $^{105}Pd/^{106}Pd$ data derived from chalcophile-rich samples by Ni-S fire assay, must be regarded as suspect due to large Cu-Ar interferences. The current column technique being employed, thus, has a great advantage over the fire-assay technique employed by Ravizza & Pyle (1997) as Cu is one of the metals which is largely removed by the

HF/HCl wash elution step, thus eliminating it as a serious cause of interference. Ru data obtained by fire assay must also be treated with caution due to the large problems associated with Ni-Ar interferences on most Ru isotopes. Again, this problem is overcome when using the Carius tube digestion as large amounts of Ni are not introduced into the system.

Another limitation of the fire assay method is that Re cannot be reliably measured. This is due to large and variable Re blanks associated with the fusion reagents, variable partitioning of the Re into the sulfide melt and incomplete isotopic equilibration of the spike and sample during fusion (Ravizza & Pyle, 1997). Therefore Re/Os and other PGE data cannot be obtained on the same sample by fire assay, thus precluding Re-Os geochronological work. It is dangerous to use Os and Re data from different cuts of the same sample powder, as the nugget effect can lead to erroneous Re/Os ratios (Ravizza & Pyle, 1997). Accordingly, perhaps the greatest advantage of the column method is that calculation of the PGE concentration and geochronology by Re/Os dating, can all be carried out on the same sample aliquot.

Lastly, the blanks associated with the column-Carius tube procedure are generally an order of magnitude better than those associated with Ni-S fire assay and other digestion techniques (Fig 5.11). As shown by Shirey and Walker (1994) and McDonald (1998), heterogeneity of PGEs will vary greatly in different rock types. Ordinary Carius tubes are mostly limited to sample sizes of c. 5 g (Shirey and Walker, 1994) and so one limitation of Carius tube digestions is that the technique will be subject to greater sampling errors than fusion techniques capable of digesting much larger sample sizes.

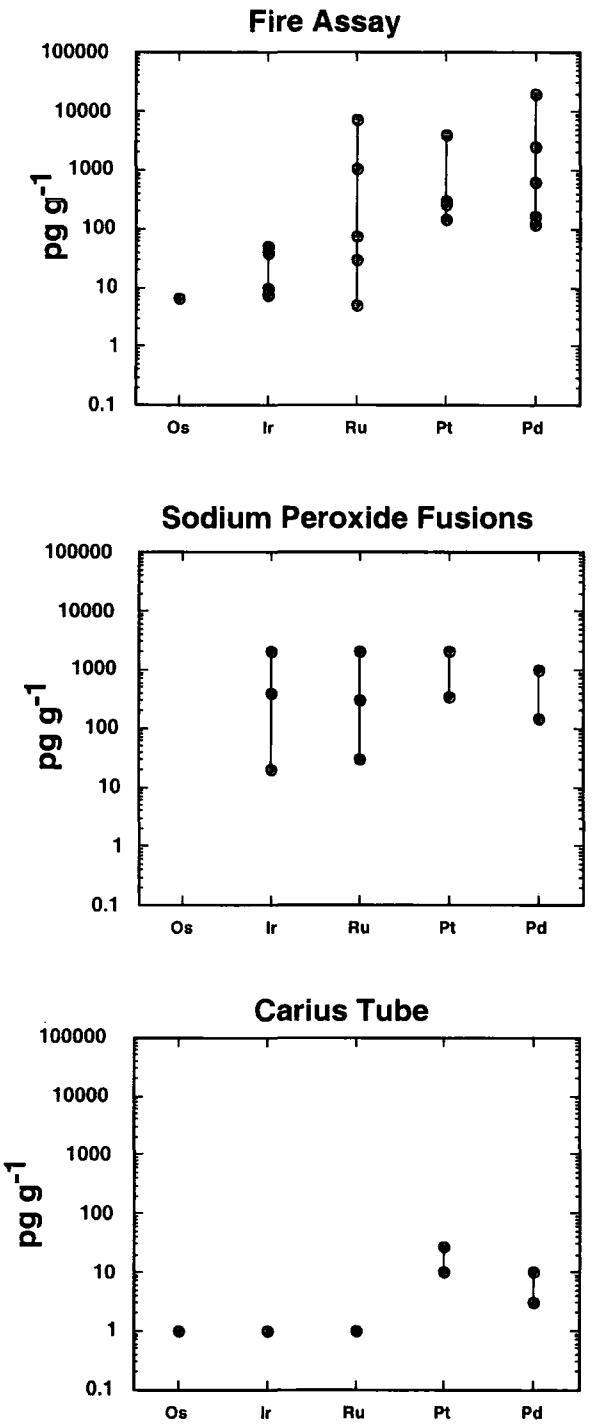

Fig 5.11 Comparison of total procedural PGE blanks in pg/g for Ni-S fire assay, sodium peroxide fusion/acid dissolution and Carius tube digestions Only methods that obtain multiple PGEs are illustrated. Dots show individual blanks for a range of studies. Data for Ni-S fire assay from (Jackson *et al.*, 1990; Juvonen *et al.*, 1994; Parry, 1980; Pattou *et al.*,1996; Ravizza and Pyle, 1997; Sun *et al.*,1993) and Woodland (this thesis). Sodium peroxide/acid dissolution data from (Enzweiler *et al.*,1995; Evans *et al.*, 1993; Gueddari *et al.*, 1996; Yi and Masuda, 1996). Carius tube data from this study plus lower points for Pt and Pd from Rehkämper & Halliday, 1998 (from Pearson and Woodland, 2000)

5.14 Overview of Anion-Exchange Chromatography

The objective in developing this Carius-tube digestion, chromatography-preconcentration technique, was to separate as many PGEs as possible from their matrix. This enhances detection limits by reducing the number of masses that must be measured during analysis, while at the same time being able to separate both Re and Os from the same dissolution. From the experiments detailed in this chapter, it is concluded that this PGE analytical technique compares very favourably with existing analytical methods for the volcanic rocks analysed and allows routine precise analysis of rocks with very low (<<1 ppb) abundances of PGEs.

Analytical reproducibility is dependent on PGE levels and rock type. This method allows confidence to be placed in inter-element PGE fractionations in rocks with <<1ppb of a given PGE. This procedure also offers the opportunity to obtain both Re-Os isotopic measurements and PGE analysis (except Rh) on very low abundance rocks that may not be amenable to other methods of analysis. A feature of significant note is the low variation in Carius tube blanks reported compared to those of other techniques (Fig 5.11). This allows accurate quantitation of very low abundance samples, provided that they are homogenous on the scale of sampling.

Procedural blanks are largely reagent dependent. Os blanks over the period of this study ranged from <1 pg to 9 pg, depending on specific batches of reagents. Ir blanks are generally close to, or below 1pg, Ru and Re are <10 pg, while Pd is close to 10 pg. Procedural detection limits (3* std deviation) of c. 3 pg/g for Os and Ir, 5 pg/g for Re, Ru and Pd and 15 pg/g for Pt. These levels are adequate for most silicate magmatic rocks and sediments and are considerably better, by several orders of magnitude, than most sodium peroxide or Ni-S fusion procedures, with the exception of those reported by Ravizza and Pyle (1997).

It is thus concluded that the technique described in this chapter is suitable for analysis of a range of low PGE abundance geological samples. As such, this procedure (Elution Scheme 2) is used for analysis of the geological samples discussed in Chapter 6 and Chapter 8.

6: Platinum Group Element Geochemistry of West Greenland Picrites

6.1 Objective in Analysing West Greenland Picrites

Prior to examining PGE behaviour in a complex subduction zone environment, it was decided to evaluate their behaviour in a simpler tectonic setting where there is no possible subduction influence. In addition, a suite of rocks were required with relatively high PGE contents to ensure high data quality and reproducibility, from which conclusions about PGE distribution could be confidently drawn. For these reasons a suite of twelve fresh, relatively uncontaminated West Greenland picrites were selected to provide a "baseline" for PGE behaviour during simple melting with which the subduction zone rocks could be compared.

6.2 Introduction and Geological Setting

Rifting between Greenland and Canada during the early Tertiary resulted in almost simultaneous eruption of voluminous flood basalts in West Greenland, East Greenland, Scotland, and the Faeroe Islands and along the eastern margin of Baffin Island. The North Atlantic Tertiary Volcanic region is thus one of the world's major flood basalt provinces. Highly magnesian picritic lavas are unusually common in this province and thus provide a unique opportunity to study primitive magmas. The picrites are presumably formed by high temperature, high degree partial melts which have not undergone much crystallisation within, or interaction with, the continental crust (Holm *et al.*, 1993 and references therein).

Given the factors outlined above, the Greenland picrites were considered to be ideal candidates for PGE analysis as the primitive nature of the rocks should ensure quantifiable PGE abundances. In addition, it is believed that PGE studies may help to understand the degree of melting, the extent of plume-depleted mantle interaction and the nature of the plume-source region. In particular, several Re-Os and Pt-Os isotopic studies have suggested that some plumes may entrain minor amounts of outer-core material (Brandon *et al.*, 1998). PGE studies may help to address this possibility. Finally, the study of picrites from an enriched plume-source

will serve as an excellent comparison to the picrites from Grenada which have no plume influence.

The samples analysed in this study for PGEs were GGU samples provided by L. Larsen. Major element data for these samples was also provided by L. Larsen, as there was insufficient sample-powders to permit XRF analysis at Durham. All samples were however analysed for trace elements at Durham using ICP-MS (see Appendix I, pvii & viii). The samples (Table 6.1) are from a suite of tholeiitic picrites exposed on the Nuussuaq Peninsula and North Disko Island, off the West Greenland coast (L.Larsen pers. com. See Fig 6.1). The samples belong to the Vaigat Formation, which at 61Ma are the earliest Tertiary rocks in West Greenland (Graham *et al.*, 1998; Fig 6.1). The samples analysed for PGEs and the stratigraphic units to which they belong are listed in Table 6.1.

Sample Name (this study)	Original Sample Name (Graham *et al.*, 1998)	Stratigraphic Unit
Gp 8	GGU 113333	Ordlingassoq
Gp 9	138228	
Gp 5	332788 *	
Gp 6	332828 *	
Gp 7	362149 *	Naujánguit
Gp 10	264217	
Gp 3	332771	
Gp 11	113210	
Gp 1	400444	Anaanaa
Gp 12	400457 *	
Gp 2	400492	
Gp 4	408001.233	

Table 6.1 List of samples analysed for PGEs (N.B. Samples marked with * analysed for He isotopes Graham *et al.*, 1998)

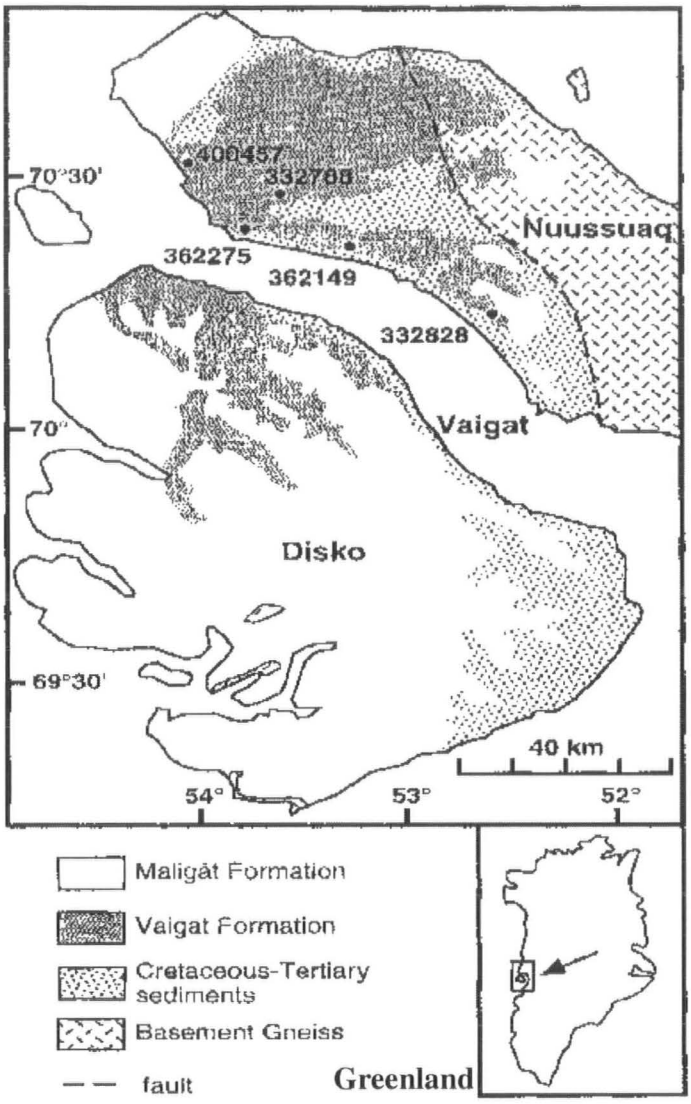

		GGU Sample No
Maligat Formation	feldspar (-olivine-augite)-phyric tholeiitic basalts	
Vaigat Formation	**Ordlingassoq Member** picrite lavas and hyaloclastites	332828 332788
	Basalt members	
	Naujanguit Member picrite lavas and hyaloclastites with horizons of contaminated basalts	362149 362275
	Anaanaa Member picrite and basalt lavas and hyaloclastites	400457

Fig 6.1 Location map and stratigraphy for the West Greenland picrites (after Graham *et al., 1998)*

6.3 Geochemical Signatures of the West Greenland Picrites

6.3.1 Major and Compatible Trace Elements

The samples analysed are typical tholeiitic picrites (Figs 6.2 & 6.3; see Appendix I, for major element data) and would seem to have undergone some minor olivine fractionation (or accumulation) as Ni content clearly diminishes with decrease in MgO (Fig 6.4).

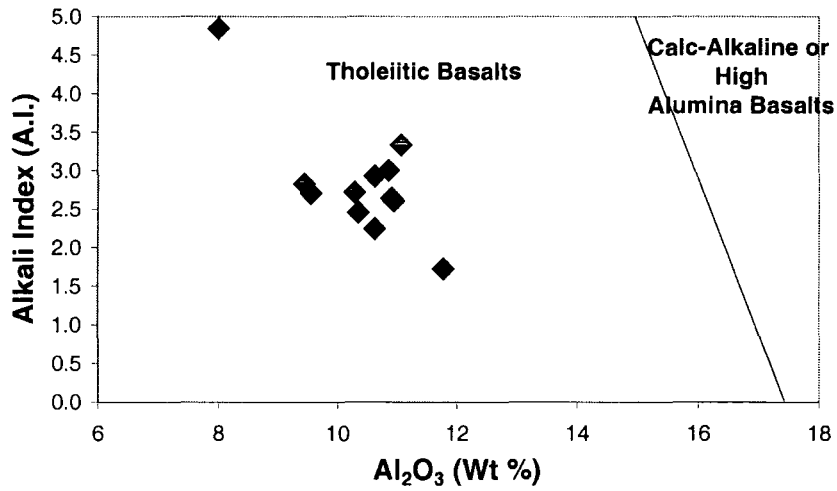

Fig 6.2 Diagram of alkali index vs wt. % Al_2O_3 for the classification of tholeiitic basalts (A.I. = $(Na_2O + K_2O)/(SiO_2 - 43) \times 0.17$; from Wilson, 1989)

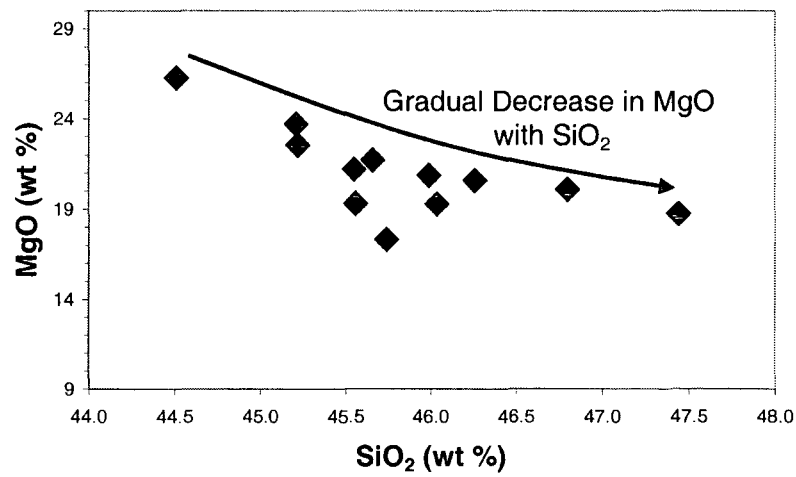

Fig 6.3 MgO vs SiO_2 diagram for WGPs to illustrate their highly picritic nature

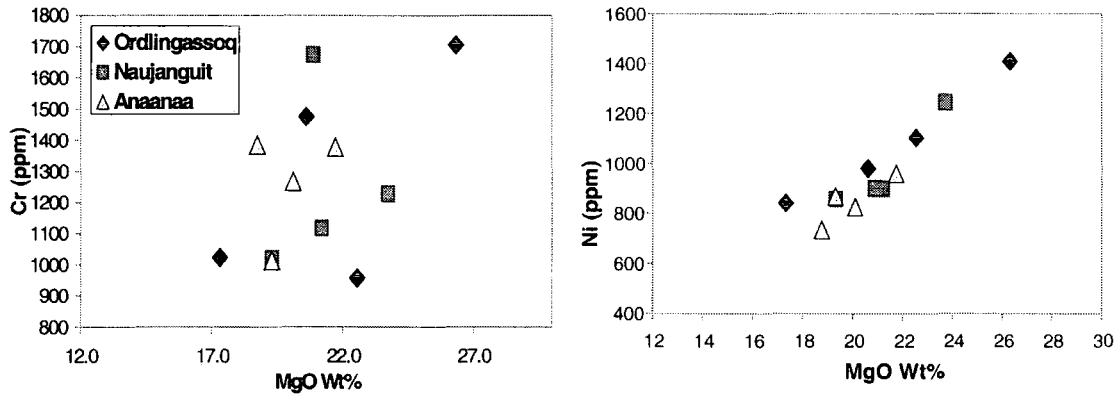

Fig 6.4 Correlation between MgO, Cr and Ni within WGPs as an index of fractionation (Cr & Ni data this project; MgO data from Larsen pers. comm.)

Following analysis of a large sample set of picrites from the Vaigat formation, Lightfoot *et al.* (1997) concluded that they have been mostly influenced by olivine accumulation. This is consistent with the tight correlations between MgO, certain major element oxides, Cr and Ni (although Cr does not show particularly good correlation with MgO within the small sample-set analysed during this project: Fig 6.4; see Appendix I). Positive correlations between both Ni and Cr vs MgO based on larger datasets (Lightfoot *et al.*, 1997) suggest that the ratio of olivine to chrome-spinel fractionation remained fairly constant during crystal accumulation and fractionation (Lightfoot *et al.*, 1997). The extent of olivine fractionation and crustal residence time, however, must have been relatively minor or the picrites would not have retained their refractory compositions. Large variations in MgO and other major element contents are attributed to differences in mantle source geochemistry or to differences in degree of melting (Holm *et al.*, 1993).

Major element differences have been noted between different members of the WGP succession (Holm *et al.*, 1993). However, there is a high degree of overlap between the major element characteristics of the samples analysed in this study (Fig 6.5). The only notable differences are that the Naujánguit picrites tend to contain higher TiO_2 concentrations and that the Anaanaa picrites tend to have slightly higher SiO_2 contents than the other picrites. These factors, coupled with the fact that the Anaanaa picrites tend to have the lowest Ni contents, suggest that they may have undergone slightly more olivine fractionation than the other picrites.

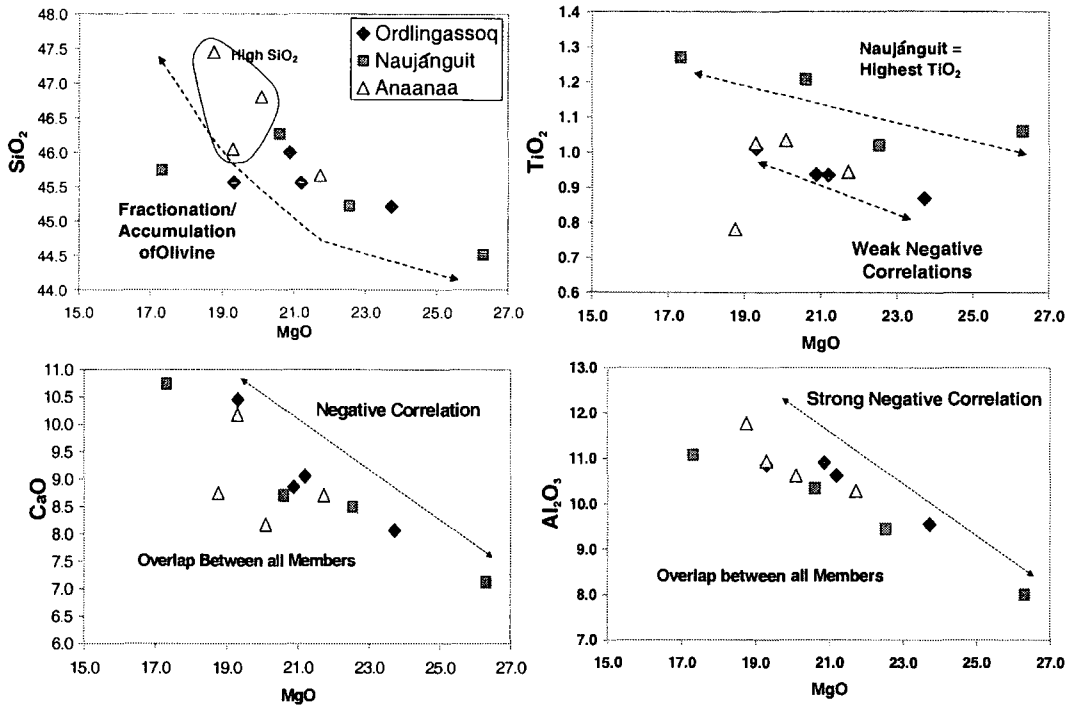

Fig 6.5 Selected major elements vs MgO for the Members of the Vaigat Formation

6.3.2 Trace Element Signatures for the West Greenland Picrites

Comparison of normalised trace element signatures is often enlightening as to the depletion or enrichment of potential magma source regions. Thus, full trace element spidergrams (after Thompson *et al.,* 1984) are presented, with the elements in order of increasing compatibility from left to right (Fig 6.6 and 6.7). Both chondrite and MORB normalised plots (after Pearce and Peate, 1995) are shown for comparison. Examination of all the data leads to several observations. Firstly, the compatible and chalcophile element concentrations and patterns are almost identical between samples and between the different members. These suggest they were derived by similar degrees of mantle melting and have had similar fractionation histories. Cr and Ni are particularly enriched relative to MORB, as would be expected for primitive lavas produced by high enough degrees of mantle-melting to cause removal of refractory metallic sulfides (i.e. > 25%).

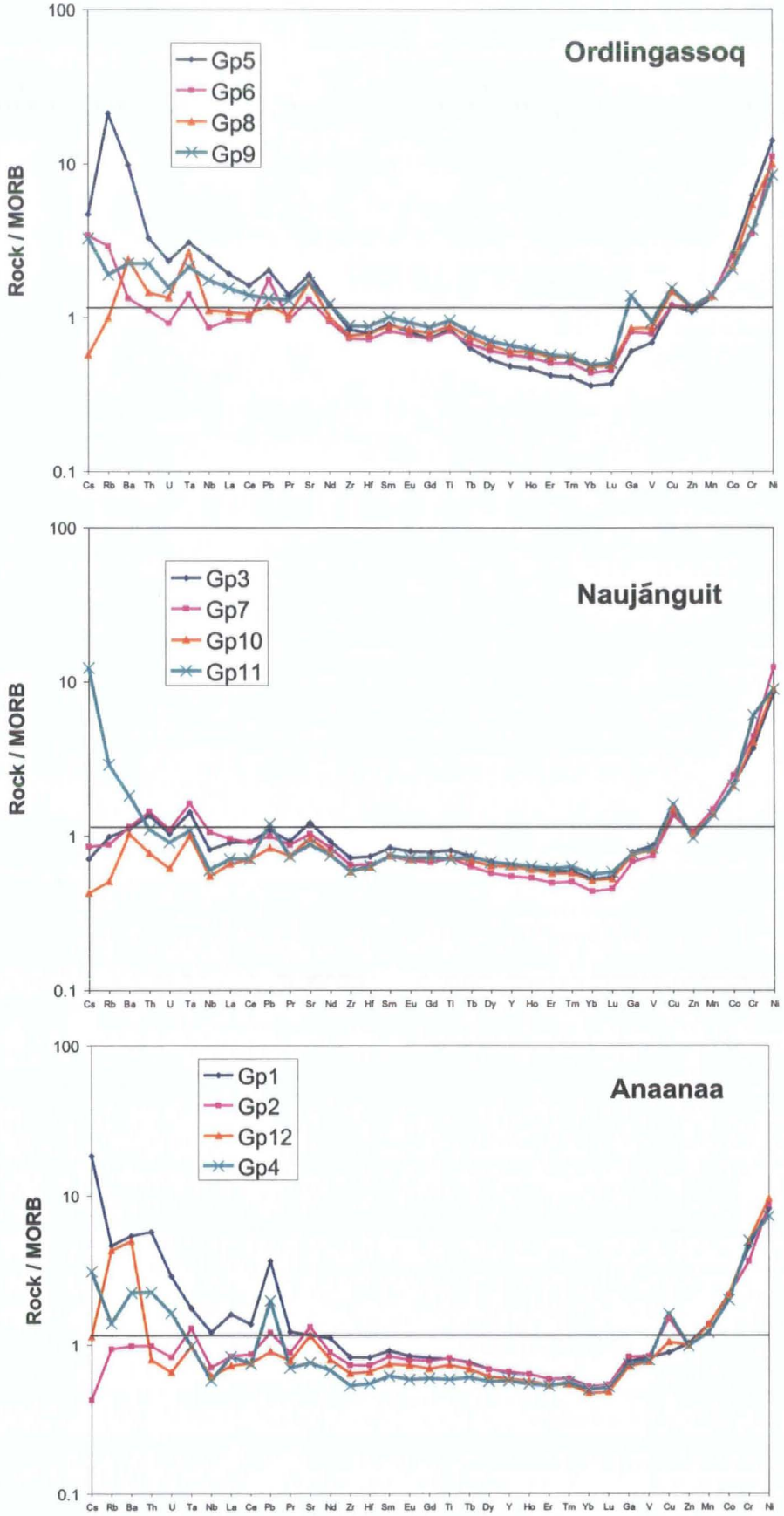

Fig 6.6 MORB-normalised extended trace element plots for respective picrite members of the Vaigat formation West Greenland. Order and normalisation values after Pearce and Parkinson, (1993)

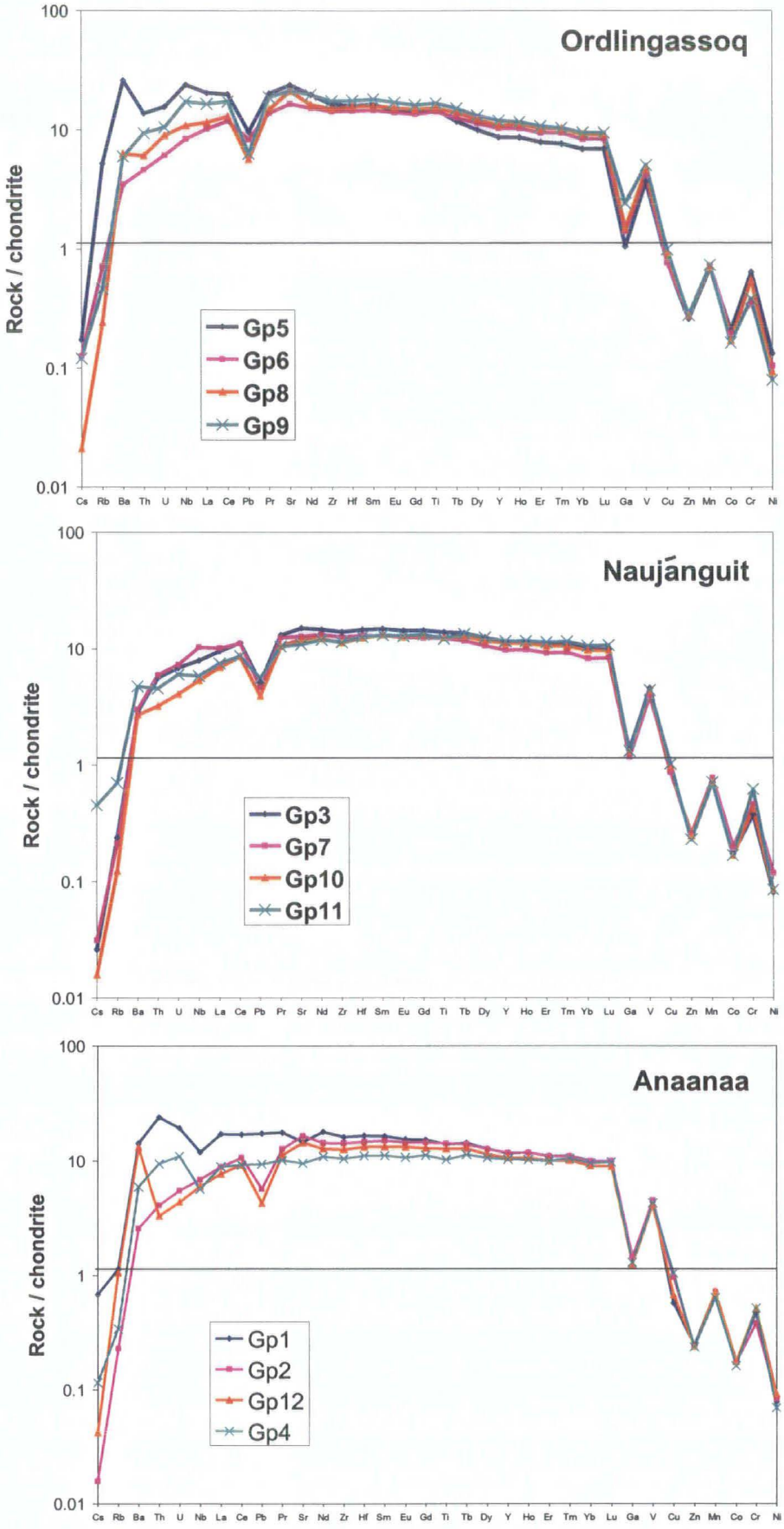

Fig 6.7 Chondrite-normalised extended trace element plots for respective picrites of the Vaigat formation, West Greenland. Element order and normalisation values after Mcdonough and Sun, (1995).

All of the WGPs contain lower concentrations of the REEs than MORB and accordingly higher concentrations of the REEs than chondrite. Compared to MORB, the WGPs have relatively flat to slightly LREE depleted patterns. The Naujánguit group has the flattest MORB-normalised REE patterns and has similar incompatible element concentrations to MORB (except for Gp11). This provides support to the model of Graham *et al.* (1998) based on both trace element and isotope data, that the Naujánguit group has a greater MORB-like component than the Ordlingassoq Member, which has a more pure plume signature. The Ordlingassoq member is more enriched in LREEs and incompatible elements possibly through addition of a fertile plume component to the MORB source (Graham *et al.*, 1998).

The Anaanaa Member has a more variable signature. The REE series are all depleted relative to MORB, but some samples are more enriched in LREE than others. Except for Gp 2, the picrites of the Anaanaa Member are enriched in the more incompatible elements relative to MORB. The more variable signatures may result from the fact that the Anaanaa Member represents some of the earliest plume-related volcanics. These may have been generated by more variable degrees of partial melting than the later Members or from variable mixing of plume and MORB-source mantle.

6.3.3 Sr and Nd Isotope Signatures of the West Greenland Picrites

Previously unpublished Sr and Nd data has been used in section 6.3.3 which was provided by L.Larsen pers. com. There is a lack of correlation between major elements and Sr-Nd isotopes which suggests that significant contamination through assimilation-fractional crystallisation (AFC) processes within the crust has not occurred. The Sr and Nd isotope compositions of the Ordlingassoq picrites are slightly enriched relative to MORB. The basal Naujánguit picrites generally have slightly more enriched isotope compositions than the Ordlingassoq picrites (Fig 6.8).

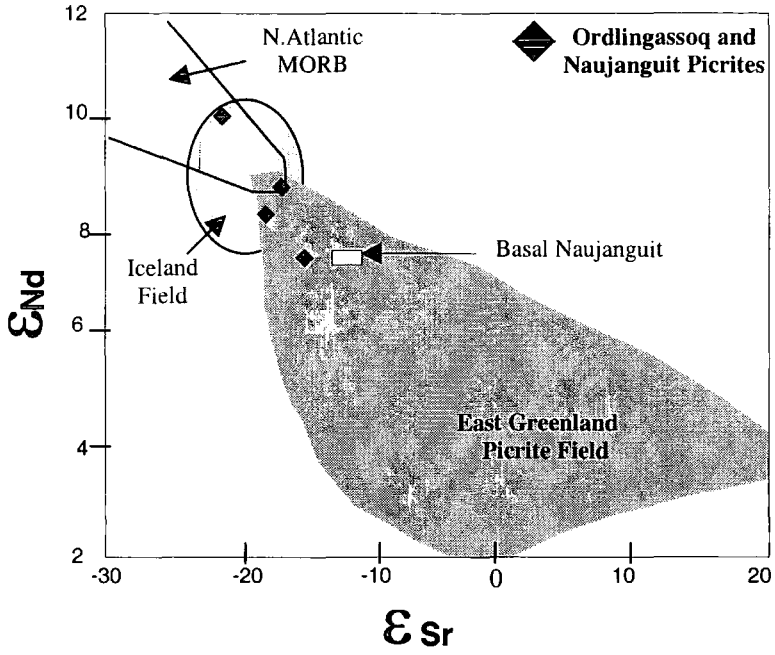

Fig 6.8 ε_{Nd} vs ε_{Sr} for West Greenland picrites. Data from Larsen (pers. comm.). Reference fields for East Greenland and Iceland from Holm *et al.*, 1993. Note – no isotope data available for Anaanaa Member picrites.

There is a significant overlap between the Sr and Nd isotopic compositions of the Ordlingassoq and Naujánguit picrites and modern Icelandic lavas (Graham *et al.*, 1998; Holm *et al.*, 1993). Holm *et al.* (1993) note a corresponding enrichment of the LREE and other highly incompatible elements in the Ordlingassoq picrites relative to those of the Naujánguit Member. Indeed, Ordlingassoq picrites analysed in this study generally have higher LREE abundances than the Naujánguit Member. The Naujánguit Member has the lowest LREE abundances of all three members. In addition, the Naujánguit Member exhibits the most constant REE patterns between different samples.

The Anaanaa Member has the most variable MREE abundances (see Fig 6.9). The HREE signatures of the picrites from all Members are very similar, although the Ordlingassoq Member tends towards lower HREE abundances than the other Members. Thus, the Ordlingassoq Member shows the highest LREE/HREE ratios of all the Members. Fractionation of this nature is often taken to infer the presence of garnet in the magma source region. The lack of any Sr or Eu anomalies is further evidence for an absence of plagioclase fractionation and minimal crustal contamination.

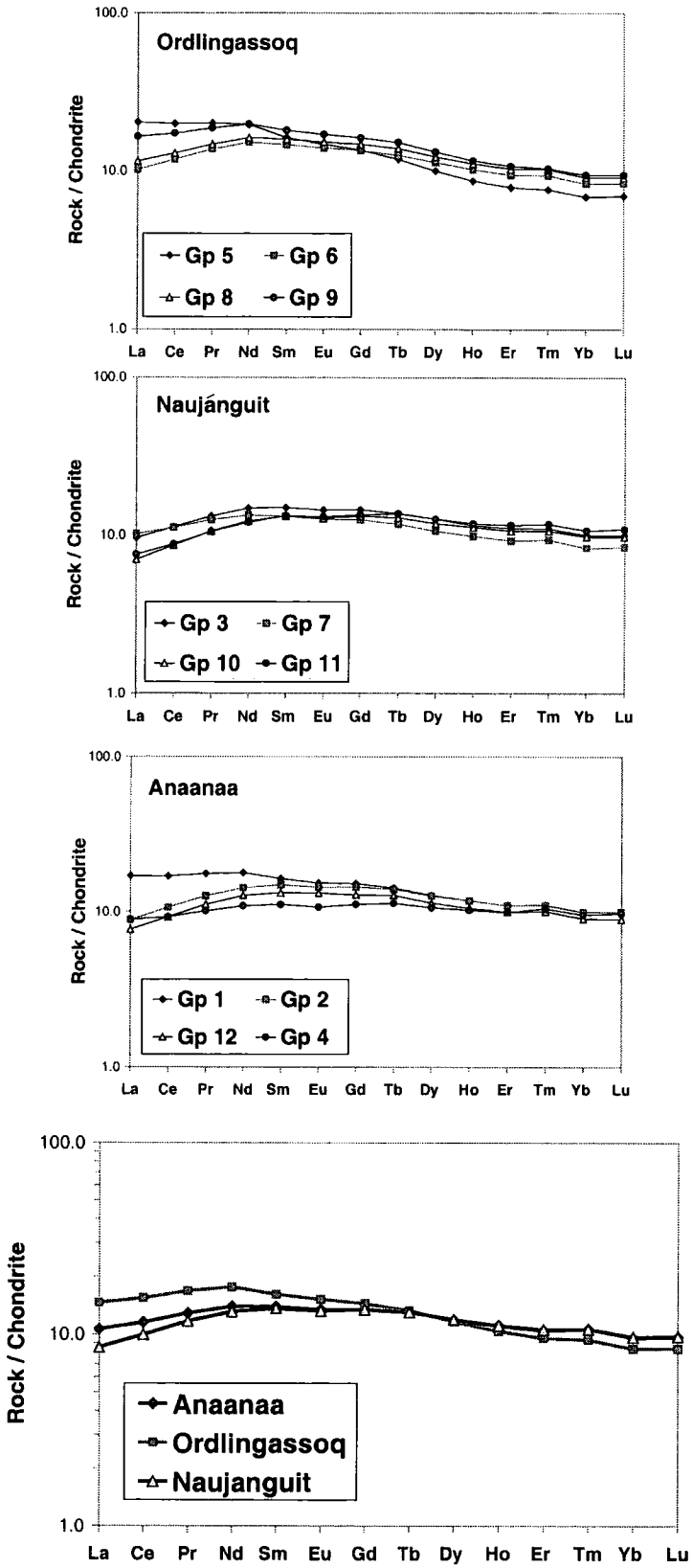

Fig 6.9 REE patterns for samples from each Member and plot of average REEs for each Member (note averages influenced by outliers esp. Gp1 in Anaanaa Member)

		La/Sm	$^{87}Sr / ^{86}Sr$
Ordlingassoq	Gp 5	2.02	0.7035
	Gp 6	1.11	0.7030
	Gp 8	1.16	0.7033
	Gp 9	1.46	0.7034
Naujánguit	Gp 3	1.03	0.7032
	Gp 7	1.24	0.7030
	Gp 10	0.84	0.7029
	Gp 11	0.91	0.7032
Anaanaa	Gp 1	1.67	0.7048
	Gp 2	0.95	0.7032
	Gp 12	0.93	0.7031
	Gp 4	1.28	0.7045

Table 6.2 La/Sm and Sr-isotope values used in Fig 6.11. Sr-isotope data from Larsen (pers. comm.)

The observed LREE/HREE variations can be partially explained in terms of mantle source region and degree of melting. For example, small degrees of partial melting can produce magmas with high LREE/HREE ratios, whereas source depletion can lower LREE/HREE ratios in resultant magmas. Finally, residual mantle phases (e.g. garnet) can preferentially retain HREEs over LREEs. The greater HREE depletion seen in the Ordlingassoq Member (relative to MORB and to the other Members) may be due to retention of the HREEs in garnet as melting in upwelling mantle plumes begins in the garnet-lherzolite zone. If the Naujánguit Member does have a MORB-like mantle component, it may have been generated by higher degrees of melting at shallower depths (within the spinel lherzolite zone). This explains the flatter REE patterns of the Naujánguit Member as HREEs would not have been retained within garnet in its source. LREE/HREE fractionation can also be generated through assimilation of LREE-enriched crustal material. Thus, the extent to which crustal contamination may have affected the geochemistry of the WGPs is discussed (Section 6.4).

6.4. Evaluation of Crustal Contamination Component in West Greenland Picrites

Certain samples (namely Gp1-Anaanaa Member, Gp5 + Gp9-Ordlingassoq Member) have elevated LREE concentrations. For Gp1 and Gp9 this corresponds to enrichment in the highly incompatible LILEs. The source of this anomaly is not certain and whilst enrichment in Cs and Rb may indicate minor crustal contamination, the enrichment in LREEs is relatively small. In order to try to determine whether crustal contamination is responsible for the variation seen, La/Sm vs Rb and La/Sm vs $^{87}Sr/^{86}Sr$ plots have been constructed. This problem is further addressed in Section 6.6 by the use of Re-Os isotopes – where crustally contaminated samples would be expected to show higher $^{187}Os/^{188}Os$. There is no correlation between high La/Sm and high Re concentrations.

Cs and Rb may be mobile during weathering, however, these Greenland samples were particularly selected due to their fresh nature. There is some correlation between both Cs and Rb and LREE enrichment in all Members. The Anaanaa Member shows the most significant correlation between Cs and La/Sm (Fig 6.10). This implies that all Members and particularly the Anaanaa Member may have undergone some crustal contamination. Alternatively, the LREE enriched mantle component (plume?) was also enriched in LILEs.

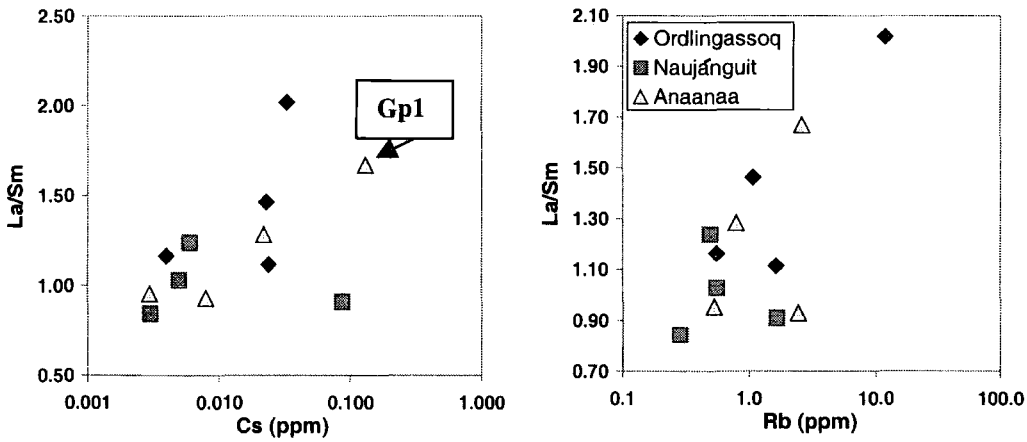

Fig 6.10 La/Sm vs Rb and Cs, as a measure of crustal contamination. N.B. Log scale used for Cs and Rb axes. Data for Cs and Rb well above instrumental detection limits (see Appendix I), therefore data is believed to reflect real differences in sample composition.

The Naujánguit picrites have the least radiogenic and most homogenous Sr-isotope characteristics in conjunction with their homogenous REE signatures. The Ordlingassoq samples have much greater LREE variation. Some of the LREE scatter in Ordlingassoq samples may be due to crustal contamination (i.e. 0.5-1%; Fig 6.11), however, the limited range in Sr-isotope compositions implies that other factors also influence LREE concentrations.

The Anaanaa group has the most heterogeneous Sr-isotope signatures, varying from Naujánguit-like ratios, to much higher $^{87}Sr/^{86}Sr$ ratios. This indicates that the Anaanaa picrites were probably derived from an isotopically similar source region to the Naujánguit picrites, but were later contaminated by crustal material which elevated the $^{87}Sr/^{86}Sr$ ratio. This accords well with the fact that Gp1 (Fig 6.11) has the highest Cs concentrations and $^{87}Sr/^{86}Sr$ ratio. The Sr-isotopes suggest that between 5 and 10% crustal contamination (assuming $^{87}Sr/^{86}Sr$ of crust = 0.71, Sr concentration 300ppm) of a primitive melt (e.g. Gp10; Fig 6.11) is required to generate the most radiogenic Sr-isotope ratios seen in the Anaanaa Member. This is rather more crustal assimilation than is suggested by other trace element data and Os-isotope data however (Pearson *et al.*, 1999).

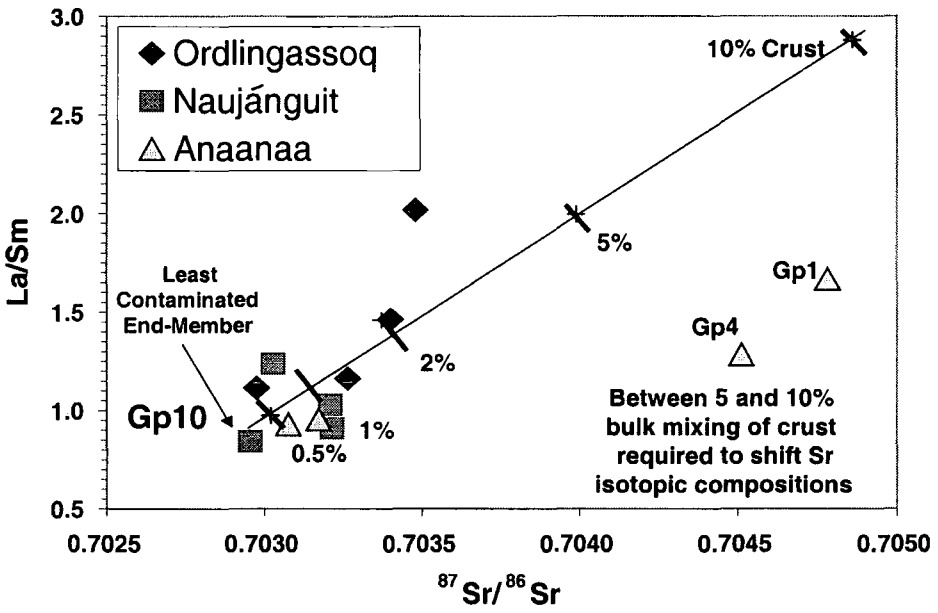

Fig 6.11 La/Sm vs $^{87}Sr/^{86}Sr$, as an index of crustal contamination. Sr-isotope data from Larsen (unpubl.). Symbols as Fig 6.10.

Thus, in light of the combined REE-LILE-Sr-isotope evidence, it is suggested that certain picrites (particularly from the Ordlingassoq and Anaanaa Members) have suffered some crustal contamination. It is uncertain exactly how much contamination has occurred as the compositions of the alleged contaminants are unknown. The low natural concentrations of the incompatible elements in the picrites render them susceptible to elemental and isotopic contamination by continental crust (Holm *et al.*, 1993). Since however, only a few samples are actually enriched in incompatible elements relative to MORB and the picrites have retained their highly unfractionated compositions, it seems that contamination was probably minor. Holm *et al.* (1993) conclude that the picrite melts have undergone negligible crustal contamination, but instead have inherited their trace element characteristics from their source regions, as would be expected for moderate to high degrees of melting. It is proposed that the picrites were able to rise to the surface relatively interrupted and with little lithospheric interaction because of the active rifting that was present when the plume material first arrived (Holm *et al.*, 1993 and Graham *et al.*, 1998 and references therein).

6.5 Petrogenesis of the West Greenland Picrites

Modelling of the major oxides of the WGPs indicates that they were derived by high degrees of melting from a source similar to that of the Icelandic picrites (Graham *et al.*, 1998). High $^{3}He/^{4}He$ ratios in the picrites also confirm a deep (lower mantle or core-mantle boundary?) plume signature within West Greenland, attributed to the presence of the Early Iceland plume (Graham *et al.*, 1998). These features and the high MgO contents of the picrites suggest that they were derived from very hot plume material below the continental lithosphere. The inferred parental magmas had MgO between 14.4 and >19 wt % and SiO_2 near 46 wt %. This indicates an origin by 25% partial melting of mantle at a temperature of 1540-1600°C and an approximate depth of 60-112Km, within the garnet stability field (Holm *et al.*, 1993; Lightfoot *et al.*, 1997; Graham *et al.*, 1998 and references therein).

In addition to the plume source, it appears that some MORB mantle was involved in the origin of the picrites, probably by mantle-head entrainment. MORB influence on geochemical signatures appears to decrease with time and so is less pronounced in the Ordlingassoq than in the Naujánguit picrites. Correspondingly the Anaanaa picrite analysed for He has the highest proportion of a depleted mantle end-member in terms of He, Pb and Nd isotopes (see Graham *et al.*, 1998, Fig 4). The MORB component diminished with time as more plume material rose and displaced it. Thus, the stratigraphically higher picrite (e.g. Ordlingassoq Member) may represent a purer Icelandic plume composition, relatively undiluted by MORB source mantle, or other lithospheric materials (Holm *et al.*, 1993 and Graham *et al.*, 1998 and references therein).

6.6 Re-Os Isotope Systematics of West Greenland Picrites

6.6.1 Introduction

The addition of the Re-Os isotope system to the study of the chemical evolution of the mantle is important because of its unique properties. Re and Os unlike elements used in other isotope-systems, are both siderophile and chalcophile. Os-isotopic studies have proved particularly useful in tracing recycled material input within mantle sources. This is because Os is compatible but Re is mildly incompatible during mantle melting. Thus, mantle partial melts will have high Re-Os ratios and evolve high $^{187}Os/^{188}Os$ ratios with time (Shirey and Walker, 1998). Recycling of oceanic crust and sediments back into the mantle via subduction zones can therfore potentially produce a mantle reservoir with high $^{187}Os/^{188}Os$; a signature which can be recognised in some plume-derived OIBs and CFBs (Walker *et al.*, 1997).

Another reservoir which could potentially contribute a radiogenic Os-isotope signature to plume material, is the outer core. It is believed that the outer-core may have become progressively more enriched in ^{187}Os with time, as the inner core grows and preferentially incorporates Os over Re. Thus, deep-seated plumes that originate at the core mantle boundary may be intrinsically radiogenic if they incorporate an outer-core component (Shirey, 1997). Support for this theory of plume origin is

provided by a limited amount of coupled ^{187}Os and ^{186}Os data in OIB, where the ^{186}Os enrichment is attributed to decay of ^{190}Pt (Brandon *et al.*, 1998). The amount of core-material entrained within respective plumes is envisaged to be relatively small, as the core is enriched in Os by a minimum factor of approximately 300 (Walker *et al.*, 1997) and Re enriched approximately 600 times (Hauri and Hart, 1997) relative to the mantle. On the basis of Re and Os abundances in OIB, Hauri and Hart (1997) suggest an upper limit of ~0.2 wt% addition of core material in plumes to account for observed geochemical signatures.

Further evidence for limited exchange of mass between the mantle and core is provided by Re/Yb ratios. MORB and OIB Re/Yb ratios are very similar. This is inconsistent with the incorporation of significant amounts of metallic core material into mantle plumes and isolation of the upper mantle from the core, as this would greatly increase the Re/Yb ratio of OIB relative to MORB (Hauri and Hart, 1997). OIB typically have lower Re contents than MORB (i.e. mean MORB Re = 0.926 ppb, mean OIB Re = 0.377 ppb) which is the opposite of that expected for an incompatible element whose concentration should be controlled by the extent of partial melting (Righter and Hauri, 1998). Greater retention of Re in sulfides during OIB formation is ruled out, as oxygen fugacity conditions favour enhanced partitioning of Re into sulfide in MORB source, rather than OIB source. Thus, another phase must be responsible for causing the differing Re abundances in MORB and OIB (Righter and Hauri, 1998).

Similarity in the behaviour of Re and Yb during mantle melting in OIB have led to the suggestion that, like Yb, Re is compatible with garnet during mantle melting. Experimental studies (Righter and Hauri, 1998) between garnet and silicate melt at 1250 – 1350°C confirm that Re is compatible in garnet. Thus, it is possible that the presence of garnet in the OIB source reservoir is responsible for the low Re content of OIB. Garnet however, is not a stable phase at the depths of MORB production (i.e. garnet stability field = >60Km). Thus, Re behaves incompatibly during MORB formation and is correspondingly enriched in MORB relative to OIB (Righter and Hauri, 1998). Coupled Re-Yb behaviour in OIB thus argues against significant core-mantle interaction in OIB as incorporation of a significant amount of core material would greatly increase the Re/Yb ratio of OIB.

Mass balance calculations reveal that the mass of Re in the primitive mantle cannot be balanced by the amount of Re in the continental crust and the depleted mantle. This leads to the assumption that there is an unidentified Re-rich reservoir, the most likely candidate being eclogitised, garnet-bearing, subducted oceanic crust in the deep mantle (Righter and Hauri, 1998). The existence of a reservoir with high Re-Os, where Re is a compatible phase, is consistent with the observed low Re, high Os-isotopic compositions of OIB (Righter and Hauri, 1998).

Crustal contamination can also potentially affect the Re-Os ratios and Os-isotopic compositions of a melt, as crust has higher Re/Os than the depleted mantle. This is predominantly due to the very low concentrations of Os in the crust rather than high Re concentrations in the crust. Very large degrees of assimilation are thus required to affect absolute Re and Os concentrations. Magmas with Os concentrations of 0.5-1ppb are considered relatively robust to crustal contamination because of the low crustal Os-content. Therefore, variable Os-isotopic compositions within high-Os lava suites probably reflect source heterogeneity rather than contamination (Walker *et al.*, 1998).

6.6.2 Application of Re-Os System to West Greenland Picrites

The WGPs are ideal for Re-Os studies because of their high Os-contents and limited crustal interaction which limits any contamination that may mask source compositions. In addition, it is hoped that study of Re-Os systematics may provide information which can help constrain the behaviour of the other PGEs in plume-derived magmas.

Re data were obtained via Carius tube-anion exchange chromatography chemistry and analysis by ICP-MS (as outlined in Chapter 5). Os data were obtained on the same sample aliquot. Samples were processed via Carius-tube digestion, followed by HBr-solvent extraction and micro-distillation (carried out by the author). High precision Os-isotopic ratios were then obtained by Graham Pearson and Gordon Irvine (on behalf of the author) using N-TIMS at the Dept. of Terrestrial Magnetism, Carnegie Institution of Washington (for procedure see Pearson *et al.*, 1995).

6.6.3 Comparison of Re and Os abundances in West Greenland Picrites with other Environments

In contrast to full PGE data, there is a relatively large database of Re-Os abundances in a range of different rock-types, resulting from the growing popularity of Re-Os isotope studies. Fig 6.12 places the WGPs into a global picture concerning their relative Re-Os abundances. A comparison of Re-Os concentrations within similar picritic and komatiitic rocks is also presented (Fig 6.13).

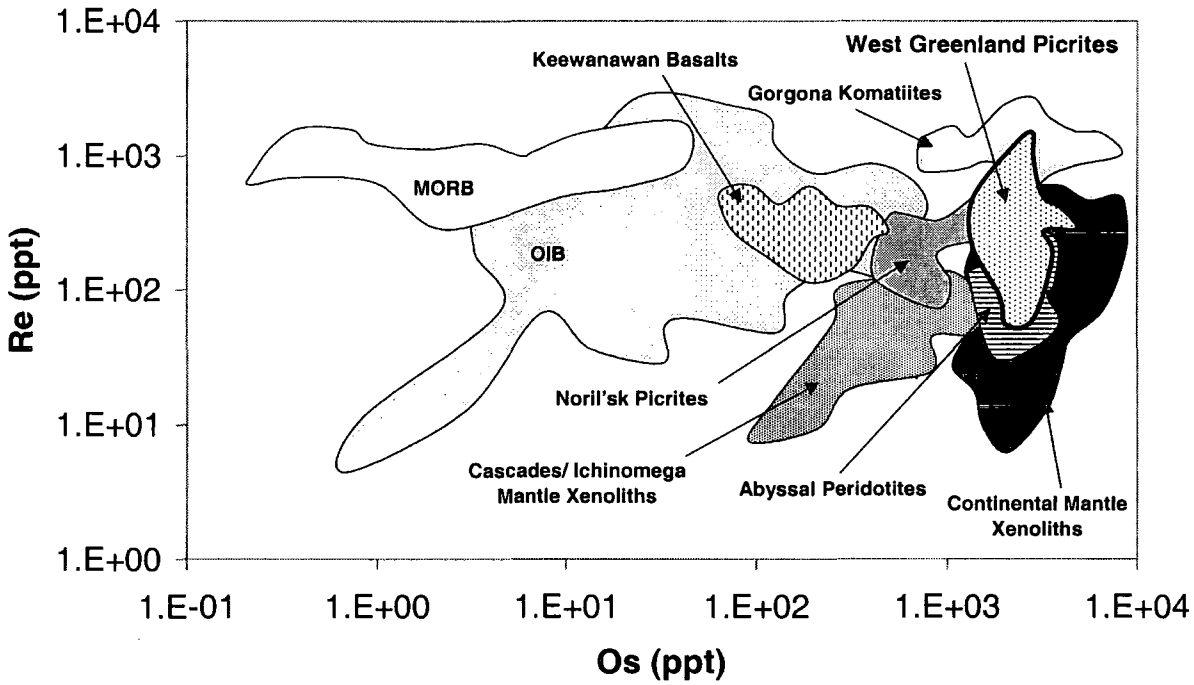

Fig 6.12 Re–Os abundances of West Greenland picrites compared to other major rock types (data from Brügmann *et al.*, 1987; Shirey, 1997; Brandon *et al.*, 1996)

The WGPs have much higher Os contents than MORB, OIB and the Keewanawan continental flood basalts (CFBs). This may be because the trace phase hosts for Os within the mantle did not participate in melting within MORB, OIB and CFB since they are not presumed to be generated at >25% melting as are the WGPs (Holm *et al.*, 1983; Wilson, 1989). Alternatively, Os-rich sulfides and/or alloys may have fractionated from the melts prior to eruption removing Os from the melt. The first suggestion most probably applies to MORB, whereas the second suggestion is more applicable to OIB and CFB.

There is a considerable amount of overlap in Os-abundance between the WGPs and the other high MgO lavas: the Gorgona komatiites and Noril'sk picrites (Fig 6.12). This suggests similarity both in the mantle source Os concentrations and degree of melting in these high MgO rocks. Slightly lower Os abundances in the Noril'sk picrites may well be due to increased fractionation in these rocks. Interestingly there is also overlap between the WGPs and the residual products of mantle melting namely, abyssal peridotites (i.e. Depleted MORB Mantle) and continental xenoliths.

MORB has higher overall abundance of Re than most other rock-types including the WGPs. This might indicate the presence of garnet in the source regions of the OIB, CFB and WGPs. Coupled evidence of HREE depletion however, is necessary to prove or disprove this theory. Komatiites have high MORB-like Re concentrations, despite the fact that like OIB, they are probably plume derived. Thus, it is suggested that if komatiites are derived from a similar garnet-bearing source to OIB, then they are produced at sufficiently high degrees of melting to remove garnet and thus release any contained Re.

Residual mantle rocks (i.e. abyssal peridotites and supra-subduction mantle wedge- represented by Ichinomegata and Cascades mantle xenoliths) contain less Re than the WGPs (Fig 6.12). This is to be expected as Re is mildly incompatible during mantle melting. By contrast, the sub-continental mantle xenolith Re abundances are highly variable and overlap the range of WGP Re concentrations. The variability in Re abundances may be due to heterogeneous metasomatism of the sub-continental lithosphere (Pearson *et al.,* 1995). In general, melt-depleted lithospheric mantle constitutes an important reservoir of low Re/Os material (Shirey and Walker, 1998). These differences in Re-Os compatibility ensure that Re/Os isotope ratios of rocks generated in different tectonic environments are quite distinct (Table 6.3). Thus, the modern mantle is quite heterogeneous, containing both supra- and sub-chondritic Os-isotopic reservoirs (e.g. OIB > chondrite ≡ upper mantle > MORB Source; Walker *et al.,* 1997).

	Re (ng/g)	Os (ng/g)	Re/Os
CI - chondrite	39.5	492	0.08
Fertile Mantle	0.25-0.30	2.8-3.4	0.40
Depleted Mantle	0.05-0.14	0.8-9	0.06-1
Komatiite	0.5-1.5	0.5-6	1-6
OIB	0.1-1	0.01-0.5	20-3,000
MORB	0.5-2	0.001-0.05	100-5,000
Av. Continental Crust	<1	<0.05	~50
Black Shale	517	2.46	18,780
West Greenland Picrites (WGP)	0.06-0.47	1.50-3.88	0.03-0.45
East Greenland Picrites	0.06-0.48	1.25-2.79	0.02-0.39

Table 6.3 Typical Re and Os abundances and Re/Os ratios (from Shirey and Walker, 1998 and references therein, except CI-chondrite, Jochum, 1996, West Greenland picrites – this project, and East Greenland picrites, Brooks *et al.*, 1999).

The Re/Os ratios for the WGPs overlap the range of the East Greenland picrites which provides good evidence of their derivation from the same mantle source region (Table 6.3). The only other Re/Os ratios that are comparable to the WGPs are those of the fertile mantle and chondrites, which is again a good indication of their primitive nature and derivation from a fertile source. The higher Re/Os ratio of OIB compared to the WGPs indicates that OIB are either produced by lower degrees of partial melting, or have undergone more fractionation than the WGPs.

There is a surprisingly large range of Re-Os concentrations within picritic rocks (Fig 6.13). Compared to many of the other picrites, the WGPs have a relatively restricted composition. Most of the other high MgO rocks show a high degree of variability in Os-content for relatively restricted Re variation. It is probable that much of this variation in Os-content may be due to varying amounts of fractionation of such phases as olivine and chromite since the West Greenland picrites which show some of the highest Os-contents, are known to have undergone some olivine fractionation (Holm *et al.*, 1993). In order to test this theory, MgO contents (as an index of differentiation) for the respective picrites (where data are available) are shown plotted against their Os-contents to see if there is any correlation (Fig 6.14).

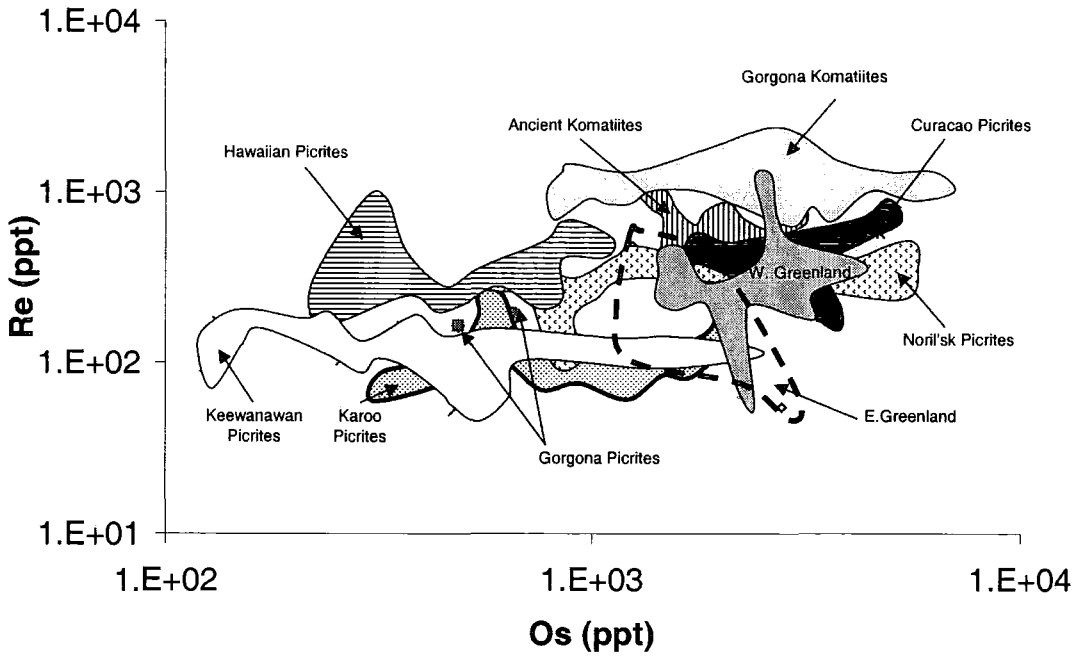

Fig 6.13 Re-Os abundances for a range of high MgO (picritic and komatiitic) rock types (data from Brügmann *et al.*, 1987, Brooks *et al.*, 1999, Walker *et al.*, 1998, Martin *et al.*, 1994)

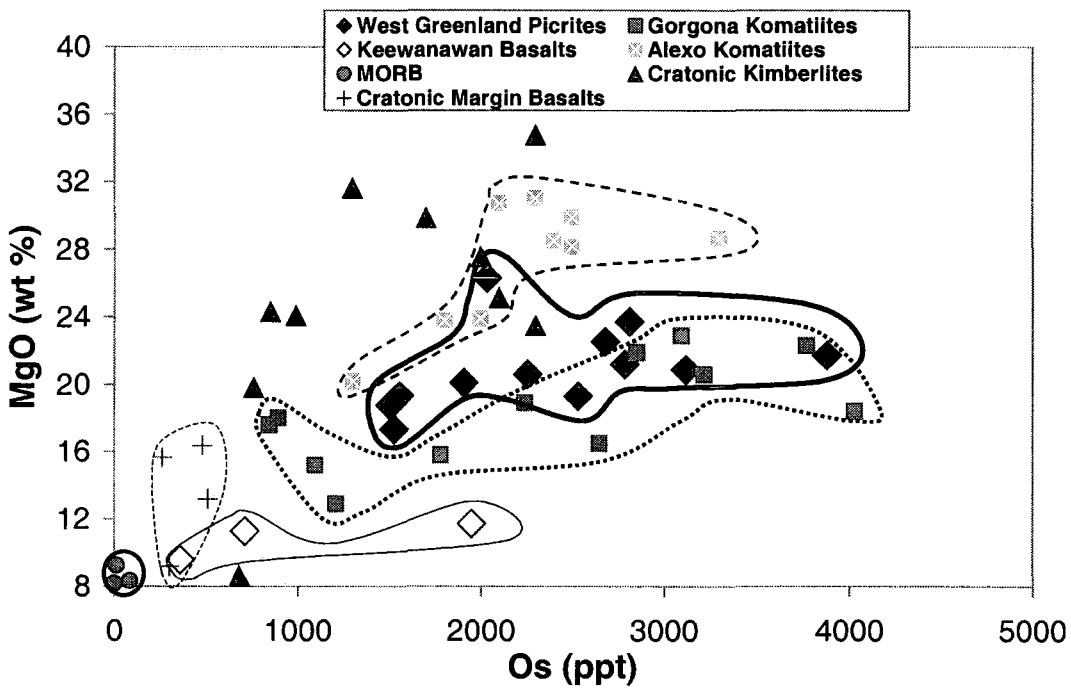

Fig 6.14 MgO contents vs Os contents for kimberlites and a range of picritic rock types (data from McDonald *et al.*, 1995; Brügmann *et al.*, 1987; Shirey, 1997)

In general, the basalts and MORB (shown for completeness) have low MgO and Os due to differentiation. For the high MgO rocks there seems to be significant similarity between the Os contents for a wider range of MgO contents. Higher MgO (and hence more primitive/less differentiated) rocks such as the Alexo komatiites do not necessarily have higher Os contents (Fig 6.14). This indicates that increasing melt fraction does not result in a corresponding increase in Os. Thus, Os-bearing phases within the mantle (alloys?) must be extremely refractory during even high degree partial melting.

The similarity between the komatiites and WGPs is compelling evidence that the West Greenland source underwent a high degree of partial melting. In addition, fractionation within the WGPs must have been minimal and does not appear to have greatly affected the Os-budget of the whole rock. As some olivine is known to have crystallised from the WGPs (Holm *et al.*, 1993) this may suggest that some of the estimated $D^{Os}_{olivine\text{-}melt}$ values (e.g. 1.8; Brügmann *et al.*, 1987) may be too high in relation to this particular environment and conditions. Further, it may lend support to the hypothesis that Os is co-precipitated with olivine, rather than being compatible in it.

6.6.4 Re-Yb Signatures of the West Greenland Picrites

Re and Yb behave similarly during mantle melting and are both presumed to be compatible with garnet (Righter and Hauri, 1998). Thus, plots of Re versus Yb can help evaluate the mineralogy of magma source regions (Fig 6.15). There are no significant differences in Re-Yb systematics between the three Members of the Vaigat formation (except for one outlier from the Ordlingassoq Member and one outlier from the Anaanaa Member). This may suggest that there were no great differences in the compositions of the sources of the different Members. Most of the WGPs plot within the field defined by OIB on the Re-Yb plot and are displaced towards lower Re and Yb than MORB.

The similarity in Re-Yb characteristics between OIB and the WGPs is unsurprising since they are all derived from a mantle plume source. Many picrites and OIB have lower Re and Yb contents than MORB. As noted earlier, this is consistent with the theory that OIB are derived from regions in which garnet is a

stable phase, whereas MORB are not. The Re contents of MORB however, are consistent with the presence of small amounts of sulfide liquid in the residual mantle during melting (Righter and Hauri, 1998). The positive trends shown by komatiites and the ferro-picrites suggest derivation from a source that contained neither residual sulfide nor garnet as a result of high degrees of melting (Righter and Hauri, 1998). The OIB Re-Yb characteristics (Fig 6.15) have been modelled by Righter and Hauri (1998) using equilibrium melting of mantle with residual sulfide (0.088%) and garnet (0-14%).

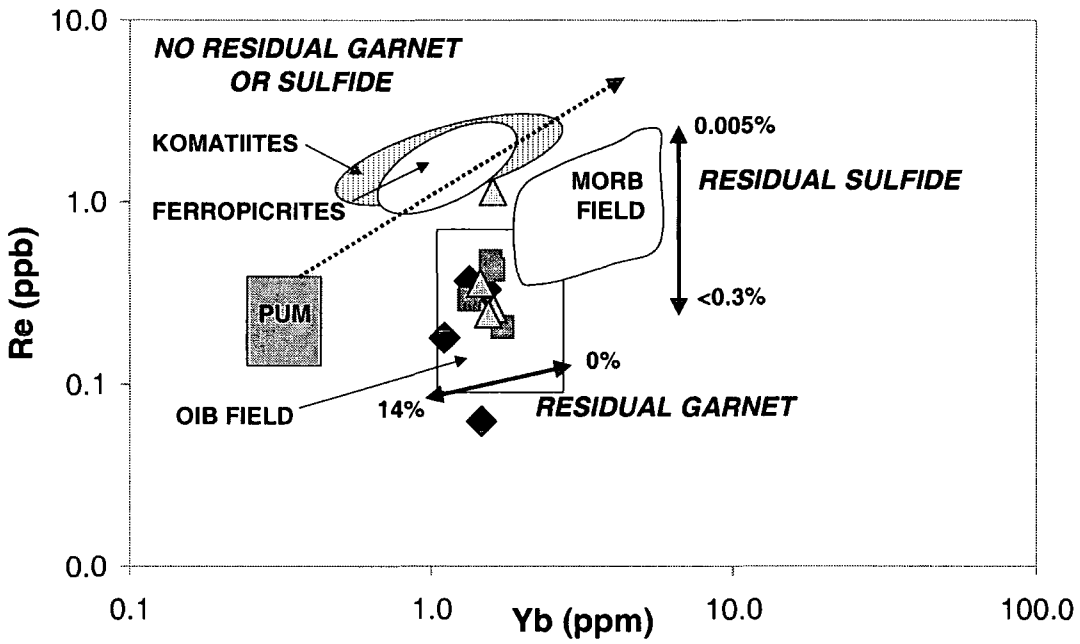

Fig 6.15 Re vs Yb diagram for West Greenland picrites. Vectors to illustrate the effects on Re & Yb concentrations in rocks generated by melting of a source containing variable amounts of garnet or sulfide are illustrated. Dotted line represents expected trend for equilibrium melting of peridotite (Fields and % residual sulfide/garnet lines from Righter and Hauri, 1998; WGP symbols as in other plots).

The comparable behaviour of OIB and the WGPs suggests that they do indeed have a common phase in their source region in which Re and Yb are both compatible. Whether this phase is garnet or sulfide, will be discussed later in context of the HREE, PGE and chalcophile element signatures of the WGPs.

6.6.5 Os-Isotope Systematics

The percentage difference between the Os isotopic composition of a sample and the average chondritic composition for a specified time is represented by gamma (γ) Os:

$$\gamma_{Os\,(t)} = \{[(^{187}Os / {}^{188}Os_{\,sample\,(t)}) / (^{187}Os / {}^{188}Os_{\,chon\,(t)})] - 1\} \times 100.$$

For the purpose of calculation of the γ_{Os} values for the WGPs, the eruption age (t) was assumed to be 60.5Ma (Holm *et al.*, 1993). Values of $^{187}Os/^{188}Os_{\,sample}$ were measured by N-TIMS and $^{187}Os/^{188}Os_{chondrite}$ was taken to be 0.12751 (Shirey and Walker, 1998). Samples with positive γ_{Os} are often described as radiogenic or enriched and imply derivation from a source with long-term elevated $^{187}Re/^{188}Os$. Samples with negative γ_{Os} are often described as depleted or unradiogenic and imply derivation from a source with long term low $^{187}Re/^{188}Os$ (Shirey and Walker, 1998). A plot of γ_{Os} for the West Greenland Picrites compared to other major rock-types is shown in Fig 6.16.

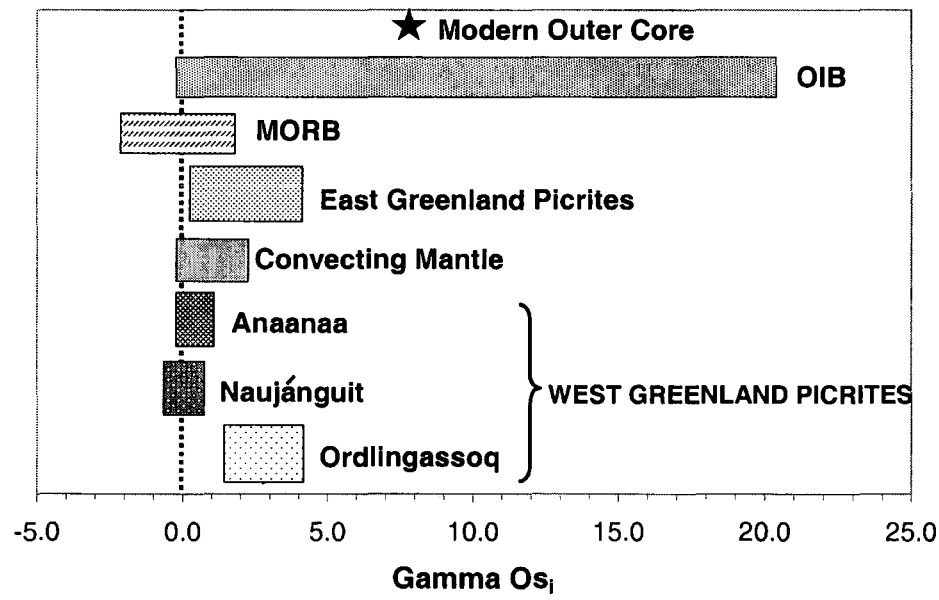

Fig 6.16 Comparison of γ_{Os} values in West Greenland picrites with γ_{Os} from other major rock types (Data Sources for γ_{Os} Values = Brooks *et al.*, 1999 (East Greenland picrites); Shirey and Walker, 1998 (MORB, OIB, mantle, outer-core).

Within the West Greenland Vaigat Formation the different Members show slightly different γ_{Os} signatures. There is considerable overlap between the Naujánguit and Anaanaa Members, whereas the Ordlingassoq Member is displaced to higher, positive values of γ_{Os} (Table 6.4). The Anaanaa and Naujánguit Members fall entirely within the γ_{Os} range defined by MORB and partially within the range defined by OIB. The Ordlingassoq Member picrites conversely fall entirely within the range of γ_{Os} values defined by OIB, but only partially within the field defined by MORB. This may suggest that the Ordlingassoq picrites have a more prominent "OIB" or plume component than the other Members, which show stronger MORB-signatures. This is consistent with the Anaanaa and Naujánguit Members being formed at the onset of plume activity, whereas the Ordlingassoq Member was formed later when plume activity was more established (Graham *et al.*, 1998).

		Re/Os	**$^{187}Re/^{188}Os$**	**$^{187}Os/^{188}Os$**	**γ_{Os}**
Ordlingassoq	G.P. 5	0.088	0.4271	0.1312	2.78
	G.P.6	0.137	0.6592	0.1306	2.13
	G.P.8	0.028	0.1337	0.1296	1.72
	G.P.9	0.216	1.0423	0.1332	3.88
Naujánguit	G.P.3	0.274	1.3177	0.1284	-0.14
	G.P.10	0.169	0.8154	0.1277	-0.27
	G.P.11	0.066	0.3176	0.1273	-0.23
	G.P. 7	0.103	0.4975	0.1281	0.32
Anaanaa	G.P.1	0.136	0.6549	0.1281	0.18
	G.P.2	0.449	2.164	0.1302	0.66
	G.P.4	0.161	0.7771	0.1282	0.8
	G.P.12	0.093	0.4457	0.1277	-0.02

Table 6.4 Re-Os isotopic data for West Greenland picrites

There is a great similarity between the γ_{Os} values of the West and East Greenland picrites (Brooks *et al.*, 1999). Almost identical maxima are reached by the

East Greenland picrites and the Ordlingassoq Member; with the Anaanaa and Naujánguit Members plotting to slightly less radiogenic compositions. This lends support to a common source for the plume, which created both the West and East Greenland picrites.

The more radiogenic nature of the Ordlingassoq picrites compared to MORB and the convecting mantle indicates the presence of a high Re/Os source component within the West Greenland source. This appears common to all OIB sources and is presumed to be either recycled oceanic crust or, a component derived from the outer core (Shirey and Walker, 1998). The γ_{Os} of the outer core is predicted by using experimental Re-Os Kds and assuming ~6% core crystallisation over 4.5Ga (Shirey and Walker, 1998). The typical γ_{Os} value of the modern outer core (Fig 6.16) is considerably more radiogenic than either the West or East Greenland picrites. Thus, if there was any contribution of ^{187}Os-enriched material from the core-mantle boundary to the source of the ancestral Iceland plume, it must have been relatively minor. The low overall concentrations of Re observed within the WGPs concurs with this last statement as the outer core is presumed to have been enriched in Re during cooling of the inner core. Thus, any significant core-mantle boundary contribution might be expected to raise Re abundances in the resultant plume.

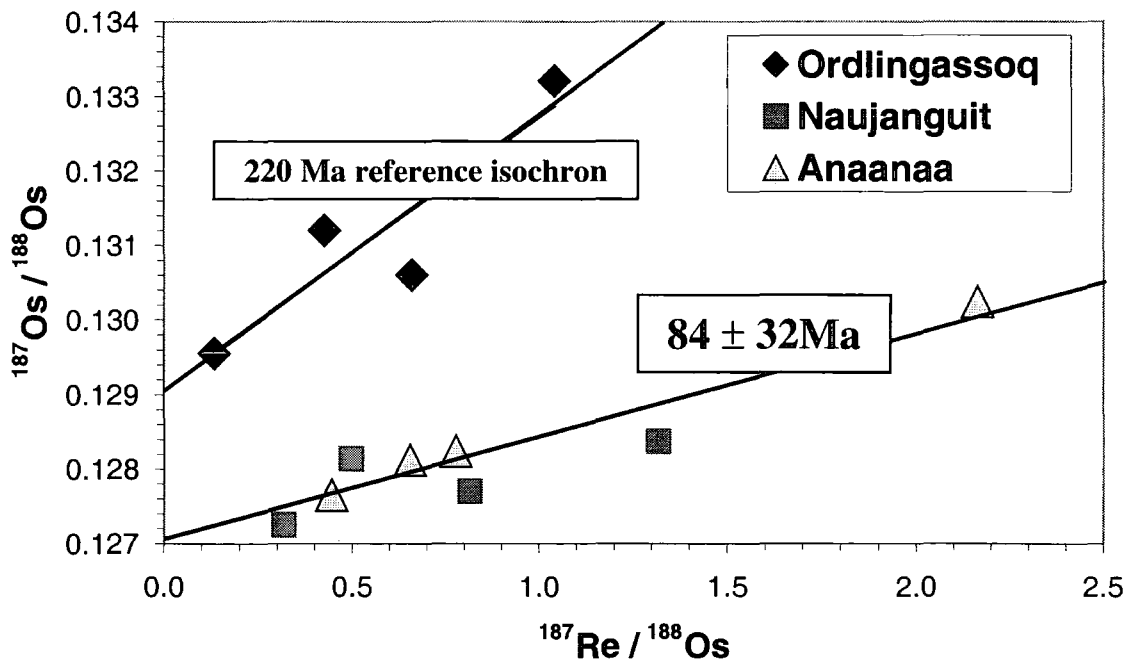

Fig 6.17 Re-Os isochron diagram for West Greenland picrites

Re-Os isochron plots for the WGPs define two separate correlations (Fig 6.17). The shallower of the two is within error of the 60Ma eruption age of the picrites (84±32Ma; Pearson *et al.*,1999). The Ordlingassoq Member plots on a separate isochron with a steeper slope as it has higher values of $^{187}Os/^{188}Os$ than the other Members. From the intercept of the isochrons with the Y-axis, initial $^{187}Os/^{188}Os$ ratios of the WGPs are estimated at between 0.1271 (Anaanaa and Naujánguit Members) and 0.1291 (Ordlingassoq Member).

These initial $^{187}Os/^{188}Os$ ratios of the WGPs fall precisely within the range of the convecting upper mantle (0.127-0.129: as defined by fertile peridotite xenoliths and MORB, Shirey and Walker, 1998). Additionally a $^{187}Os/^{188}Os$ of 0.127 corresponds with the average modern $^{187}Os/^{188}Os$ of chondritic meteorites (Shirey and Walker, 1998). This may suggest that the Anaanaa and Naujánguit Member source regions have evolved identically to chondrites over time and have been in a closed-system. The higher $^{187}Os/^{188}Os_i$ ratios (i.e. enhanced radiogenic component) of the Ordlingassoq Member may imply that it was derived from a separate source, with higher time integrated Re/Os. Alternatively the Ordlingassoq Member could be derived from a similar source to the other Members, but one which has incorporated either more outer core material or recycled oceanic crust. The high Os-contents of the picrites make them relatively impervious to crustal contamination and over 10% crust would be needed to generate the radiogenic Os-compositions observed (Pearson *et al.*, 1999).

Roy-Barman and Allègre (1995) have noted that a general lack of correlation is observed between Re concentration and Os-isotope ratios in both MORB and OIB. Comparable plots for the WGPs (Fig 6.18) illustrate that there is a corresponding lack of correlation in the Anaanaa and Naujánguit Member picrites and a weak positive correlation in the Ordlingassoq picrites. Weak positive correlations between Re and Os-isotopes might be expected if $^{187}Os/^{188}Os$ concentration reflects the time-integrated Re concentration of the source (i.e. by decay of Re in oceanic crust, or in the outer core). The general absence of positive correlation in the Naujánguit and Anaanaa Members indicates, however, that the Re concentration of lavas does not mainly reflect the composition of the mantle source but is more strongly controlled by magmatic processes. Further evidence of this is provided by Re-Os concentration

diagrams (e.g. Fig 6.12 & 6.13), where lavas are distributed according to their petrological types.

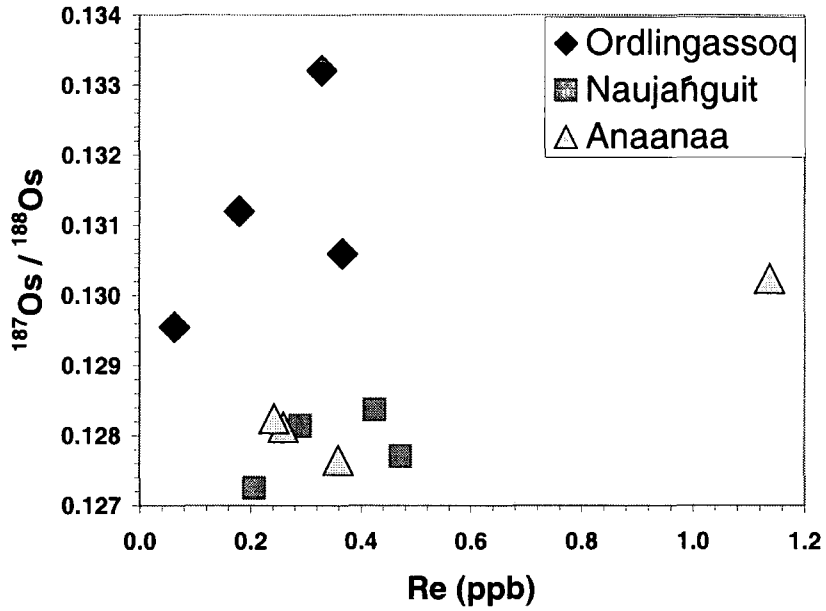

Fig 6.18 $^{187}Os/^{188}Os$ vs Re concentration for West Greenland picrites

In Section 6.2 it was noted that Os-isotopic signatures vs Cs (or Rb) might be a good indicator of possible crustal contamination in the WGPs as certain samples (e.g. Gp1 and Gp4 of the Anaanaa Member) indicate a degree of contamination. A plot of $^{187}Os/^{188}Os$ against Cs, however, does not provide any conclusive evidence (Fig 6.19). There is a slight trend of increasing Cs with increasing $^{187}Os/^{188}Os$ for the Ordlingassoq Member, but samples from the Anaanaa and Naujánguit Members show no correlation between high Cs and high $^{187}Os/^{188}Os$. In fact, Gp1 which has the highest $^{87}Sr/^{86}Sr$ composition, has one of the lowest $^{187}Os/^{188}Os$ ratios. Thus, if the high Sr-isotopes ratios are produced by crustal contamination, the Os-isotope ratios do not appear to be as sensitive to small degrees of assimilation and thus do not identify a crustal component. This is further evidence that variation in Os-isotope systematics of the WGPs is source-controlled, rather than influenced by later magmatic and AFC processes. The enriched Sr and LILE signatures in the WGPs may reflect interaction with enriched lithospheric mantle (L. Larsen pers. comm., 1999).

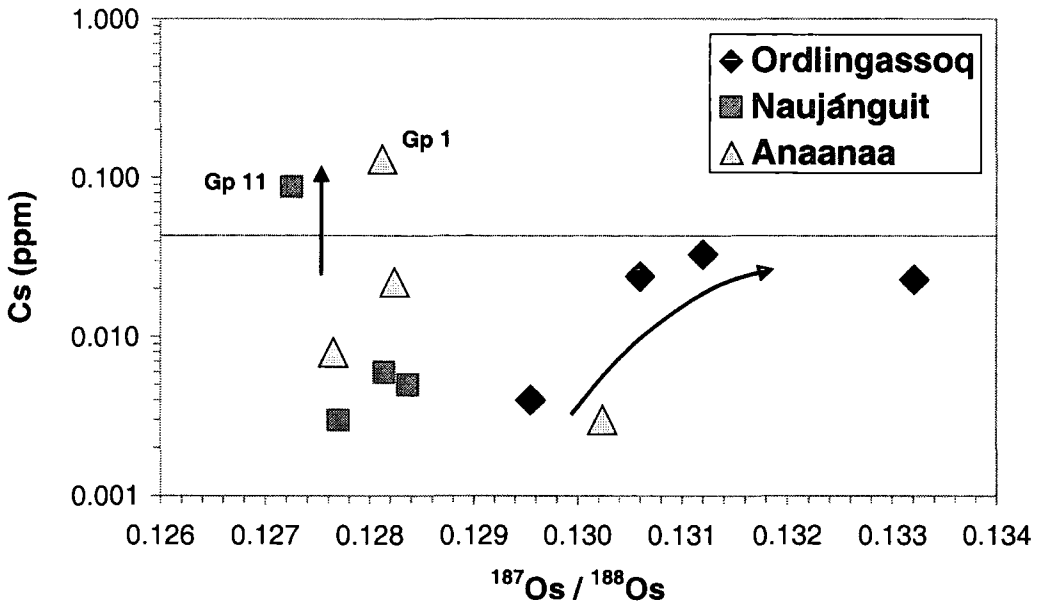

Fig 6.19 $^{187}Os/^{188}Os$ vs Cs as an index of crustal assimilation – (Rb shows similar, but less well defined characteristics)

Initial conclusions that can be drawn from the Re-Os data are:

1) The Re-Os isotopic compositions of the picrites are quite homogenous, with subtle differences between the different Members.

2) The near-chondritic Os-isotope abundances and low initial γ_{Os} values of the Naujánguit and Anaanaa Members, imply that minimal interaction has taken place with either recycled crust, or with the outer core.

3) The Ordlingassoq Member is systematically more enriched in $^{187}Os/^{188}Os$ than the Naujánguit and Anaanaa Members and may have interacted most with an ancient Re-enriched source with elevated $^{187}Os/^{188}Os$.

4) Very little interaction is thought to have taken place between the SCLM and the picrites as the low γ_{Os} values of the SCLM below Greenland (-13 to –20; Brooks *et al.*, 1999) would have reduced the γ_{Os} values of the picrites if significant assimilation had occurred. Some of the radiogenic $^{87}Sr/^{86}Sr$ signature could be inherited from such a source however.

5) Study of the Re-Os isotopes alone, indicate minor interaction of the WGPs with a ^{187}Os-enriched component in their source region, but they are not conclusive.

6) In order to investigate whether other processes such as magmatic-segregation of sulfides have affected relative Re-Os abundances, it is considered necessary to investigate the full PGE-signatures of the WGPs.

7) The high ^{3}He/^{4}He ratios (Graham *et al.*, 1998) of the WGPs are highly suggestive of a lower mantle/core-mantle boundary signature. Studies of ^{186}Os isotopes (from Pt decay in the outer core) however, are necessary to confirm a core source for the radiogenic ^{187}Os/^{188}Os signatures. Such work is currently under way (Pearson *et al.*, 1999).

6.7 PGE Analysis of West Greenland Picrites

6.7.1 Reproducibility of Data

All samples were processed via the Carius-tube, anion exchange procedure outlined in Chapter 5. 1g samples were digested and reproducibility of the data was monitored by analysing 3 of the 12 samples in duplicate. PGE abundance plots for the replicates with typical error bars (2 σ) are shown below, along with a tabulation of the reproducibilities (2 x Stdev as a % of the average of the replicates).

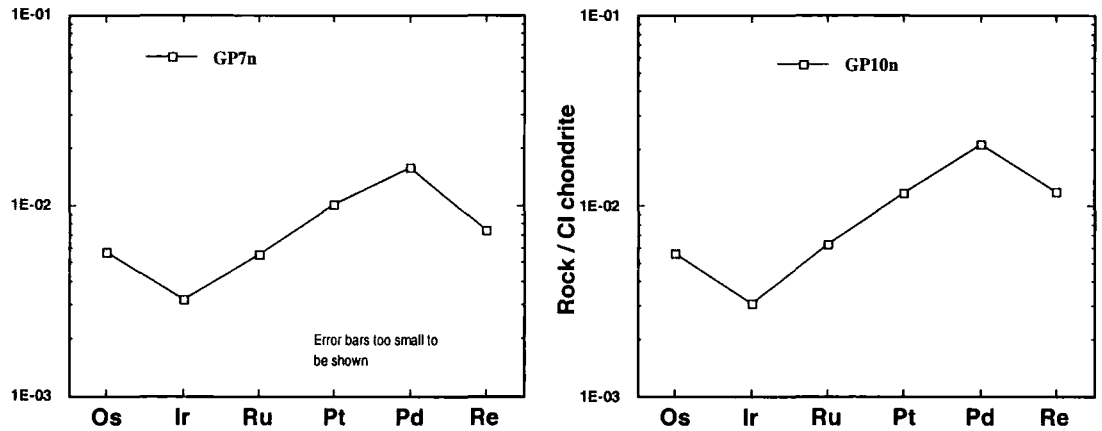

Fig 6.20 Errors on replicate analyses of two West Greenland picrites – Error bars smaller than size of symbol

The reproducibility achieved for the WGPs is significantly better than the reproducibility obtained for most elements in standard rock replicate analyses (Table 6.5). This suggests either that these sample powders have been better homogenised than the standards, that the PGEs are less affected by the nugget effect within these picrites, or that the PGE host phases are more susceptible to complete dissolution within the picrites. Whatever the reason, confidence may be placed in the high quality of the data for all PGEs within this dataset and thus in inferences regarding their relative abundances.

	Re	Os	Ir	Ru	Pt	Pd
G.P.5a	0.18	2.03	1.08	3.14	6.27	4.20
G.P.5b	0.18		1.11	2.95	6.01	4.48
ERROR (2σ%)	**0.79**		**3.66**	**8.74**	**5.98**	**8.97**
G.P.7a	0.30	2.90	1.58	3.91	9.95	8.57
G.P.7b	0.29	2.72	1.49	3.66	9.91	8.74
ERROR (2σ%)	**4.09**	**9.20**	**8.20**	**9.30**	**0.62**	**2.82**
G.P.10a	0.48	2.78	1.48	4.26	11.42	11.58
G.P.10b	0.46	2.79	1.46	4.28	11.44	11.50
ERROR (2σ%)	**6.18**	**0.81**	**2.05**	**0.81**	**0.18**	**0.99**

Table 6.5 Reproducibility on duplicate analyses of West Greenland picrites- concentrations in ppb

6.7.2 PGE Concentrations

The PGE concentrations measured in all the Greenland samples and the stratigraphic Unit to which they belong, are tabulated (Table 6.6). Initial examination of this dataset suggests the following:

1) There is no great variation in PGE concentrations between the different stratigraphic units.

2) The Picrites of the Naujánguit Member tend to have slightly higher PGE concentrations than the other units, particularly for Pd.

3) One picrite from the Anaanaa Member (G.P.2) has anomalously high Re concentrations, whilst one picrite of the Ordlingassoq Membr (G.P.8) has anomalously low Re. This variability may be due to the greater mobility of Re during alteration compared to the other PGEs.

4) PGE concentrations are least variable and generally of lowest abundance within the Ordlingassoq Member.

	Sample	Re	Os	Ir	Ru	Pt	Pd
Ordlingassoq	G.P. 5	0.18	2.03	1.09	3.05	6.14	4.34
	G.P.6	0.37	2.68	1.36	3.20	9.41	6.69
	G.P.8	0.06	2.26	1.19	3.31	9.54	6.66
	G.P.9	0.33	1.52	0.81	2.55	8.76	7.14
	Average	0.24	2.12	1.12	3.03	8.46	6.21
	stdev	0.14	0.48	0.23	0.33	1.58	1.26
Naujánguit	G.P.3	0.43	1.55	0.93	3.00	9.59	10.95
	G.P.10	0.47	2.79	1.47	4.27	11.43	11.54
	G.P.11	0.21	3.12	1.64	4.41	13.00	10.90
	G.P. 7	0.29	2.81	1.53	3.79	9.93	8.66
	Average	0.35	2.57	1.39	3.87	10.99	10.51
	stdev	0.12	0.69	0.32	0.64	1.56	1.27
Anaanaa	G.P.1	0.26	1.91	0.94	2.63	7.48	6.97
	G.P.2	1.14	2.53	1.33	3.26	10.69	10.30
	G.P.4	0.24	1.50	0.80	2.99	9.53	8.74
	G.P.12	0.36	3.88	1.94	3.61	11.16	9.35
	Average	0.50	2.46	1.25	3.12	9.71	8.84
	stdev	0.43	1.04	0.51	0.41	1.64	1.40

Table 6.6 PGE concentrations (ppb) for West Greenland picrites

These conclusions are further illustrated by chondrite-normalised plots for each of the above members (for normalising values see Page 288). The main points to draw from these patterns are that they are lower in overall abundance than chondrite, but relatively flat due to their primitive nature. The slopes are due to apparent Ir depletion (compared to Os) and a slight enrichment in the PPGEs, as would be expected for a partial melt. The shapes of the PGE patterns are remarkably similar for all of the Members of the Vaigat Formation with Re showing the most variation. The Ordlingassoq Member tends to show slightly flatter patterns than the other members, which ties in well with the observations from major element data that this member has the purest plume-signature.

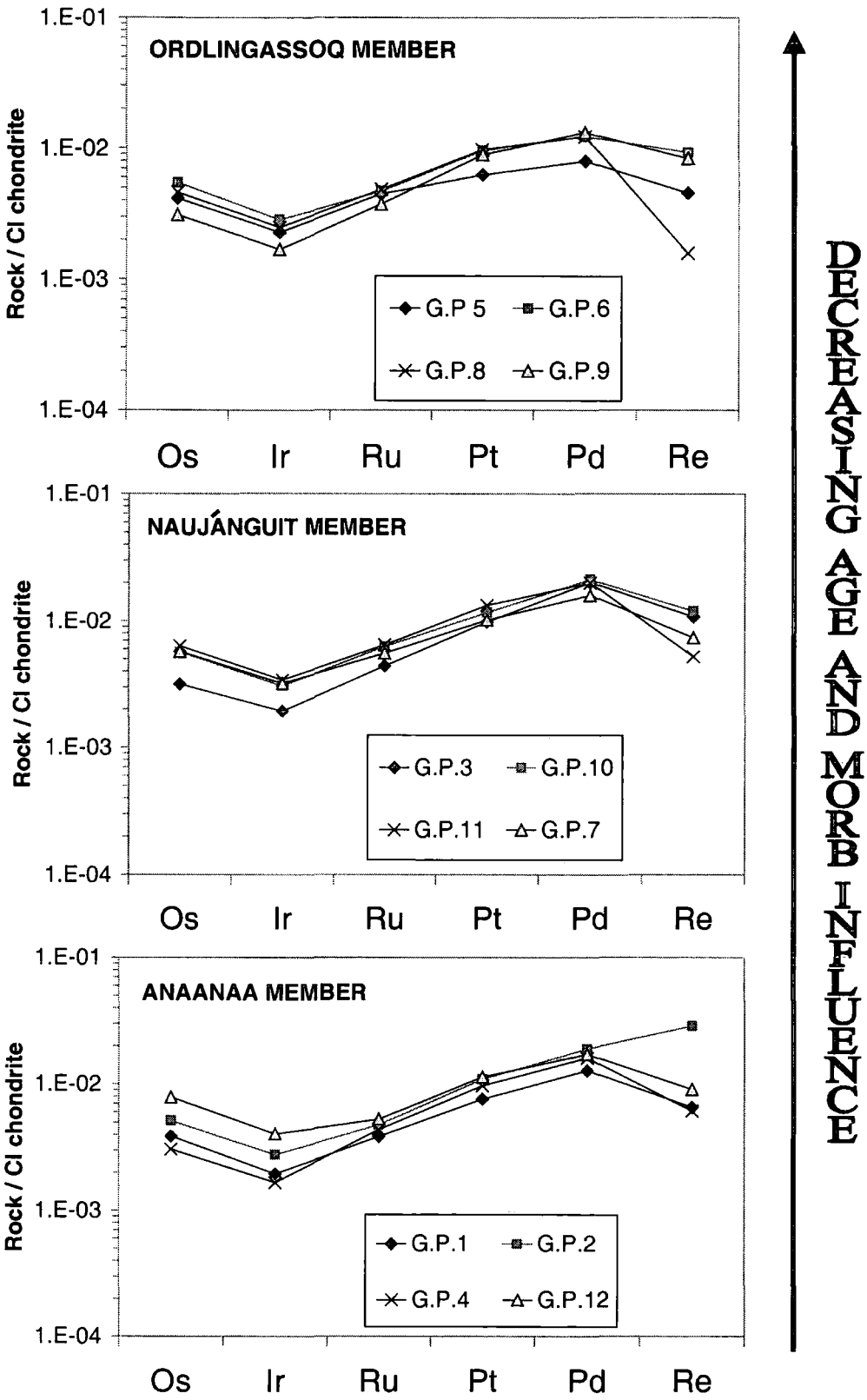

Fig 6.21 Chondrite-normalised PGE patterns for each of the Members of the Vaigat Formation

6.7.3 Comparison of West Greenland Picrite Inter-PGE Ratios with Magmas from Other Tectonic Environments

As there are a lack of complete PGE datasets for magmas from different tectonic environments, it is often useful to compare PGE ratios rather than PGE patterns. Some of the most commonly used PGE inter-element ratios are shown in Table 6.7.

Sample	Os/Ir	Ru/Ir	Pt/Ir	Pd/Ir	Pt/Pd
Ordlingassoq (average)	1.90 ± 0.05	2.76 ± 0.33	7.83± 2.21	5.82 ± 2.1	1.37 ± 0.1
Naujánguit (average)	1.83 ± 0.11	2.83 ± 0.33	8.14 ± 1.62	8.0 ± 2.71	1.05 ± 0.15
Anaanaa (average)	1.96 ± 0.07	2.72 ± 0.79	8.44 ± 2.57	7.75 ± 2.51	1.10 ± 0.07
MORB	~0.37 - 0.87	0.11	25.24	~ 56 - 100	0.45
Cont. Thol.		2.6	65.4	97	0.67
Indian Ocean OIB		0.6 - 3.82	17.7-100	25.4 - 351	0.26 – 1.4
Alkali OIB	0.78		8.39	4.83	1.74
Tholeiitic OIB		3.85	97.5	101.06	1.25
Kimberlites (on-craton GpI)	1.29	2.49	4.07	2.88	1.41
Kimberlites (off-craton)	0.79	1.85	16.3	10.2	1.60
Komatiites	0.79	2.5	7.5	5.04	1.48
Abyssal Peridotites	1.04	2.04	3.3	1.86	1.84
Upper Mantle	1.01	1.48	2.06	1.16	1.5

Table 6.7 Summary of mean inter PGE ratios and comparison with other mantle-derived rocks. Data sources McDonald *et al.*, 1995 and References therein + Ravizza and Pyle, 1997 (additional MORB & alkali basalt data), Fryer and Greenough, 1992 (Indian Ocean OIB data) and Snow and Schmidt, 1998 (abyssal peridotite data).

IPGE ratios within the WGPs are very similar, perhaps indicating that their mantle source is homogeneous with regard to IPGE distribution. A plot of Os vs Ir for the picrites illustrates the constancy of the Os/Ir ratio and the strong positive correlation between their abundances (a best fit linear regression line plotted through this data has an R^2 value of 0.98). When compared to other mantle-derived rocks, the WGPs most closely resemble other high MgO lavas (e.g. komatiites) except in their Os/Ir ratio (Table 6.7).

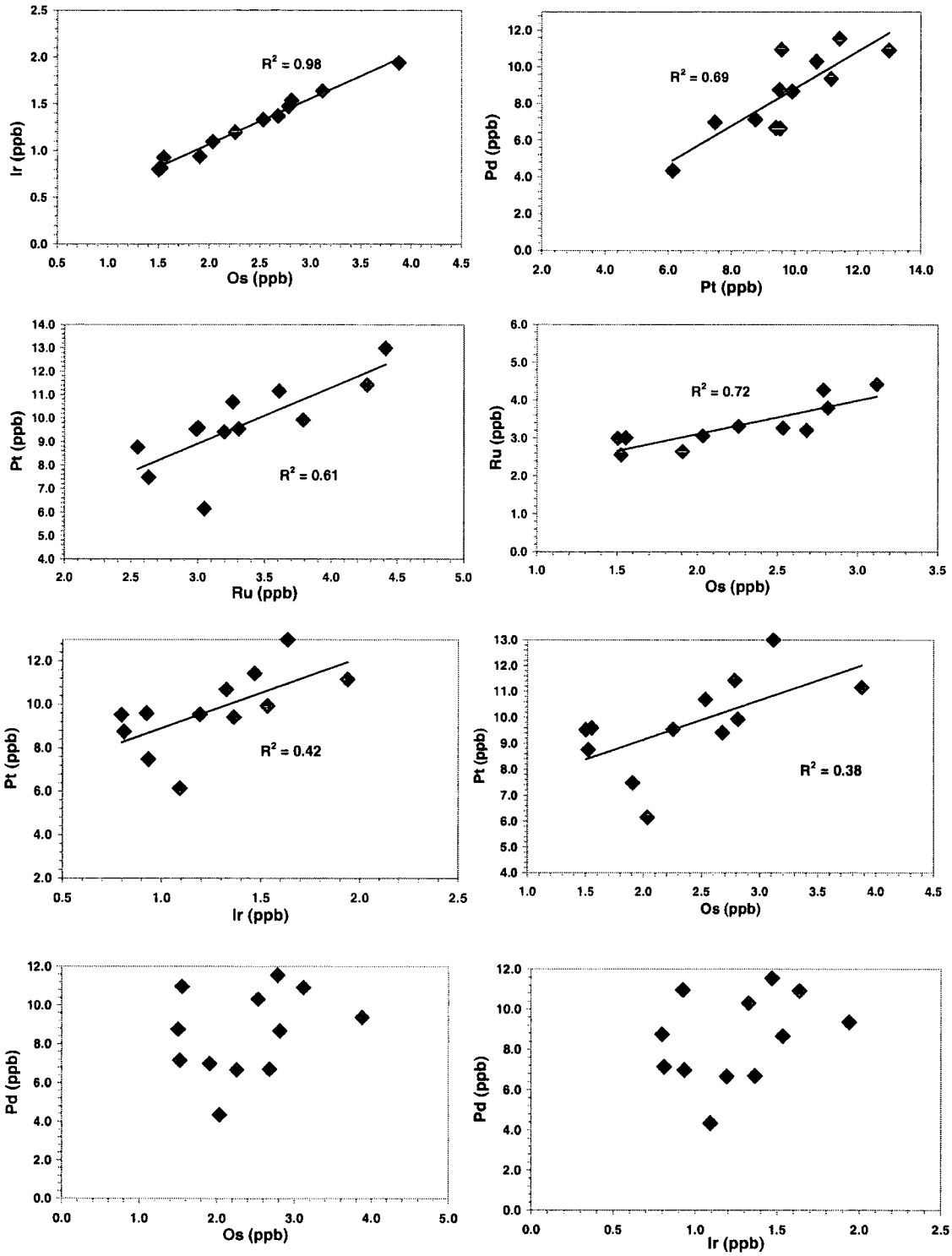

Fig 6.22 Basic PGE ratios for West Greenland picrites

The WGPs have higher Os/Ir ratios than any other rock-types (Table 6.7; Fig 6.23, 6.24). As the Os/Ir ratio of the WGPs is approximately twice that of the upper mantle (Fig 6.23) this may provide evidence that the picrites were derived from a source somewhat different from typical mantle. Alternatively, it may be that data quality where Ir and Os were obtained on the same sample aliquot in the past was poor and as such, subtle differences in Os/Ir ratios have not been recognised.

Conversely, the Os/Ir ratios of the WGPs may imply that during magma generation, Os was preferentially enriched in the melt relative to Ir, by almost a factor of 2. As values of $D_{sulfide\text{-}silicate\ melt}$ are almost identical for both Os and Ir, this could be evidence that either the IPGEs are not contained within sulfides, or that published D values are not correct under all mantle-melting conditions (e.g. differ in response to changes in fO_2).

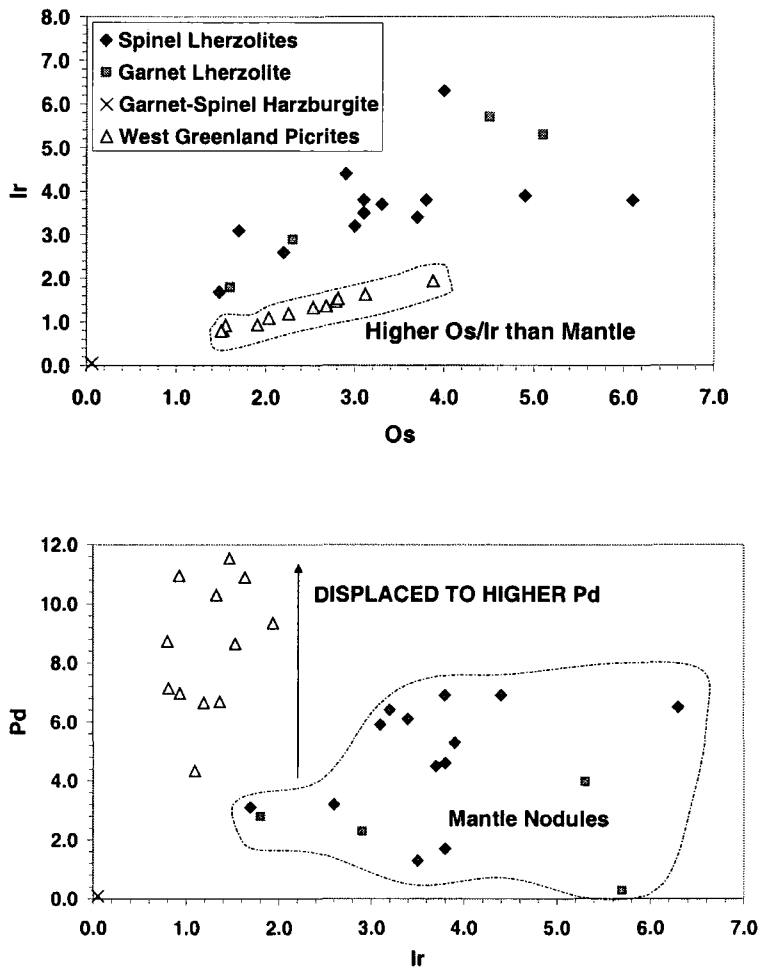

Fig 6.23 Comparison of PGE ratios in West Greenland picrites with those in mantle nodules (data from Morgan *et al.*, 1981)

Further examination of PGE relationships (Fig 6.22) confirms the strong covariance of the IPGEs. Ru as well as Ir shows a strong positive correlation with Os, suggesting that Ir, Os and Ru abundances may be controlled by the same factors.

Pd behaves differently to Pt during mantle melting: whereas Pt covaries positively with the IPGEs, there is absolutely no relationship between Pd and IPGE concentrations within the WGPs (Fig 6.22). This implies that either Pd is hosted within different mantle phases to the IPGEs, or that Pd has very different partition coefficients for mantle phases compared to the IPGEs. Pd is moderately incompatible during mantle melting (especially in S-depleted conditions). This is illustrated by the fact that Pd is enriched in melts relative to mantle restites (Fig 6.23).

The Pt/Pd ratios obtained for the Greenland picrites are more variable than Os/Ir. There is however, a positive correlation between Pt and Pd (R^2 value of the linear regression line for this data is 0.69; Fig 6.22). Thus, Pt appears to show a range of behaviour during magma genesis, having features in common with both the IPGEs and Pd. Pt may therefore be hosted in a variety of different phases (possibly in alloys with the IPGEs, but also within sulfide the probable mantle host for Pd). There are several reasons why the Pt/Pd ratios may show greater variability than the Os/Ir ratios including:

1) Greater source heterogeneity with regard to Pt and Pd.

2) Pt and Pd can be remobilised during secondary alteration processes much more readily than the IPGEs.

3) A small amount of crustal contamination would be likely to affect the Pt/Pd ratios more than the Os/Ir ratios due to the higher abundances of PPGEs within the crust. This is unlikely to be an issue in the WGPs as they have undergone only minimal crustal contamination.

4) Pt and Pd may be more strongly fractionated from each other during differentiation, than are Ir and Os.

The picrites of the Ordlingassoq Member have lower PPGE/IPGE ratios than the other Members. This is indicative of higher degrees of partial melting in the Ordlingassoq Member (if Pt and Pd are released from mantle sulfides at intermediate degrees of melting, whereas Os, Ir and Ru are retained in alloys and only released at

higher melting fractions; Fryer and Greenough, 1992). The Pt/Pd ratios of the WGPs are intermediate between those of the more evolved rocks (i.e. MORB) and those of the primitive rocks (i.e. komatiites/upper mantle). This implies that there has been greater Pt-Pd fractionation within the picrites than in the most primitive rocks. This is probably due to Pd enrichment of the melt during early crystallisation.

The WGPs have very similar Pt/Pd ratios to kimberlites although much higher overall concentrations of both elements (Fig 6.224)

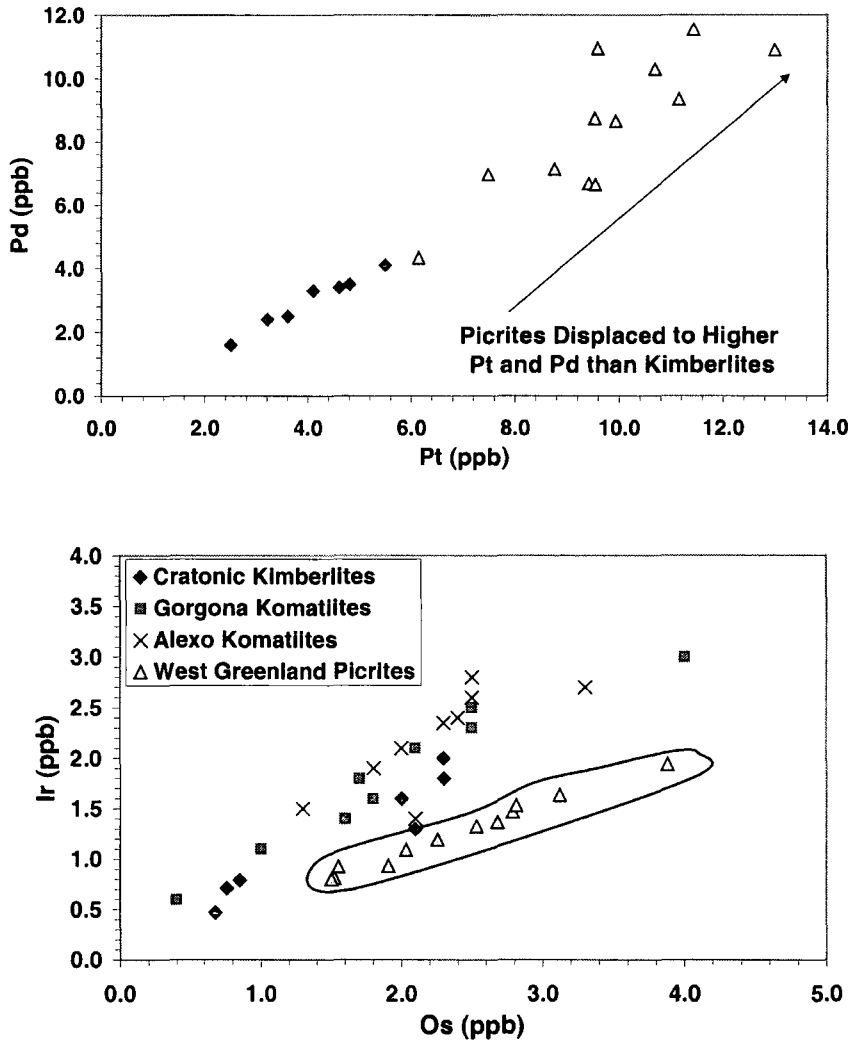

Fig 6.24 Comparison of PGE ratios in ultramafic rocks with the West Greenland picrites

(Similar plots for Os-Ru and Os-Pd do not discriminate between the WGPs, komatiites and kimberlites). Data for cratonic kimberlites from McDonald *et al.*, 1995 and data for komatiites from Brügmann *et al.*, 1987.

6.7.4 Correlation Between PGEs and Major/Rare Earth Elements

6.7.4.1 PGEs vs Mg No.

Plots of the PGEs vs Mg No. are presented (Fig 6.25). Mg No. is used as an index of fractionation in order to ascertain whether any systematic variations of PGEs occur during fractionation. Mg No. is calculated using the equation:

$$\text{Mg No.} = 100\ (\text{wt\% MgO} / \text{EW}) / ((\text{wt\% MgO} / \text{EW}) + (\text{wt\% FeO} / \text{EW}))$$

(Where EW = Elemental weight (40.3 for MgO; 71.8 for FeO); (Ragland, 1989).

Correlations exist between Os, Ir and Mg No. within the Anaanaa and Naujánguit Members. There is very little correlation between these elements however in the Ordlingassoq picrites. The correlated decrease in IPGEs with fractionation is characteristic of removal of these elements with early crystallising olivine or an associated phase.

Ir and Os are thought to exist in the mantle as Os-Ir alloys (Keays, 1995). During partial melting, the tiny alloys are freed from their sites and "float off" in the newly generated magma. Separation of silicate (e.g. olivine) and oxide (e.g. chromite) phases drag the tiny alloys down with them, explaining why olivine-rich rocks are often enriched in Ir and Os (Keays, 1995). Although there is some strong evidence for existence of refractory metal alloys in the mantle, high Os and Ir contents have also been found to exist within sulfides in mantle xenoliths (Pearson *et al.*, 1998). This suggests that sulfide may also be a major host for the IPGEs in the mantle. Dominance of sulfide or alloys is probably dependent on prevailing fS_2 and fO_2 mantle conditions at the time of magma generation (Ballhaus, 1995; see Section 1.7)

The almost identical behaviour of Os and Ir in the WGPs would certainly seem to suggest that Os and Ir coexist in the same mantle phase, be it sulfide or alloy. In addition, the PGE data suggest that the Ordlingassoq picrites may have undergone less systematic olivine (+IPGE-rich phase?) fractionation than the Anaanaa and Naujánguit Picrites.

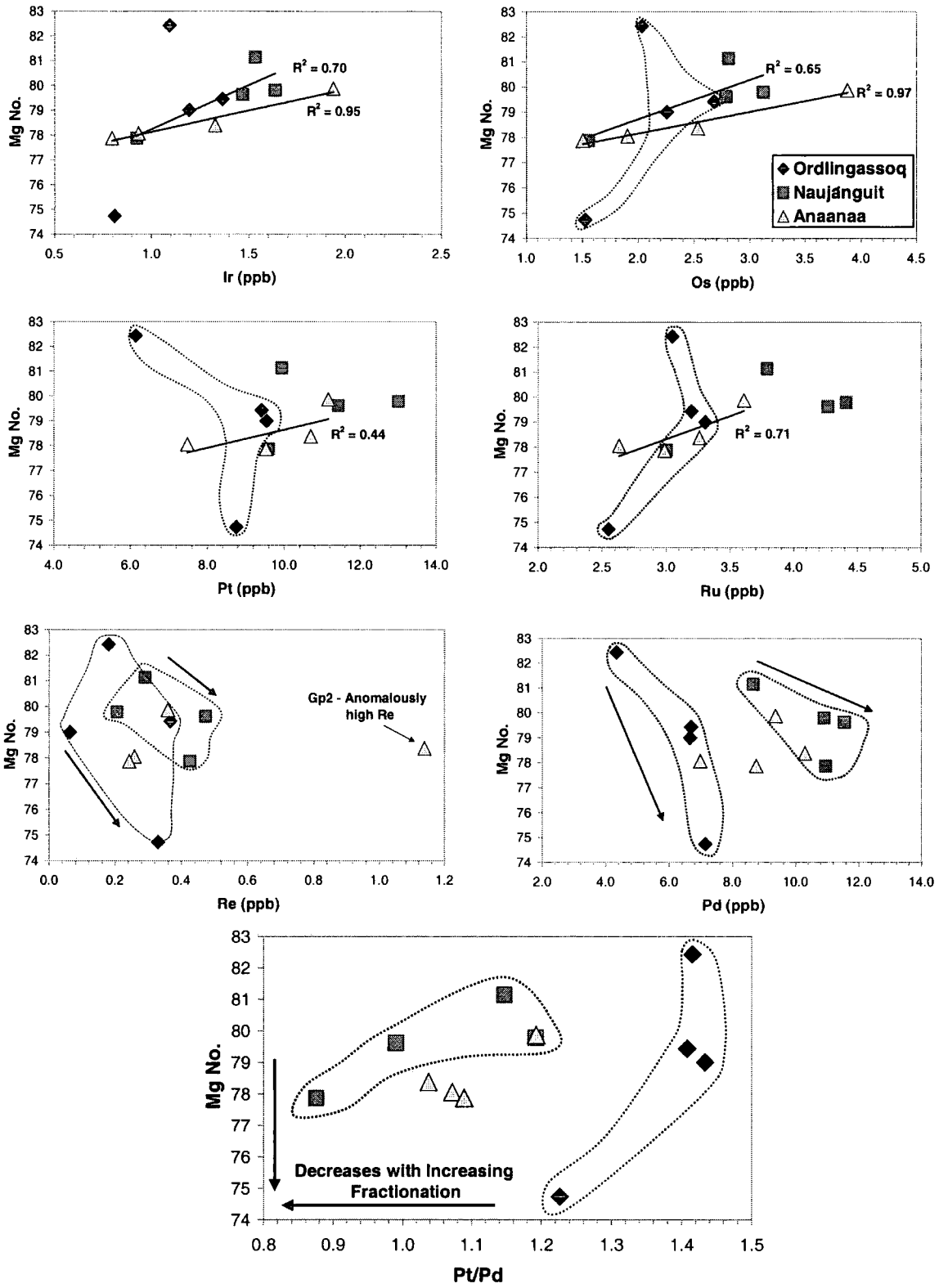

Fig 6.25 Mg No. vs PGE concentrations for the Vaigat Formation of West Greenland

Pt and Ru show weaker positive correlations with Mg No. (except for the Ordlingassoq Member) than Ir and Os. However, this still implies that Ru and Pt may be mildly compatible with early crystallising phases. Pt is known to show some affinity for chromite (Keays, 1995). Pd and Re show poor inverse relationships with Mg No. This is because they are more incompatible than the other PGEs during crystallisation (under S-undersaturated conditions) and partition into the residual melt, rather than into cumulus phases. This is illustrated by the Pt/Pd vs Mg No. plot, where Pt/Pd decreases with progressive fractionation.

6.7.4.2 PGEs vs Major Elements

Other selected major element vs PGE plots are shown where trends were recognised (Fig 6.26). In general, the PGEs do not correlate as strongly with any of the other major elements as they do with Mg. In brief, Re and Pd show a weak positive correlation with Ca, Ir shows a weak negative trend and Pd shows no correlation. With Ti, Ir forms a negative correlation, however Pt, Pd and Re show weak negative correlations across the range of all picrites, no definite trends are seen within discrete Members. PGE plots vs alkalis (i.e. K_2O + Na_2O) show highly variable Re, Pd and Pt for little change in alkali concentration. Ir exhibits a negative correlation with alkalis which may be due to their relative incompatibility differences (e.g. alkalis may build up in residual melt, after Ir has been removed). Re and Pd show no correlation with Al_2O_3, Ir concentration is highly variable for a limited range in Al_2O_3 concentration, whereas Pd forms a weak positive correlation with Al_2O_3.

A lack of correlation between the PGEs and the major elements is not unusual (e.g. Sylvester *et al.,* 1998) and may be attributed to the distribution of PGEs during mantle melting being controlled by phases other than silicates (i.e. sulfides or alloys). The following trace element signatures are thus investigated to try to deduce other parameters to which the PGE abundances may be linked.

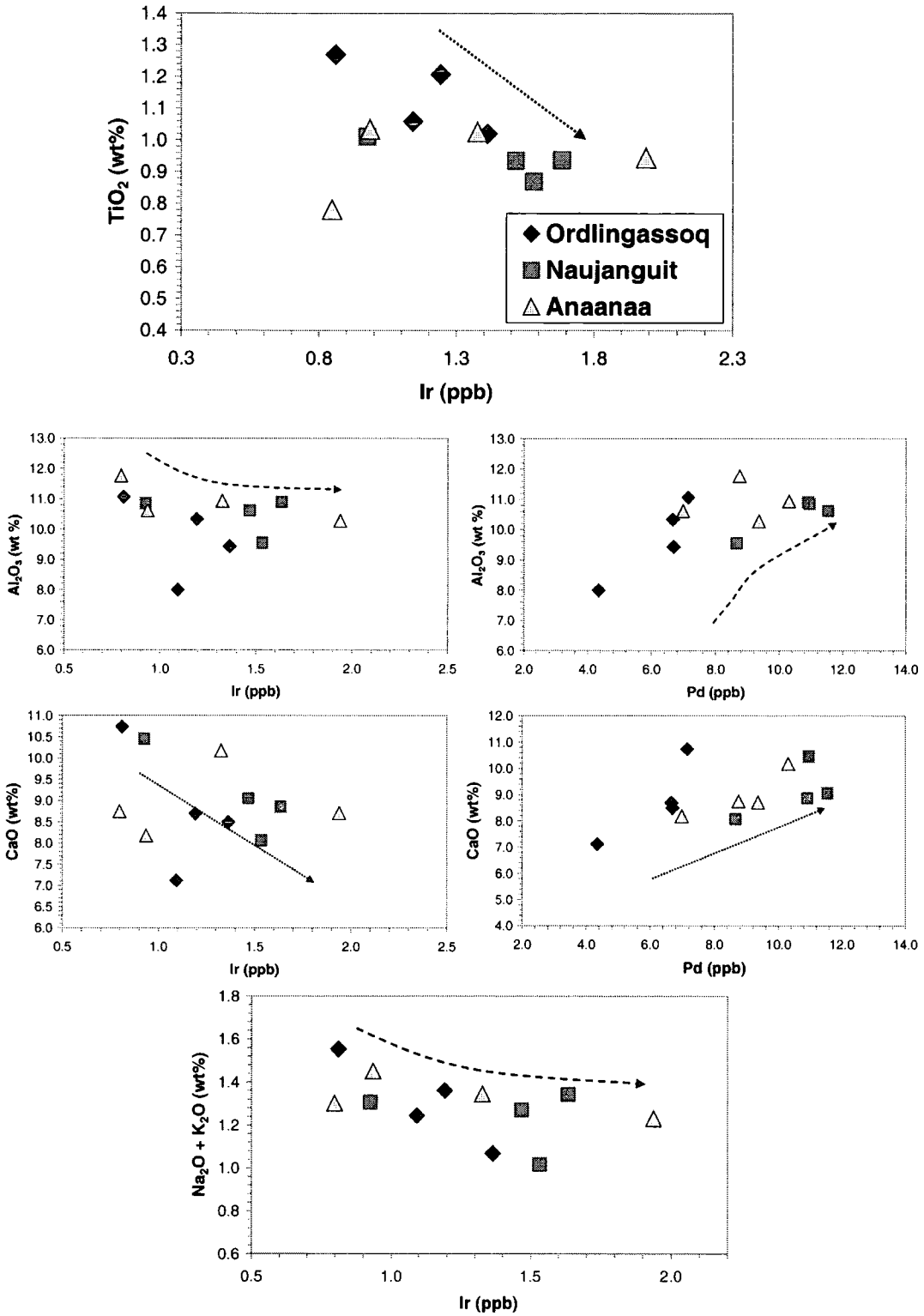

Fig 6.26 Selected major element plots vs PGEs for the Vaigat Formation of West Greenland

6.7.4.3 PGEs vs La/Sm

La/Sm will be considered as this ratio is useful in determining degree of partial melting involved in magma generation. High La/Sm values are thought to represent low degrees of partial melting, evolving to lower values as the percentage of mantle melting increases (Fryer and Greenough, 1992).

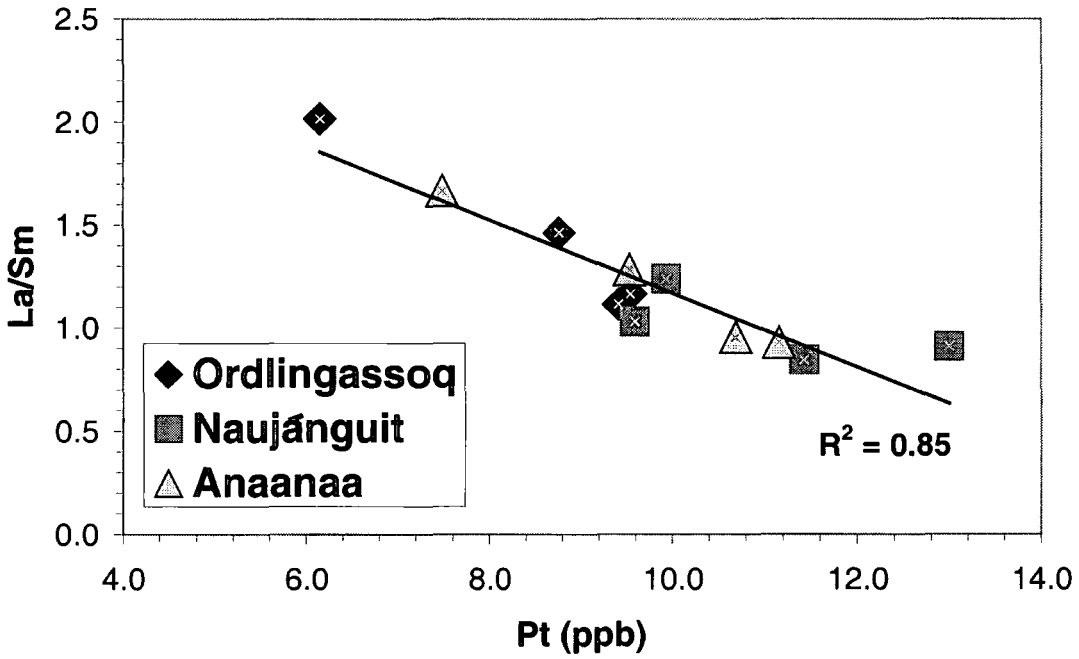

Fig 6.27 Variation in La/Sm with Pt concentration for picrites of the Vaigat Formation

There are strong inverse correlations between Pt (R^2 0.85), Pd (R^2 0.7) and La/Sm ratio (Fig 6.27). This means that the higher the degree of mantle-melting the more Pt is released into the melt. This illustrates that Pt behaves in a mildly compatible manner during mantle melting. The poorer correlations between Pd and La/Sm may result as Pd is probably more incompatible than Pt and is probably more affected by small changes in degree of partial melting. Alternatively Pd may be more mobile than Pt during eruption of the lavas (i.e. affected by degassing of the lavas). The fresh nature of the Vaigat Formation picrites (Graham *et al.*, 1998) tends to imply the Pd has not become fractionated relative to Pt during late-stage alteration.

The degree of correlation between the PGEs and La/Sm varies in the order Pt> Pd> Ru≥ Re> Os & Ir, where Os and Ir show no significant correlation with La/Sm. The inference that can be drawn from this is that IPGE concentrations are not significantly affected by minor changes in degree of partial melting. As previously mentioned, this is good evidence that the IPGEs are hosted in different, more refractory mantle phases than Pt or Pd.

A plot of Pd/Ir vs La/Sm (Fig 6.28) shows very little correlation, except in the Naujánguit group. Pd behaves more incompatibly during mantle melting than Ir (and Os) and is thus removed by smaller degrees of melting. This difference in behaviour is attributed to the fact that Pd is held within mantle sulfides which completely dissolve by intermediate percentages of melting (Fryer and Greenough, 1992). Since however, all PGEs show evidence of concentration in mantle sulfides (Jagoutz *et al.*, 1979) this supports the hypothesis (Ballhaus, 1995) that following sulfide dissolution within the shallow mantle, refractory Os-Ir-Ru alloys can be stabilised and thus retained within the source. Pt and Pd by contrast behave incompatibly and remain within the silicate melt.

Similar La/Sm relationships have also been noted in Indian oceanic island basaltic rocks, although overall concentrations of PGEs are more variable (i.e. Ir ~ 0.02-0.27ppb, Pd ~ 0.81-18.4) and Pd/Ir ratios are elevated relative to West Greenland (Fryer and Greenough, 1992). The reason for the differences in Pd/Ir ratios between these environments is probably due to differences in extent of partial melting and fractionation.

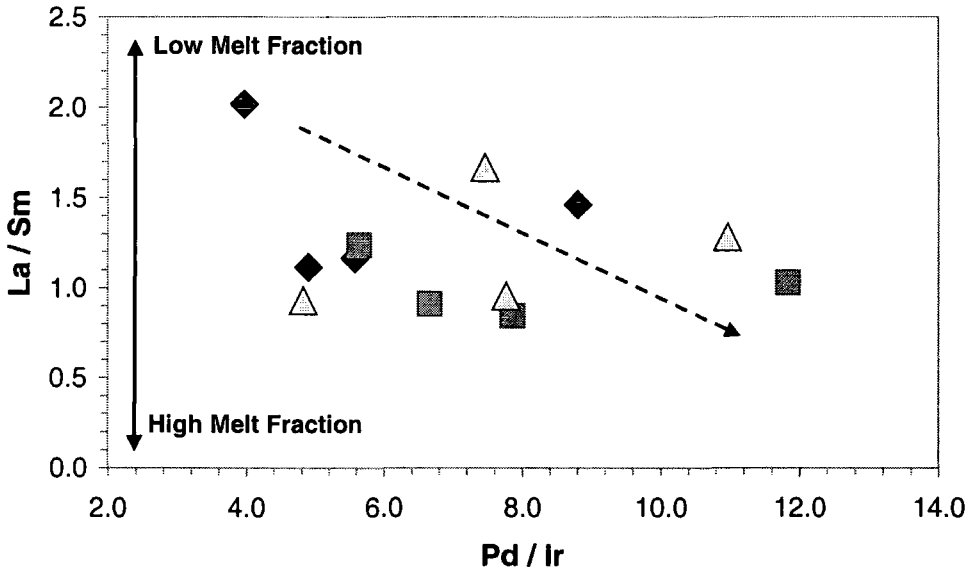

Fig 6.28 La/Sm vs Pd/Ir plot for picrites from the Vaigat Formation (arrow indicates weak negative correlation).

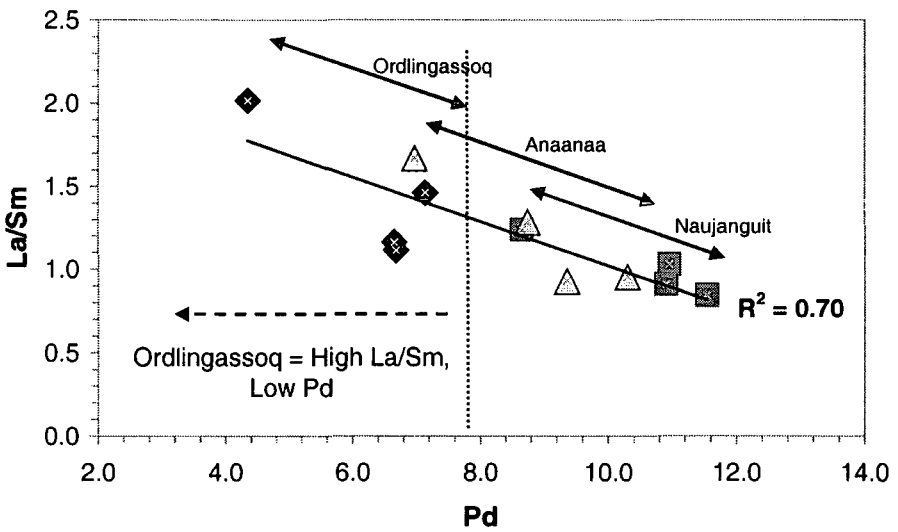

Fig 6.29 La/Sm vs Pd plot to illustrate variability (of melt fraction?) between picrites of the Vaigat Formation (Pd in ppb).

There is a tendency for the Ordlingassoq Member picrites to have highest La/Sm, but lowest Pd contents (Fig 6.29) suggesting derivation by lower degrees of mantle-melting. This is at odds with other evidence (i.e. high IPGE/PPGE ratios) that the Ordlingassoq Member was produced by higher degrees of melting, although this

signature is also consistent with lower degrees of fractionation. This highlights one of the problems in evaluating PGE data as the highly compatible nature of the IPGEs makes them prone to fractionation, which can disguise the mantle IPGE/PPGE signatures.

Assuming that the high La/Sm-low Pd signature particularly of Gp5 (of the Ordlingassoq Member) is not partial melting related and not dominated by crustal contamination (<4% crustal contamination; Fig 6.11), it could be derived from contamination of this sample by an enriched sub-continental lithospheric mantle (SCLM) component during ascent to the surface. The high $^{187}Os/^{188}Os$ composition of Gp5 tends to argue against this, however, as such SCLM tends to have unradiogenic Os-isotopic compositions due to ancient Re-depletion (Pearson *et al.*, 1998). Instead therefore, the La/Sm and radiogenic Os-isotopic signatures of certain Ordlingassoq Members may suggest more influence of a recycled component in their source region.

6.7.4.4 PGEs vs Other Incompatible Elements

The PGE abundances within the WGPs were compared with highly incompatible elements (e.g. Nb) to deduce whether the La/Sm signature was predominantly melt-fraction (or fractionation) controlled and the possible influence of crustal contamination (e.g. Cs, Rb).

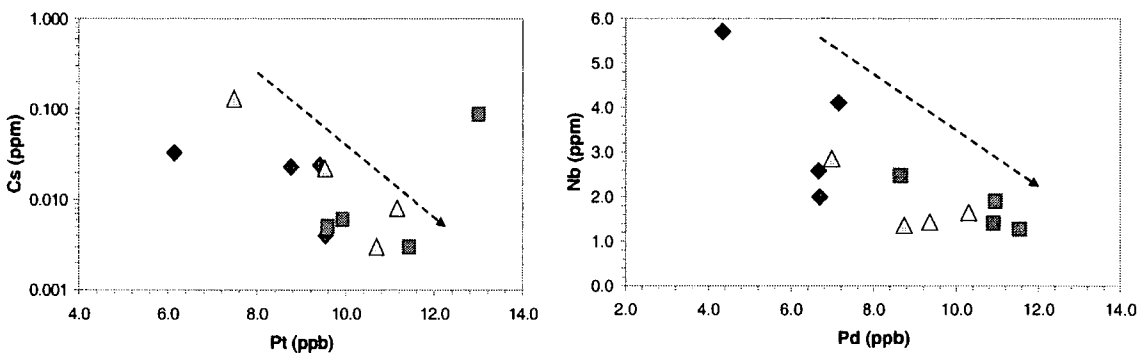

Fig 6.30 Variation of incompatible elements with PGEs

Cs and Rb show almost identical variation with the PGEs. Neither show any correlation with Os and Ir, but they correlate inversely with Re, Pt and Pd (Fig 6.30).

Pd and Re show similar inverse correlations with Nb. Ir and Os show weaker negative correlations with Nb (Fig 6.30). This behaviour is somewhat unexpected as Nb often positively correlates with Pd as they are both incompatible elements. In the WGPs however, there is no evidence of such a relationship. Therefore, differences in Nb concentration between samples are likely to reflect variation in source composition.

6.7.5 Variation of PGEs with other Chalcophile/Siderophile Elements

In addition to comparison of the PGE-signatures of the WGPs, to LILEs and REEs, it is important to compare them to both compatible and chalcophile elements. This is because the IPGEs are typically associated with compatible elements and because the PPGEs have chalcophile affinities (Keays, 1995).

Extended PGE plots can be drawn to include Ni and Cu because of their comparable behaviour during geological processes (e.g. Fryer and Greenough, 1992). Such a plot is illustrated below for the WGPs, where an average pattern for each of the Members has been constructed. Although the convention has often been to normalise such plots to primitive mantle (e.g. Fryer and Greenough, 1992), the plot in this case is normalised to chondrite (McDonough and Sun, 1995). This is to maintain consistency with other PGE patterns drawn during this study and also as primitive mantle normalisation factors are highly variable.

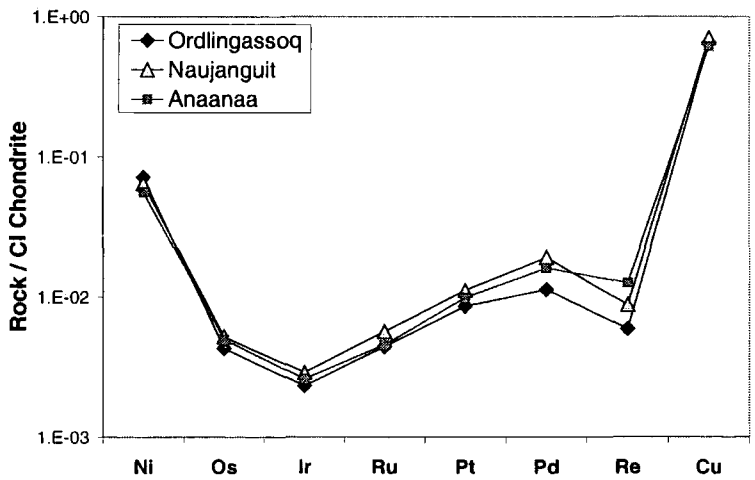

Fig 6.31 Chondrite-normalised extended Ni-PGE-Cu plots for averages of each Member of the Vaigat Formation. Normalisation values after McDonough and Sun (1995)

The patterns obtained for West Greenland are compared with patterns from different environments to determine if there are any systematic differences in chalcophile and siderophile element abundances. In general, there is a scarcity of full PGE data for picritic rocks. However, patterns from other relevant environments are illustrated to place the picrite data in context (Fig 6.32).

The WGPs plot almost entirely within the field defined by the Gorgona komatiites (Brügmann *et al.,* 1987) as do the cratonic kimberlites (Fig 6.32a). The exception is for Re, which plots to slightly lower abundances than komatiite. By comparison, the WGPs tend to have higher concentrations of the PPGEs (Pt and Pd) than cratonic kimberlites. This may suggest that high MgO rock-types are produced by similar, high degrees of partial melting. The percentage melt fraction generally thought to be required to generate komatiites is in excess of 30% (Keays, 1995). The higher concentrations of PPGEs in the WGPs relative to kimberlites, may result as the WGPs are probably generated by higher degrees of melting. Considering however, the complex petrogenesis of kimberlites and the fact that they are mixtures of different source region melts, it is unwise to draw too many conclusions from their PGE signatures in relation to WGP petrogenesis.

The Ni contents of the WGPs are lower than PUM. Conversely, MORB and OIB have significantly lower Ni-contents than the WGPs. This is consistent with OIB/MORB production as lower degree melts and them having undergone more olivine fractionation than the WGPs (also illustrated by their lower MgO contents). The WGPs tend to have slightly higher Cu contents than MORB. This is probably related to the S-saturated nature of the MORB source as Cu distribution is predominantly controlled by sulfide phases (Hamlyn *et al.,* 1985). The differences in S-saturation between MORB and the WGPs will be discussed in more detail later. There is overlap in Cu-concentrations found in OIB and the WGPs which is expected, since both groups of rocks are plume-derived. Some OIB compositions plot to higher Cu-concentrations than the WGPs, but this is probably related to extent of fractionation as Cu is incompatible provided a melt is S-undersaturated (Keays, 1995).

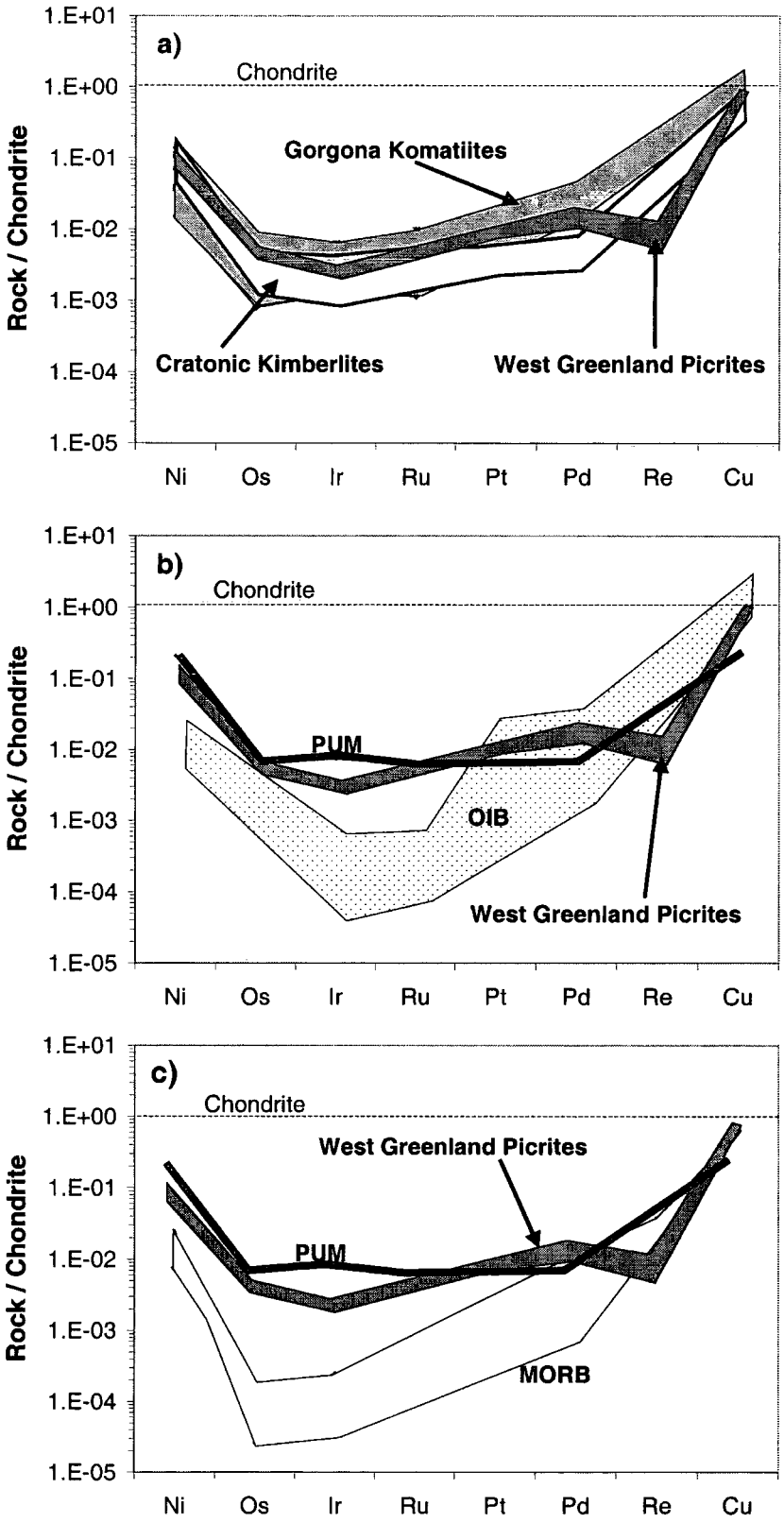

Fig 6.32a-c Chondrite-normalised extended PGE-siderophile element plots for WGPs compared to a) komatiites and kimberlites (Data from McDonald *et al.*, 1995; Brügmann *et al.*, 1987) b) PUM and OIB (Data from Sun and McDonough, 1995; Fryer and Greenough, 1992) c) PUM and MORB (Data from McDonough and Sun, 1995; Hertogen *et al.*, 1980).

Relative to OIB, the WGPs are significantly enriched in Ir and Ru and marginally enriched in Os, whereas the concentrations converge for the PPGEs and Re (Fig 6.32b). The higher IPGE (and Ni) abundances probably result from higher degrees of melting in the WGP-source and may be produced by lower degrees of fractionation in the WGPs compared to OIB. Re is depleted in the WGPs compared to PUM, OIB and MORB. Two explanations exist for this signature: either Re is depleted in the WGP-source because of a previous melt-extraction event (which explains the pattern relative to PUM), or Re is enriched in the more evolved basalts relative to the WGPs as a result of its incompatible behaviour (which explains the MORB and OIB patterns).

Further comparisons of individual PGE-contents in relation to each of the siderophile and chalcophile elements are now considered, in order to understand the fractionation history and S-saturation status of the WGP magma.

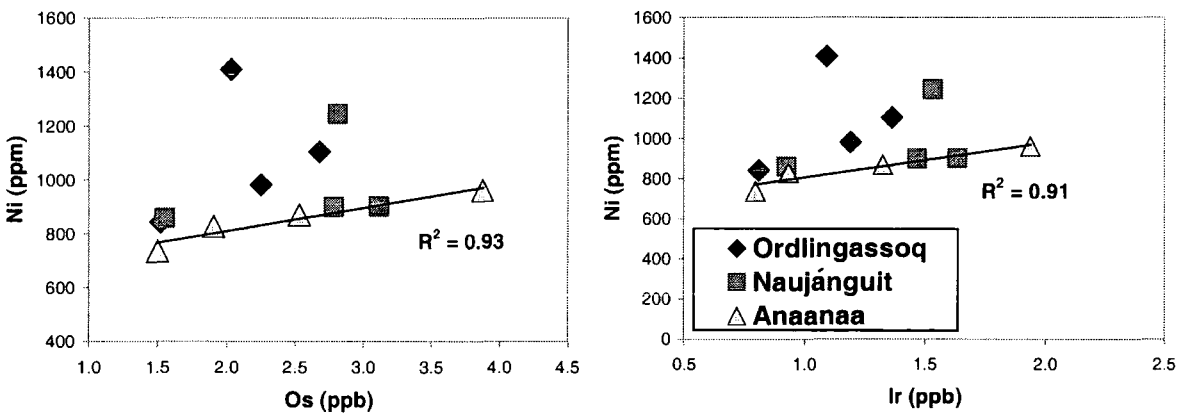

Fig 6.33 Compatible element variation; Ni vs Os and Ir

There is a positive correlation between both Os and Ir, and Ni, especially in the Anaanaa Member. The similarity of the plots (Fig 6.33) indicates identical behaviour for Os and Ir. Ir and Os are most strongly correlated with Ni in the Anaanaa Member and show a wide variation in concentration, for little change in Ni. These plots coupled with the strong correlations between Ir, Os and Mg No. indicate that olivine fractionation played an important role in Ni, Ir and Os distribution, particularly in the Anaanaa Member. Plots of Ru-Ni, Pt-Ni and Re-Ni do not show

any strong correlations, with significant overlap between the different stratigraphic Members. Thus, while Ir and Ru co-crystallise with olivine (possibly as alloys), Pt and Ru do not. Since Pt and Ru do not show negative correlation with Ni (like Pd) this indicates that they are not highly incompatible during early cumulate formation. Thus, it is proposed that crystallisation of Pt and Ru may instead be governed by a silicate phase other than olivine.

Pd-Ni plots show strong negative correlations, except within the Anaanaa Member (Fig 6.34). This is probably caused by differences in Ni and Pd compatibility with phases crystallising from the picritic melt, particularly olivine, with which Ni is compatible. Pd by contrast, does not enter such silicate phases during fractionation of silicate melts and is instead controlled by the behaviour of S and sulfide melts (Keays, 1995). Constant Ni for highly variable Pd contents, have been observed within Western Australian komatiite-cumulates (Keays, 1995) as well as within the Anaanaa Member. Keays (1995) attributes this trend to the fact that that Ni entered olivine in fixed proportions, while the Pd content of the cumulates varied in direct proportion to the amount of trapped interstitial melt (Keays, 1995).

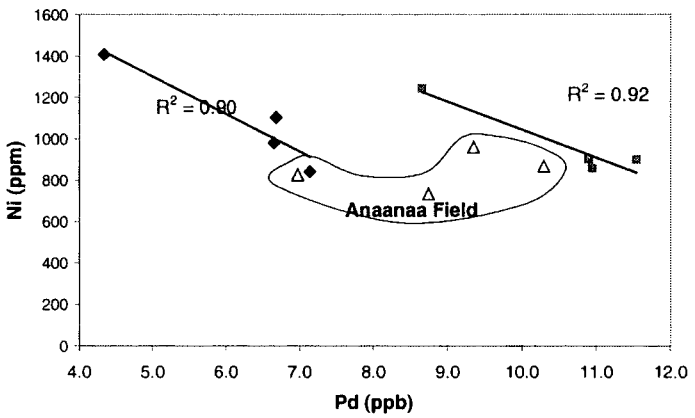

Fig 6.34 Variation in Ni vs Pd for the Members of the Vaigat Formation

The trends of depletion of the magma in Ni and in the heavier PGEs, particularly Ir and Os, due to early olivine fractionation and incompatibility of Pd and Re with olivine, concurs with the order of fractionation modelled by Keays (1995; see Fig 6.37). Cr-PGE plots might be expected to show correlation since all

are thought to be highly compatible with early crystallising phases. There are however no significant relationships. Thus in the Vaigat Formation the PGEs did not co-crystallise with Cr.

There is little or no correlation between Co and any of the PGEs, except for Pd. Within the Co-Pd plot, the different Members form discrete fields with little overlap. The Naujánguit and Ordlingassoq Members, unlike Anaanaa member, have trends of decreasing Co with increasing Pd.

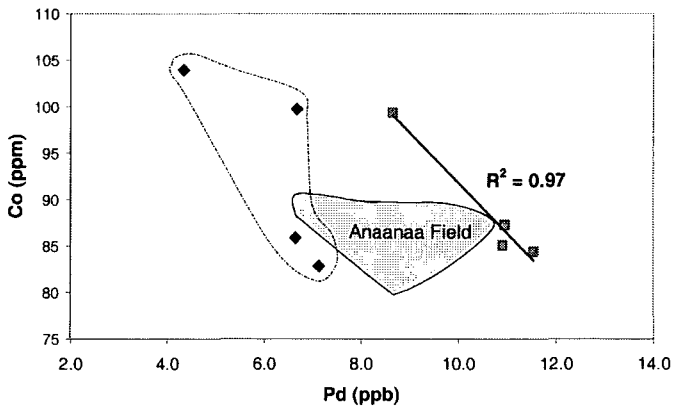

Fig 6.35 Variation of Co and Pd in the picrites of the Vaigat Formation

Cu-PGE plots are not good discriminant diagrams for the different Members, nor do they show well-developed trends for most of the PGEs. Ru within the Naujánguit Member shows a weak positive correlation with Cu, as does Pd within all of the Members. This is as expected since Pd and Cu are both chalcophile elements. The fact that the IPGEs and Re do not exhibit such correlations, indicates that they are not behaving in a strongly chalcophile manner or being governed by the same sulfide phases as Cu and Pd. Recent modelling of basalts from the Newer Province, Australia, suggests that $D_{sulfide/silicate}$ for Pd may be ten times higher than for Pt (Vogel and Keays, 1997). This would explain the observed differences in behaviour of Pd and Pt in the WGPs.

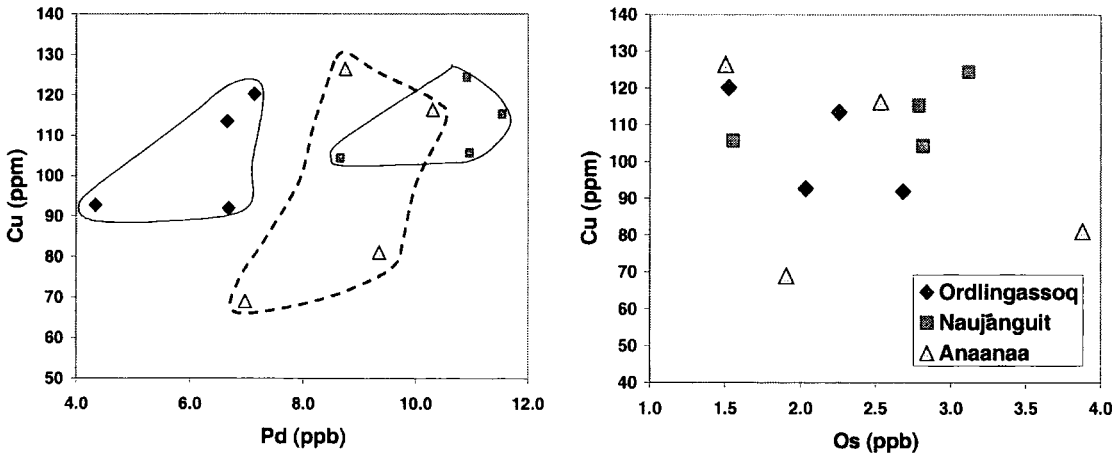

Fig 6.36 Cu vs Pd and Os for the picrites of the Vaigat Formation

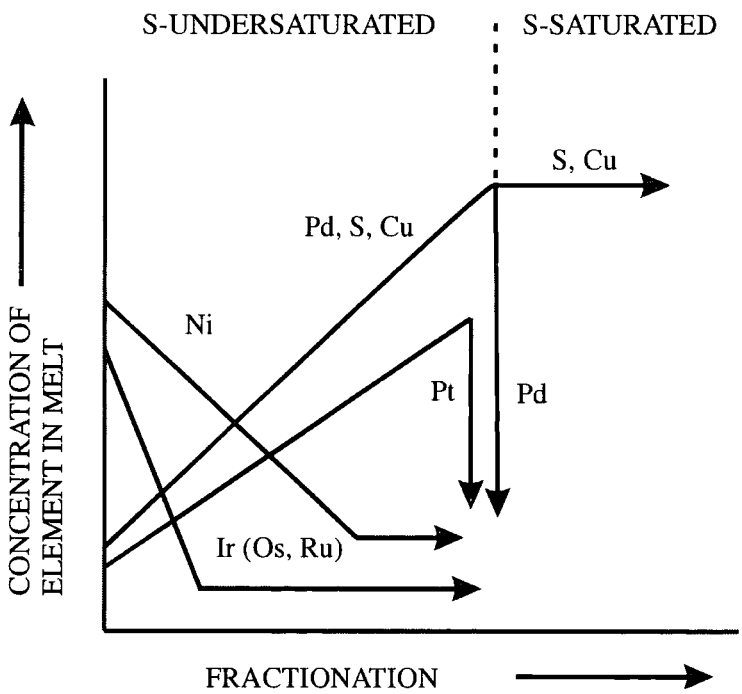

Fig 6.37 Variation of base and precious metals in magmas as a function of fractionation (From Keays, 1995)

6.8 Importance of S-Saturation in Determining West Greenland Picrite PGE Signatures

The timing of S-saturation within magma is crucial in determining the PGE concentrations and inter-element ratios within the final crystallising assemblage. For example, a melt must be undersaturated in PGEs at the time of generation in the mantle and during transport to higher crustal levels, if it is to maintain high PGE concentrations upon emplacement. This is because of the high partition coefficients of the PGEs between sulfide liquid and silicate melt. Thus, as soon as a magma becomes S-saturated and an immiscible sulfide liquid forms, all PGEs will be scavenged by this sulfide liquid and thus removed from the melt (Brooks *et al.*, 1999 and Vogel and Keays, 1997).

Economic PGE deposits such as the Platinova Reef of the Skaergaard intrusion are thought to have formed from high MgO magmas derived during high degrees of melting of a S-undersaturated source. In these situations the PGEs (particularly Pt and Pd) are able to build up to economic quantities in the melt before S-saturation finally causes the precipitation of sulfides highly enriched in PGEs (Brooks *et al.*, 1999).

S is a strongly incompatible element and so is easily depleted in mantle sources during even low degree melting episodes. Thus, magmas generated by melting of sources already depleted in S by a previous melting episode (e.g. boninites) are typically S-undersaturated. At 25% partial melting all S is thought to be dissolved in the melt (Keays, 1995). Hence, magmas formed at precisely this degree of melting of a fertile source will be S-saturated (and contain maximum Pd contents of ~12ppb, Fig 6.38). Higher degrees of melting however, result in magmas that are undersaturated because of dilution of the S by the increasing silica content of the melt (Keays, 1995). Komatiites are therefore typically derived from S-undersaturated primary melts.

The plots (Fig 6.38) illustrate the behaviour of Pd during mantle melting and how it is closely linked to S-saturation. In A) the Pd content within the mantle residue increases with the degree of partial melting, as long as the upper mantle residue contains S. At >25% partial melting however, all mantle sulfide is dissolved and there is total S-depletion of the mantle. At this point all Pd will also enter the

melt and so become depleted in the mantle residue. B) illustrates that as long as sulfides remain in the source regions of partial melts, Pd will be depleted in the resulting melt. Once sulfide is removed from the source however (>25% melting), melts contain appreciable Pd which then slowly decreases with increasing partial melting, once the S-saturation limit is passed (Keays, 1995).

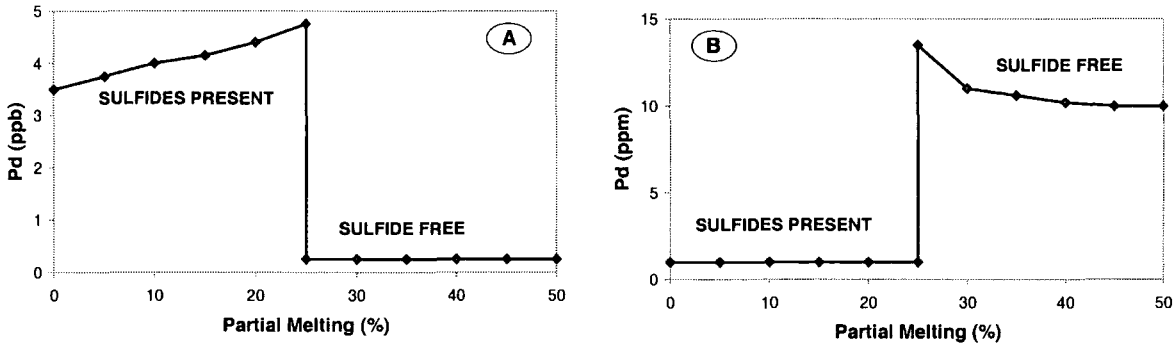

Fig 6.38 Variation of Pd A) In upper mantle residues produced by varying degrees of partial melt extraction, B) In melts generated by varying degrees of partial melting of the upper mantle (from Keays, 1995).

The situation is obviously not so clear-cut for the IPGEs during partial melting as although they are hosted within mantle sulfides, partial melting (even >25%) and S-dissolution does not necessarily remove the IPGEs from the mantle. This is clearly illustrated by residual mantle xenoliths which still contain high Os-Ir concentrations despite depletion in the PPGEs (e.g. Morgan *et al.*, 1981).

Knowing whether S-saturation has taken place during a magma's history is not only important to the discovery of magmatic sulfide deposits, but, it also provides information that can be used to characterise and constrain the type of mantle source (Vogel and Keays, 1997). In order to determine whether a suite of rocks is formed from fertile, S-undersaturated magma or from S-saturated magma, various discriminant diagrams can be drawn. Those commonly used are Pd vs Se (where Se forms a direct analogue of S-concentration) or Pd vs Cu (when S or Se data are not available). Cu and Pd, being highly chalcophile, should be strictly controlled by S-concentration (Vogel and Keays, 1997 and Brooks *et al.*, 1999).

The WGPs were derived from a S-undersaturated source, if the empirically derived S-saturation line is assumed to be correct (Brooks *et al.*, 1999; Fig 6.39). Interestingly, the WGP and Skaergaard fields partially overlap. The East Greenland basalts plot closer to the S-saturation line than the WGPs. This is to be expected though, as the basalts have undergone more fractionation than the WGPs and fractionation pushes melts towards S-saturation because of decrease in temperature (Vogel and Keays, 1997). The comparable West and East Greenland fields add support to the hypothesis that they were derived from the same source, namely, the ancestral Iceland plume. Obviously the lavas extruded in both East and West Greenland were derived from a S-undersaturated melt generated through >25% partial melting of a S-undersaturated source (shown by elevated Pd concentrations).

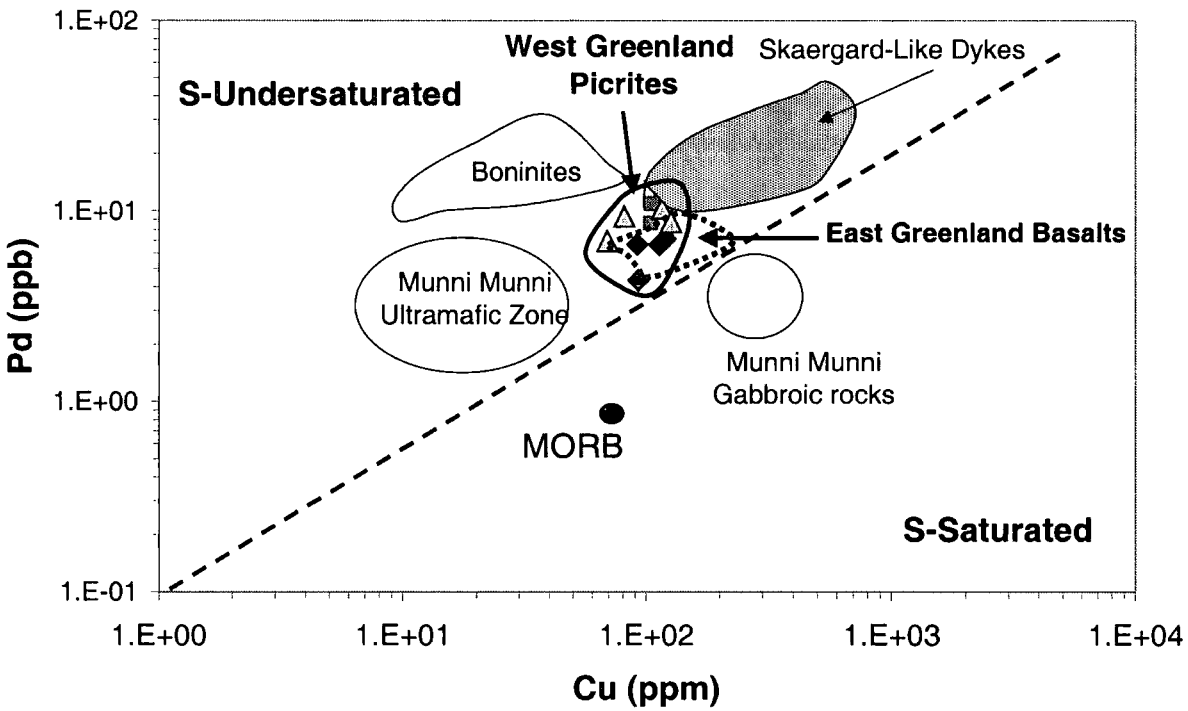

Fig 6.39 Pd vs Cu discriminant diagram between the fields formed by S-saturated magmas (e.g. MORB) and the field of rocks formed by S-undersaturated magmas (e.g. West Greenland picrites). Fields and empirically-derived S-Saturation line, taken from Vogel *et al.*, 1999 and Brooks *et al.*, 1999.

The S-depletion may be due to either: high degrees of partial melting (which would probably be expected in a plume regime) or due to previous melt extraction

from the mantle source of the Greenland picrites. The fact that immiscible sulfides probably did not separate from the picrites (possibly due to rapid magma quenching on extrusion?) may account for the homogeneity between replicate PGE signatures in the WGPs. Such conditions may limit the "nugget effect" as Pd is actually still dissolved within the melt, rather than held in immiscible S-droplets.

Vogel and Keays (1997) have devised a simple method to estimate partial melt fraction removed from the mantle using the equation:

$$(1 / F) \times 4.4\text{ppb} = \text{Amount of Pd expected in S-undersaturated Melt}$$

Where F is the partial melt fraction removed from the mantle and 4.4ppb is the reported value for Pd concentration in the mantle.

Using this approach, Vogel and Keays (1997) estimated that tholeiitic magmas generated at ~24% partial melting, should be expected to contain 18ppb Pd if they remained S-undersaturated during their approach to the surface. In reality such rocks typically contain ~1ppb, so they consider this as evidence that such rocks must have undergone S-saturation prior to extrusion. Applying this logic, komatiites derived from ~30% mantle melting (which generally plot as S-undersaturated), should exhibit concentrations of ~14.5ppb Pd. In fact, komatiites span a range of ~8-24ppb Pd (e.g. Gorgona, Brügmann *et al.*, 1987) and so only partially agree with this simplistic model.

Considering the WGPs, unfeasibly high degrees of melting are required to produce the observed Pd abundances (i.e. 62-100% melting for Ordlingassoq, 38-51% melting for Naujánguit and 42-63% melting for the Anaanaa Member). Thus, either some sulfide must have been removed from the melt prior to extrusion (which seems unlikely given the S-undersaturated nature of the picrites), or the above equation is flawed in being a gross over-simplification of mantle melting.

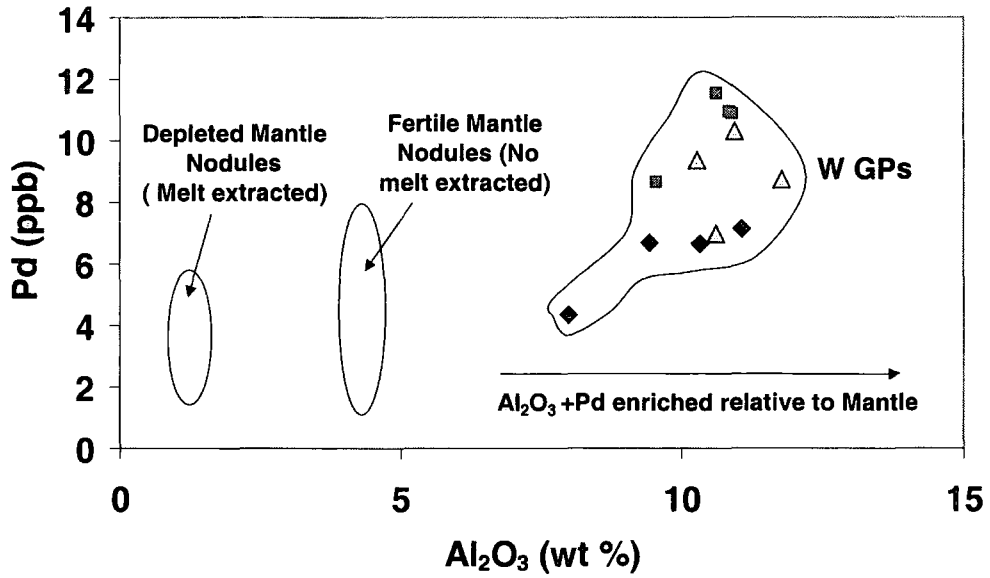

Fig 6.40 Scattergram showing Pd and Al_2O_3 contents of upper mantle nodules (spinel lherzolites) VNP Province, Australia (xenolith fields from Keays, 1995).

The high Al_2O_3 and Pd concentrations of the WGPs compared to those in the mantle nodules (Fig 6.40) illustrate that they are partial melts of the mantle in which incompatible elements are enriched, relative to the residues of the melting process. The high Pd concentrations may also be explained if PGEs have been contributed from a more PGE-rich source than average upper mantle.

More complex diagrams involving chalcophile element ratios can be drawn which form good discriminant plots of tectonic environment (Vogel *et al.*, 1999). On a Pd/Ir vs Ni/Cu plot, the WGPs form a discrete field which lies on a continuum between mantle, komatiites and high MgO basalts (Fig 6.42). This line is probably a partial melting trend. Interestingly, since they are both plume-derived rocks, the WGPs are quite separate from the CFB field. The CFBs have a more fractionated signature, probably due to greater separation of early crystallising phases during ponding at the base of the lithosphere, whereas the WGPs were able to rise almost uninterrupted to the surface.

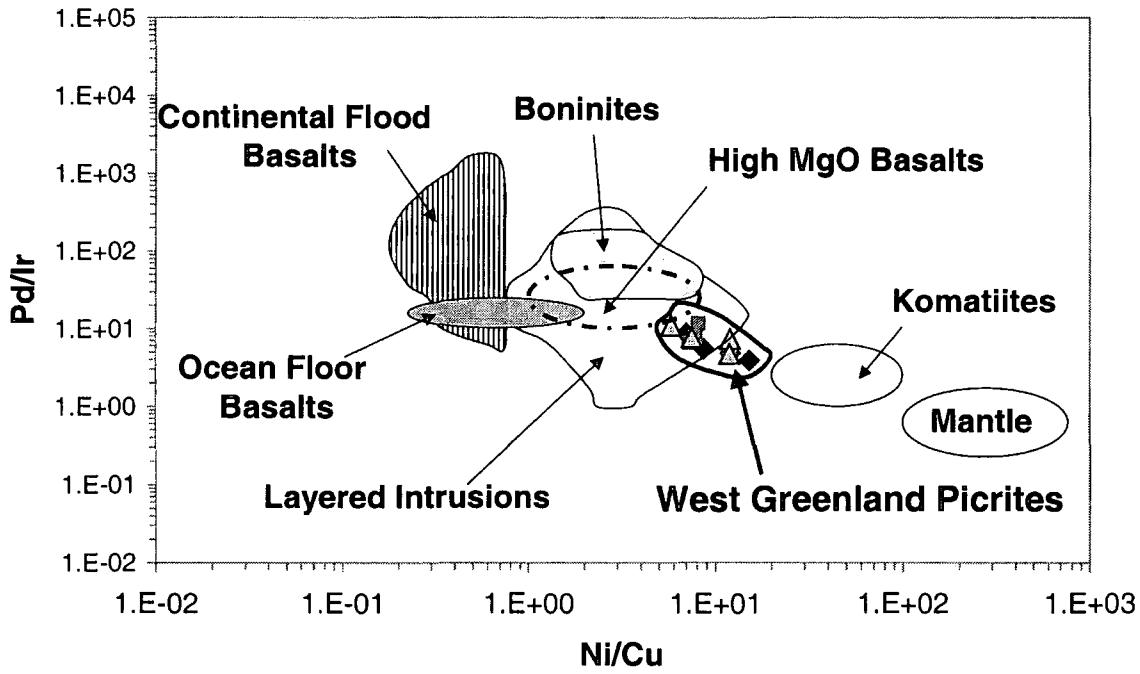

Fig 6.42 Pd/Ir vs Ni/Cu diagram (after Vogel *et al.*, 1997), showing the relative global position of WGPs. Note linear trend between high MgO basalts, back to mantle passing through WGPs and komatiites

6.9 Summary of Important Implications from West Greenland Picrite Data

6.9.1 General Geochemistry

The WGPs were produced 61Ma ago by magmatism associated with the ancestral Iceland plume during the onset of rifting at the Greenland margin. The picrites of the Ordlingassoq, Naujánguit and Anaanaa Members comprise the earliest Tertiary volcanics of the Vaigat formation and show subtle geochemical variations.

All three Members show a decrease in MgO (and Mg No.), Ni and Cr with increasing SiO_2, highlighting that the picrites underwent some olivine and possibly chrome spinel fractionation. Marginally higher SiO_2 and lower Ni in the Anaanaa samples indicate it may have undergone slightly more fractionation than the other Members or experienced slightly different melting conditions. No other significant major element variations were recognised between the different Members, suggesting relatively constant conditions during magma-genesis.

All Members show HREE depletion relative to MORB. Differences in REE abundances allow some discrimination to be drawn between the members:

1) The Anaanaa Member has the most variable MREE signatures and is intermediate to the other two members in terms of LREE concentrations.
2) The Naujánguit Member has the flattest (most MORB-like) REE signatures and the lowest LREE concentrations of all the members. The Naujánguit and Anaanaa members have identical HREE signatures.
3) The Ordlingassoq Member has the highest LREE/HREE ratios of all the Members (due to both LREE enrichment and HREE depletion compared to the other Members). This suggests that garnet may have played a more prominent role in evolution of the Ordlingassoq member.

The Naujánguit Member generally shows the most depleted LILE-signatures. Enrichment in highly incompatible elements (i.e. Cs and Rb) corresponds to enrichment in the LREEs for certain samples in the Anaanaa and Ordlingassoq Members. For the Anaanaa Member, enrichment in Cs partially correlates with Sr-isotope enrichment, suggesting there may have been an element of crustal contamination. Mixing calculations however, indicate that large amounts of crust (5-10%) would be needed to create the most radiogenic Sr-isotopic compositions observed. This is not compatible with the other LREE and LILE element signatures. Lack of correlation between Os-isotopes and LILE enrichment confirms that crustal contamination is not significant. It is possible that radiogenic Sr and LREE enrichment (in the Ordlingassoq Member) reflects interaction with enriched subcontinental lithospheric mantle.

Significant overlap occurs between ε_{Nd} and ε_{Sr} signatures for West and East Greenland picrites and Icelandic volcanics, confirming their common plume source (Holm *et al.*, 1993). Thus, it is probable that the ancestral Iceland plume produced the WGPs. Variable mixing between MORB source mantle and a plume component controls the REE signatures of the Vaigat Formation. The Naujánguit Member has preserved the clearest MORB-source signature in terms of REEs. The Ordlingassoq

Member becomes more dominated by a LREE, LILE-enriched plume component, derived from within the garnet stability field.

6.9.2 Re-Os Geochemistry of West Greenland Picrites

The WGPs have similar Os contents to other high MgO rock types such as komatiites. This suggests that high degrees of melting (>25%) were responsible for WGP production. Re abundances in the WGPs are comparable to kimberlites and other picrites, but lower than OIB and MORB, indicating that significant fractionation of the WGPs has not occurred. Lower abundance of Re in the WGPs than in komatiites, suggests that some Re may have been retained in the source region of the WGPs, possibly within garnet. This is confirmed by Re-Yb plots where the WGPs plot within the field defined by OIB, containing 0-14% residual garnet in the source (after Righter and Hauri, 1998). Despite the variations in HREE patterns of the different Members, Re-Yb data point to a minor, homogenous garnet-content in the source regions of the different members.

The Ordlingassoq Member picrites are significantly more enriched in radiogenic Os than the other Members. As the Ordlingassoq picrites do not show any evidence of increased crustal assimilation, this radiogenic component may be plume-derived. The γOs values derived for the different Members confirm that the Ordlingassoq group has closer affinity to OIB, whereas the Naujánguit group has greater isotopic affinity with MORB. The Anaanaa Member overlaps both OIB and MORB γOs fields. This concurs with the source proposed for each Member based on other trace element data. The source of the radiogenic Os component in the Ordlingassoq group cannot be conclusively proven. It is proposed that the Re-Os systematics have been predominantly controlled by the mantle source rather than any AFC processes, but whether the ancient Re-enriched source was recycled crust or outer core is uncertain. The contribution from this source is presumed to be relatively minor because of the low overall Re (and Pt) content of the WGPs and their low γOs values compared to other OIBs.

6.9.3 PGE Signatures and Behaviour within the West Greenland Picrites

The WGPs define relatively flat chondrite-normalised PGE patterns, consistent with their derivation from high degrees of mantle melting. There are only subtle variations between the PGE patterns of the different Members, with the Ordlingassoq Member having the least variable PGE patterns and lowest overall concentrations. The Anaanaa group has the most variable PGE patterns; particularly for the IPGEs, whereas the Naujánguit group has overall slightly higher PGE concentrations particularly for Pd. The IPGE variation in the Anaanaa group may be related to the slightly higher degrees of fractionation hypothesised.

In terms of their PGE ratios, each of the Members are generally within error of each other, again illustrating the homogeneity of the PGE distribution. The WGPs most closely resemble other high MgO rock-types in terms of PGE-ratios, although Os/Ir is considerably higher in the WGPs than other rock types. It is thus probable that in rocks which have undergone limited fractionation the PGE signatures will be governed by degree of partial melting. There are good correlations between the IPGEs (particularly Os and Ir), intermediate correlations between the IPGEs and Pt, intermediate correlations between Pt and Pd, and no correlations between the IPGEs and Pd, or Re. This illustrates that the IPGE-distribution is controlled by a different set of factors to that of Pd and Re, and that Pt behaves in a manner intermediate to the other two groups.

In general, there is very little correlation between the major elements and PGE abundance. This is attributed to PGE melting/fractionation behaviour being dominantly controlled by phases other than silicates. Re is the exception as it may be compatible with garnet during mantle melting. PGE distribution does relate to Mg No. however. Strong positive correlations occur between Os, Ir and Mg No. in the Anaanaa and Naujánguit Members. This confirms previous observations that the IPGEs are either compatible in or co-crystallise with cumulate phases such as olivine, possibly in the form of metallic alloys. Intermediate correlations between Pt and Ru, and Mg No. point to moderate compatibility with early crystallising phases. No correlation exists between Pd and Mg No. This illustrates two points: firstly that Pd is highly incompatible during early silicate crystallisation and secondly that Pd

behaves in a significantly different manner to all of the other PGEs (including Pt) during petrogenetic processes.

Correlation of Pt with La/Sm implies that Pt abundance in the WGPs might be controlled by degree of melting. No relationship exists between the IPGEs and La/Sm, which implies that over the observed melting trend the IPGEs behaved in a more compatible manner. Based on these observations, it is proposed that Pt and Pd are contained within different mantle-phases to Os and Ir, at least within the WGP source.

Plots of chalcophile elements vs the PGEs most effectively constrain the phases that have controlled PGE distribution in the WGPs. Positive correlation between Os, Ir and Ni, suggest that olivine fractionation (or a trace phase that crystallises at the same time as Os) has strongly controlled the distribution of Os and Ir, particularly in the Anaanaa Member. Poor correlation between Ru, Pt, Re and Ni suggests that their distribution is not olivine controlled. This is particularly interesting for Ru, which is often assumed to behave in a similar manner to Ir and Os. Pd conversely, shows strong inverse relationships with Ni, confirming that Pd behaves in an incompatible manner during early olivine crystallisation.

There is weak positive correlation between Pd and Cu, another mildly incompatible chalcophile element. Increase of the chalcophile elements in a melt may only occur if the melt is S-undersaturated. It has been shown that the WGP parental magma was indeed S-undersaturated at time of eruption. This implies high degrees (>25%) of melting in the mantle. At these high degrees of melting, all of the sulfide (and Pd-Pt) might be expected to dissolve into the melt, explaining the high PGE-concentrations in the WGPs. The WGP melt obviously did not become S-saturated at any point during its ascent or it would have precipitated its PGE-load. The chalcophile and PGE abundances (and hence S-saturation conditions) of the West and East Greenland picrites are very similar. Therefore, as in the Skaergaard intrusion of East Greenland, it might be considered that there is a potential for economically viable PGE deposits within West Greenland.

7: Geochemistry of Grenada Volcanic Rocks

7.1 Introduction

The island of Grenada is situated at the Southern end of the Lesser Antilles arc (Fig 7.1). The Lesser Antilles is an intra-oceanic arc which has developed over the past 40 million years as a result of westward subduction of the Atlantic plate beneath the Caribbean plate. It extends some 850km along the eastern edge of the Caribbean Plate, beneath which Atlantic Ocean crust of Cretaceous to Jurassic age is being subducted at a rate of 2.2–3.8cm/a. The Benioff zone has an average dip of 45° and is at a depth of 100-120km beneath the volcanic arc. The crust beneath the arc is about 30km in thickness and has typical island arc and oceanic crustal seismic velocities (White and Dupré, 1986) and references therein). Two major periods of vulcanicity have formed the Lesser Antilles arc over the past 40Ma. In the north, following the initial period of Pre-Miocene vulcanism, the axis of the arc migrated westward prior to the Miocene - Recent activity (Arculus, 1973) giving the two distinct arcs in this region (Fig 7.1). In the south however, the centres of the Tertiary and Quaternary vulcanism coincided and thus the Southern Lesser Antilles arc is regarded as mature (Davidson and Harmon, 1989).

Grenada was selected as a suitable area to study the behaviour of PGEs in an arc-system as the geochemistry of the volcanics has been well characterised (Thirlwall *et al.*, 1994, 1996; Turner *et al.*, 1996). Grenada is unusual amongst intra-oceanic island arcs in that highly magnesian (10-15% MgO) basalts are common (Arculus, 1973). These high MgO lavas represent a suitable starting point for characterising the PGE signatures of arc rocks, as they should contain measurable quantities of the PGEs. In addition, the occurrence of cumulate blocks within some Grenada lavas presents an ideal opportunity to directly observe the possible effects of crystal fractionation on PGE abundances and inter-element ratios.

These near-primary lavas show a wide variation in chemistry, from tholeiites with near-flat REE patterns to SiO_2 undersaturated basalts. They are associated with low-Mg basalts and andesites by open and closed system fractionation processes

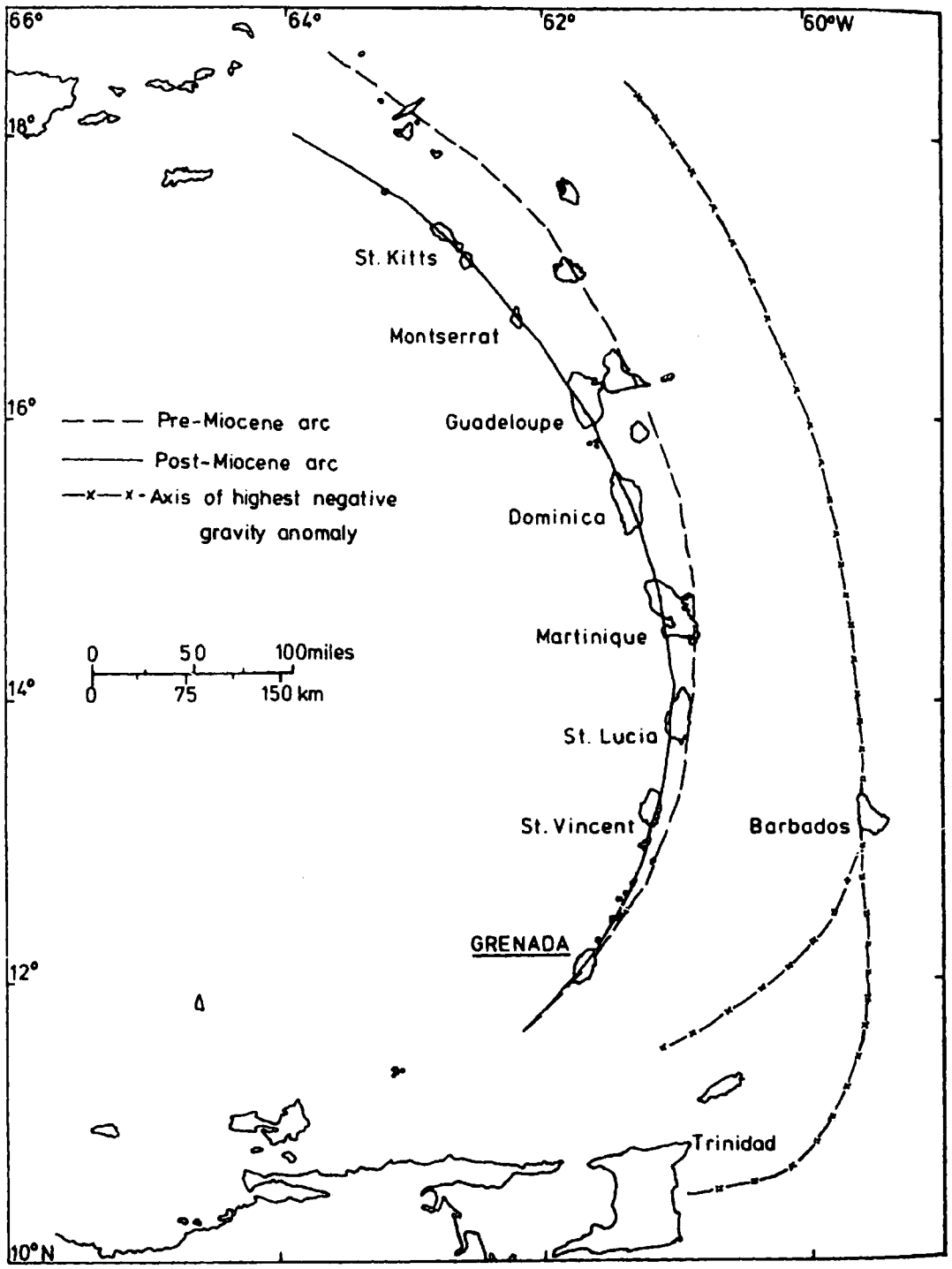

Fig 7.1 Location Map for The Lesser Antilles Arc (Note positions of both Pre and Post-Miocene Arcs) (from Arculus, 1976).

(Thirlwall *et al.*, 1994). Thus, Grenada also represents an ideal system in which to observe the behaviour of the PGEs during fractionation in an arc system. Finally, the presence of picritic magmas on Grenada provides a rare opportunity to determine the PGE signature of the sub-arc mantle, as the picritic lavas have undergone relatively little chemical modification since their derivation from the mantle wedge. Such magmas are probably relatively unaffected by crustal contamination, as this would lead to cooling and olivine precipitation (White and Dupré, 1986). The unusual alkalic geochemistry of Grenada has been linked to the tectonic setting of the island near the lateral edge of the subduction zone where hinge faulting occurs (Wilson, 1989).

7.2 General Geology of Grenada

The geology of Grenada was first described by Martin-Kaye (1969). The next extensive study was conducted by Arculus (1973) who mapped many of the geological formations on Grenada. No pre-Tertiary horizons have been discovered on Grenada, the post Miocene volcanics being underlain by a tectonically disturbed series of volcano-sedimentary rock units (Tufton Hall Formation; Fig 7.2). The Miocene - Recent volcanics were mapped by Arculus (1973) and subsequently subdivided into a number of main volcanic centres (Fig 7.10) based on field, petrological and geochemical evidence. The main volcanic centres identified on Grenada are given in Table 7.1.

Centre		**Probable Period of Activity**
Mt. St. Catherines	(MSC)	? 50,000 - 20,000yrs
Mt. Granby-Fedon's Camp	(MGF)	? 1 Myrs - ?50,000yrs
Sinai - Mt. Maitland – Mt. Moritz	(SMM)	2 -1 Myrs
South East Mnt.	(SEM)	? 2 Myrs
Southwest Grenada	(SWG)	4-3 Myrs
Northern Domes	(ND)	? 4 Myrs

Table 7.1 Probable eruption ages of the main Grenadian volcanic centres (Arculus, 1973)

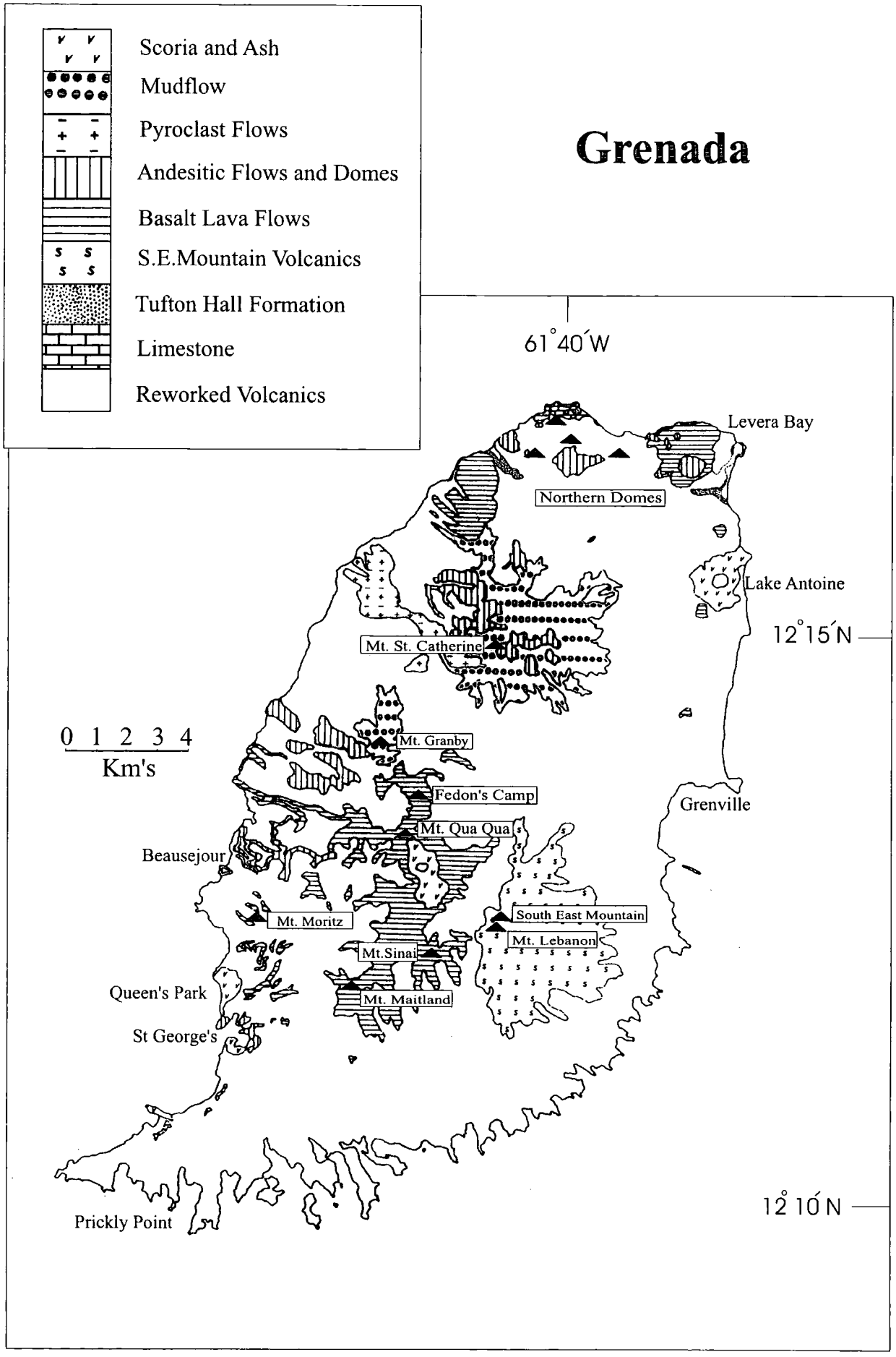

Fig 7.2 Geological Map of Grenada (after Arculus, 1973)

The eruption order and ages proposed above are based on field observations and K-Ar dating (Arculus, 1973). Grenada volcanic activity was characterised by the eruption of lava flows and pyroclastic falls. A prominent feature of Grenadian geology is the large surface area of the island occupied by secondary or reworked volcanic detritus, redistributed from its original proximity to the main volcanic centres by the heavy rainfall on Grenada (Arculus, 1973). Exposure is poor on Grenada as a result of heavy tropical vegetation

7.3 Classification of Grenadian Volcanics

Most of the lavas in the Lesser Antilles, including those on Grenada, belong to the calc-alkaline suite (Arculus, 1973). Initial classifications of Grenada rocks were based on both geochemical and petrological evidence. Arculus subdivided the volcanics according to weight percentage silica (Fig 7.3). Obvious mineralogical features (such as abundance of olivine or clinopyroxene) were then added as prefixes to the appropriate names.

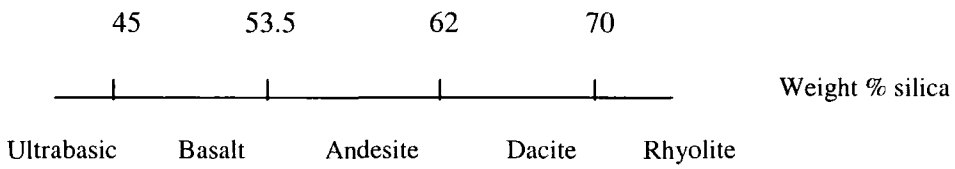

Fig 7.3 Class divisions of volcanic rocks used by Arculus (1973)

Although Arculus (1976) recognised the petrographic and some geochemical differences between the basic lava suites, the marked chemical differences now used to classify Grenadian lavas only became clear when systematic errors were discovered in the major element data produced by Arculus (Thirlwall and Graham, 1984; Thirlwall *et al.*, 1996). As such, the Grenada basalts were further subdivided into an M-series (magnesian and olivine microphyric) and a C-series (calcic and clinopyroxene phyric) by Thirlwall and Graham (1984). The geochemical signatures of these respective series will be discussed further in section 7.7.

7.4 Petrology of Grenada Volcanics

The volcanic rocks of Grenada are characterised by a compositional continuum from picrites, to basalt and andesite, and by the occurrence of basic cumulate blocks. The typical petrological features of each of the major rock types are illustrated in the following section, with examples from samples collected during this project. Microprobe analyses of the constituent minerals within the volcanics were beyond the scope of the project and thus compositions of the minerals are inferred from reference to the extensive petrological and mineralogical studies of Arculus (1973; 1976; 1978).

7.4.1 The Picrites and Basalts

The picrites and basalts are predominantly composed of olivine, clinopyroxene, plagioclase and spinel, with textures varying from microphyric to coarsely porphyritic. Arculus (1973) noted that the gradational nature of the compositional variation between the picrites and basalts is reflected to some extent in their petrography and mineralogy. Figs 7.4-7.6 illustrate the typical mineralogy of the picrites and basalts. The picritic rocks analysed during this study (e.g. Fig 7.4) all have broadly similar mineralogies, with varying modal proportions of the major phenocryst phases: olivine, ± cpx, ± plagioclase feldspar. Well-developed prismatic olivine is common and forsteritic (Fo_{90-75}) in composition (Arculus, 1973). The olivines sometimes show orange iddingsitic alteration depending on the freshness of the sample. This feature leads to the petrological classification of the M-series as olivine microphyric. Arculus (1973) identified modal nepheline within the groundmass of some picritic samples with the use of a microprobe, thus, some Grenada picrites are mildly silica undersaturated in composition.

Within the basalts (Figs 7.5 & 7.6) calcic augite phenocrysts commonly showing complex oscillatory zoning become a more prominent phenocryst phase. These augite crystals sometimes demonstrate a darkening in colour from core to rim, which corresponds to increasing enrichment in Ti (Arculus, 1978). Olivines within the C-series basalts (Fig 7.5) are slightly less forsteritic (Fo_{85-71}) in composition than those in the picrites (Arculus, 1973). Typical M-C transitional basalts (Fig 7.6) contain zoned clinopyroxene phenocrysts similar to those of the C-series basalts.

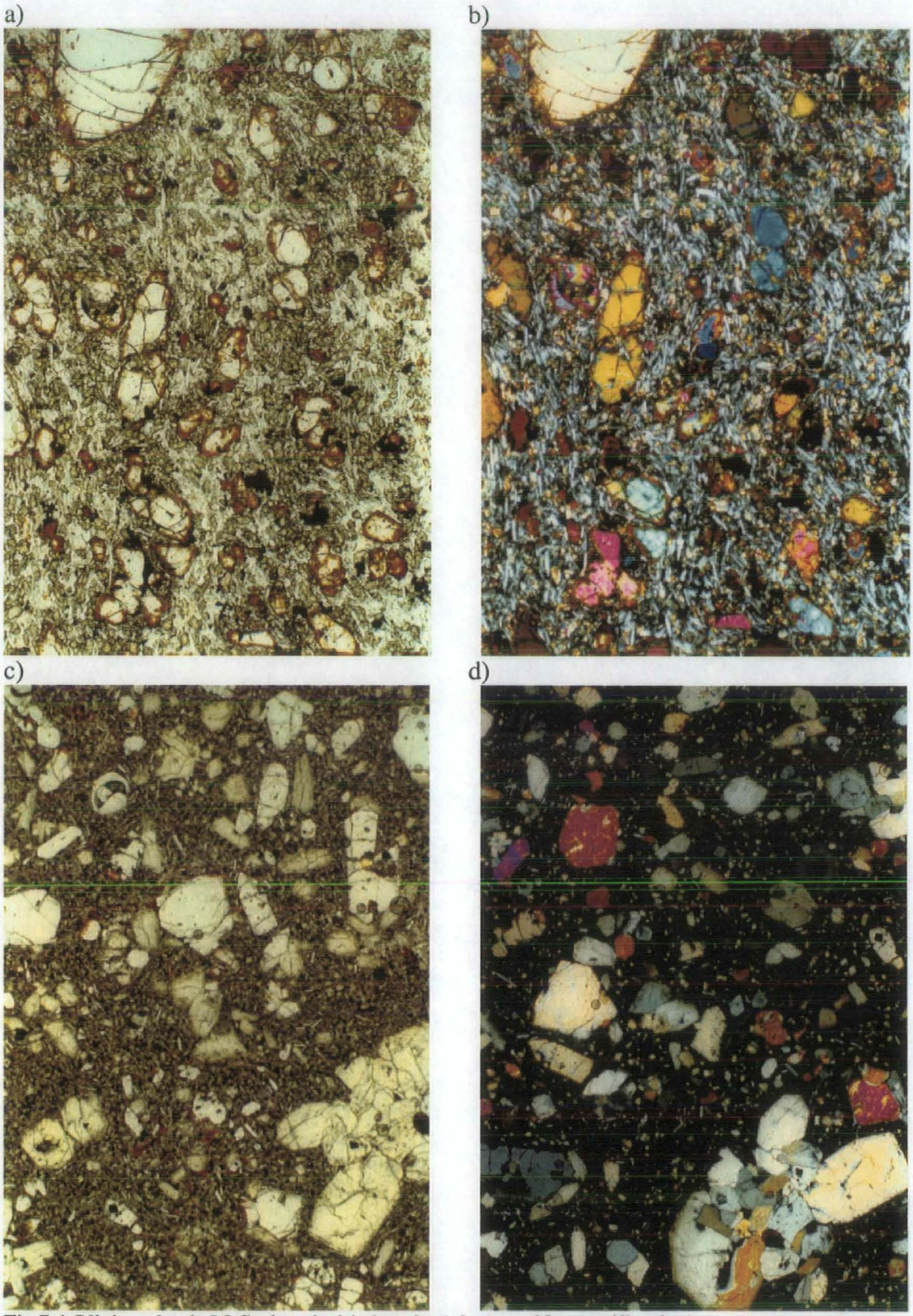

Fig 7.4 Olivine phyric M-Series picritic basalts (photos x 10 magnification)
a) & b) Gd 14 – Olivine phyric, picritic basalt (M-Series). Note euhedral olivine phenocrysts (with orange iddingsite rims), aligned in flow-textured groundmass of plagioclase laths, pyroxene and opaques.
c) & d) Gd 16 – Porphyritic M-Series picrite. Main phenocryst phases are olivine and clinopyroxene (pale green body colour). Microcrystalline groundmass contains plagioclase laths and finely disseminated opaques.

a)

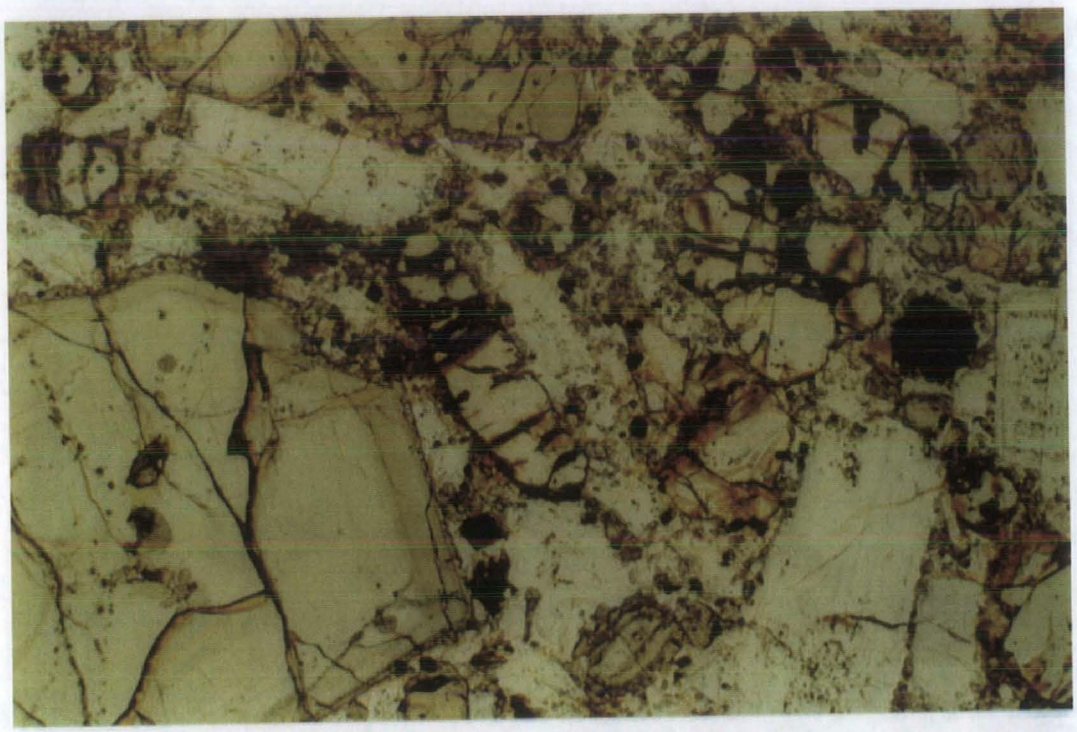

b)

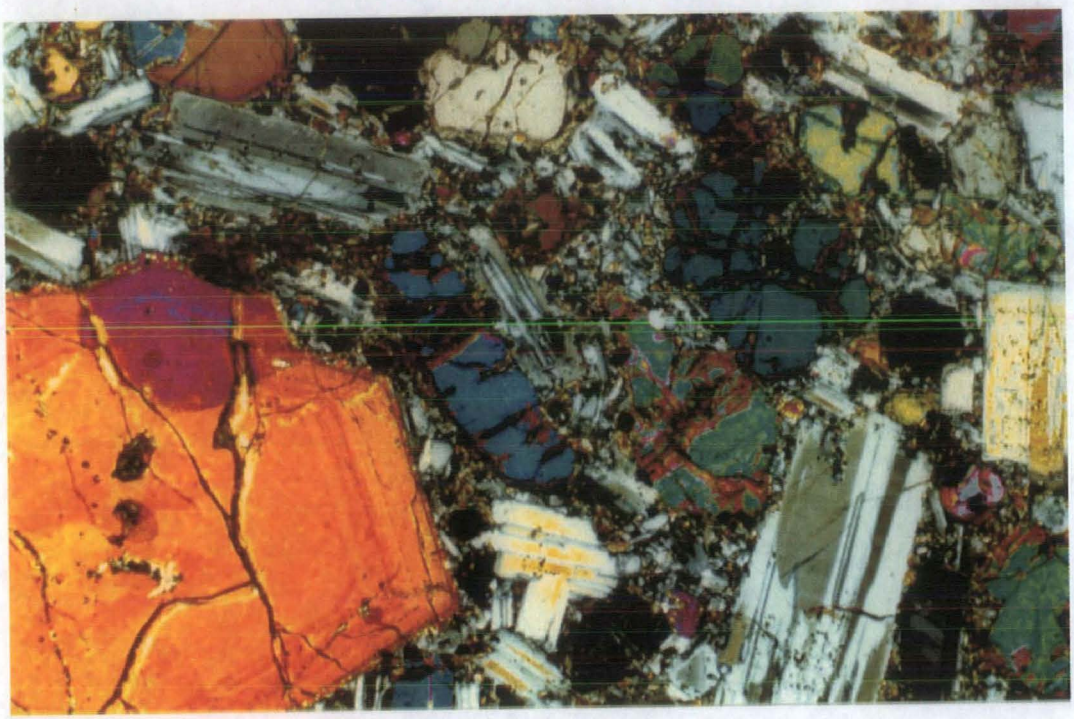

Fig 7.5 Olivine – clinopyroxene phyric M-C transitional basalt (photos x 10 magnification)

a) & b) Gd 5 – Note presence of large oscillatory zoned clinopyroxene (cpx) phenocryst, prismatic iddingsitized olivine phenocrysts and oscillatory zoned plagioclases (shown by melt inclusions in p.p.). Groundmass consists of fine plagioclase and pyroxene. Opaques occur predominantly within the groundmass.

a)

b)

c)

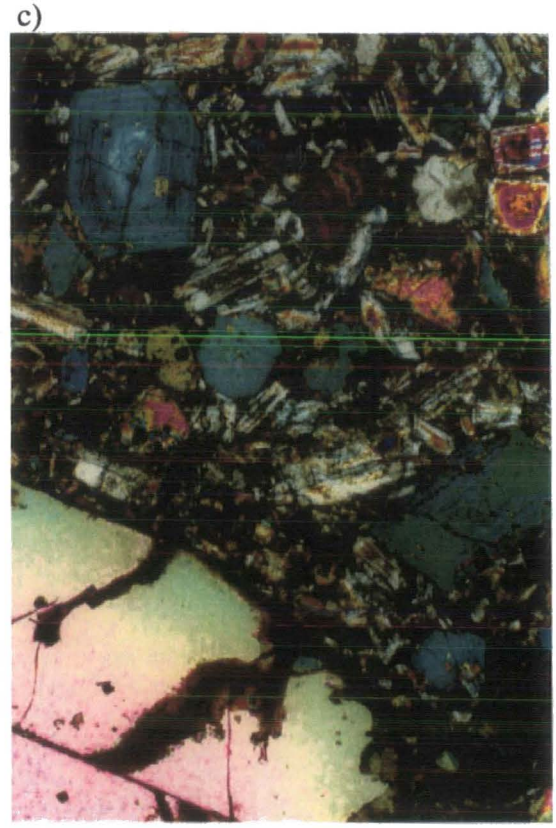

Fig 7.6 Clinopyroxene phyric C-series basalts
a) Photo of a typical C-Series basalt in hand specimen, cpx phenocrysts commonly 5mm in size.
b) & c) – Gd21 (photos x 10 magnification). Oscillatory and sector zoned cpx's are the main phenocryst phase (note paler colour of cores). Occasional isolated olivine crystals also occur (up to 1cm in size) – suggesting importance of olivine in the fractionating assemblage from which the C-Series are evolved. Opaques are widespread within both phenocrysts and groundmass.

The M-C series also contain a higher modal abundance of olivine, which probably accounts for their generally more magnesian composition. Glomeroporphyritic clusters of clinopyroxene, olivine and plagioclase often occur within the porphyritic basalts and the picrites. Glomerocrysts have the same composition as phenocrysts and probably represent cognate crystal accumulations, rather than xenocryst clusters (Arculus, 1973). Plagioclase crystals again have high An content ($An_{>80}$) and oscillatory zoning characteristic of calc-alkaline rocks. Some Grenadian basalts also contain amphibole (Arculus, 1973), although none was found in the samples analysed in this study.

7.4.2 The Cumulates

Plutonic blocks composed of variable proportions of plagioclase feldspar, amphibole, olivine, clinopyroxene and magnetite are found in several localities in Grenada (Arculus, 1973). The samples analysed in this study were recovered from Prickly Point in south-west Grenada (Fig 7.10) and are of two contrasting types (Fig 7.7 & 7.8). Fig 7.7 illustrates the first type of cumulate (e.g. Gd2 & Gd3) which consists of plagioclase, amphibole and opaques. This sample has an equigranular texture with the amphibole poikilitically enclosing the plagioclase and opaques, suggesting that amphibole crystallised last. The second type of cumulate (Gd1, Fig 7.8) consists predominantly of coarse (1-2cm) amphibole crystals held together by altered intercumulus glass. The thin section illustrates how the amphibole poikilitically encloses clinopyroxene, opaques and another minor phase (extensively iddingsitized olivine). The intercumulus glass is highly altered but contains microlites of feldspar.

The cumulate-block plagioclase is generally more calcic (An_{89-96}) than any of the phenocrysts in the lavas (Arculus, 1978) and there is a noticeable lack of zoning in cumulate plagioclase and clinopyroxene phenocrysts when compared to the lavas. The modal abundance of amphibole (pargasitic hornblende) is much greater in the cumulates than in any of the lavas on Grenada and may probably relates to the instability of amphibole at low-pressures in the lavas (Arculus, 1978).

a)

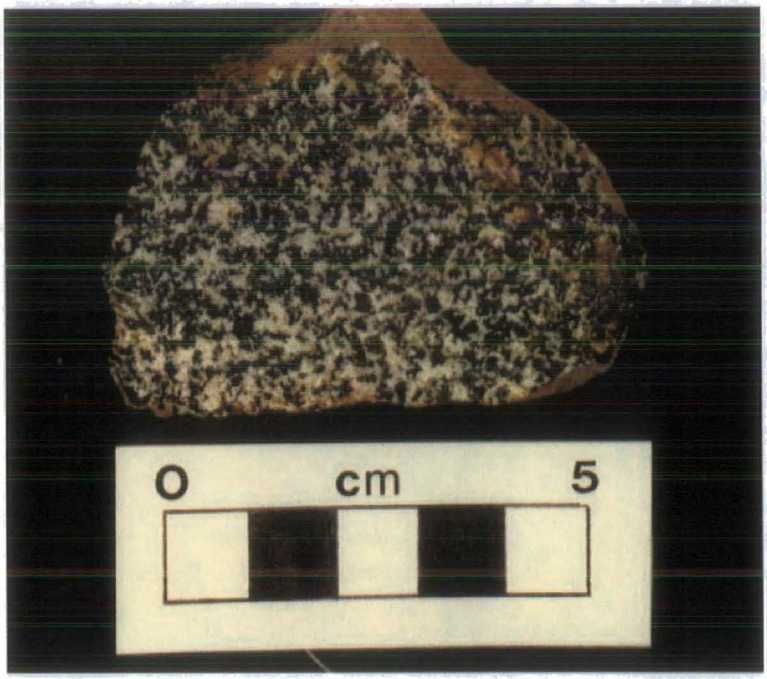

a)

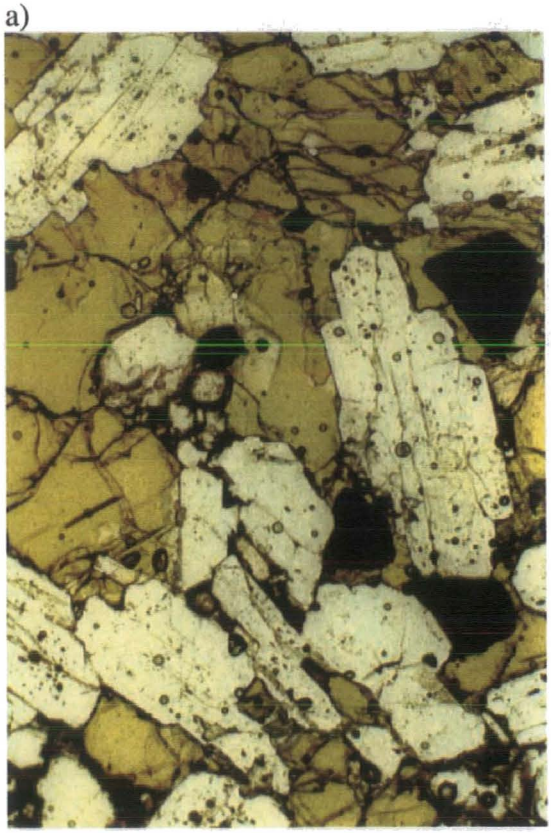

b)

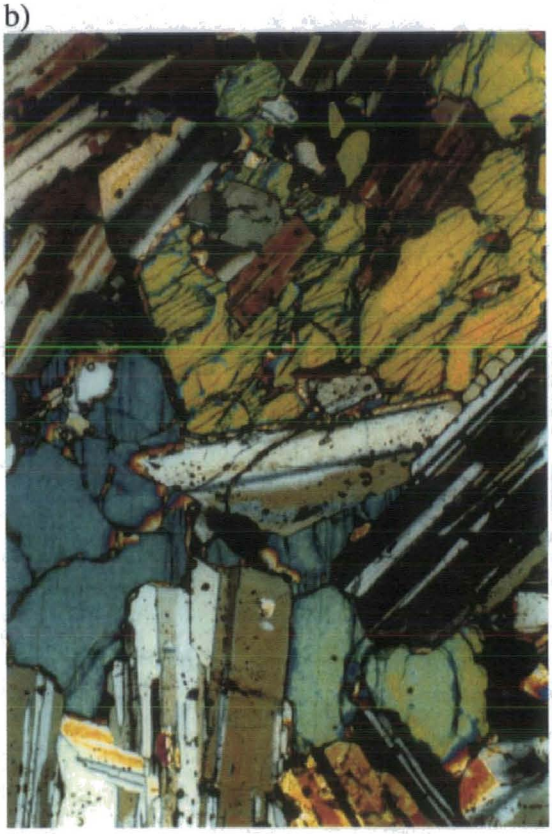

Fig 7.7 – Plagioclase-amphibole rich cumulate
a) Specimen Gd3 in hand specimen (Gd2 = identical mineralogy, but slightly finer grain size) b) & c) Gd 3 (photos x 10 magnification). Equigranular cumulate texture is apparent. Amphibole (green in plane polars) poikilitically encloses plagioclase crystals. Fine opaques are included within the plagioclases, whereas later, more euhedral opaques are included within amphibole.

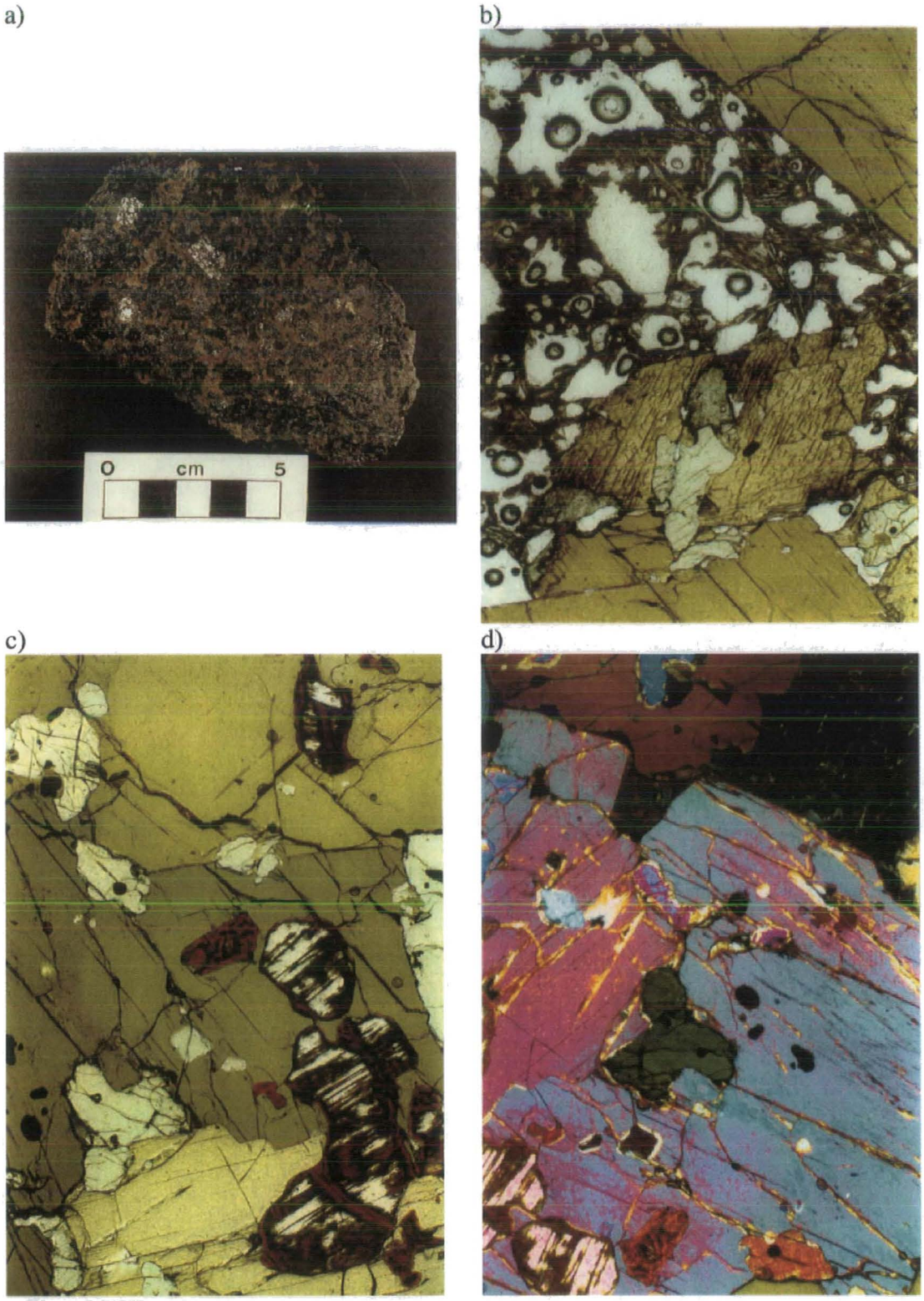

Fig 7.8 Amphibole-rich cumulate
a) Gd1 in hand specimen. Large amphibole crystals are poorly bound by highly altered intercumulus glass.
b) Gd1 (photos x 10 magnification) showing intercumulus glass in plane polars Note quench textured plagioclase crystals (glass appears almost isotropic under cross polars).
c) & d) Gd1 (photos x 10 magnification). Large amphibole crystals, poikilitically enclose smaller cpx crystals (paler green in plane polars.) and opaques. cpx's in cumulates do not show oscillatory zoning and have opaque inclusions. Note presence of another highly altered phase (possibly iddingsitized olivine – in disequilibrium with cumulate assemblage).

7.4.3 The Andesites

The dominant phenocryst phases within the andesites of Grenada are plagioclase feldspar, clino- and orthopyroxene, amphibole and magnetite. Characteristically, the andesites are extremely porphyritic with abundant oscillatory-zoned plagioclase feldspars (Fig 7.9). The absence of olivine in the groundmass and as a phenocryst mineral in many andesitic compositions, indicates that olivine is no longer a stable component of the andesitic assemblage. Fig 7.9 illustrates and compares two of the different andesite-types found on Grenada. Fig 7.9 (a+b) is a basic andesite (ca. SiO_2 >50%, Thirlwall *et al.,* 1996) and contains a high proportion of sector-zoned clinopyroxene. Fig 7.9 (b+c) is referred to as a high SiO_2 andesite on the basis of its major element chemistry (ca. SiO_2 >58%, Thirlwall *et al.,* 1996). The felsic nature of this rock is obvious, plagioclase being the main constituent of both groundmass and phenocryst phases. A resorbed amphibole phenocryst in this sample implies that amphibole was unstable in the magma.

7.4.4 Distribution and Variation of Opaque Phases Across the Fractionation Suite

Opaque phases are widely distributed throughout the compositional range of rocks analysed on Grenada (Figs 7.4-7.9). There is a wide range of compositional variation in Grenadian spinels from chrome-free, to chromite, to titaniferous magnetite, even within a single section (Arculus, 1978). In the Grenada basalts, the Cr- and Al-rich spinels occur predominantly as inclusions within silicate phenocrysts and titaniferous magnetite is the groundmass composition. Titaniferous magnetite is also the main opaque phase within Grenada andesites. Arculus (1978) suggests that a spinel solid solution was an early crystallising phase and that there was no hiatus in spinel fractionation during differentiation of the suite. The abundance of magnetite is greater in the cumulates than in the supposed equivalent lavas, probably as a result of gravity sorting (Arculus, 1978).

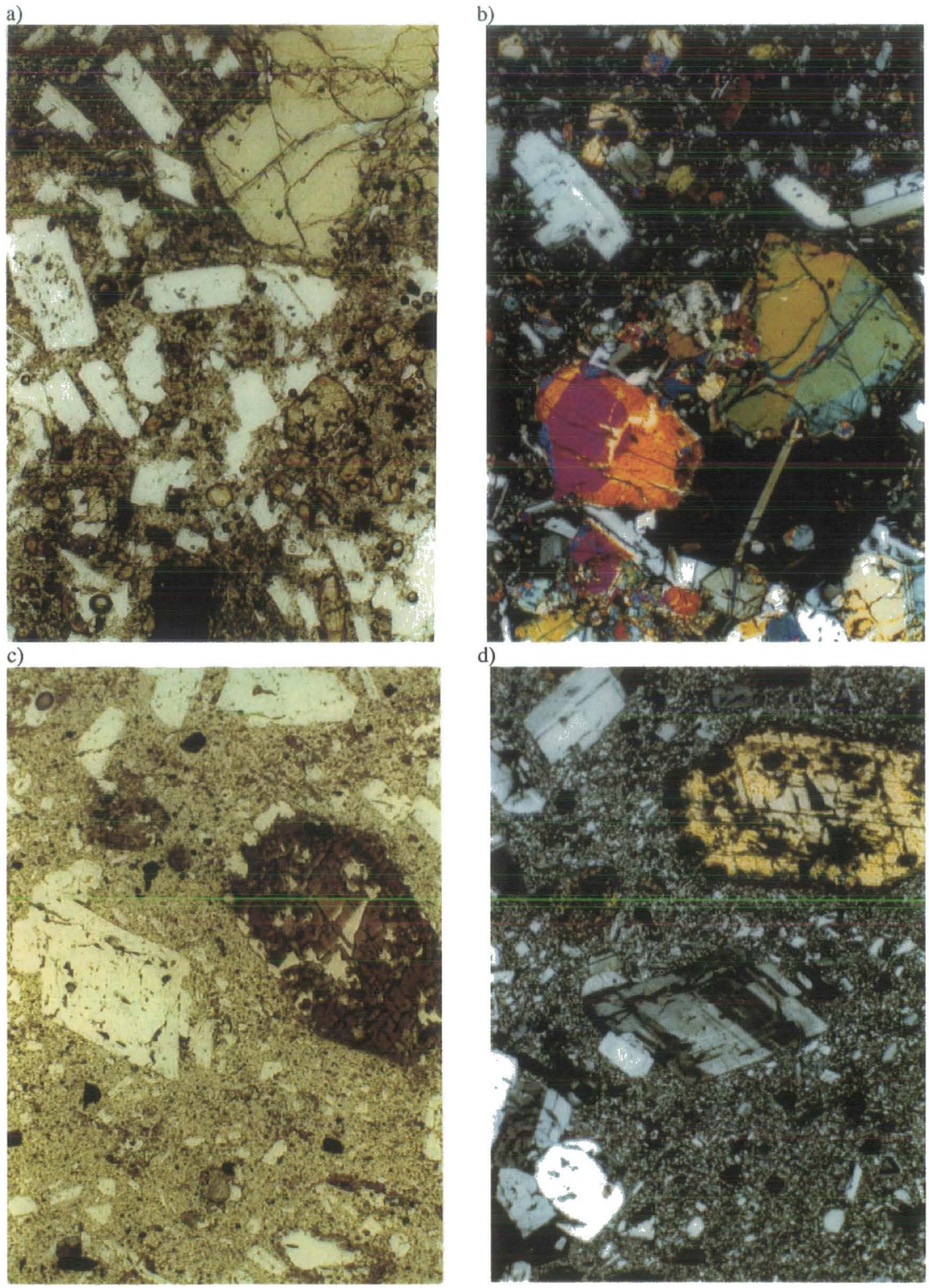

Fig 7.9 Andesites
a) & b) Gd17; Basic Andesite (photos x 10 magnification). Main phenocryst phases are plagioclase (sometimes zoned), opaques (some with cubic form) and cpx (showing sector rather than oscillatory zoning). Cpx crystals have a glomeroporphyritic texture. The groundmass consists of plagioclase and pyroxene microlites and has been sericitically altered. c) & d) Gd25; High SiO_2 Andesite (photos x 10 magnification). The assemblage is dominated by felsic minerals. The main phenocryst phases are plagioclase (sometimes showing zoning) and quartz. Also present however are occasional, badly corroded amphibole phenocrysts. Opaques present in groundmass, but less abundant than in other specimens.

7.5 Sample Collection

With the exception of samples AMG 6078, 6103 and 6157 (provided by M. Thirlwall) all samples were collected during March 1997 by the author and have the prefix Gd (for Grenada). The samples collected in this study belong mostly to the MGF and SMM centres (assignation being based on proximity to these centres; Fig 7.10). Determination of exact provenance of samples is difficult due to poor exposure. Samples collected at Prickly Point, although in the vicinity of the SWG volcanic centre, are probably derived from the younger SMM centre (e.g. the cumulus blocks Gd1, Gd2 & Gd3) based on the observations of Arculus (1973). The basalt sample Gd5 analysed during this project was also collected from Prickly Point, but because of its M-C transitional chemistry is probably derived from the MGF centre.

7.6 Compositional Variation of Samples Analysed

A suite of rocks spanning the compositional range on Grenada were selected for analysis of PGEs. Particular interest was focussed on the more picritic compositions in order to form a comparison with the picrites analysed from Greenland (Chapter 6). The samples analysed for PGEs are listed in Table 7.2 Classification of the rocks analysed is based on both petrological and geochemical evidence. The main petrological features of the sample set were illustrated (Fig 7.4-7.9) and discussed earlier in this chapter and are summarised in Table 7.2. The volcanic centres from which the samples were collected are also illustrated in Table 7.2. The full major and trace element chemistry of the Grenada lavas analysed are presented in Appendix I. All XRF and REE analyses (by ICP-MS) were carried out by the author at Durham (with the exception of AMG 6078, 6103 and 6157 - data in Thirlwall *et al.*, 1996). Details of XRF and ICP-MS sample preparation are also presented in the Appendices.

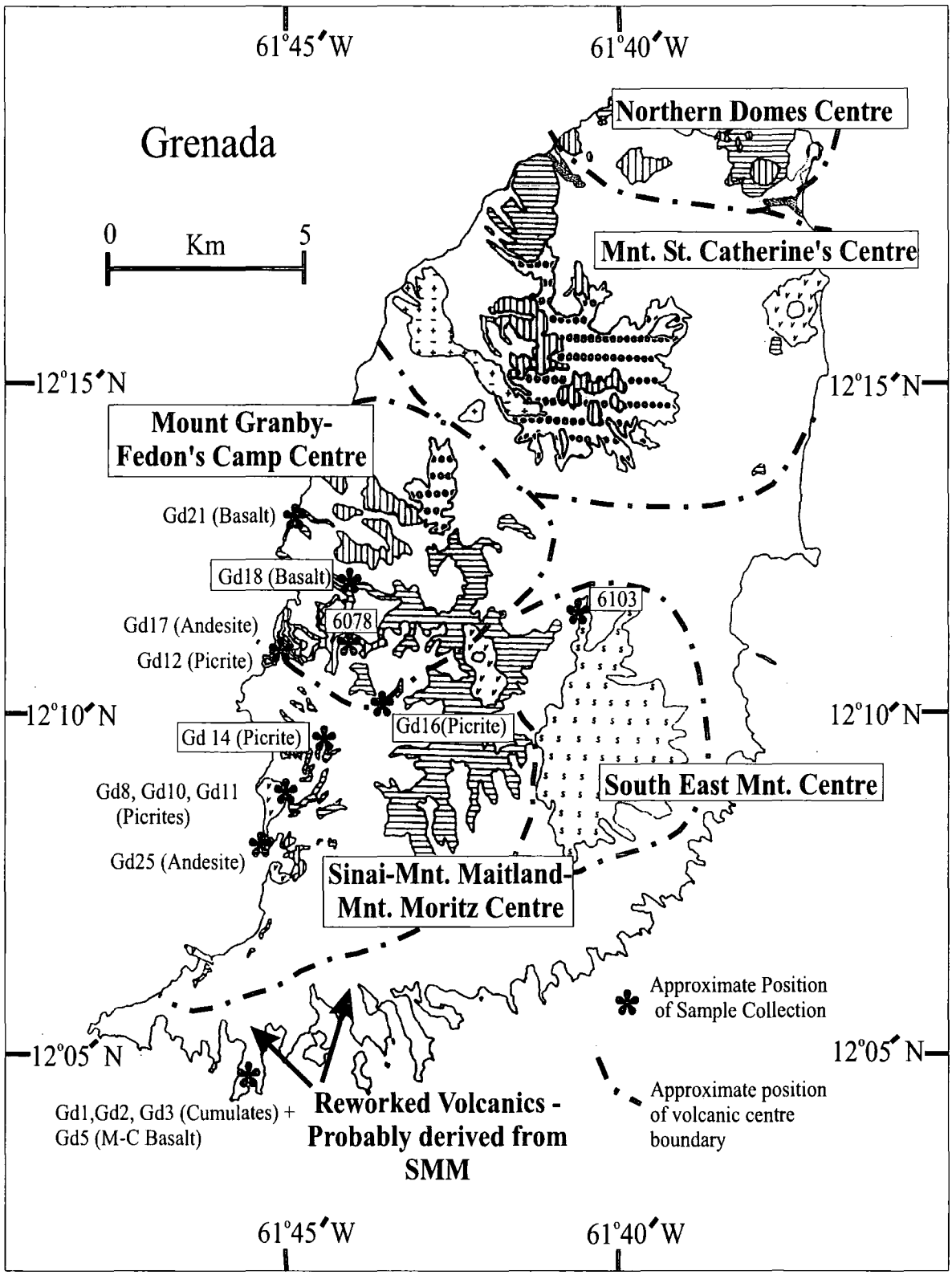

Fig 7.10 Map of Grenada showing approximate sample locations for samples analysed

7.7 Geochemical Classification of Grenadian Volcanics

7.7.1 Introduction

All of the samples from Grenada analysed during this project belong to the calc-alkaline group of rocks (Fig 7.11). On Grenada, the rocks range in composition from mildly undersaturated basanitoids (most basalts have less than 1-2% normative nepheline) (Thirlwall and Graham, 1984), to silica-saturated (modal quartz-bearing) andesites and dacites (Arculus, 1973). Although early classification schemes for Grenada basalts were based on normative parameters (Arculus, 1976), better subdivisions of the Grenadian suites became possible based on major element, trace element and isotopic differences (e.g. Thirlwall and Graham, 1984).

	Series	Basic Petrology and Composition	Volcanic Centre	Figure
Gd17	M-series	Basic andesite (<9% MgO, > 51% SiO_2)	MGF	7.9
Gd25	M or C-series	High SiO_2 Andesite (<3.5% MgO),	MMM	7.9
Gd1	Cumulate	Hornblende rich	MMM ?	7.8
Gd2	Cumulate	Plag - amphibole	MMM ?	
Gd3	Cumulate	Plag - amphibole	MMM ?	7.8
Gd8	M-series, low La/Y	Picrite - > 11% MgO, <48% SiO_2	MMM	
Gd10	"	"	MMM	
Gd11	"	All M-series picrites olivine phyric	MMM	
Gd14	"	"	MMM	7.4
Gd12	M-series, High La/Y	Picrite	MGF	
Gd16	"	"	MMM	7.4
Gd5	M-C transitional ?	Basalt - > 47% SiO_2, ~11% MgO	?	7.5
Gd21	C-Series	Basalt <9% MgO	MGF	7.6
Gd18	C-Series	(all C-series basalts cpx phyric)	MGF	
6078	M-series, High La/Y	Picrite	MGF	
6103	"	"	SEM	
6157	Low La / Y	M-C transitional Picrite	MGF	

Table 7.2. Classification of Grenada samples analysed, series divisions after Thirlwall *et al.* (1996)

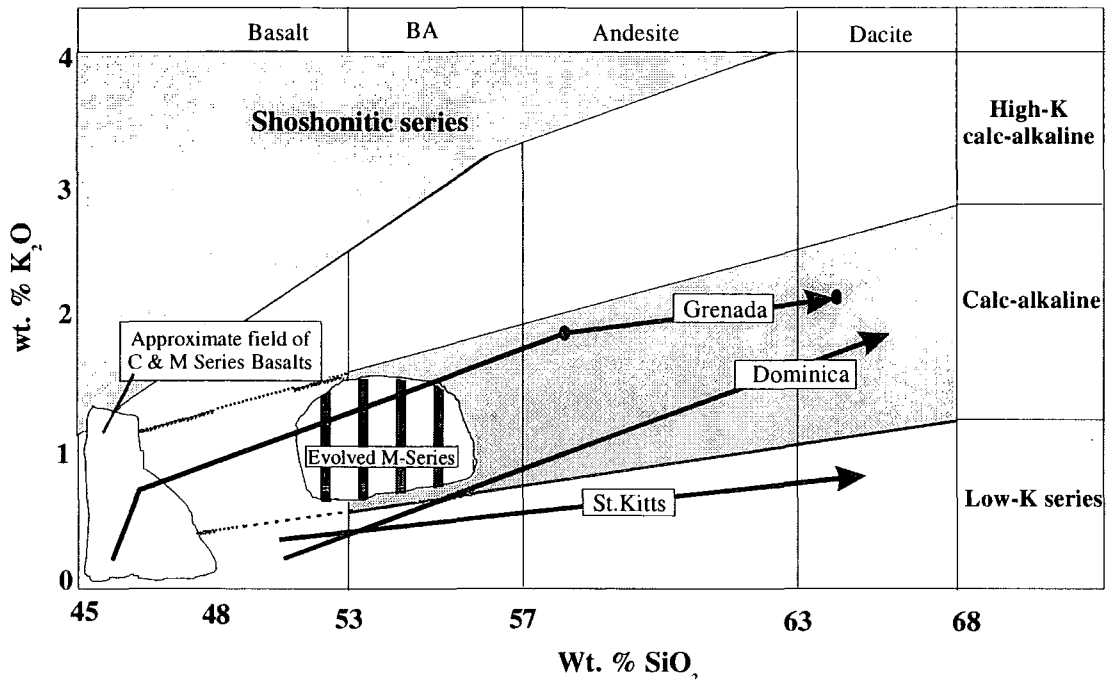

Fig 7.11 Comparison of Grenada lavas to those from other islands in the Lesser Antilles arc (from Wilson, 1989)

7.7.2 Major Element Characteristics of Grenadian Rocks

Simple SiO_2 vs MgO plots do not adequately represent the diversity of basaltic compositions on Grenada as MgO rapidly increases for only a minor change in SiO_2 across the transition from basalts to picrites. The use of a MgO vs CaO plot, however, proves to be a good discriminant, as at least two separate groups (and one transitional group) form discrete clusters (Fig 7.12). This discrimination forms the basis of the subdivision between the C and M series of Grenada as defined by Thirlwall *et al.* (1996).

The M-series picrites have more Mg-rich and often less calcic compositions than the C-series. The Mg-characteristics are either due to increased accumulation of Mg-rich olivine phenocrysts within the M-series, or greater removal of olivine from the C-series compared to the M-series. The trend of Ca-enrichment and then depletion within the C-series (relative to the M-series) must be due to differential amounts of accumulation and fractionation of cpx and plagioclase from the melt, as implied by the presence of large cpx-phenocrysts and plagioclase crystals.

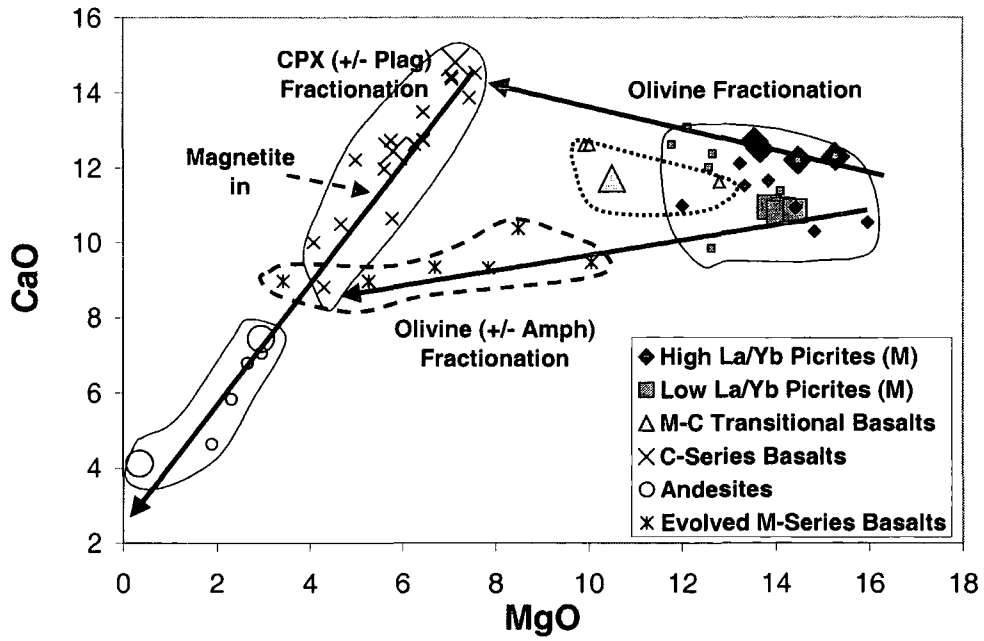

Fig 7.12 Harker-type major element diagram illustrating the subdivision of the C and M-series of Grenada – Large symbols are for data analysed during this study, small symbols represent data from Thirlwall *et al.* (1996).

During fractional crystallisation of the M-series (Fig 7.12) Mg rapidly decreases for relatively little change in the Ca-content. This suggests that M-series compositional variation arises because of olivine fractionation/accumulation, rather than cpx removal from the magma. Both M- and C-series magmas can evolve towards andesitic compositions via fractionation of the phases shown in Fig 7.12.

Variation of Na_2O, Fe_2O_3 and SiO_2 (Fig 7.13) illustrate that between 6 and 16% MgO, the fractionation trends defined by the M-series picrites, M-C transitional basalts and C-series basalts remain relatively flat, with large decreases in MgO for only minor increase in the other elements. This is due to the overriding effect of olivine fractionation which rapidly depletes MgO with little effect on the other major elements. At less than 6% MgO, Na_2O and SiO_2 rapidly increase with decreasing MgO through the C-series basalts and andesites as fractionation proceeds. Conversely, Fe_2O_3 rapidly decreases with decreasing MgO past 6% MgO. This happens midway through fractionation of the C-series and probably marks the beginning of magnetite fractionation, which then continues throughout the evolution of the magmas towards andesitic compositions.

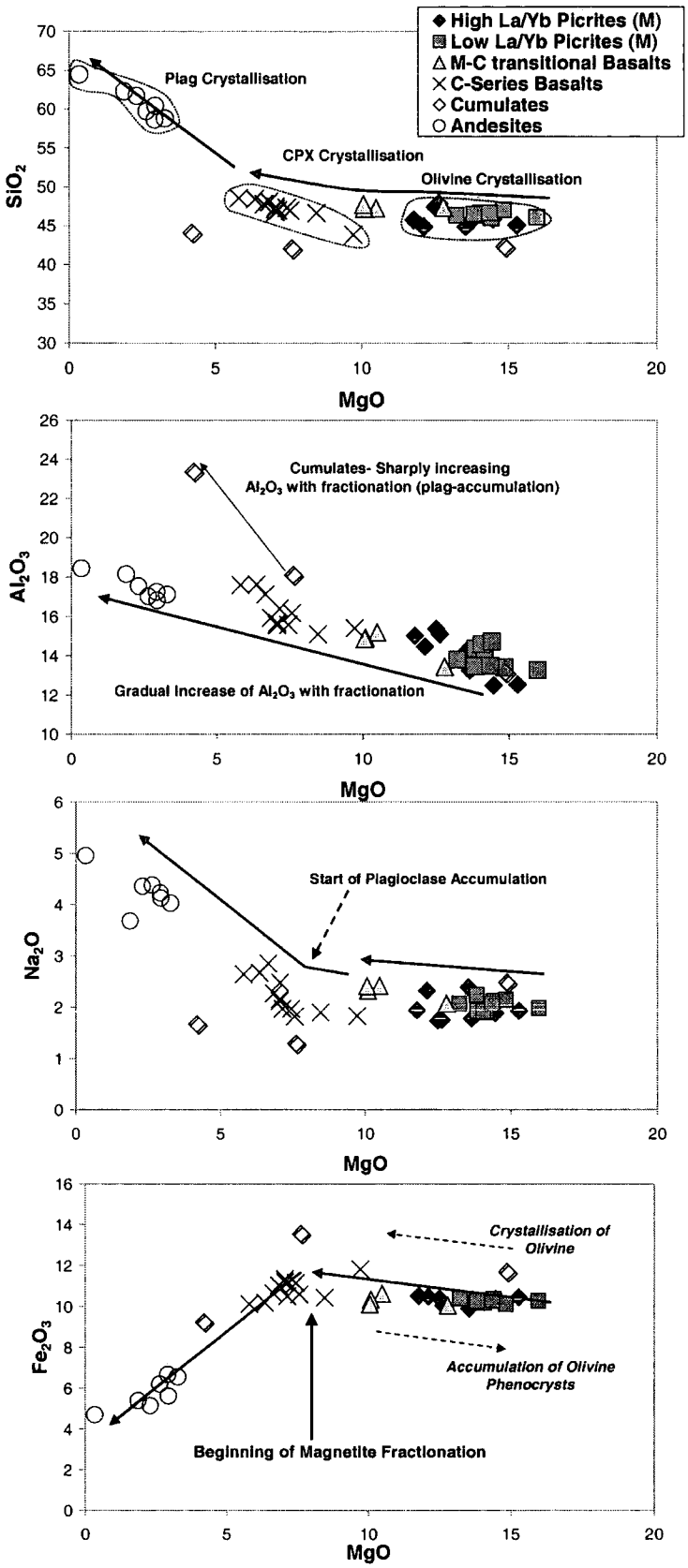

Fig 7.13 Harker-type diagrams for selected major elements

The Al_2O_3-contents of the Grenada lava suite systematically increase with decreasing MgO due to the incompatibility of Al during olivine fractionation. A sharp increase in Al_2O_3-content is observed within the cumulates as fractionation proceeds. This is attributed to the observed accumulation of plagioclase phenocrysts. The trends of Mg enrichment/depletion within the M-series picrites and C-series basalts can be attributed to one of two processes:

1) enrichment- due to accumulation of Mg-rich olivine phenocrysts within the melt; or,

2) depletion- due to removal of Mg-rich olivine phenocrysts from the melt.

It is assumed that variation in MgO concentrations of the M-series picrites is mainly due to variable degrees of olivine accumulation rather than fractionation. This is based on the modelling and Mg No. calculations of Arculus (1976) which suggest that "extensive fractionation of any one phase, or combination of phases, such as garnet, cpx, opx or olivine has not occurred". The presence of ubiquitous olivine phenocrysts within the M-series confirms that their accumulation may be the cause of variation in Mg-concentrations within the M-series. The M-C basalts and C-series basalts lie along a continuum from the M-series basalts with decreasing MgO (Fig 7.13). The M-C basalts and C-series basalts, however, contain a lower proportion of olivine phenocrysts than the M-series picrites (Table 7.3). It is suggested that the major element characteristics of the M-C basalts can be explained by approximately 7.3% fractionation of olivine from an M-series picritic melt, whereas the C-series basalts can be generated by fractionation of up to 16% olivine from a similar M-series picritic melt (Thirlwall *et al.,* 1996).

In order to determine the effect of olivine accumulation/fractionation on the whole-rock MgO concentrations, the percentage of olivine phenocrysts within each of the samples analysed during this study has been estimated (Table 7.3).

The composition of the primary melt, prior to olivine accumulation can be calculated using the Lever Rule (Albarède, 1995):

Conc. Primary Melt = Frac.Ol x Conc.Ol. + (1- Frac.Ol.) x Conc.Residual Melt

(where Frac.Ol = % of olivine phenocrysts, as a mass-fraction), Conc.Ol = Wt% MgO in olivine and Conc.Residual Melt = whole rock MgO)

Sample Name	Series	W.R. MgO Content (wt %)	% of Olivine Phenocryts	~ Fo Number	Wt% MgO in Olivine
Gd8	M-series Picrite - Low La/Yb	13.86	~10%	85	44.8
Gd10	"	14.15	5-10%	85	44.8
Gd11	"	14.06	12%	85	44.8
Gd14	"	14.41	20%	85	44.8
Gd12	M-series Picrite - High La/Yb	13.66	10-15%	85	44.8
Gd16	"	13.55	~5%	85	44.8
Gd5	M-C transitional Basalt	10.49	8%	82.5	43
Gd21	C-Series Basalt	7.15	<2%	78	40.6
Gd18	C-Series Basalt	5.8		78	40.6

Table 7.3 Compilation of approximate olivine phenocryst content and composition of M-series picrites and C-series basalts. Percentage of olivine phenocrysts estimated from thin sections (Fo numbers and corresponding Wt% MgO of olivines, after Arculus, 1973, 1978).

Approximate primary melt MgO compositions (wt%) are thus estimated at between 6.8% and 11.9% for the M-series picrites (the former value representing removal of 20% olivine and the latter value removal of 5% olivine). This suggests that some of the M-series "picrites" are only picritic in nature because of excess olivine accumulation. For the M-C transitional basalt, removal of ~8% olivine phenocrysts generates a primary melt composition of 7.7% MgO. In contrast, for the C-series basalts, the calculated primary melt composition after removal of <2% accumulated olivine phenocrysts is 6.5% MgO. Thus, removal of a significant proportion of the olivine phenocrysts from a high MgO M-series melt would seem to be capable of producing magmas with the approximate MgO composition of the more evolved C-series basalts, as suggested by Thirlwall *et al.* (1996).

There is not a straightforward linear relationship between % of olivine phenocryst accumulation and MgO content within the M-series picrites (Fig 7.14). The constancy of the MgO-concentration of the picrites despite variation in olivine-phenocryst abundance implies that a primary high-MgO melt may have existed and

that olivine accumulation is not the main controlling factor in determining M-series lava MgO content. It is noted that caution must be exercised in estimating initial MgO compositions via % phenocryst accumulation, as estimate of phenocryst abundance will vary widely across a given sample, depending on the exact location of the given cross-section.

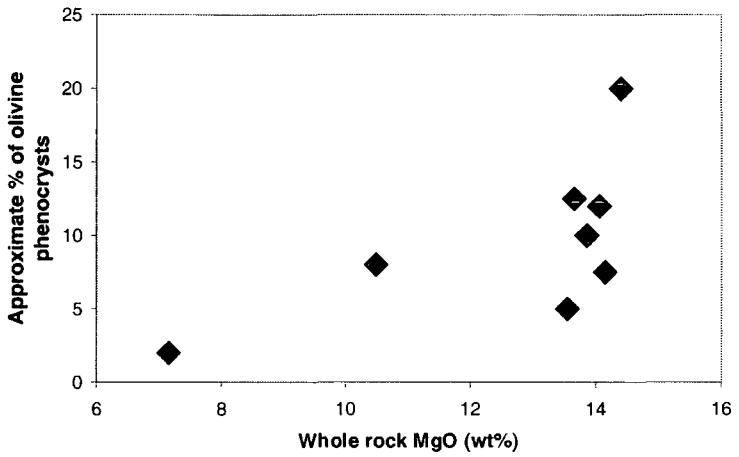

Fig 7.14 Plot of whole rock MgO composition vs % of accumulated olivine phenocrysts for samples listed in Table 7.3

7.7.3 Compatible Trace Element Signatures

The elements, Ni, Cr, V and Sc will be considered as compatible elements due to their high affinities for the early crystallising phases within the Grenada assemblage. Positive correlation exists between Ni and Cr, with MgO (Fig 7.15). The C-Series basalts have much lower overall concentrations of Ni and Cr than the M-Series. This clearly illustrates that the C-Series are not primary mantle melts and that fractional crystallisation of olivine and chrome-spinel has probably played an important role in their evolution. Conversely, the high MgO values and high concentrations of both Cr and Ni within the M-Series picrites imply that they are more representative of primary mantle melts. Some olivine fractionation (accumulation) has obviously taken place within the M-series picrites based on petrological evidence.

Sc and V concentration increases with decreasing MgO for samples with between 16 and 6% MgO (Fig 7.15). This is probably due to build up of Sc and V within the melt as a result of their incompatibility with olivine, the main early crystallising phase. As Sc and V are mildly compatible with spinel, this also suggests that a significant amount of spinel did not crystallise during early M-series fractionation. V and Ti concentrations within the melt continue to rise with decreasing MgO, until ~6% MgO (within the C-series basalts), after which point there is rapid depletion of both elements with decreasing MgO. This marks the onset of magnetite/titano-magnetite crystallisation which continues throughout the evolution of the andesitic rocks. The sharp Ti depletion within the andesitic lavas (coupled with Er/Yb ratios, Thirlwall and Graham, 1984) also suggests the importance of amphibole fractionation in the evolution of the M-Series andesites. The petrological evidence of such a process is provided by the cumulates (particularly Gd1) illustrated in Fig 7.7 and 7.8.

Sc undergoes rapid depletion within the C-series basalts and then continues to fall more steadily with decreasing MgO through to the andesites. This depletion of Sc (coupled with decrease in Fe and Ca, and increase in Si, Al and Na) in the C-series suggests the dominance of clinopyroxene in the fractionating assemblage. This concurs with the presence of clinopyroxene phenocrysts in the C-series basalts (Thirlwall and Graham, 1984). Fractionation of amphibole and plagioclase in addition to pyroxene during formation of the andesites, probably accounts for the rapid depletion of Sc between the C-series and the more andesitic compositions.

7.8 Trace Element Signatures of the Grenadian Volcanics

7.8.1 Introduction

The volcanic series from Grenada show the typical features of an island arc series: enrichment in the fluid-mobile elements (U, Sr, Ba) and relative depletion of the high field strength elements (HFSE) (Nb, Ta, Zr, Hf). Elements are placed in order of increasing compatibility with a fertile spinel-lherzolite mantle (from left to right; Fig 7.16) after Pearce and Parkinson (1993). Such plots are of most use for

basaltic rocks as they highlight elemental concentrations relative to MORB and thus differences in the composition of the source components and extent of mantle melting. Plots of more evolved rocks will reflect AFC processes and so are not easily interpreted in terms of mantle derivation. Thus, in the following section most of the description is focussed on the picritic and basaltic composition rocks, although spidergrams for the more evolved rocks are also presented for completeness.

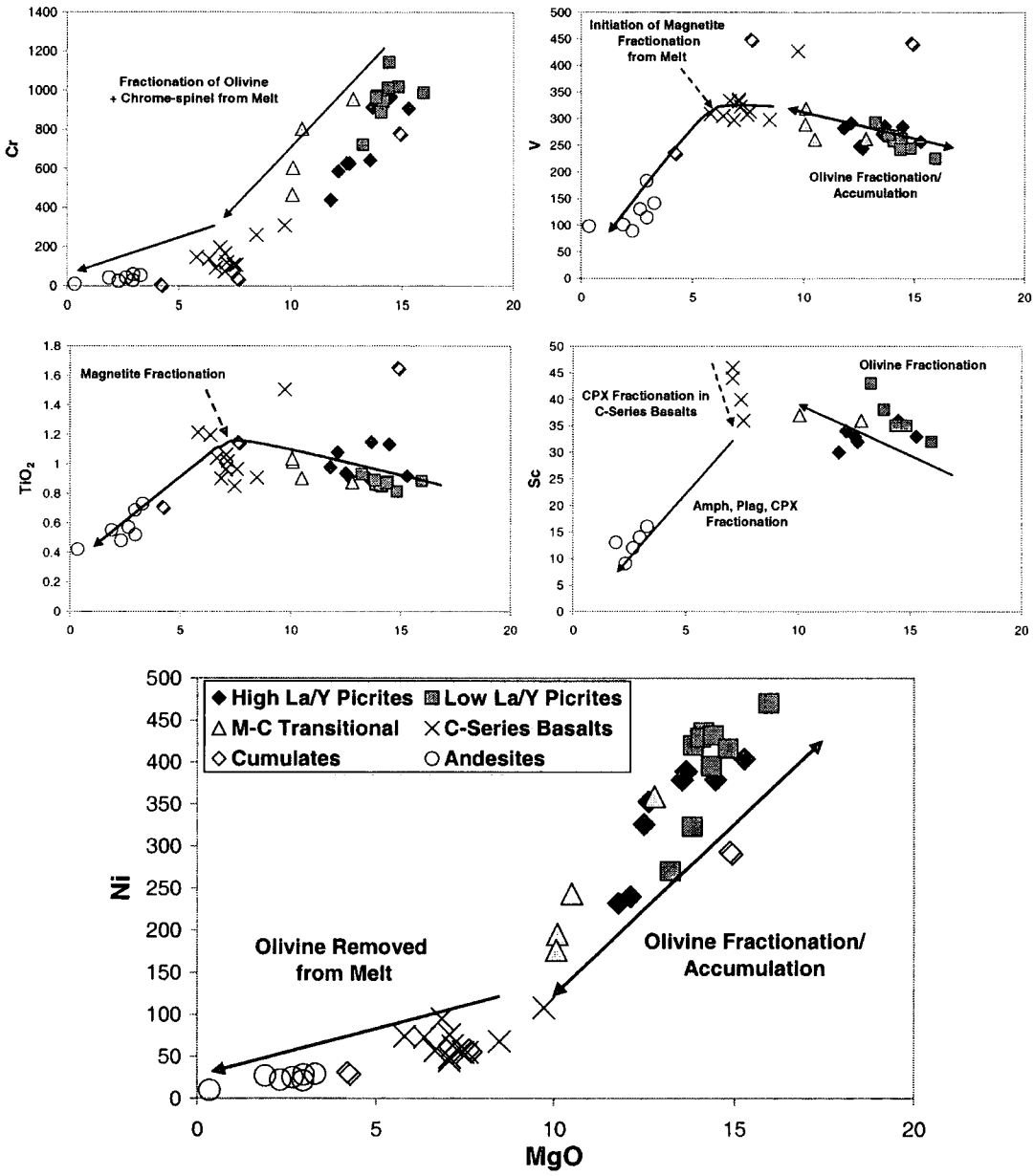

Fig 7.15 Compatible element (and Ti) variation digrams for Grenada volcanics (oxides as wt %, elements as ppm)

7.8.2 M-series Picrites

The picrites fall into two distinct groups on the basis of their trace element patterns. This division was recognised by Thirlwall *et al.* (1996) who sub-divide the picrites into low and high La/Y groups (Section 7.9.1). To a first approximation the following can be noted:

1) The picrites are enriched in large ion lithophile (LILE) and fluid-mobile elements relative to MORB, with the pattern of enrichment generally increasing as incompatibility increases. This strongly suggests a subduction-derived fluid component has modified the mantle source from which the picrites are generated.

2) The compatible elements (especially Ni and Cr) are highly enriched relative to average N-MORB, suggesting that the picrites are relatively primitive and have not undergone extensive fractionation. The close correlation between the high and low La/Y picrite compatible element concentrations, implies that the elemental differences between these two groups are not due to differing degrees of fractionation.

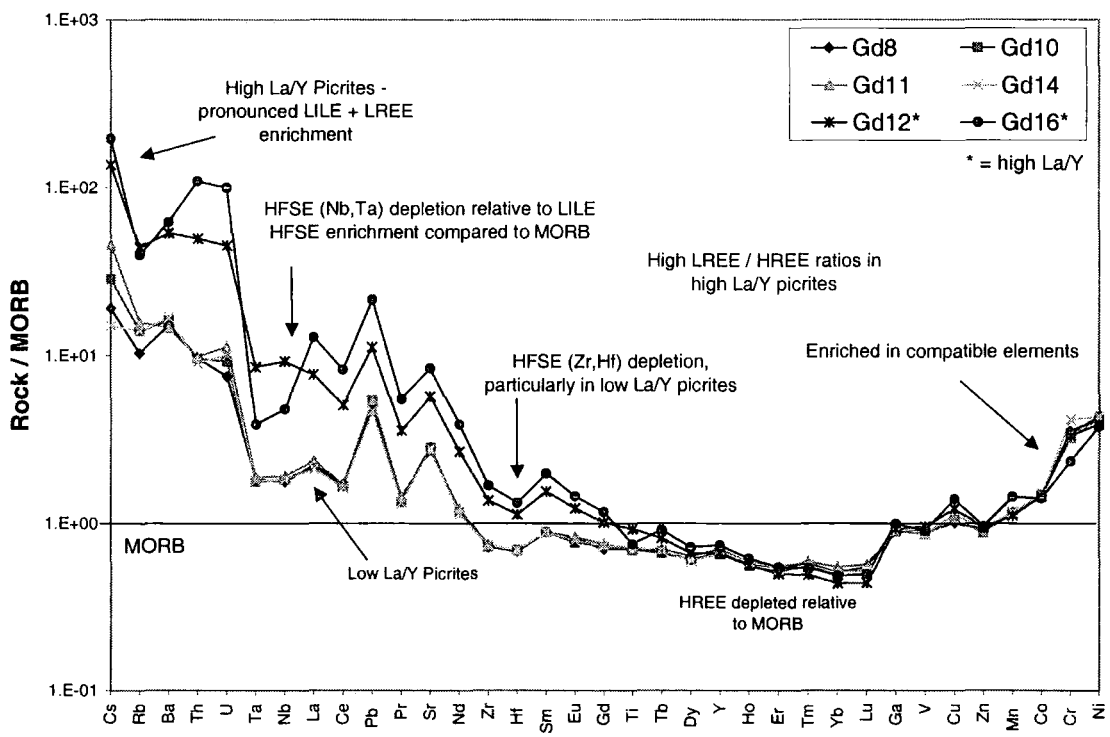

Fig 7.16 MORB-normalised trace element spidergram for M-series picrites of Grenada (Normalising values taken from Pearce and Parkinson (1993) where available and from Sun and McDonough (1989).

3) The HFSE are depleted relative to the LILE and LREE. This probably reflects enrichment of the LILEs rather than actual HFSE depletion. This is to be expected as the HFSE behave more conservatively than the LILEs during slab dehydration (Pearce and Peate, 1995).

The HFSE behave in an incompatible manner during mantle melting. Thus, the enrichment of HFSE relative to MORB within the high La/Y picrites may suggest that the picrites were produced by a lower degree of melting than that which generated MORB. This is perhaps unlikely as fluid addition (indicated by the high LILE- abundances of this group of picrites) from the dehydrating slab acts to lower the solidus of the mantle wedge and thus promote melting (Wilson, 1989). Less melting of the mantle wedge above a subduction zone relative to MORB might occur however, if the thickness of the arc crust is sufficient to impede decompression melting which occurs during MORB generation. As the crust beneath Grenada is ~30km thick, this condition may be relevant.

Alternative means by which HFSE enrichment relative to MORB may have arisen in the high La/Y picrites include:

a) enrichment of the mantle source, through "feeding" of fertile mantle into the system enabled by the location of Grenada at the hinge zone of the subduction system,

or, b) enrichment of the mantle in HFSE from the subducting slab, which is more likely to happen if melting rather than dehydration of the slab takes place (Pearce and Peate, 1995).

4) The Grenada picrites show progressive enrichment in mantle-derived elements with increasing incompatibility of these elements. Pearce and Parkinson (1993) argue that Nb, Zr, Y, Yb and Ti are dominantly mantle-derived (although Nb and Zr may be released from the subducting slab if melting rather than dehydration occurs (Pearce and Peate, 1995). In the high La/Y picrites Zr, Hf, Ta and Nb are all above MORB concentrations (and have higher Zr/Hf and lower Ta/Nb than MORB). This has been attributed to small degrees of melting of a mantle source with residual garnet or to an enriched mantle source (Pearce and Parkinson, 1993 and references therein). The low La/Y picrites conversely contain lower Zr-Hf concentrations than MORB, but the Zr-Hf pattern parallels MORB implying that their HFSE signature is

mantle rather than slab-derived. This suggests that either the mantle below Grenada is heterogeneous and variably enriched in fluids and/or slab melts, or that there are variations in degree of partial melting.

5) The HREE patterns are very similar for both the high and low La/Y groups and are depleted relative to MORB (particularly for Yb). This suggests that there might be a residual phase (e.g. garnet?) within the supra-subduction zone mantle which is not present in MORB source mantle.

7.8.3 C-series Basalts

The following observations and initial assumptions are noted from consideration of Fig 7.17

1) The M-C transitional basalt differs from the C-series in a number of ways. Firstly, it has much higher concentrations of Ni and Cr. This suggests that either the C-Series basalt has undergone higher degrees of fractionation (of olivine and spinel?) or that the M-C series contain a higher percentage of accumulated olivine. Secondly the M-C basalt and C-series basalts have similar transitional metal and HREE concentrations, but the M-C basalt has generally lower HFSE (more depleted source?) and LILE concentrations than the C-series basalts.

2) The Zr-Hf pattern within the M-C basalt (Gd5) is parallel, but depleted relative to MORB. This implies that these elements are dominated by a mantle signature and not influenced by input from the subduction zone (Pearce and Parkinson, 1993).

3) The C-series basalts are enriched in MREE relative to MORB, whereas the HREE are depleted relative to MORB. This may be due either to the presence of HREE-compatible phases in the mantle source (i.e. garnet) or within the C-series fractionating assemblage (i.e. cpx).

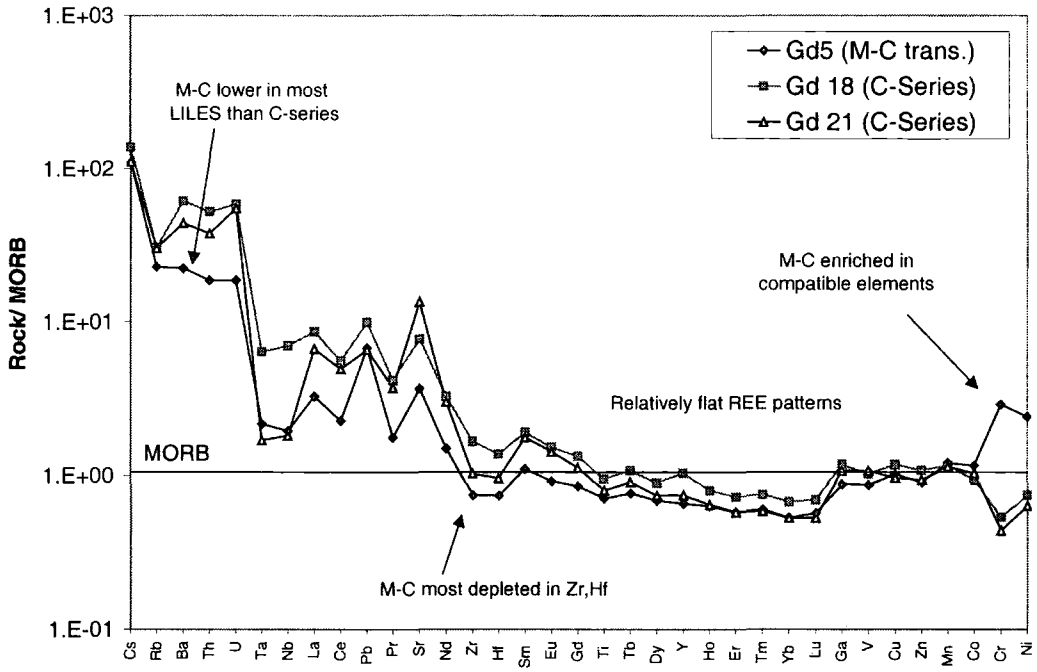

Fig 7.17 MORB-normalised trace element spidergram for M-C and C-series basalts of Grenada (Normalising values taken from Pearce and Parkinson (1993), where available and from Sun and McDonough (1989)).

7.8.4 Cumulates

1) Compatible element patterns for the cumulates diverge between the amphibole-rich cumulate Gd 1 and the plag-amph cumulates Gd2 & Gd3. Gd1 shows an enrichment in Cr and Ni, (and a similar pattern to the M-Series picrites), whereas Gd2 & Gd3 show a depletion in Cr and Ni. This suggests that Gd1 is derived from fractionation of a more primitive magma than the other cumulates (e.g. M-series picrite-type magma). Thus, the evolved M-Series lavas of Grenada seem likely to have formed by crystallisation of amphibole from a picritic parent. This is also an interpretation suggested by Thirlwall *et al.* (1996). Gd2 & Gd3 conversely must be formed from crystallisation of a less picritic parent, which has already undergone some fractionation (e.g. C-series basalt?).

2) All cumulates show Ti-enrichment. This is probably due to the presence of both titaniferous magnetite and amphibole within these rocks. V is also correspondingly high, confirming the importance of magnetite in this assemblage.

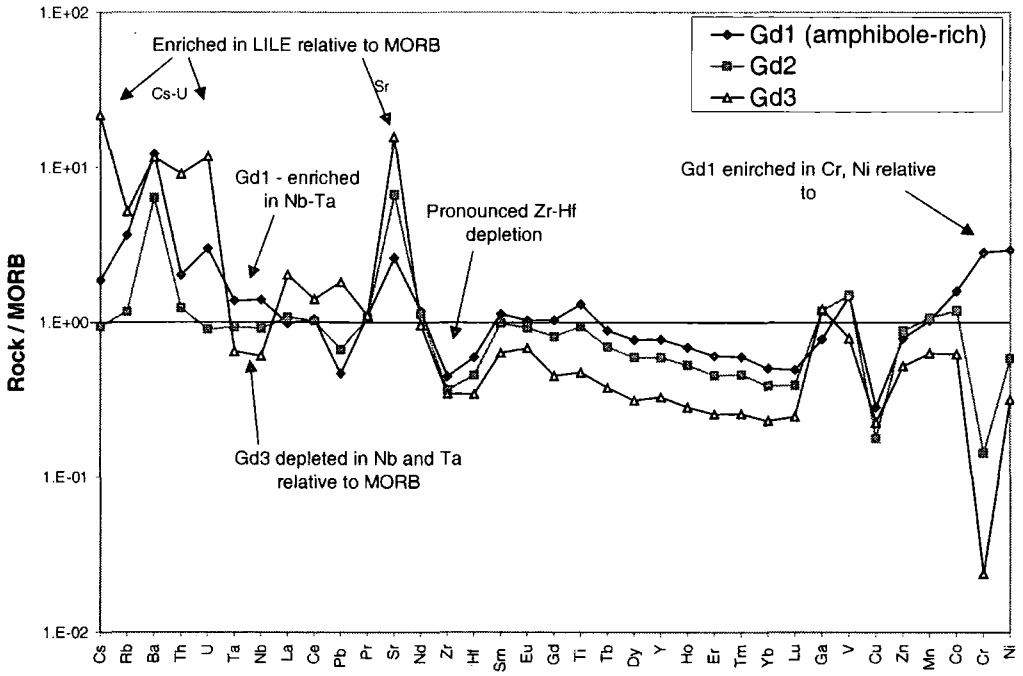

Fig 7.18 MORB-normalised trace element spidergram for cumulates of Grenada (Normalising values taken from Pearce and Parkinson (1993) where available and from Sun and McDonough (1989)).

3) The HFSE distribution in the cumulates is effected by amphibole abundance. Nb and Ta are enriched in the hornblende-rich cumulate Gd1 relative to the other cumulates, confirming that they are mildly compatible with amphibole. The differential compatibility of Zr and Hf with amphibole is demonstrated by the fact that Zr and Hf become increasingly fractionated as amphibole content within the cumulate increases.

4) Gd2 & Gd3 have a pronounced Sr-peak which probably reflects the high proportion of plagioclase within their mineral assemblage.

5) All cumulates are depleted in Cu, a feature not seen in any of the "parental" lavas. Cu content is a strong indication of S-saturation conditions in a magma, as Cu is immediately precipitated as sulfide when a magma becomes S-saturated (Keays, 1995). Thus, S-saturation and Cu (PGE?) removal from the magmas may have taken place prior to formation of the cumulates. Alternatively, conditions during formation of these cumulates may not have been suitable for Cu-fractionation (S-undersaturated?) and so Cu may have remained in the melt. In this situation Cu-

enrichment would be expected in the residual melts from which the cumulates have been removed (i.e. andesites).

7.8.5 Andesites

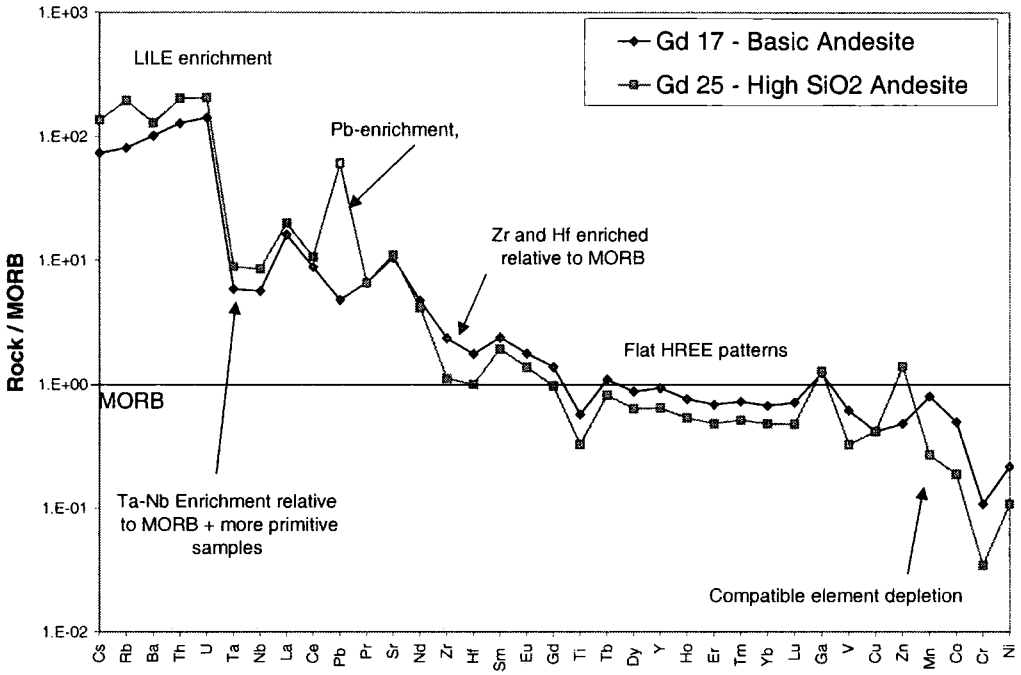

Fig 7.19 MORB-normalised trace element spidergram for andesites of Grenada (Normalising values taken from Pearce and Parkinson (1993), where available and from Sun and McDonough (1989).

1) The andesites show the overall pattern of incompatible (LILE) enrichment and compatible element depletion that would be expected in evolved rocks.

2) Gd 25 has a peak for Pb. As it is the most evolved rock analysed, this may be due to crustal contamination caused by increased crustal residence time (isotopic data would be necessary to confirm this) as well as from slab input.

3) Both andesites are relatively Ti depleted, this is probably due to removal of magnetite and amphibole in the earlier crystallising assemblages (e.g. cumulates).

4) Nb, Ta, Hf and Zr are markedly enriched within the andesites compared to the cumulates. This implies that the HFSEs behaved in an incompatible nature during cumulate formation and become enriched in the residual andesitic melts.

7.9 Detailed Examination of Trace Element Data

The trace element data obtained for the rocks of Grenada will now be considered in more detail within the respective groupings of REE, HFSE and LILE.

7.9.1 Rare Earth Element Signatures

The volcanic series of Grenada show variable amounts of LREE enrichment. This can be monitored by both the LREE/MREE ratio: La/Y and the LREE/HREE ratio: La/Yb (Thirlwall *et al.*, 1996). Within the picrites there is a wide range of LREE enrichment which allows both high and low La/Y and La/Yb groups to be defined (Thirlwall *et al.*, 1996). The least LREE enriched group has La/Y <0.7 and La/Yb <7, whereas the more LREE enriched group has La/Y >0.7 and La/Yb >9. The high La/Y, La/Yb picrites are also characterised by higher concentrations of most incompatible elements, generally higher concentrations of CaO and lower SiO_2, than the low La/Y group (Thirlwall *et al.*, 1996). Accordingly both high- and low-La/Yb and La/Y groups can be recognised within the evolved M-series basalts and andesites as a result of fractionation from high- and low-La/Yb and La/Y picritic parents. All of the most differentiated samples, however, have La/Y >1 probably due to amphibole crystallisation (Thirlwall *et al.*, 1996).

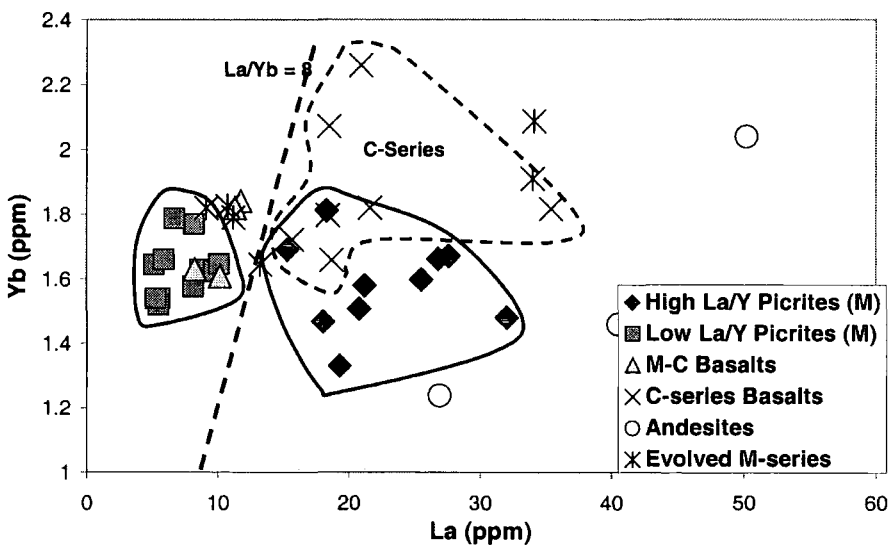

Fig 7.20a Plot of La/Yb illustrating the subdivision of the high and low La/Yb M-series picrites

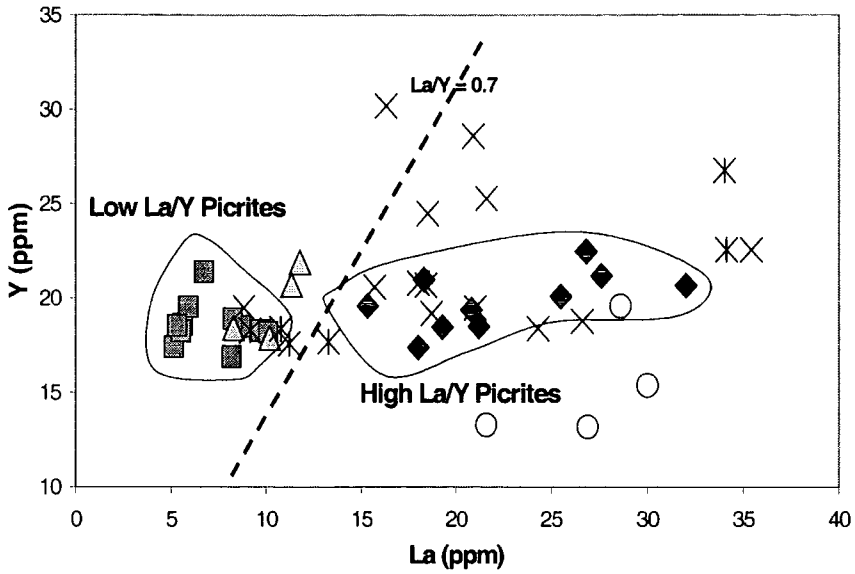

Fig 7.20b Plot of La/Y illustrating the subdivision of the high and low, La/Y M-series picrites

The subdivisions of these (and all other) groups, based on their La/Y ratios and MgO, SiO_2 concentrations are illustrated below. Each of the geochemical subgroups are present at each of the volcanic centres with the exception of the M-C transitional group which is only present at the MGF centre. Thus, similar petrogenetic processes transpired on several occasions at different centres (Thirlwall *et al.*, 1996).

Rock type	Series	MgO	SiO_2	La/Y	La/Yb	Subgroup
Basalts	C	<7.5%	>47%			
Picrites	M	>11%	<48%	>0.7	>9	High La/Y
Picrites	M	>11%	<49%	<0.7	<7	Low La/Y
Evolved basalts/ basic andesites	M	<10%	>50%	>0.7	>9	High La/Y
Evolved basalts/ basic andesites	M	<9%	>51%	<0.7	<7	Low La/Y
High SiO_2 Andesites		<3.5%	>58%	>1	>9	High La/Y
Transitional basalts	M-C	>9.9%	<48%	<0.7	<7	Low La/Y

Table 7.4 Geochemical subdivisions of Grenada volcanic rocks (after Thirlwall *et al.*, 1996) N.B. La/Y, La/Yb of C-series generally high, but can be quite variable.

The C-series basalts tend to show enrichment in the LREEs of a similar nature to the high La/Y picrites (Fig 7.21). The M-C basalts show LREE enrichment relative to the low La/Y picrites, but depletion relative to the high La/Y picrites and C-series basalts. There is little variation in the shape of the HREE patterns (Dy – Lu), between the C and M-series suggesting that the fractionating phases within the C-series basalts did not cause any HREE fractionation. The HREE of all Grenada lavas are depleted relative to MORB, but consistent throughout the different series. This suggests that each of the Grenada series were probably derived from a similar, possibly garnet-bearing source. Although Ce is depleted relative to La in the spidergrams it is not depleted with respect to Pr or Nd. The absence of a Ce anomaly (Peate and Pearce, 1998) suggests that pelagic sediment input to the subduction zone is not an important factor in controlling the chemistry of the Grenada lavas.

There are several possible reasons for the observed LREE element enrichment within the high La/Y picrites. Firstly, it could be related to degree of partial melting, where high La/Y would represent a smaller average melt fraction. Secondly, it could be related to variable degree of hydrous fluid input, where high La/Y would reflect increased fluid input from the subducting slab. This problem will be further addressed by comparison of the REE signatures with isotopic and other trace element data in section 7.9.4

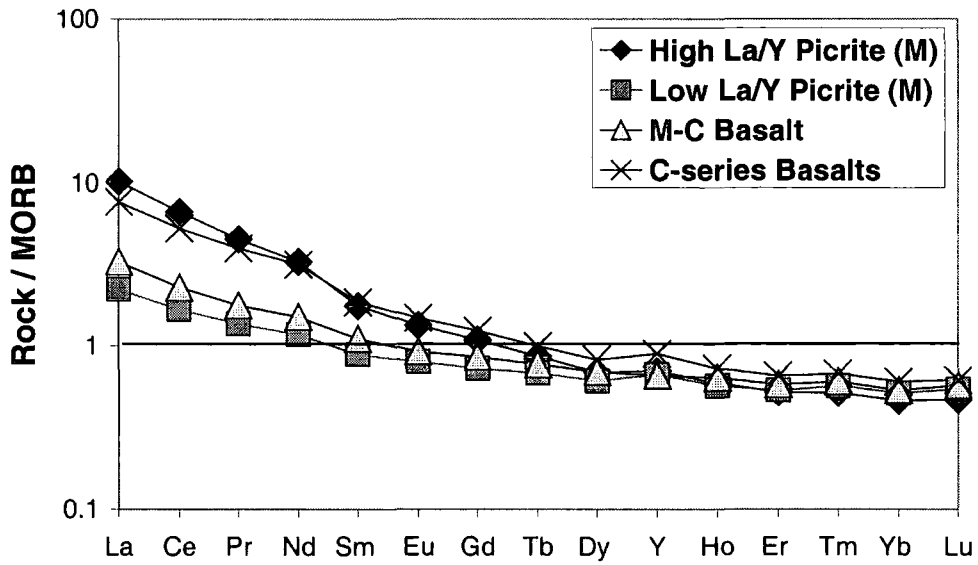

Fig 7.21 MORB normalised patterns for the main Grenada lava series (the lines were generated from average group compositions)

7.9.2 High Field Strength Elements

Within a subduction system the HFSE are those elements for which there is no detectable slab signature to the source of arc volcanism. Thus, they can be used to obtain information about the composition of the sub-arc mantle and place constraints on the melting conditions within the mantle wedge. Of these, the most geologically important HFSE are Ta, Nb, Zr, Hf and Ti (in descending order of incompatibility, Pearce and Peate, 1995). Variation in HFSE ratios (e.g. Nb/Ta, Zr/Hf) can be useful in determining relative enrichment or depletion of a source region. For example, Ta is more incompatible than Nb during mantle melting and thus low Nb/Ta ratios will be obtained at low degrees of melting. Such HFSE ratios are illustrated below for the M-series picrites and C-series basalts of Grenada:

	MORB	Chondrite	Low La/Y Picrite	High La/Y Picrite	C-Series Basalt
Nb/Ta	17.9	17	18	20.2	17.5
Zr/Hf	36.09	36	38	44	37

Table 7.5 Comparison of HFSE ratios in Grenada lavas (average) with MORB and chondrite (MORB ratio after Pearce and Parkinson, 1993, chondrite ratio from Sun and McDonough, 1989)

Comparison of HFSE ratios (Table 7.5, Fig 7.22) illustrates that the high La/Y picrites have higher Zr/Hf and Nb/Ta ratios than both the low La/Y picrites and the C-series picrites. The C-Series basalts show very similar ratios to the low La/Y picrites and to both MORB and chondrites. This may suggest that the C-series basalts and low La/Y picrites were derived from mantle of a similar composition which, by comparison with MORB, had not been significantly altered by subduction components. The high La/Y picrites would seem to be enriched in the more compatible HFSE given the ratios illustrated above. This might suggest that the high La/Y picrites were derived from a more depleted source than the other lavas. Interestingly, the Zr/Hf, Nb/Ta ratios of the high La/Y picrites are very similar to those within shoshonitic lavas from the North Northern Seamount Province of the Marianas Trench (Zr/Hf up to 48, Nb/Ta up to 25; Peate and Pearce, 1998). Thus, high HFSE ratios may be a common feature of some alkalic arc magmas.

Interpretation of source enrichment or subduction component on HFSEs alone is very difficult as they may be affected by a number of factors. Firstly, the HFSE can be retained within and fractionated by trace mantle phases (i.e. amphibole). Secondly, HFSE content can be affected by variable degrees of subduction input, particularly via slab-derived siliceous melts rather than slab-derived aqueous fluids, as the HFSE are unlikely to be mobilised by aqueous fluids (Pearce and Peate, 1995). Lastly, pre-existing mantle-wedge enrichment or depletion, or extent of partial melting can affect HFSE content and ratios.

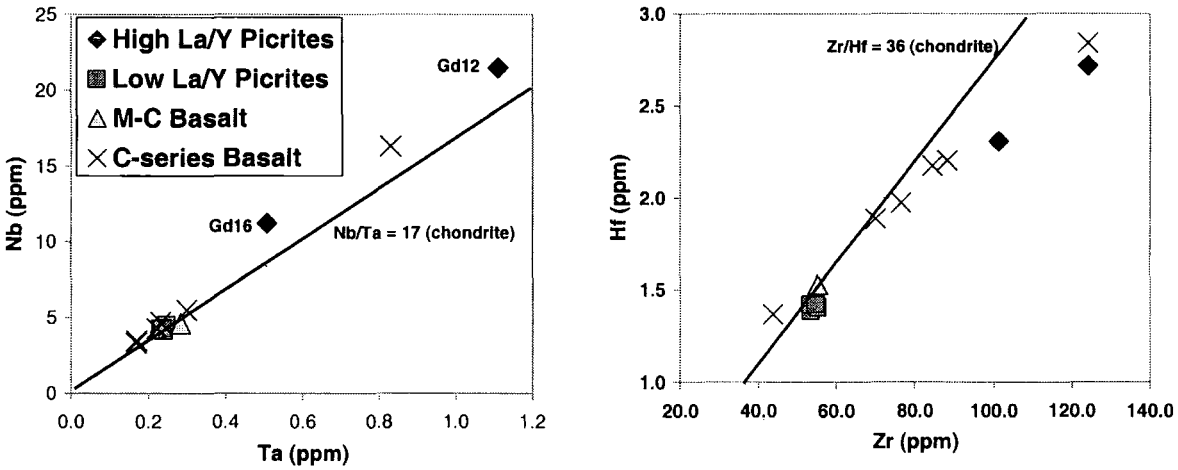

Fig 7.22 Comparison of HFSE ratios in picrites and basalts

7.9.3 Large Ion Lithophile Elements

The LILEs are fluid mobile highly incompatible elements. Within the LILE series however, relative variations in fluid mobility can be useful in determining arc magma-genesis. The series consists of the more fluid-mobile elements (Cs, Ba, Rb, Pb, K and Sr) and the less fluid-mobile element (Th and U). The LREEs La, Ce and Nd are often considered as part of the latter group when considering fluid signatures.

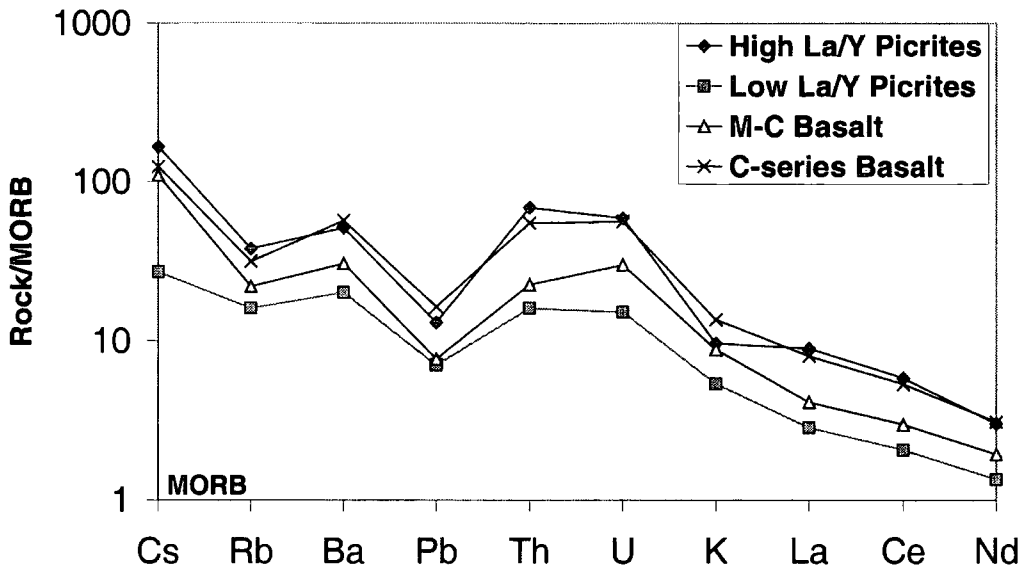

Fig 7.23 Extended LILE spidergram for the main Grenada rock types (each line represents an average of at least 3 samples of the magma-series shown). MORB-normalisation values after Pearce (1982). Data for average compositions compiled from this study and Thirlwall *et al.*, (1996) and Thirlwall and Graham (1984). N.B. Cs-point for low La/Y picrites based on two analyses only.

LILEs (and the fluid-mobile LREE) are enriched relative to MORB within all of the Grenada rock-types (Fig 7.23). This is characteristic of subduction-related rocks derived from a MORB-source mantle, modified by hydrous fluids from the subduction zone. The different rock-types show very similar patterns but varying overall concentrations of LILEs. This suggests that they were generated from sources containing differing amounts of LILE-enriched fluid, but, that the fluid composition was the same in each of the sources. The nature and amount of fluid addition will be further addressed using incompatible ratio plots in Section 7.9.4.

7.9.4 Constraining Relative Subduction/Source Contributions to Lava Signatures

Diagrams of the form M/Yb versus Nb/Yb, where M maybe a LILE, LREE or HFSE, help to quantify the extent and nature of enrichment of the respective element M (Peate and Pearce, 1998). In this type of plot it is assumed that there is no contribution of Nb and Yb from the slab and that the composition of the wedge prior

to addition of a subduction component would have plotted within the MORB array (Peate and Pearce, 1998). Following these assumptions, any displacement of data from the MORB array is presumed to be due to addition of a subduction component to the wedge. Sub-horizontal variations parallel to the MORB array are controlled by source depletion or enrichment, where low Nb/Yb represents a depleted mantle wedge (Peate and Pearce, 1998; Pearce and Peate, 1995). The varying data trends that can be obtained and their suggested implications are illustrated below in a simplified manner (after Pearce *et al.*, 1995).

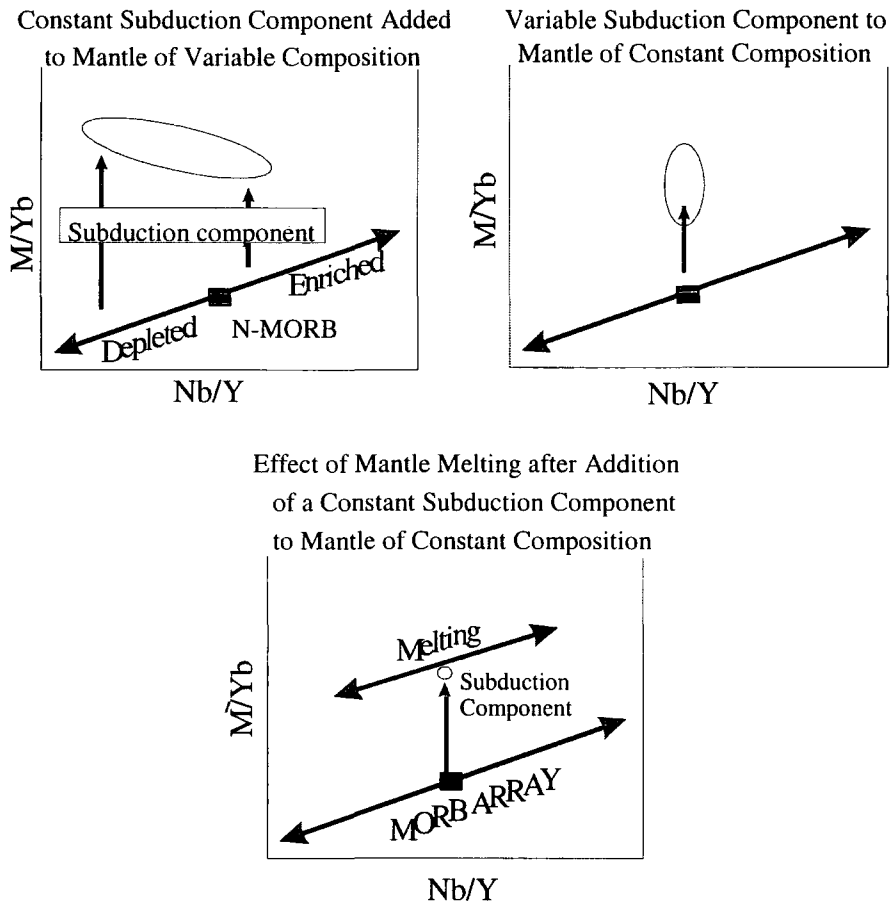

Fig 7.24 Plots of M/Yb vs Yb/Nb to discriminate between subduction components and source enrichment/depletion in subduction related rocks (after Pearce *et al.*, 1995).

A range of elements of varying fluid mobility have been plotted using the convention outlined above. The elements were chosen to span the range of fluid

mobilities with K > Ba > La > Th. These elements were also chosen as K and Ba are known to have a high contribution from the subducting slab.

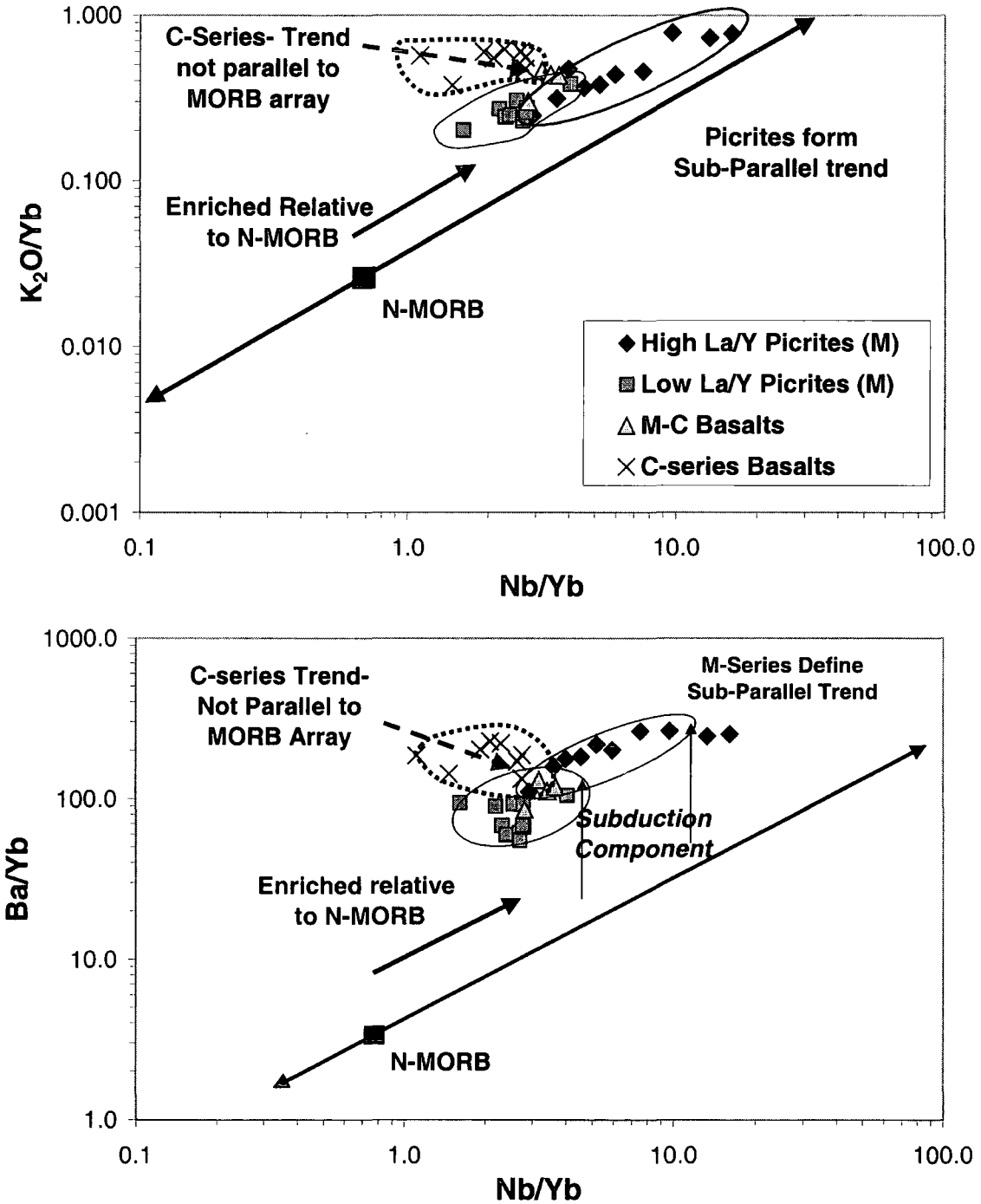

Fig 7.25 a) Behaviour of the fluid-mobile elements a) K_2O/Yb vs Nb/Yb and Ba/Yb vs Nb/Yb (N-MORB and MORB-array from Pearce *et al.*, 1995).

The K_2O and Ba plots indicate that a slab-derived LILE-enriched fluid has been added to the mantle below Grenada. All lava series plot to the right of N-MORB on the MORB array and are thus enriched relative to N-MORB. Most of the M-series picrites and the M-C basalt form a sub-parallel trend relative to the N-MORB array. Therefore, variation in K_2O and Ba abundance in the picrites can be attributed to variable degrees of melting of the mantle wedge after enrichment by a constant subduction component. The C-series do not form a trend parallel to the MORB-array and are displaced to higher values of K_2O/Yb and Ba/Yb than the M-series picrites. Thus, the C-series may contain a higher percentage of subducted material than the M and M-C series. The negative slope of the C-series dataset indicates that they were formed by addition of a constant subduction component to a more variable source region than that of the M-series.

The high La/Y picrites again form sub-parallel trends with the MORB array in the Th/Yb-Nb/Yb plot (Fig 7.25b). The low La/Y picrites and C-series basalts however, form more diffuse groups above from the MORB array. This pattern suggests that the subduction component for Th added to the mantle may have been less constant than it was for both K and Ba. This may be related to the less fluid-mobile nature of Th, the distribution of which might be controlled by siliceous melts rather than aqueous fluid (Pearce pers.comm.). Conversely, the La data shows the sub-parallel trend with the MORB array characteristic of the K-plot, confirming the fluid-mobile nature of this LREE.

In conclusion, the plots of Fig 7.25 suggest that the M-series picrites and M-C transitional basalts were formed by variable degrees of melting of a mantle source enriched by a constant LILE/LREE enriched component. The higher Nb/Yb ratios of the high La/Y picrites suggest that they were derived from a less depleted mantle source than the low La/Y picrites. The C-series basalts have a more variable signature than the M and M-C series lavas. They could have originated from mantle of similar composition to that of the low La/Y picrites (shown by Nb/Yb), but more enriched in a subduction component.

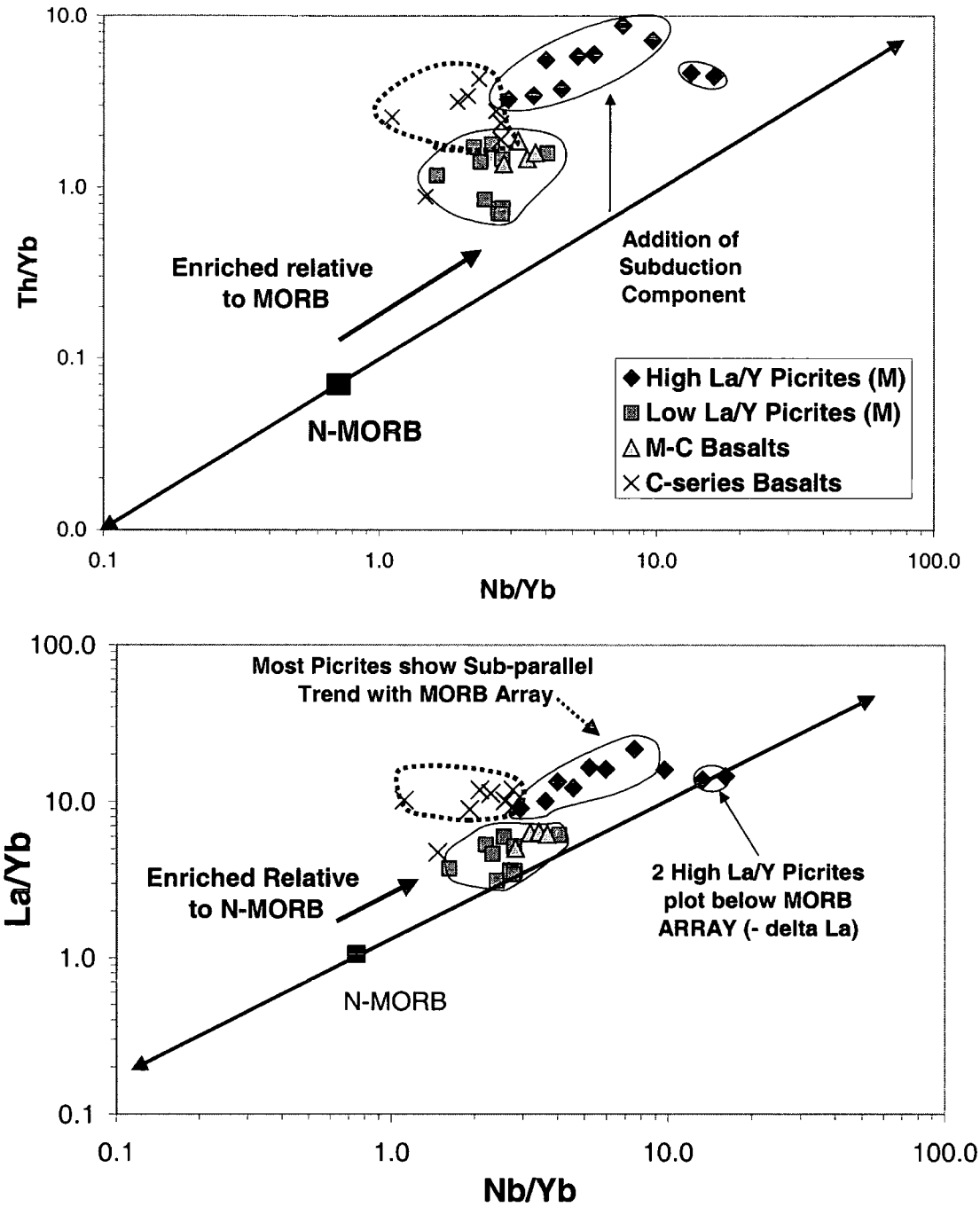

Fig 7.25b Behaviour of the fluid-mobile elements a) La/Yb vs Nb/Yb and Th/Yb vs Nb/Yb (N-MORB and MORB-array from Pearce *et al.*, 1995).

7.9.5 Delta (Δ) La

In order to determine the exact nature of the subduction component, the influence of the pre-existing mantle depletion/enrichment must be removed from the equation. This has been done by calculating ΔLa: the relative displacement of samples from the MORB array towards the subduction component. The procedure of using ΔLa is modified from the ΔNb notation of Fitton *et al.* (1997). ΔLa is preferred

to element ratio plots (e.g. La/Yb, Nb/Yb) as an estimate of subduction component contribution to the mantle wedge, as the effects of pre-existing source depletion/enrichment (as monitored by Nb/Yb) are removed from the system. Having eliminated the contribution from mantle wedge depletion/enrichment, ΔLa variation can be correlated with isotopic evidence to identify the subduction component as sediment or fluid derived.

ΔLa is calculated using the following equation:

$$\Delta La = -0.112 + \log(La/Yb) - 1.185 \times \log(Nb/Yb)$$

where La/Yb and Nb/Yb are measured sample ratios and the values (-0.112 & 1.185) are derived from the equation of a straight line defined by an average N-MORB array on a La/Yb vs Nb/Yb plot (Pearce *et al.*, 1995). La deficiency or enrichment relative to the N-MORB array, is thus expressed in terms of ΔLa >0 = enrichment, whereas ΔLa <0 = deficiency.

Almost all of the Grenadian samples are enriched in La relative to N-MORB, except for 2 of the high La/Yb M-series picrites (Fig 7.26). There is a good deal of overlap between ΔLa compositions for the high and low M-series picrites and the M-C basalts. However, the C-series tend to plot to slightly higher ΔLa-values, suggesting they have been more enriched in a high-La subduction component.

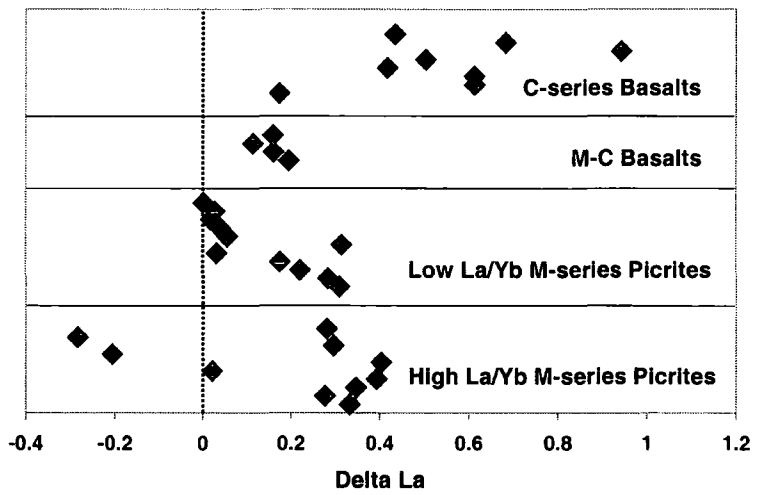

Fig 7.26 Variation of ΔLa within the respective primitive rock types of Grenada

In order to try to identify the nature of this subduction component, ΔLa has been plotted against Sr and Nd isotope ratios. Only data for rocks of picritic and basaltic composition have been plotted as the mantle signature is probably masked by the effects of AFC processes within the more evolved rock types. Data points are limited due to a lack of published isotope data for samples with corresponding REE data. All isotope data are taken from Thirlwall *et al.* (1996).

On each of the isotope vs ΔLa plots, two particular samples of interest are plotted. These are sample 509, a high La/Yb picrite and sample 310a, an evolved M-series andesite. Sample 509 has been identified by Thirlwall *et al.* (1996) on the basis of its isotopic characteristics as an end-member sample, representing the largest observed sediment contribution from the subduction zone. Incorporation of subducted sediment in the lava source, or crustal assimilation, would have the effect of decreasing the $^{143}Nd/^{144}Nd$ ratio, whilst simultaneously increasing the $^{87}Sr/^{86}Sr$ ratio. Input of fluids from the subduction zone rather than bulk sediment, would act to raise the Sr-isotope ratios and ΔLa at constant Nd compositions. Sample 310a is considered another end-member as it has suffered a high degree of crustal contamination (Thirlwall *et al.*, 1996). Thus, sample 310a is plotted in Fig 7.27 to illustrate the effect that crustal contamination would have on each of the isotope ratios.

ΔLa vs Nd-isotope plots form a very good discrimination between the respective M-series picrites (Fig 7.27a). The high La/Yb picrites plotting towards lower $^{143}Nd/^{144}Nd$ than the low La/Yb picrites. The low La/Yb picrites generally form a much tighter cluster of points than the high La/Yb picrites. This perhaps suggests that the subduction component added to the source of the low La/Yb picrites was more homogenous than to the source of the high La/Yb picrites. There is a large variation in ΔLa for relatively little change in $^{143}Nd/^{144}Nd$ within the low La/Yb picrites. This suggests that variation within the low La/Yb group may be due to varying amount of fluid input, rather than to variation in sediment contribution.

The M-C basalts plot as a tight cluster within the low La/Yb picrites (Fig 7.27a), suggesting a common subduction-component input. The C-series basalts, however, are displaced to high ΔLa values and have some of the highest $^{143}Nd/^{144}Nd$ ratios.

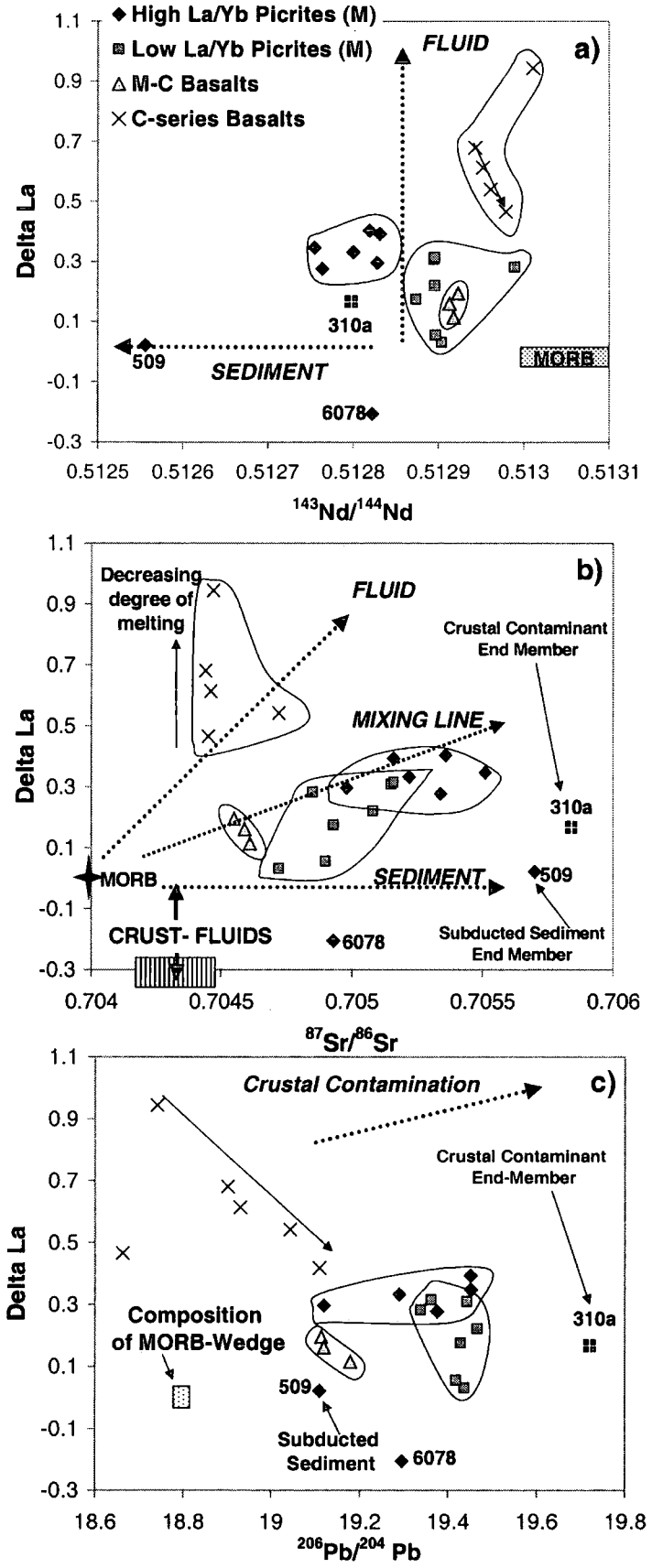

Fig 7.27 Nd, Sr and Pb isotopes vs ΔLa for M-series picrites, M-C basalts and C-series basalts of Grenada (isotope data from Thirlwall *et al.*, 1996)

This suggests that the C-series basalts may be extracted from a source with higher subducted sediment content than the M-series picrites. All Grenada lavas have $^{143}Nd/^{144}Nd$ lower than Atlantic MORB and the range in $^{143}Nd/^{144}Nd$ ratios can be generated by a variable contribution of up to 2% sediment (of local sea-floor composition) within the Grenada source (Thirlwall *et al.*, 1996). The crustally contaminated sample 310a in Fig 7.27a, plots in the same range as the picrites and is not displaced to low $^{143}Nd/^{144}Nd$ like sample 509. This suggests that variation in $^{143}Nd/^{144}Nd$ ratios is indeed due to variable subducted sediment contribution, rather than high-level, arc-crust assimilation.

The plot of $^{87}Sr/^{86}Sr$ vs ΔLa effectively shows the opposite of the Nd-plot, with the high La/Yb picrites plotting to more radiogenic Sr-signatures (Fig 7.27b). This confirms the greater importance of sediment within the high La/Yb picrite source. Within the low La/Yb picrites, there is a general trend of increasing ΔLa with increasing $^{87}Sr/^{86}Sr$. This is indicative of mixing between MORB-source mantle and an increasing fluid- (and/or sediment) component. The high La/Yb picrites define a more sub-horizontal trend towards increasing $^{87}Sr/^{86}Sr$ and towards sample 509, the sample with the clearest sediment contribution. This suggests that subduction-related sediment rather than fluid may dominate their signature.

The M-C basalts have the most restricted range of isotopic compositions and show a decrease in ΔLa with increasing $^{87}Sr/^{86}Sr$ (increasing sediment input?). If La distribution is controlled primarily by fluids rather than sediment, this may be related to the trend observed by Thirlwall *et al.* (1996), where fluid modification of the mantle seems to decrease with increasing sediment input. The C-series basalts show almost uniform, low $^{87}Sr/^{86}Sr$ ratios for a wide variation in ΔLa values. This suggests that their variation is dominated by fluid, rather than sediment input to the mantle source. Thirlwall *et al.* (1996) suggest that such low $^{87}Sr/^{86}Sr$ ratios could be obtained by addition of fluids derived from altered oceanic crust, rather than from sediments.

On the ΔLa vs $^{206}Pb/^{204}Pb$ graph, the sample 310a plots to much higher $^{206}Pb/^{204}Pb$ than all of the other samples due to crustal contamination (Thirlwall *et al.*, 1996; Fig 7.27c). This illustrates that the primitive M and C-series picrites and basalts have undergone minimal crustal contamination when compared to more

evolved Grenadian samples. Most of the M and M-C lavas plot to more radiogenic compositions than that of sample 509, the proposed high-sediment end-member. Thus it seems likely that all samples have undergone a small degree of crustal contamination. Indeed, Thirlwall *et al.* (1996) conclude that the lead isotope compositions of Grenada are largely controlled by high level crustal assimilation. This is because the $Pb_{(picrite)}/Pb_{(crust)}$ ratio is much lower than the corresponding ratio for Sr or Nd, and is thus more sensitive to late-stage crustal contamination. The distinct Pb-isotopic characteristics of the C- and M-series suggest that they may be formed from isotopically distinct sources.

The new approach of using ΔLa as an index to estimate subduction-component contribution in conjunction with isotope data (Thirlwall *et al.*, 1996), has proved extremely useful. Following, these studies the following conclusions can be suggested:

1) A progressively greater sediment contribution, coupled with increasing melt fractions from the C-series, through the low La/Yb picrites to the high La/Yb picrites can successfully explain the Nd-ΔLa plots. Thirlwall *et al.* (1996) also note that melt fraction broadly decreases with amount of subducted sediment in the source.

2) Mixing of sediment and slab derived fluids can explain the M and M-C series Sr-isotope characteristics. The high La/Yb picrites may be influenced more by the sediment than the fluid input.

3) The Sr-signature of the C-series basalt can be generated by variable degrees of interaction with fluids derived during dehydration of oceanic crust.

4) The higher ΔLa of the C-series basalts relative to that of the M-series picrites, may suggest the C-series are derived from smaller average melt fractions than the M-series picrites, or that the C-series basalts have been more enriched by LREE-LILE bearing fluids than the M-series.

5) The Pb-isotope data suggest that even the most primitive M-series picrites have undergone a minor amount of crustal assimilation.

7.10 Summary of Petrogenetic Processes Responsible for Production of Grenadian Volcanics

7.10.1 Introduction

In order to try to understand the behaviour of the PGEs within the Grenada volcanic system, a number of parameters regarding the evolution of the Grenadian volcanics must be outlined, namely:

What is the character of the mantle wedge?

How is this source modified by the subduction component?

What degree of melting is responsible for the production of the Grenadian volcanics?

How do these primitive melts evolve during ascent to the surface?

Does crustal assimilation play an important role in determining the volcanic signatures?

What are the approximate magma chamber residence times beneath Grenada?

The above questions will be considered using information obtained via the trace-element studies in Chapter 7 and from the literature where appropriate.

7.10.2 What is the character of the mantle wedge?

There is no evidence that the mantle wedge below Grenada is more depleted in the HFSE than the source of MORB (Thirlwall, *et al.*, 1994). This is consistent with the absence of back-arc spreading (Turner *et al.*, 1996). This can be illustrated by the Nb/Ta and Zr/Hf ratios (Table 7.5) which are generally equivalent to MORB. Ti is depleted in picritic melts relative to the REEs which suggests the presence of a phase with a high K_d for Ti (but not Nb) within the mantle wedge or subducting slab. Thus, there is modelled to be residual amphibole in the source region below Grenada (Thirlwall *et al.*, 1994).

Enrichment in LILEs and LREEs relative to MORB in the near primary melts of Grenada implies that the MORB-source type mantle has been enriched by fluids released from the subducting slab. The HREEs tend to be depleted relative to the

LREEs and MORB (in even the most picritic rocks; Fig 7.21). One explanation for this observation is that garnet is a stable phase in their source region. Arculus (1976) suggests that fractional crystallisation cannot satisfactorily explain the REE patterns obtained and that they must be determined by source composition and degree of melting of that source. Shimizu and Arculus (1975) suggest that the REE distribution in Grenadian lavas can be obtained via partial melting of a garnet-lherzolite source. The variations in primary melt compositions were thus attributed by Shimizu and Arculus (1975) to factors such as variable degrees of melting, or variable fluid enrichment, rather than the presence of exotic mantle components (i.e. OIB) within the mantle wedge.

7.10.3 What degree of melting is responsible for the production of the Grenadian volcanics?

Current opinion (Turner *et al.*, 1996; Thirlwall *et al.*, 1994) favours a model whereby Grenadian volcanics were generated by approximately 10-15% partial melting of the mantle wedge, which presumably had a pre-subduction chemistry similar to that of Atlantic N-MORB. The degree of melting below Grenada is thus significantly lower than that postulated for other intra-oceanic arcs (e.g. Marianas – 20-25% partial melting; Peate and Pearce, 1998). This has been attributed to the fact that the Lesser Antilles is built on thicker lithosphere than younger arcs (e.g. Tonga) which impedes decompression melting (Pearce and Parkinson, 1993). However, within the mantle wedge input of fluids into fertile, average temperature MORB mantle, at depths shallower than ~100km, should depress the mantle solidus sufficiently to initiate melting even without decompression (Pearce and Parkinson, 1993).

Lower degrees of partial melting would explain the relative enrichment in LILEs and thus alkalic nature of the Grenadian suite. Unlike other volcanic arcs characterised by alkaline rocks, the depth to the Benioff Zone below Grenada is relatively shallow (110-120Km; Sigurdsson *et al.*, 1973). Thus, the likely depth of melt generation may be shallower and the melt column shorter than in other arcs. Generation of a smaller average melt fraction than in most arcs and thus a lower melt production rate, may result in a shorter lifetime for Grenadian magma chambers,

limiting the time available for fractionation and accounting for eruption of the picrites (Thirlwall *et al.*, 1996).

Using La/Yb as a measure of degree of partial melting indicates that the low La/Yb picrites of the M-series were generated in larger mean melt fractions than the high La/Yb M-series picrites. The C-Series basalts were generated by a wider range of partial melt fractions, generally tending towards the higher melt fractions postulated for the low La/Yb M-series picrites.

7.10.4 How is the mantle source modified by the subduction component?

Volcanic arc basalts are all characterised by selective enrichment in incompatible elements of low ionic potential, thought to be due to the input of aqueous fluids from subducted oceanic crust into their mantle source regions. Calc-alkaline and alkalic lavas, such as those from Grenada, are also enriched in Th and the LREE, possibly due to contamination of their source by a melt derived from subducted sediment (Pearce, 1982). Variations in primary melt compositions on Grenada are attributed to modification of the mantle source by slab derived components of which there are two end-members, aqueous fluids and subducted sediment. Differences in contribution from these components are believed responsible for the variations observed on Grenada and will be considered in more detail below:

1) **Variation in the amount of hydrous fluid component in the source**

Thirlwall *et al.* (1996) conclude that hydrous fluids, derived from dehydration of both sediments and altered subducted basaltic crust, led to mantle enrichment in Sr, Ba, U, K, Rb and, to a lesser extent, LREEs (Fig 7.23). The hydrous fluid component (inferred from Sr/Nd ratios and ΔLa, Fig 7.27) generally increases from the M-Series, through the M-C Series, to the C- Series.

2) Variations in the amount of subducted sediment present in the source

Estimates of sediment contribution to the mantle vary from 15% (Turner *et al., 1996*) to <2% (Thirlwall *et al.*, 1996). The former value was calculated on the basis of Th-immobility in fluids and is now believed to be in error (Turner pers. comm.). The latter estimate however, was calculated on the basis of variation in

$^{143}Nd/^{144}Nd$ (at constant $^{106}Pb/^{204}Pb$ and $^{87}Sr/^{86}Sr$) and seems to better explain some of the compositional variation seen in the Grenada volcanics (e.g. Table 7.6).

Series	Sediment in Mantle Source
C-series Basalts	0.2%
Low La/Y Picrites (M-series), M-C Transitional lavas	0.4%
High La/Y Picrites (M-series)	0.8-1.4%

Table 7.6. Calculated amount of sediment contribution in the sources of the respective Grenada lava series (Thirlwall *et al.*, 1996).

It may be noted that the amount of sediment in the M-series source increases as the inferred melt fraction decreases (i.e. high La/Y = lowest inferred melt fraction). Thus, Thirlwall *et al.* (1996) suggest that smaller melt fractions may imply shorter melting columns with the melt being mainly extracted from highly sediment-metasomatized mantle nearest to the wedge-slab interface.

7.10.5 How do these primitive melts evolve during ascent to the surface?

After generation within the asthenospheric part of the mantle wedge, lherzolite diapirs rise buoyantly towards the surface. At some point, segregation of primary magmas will take place, which then rise towards the earth's surface along a variety of ascent paths. Both geophysical and petrological evidence indicate the presence of high level magma reservoir systems within the crust and upper mantle of island arcs, in which the primary magmas may pond and fractionate (Wilson, 1989).

The presence of cumulate plutonic blocks on Grenada, with the low-pressure assemblages of plagioclase and amphibole, suggests that fractionation has taken place in high-level magma chambers. The presence of plagioclase feldspars constrains their depth of crystallisation to less than about 30km as plagioclase does not readily crystallise from basic melts at greater depths (Powell, 1978). Using mineral geothermometry, Powell (1978) has calculated that the nodules crystallised in the temperature range 1100-1200°C. Furthermore, Powell (1978) estimates that the anorthite-bearing nodules of Grenada crystallised at a pressure of ~3Kbars, which

approximates to 10km depth. Amphibole although uncommon as a phenocryst phase in the erupted magmas is a common cumulate-mineral. Thus, it is clearly a stable crystallising phase from volatile-rich basic magmas at depth, but, becomes unstable and is subsequently resorbed as the magmas ascend towards the surface (Fig 7.9c).

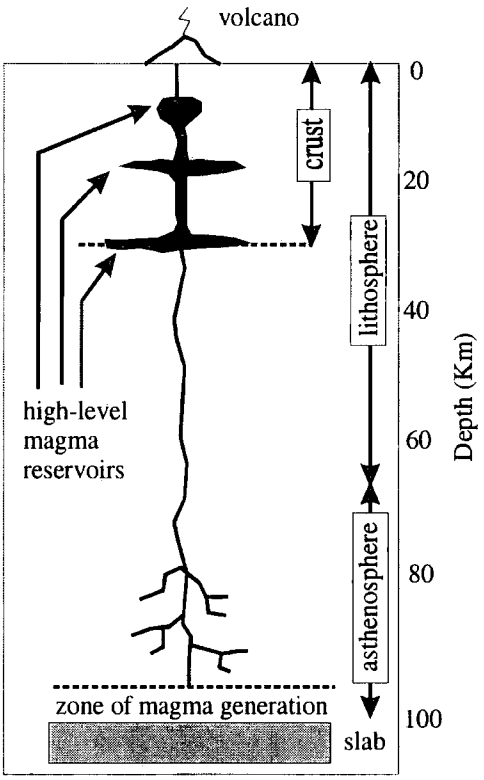

Fig 7.28 Magma reservoir system beneath a mature island arc with ~ lithospheric thickness inferred beneath Grenada (ca. 30Km) – a series of interconnected reservoirs fed from the zone of magma generation feed to higher-level and crustal storage chambers (from Wilson, 1989)

It is probable that the anorthite-bearing cumulates (e.g. Gd2 & Gd3), represent late stage fractionation processes and not products of initial fractionation from the picritic parent magmas as indicated by their low compatible element concentrations (Fig 7.18). Thirlwall *et al.* (1996) suggest that olivine fractionation is responsible for producing the range in more evolved volcanics seen in Grenada. Indeed, major element Harker diagrams (Fig 7.29) illustrate strong negative correlations between both Ni and MgO, and SiO_2 which suggests a strong olivine control during fractionation (Sigurdsson *et al.*, 1973). However, cumulates Gd 2 &

Gd3, studied within this project lack olivine. Thus, olivine fractionation must have happened at an earlier stage, with these olivine-bearing cumulates not being brought to the surface, because of formation in deeper magma chambers. The amphibole-rich cumulate, Gd1, lacks anorthite, but contains some heavily altered olivine. Thus, it may be produced from a more mafic magma than that responsible for precipitation of Gd 2 & Gd3. This is consistent with the suggestion of Thirlwall *et al.* (1996) that the evolved M-Series was produced via fractionation of amphibole and with the observation that Gd1 contains a much higher concentration of compatible elements.

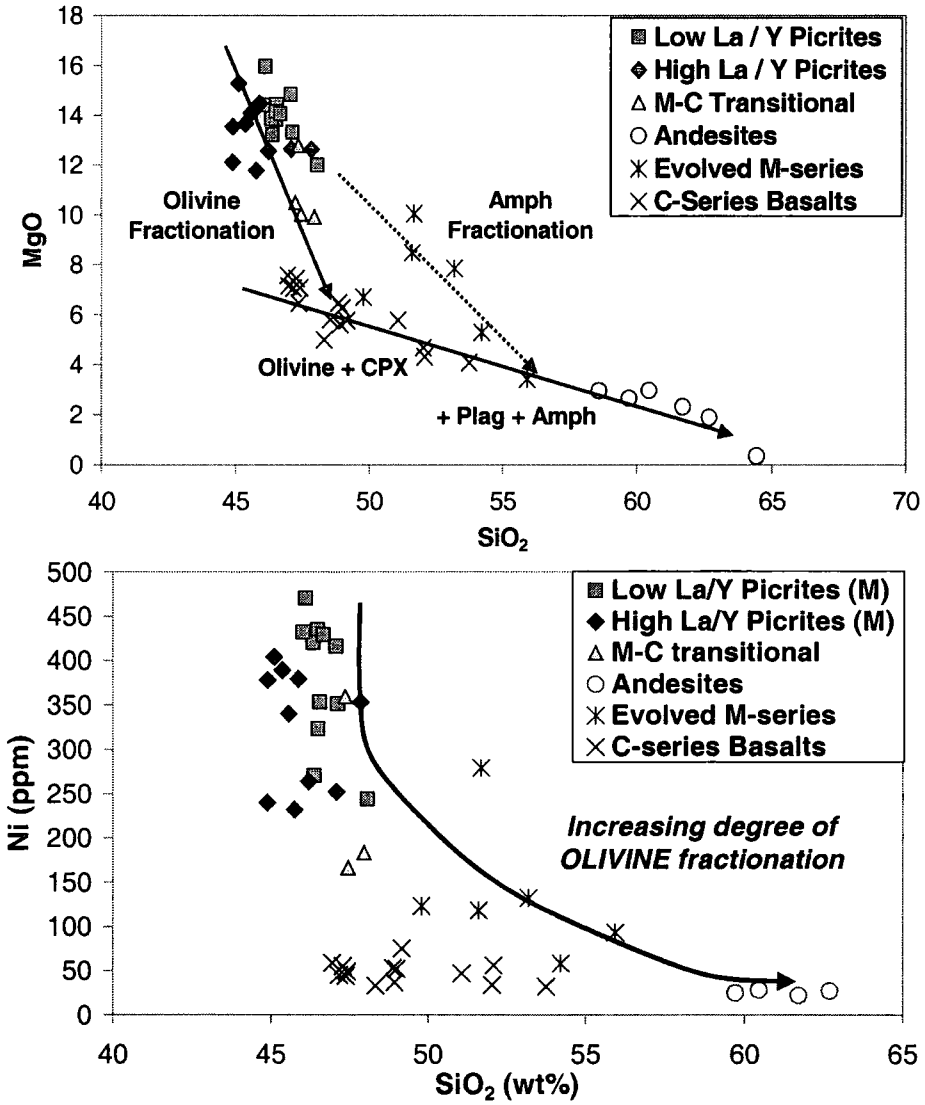

Fig 7.29 Ni and Mg vs SiO_2 as a measure of fractionation and indication of olivine control on fractionation

Thirlwall and Graham (1984) have determined that all C-Series magmas were generated by high-level fractionation of high-Ca magmas. These magmas cannot however, be in equilibrium with the mantle and must themselves be products of an earlier stage of fractionation of more mafic compositions within or close to the base of the crust. The presence of high-Mg cores in C-series clinopyroxene phenocrysts provides further evidence of generation from a more picritic parent. They conclude that high-level fractionation of clinopyroxene and plagioclase with minor olivine and magnetite was the dominant process controlling evolution of the Grenada C-series magmas.

This was accompanied by minor assimilation of material from the arc crust, producing the systematic increases in $^{206}Pb/^{204}Pb$ with fractionation and variations in the incompatible element ratios. The high silica andesites (>58% SiO_2) lie on extensions of C-series AFC correlations and so would appear to be produced via assimilation and amphibole dominated fractionation from C-Series parents (Thirlwall *et al.,* 1996). Thus, fractional crystallisation of olivine, clinopyroxene and spinel takes place at higher temperatures and at lower temperatures these phenocrysts are joined by amphibole and plagioclase to produce the trend towards increasing silica saturation (Arculus, 1976). Cumulates such as Gd2 & Gd3 represent the products of late-stage C-Series fractionation to produce andesites.

7.10.6 Does crustal assimilation play an important role in determining the volcanic signatures ?

The crust beneath Grenada consists of a disturbed Tertiary basement composed of volcanic-sedimentary units, overlain by younger undisturbed volcanic units. No units below this basement are exposed and the rest of the crust is thought, on the basis of seismic evidence, to consist of oceanic crust (Arculus, 1978). Assimilation of shallow crust is ubiquitous in Grenada high MgO magmas. This has been concluded through a variety of observations (Fig 7.27, Thirlwall *et al.,* 1996; Thirlwall and Graham, 1984). Firstly, the presence of ^{18}O enriched quartz xenocrysts within the basic andesites suggests that there is assimilation of high-level crustal material during fractionation of picrites to form the evolved M-series lavas. Furthermore, the variations in isotope and trace element ratios on Grenada can be

effectively modelled by mixing with a crustal component identified from the quartz-xenocrysts (Thirlwall *et al.*, 1996).

Secondly, isotopic evidence points to the importance of crustal assimilation. There is generally a strong negative correlation between $^{206}Pb/^{204}Pb$ and MgO, Cr, Ni, Sc and degree of fractionation in the C-Series basalt. Weaker correlations are also recognised between Sr, Nd and indices of fractionation. Thus, with increasing fractionation, the lavas acquire more radiogenic Pb and Sr, and less radiogenic Nd. This suggests the operation of AFC processes (Thirlwall and Graham, 1984). The crustal assimilant is required to have high $^{206}Pb/^{204}Pb$ (20.3) and high Sr/Nd, and generates the wide spread in $^{206}Pb/^{204}Pb$, Pb/Nd and $^{87}Sr/^{86}Sr$ at near constant $^{143}Nd/^{144}Nd$ in most Grenada magma groups (Thirlwall *et al.*, 1996). The degree of crustal assimilation varies between the respective series and is summarised below (Table 7.7).

Series	Amount of Crustal Assimilation
Picrites	2-5%
M-Series Basic Andesites	~8-12%
M-C Transitional	~3%
C-Series	"Minor" assimilation ?

Table 7.7 Postulated amounts of bulk crustal assimilation required to produce isotopic signatures of the corresponding lava series (from Thirlwall *et al.*, 1996; Thirlwall and Graham, 1984).

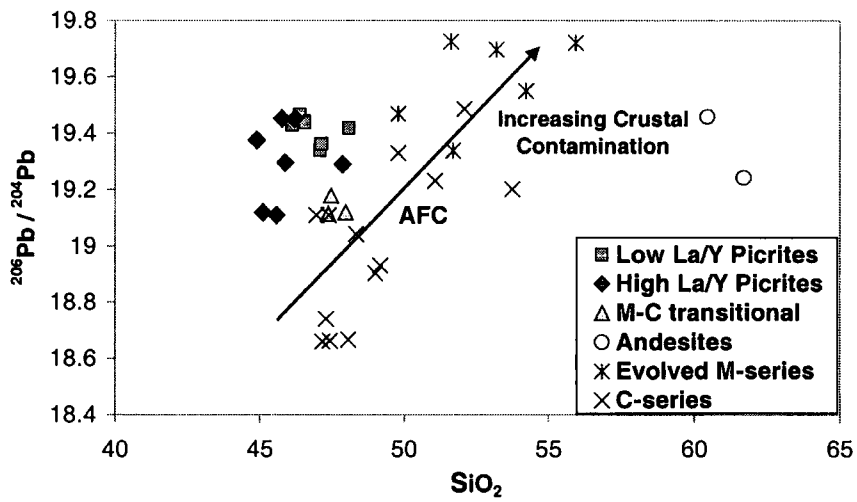

Fig 7.30 Increase in radiogenic Pb with SiO_2 - indicating AFC processes (data from Thirlwall *et al.*, 1996)

7.10.7 What is the approximate magma chamber residence time beneath Grenada?

Turner *et al.* (1996) have modelled magma chamber residence times based on the whole Lesser Antilles Arc using U-Th disequilibria and Sr isotopes. They have constrained the maximum time for fluid transport through the mantle wedge to ~90Ka. Since U-Th mineral isochrons indicate that the magmas resided in the crust for ~50Ka prior to eruption, this leaves only ~40Ka for transport from the slab to the crust. This requires an ascent rate >1m/yr and would necessitate channelled flow through the mantle wedge.

As previously mentioned, the abundance of highly picritic magmas may be due to short residence times within their associated magma chambers below Grenada. Since even the picrites have undergone minor crustal assimilation (Thirlwall *et al.*, 1996), there must have been some ponding of these picritic magmas at crustal levels. No studies have been conducted on Grenada aimed specifically at estimating magma residence times. Thus studies on the magma chamber conditions on the neighbouring island of St. Vincent will be considered instead.

Cumulate formation and fractionation on St. Vincent is an extremely important petrogenetic process. Cumulate nodules composed predominantly of plagioclase, olivine, pyroxene (cpx and opx), ± Cr-spinel, ± titanomagnetite are unusually abundant (Heath *et al.*, 1998[a]). U-Th isochrons for the Soufriere volcano on St. Vincent reflect long magma residence times for both the crystals and co-existing melt. It is suggested that recent lavas from this volcano were all derived from magma that was generated in the mantle wedge and transported into a crustal magma chamber ~60,000y ago, over which time it remained at a constant temperature close to its liquidus. This was probably facilitated by insulation of the chamber from the country rock by thick deposits of cumulate-crystal mush around the walls of the chamber. This is a particularly long residence time for an arc and may be due to the thick arc-crust below the Lesser Antilles. There seems to be a consensus however, that ~30Ka is an average transit time for melts through the mantle wedge (Heath *et al.*, 1998[b]).

Long residence times may characterise more evolved lavas that develop on thick arc crust (Heath *et al.*, 1998[b]), such as the evolved M-series and high SiO_2

andesites of Grenada. However, the lack of fractionation in the M-series lavas seems hard to reconcile with such a model. Instead, the primitive lavas of Grenada may have behaved more like tholeiitic arc lavas, which are inferred to have minimal crustal residence times (Heath *et al.*, 1998[b]). Further investigation, such as comparison of U-Th isotopic composition between primitive and evolved lavas would obviously be required to resolve this problem.

7.10.8 Summary of Proposed Grenada Petrogenesis

Ultimately all magmas on Grenada were derived by fractional crystallisation from picrites with ca. 15% MgO. These primary magmas erupted essentially unaffected by fractionation although slightly contaminated by crustal assimilation, as the M-series picrites. The M-series picrites have variable La/Y signatures caused by differing degrees of source partial melting and variable enrichment of the source in incompatible elements from slab-derived fluids. Amphibole-dominated crustal fractionation of these picrites (Fig 7.31) produces evolved M-series basalts and andesites in which both high and low La/Y groups can also be recognised (Thirlwall *et al.*, 1996).

The most primitive C-series basalts (7.5% MgO) have mineralogy and chemistry consistent with an origin by fractionation of 16% olivine from picrites, predisposed to olivine fractionation by high contributions of fluid in the magma source. These picrites have similar major element compositions to M-series picrites, but are more enriched in LILEs (Thirlwall *et al.*, 1996). More evolved C-series basalts are derived via further fractionation of augite and plagioclase (with minor olivine and magnetite). High SiO_2 andesites are the end-product of C-series differentiation via amphibole-dominated fractionation and AFC (Arculus, 1978). The various stages of fractionation involved in producing the range of volcanic products on Grenada are illustrated schematically in Fig 7.31.

A group of lavas transitional to the M and C series has been identified at one particular volcanic centre (MGF). The evolution of this group is attributed to the transitional nature of both fluid and subducted sediment contribution to its source. LILE-enriched fluid contribution to the mantle source for the various series is

postulated to increase in the order C-series > M-C series > M-Series. Conversely, sediment contribution is thought to increase in the order M-series (high La/Y) > M-C > M-series (low La/Y) > C-series (Fig 7.27). All of the Grenada lavas have undergone some crustal assimilation with the andesites being demonstrably generated by AFC processes (Thirlwall *et al.*, 1996). Strong variability in trace element characteristics between volcanic centres, suggests that each of the volcanic episodes was associated with individual melting events in the upper mantle, which resulted in variable trace-element geochemistry (Arculus, 1976).

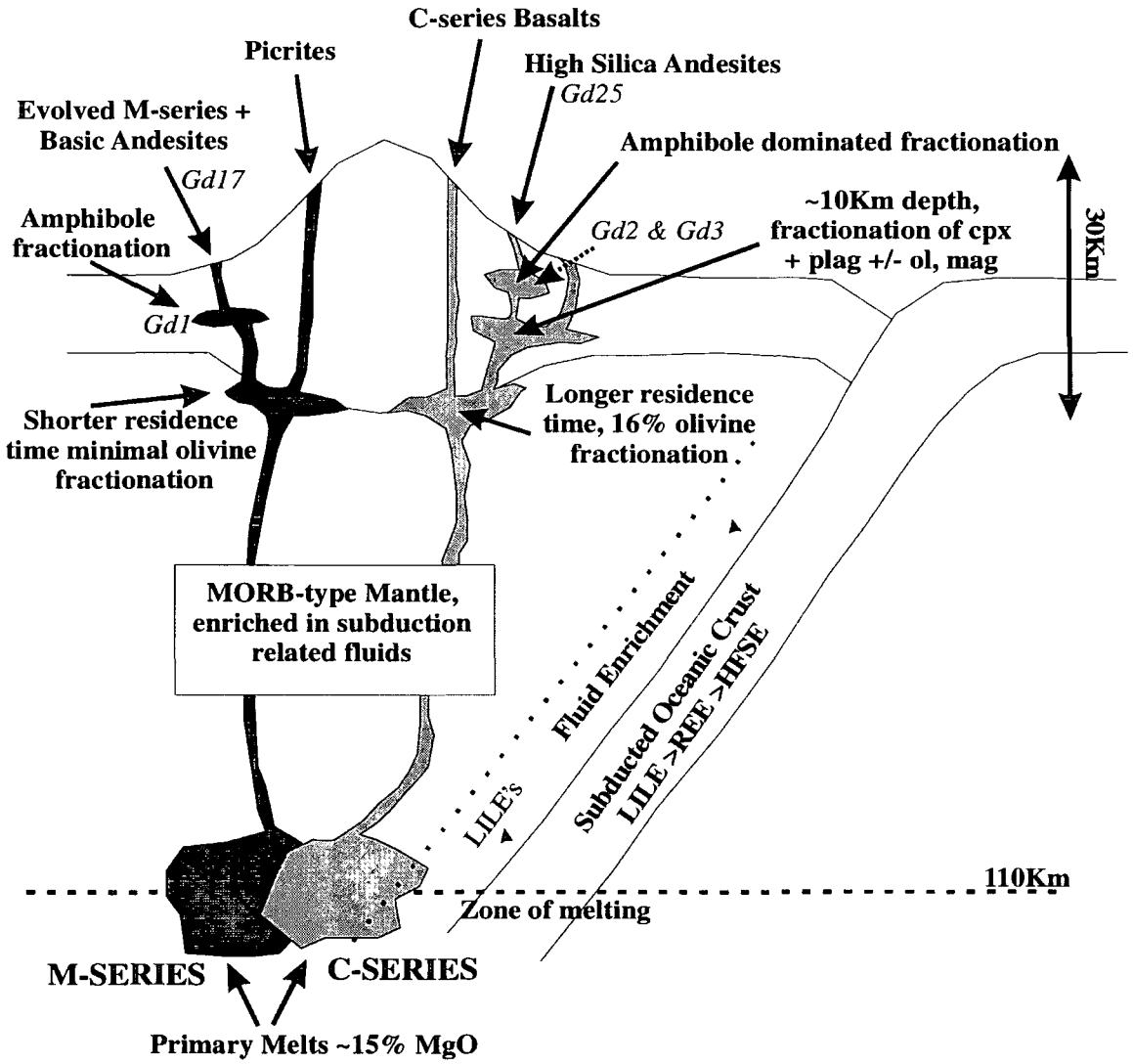

Fig 7.31 Schematic illustration of arc-plumbing below Grenada and the stages of fractionation involved in generating the range of lava compositions found on Grenada

8: PGE Signatures Within Subduction Related Lavas – Comparison between Grenada, Lesser Antilles Arc and the Izu-Bonin Arc

8.1 PGE Behaviour in Subduction Systems – Previous Work and Aims of this Study

PGE data for subduction-related rocks in the literature are largely restricted to boninites (i.e. Pd and Ir, Hamlyn *et al.*, 1985; Re-Os, Parkinson *et al.*, 1998) and to peridotite nodules of likely sub-arc mantle wedge provenance (Brandon *et al.*, 1996; Parkinson *et al.*, 1998[a, b]; Rehkämper *et al.*, 1997).

Recent Os-isotope studies of mantle peridotite xenoliths from subduction zones present conflicting pictures of the origin and evolution of the sub-arc mantle wedge. Parkinson *et al.* (1998[b]) note that mantle peridotites from both the Izu-Bonin forearc and from Grenada have unradiogenic Os. The unradiogenic Os-isotope compositions are attributed to ancient melt depletion events within the mantle that are not recorded by incompatible lithophile isotope systems. Thus the Os-isotopes and PGEs may preserve unique information about previous mantle depletion episodes. The residues of such melting events are less dense than fertile mantle and thus difficult to subduct, so survive mantle homogenisation by convection. The presence of such old depleted mantle in these modern arc systems has led to the suggestion that subduction zones may act as "graveyards" for old oceanic lithosphere (Parkinson *et al.*, 1998[a]).

It has been suggested (Parkinson *et al.*, 1998[a]) that arc melts rising through such depleted mantle should acquire an equally unradiogenic signature. Thus, the presence of unradiogenic Os-isotope compositions in arc lavas would provide conformation of the "graveyard" theory. Part of this study will be to attempt to address this question through analysis of six Grenada samples for Os-isotopes. In addition, it is the aim of this Chapter to consider whether the other PGEs support such a theory. The effect of subduction zones on the mantle PGE budget is also considered by comparison of the PGEs with REEs and fluid mobile elements. Any

correlations would be significant since it has previously been claimed that PGE behaviour is largely decoupled from REE depletion/enrichment events (Pattou *et al.*, 1996, Rehkämper *et al.*, 1997). Correlation of PGEs with lithophile element behaviour within the subduction environment might suggest that PGE-behaviour is modified in the halogen-rich, hydrous mantle wedge above subduction zones.

In contrast to the findings of Parkinson *et al.* (1998[a]) peridotite xenoliths thought to have sampled the arc mantle wedge from Ichinomegata, Japan and Simcoe, Cascades, indicate that some sub-arc mantle wedges may be enriched in radiogenic Os (Brandon *et al.*, 1996). This radiogenic Os is thought to be fluid-derived: either from dehydration of oceanic crust or sediments which have elevated $^{187}Os/^{188}Os$ (but low total Os i.e. <500ppt) compared to present-day mantle. In light of this observation, Brandon *et al.* (1996) propose that Os may be mobile during slab dehydration or melting. The volatility of all PGEs is known to increase in Cl-rich, oxidising systems, so slab-derived melts may be particularly effective at transporting PGEs. In terms of overall Os-concentration, the peridotite xenoliths are substantially depleted (i.e. 720-894ppt) relative to other peridotites (1-5ppb; Shirey and Walker, 1998). Thus, Brandon *et al.* (1996) suggest that Os may behave in a mildly incompatible manner as a result of destabilisation of sulfide phases in the oxidising regime of the subduction environment.

Rehkämper *et al.* (1997) have analysed a suite of harzburgites believed to be the residues from a supra-subduction zone environment. These samples are believed to have suffered repeated episodes of melt extraction, combined with re-enrichment by silicic melts from the subduction zone. The harzburgites have steep, fractionated (Pt-Pd depleted) patterns, considered to be due to enhanced transport of the more-fluid mobile PGEs (Pt and Pd) in the fluid-rich subduction environment (Rehkämper *et al.*, 1997). Since the residues from such hydrous melting in supra-subduction environments have low Pd/Ir, Pt/Ru ratios, it might be expected that arc-lavas would show correspondingly high ratios. This point will be addressed by considering the appropriate ratios observed within the Grenada suite.

Analysis of the Grenadian picritic lava suite provides a unique opportunity to evaluate the above arguments as the PGE-characteristics of this primitive suite, should be relatively unmodified compared to other arcs. If, as Brandon *et al.* (1996)

propose, Os is particularly mobile within the subduction environment and has been stripped from the wedge during metasomatism, a corresponding enrichment of Os (and the other PGEs?) should be observed within the resultant lavas. Failure of the picrites to show such enrichment may lend support to the theory of Parkinson *et al.* (1998[b]) that PGEs within the sub-arc wedge have been depleted by ancient melting events.

Brandon *et al.* (1996) require the addition of 7-15% of a subduction component (of which ~5% is sediment, at Os ~225-290ppt) to a depleted mantle source to account for the observed Os concentrations. Thus, the PGE concentrations of representative sediments from the Atlantic plate have been determined to evaluate the maximum PGE-contribution to the Grenada sub-arc mantle from subducted sediment.

8.2. Summary of Os-Isotope Geochemistry of Grenadian Lavas

Os-isotopic analyses were conducted on a limited number of Grenadian lavas. Samples were micro-distilled for Os-collection (by the author at Durham) and analysed by N-TIMS at the Department of Terrestrial Magnetism, Carnegie Institution of Washington (by Graham Pearson and Gordon Irvine) using the methods outlined in Pearson *et al.* (1995). The Os-isotopic ratios obtained and the precision of those measurements are given in Table 8.1 with the corresponding Os-concentrations. The limited numbers of analyses indicate that the Os characteristics of the Grenada samples are lava series-dependent. The high La/Y picrites have higher $^{187}Os/^{188}Os$ ratios and lower Os concentrations than the low La/Y picrites (Fig 8.1). The M-C series picrite (AMG 6157) is unique in having a much lower $^{187}Os/^{188}Os$ ratio, but higher Os concentration than any of the other lavas (Table 8.1). The lower Os-ratio of the M-C picrite is matched by lower Sr and higher Nd ratios than in the high La/Y picrites (Table 8.1).

Sample Name	$^{187}Os/^{188}Os$ (±2RSD)	Os (ppb)	$^{87}Sr/^{86}Sr$	$^{143}Nd/^{144}Nd$
Gd1 – Cumulate	0.14618 ±0.000790	0.074		
Gd8 – Low La/Y Picrite	0.14148 ±0.000532	0.087		
Gd10 – Low La/Y Picrite	0.14263 ±0.000259	0.085		
AMG 6078 – High La/Y Picrite	0.14738 ±0.000282	0.075	0.70493	0.512822
AMG 6103 – High La/Y Picrite	0.16441 ±0.000489	0.045	0.70498	0.512828
AMG 6157 – M-C Picrite	0.13366 ±0.000211	0.302	0.70455	0.512923

Table 8.1 Os-isotopic signatures of Grenadian lavas as measured by N-TIMS (samples prefixed AMG from Thirlwall – Sr and Nd isotope data for these samples from Thirlwall *et al.*, 1996)

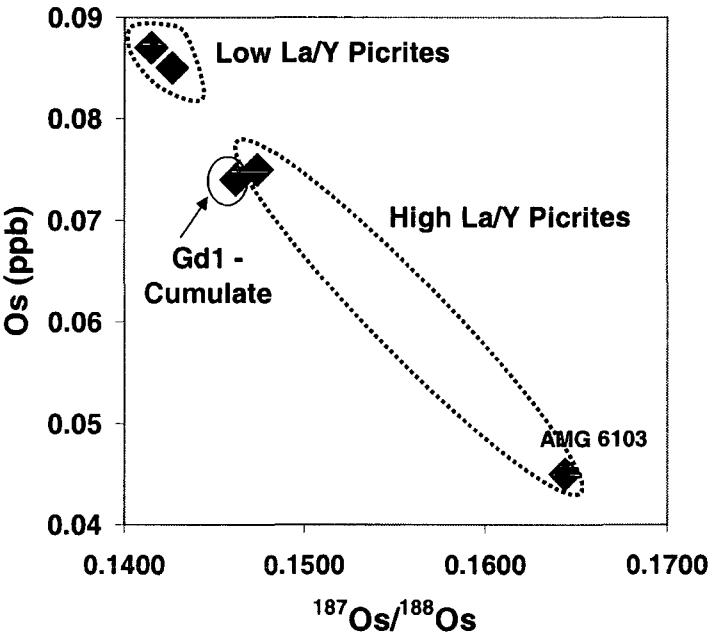

Fig 8.1 Relationship between the Os-isotope ratios and Os concentrations of the high and low La/Y picrites of the M-series of Grenada

8.2.1 Constraints on the Os Isotope Systematics of the Grenada Arc Source, from Peridotite Xenoliths

The Grenada M-series picrites and cumulate are more enriched in radiogenic Os than the sub-arc mantle wedge peridotite xenoliths recorded by Brandon *et al.* (1996), the Izu-Bonin mantle wedge harzburgites (Parkinson *et al.*, 1998[a]) and the one peridotite xenolith reported from Grenada (Parkinson *et al.*, 1998[b]; Fig 8.2). The M-C picrite, the most unradiogenic sample of the Grenada suite, has a $^{187}Os/^{188}Os$ ratio comparable to the most radiogenic sub-arc peridotites of Brandon *et al.* (1996);

(Fig 8.2). Thus, the M-series Grenada rocks are either significantly more enriched in radiogenic slab fluids than the samples analysed by Brandon *et al.* (1996) or the radiogenic signatures within the Grenada rocks are derived from an alternative source.

The Izu-Bonin harzburgites are less radiogenic than the Grenada lavas (Fig 8.2), this is consistent with their origin as residues of an ancient, mantle-melting event (Parkinson *et al.*, 1998[a]). The Izu-Bonin harzburgites partly overlap with the mantle wedge harzburgites (Brandon *et al.*, 1996), but also plot to less radiogenic compositions. This implies that the Izu-Bonin harzburgites have not been enriched by radiogenic Os-rich subduction fluids to the same degree as the Cascades and Ichinomegata mantle wedges.

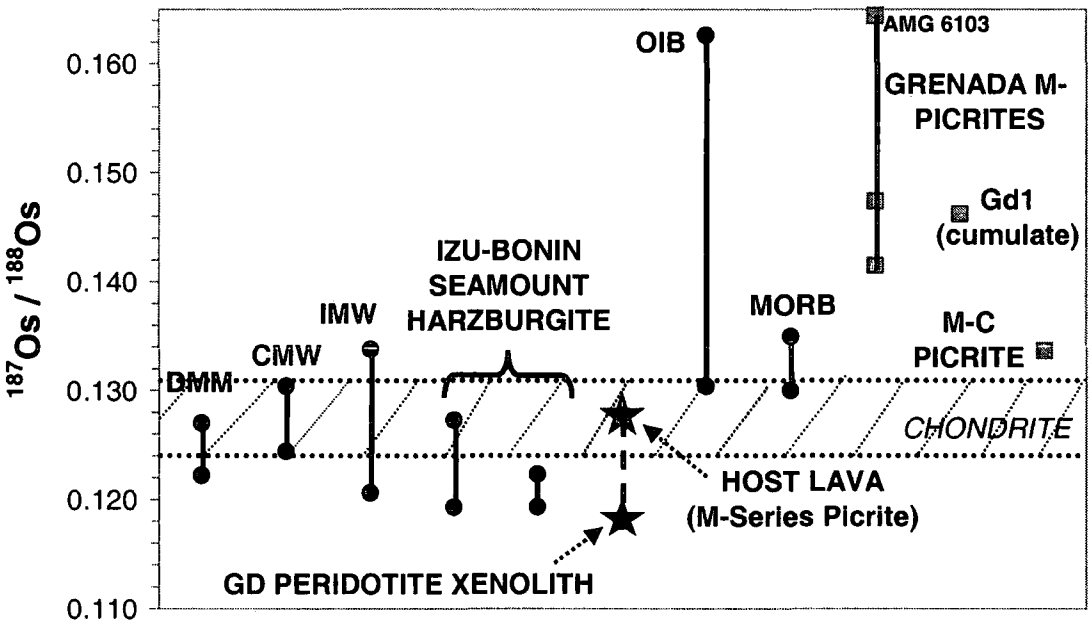

Fig 8.2 Range of Os-isotopic signatures for Grenada samples vs Izu-Bonin, with possible mantle reservoirs shown for comparison.

(DMM = depleted MORB mantle, Snow and Reisberg, 1995; CMW = Cascades mantle wedge, IMW = Ichinomegata mantle wedge, Brandon *et al.*, 1996; I.B. seamount data from Parkinson *et al.*, 1998[a]; Grenada peridotite xenolith data from Parkinson *et al.*, 1998[b]; Grenada host lava data from Parkinson, pers. comm.; Chondrite field + MORB data from Shirey and Walker, 1998; OIB data from Martin *et al.*, 1994)

All of the Grenada lavas analysed during this project are significantly more radiogenic than the single peridotite xenolith from Grenada analysed by Parkinson *et al.* (1998[b]). This xenolith is less radiogenic than both depleted MORB mantle (defined by the abyssal peridotites of Snow and Reisberg, 1995) and other analysed mantle-wedge xenoliths (Fig 8.2). Thus, parts of the Grenada sub-arc mantle wedge would appear to be highly depleted. Caution must be exercised however in basing assumptions of Grenada sub-arc composition on this one sample, as the data of Brandon *et al.* (1996) illustrates the wide variation in $^{187}Os/^{188}Os$ ratios than can exist in sub-arc lithosphere (i.e. from 0.1206 to 0.1338).

The host lava of the Grenada peridotite xenolith, is more radiogenic than the actual xenolith which it carried (i.e. host lava = $^{187}Os/^{188}Os$ of 0.1275, xenolith = $^{187}Os/^{188}Os$ of 0.118). The Os-isotopic signature of this host-lava, an M-series picrite, is lower than the M-series picrites measured during this study. This could be due to the inclusion of tiny pieces of highly unradiogenic xenolith within the lava which would act to lower its overall $^{187}Os/^{188}Os$ ratio (I. Parkinson pers. comm.). Thus, the xenolith may not represent the actual source of the lavas and it is probable that the lavas underwent only minimal interaction with this radiogenically depleted part of the mantle on their way to the surface (I. Parkinson pers. comm.).

The presence of unradiogenic xenoliths within radiogenically enriched lavas on Grenada, could fit with the marble-cake mantle model (Allègre and Turcotte, 1986) in which depleted peridotite contains enriched pyroxenitic-regions with high $^{187}Os/^{188}Os$. Such pyroxenitic veins show inverse correlation between Os (and Re?) concentration and Os-isotopic ratio (Shirey and Walker, 1998). Thus, preferential melting of these veins could potentially produce the pattern of low Re-Os, high $^{187}Os/^{188}Os$ seen in the Grenada M-series picrites. Alternatively, melting of the residues would produce magmas with lower $^{187}Os/^{188}Os$, but high Os content, the signature of the M-C series. However, such a model might be expected to produce much more dramatic elemental differences in the magma-series on Grenada. Therefore, alternative explanations for the Os-isotope systematics of the lavas are discussed below.

8.2.2 Constraints from Lavas

The $^{187}Os/^{188}Os$ range defined by the M-series lavas is considerably more radiogenic than MORB but falls within the range defined by OIB, except for AMG 6103 which is more radiogenic than OIB (Fig 8.2). The radiogenic nature of OIB is attributed to both the presence of recycled crust in the source region and to high-level crustal contamination. Overlap between OIB and MORB $^{187}Os/^{188}Os$ ranges reflects the varying importance of the three end-member components of OIB basalts: MORB, plume material and old oceanic crust. The extremely radiogenic nature of AMG 6103 suggests it was enriched by a component not present during OIB formation, possibly radiogenic slab-derived fluids. The M-C picrite is the only Grenada lava to overlap with the $^{187}Os/^{188}Os$ range of MORB. On this basis it may be suggested that the M-C picrite was either affected less by crustal contamination, or, derived from a source less enriched in radiogenic slab-derived fluids than the other Grenada lavas.

8.2.3 Source of Radiogenic Os in Grenada Lavas/Cumulates

A plot of $^{187}Os/^{188}Os$ vs $1/^{188}Os$ (Fig 8.3) approaches a reasonably straight line, especially if Gd10 is not included. Such a relationship is characteristic of two component mixing between a radiogenic, low-Os component and a relatively unradiogenic, higher-Os component. In a normal subduction environment there are two possible explanations for such a signature:

1) Mixing of a subduction component: either slab-derived aqueous fluids or assimilated sediments, with mantle.

2) Radiogenic Os could be acquired from late-stage crustal contamination, as the magmas assimilate arc crust during ascent to the surface.

Simple mixing calculations can be used to explore these possibilities. On the basis of Sr, Nd and Pb isotopes, Thirlwall *et al.* (1996) estimate that picrite lavas have experienced ~2% crustal contamination. If this crust is relatively young Tertiary arc crust then it is unlikely to have an extremely radiogenic Os isotope composition. Mixing of a crustal component with Os of ~0.03ppb and a $^{187}Os/^{188}Os$ ratio of ~1, with the different lavas analysed, indicates that it is difficult to achieve the observed

radiogenic-Os enrichment in the lavas with minor (2-5%) crustal contamination (Fig 8.3). The M-C picrite (sample 6157) is particularly robust to late stage crustal contamination as it contains 0.3ppb Os, but still exhibits a radiogenic Os-signature. Thus, although minor contamination of the Grenada magmas with arc-crust undoubtedly enriched them in radiogenic Os, it seems unlikely that this was the sole source of the ^{187}Os enrichment.

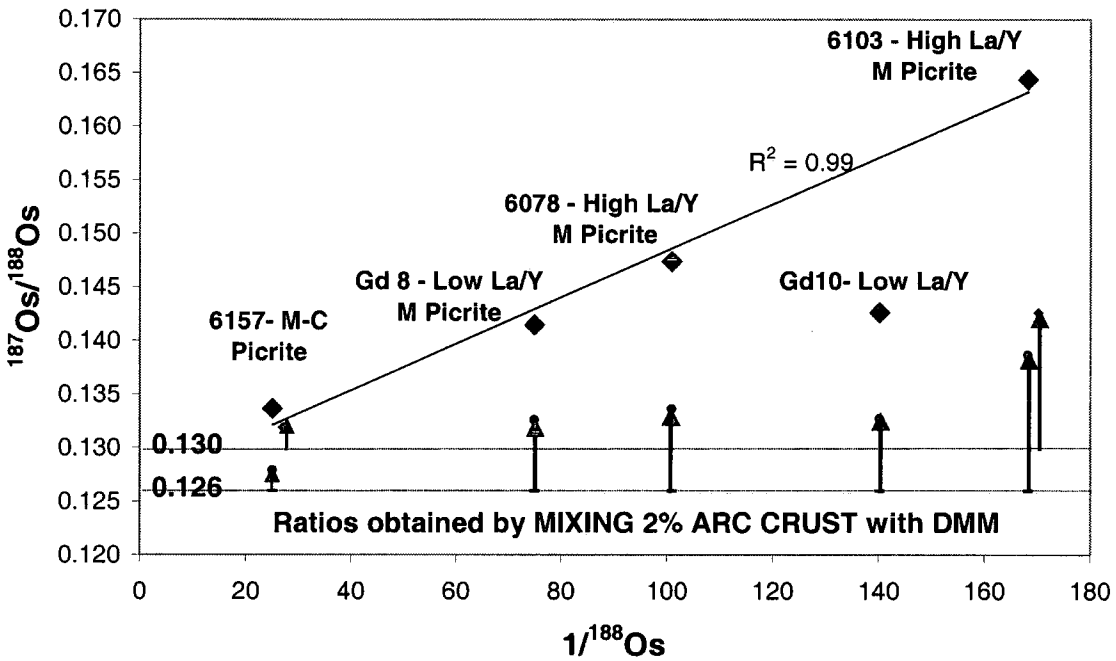

Fig 8.3 Os-isotope mixing line for Grenada samples - Effect on $^{187}Os/^{188}Os$ of mixing between arc crust and magmas derived from both a depleted mantle source ($^{187}Os/^{188}Os$ of 0.126) and from a more fertile source ($^{187}Os/^{188}Os$ of 0.13). Fractional crystallisation alone would produce a horizontal trend – the positive linear array must therefore represent a mixing line produced by a combination of AFC processes (Alves *et al.*, 1999).

Other observations are also inconsistent with crustal contamination dominating the Re-Os systematics of the Grenada lavas as variations in $^{187}Os/^{188}Os$ are not strongly correlated with Re enrichment (Fig 8.4). Thus, high Re concentration within the picrites is probably not related to crustal assimilation as this would also have elevated $^{187}Os/^{188}Os$ ratios. The low La/Y picrites have lower Re concentrations and less radiogenic Os-isotope ratios than the high La/Y picrites. Variability in Re is probably therefore, a primary feature of the different magma sources, possibly related to differences in mantle enrichment/depletion. In addition, if crustal

contamination were responsible for all of the radiogenic Os in the Grenada magmas, it is difficult to explain why the high La/Y picrites are more radiogenic than the low La/Y picrites and the M-C picrite.

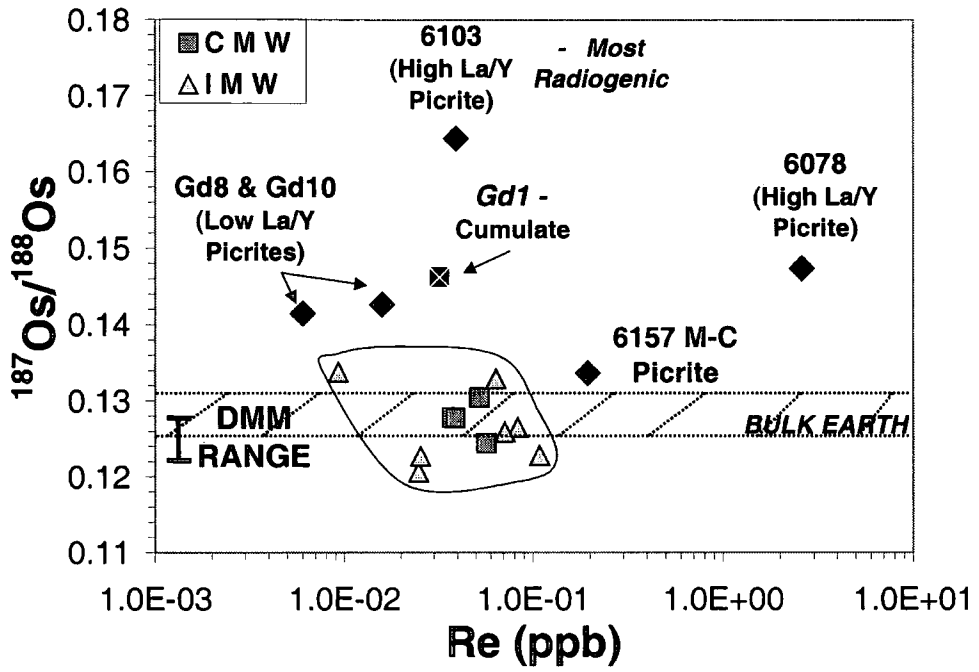

Fig 8.4 Re concentration of Grenada samples vs their Os-isotopic signature (CMW=Cascades mantle wedge, IMW=Ichinomegata mantle wedge from Brandon *et al.*, 1996. DMM range from abyssal peridotite data of Snow and Reisberg, 1995).

These arguments imply that some of the radiogenic Os in the Grenada picrites may be supplied by radiogenic Os originating from slab fluids, or from melted sediments. Hence the isotopic composition of the lavas represents a mix between DMM or more fertile mantle, and a radiogenic slab component, with minor crustal influence. The high La/Y picrites, representing smaller degree melts with a greater proportion of slab-derived fluid component, contain the most radiogenic Os (and Sr). Larger degree melts such as the low La/Y and M-C group have less radiogenic Os. It is significant that even the least radiogenic sample, the M-C picrite (6157; $^{187}Os/^{188}Os$ of 0.13366), still plots within the upper part of the range of the "enriched arc-mantle" samples of Brandon *et al.* (1996) indicating that it has incorporated slab-derived Os. The potential for high $^{187}Os/^{188}Os$ sediments being subducted and

incorporated into the Grenada lava source is high, as a large proportion of the sediments subducted below Grenada are thought to be derived from the Guyana shield (White and Dupré, 1986). Crust from an ancient craton such as this would have extremely high $^{187}Os/^{188}Os$ (~10; Shirey and Walker, 1998), and thus sediments derived from this area could be an important source of radiogenic Os in the Grenada subduction system.

8.2.4 Conclusions

The $^{187}Os/^{188}Os$ ratios of Grenada lavas are highly variable and too high to be explained solely by minor, late-stage crustal contamination. The M-C picrite which is relatively immune to crustal contamination due to its high Os-content, has $^{187}Os/^{188}Os$ ratios within the upper-range of the "radiogenic" arc peridotites of Brandon *et al.* (1996). This implies that there is enrichment of the Grenadian sub-arc mantle by sediments or slab-derived fluids. The correlation of increasing $^{87}Sr/^{86}Sr$ and decreasing $^{143}Nd/^{144}Nd$ with increasing $^{187}Os/^{188}Os$ in Grenada, from low to high La/Y M-series picrites, agrees with the conclusion of Thirlwall *et al.* (1996) that the high La/Y M-series picrites have a greater subduction component than the low La/Y picrites.

8.3 PGE Signatures of Grenadian Lavas

8.3.1 Reproducibility of Grenada PGE Data

The first PGE data obtained for the rocks of Grenada are presented in this chapter. These data form the basis of one of the first evaluations of full PGE signatures within an intra-oceanic arc (of non-boninitic character). This is due to analytical difficulties which have hampered analysis of PGEs in non-mineralised, low abundance samples in the past. Confidence is placed in the data quality as analytical blank is negligible (see chapter 5) and all Grenada samples were analysed either in duplicate or triplicate to monitor reproducibility (according to the convention outlined by McDonald, 1998).

2g sample aliquots were used where possible to reduce sampling errors. In addition, accuracy was assessed by considering the "smoothness" of the chondrite-normalised PGE patterns obtained. There has been recent debate regarding the use of normalising parameters within PGE geochemistry. Different PGE patterns (and thus interpretations) can be obtained simply by using different normalising factors (McDonald, 1998). Thus, the approach during this project has been to use the most recently determined values for C1-chondrite (Jochum, 1996) which are recommended as a possible "standard" set of normalising factors for future work (McDonald, 1998).

PGE	C1-Chondrite Concentration (ppb)
Re	39.5 ± 0.002
Os	492 ± 0.01
Ir	480 ± 0.019
Ru	683 ± 0.048
Pt	982 ± 0.038
Pd	545

Table 8.2 Chondrite-normalising values used within this chapter (all values from Jochum, 1996; except for Pd, from Naldrett and Duke, 1980)

Typical errors for a range of Grenada samples spanning the range of PGE concentrations are shown in Fig 8.4. Both concentrations and errors (2σ) are chondrite-normalised. These errors are representative of the other andesites, cumulates and picrites analysed in this study. Thus, error bars will generally not be shown on PGE-plots in the rest of this chapter for reasons of clarity. It should be noted that, in general, better reproducibility is achieved for higher abundance samples. In the case of the cumulates, however, there is greater variation between sample aliquots than in other samples. It is proposed that this is probably related to the coarse grain size of these rocks which may pre-dispose them towards more heterogeneous PGE "nugget" distribution.

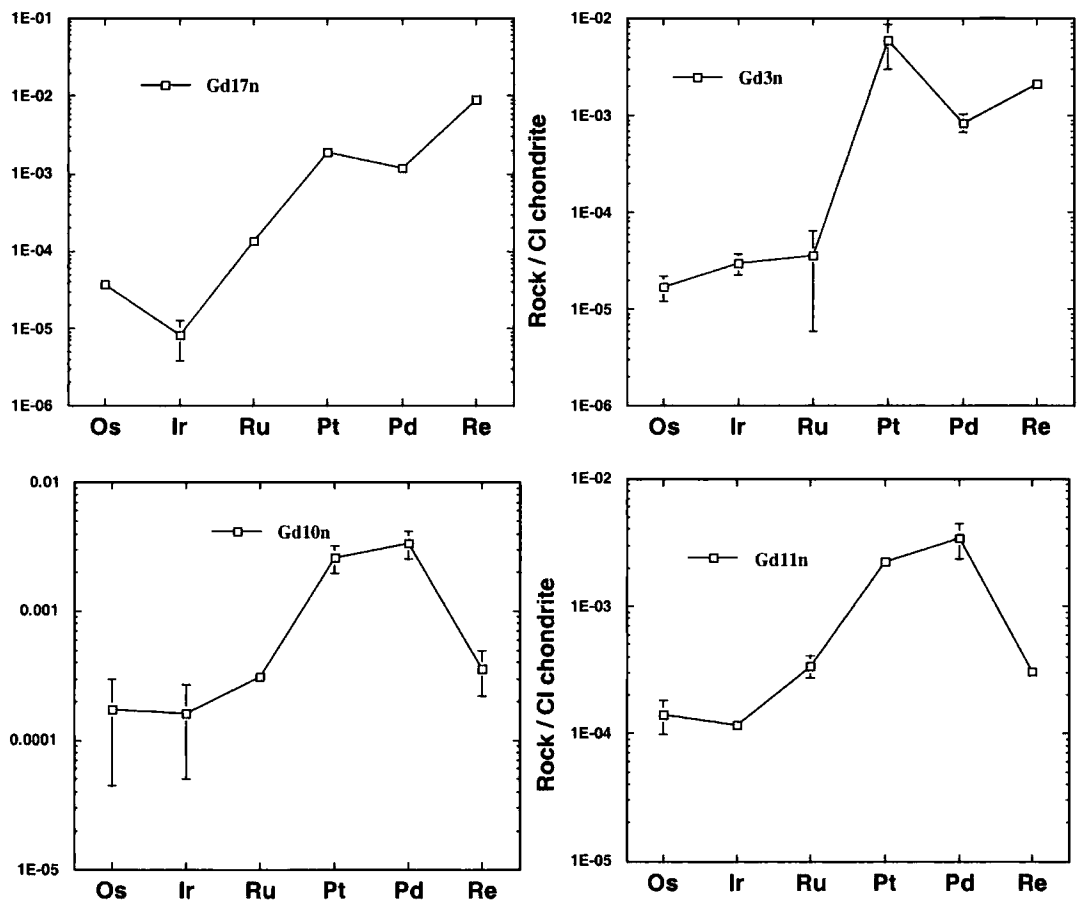

Fig 8.4 Typical errors (2σ) on replicate analyses for andesites (Gd17), cumulates (Gd3) and picrites (Gd10 and Gd11). Error bars smaller than symbol where not shown.

SAMPLE		Re	Os	Ir	Ru	Pt	Pd	No. of Replicates
Gd 17	Average (ppb)	0.36	0.018	0.004	0.092	1.896	0.655	2
	2*Stdev as %	2.0	18.6	53.7		2.6	7.6	
Gd 3	Average (ppb)	0.085	0.008	0.014	0.025	5.775	0.462	2
	2*Stdev as %	10.8	28.5	23.6	83.1	48.3	21.1	
Gd 10	Average (ppb)	0.014	0.085	0.078	0.211	2.537	1.823	3
	2*Stdev as %	38.4	74.0	68.9	3.3	24.4	23.5	
Gd 12	Average (ppb)	0.033	0.042	0.090	0.154	3.725	2.836	2
	2*Stdev as %	4.4	8.1	24.9		18.4	1.6	

Table 8.3 Typical reproducibility of Grenada samples

8.3.2 Summary of PGE Concentrations within the Grenada Suite

Comprehensive tables containing all PGE data on replicates and statistics of reproducibility between replicates are presented in Appendix II. Average PGE concentrations are not considered a good measure of the actual PGE abundance within a particular group of samples. In reality PGE-abundance can show a high degree of inter and intra-sample variability due to the occurrence of PGEs as discrete sulfides or nuggets. Thus, the PGE-ranges for each of the main groups of Grenada volcanic rocks are presented (Table 8.4).

Rock-type	Os	Ir	Ru	Pt	Pd	Re
High silica Andesite	0.016 - 0.018	B.D.L.	0.173	1.097 - 1.217	0.065 - 0.135	0.055 - 0.056
Basic Andesite	0.017 - 0.019	0.003 - 0.005	0.092	1.879 - 1.914	0.638 - 0.673	0.357 - 0.362
Hornblende-rich Cumulate	0.044 - 0.139	0.155 - 0.499	0.116 - 0.202	2.863 - 9.097	0.578 - 3.026	0.013 - 0.057
Plagioclase-bearing Cumulate	0.008 - 0.012	0.013 - 0.073	0.017 - 0.032	3.178 - 6.762	0.427 - 0.804	0.014 - 0.088
C-Series Basalt	0.012 - 0.014	0.024 - 0.037	0.038 - 0.046	1.512 - 3.146	2.518 - 7.60	0.088 - 0.102
M-C Basalt/Picrite	0.302 - 0.537	0.054 - 0.316	0.065 - 0.069	1.839 - 5.081	3.70 - 4.471	0.124 - 0.195
Low La/Y Picrite	0.054 - 0.117	0.037 - 0.166	0.064 - 0.326	1.742 - 3.858	1.113 - 2.280	0.006 - 0.018
High La/Y Picrites	0.038 - 0.075	0.048 - 0.098	0.062 - 0.171	3.117 - 3.968	1.873 - 4.015	0.012 - 0.039

Table 8.4 Concentration ranges for the samples analysed - All concentrations in ppb (B.D.L. = below detection limit ≈ to < 2ppt for Ir) N.B. The full PGE dataset, including replicate analyses for all samples are shown in Appendix II.

In terms of overall PGE abundances, the following are true,

For Os: M-C series > Picrites ≡ Hornblende Cumulate > C-Series Basalts > Plagioclase- Cumulates > Andesites

For Ir: Hornblende Cumulate > M-C series > Picrites > Plagioclase-Cumulates > C-Series Basalts > Andesites

For Ru: Hornblende Cumulate > Picrites > M-C series > C-Series Basalts > Plagioclase- Cumulates > Andesites

For Pt: Hornblende Cumulate > Plagioclase-Cumulates >M-C series > Picrites > C-Series Basalts > Andesites

For Pd: C-Series Basalts > M-C series > Picrites > Hornblende Cumulate > Plagioclase-Cumulates > Andesites

For Re: Basic Andesite > M-C series > C-Series Basalts > Plagioclase-Cumulates > Hornblende Cumulate > High SiO_2 Andesite > Picrites

8.3.3 PGE Patterns for Grenadian Volcanics

In the following discussion, absolute–concentration and C1-normalised PGE patterns are presented. Replicate analyses of the same sample are displayed on the same graph as a comparison of the reproducibility in the concentration plots. Statistics on the typical reproducibility of the data are presented in Table 8.3. Where a data-point is absent from a graph, it was considered to be unreliable (generally because of a lack of signal on Ru during analysis or due to the sample being close to, or below, detection limit).

There is variability in the steepness of the PGE patterns for the different rock types (Fig 8.5). In general, the most primitive rocks have the flattest (least fractionated) patterns (except for Re depletion). The M-series picrites: Gd8, Gd10 and Gd11, were recovered as individual bombs within a thick scoriaceous flow and thus were probably derived from the same batch of magma. There is a very close resemblance between the PGE patterns of these samples and thus it may be concluded that PGE distribution within a single restricted magma batch is relatively homogenous. Gd14 by contrast, although of the same geochemical subgroup as Gd8, Gd10 and Gd11, is from a different location (and hence magma batch?) and shows subtle differences, particularly in the slope of the IPGEs due to Ir enrichment.

The high and low La/Y subgroups of the M-series picrites show almost identical PGE patterns. Subtle differences include a tendency towards more positively sloped IPGE patterns and lower Os concentrations within the high La/Y group. This suggests that the PGEs are not strongly controlled by the same factors that control LREE enrichment. Therefore, the differences in degree of melting or amount of fluid input, responsible for La/Y variation in the picrites, were not sufficient to cause variation in PGE content between the high and low La/Y picrite groups. The M-C basalt (Gd5) and M-C picrite (AMG 6157) have PPGE patterns akin to those of the M-series picrites, but IPGE patterns that are markedly different, implying some fundamental differences in their formation or source region.

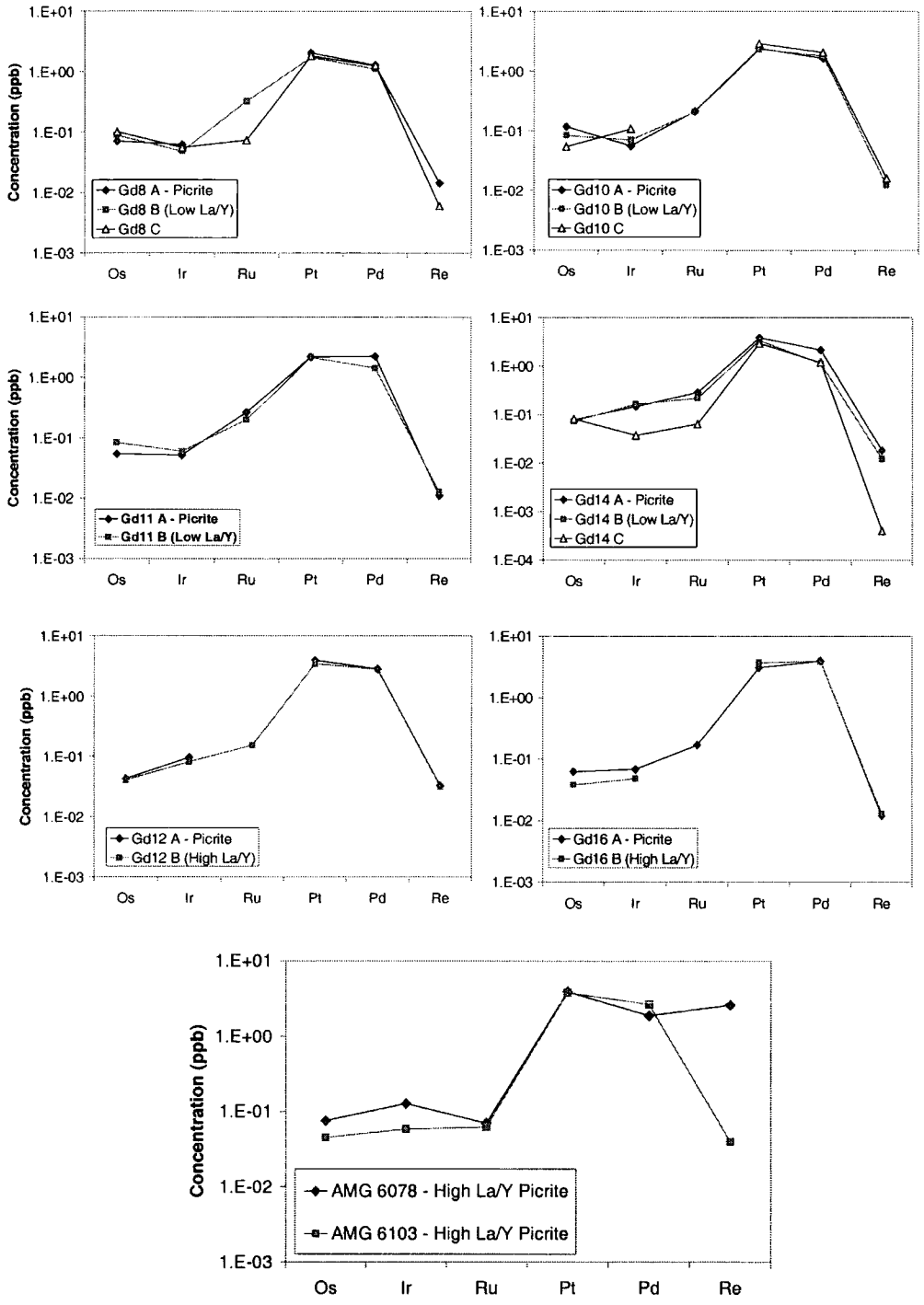

Fig 8.5a PGE patterns (absolute concentrations) for all Grenada samples analysed. N.B. High Re in Sample AMG 6078 is uncharacteristic of all other picrites and is considered suspect. Re contamination may have occurred as a result of rock-crushing in a tungsten carbide mill.

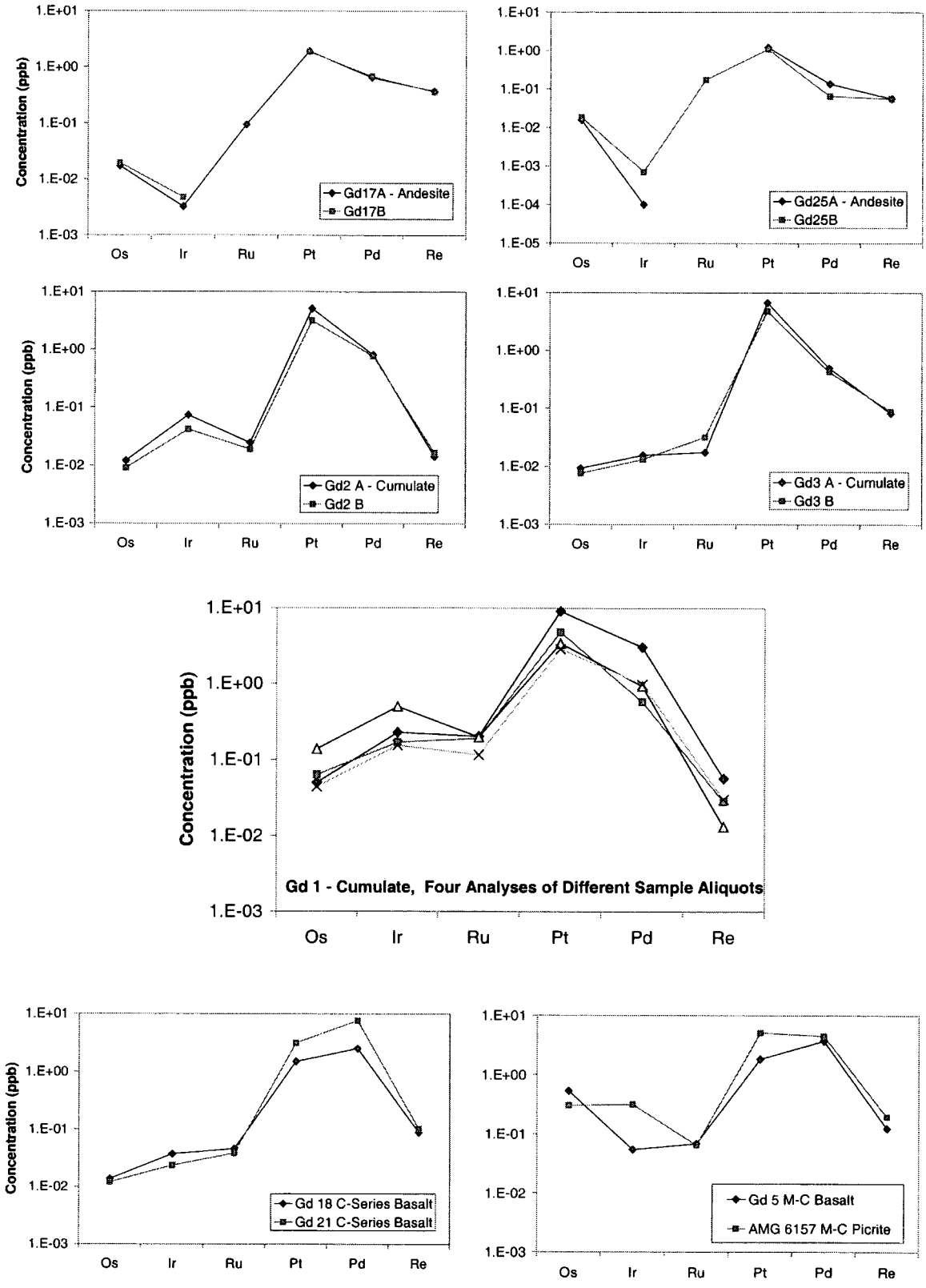

Fig 8.5b PGE patterns (absolute abundance) for Grenada samples

8.3.3.1 IPGE Variation during Fractionation

a) PICRITES and BASALTS: There are only very subtle differences in Os and Ir concentration within the M-series picrites. This indicates that Os and Ir behave very similarly during initial mantle melting. The low La/Y group has flat to slight negative-sloped patterns between Os and Ir, whereas the high La/Y group has flat, to slight positive-sloped patterns between Os and Ir. This relationship suggests either that Ir is slightly less compatible than Os during smaller degree melting events, or that Ir was enriched relative to Os in the fluids that cause corresponding La enrichment in the high La/Y picrites.

The M-C group displays unusual IPGE patterns, characterised by higher abundances of Os than those seen in any of the other groups. There was a divergence in behaviour of Os and Ir during fractionation of the M-C picrite to form the basalt. Os/Ir within the basalt is significantly higher than in the picrite (i.e. Os/Ir of 9.94 vs 0.96). Thus, a phase with which Ir was highly compatible but Os was not, presumably crystallised from the picrite prior to basalt formation. Ru was unaffected by fractionation, but is markedly depleted relative to Os within both the picrite and basalt. It is tempting to ascribe the Os-enrichment in the M-C series to metasomatic concentration of Os by Cl-rich fluids (e.g. Brandon *et al.*, 1996). However, the flat Os-Ir pattern within the picrite implies that Ir and Os behaved coherently within the mantle source. Thus, the variations in Os/Ir are probably a fractionation phenomenon.

The C-series has gentle positive slopes from Os, through Ir, to Ru (closely resembling cumulate Gd3). This must reflect the relative trend of IPGE compatibility with phases such as olivine, fractionation of which generated the C-series from more picritic parental magmas (Thirlwall *et al.*, 1996). Removal of the IPGEs presumably during early C-series fractionation, is confirmed by the lower concentration of Os, Ir and Ru in the C-series compared to the M-series picrites.

b) ANDESITES and CUMULATES: The andesites show asymmetrical V-shaped patterns from Os, through Ir to Ru. This is due to marked depletion in Ir and enrichment in Ru relative to the other IPGEs, suggesting that a phase with which Ir is particularly compatible has been removed from the melt prior to andesite formation.

Relative Ir-enrichment within the cumulates (compared to the other IPGEs) may explain the observed Ir-depletion within the andesites. Ru is significantly enriched within Gd25 compared with the cumulates (Gd2 & Gd3) and the basalts to which it is genetically related. This implies that rather than behaving in a compatible manner during fractionation (which is often inferred by comparison with Os), Ru was retained within the residual andesitic melt. This is the first time that this phenomenon has been recognised and may be related to the unusual hydrous, high-fO_2 conditions within island arc magma chambers.

Cumulates Gd1 and Gd2 exhibit similar IPGE patterns. However, there is a significant difference in overall IPGE concentration between the two different types of cumulate. It was proposed (Chapter 7) that Gd1, the hornblende-cumulate, was deposited during formation of andesites akin to Gd17 from M-series lavas. Conversely, Gd2, a plagioclase-bearing cumulate, was thought to be deposited during high level fractionation of C-series magmas during formation of highly evolved andesites like Gd25 (Fig 7.31). PGE variations corroborate this theory as Gd1 formed from a less fractionated, more basic magma, contains significantly higher quantities of PGEs than Gd2 which would have probably experienced a higher degree of PGE removal in earlier fractionation events. The low concentration of PGEs within cumulates Gd2 and Gd3 provides indirect evidence that several stages of magma pooling and fractionation have taken place before the more evolved rock types are eventually erupted at the surface.

8.3.3.2 PPGE Variation during Fractionation

a) PICRITES and BASALTS: The picrites (both M and M-C series) exhibit flat or slight negative slopes in their PGE patterns between Pt and Pd, suggesting that they are not strongly fractionated from each other during initial melting. The M-C and C-series basalts are enriched in Pd relative to the other PPGEs and thus have positively-sloped patterns between Pt and Pd, unlike any of the other rock-types. Thus, either a phase with which Pd is compatible has accumulated within the basalts or Pd has reached its maximum "solubility" within the basalt melt. Pd build-up within the basalts implies that it may be slightly less compatible than Pt in this situation.

b) ANDESITES and CUMULATES: The andesites mark a return to negative slopes between Pt and Pd. This is due to a big decline in Pd concentration, suggesting that Pd has been rapidly removed from the magma, although Pt concentration also drops overall between the basaltic and andesitic compositions. The cumulates have PPGE patterns with similar shapes to those of the andesites (i.e. with relative Pt-enrichment). Thus, Pt appears to be more compatible with one of the cumulus phases than Pd. The nature of this phase will be discussed later. The dramatic changes in Pt-Pd slope which occur as fractionation proceeds, indicates either that Pt and Pd distributions are controlled by different phases, or that they show markedly different partition coefficients for the phases that are crystallising.

8.3.3.3 Re Variation During Fractionation

Consistently low Re concentrations within the M-series picrites (except for AMG 6078) suggest that the mantle source of the M-series picrites is homogenous with regard to Re and that variation in the amount of crustal contamination between picrites is minimal. The anomalously high Re-content of sample AMG 6078 cannot easily be explained and may be the result of contamination. The consistency of the rest of the PGE-pattern with the other Grenada samples however, suggests that Re alone may have been contaminated during the sample preparation (ca. crushing in tungsten carbide, Thirlwall pers. comm.).

This signature of depletion of Re relative to the other PGEs occurs within the M-C group, the C-series basalts and the cumulates. The M-C picrite however, contains nearly an order of magnitude more Re than the M-series picrites. Since Os-isotopic studies rule out more extensive crustal contamination of this sample, compared to the M-series picrites, Re variation must be source-controlled. Re concentration increases as fractionation proceeds and peaks within the andesites, resulting in a flattening of the negative slope between Pd and Re. This confirms the incompatible behaviour of Re during fractionation.

8.3.4 Covariation of the Different PGEs during Fractionation of the Grenada Suite

Os and Ir would be expected to co-vary most strongly under normal conditions of mantle melting (e.g. correlation coefficient of 0.98 for Os-Ir, within the Greenland picrites). Such clear-cut patterns are not observed in Grenada however, as the environment is considerably more complex. Multiple fractionation events and possibly heterogeneous mantle combine to overprint the initial melting signatures, probably what is observed in the Greenland picrites. Regardless of the complications, some relationships between PGEs have been identified.

Os and Ir covary positively within the cumulates and from the C-series basalts to the M-series picrites (Fig 8.6a). The two M-C-samples plot in a separate field in which Ir and Os are negatively correlated. The andesites too are displaced from the main trend and become rapidly depleted in Ir for little change in Os. The situation is repeated between Ru and Os (Fig 8.6b), although this time Ru increases between the C-series and more andesitic compositions for relatively little change in Os-concentration. Os and Pd covary depending on the type of sample (Fig 8.6c). M-C samples have high Pd and Os, whereas the C-series have high Pd and low Os, probably an artefact of increased fractionation. The Pd concentration drops rapidly for little change in Os in the andesites, this is probably related to the fact that absolute minimal amounts of Os are retained in the melt by time the andesites are formed.

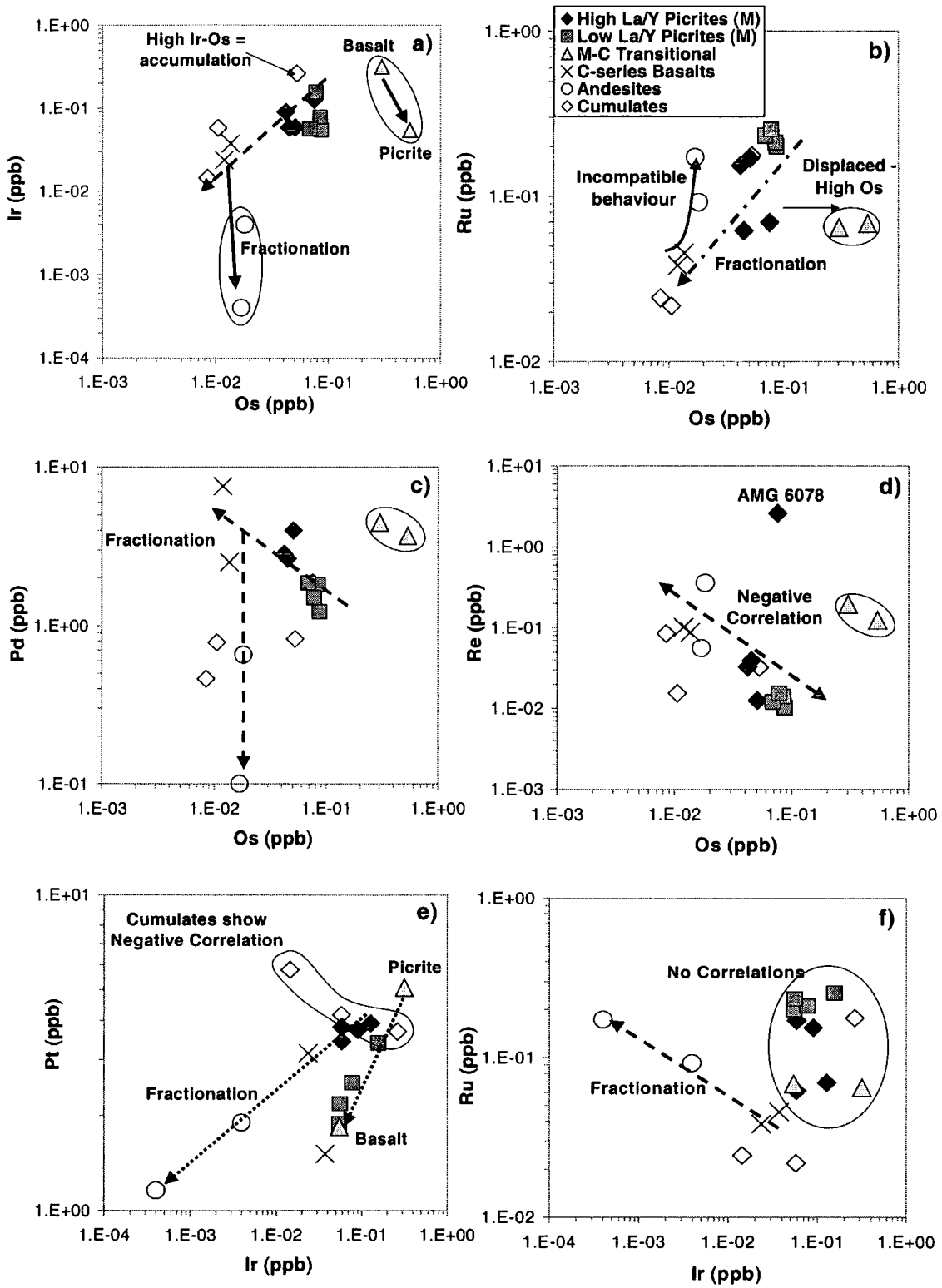

Fig 8.6 (a-f) Relative PGE variations within the Grenada fractionation suite

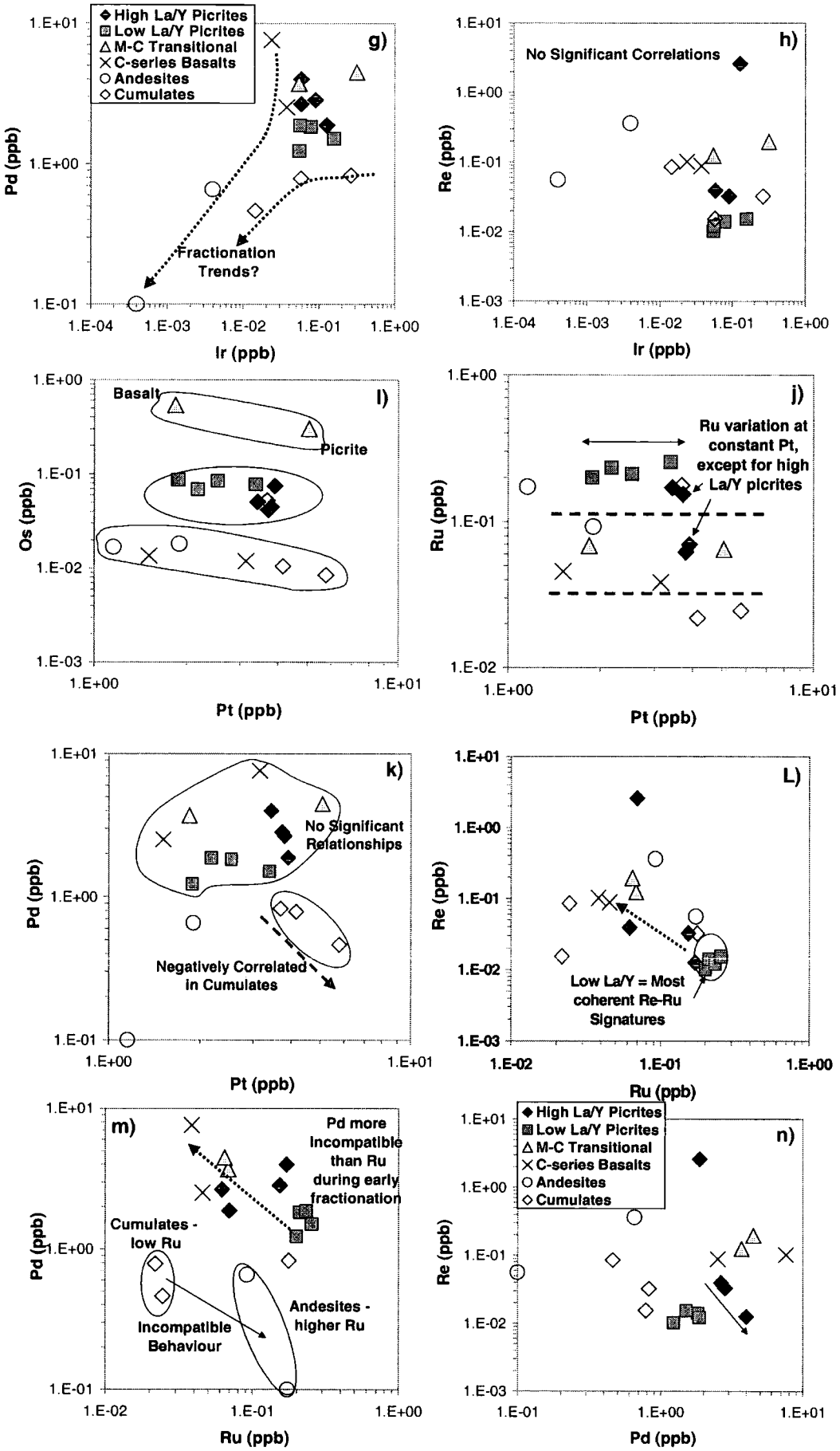

Fig 8.6 (g-n) Relative PGE variation in the Grenada fractionation suite

A negative correlation is observed between Os and Re (Fig 8.6d) from the C-series basalts through to the M-series picrites. This must be due to the well-documented incompatibility differences between Os and Re (Shirey and Walker, 1998), with Os removed in early crystallising phases (olivine) while Re is concentrated into the residual melt. The M-C group again, plot as a separate field as a result of having both high Re and Os compared to the M-series picrites. Pt and Ir concentrations within the low La/Y picrites are unrelated (Fig 8.6e) with a wide scatter of Pt-concentration at constant Ir. The high La/Y picrites form a much tighter cluster (less Pt-variation) and a positive trend, which is also seen within the andesites. Very little correlation is observed between Ir and Ru (Fig 8.6f), except within the andesites where they show contrasting behaviour (Ru behaves incompatibly, Ir behaves compatibly).

Pd and Ir concentrations are both high within the primitive rocks (Fig 8.6g), but then Ir is preferentially extracted with the cumulates. Both Ir and Pd decrease as fractionation proceeds to andesitic composition. No coherent relationship exists between Re and Ir (Fig 8.6h). Os and Ru are largely invariant (Fig 8.6i and j) with increasing Pt concentration. Thus, processes which control Pt-abundance do not affect the IPGEs. Decoupling of Pt and IPGE-behaviour therefore occurs during fractionation. Pt and Pd have systematically higher concentrations within the high La/Y picrites compared to the low La/Y picrites (Fig 8.6k). It can be inferred therefore that the processes which cause La-enrichment (i.e. higher fluid input?) may also increase Pt and Pd concentrations. Within the cumulates Pt and Pd negatively correlate. This indicates that similar experimentally calculated partition coefficients for Pt and Pd between magmatic phases may not hold true in natural systems.

Re and Pd variations vs Ru highlight the fact that the low La/Y picrites form a much more coherent group (Fig 8.6 l and m) than the other primitive rocks, which have highly variable Re and Pd. The scattered nature of Re and Pd compared to Ru within the high La/Y picrites, implies that these elements may have been variably mobilised within the high La/Y picrites. This could correspond to high slab-fluid input as suggested by the LREE enrichment. Re and Pd do not behave the same during fractionation (Fig 8.6n). In general, Re is high in the most evolved samples,

whereas Pd content decreases with fractionation. Thus, Re appears to be the more incompatible of the two elements.

8.4 Variation of PGEs in the Grenadian Suite with Major Elements

In order to determine what governs the PGE compositions and variation in the Grenada samples, the PGE data must be compared with other element data, following a similar procedure to that used in Chapter 6.

8.4.1 PGEs vs Mg No. in the Grenada Suite

Plots of PGEs vs Mg No. illustrate how PGE contents in the Grenada suite vary with fractionation. To a first approximation, all of the PGEs except Ru and Re decrease in concentration as the degree of fractionation increases through the C-series into the andesites. There is very little variation in Mg No. throughout the picrite-series despite a wide variation in PGE concentrations. Therefore, the overall PGE abundances in the near-primary lavas are probably influenced by factors other than fractionation. This also appears to be the case for the M-C lavas as, although they have slightly lower Mg Nos., they have significantly higher Os-concentrations than the M-series picrites. This suggests that the M-C lavas must be derived from discrete primary magmas rather than from fractionation of M-series lavas, as crystallisation of any olivine would be expected to deplete the magma in Os (Brügmann *et al.*, 1987) and lower the Mg No.

The cumulates are not significantly enriched in any of the PGEs compared to the primitive magmas. They show variable behaviour, with the lower Mg No. plagioclase-bearing cumulates Gd2 and Gd3 (products of C-series fractionation) showing low Ru, Pd and Os, and high Pt compared to the other samples. By contrast, Gd1 which appears much less fractionated judging by its high Mg No. (product of M-series fractionation), contains significantly higher concentrations of the IPGEs (Ir, Os and Ru) and less Pt than the other cumulates. This suggests that the plagioclase-bearing cumulates are in fact precipitated from a magma which has been previously depleted in PGEs, probably during earlier olivine fractionation. The low Ru content in Gd2 and Gd3 correlates with observed high Ru abundances in the andesites. The

inverse of this relationship is true for both Pt and Ir. Thus, it is suggested that PGE-concentration within the andesites is largely governed by extent of cumulate fractionation and hence concentration or removal of different PGEs from the magma.

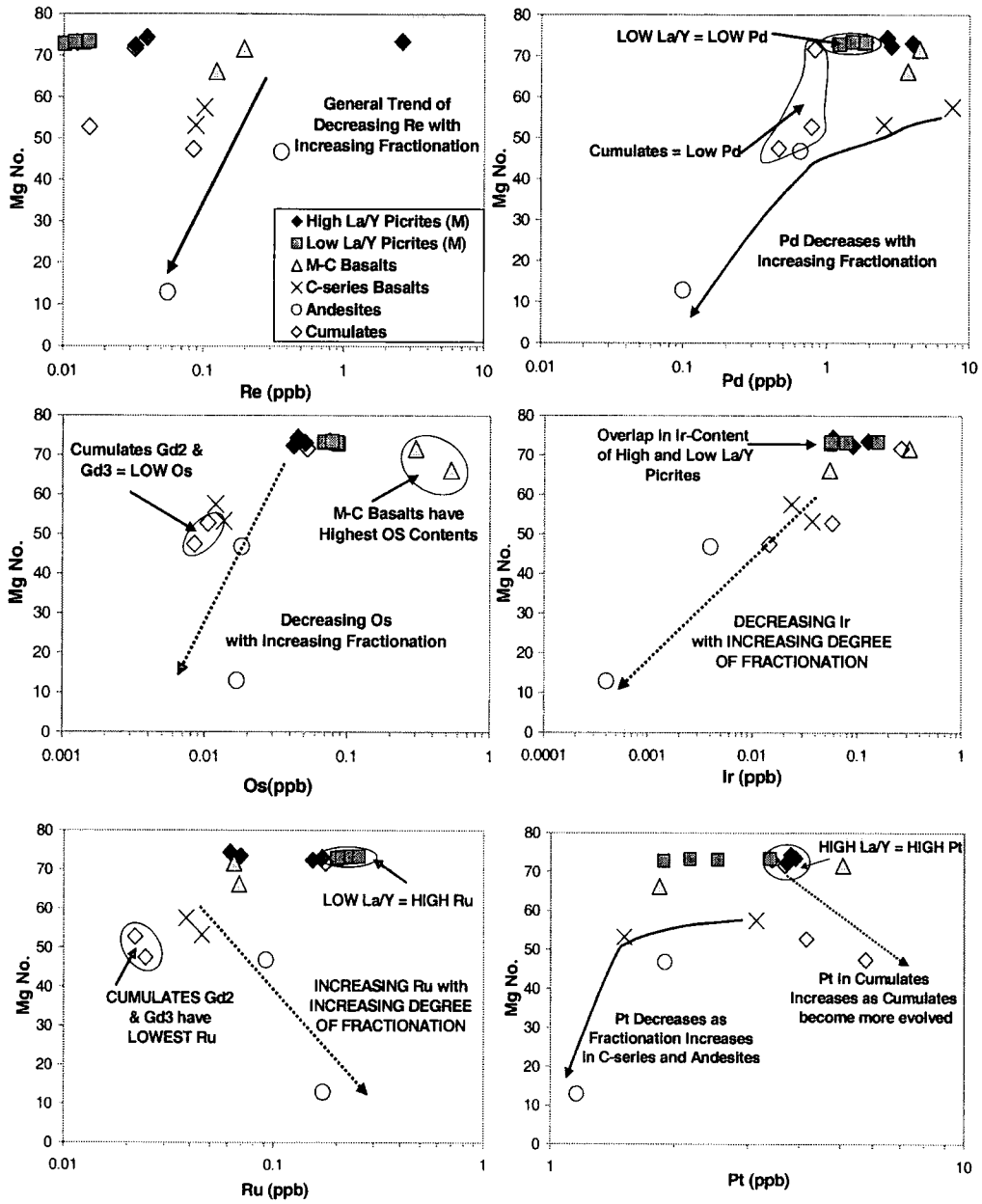

Fig 8.7 PGE variation against Mg No as an index of fractionation

The Re concentrations of the Grenada suite increase during the initial stages of fractionation (i.e. from the M-series picrites to the C-series basalts) consistent with the incompatible behaviour of Re. Further fractionation (i.e. from C-series to andesites) however, results in Re depletion within the more evolved rocks. This is contrary to expected behaviour and suggests that a phase with which Re is compatible begins to crystallise during the latter stages of fractionation

8.4.2 Correlation between PGEs and Other Major Elements within the Grenada Suite

Variation in PGE concentrations within the more primitive samples cannot easily be linked to olivine fractionation. Thus, comparison with other major elements has been undertaken to ascertain whether there is a link between PGE concentration and degree of partial melting or fractionation of another mineral phase.

8.4.2.1 Correlation of PGEs with Al_2O_3

Al_2O_3 has been chosen as an index of degree of partial melting as it is mildly incompatible during mantle melting, but not significantly fluid mobile. Thus, high Al-content in primitive melts should imply a low degree of melting. In addition, the bulk partition coefficients of Re and Al are often comparable during mantle melting (Reisberg and Lorand, 1995). Plots of Al_2O_3 vs Os, Ir and Pt do not show any significant trends. Some subtle trends do emerge, however, when Re, Ru and Pd are compared with Al_2O_3 (Fig 8.8). Fractionation from C-series basalt to andesite composition is marked by decrease in Re and Pd concentration, but increase in Al_2O_3 concentration. This may be due either to plagioclase (in which Al_2O_3 is compatible but Re and Pd are not) accumulation in the andesites, or, because Al_2O_3 is more incompatible than Pd and Re and therefore becomes concentrated in the residual melt. The fact that Re and Al become negatively correlated as fractionation proceeds, is indicative of variation in S-systematics of the magma. As Re is chalcophile but Al is lithophile, S-variation within a magma can cause the bulk partition coefficients of Al and Re to differ (Reisberg and Lorand, 1995).

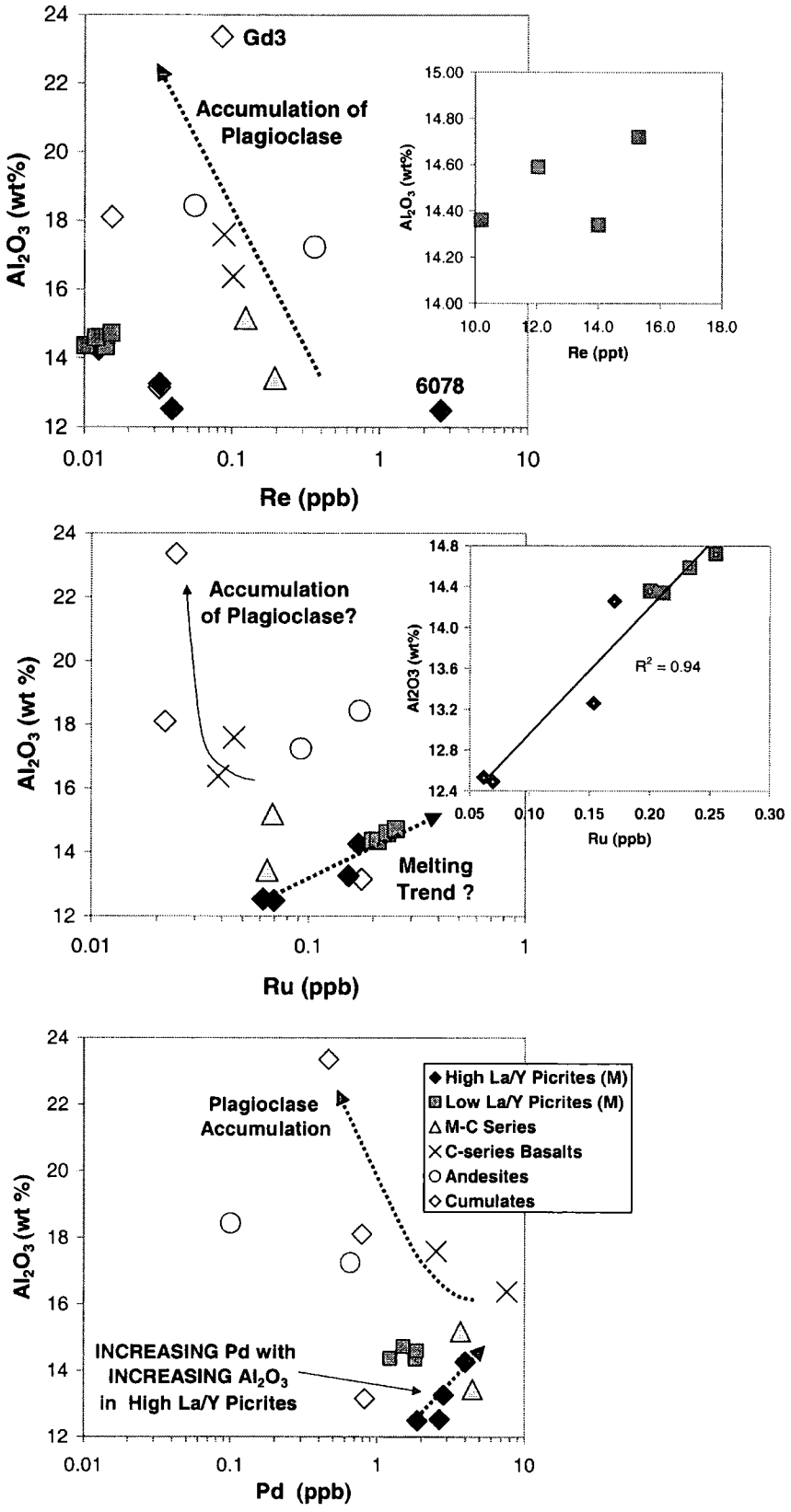

Fig 8.8 Plots of Re, Ru and Pd vs Al_2O_3 for the Grenada suite (Inset boxes show correlations within the picrite groups)

The low La/Y picrites form a much more coherent group than the high La/Y picrites as regards their Re and Al_2O_3 characteristics. Within the low La/Y picrite group Al and Re positively correlate (Fig 8.8). No such trend is observed within the high La/Y picrites. In addition, the high La/Y M-series picrites generally contain lower Al_2O_3 but, higher Re concentrations. This decoupling of the Al- and La-behaviour implies that the La (and presumably Re) are more fluid-mobile than Al. Thus, the lack of correlation between Al and Re within the high La/Y picrites indicates than in hydrous-melting conditions, Al and Re do not behave similarly.

The opposite situation is true for Al_2O_3 vs Ru (Fig 8.8). Ru correlates positively with Al_2O_3, in both the high and low La/Y picrites with Ru and Al_2O_3 being most enriched in the low La/Y picrites. Thus, Ru and Al may behave similarly during mantle melting. Presumably both elements are either extracted from their mantle source more effectively when there is less fluid input, or by higher degrees of melting. There are no significant trends for Pd and Al_2O_3 between the low and high La/Y picrite groups. Within the high La/Y group however, Pd and Al_2O_3 positively correlate.

8.4.2.2 PGEs vs TiO_2

TiO_2 is a useful indicator of magnetite fractionation. Ir decreases with decreasing TiO_2 through the C-series basalts into the andesites and also within the cumulates (Fig 8.9). This suggests either that Ir may be mildly compatible with magnetite, or that Ir is being precipitated as an alloy or within another cumulate phase, at the same time as magnetite. No significant correlations are observed between Os, Ru or Pd and TiO_2.

There is no correlation between Pt and TiO_2 except within the cumulates where Pt increases slightly for a sharp decrease in TiO_2 (Fig 8.9). This indicates that Pt was not compatible with magnetite during cumulate formation. There are no other significant correlations between TiO_2 and any of the other PGEs. This is an interesting result, as recent reports (Righter *et al.*, 1998) suggest that Re is compatible with magnetite. No evidence of this is seen by comparison of Re with TiO_2, but further comparison of Re with other magnetite-compatible elements (e.g.

V) will be conducted in section 8.6. in order to fully ascertain what phases are controlling Re distribution within the Grenada suite.

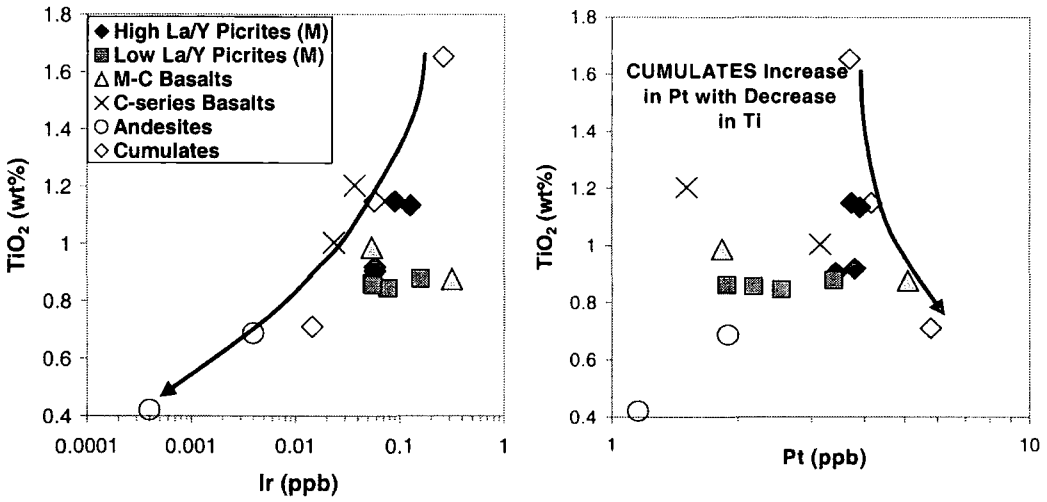

Fig 8.9 Plots of Ir and Pt vs TiO_2 for the Grenada suite

8.4.2.3 PGEs vs CaO

Ca is compatible with both plagioclase and CPX, which are important phenocryst phases formed during high level fractionation of the Grenada suite. The Pt-content of the C-series basalts increases with increase in CaO (Fig 8.10). This may be due to accumulation within the C-series magma of cumulus phases such as plagioclase and CPX with entrained PGE nuggets. The cumulates likewise, are high in both CaO and Pt. It is suggested therefore that Pt is compatible with an as yet unidentified constituent of the cumulates.

In contrast, Ru has a low concentration within the high CaO-cumulates, but reaches higher concentrations in the more evolved andesites (Fig 8.10). This suggests that the Ru and Pt are decoupled during cumulate formation, with Ru behaving in a more incompatible manner. No correlations are observed between the other PGEs and CaO however, with the M-series picrites and M-C transitional series showing highly variable PGE contents at very constant CaO concentrations. Therefore, it can be assumed that the distribution of Ir, Os, Pd, Pt and Re within the more primitive samples is not controlled by CaO-rich phases (i.e. CPX or plagioclase).

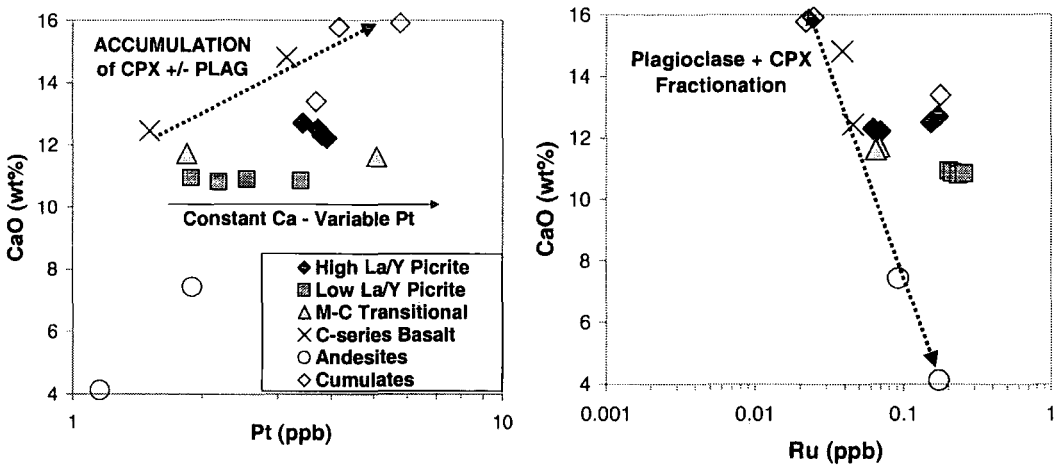

Fig 8.10 Plots of Pt and Ru vs CaO for Grenada suite

8.5 Variation of PGEs with Compatible Elements in the Grenadian Suite

Correlations between the PGEs and major elements are often absent or ambiguous, as silicate phases are not perceived to be the main phases controlling PGE distribution (Sylvester *et al.*, 1998). Instead, the PGEs generally have a greater affinity with compatible elements such as Ni, Cr, Co and V since these elements tend to have similar partition coefficients to the PGEs for certain mineral phases. For example, experimental studies indicate that Re is comparable to V and Cr in its affinity for magnetite, whereas Ru has a comparable K_d to Ni and Co in magnetite (i.e. >200; Righter *et al.*, 1998). In addition, Os like Ni, is thought to be compatible with olivine (Brügmann *et al.*, 1987). Thus, in the following section, relationships between the PGEs and Ni, Cr, Co and V are examined to try and identify likely mineral phases which are controlling PGE distribution.

8.5.1 PGEs vs Ni

Variations in Re and Pt concentration are independent of Ni variation. Hence, it can be concluded that accumulation/fractionation of olivine did not affect Re and Pt concentration within the Grenada magmas.

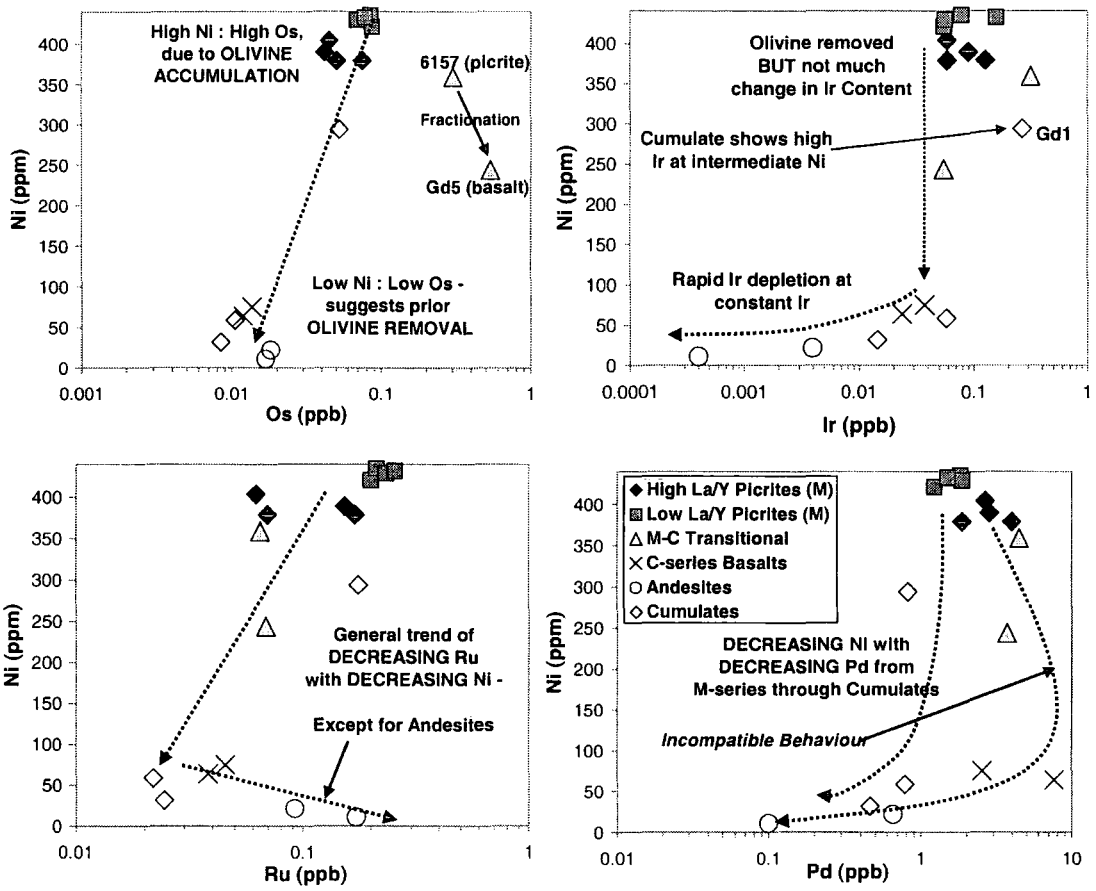

Fig 8.11 Covariation of PGEs with Ni in the Grenada lavas

The clearest correlation between olivine fractionation and corresponding PGE depletion of the associated lavas is for Os (Fig 8.11). The C-series lavas, postulated to be derived via olivine fractionation of more picritic melts, are substantially more depleted in Os and Ni than the M-series picrites. This lends credence both to the theory of C-series production via olivine crystallisation and the proposal that Os is compatible with olivine (Brügmann *et al.*, 1987) or with a phase coprecipitated with olivine. The only samples that do not conform to this trend are the M-C transitional samples which have higher Os and lower Ni than the M-series picrites. This may suggest that factors other than olivine accumulation have influenced the Os-distribution in this group. This is backed-up by the observation that the Os-content of the M-C group appears to increase with fractionation of olivine, as shown by the

decline in Mg No. Thus, specific conditions may have occurred within the M-C magma chambers under which Os did not behave compatibly with olivine.

The M-C group displays the opposite trend for Ir vs Ni (Fig 8.11), with Ir becoming depleted in the magma as olivine fractionation proceeds. In the M and C-series samples Ir-content does not fall as rapidly with decreasing Ni as does Os. Therefore, Ir abundance is probably less strongly controlled by olivine than is Os abundance. Within the more evolved samples Ir content decreases rapidly for very little change in Ni concentration. Thus, phases other than olivine are responsible for Ir depletion in the melt. For example, cumulate Gd1 which is predominantly composed of amphibole, has one of the highest Ir contents, indicating that Ir in this instance was precipitated from the melt during accumulation of amphibole phenocrysts.

Ru becomes depleted during olivine fractionation between the C and M-series (Fig 8.11) suggesting mild compatibility with olivine. As fractionation proceeds, however, and andesites are formed, the behaviour of Ru changes and it becomes incompatible with the crystallising phases. Pd conversely, behaves in a mildly incompatible manner during olivine fractionation as the concentration of Pd does not decrease between the M-series picrites and C-series basalts. The Pd content of cumulate Gd1 is also low, suggesting that Pd was not precipitated from the melt with amphibole during M-series fractionation. Between the C-series and the andesites, there is rapid depletion of Pd (in a similar manner to Ir), suggesting that Pd was precipitated from the melt. This may be related to S-saturation within the melt, the implication being that S-saturation was reached in high-level magma chambers between formation of C-series basalts and andesites. This may be related to assimilation of crust which can push a magma towards S-saturation (Keays, 1995).

8.5.2 PGEs vs Cr, V and Co

8.5.2.1 PGEs vs Cr

Other phases that have been proposed to affect PGE distribution are chromite and magnetite (Keays, 1995; Righter *et al.*, 1998). Plots of the PGEs vs Cr, show very

similar patterns to the PGE vs Ni plots for the C, M-C and more evolved rock types. This suggests that depletion in PGEs probably occurs in conjunction with poly-minerallic cumulate segregation from the magma, rather than with any one particular mineral phase. Within the picritic rock types there are wide variations in PGE-content at relatively constant Cr. Thus, it can be concluded that presence of phases such as chrome-spinel do not govern PGE distribution in the picrites.

8.5.2.2 PGEs vs V

Likewise, there is very little variation of V across the span of PGE concentrations in the picrites (Fig 8.12). This suggests that magnetite is not responsible for PGE variation in the picrites either.

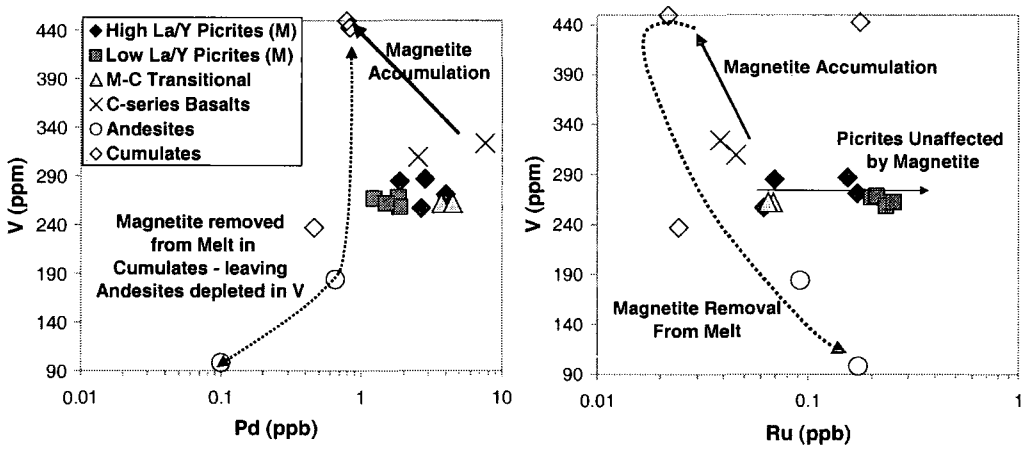

Fig 8.12 Variation of Pd and Ru content with V as an index of magnetite fractionation/ accumulation

The absence of a significant correlation between the picrite-PGEs and V may be because magnetite fractionation only began during formation of the C-series (inferred from the major element and trace element data). Between the C-series and the more evolved cumulates, a trend of increasing V is observed which is probably related to accumulation of magnetite within the cumulates. This accumulation correlates positively with Pt and Ir, negatively with Pd and Re and there is no correlation for Ru and Os. This suggests that Pt and Ir may be compatible with

magnetite, whereas Pd and Re are incompatible. This contrasts with experimental results (Righter *et al.,* 1998). There is a decrease in all PGEs (except Ru) and V as fractionation proceeds towards andesite formation. Thus, the PGEs (except Ru) and magnetite are quantitatively removed from the late-stage melts during high-level cumulate formation.

8.5.2.3 PGEs vs Co

Ir shows a strong positive relationship with Co concentration in the Grenada series (Fig 8.13). Similar relationships are observed for Ru and Pd, whereas no correlation is observed between Os and Pt, and Co. The only PGE to show a negative correlation with Co is Re (Fig 8.13). It has been noted (Righter *et al.,* 1998) that Ru shows similar partitioning to Co into magnetite. Earlier observations between V and the PGEs, however, imply that magnetite is not a controlling phase on PGE distribution.

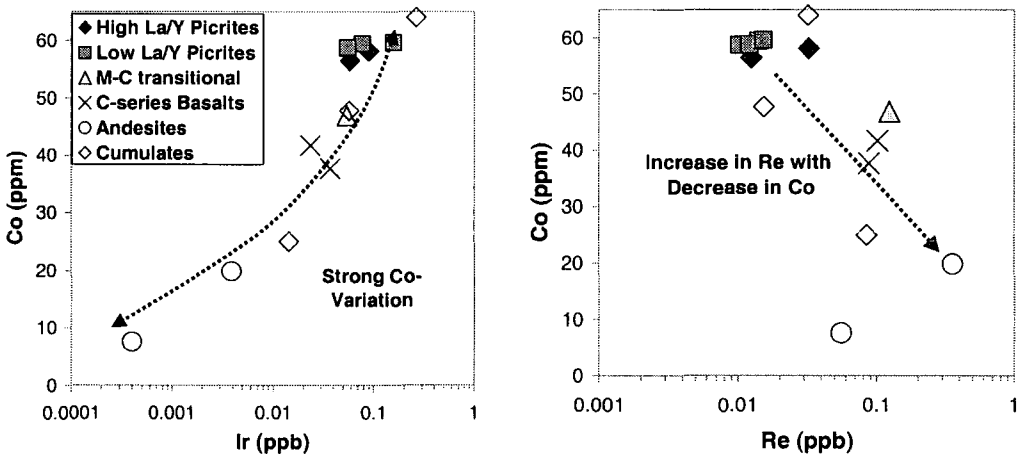

Fig 8.13 Covariance of PGEs with Co in Grenada samples

The behaviour of the PGEs vs Co is markedly different in the Grenada samples compared to the Greenland samples. In the Greenland suite there was no correlation between Co and any of the PGEs, except Pd with which it correlated negatively. Thus, it seems that the behaviour of Co is dependent on specific magmatic conditions, probably fO_2 and fH_2O as these would dictate the oxidation

state of Co and thus its compatibility with co-crystallising phases. Re and Ru partition coefficients are also known to be affected by fO_2 since they form multi-valent cations (Righter *et al.,* 1998). Thus, differential behaviour of the PGEs between the Greenland and Grenada systems may in part be explained by variation in magma fO_2 conditions, which in turn affect the partition coefficients of certain PGEs for other crystallising phases.

8.6 Variation of PGEs with Incompatible and Fluid-Mobile Elements in the Grenada Suite

Variation of PGE concentrations, particularly within the picritic rocks, cannot easily be linked to fractionation of mineral phases. Variation may therefore, instead be linked to conditions which prevailed during the genesis of the magmas within the mantle. Os-isotope variation suggests the input of radiogenic Os to the subduction zone, probably from slab-derived fluids. In order to better constrain the relative roles of fluid enrichment from the subduction zone vs degree of partial melting in the Grenada source, the PGEs are plotted against a variety of incompatible elements, chosen for their use in identifying specific processes.

8.6.1 Variation of PGEs with Nb – an incompatible element with minimal subduction zone dependence

As Nb is a fluid-immobile incompatible element it should be most enriched in small degree melts. Additionally, Nb may be used as a measure of mantle depletion, as it will be depleted in mantle that has suffered previous melting events. Correspondingly, Nb is enriched within the high La/Y picrites (probably generated at small melt fractions), but relatively depleted in the low La/Y picrites (larger melt fractions), (Fig 8.14). Alternatively the low La/Y picrites and the M-C series may be derived from a source previously and homogeneously depleted in Nb, relative to that of the high La/Y picrites. There is overlap in Ir-Os concentrations at variable Nb between the high and low La/Y picrites. Thus, the events which caused Nb depletion/enrichment did not affect the IPGE budget of the primitive melts. Within the high La/Y picrites, Ir and Os concentration stays constant whilst Nb is highly

variable. Conversely, the low La/Y picrites and M-C samples have highly variable Os and Ir concentrations, but lower and more constant Nb concentrations than the high La/Y picrites (Fig 8.14).

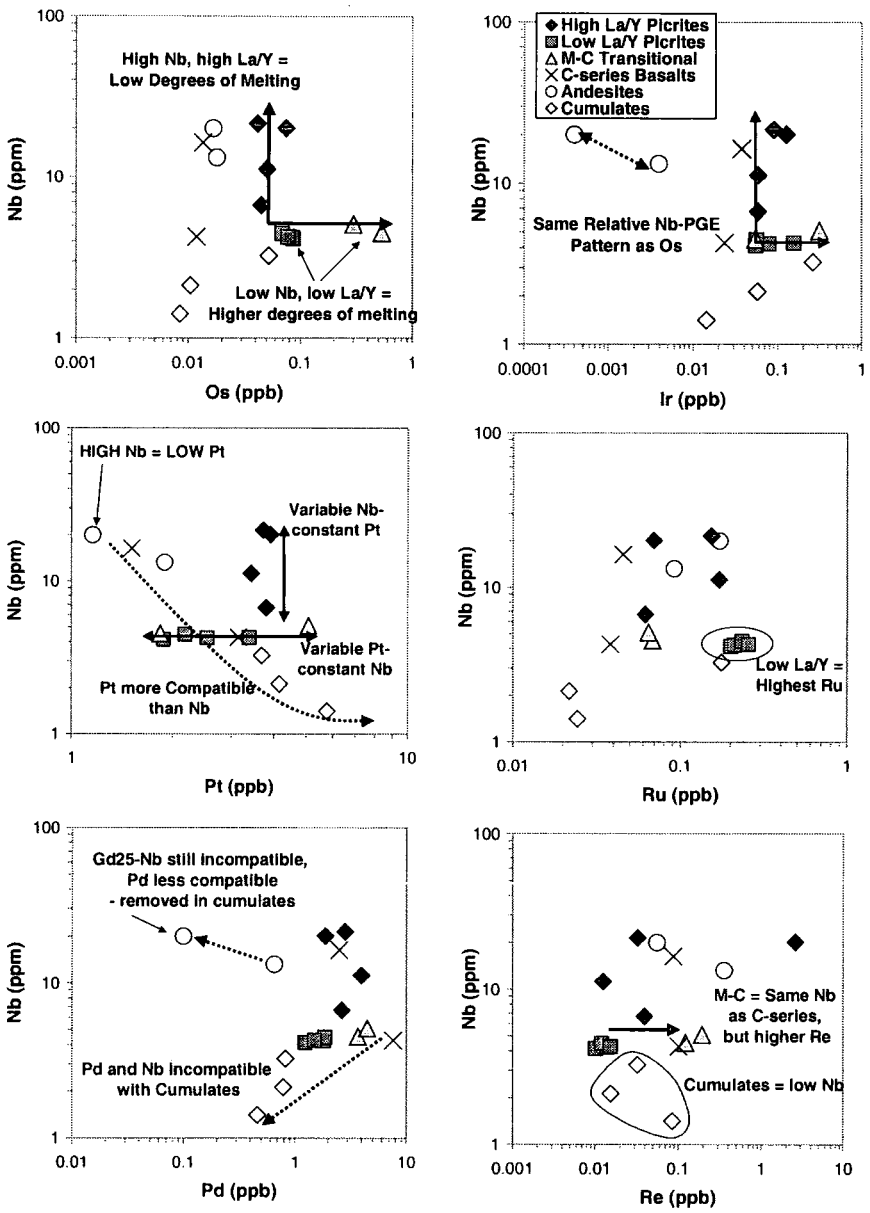

Fig 8.14 Plots of PGEs vs the incompatible element, Nb for Grenada samples

The plots of Pt and Pd vs Nb illustrate that Pt and Pd are enriched in the high Nb, high La/Y picrites, compared to the low La/Y picrites and the M-C series. Correlated depletion of both Pt-Pd and Nb in the low La/Y picrites suggests they may be derived from a more depleted source than the high La/Y picrites. Conversely,

it may be that the PPGEs are more readily mobilised in the fluid-rich melts that generated the high La/Y signature. A negative correlation between Nb and Pd in the more evolved rocks illustrates that Pd, unlike Nb, does not behave in an incompatible manner during fractionation. Nb is more incompatible than the PGEs (except Ru), as it continues to be enriched in the melt (i.e. Gd25) after PGE concentration has begun to diminish.

8.6.2 Variation of PGEs with Fluid Mobile Elements

8.6.2.1 PGEs vs La/Y

No consistent Os and Ir variations were observed with La/Y variation. Therefore, it can be concluded that the events which cause La/Y variation (i.e. differing degrees of fluid input) did not greatly affect Os and Ir concentrations. Pt and Pd abundances tend to be higher in the high La/Y picrites, implying increased mobility in sources with a higher fluid input. Re and La/Y show some positive correlation between the low La/Y picrites, through the M-C series, to the most Re-enriched high La/Y picrite (Fig 8.15). Thus, Re may, like Pt and Pd, be enriched in magmas that have a higher fluid-component in their source. Ru demonstrates opposing behaviour as it is most enriched in the low La/Y picrites.

8.6.2.2 PGEs vs Ba

Re and Pd show weak positive correlations with Ba (Fig 8.16). There is also a tendency of the high Pt samples to show high Ba. Again, Os, Ir and Ru do not show significant correlations with Ba. It can be concluded that subduction-derived fluids responsible for mild enrichment of Ba and La in the Grenadian magmas have also enriched Re, Pd and Pt. Thus, under subduction zone conditions particular PGEs may be selectively mobilised by fluids.

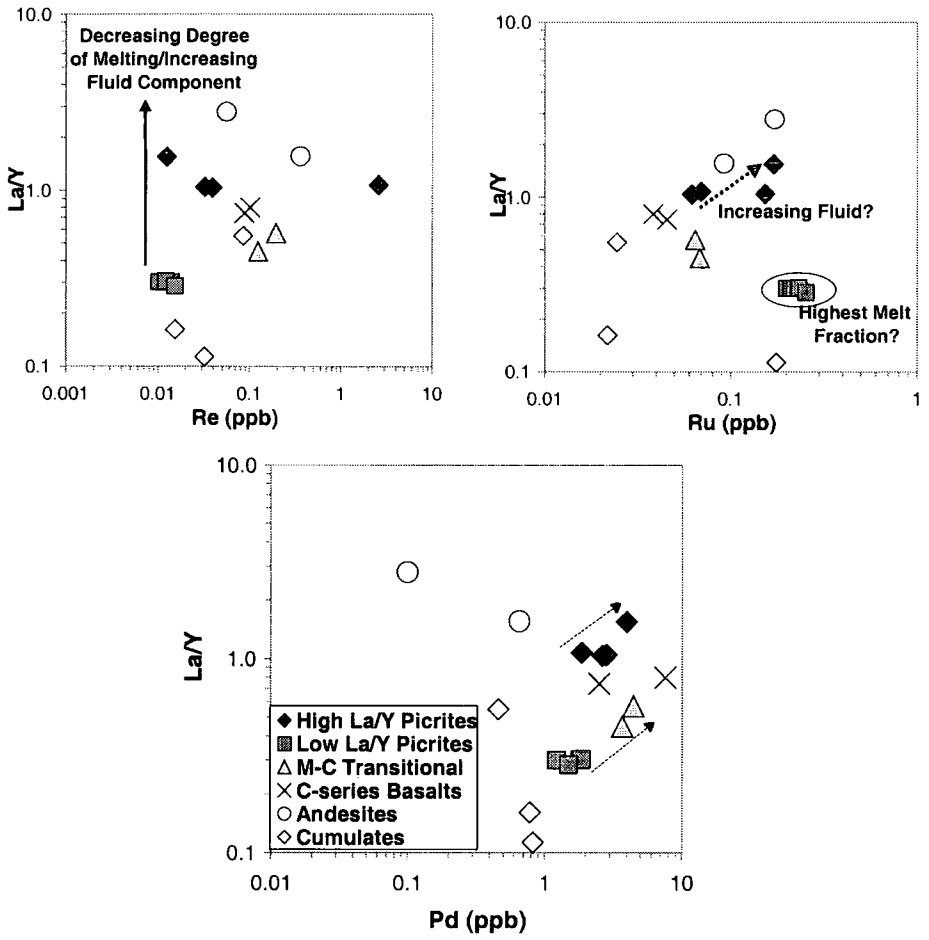

Fig 8.15 Variation of Re, Ru and Pd with La/Y ratio (dashed arrows are suggested trends of increasing La/Y with PGEs within specific sample groups)

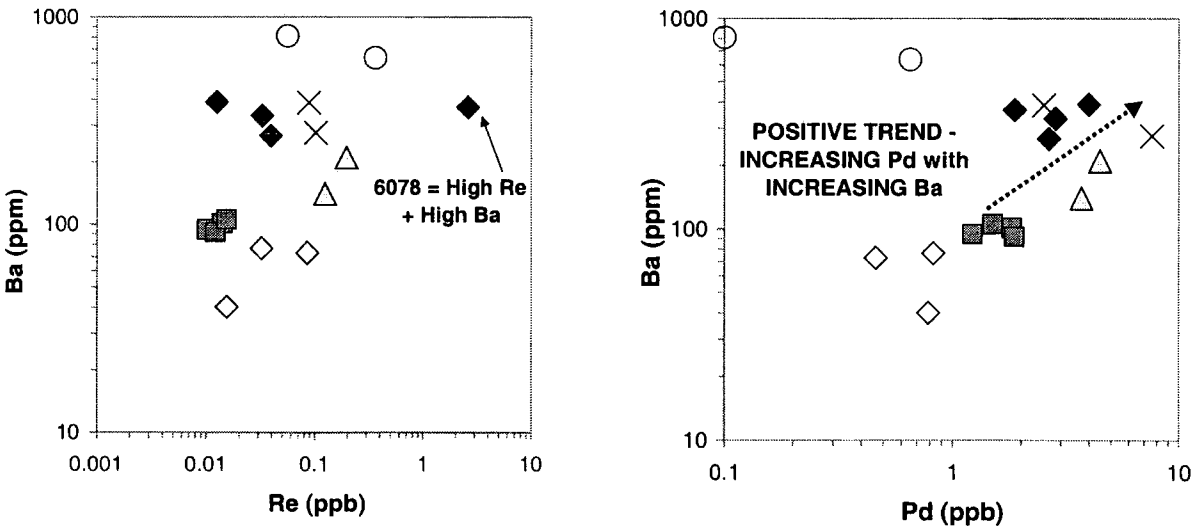

Fig 8.16 Variation of PGEs with Ba in Grenada samples

8.7 Contribution to the PGE Budget of the Grenada Subduction Zone from Local Sediments

8.7.1 Introduction

Evaluation of sediment subduction through the geochemical study of an island arc magma requires a knowledge of the composition of the sediments potentially being subducted beneath the arc (White *et al.*, 1985). Data on PGE-concentrations in sediments however are very limited and generally restricted to studies of the K-T boundary layer (e.g. Tredoux *et al.*, 1989), to black shales and to Mn-nodules (e.g Ravizza and Pyle, 1997). This is again due to the analytical difficulties in measuring PGE-concentrations in rocks that are not enriched. Data on PGE-concentrations in average non-metalliferous, non-K-T boundary sediments, more typical of the bulk-sediment recycled into the mantle via subduction zones, was thus unavailable in the literature. As a step towards evaluating whether sediment recycling is an important source of PGEs within the Grenadian sub-arc mantle, several type-sediments have been analysed.

8.7.2 Nature of the Sediments Subducted below Grenada

Sediment character and thickness varies from south to north along the Lesser Antilles arc with thick terrigenous sediments of the south (~5km thick) giving way to much thinner (<800m) pelagic sediments in the north. In the south, most of this material is derived from South America and deposited on the sea floor by turbidity currents. Thus, sediments in front of the Lesser Antilles arc (particularly the southerly islands, such as Grenada) contain unusually radiogenic Pb and Sr compared to other marine sediments, probably due to a component derived from the Archaean Guyana Shield (White *et al.*, 1985). The strong similarity between the Pb isotopic compositions of the Lesser Antilles volcanics and sediments in front of the arc provide strong evidence that sediment is contributing to the arc source (White *et al.*, 1985). In Section 8.2, it is proposed that incorporation of ancient crustal material into the Grenada source is the most plausible explanation for the elevated Os-isotopic signatures within the picritic lavas of Grenada.

ODP Leg 543 drilled several sites to the west of the Lesser Antilles, on the associated accretionary prism. The most southerly sediments sampled and thus most representative of material being subducted below Grenada (two piston core samples) were analysed for PGEs. These samples are not metalliferous and are assumed to represent "normal" sediments. In addition, a Mn-rich sample was analysed as a possible PGE-enriched end-member sediment. The lithologies of the sediments analysed are summarised in Table 8.5.

Sample Name and Site	Lithology
V24-260: 643-646cm (12° 80' N, 57° 80'W)	An interbedded series of foraminiferal clay and sandy layers, made up of medium sized angular and subangular quartz. Some chlorite and large planktonic forams present.
RC13-175: 162-164cm (11° N, 57° 75'W)	Clayey sand, pale yellowish brown and olive-grey in colour. Slightly friable and homogeneous, with a low carbonate content. Consists of abundant quartz, mica, mafic minerals, rare planktonic and benthonic forams and siliceous spicules
543A : Core 27: 27-28cm (15° 42' N, 58° 39' W)	Orange-coloured, compacted, fine clays with dark-brown/black Mn-spots and layers

Table 8.5 Summary of lithological characteristics of sediments analysed for PGEs (descriptions from Initial Reports of the DSDP Leg 78A)

8.7.3 PGE Signatures of Typical Sediments Subducted Below Grenada

Sediments were analysed by Carius-tube digestion (2g samples) and anion-exchange chromatography, an additional decarbonation step was added prior to digestion (Chapter 5). Os was not recovered from the sandy-samples (13-175 and 24-260) as it was not quantitatively extracted from these sediments using the normal solvent extraction procedure.

	Os	Ir	Ru	Pt	Pd	Re
543: Mn-1	1.073	0.294	0.302	3.037	6.019	0.041
543: Mn-2	0.830	0.328	0.342	3.109	5.835	0.048
13-175		0.002	0.017	0.211	0.029	0.137
24-260		0.013	0.034	0.510	0.376	0.056

Table 8.6. Concentration of PGEs (ppb) in typical Atlantic plate sediments subducted below Grenada

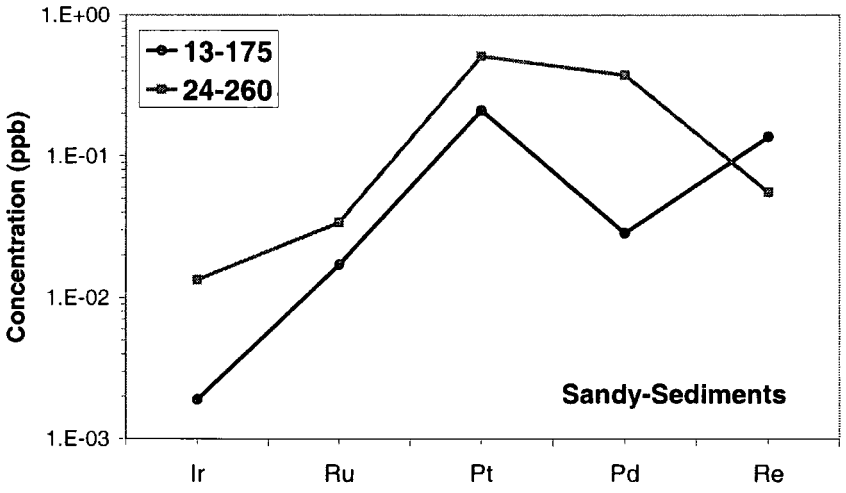

Fig 8.17 PGE-patterns (absolute abundance) for non-metalliferous sediments

The sandy-samples (13-175, 24-260) although lithologically similar, contain different concentrations of PGEs (Table 8.6). Sample 13-175 is lower in all PGEs except Re, than sample 24-260. The large variations in Pd and Re content between the two samples may reflect the greater mobility of these PGEs compared to the heavier PGEs in the sedimentary environment. The steep positive PGE patterns between Ir and Pt may reflect the derivation of these sediments from evolved crustal material, with the flattening of the Pd-Re pattern due to secondary alteration within the sedimentary pile.

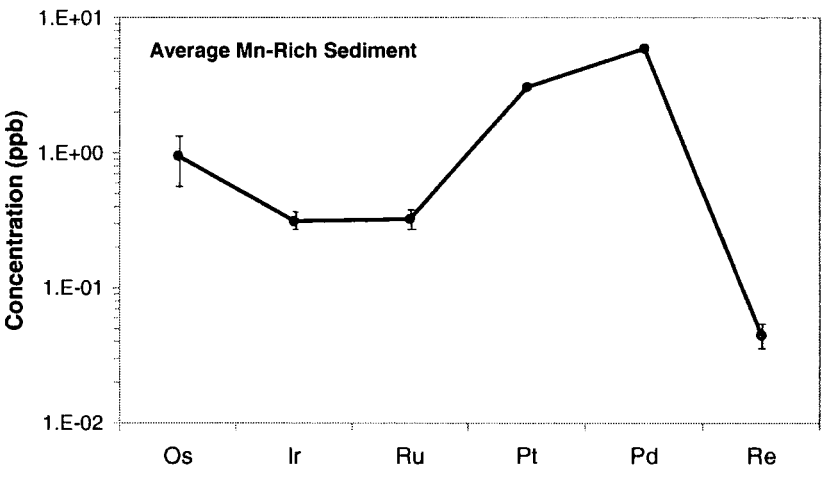

Fig 8.18 PGE pattern (absolute abundance) for Mn-rich sediments – error bars shown (1σ) illustrate the reproducibility achieved between two separate digestions of the same sample

The Mn-rich sediments have very different shaped PGE patterns to the sediments of terrigenous origin (Fig 8.18). Os is enriched relative to Ir and Ru, as are Pt and Pd. Re shows a marked depletion within the Mn-rich sediments. This pattern must be related to the preferential scavenging of certain PGEs from the seawater during sediment deposition. The Os/Ir ratios (2.5-3.6) and Pd/Pt ratios (1.9-2) of the Mn-rich sediments analysed during this project overlap with the Os/Ir ratios (2-3.5) and Pd/Pt ratios (1.8-4.8) of reducing sediments from the continental margin of Oman reported by Ravizza and Pyle (1997). They interpret these high ratios as evidence of authigenic Os and Pd enrichment under reducing conditions. The strong Re-depletion suggests that Re behaves incompatibly during Mn-rich sediment formation under reducing conditions.

Comparison of the relative C1-normalised PGE patterns obtained for both the sediments and the most primitive Grenadian lavas, reveals that the sandy sediments are depleted in all PGEs (except Re) relative to the M-series picrite (Fig 8.20). Conversely, the Mn-rich sediment is enriched in all PGEs relative to the M-series picrite. The shape of the overall patterns is very similar between the M-series picrite and the Mn-rich sediment as regards their relative Re depletion. The M-C picrite contains significantly higher Re concentrations than any of the sediments, but is of comparable Ir, Pt and Pd concentration to the Mn-rich sediment.

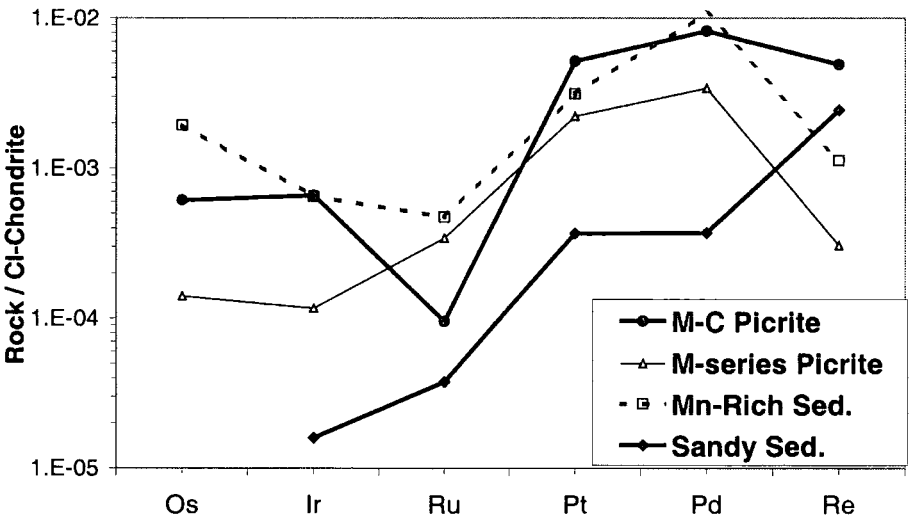

Fig 8.20 Chondrite-normalised PGE-patterns to illustrate the differences in shape and overall concentration between typical Grenadian subducted sediment and Grenada picritic lavas.

8.7.4 PGE Input to Grenadian Mantle Source from Sediments

In principle, a maximum of only 2% bulk sediment mixed into the mantle source is required to generate the entire range of isotopic compositions from the Lesser Antilles (Davidson, 1986; Thirlwall *et al.*, 1996). Due to the strong contrast in trace element concentrations between mantle and sediment, only small proportions of contaminant are required to produce large changes in isotope ratios (Davidson, 1987). The mineralogy and water content of sediment on the subducted slab suggest that it will melt before the oceanic crust and produce partial melts richer in incompatible elements than the initial sediment was. Thus, even less melt than bulk sediment would be required to shift the isotopic compositions of resultant magmas (Davidson, 1986).

Variation of isotopic signatures in a subduction environment requires only minimal sediment input. In order to significantly influence the actual concentration of elements within the mantle via subduction however, a far larger proportion of sediment input would probably be required, especially if the elements in question are not particularly incompatible during slab dehydration. Simple mixing calculations have been performed to estimate the effect that ~2% sediment mixing would have on Pd and Ir concentration within the picrites.

	Conc in Picrite (ppb)	Picrite Conc + 2% Mn-sediment	Picrite Conc + 2% Sandy sediment
Pd	2.84 ± 0.05	2.90ppb	2.79ppb
Ir	0.090 ± 0.02	0.089ppb	0.088ppb

Table 8.7 Effect on PGE concentrations in an average picrite of mixing with 2% of a Mn-rich sediment and 2% of a sandy sediment – errors are 2σ

The effect on PGE concentration of mixing low quantities of sediment into melts of picritic composition is minimal. The difference is within the error on the original PGE-analysis of the picrite (Table 8.7). Thus, concentration-mixing calculations are of limited use and isotopic calculations of sediment mixing are preferred to estimate amount of subduction-derived component in the arc-lava source.

8.8 PGE-Signatures of Boninitic Lavas from the Izu-Bonin Forearc: *(A comparison to Grenada arc lavas)*

8.8.1 Introduction to Izu-Bonin Geology

The Izu-Bonin-Mariana subduction system is the largest intra-oceanic arc in the world. The region has evolved as a complex system of intra-oceanic arcs, basins and trenches since westward subduction of the Pacific Plate started in the early-middle Eocene (Murton *et al.*, 1992 and references therein). The samples analysed during this study were recovered during ODP Leg 125 at Site 786B. This Site is located in the forearc section of the Izu-Bonin system. The forearc is approximately 150-200Km wide and lies between the active volcanic arc and the Izu-Bonin trench, which marks the boundary between the Pacific and Phillipine-Sea plates (Fig 8.20) (Murton *et al.*, 1992 and references therein).

A complex boninitic volcanic edifice was drilled at Site 786B. The basal sequence consists of low-Ca boninite intrusive sheets, overlain by low-Ca boninite pillow lavas. These in turn are overlain by intermediate-Ca bronzite andesites, low-Ca bronzite andesites, andesites, dacites and rhyolites. The basal sequence is ~41Ma old and is interpreted as an oceanic forearc basement upon which is built the more evolved volcanic edifice of the overlying sequence. The Eocene forearc basement and edifice are cut by dykes of intermediate-Ca and high-Ca boninite (i.e. ICB and HCB) composition (Pearce *et al.*, 1992[a]). During this study, representative samples of both the volcanic edifice and the dyke-suite have been analysed for PGEs (Table 8.8). The phenocryst assemblages of the groups analysed are shown in Table 8.9

Sample Name	Core Name	Core Interval (cm)	Magma Type	Character
I.B.1	1R-1	75-79	ICBrzA	Volcanic Edifice
I.B.5	5R-2	69-71	HCB	Dyke
I.B.21	21R-2	28-32	R	Volcanic Edifice
I.B.40	40R-2	83-90	HCB	Dyke
I.B.67	67R-1	56-59	ICB	Dyke

Table 8.8 Depth intervals and composition of samples from ODP Leg 125, Site 786B, subsequently analysed for PGEs (this study);(Pearce *et al.*, 1992[a]).
(Abbreviations: *ICBrzA* = Intermediate-Ca, bronzite-andesite. *HCB* = High-Ca boninite. *ICB* = Intermediate-Ca boninite. *R* = Rhyolite)

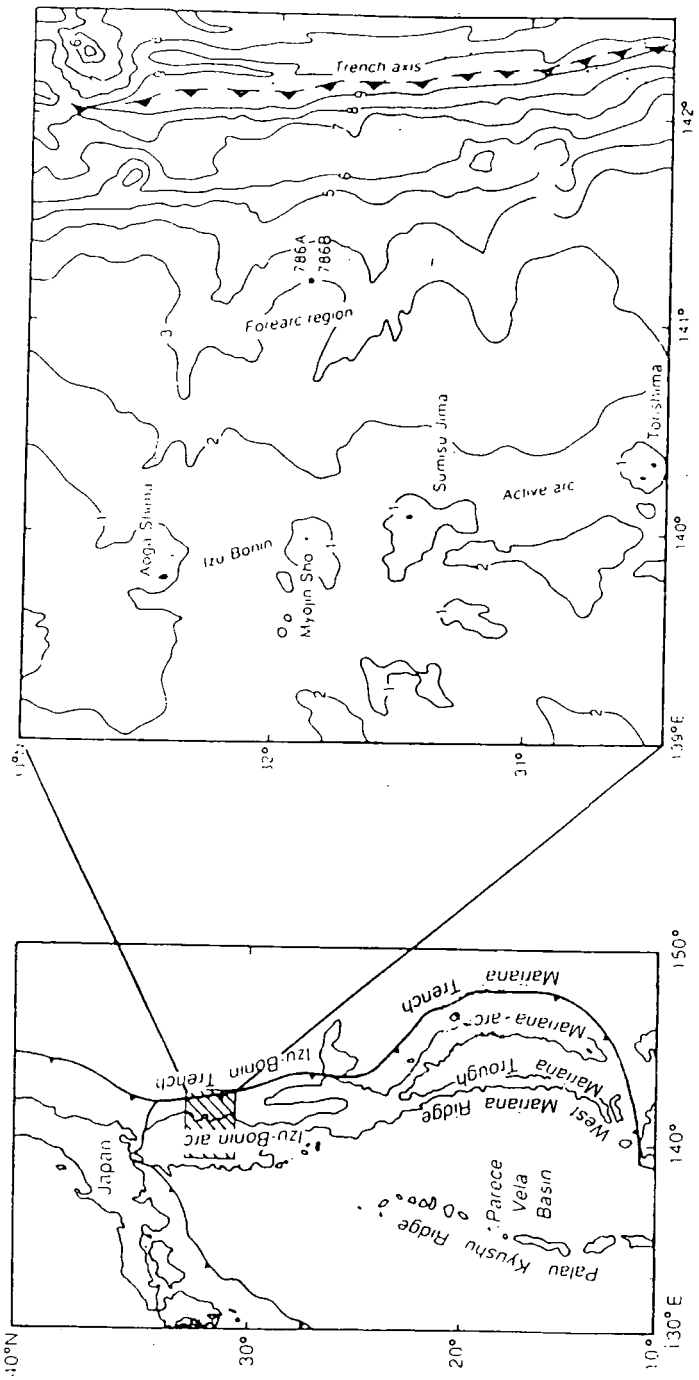

Fig 8.21 Location of the Izu-Bonin arc and the position of drill site 786B, ODP Leg 125 (after Murton *et al.*, 1992)

Group Name	Phenocryst Assemblage
ICB	1-5% altered Ol, 5-10% OPX, 2-4% altered CPX, 0-10% altered Plag, trace Cr-Spin.
HCB	Altered Ol, trace OPX, 1-3% altered CPX, trace Plag, dark-red Cr-Spin.
ICBrzA	0-1% altered Ol, 6-20% OPX, 3-10% CPX, 5-15% resorbed Plag, trace Cr-Spin.
R	Trace OPX, trace CPX, <3% resorbed Plag, trace Qtz, Mag phenocrysts common.

Table 8.9 Summary of phenocryst assemblages of the Site 786 groups (from Pearce *et al.*, 1992[a]).

8.8.2 Outline of the Geochemistry of Samples Analysed

Major and trace element data (from Pearce *et al.*, 1992[a]) are presented in Appendix I. The groups outlined above were classified primarily on their MgO, SiO_2 and CaO contents, although other significant differences do occur in their trace element geochemistry, particularly for the compatible elements Ni and Cr (Pearce *et al.*, 1992[a] and references therein). The MgO concentration decreases in the order ICB, HCB, ICBrzA, R, whilst SiO_2 increases in the order HCB, ICB, ICBrzA, R. For CaO, the inverse of the SiO_2 trend is observed (Fig 8.22).

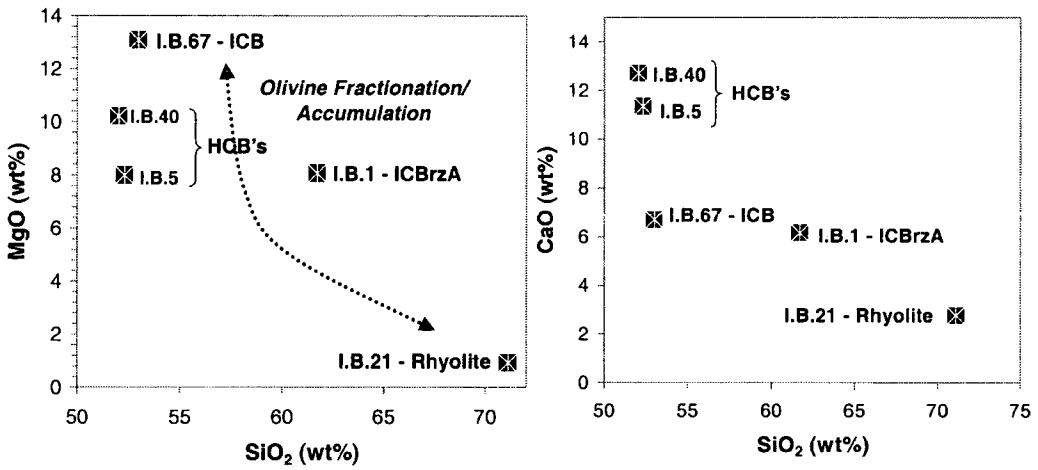

Fig 8.22 MgO and CaO vs SiO_2 for Izu-Bonin samples (data from Pearce *et al.*, 1992)-showing characteristic boninite high MgO – high SiO_2 compositions.

Trace element data reveal that the evolved rock types can be related by fractionation and/or accumulation of the observed mineral phases back to one of the boninite groups (Pearce *et al.*,1992[a]). The HCBs often have lower Ni and higher Cr than the ICBs (although there is overlap in the ICB and HCB Ni-Cr abundances for

the samples analysed in this study). This may be due to the greater degree of olivine accumulation within the ICBs (Table 8.23), or greater olivine fractionation from the HCBs.

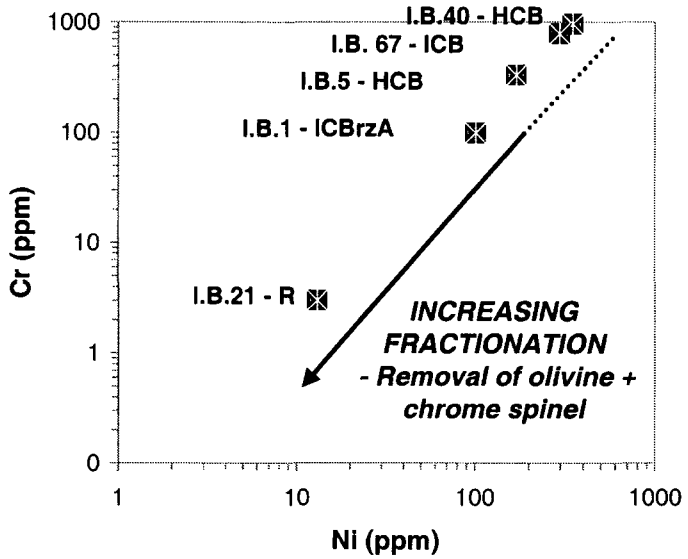

Fig 8.23 Ni vs Cr, for Izu-Bonin samples (Data from Pearce *et al.*, 1992[a] and Murton *et al.*, 1992)

The boninites show enrichment in LILEs, LREEs and certain HFSEs relative to Ti, Y and the HREEs (e.g. Yb), reflecting addition of a subduction component to the boninite source region (Fig 8.24). The HREEs, Ti and Y are depleted relative to MORB (Pearce *et al.*, 1992[a]) confirming that boninite genesis requires a depleted rather than a fertile mantle source (Murton *et al.*, 1992). The low concentration of Nb (Fig 8.24) in the boninites also indicates that the oceanic lithosphere prior to onset of subduction was not enriched by any asthenospheric OIB component (Pearce *et al.*, 1992[b]). Hf and Zr-enrichment relative to Ti and Sm, implies either that amphibole played an important role in the genesis of the boninites (Murton *et al.*, 1992), or that the subduction component was enriched in Hf and Zr relative to Ti and Sm (Pearce *et al.*, 1992[b]).

The overall melting regime in which the boninites were generated has been constrained to shallow depths (~30km) and high temperatures (1250°C). The geochemical compositions observed can be explained by remelting above a subduction zone of depleted MORB mantle (Fig 8.25). Thus, it is assumed that the boninite source had lost 10-15wt% of melt at a ridge, before undergoing a further 5-10wt% melting at the onset of subduction (Pearce *et al.*, 1992[b]).

It is thus envisaged that the boninites were generated by decompression melting of a diapir of metasomatised residual MORB mantle, leaving harzburgite as the depleted residue from the second supra-subduction stage of melting. The composition of the harzburgites suggest a total of 25% melting with respect to fertile MORB mantle (Pearce *et al.*, 1992[b]). Isotopic data (εNd) suggest that the ICB may have been produced from a more refractory lithosphere than the HCB (Pearce *et al.*, 1992[a]).

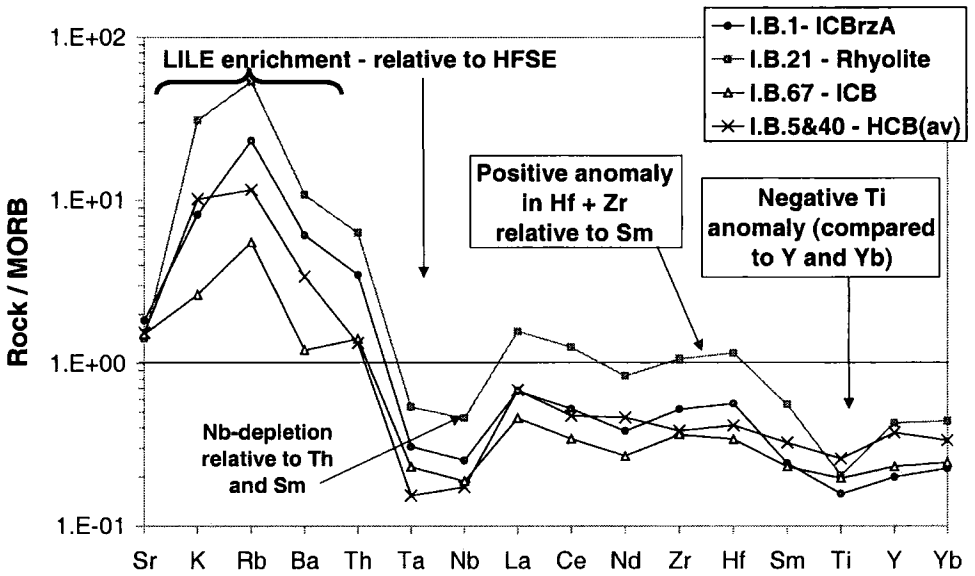

Fig 8.24 MORB-normalised trace element patterns for the Site 786B Izu-Bonin samples (After Pearce *et al.*, 1992[b]) – Data from Pearce *et al.* (1992[a]) and Murton *et al.* (1992).

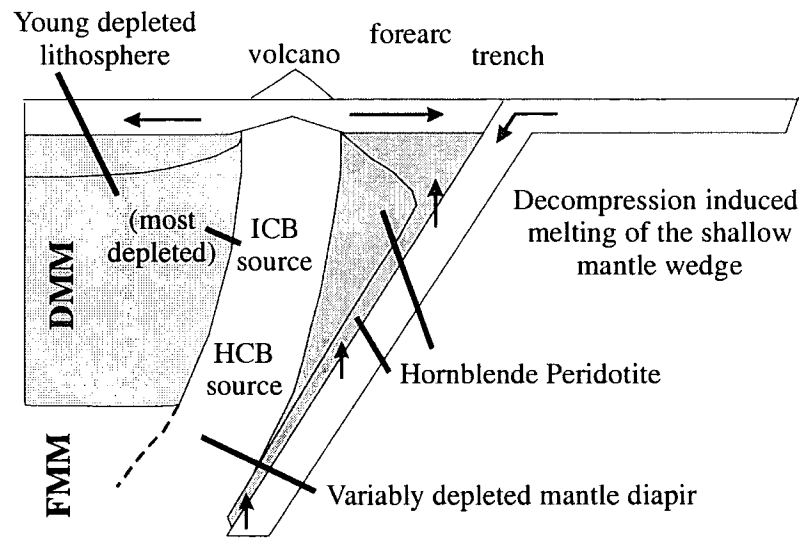

Fig 8.25 Simplified tectonic model of boninite production (after Pearce *et al.*, 1992[a])

8.8.3 PGE Patterns and Abundances in Izu-Bonin

The PGE abundances (ppb) of the Izu-Bonin suite analysed by Carius-tube, anion exchange chromatography during this study are presented below. The data quality was again assessed by running a duplicate analysis of one of the samples. Sufficient quantities of rock powder were not available to permit a duplicate analysis of each sample as was conducted on the Grenada samples. The reproducibility achieved for duplicate sample I.B.67 is illustrated graphically in Fig 8.26. 2g aliquots of all samples were analysed to improve on sampling statistics.

	Type	Os	Ir	Ru	Pt	Pd	Re
I.B. 1	ICBrzA	0.023	0.025	0.242	3.312	7.219	0.247
I.B. 5	HCB	0.031	0.104	0.123	1.887	1.187	0.264
I.B. 21	Rhyolite	0.005	0.002	0.020	0.175	1.016	0.419
I.B. 40	HCB	0.049	0.107	0.250	1.536	3.682	0.344
I.B. 67A	ICB	0.043	0.080	0.153	5.765	3.533	0.195
I.B. 67B	ICB	0.024	0.074	0.196	6.268	3.444	0.200
I.B. 67	**Average**	**0.033**	**0.077**	**0.175**	**6.017**	**3.489**	**0.198**
I.B. 67	**Stdev**	**0.014**	**0.005**	**0.030**	**0.355**	**0.063**	**0.004**
1 σ error as %		**41.49**	**5.99**	**17.25**	**5.91**	**1.80**	**1.86**

Table 8.10 PGE abundances in Izu-Bonin samples, all values in ppb (Abbreviations: *ICBrzA* = Intermediate Ca, bronzite, andesite. *HCB* = High Ca-boninite. *ICB* = Intermediate Ca-boninite)

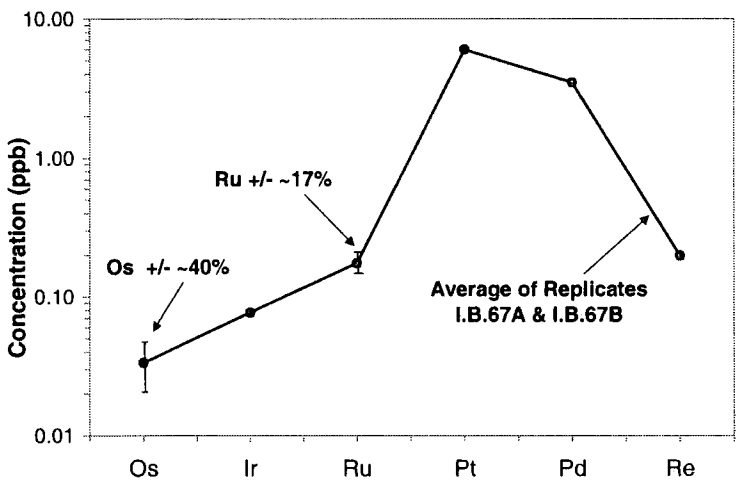

Fig 8.26 Typical errors (1σ) achieved for Izu-Bonin PGE analyses – Error bar smaller than size of symbol where not shown

8.8.3.1 Differences in PGE Patterns between the Izu-Bonin Andesite and Rhyolite

The Izu-Bonin samples exhibit steep (PPGE-enriched) C1-normalised PGE patterns. This accords well with previous observations that boninites are characterised by high Pd/Ir ratios (Hamlyn *et al.*, 1985). PGE concentrations markedly decrease between the ICBrzA and the rhyolite (Fig 8.27). Pd does not show evidence of incompatible chalcophilic behaviour during fractionation as it sometimes does in other magmatic systems. The drop in PGE concentration is matched by decrease in Ni, highlighting their comparable siderophilic, compatible behaviour during fractionation of early phases such as olivine. In contrast, Re concentration increases from the andesite to the rhyolite. This illustrates the contrasting incompatible behaviour of Re compared to the other PGEs. The Pd/Re ratio is correspondingly much higher within the andesite than the rhyolite.

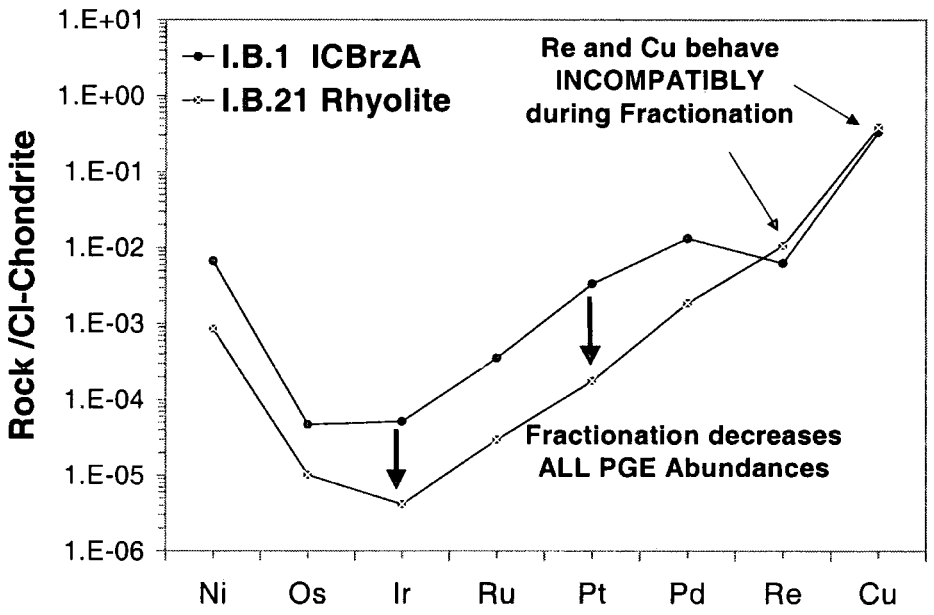

Fig 8.27 Contrasting PGE patterns for an Izu-Bonin andesite and rhyolite

The Os/Ir ratio of the rhyolite is noticeably higher than in the andesite. This variation of Os/Ir with fractionation is also seen on Grenada and implies that fractionation of Os from Ir takes place within high-level magma chambers, probably related to differential compatibility with one of the crystallising phases. Of the

phenocryst phases within the rhyolite (Table 8.9) magnetite would seem the most likely candidate for causing PGE fractionation as olivine is absent. Thus, the observed high Os/Ir within the rhyolite is unlikely to be due to accumulation of olivine which might act to boost the Os concentration and instead may suggest that Ir has been partially removed from the melt, possibly by co-precipitation with magnetite.

8.8.3.2 Differences in PGE Patterns between the Izu-Bonin ICBs and HCBs

The IPGE concentrations of the ICB and HCB groups are very similar. Thus, although the ICB are thought to be derived from more refractory lithosphere than the HCB (Pearce *et al.*, 1992[b]), the abundances of the IPGEs were not significantly affected by previous low-degree melting events. By comparison, there is much greater inter-sample variation within the PPGE-group. The ICB, I.B.67, has markedly higher Pt concentration than the HCB, which have identical Pt concentrations. The HCBs have variable Pt/Pd however. This may suggest that Pd has been variably mobilised and removed from the metasomatised lithosphere beneath the Izu-Bonin forearc.

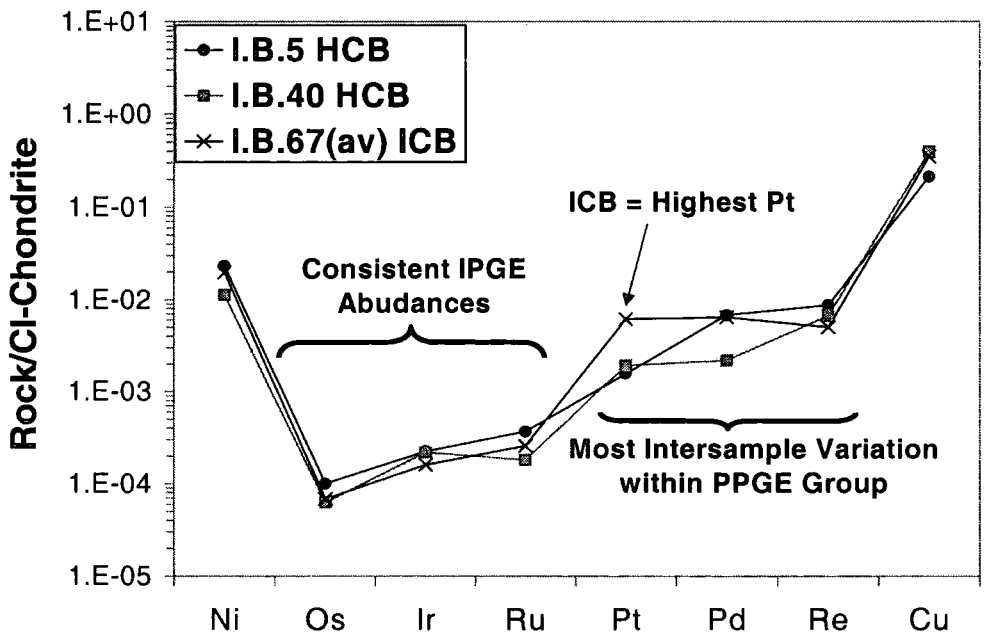

Fig 8.28 Contrasting PGE patterns for the high-Ca boninites (HCB) and intermediate-Ca boninite (ICB) from Izu-Bonin

8.8.3.3 Comparison of PGE Patterns between the Whole Izu-Bonin Fractionation Suite

Ir is only enriched relative to Os within the more primitive samples and becomes increasingly depleted relative to Os as fractionation proceeds (Fig 8.29). Pd reaches some of its highest concentrations within the more evolved rocks, while Cu stays relatively constant throughout the Izu-Bonin fractionation series. This strongly suggests that the magmas did not become S-saturated during fractionation. Thus, sulfide is not a major control on PGE abundances in this magmatic suite.

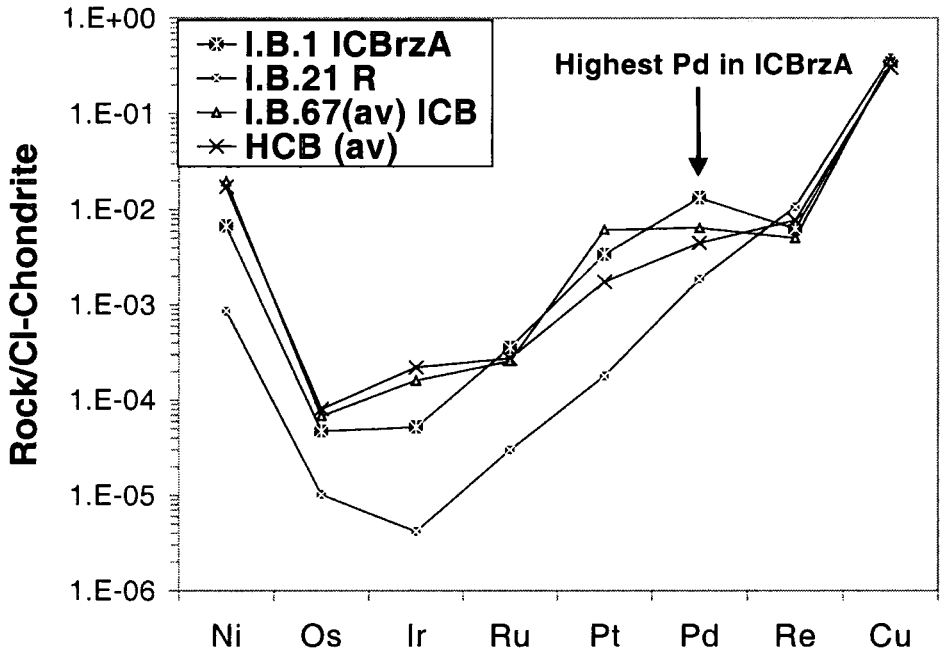

Fig 8.29 Variation of PGE concentration throughout the Izu-Bonin fractionation suite (HCB is an average of I.B.5 and I.B.40)

Apart from Ir-depletion and Pd-enrichment in the andesites, the PGE-patterns and concentrations within the boninites and the andesite are otherwise similar. This suggests that most of the PGEs did not behave compatibly during the initial stages of fractionation. This is particularly true for Ru (Fig 8.29) and was also the case in the Grenada andesites, where Ru concentration increased in the more evolved andesite. This suggests that there are significant differences in the behaviour of Ru compared to Ir and Os, which are usually depleted in andesites.

8.8.4 Correlation of Inter-PGE Variation for Izu-Bonin Samples

There is greater correlation between the individual PGEs within the Izu-Bonin samples than there is within the Grenada samples, with definite correlation between the PGE contents through the fractionation series of the ICB, to the andesite, to the rhyolite. The HCBs tend to plot away from this main trend due to lower Pt and Pd, and higher Re concentrations than the ICBs (Fig 8.30). Positive correlations are observed between Os-Ir, Os-Pt and Ir-Pt. Negative correlations are observed between Os-Re and Ir-Re. No significant correlations are observed between Pd-Re and Os-Re. The situation is slightly more complex when the IPGEs are plotted against Ru or Pd. There is often initially a negative correlation as Ru (or Pd) continues to build up within the andesitic melt after the IPGE concentration begins to diminish. Then however, the correlation from andesite to rhyolite becomes positive as both Ru and the IPGE concentration within the melt rapidly declines. This serves to illustrate that Ru and Pd behave in a slightly more incompatible manner during initial fractionation than Os, Ir and Pt.

8.8.5 Variation of PGEs with Mg No.

There are positive correlations between Os, Ir and Mg No., which also correlate with decrease in Ni-content (Fig 8.31). This indicates that olivine (or a phase co-crystallising with olivine) plays an important role in the Izu-Bonin series evolution, as well as in the Grenada suite. Olivine phenocrysts are certainly observed in the Izu-Bonin suite, particularly within the boninites (Table 8.9). Pt also shows a positive correlation with Mg No., implying that its removal from the melt is related to fractionation. Unlike Ir and Os, however, there is not such a good correlation with Ni-content (i.e. highest Pt occurs in the andesite which has low Ni) suggesting that olivine is not the dominant controlling phase. A plot of Pt vs Cr (Fig 8.31) shows better correlation between the ICB, andesite and rhyolite implying that fractionation of chrome spinel (a common phenocryst phase; Table 8.9) may be more important in controlling Pt-distribution.

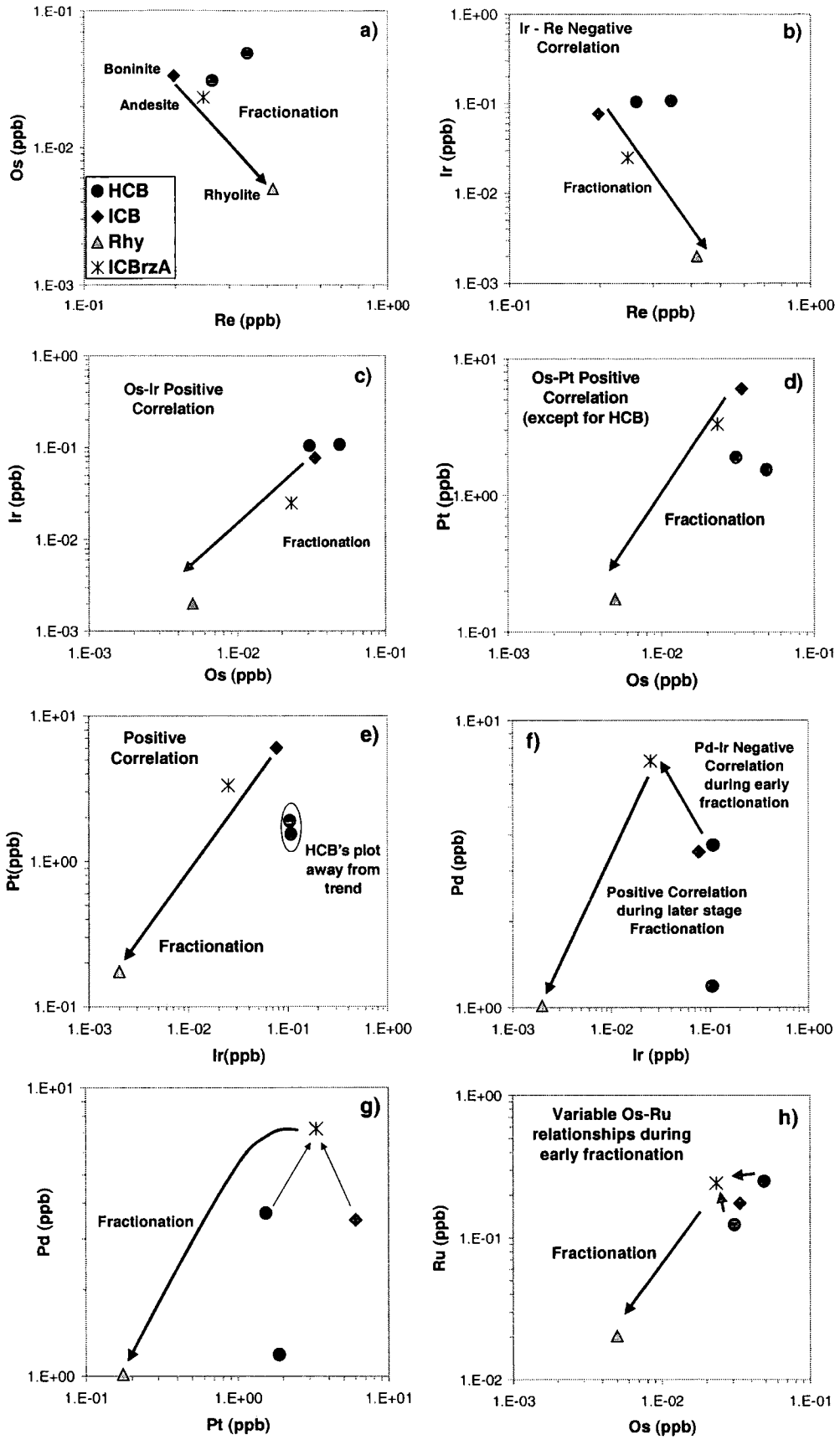

Fig 8.30 Inter-PGE variation plots for the Izu-Bonin samples (HCB = high Ca boninite, ICB = intermediate Ca boninite, Rhy = rhyolite, ICBrzA = andesite)

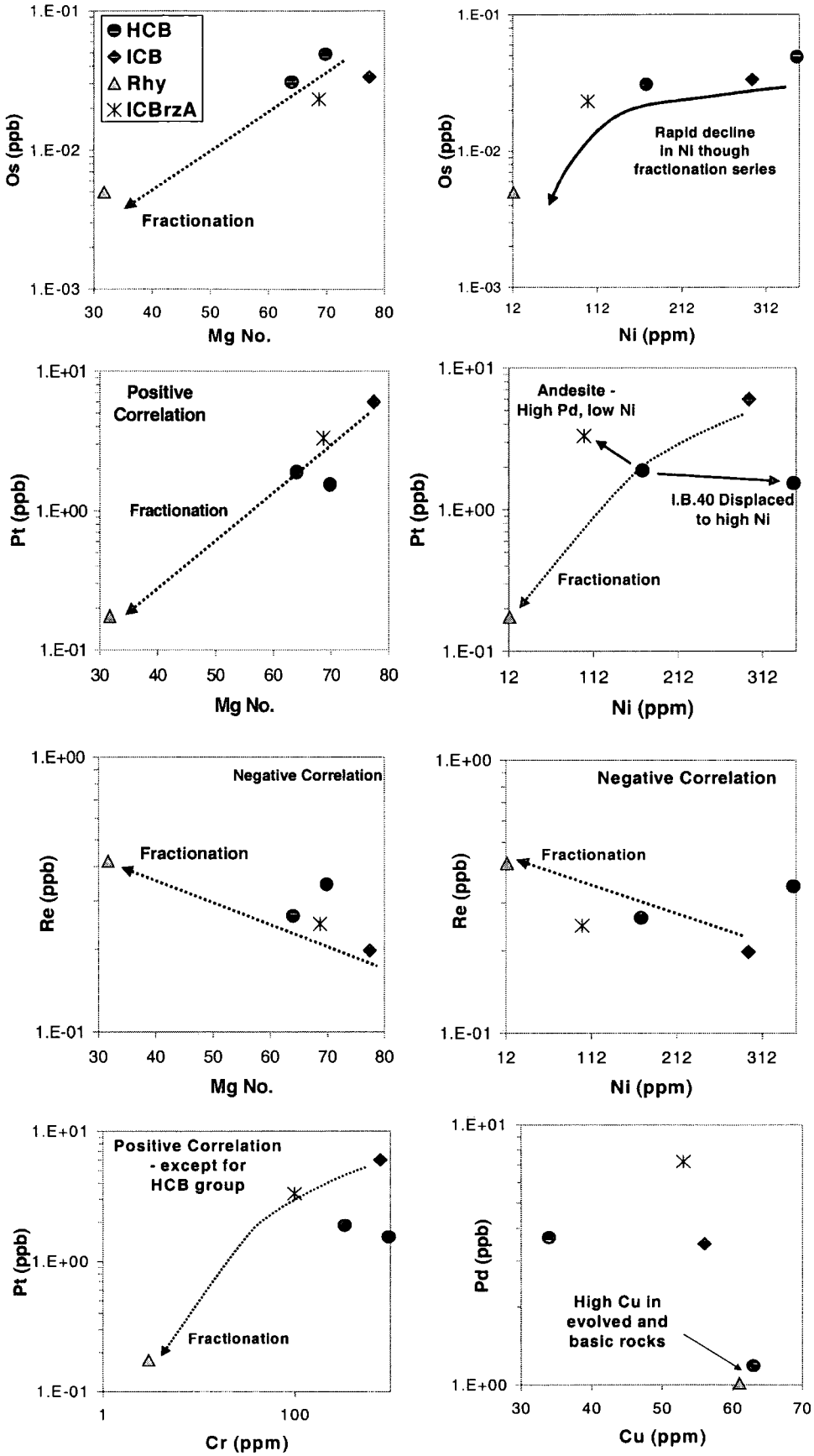

Fig 8.31 PGEs vs indices of fractionation

There is little correlation between Pd and Ru, and Mg No., except that both are enriched in the lower Mg No. andesites compared to the boninites. The same trend is observed between these same elements and Ni. This highlights the point that Pd and Ru behave very similarly within the boninite suite, neither being controlled by olivine fractionation. Pd distribution is also independent of Cu (Fig 8.31), with high Cu and low Pd being observed in both a boninite and a rhyolite. The high Cu concentration within the most evolved rock type indicates that magma was not S-saturated. Therefore, Pd distribution must be governed by a phase other than sulfide. The same is true for Re. Pd and Re show little correlation with V in the andesite and boninites. However, the rhyolite is markedly depleted in Pd, Re and V. This confirms that magnetite only became a significant fractionating phase between formation of the andesite and rhyolite. This is backed up by the presence of common magnetite phenocrysts within the rhyolite (Table 8.9). Thus, it is tentatively suggested that Pd and Re may co-crystallise, or be compatible with magnetite during the late stages of fractionation.

8.9 Comparison between PGE Signatures of Grenada and Izu-Bonin: Contrasting Subduction Systems

8.9.1 PGE Ratios

In this section, the PGE-ratios of Grenada and Izu-Bonin will be considered to see if any differential fractionation of the PGEs is obvious between the two tectonic environments and if this in turn can be related to conditions during their genesis. It should be noted that PGE ratios (particularly within the Grenada Suite) can be highly variable between samples of the same series or group. The ratios shown in this case are taken from the average of the replicates of the samples shown, which themselves were chosen to represent an average ratio for their group or series.

8.9.1.1 Primitive Samples

The primitive sample inter-element PGE ratios most closely represent the ratios of the mantle sources from which the samples were derived, although they will of course have been slightly changed as both Grenada and Izu-Bonin samples have undergone some fractionation. Os/Ir ratios within the Grenada picrites are noticeably higher than in the Izu-Bonin boninites (Table 8.11). The lower Mg Nos. of the boninites imply that they have undergone more olivine and probably Os fractionation, that the Grenada picrites.

Primitive Rocks	Os/Ir	Pt/Pd	Pt/Ru	Re/Os	Pd/Ir
Gd: Low La/Y picrite (Gd11)	1.23	1.17	9.09	0.18	33.42
Gd: High La/Y picrite (Gd16)	0.87	0.86	20.0	0.25	68.35
Gd: M-C picrite (AMG 6157)	0.96	1.14	100.0	0.64	14.16
IB: ICBoninite (I.B. 67 av)	0.44	1.72	33.33	5.92	45.46
IB: HCBoninite (I.B.5+40 av)	0.38	1	9.09	7.82	22.89
Supra-subduction harzburgite		***1.66***	***0.34***		***1.28***
Mantle wedge				***0.089***	

Table 8.11. Key PGE ratios for primitive rocks of Grenada and Izu-Bonin (supra-subduction harzburgite data from Rehkämper *et al.*, 1997; Mantle wedge data from Cascades and Ichinomegata peridotite xenoliths, Brandon *et al.*, 1996).

An alternative hypothesis for the increased Os/Ir of the Grenada picrites compared to the boninites is that Os has been selectively enriched within the Grenada rocks. This might add weight to the theory of Brandon *et al.* (1996) that Os is selectively mobilised in subduction zones relative to Ir. The reason for enrichment within the picrites relative to the boninites is uncertain, but may be linked to the fact that the Grenada picrites are derived from a more volatile-rich or hydrous magma source. This is demonstrated by the prevalence of amphibole phenocrysts within the Grenada suite, which are absent in the boninite suite.

It has been assumed that Os and Ir behave in an almost identical manner during mantle melting due to the near uniform Os/Ir ratios of ~1 that are observed within both mantle residues and high degree partial melts (e.g. komatiites of Brügmann *et al.,* 1987). The new data obtained during this study clearly illustrate that this is not the case when a more complex system such as a subduction zone is considered. Without the analysis of mantle peridotite xenoliths from the areas under study, it is impossible to say whether the Os/Ir fractionation is a result of mantle melting processes or later magma chamber processes.

Re/Os is markedly higher within the boninites than in the Grenada picrites. This is because of relative enrichment of Re within the boninites. The Re/Os ratios are considerably higher in the arc lavas than in the postulated mantle-wedge residue (Table 8.11). This suggests that Re is selectively mobilised during arc-magmagenesis relative to Os. This is as expected as Re is moderately incompatible during mantle melting (Shirey and Walker, 1998). For the other PGE-ratios shown in Table 8.11, there is a considerable overlap between the boninites and picrites. This illustrates that the PPGEs may be less sensitive to differences in the subduction environment than the IPGEs.

The Pd/Ir and Pt/Ru ratios of the supra-subduction harzburgite (Rehkämper *et al.,* 1997) are considerably lower than the corresponding ratios for the subduction lavas. Rehkämper *et al.* (1997) attribute the low ratios in the harzburgitic residues to the fact that Pt and Pd have greater transport efficiency in fluids released from the subducting slab than do Ir and Ru. The results (Table 8.11) confirm this theory, as both arc-lavas are enriched in the PPGEs relative to the IPGEs. Furthermore, the Pt/Pd ratios of the arc lavas are similar to, or slightly lower than, the harzburgitic

residue. This indicates that these elements behave in a similar way during fluid mobilisation, although Pd may sometimes be mobilised more readily.

8.9.1.2 Intermediate Samples

Comparison of PGE ratios between the primitive rocks (Table 8.11) and the intermediate rock types (Table 8.12) highlights several differences. Firstly, the Os/Ir ratios of all samples are fractionated compared to their supposed "parental" melts. The Os/Ir ratio falls from the picrites to the Grenada C-series basalts. The M-C basalt Os/Ir is increased by an order of magnitude from the M-C picrite. The Izu-Bonin Os/Ir ratio also rises between the boninite and andesite. This illustrates that the compatibility and behaviour of Ir and Os are highly dependent on individual magma chamber conditions and possibly on the presence of specific fractionating phases. The M-C basalt is clearly anomalous compared to the other arc rocks judging by its elevated Os/Ir and low Re/Os, Pd/Ir signature. The M-C basalt more closely resembles the high La/Y picrite (Table 8.11) in terms of its Re/Os and Pd/Ir ratios. The M-C basalt also has more MORB-like PGE ratios than any of the other intermediate arc rocks, except for its Os/Ir and Re/Os ratios which are affected by the very high concentrations of Os within the M-C group.

Intermediate Rocks	**Os/Ir**	**Pt/Pd**	**Pt/Ru**	**Re/Os**	**Pd/Ir**
C-series Basalt (Gd21)	0.51	0.41	100.0	8.53	323.24
M-C Basalt (Gd5)	9.90	0.50	25.0	0.23	68.13
ICaBrzA (I.B. 1)	0.93	0.46	14.29	10.64	289.92
MORB	***0.85***	***0.49***	***22.5***	***170***	***51***

Table 8.12 Key PGE ratios for intermediate rocks of Grenada and Izu-Bonin (MORB data from Ravizza and Pyle, 1997 and Plessen and Erzinger, 1997)

Apart from the M-C basalt, the intermediate arc rocks from both Grenada and Izu-Bonin are marked by Pd/Ir ratios that are elevated compared to the more primitive samples and MORB. High Pd/Ir ratios are a characteristic feature of low-Ti boninitic magmas and have been attributed to early Ir-depletion related to fractionation of olivine, chromite and CPX, while Pd remains in the residual S-

undersaturated melts (Hamlyn *et al.*, 1985). Further consideration will be given to the S-saturation conditions within the respective Grenada and Izu-Bonin magmas in Section 8.9.3. The Pt/Pd and Re/Os ratios of the Izu-Bonin andesite and C-series basalt are very similar. Thus, it can be inferred that these elements behave in a similar manner during fractionation within both the Grenada and Izu-Bonin arcs. Re/Os ratio increases during fractionation for both the Izu-Bonin and Grenada suites.

8.9.1.3 Evolved Samples

The Pd/Ir and Re/Os ratios of the evolved Grenada samples are much lower than those of the Izu-Bonin rhyolite. Pd/Ir ratio is lower within the Grenada andesites than in the C-series basalt. This drop may suggest that S-saturation conditions changed within the Grenada magma causing Pd-precipitation. The Izu-Bonin Pd/Ir ratios conversely increase during fractionation, implying that the magma remained S-undersaturated.

The high Os/Ir ratios of the Grenada andesite reflect the fact that Ir has been extracted from the melt to a point where it is below detection limit (<1ppt), rather than Os-enrichment. The Pt/Ru ratios have fallen with fractionation in both arc suites and this reflects relative Ru enrichment in the evolved samples. The Pt/Pd ratios show contrasting behaviour between the Grenada and Izu-Bonin samples. Fractionation at Izu-Bonin lowers the Pt/Pd ratio whilst fractionation at Grenada significantly raises the Pt/Pd ratio.

Evolved Rocks	Os/Ir	Pt/Pd	Pt/Ru	Re/Os	Pd/Ir
Basic Andesite (Gd17)	4.61	2.89	20.0	19.77	165.92
High SiO_2 Andesite (Gd25)	42.13	11.56	6.67	3.32	250.13
Rhyolite (I.B. 21)	2.5	0.17	8.33	83.7	507.85

Table 8.13 Key PGE ratios for evolved rocks of Grenada and Izu-Bonin

8.9.2 Comparison between PGE Patterns for Grenada and Izu-Bonin

8.9.2.1 Grenada Andesites vs Izu-Bonin Andesites and Rhyolite

The andesite Gd25 is depleted in Ir, Pd and Re compared to the rhyolite from Izu-Bonin, which may suggest that larger degrees of fractionation produced the Grenada suite. The differential behaviour of Pd between the different rock types indicates that a particular phase with which Pd is compatible crystallises from the Grenada suite, but not the Izu-Bonin suite. The most obvious difference between the cumulate and phenocryst mineralogies of the two suites is that amphibole is ubiquitous within the evolved Grenada suite, but apparently absent from the boninite suite (Table 8.9). It was previously noted (Sec. 8.3.2) that Ir is particularly enriched within the hornblende-cumulate Gd1. Thus, Ir and Pd are either compatible with amphibole, or they are predisposed to fractionation within hydrous melts, of which amphibole is an indicative phase. Despite these differences and considering that the Izu-Bonin and Grenada lavas are derived from dynamically different subduction environments, the overall shape of the PGE-patterns (particularly in Fig 8.32b) is remarkably similar. The Izu-Bonin andesite is more comparable in terms of PGE abundances and patterns with the C-series basalt group of Grenada (Fig 8.33b), rather than Grenada andesites.

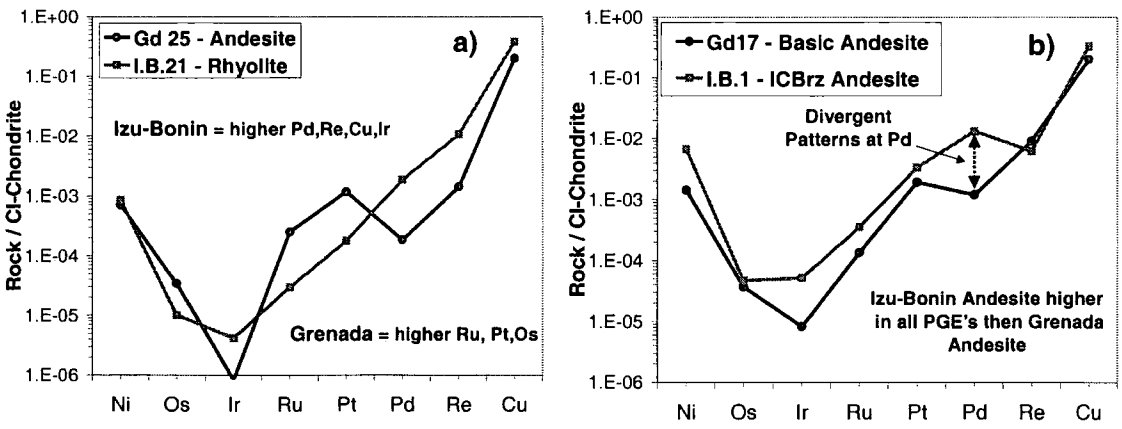

Fig 8.32 Comparison of PGE patterns between the more evolved rocks of Grenada (sample prefix Gd) and Izu-Bonin (sample prefix I.B.)

8.9.2.2 Grenada M-C and C-series samples vs Izu-Bonin Andesites and Boninites

The C-series basalt has slightly lower overall PGE abundances than the I.B. andesite. This probably reflects a higher degree of fractionation of the PGE phases from the intermediate Grenada lavas compared to the Izu-Bonin lavas. The M-C basalt is enriched in the IPGEs but depleted in the PPGEs relative to the Izu-Bonin andesite. The IPGE-enrichment is mirrored within the M-C picrite (compared with the boninitic magmas) and is thus probably a primary feature of the M-C group rather than an artefact of fractionation processes.

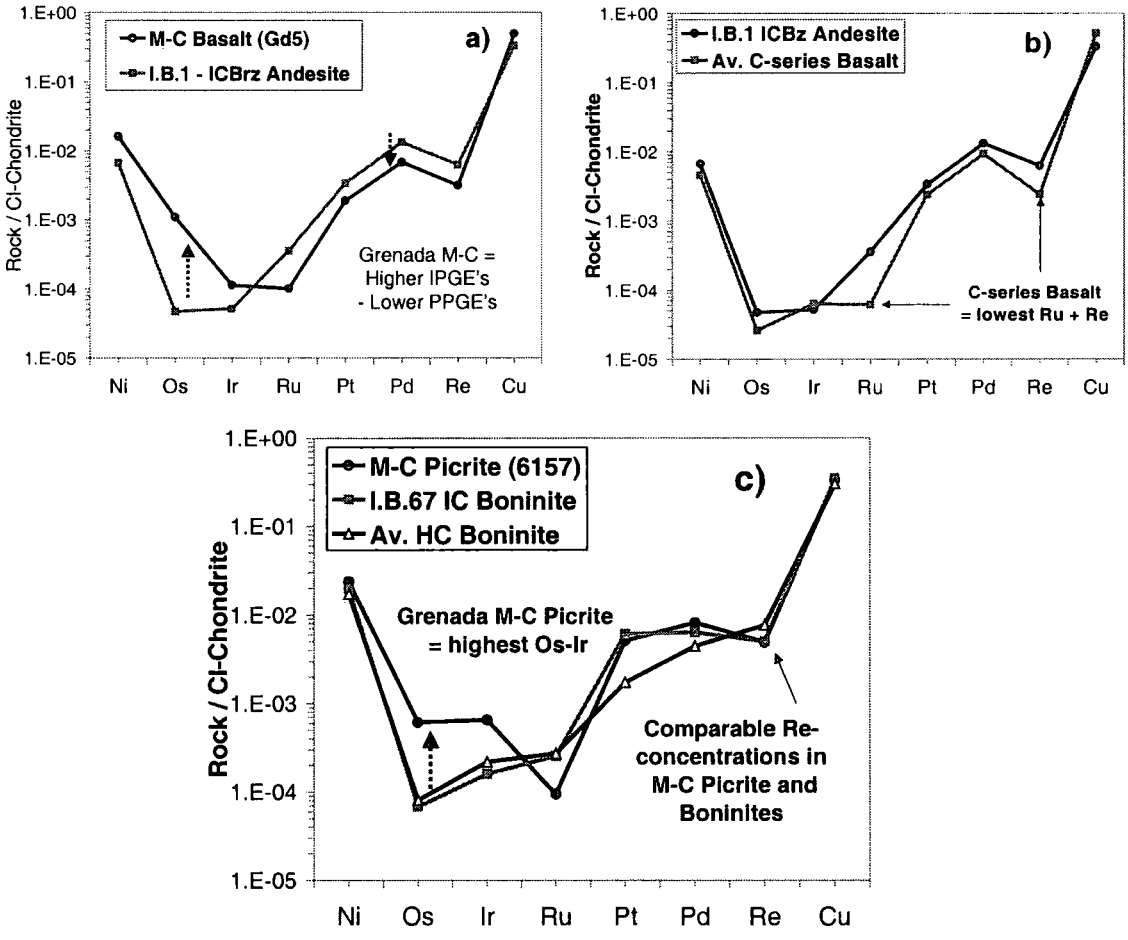

Fig 8.33 Comparison of PGE patterns between Grenada and Izu-Bonin samples (I.B. = Izu-Bonin, M-C and C-series = Grenada)

The M-C picrite and basalt contain more Os and Ir than the other Grenada picrites and the boninites. This could be achieved via the following conditions or processes:

a) If the M-C group were derived from a more residual mantle source than both the M-series of Grenada and the Izu-Bonin boninites (i.e. Os-Ir concentrated in residua by a previous melting episode). Presence of some residual mantle in the Grenada sub-arc wedge is confirmed by the existence of a depleted harzburgitic nodule in the Grenada lavas (Parkinson *et al.*, 1998[b]). However, since the boninites are also supposed to be derived from a depleted mantle-source, this cannot explain the discrepancy in Os and Ir concentrations between the M-C series and the boninites.

b) If the M-C picrites were generated by significantly higher degrees of partial melting than the boninites, in which refractory IPGEs were more effectively removed from the mantle. The Grenada lavas and the Izu-Bonin boninites are both thought to be generated by 10-15% mantle melting (Thirlwall *et al.*, 1996) although the boninites are thought to be derived from a more refractory source (Pearce *et al.*, 1992). It is speculated that the Izu-Bonin suite is generated at slightly higher temperatures than the Grenada suite (i.e. 1250°C vs 1100°C), thus, the lower Os-Ir within the boninites is contrary to expectation. This implies that the PGE-distribution in the M-C group of Grenada compared to the boninites is controlled by factors other than degree and temperature of melting.

c) If as Brandon *et al.* (1996) suggest, Os (and Ir?) are readily mobilised in halogen-rich subduction fluids and stripped from the mantle to be enriched in arc lavas. In this case, the mantle source of the M-C group must have interacted with fluids more than either the M-series of Grenada or the boninites.

An increased subduction component in the M-C group relative to the other Grenada series is not obvious from either REE or isotopic evidence. This does not dismiss the theory that Os may be mobilised and consequently enriched by fluids, as decoupling of PGE-REE signatures is a well-recognised phenomenon (Pattou *et al.*, 1996). However, since the M-C picrite has a less radiogenic Os-signature than the M-series picrites, preferential enrichment of Os (and Ir?) in the M-C series through fluid involvement in the Grenada mantle wedge is not considered viable.

Differences in the amount of hydrous fluid-component in the sources of boninites and the M-C series could account for the Os-Ir variations observed between these groups. There may be less aqueous fluid within the boninite source as they are generated at much shallower depths than the Grenada suite (i.e. 30 Km vs 100Km) (Thirlwall *et al.,* 1996; Pearce *et al.,* 1992). Thus, the boninites are formed at depths where amphibolitized subducting oceanic lithosphere is a stable phase. Breakdown of amphibole however, occurs at the depth of Grenada-magma generation and is thought to be one of the main sources of aqueous fluid to the mantle wedge above the subducting slab (Wilson, 1989).

8.9.2.3 Grenada Picrites vs Izu-Bonin Boninites

In general the shapes of the PGE-patterns defined for the Grenada picrites and Izu-Bonin boninites are very similar (Fig 8.34). Almost identical Ni and Cu concentrations are observed in the different rock types, which suggests that they cannot have had very different fractionation histories, been generated from significantly different source regions, or been subject to vastly different S-saturation conditions.

The most significant difference between the boninites and Grenada picrites is in their Re concentrations. This Re-depletion is evident in each of the more primitive Grenada lavas except the M-C series (Fig 8.33c). The low concentrations of Re may indicate the existence of a negative Re anomaly within portions of the Grenada mantle wedge. This could provide evidence that the Grenadian sub-arc mantle has experienced a previous, low-degree melt depletion event in which Re, the most incompatible of the PGEs was removed. Alternatively, Re could have been preferentially retained within the mantle source of the Grenada M-series picrites.

The ICBs contain significantly higher concentrations of Pt and Pd than the low La/Y picrites. This cannot easily be related to variation in melt fraction as higher Os and Ir contents (suggesting higher degree of melting?) are found within the low La/Y picrite. The Pt and Pd concentrations of the high La/Y picrites and the ICBs however, are more comparable. This is probably due to enrichment of Pt and Pd by fluids within the high La/Y group.

The Grenada picrites generally have higher Os-concentrations than the boninites. This, coupled with the lower MgO compositions and presence of skeletal olivine phenocrysts in the boninites (ca. 8-13%, Pearce *et al.*, 1992) implies that the boninites may have had more Os removed with olivine during early fractional crystallisation than did the Grenada picrites.

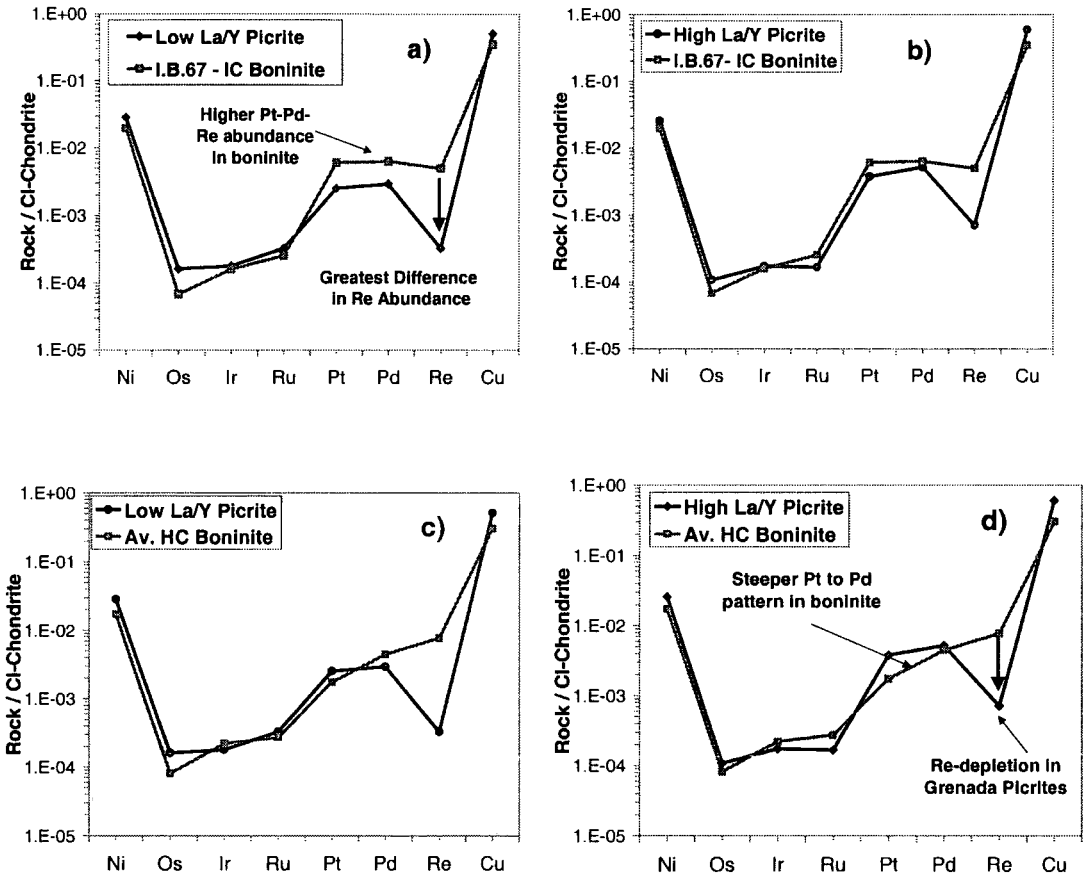

Fig 8.34 Comparison of the Grenada high and low La/Y picrites of the M-series, with the high Ca (HCB) and low Ca (LCB) boninites of Izu-Bonin

8.9.2.4 Conclusions from Comparison of Izu-Bonin and Grenada PGE Patterns

PGE patterns have been obtained for the lavas of the Izu-Bonin forearc and the Lesser Antilles arc which have a striking resemblance. This implies that the PGEs are relatively robust to variations in subduction environment, such as differential fluid and sediment input to their mantle sources. Os concentrations are

higher in the Grenada magmas than in the boninites, whether this is due to increased olivine/Os fractionation in the boninites or fluid-enrichment of Os in the Grenada rocks is uncertain.

The boninites of Izu-Bonin are generated by shallow, subduction-related melting of depleted mantle wedge (Pearce *et al.*, 1992). The Izu-Bonin PGE concentrations are not however significantly depleted relative to the Grenadian picrites and in fact Re, and sometimes Pt and Pd, are markedly enriched within the boninites. Thus, either the postulated initial melt extraction event at Izu-Bonin did not remove any PGEs from their mantle site or the Grenada sub-arc mantle has also undergone a similar depletion event.

The M-C group of Grenada have unique IPGE characteristics that cannot easily be explained by variable degrees of partial melting or fluid influence. Thus, blocks of mantle with distinct PGE-characteristics may be present in the sub-arc mantle wedges of subduction zones. This may well explain why the M-C group is restricted to one specific volcanic centre (MGF) on Grenada. Persistence of heterogeneous mantle signatures to the surface may imply rapid channelled flow of lavas. Indeed, Thirlwall *et al.* (1996) suggest that shorter melting columns and shorter magma-chamber residence times beneath Grenada than other arcs, may well account for the high proportion of picritic lavas erupted at the surface.

It is thus proposed, on the basis of comparison between Izu-Bonin and Grenada, that intra-oceanic, subduction-related volcanic rocks may have universally similar PGE patterns. As such, PGE patterns may provide another useful geochemical tool in identifying arc volcanics within the geologic record. Further analyses of volcanic rocks from different intra-oceanic arcs need to be conducted to test the above hypotheses.

8.9.3 Comparison of Sulfide Saturation Conditions in Grenada and Izu-Bonin Magmas

8.9.3.1 Constraints on Grenadian Magmas

One of the best ways to constrain the relative timing of S-saturation within a magma series is to study the behaviour of the PGEs compared to the highly chalcophile element Cu, which is immediately precipitated from a magma once S-saturation occurs (Keays, 1995). Decrease in Ni, Os, Ir and Ru from the M and M-C series to the C-series reflects the fact that the IPGEs exhibit siderophilic behaviour during fractionation. Pd, Re and Cu concentrations within the C series basalts are equal to, or greater than, the M and M-C series, reflecting the more chalcophilic nature of these elements during fractionation. The high Os and Ir content of the M-C group is not matched by high Ni-content. Thus, Ir and Os are not concentrated in this group because of higher olivine accumulation.

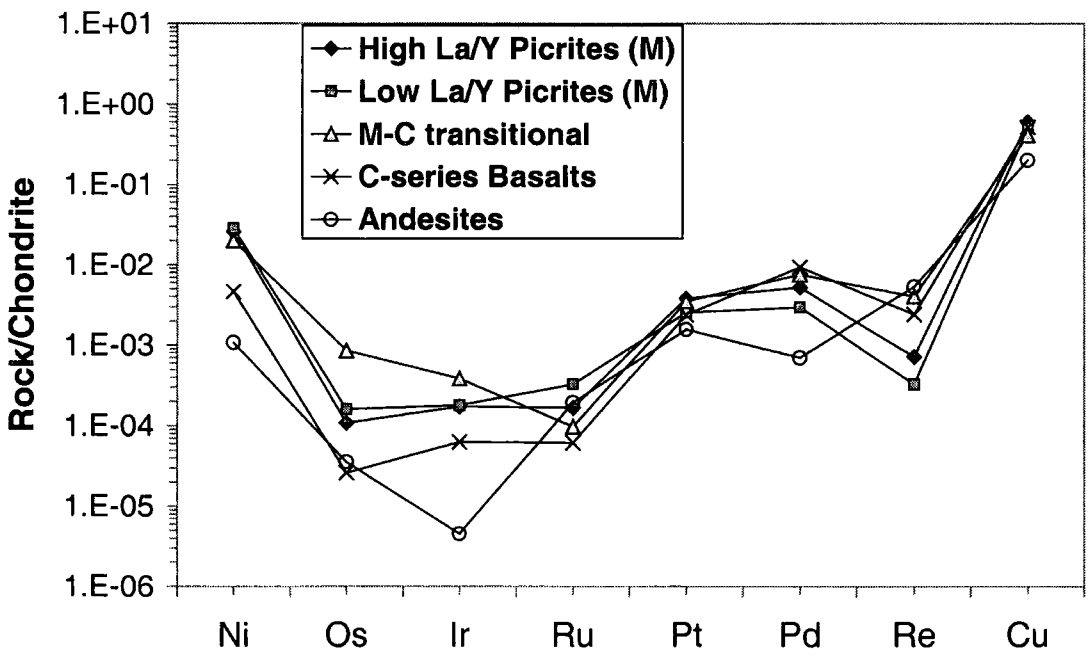

Fig 8.35 Comparison of chalcophile-siderophile and PGE variation through the Grenada suite

There is a large decrease in Cu-concentration between the primitive rocks (C-series basalts and M-series picrites) and the more evolved rocks (andesites; Fig 8.35). Thus, it is suggested that S-saturation must have occurred within high-level magma chambers during andesite formation. The cumulates do not however, contain the "missing" Cu. Thus, they must have formed prior to S-saturation. Abundance of PGEs and Cu in both the cumulates and andesites, indicates that Pt and Ir partition into the cumulates rather than the andesitic-melts, whereas, Ru, Re and Cu partition into the residual melt. Os and Pd show variable but similar concentrations within both andesites and cumulates. Thus, Re and Ru behaved in the most incompatible manner during cumulate formation.

Within the more primitive samples, Re concentration increases as Cu-content decreases (Fig 8.36). This implies that phases other than sulfide may govern Re partitioning in hydrous melts. Such a trend is also observed for Pt within the C and M-C basalts. The opposite trend, however, is observed for Pt within the low La/Y picrites, while the high La/Y picrites maintain constant Pt at variable Cu. The variable behaviour of Pt in the different primitive rocks indicates that Pt partitioning (into sulfides with Cu) may be dependent on subtle differences in magma-chamber or melt conditions.

Cu variation within the primitive samples is somewhat independent of Ir and Os concentration. The C-series basalts contain less Os than M-series picrites, but comparable Cu contents. This lends credence to the theory that Os-depletion within the C-series is controlled by a silicate phase(s) (i.e. olivine), rather than sulfide phases. Ru concentrations within the high and low La/Y picrites increase with increase in Cu. Thus, Ru and Cu behave in a similar, incompatible manner. Pd however, does not positively correlate with Cu (Fig 8.36). This is contrary to observations in other magmatic systems (e.g. Keays, 1995) that Pd is the most incompatible and chalcophile of all the PGEs. Thus, Pd-behaviour and partitioning may be dependent on H_2O and O_2 conditions within a magma, even though as a mono-valent cation, the oxidation state of Pd itself will not vary (Righter *et al.*, 1998).

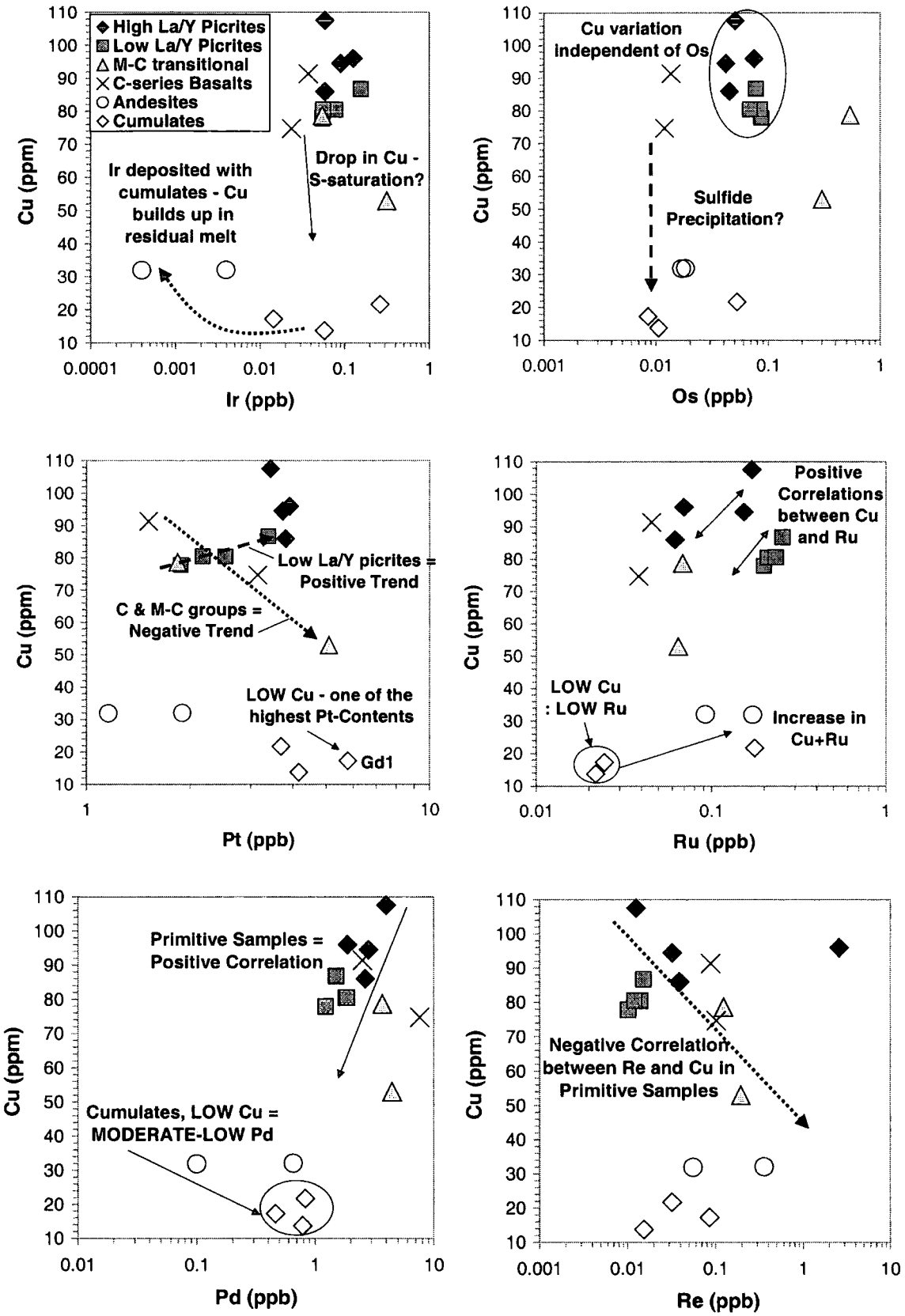

Fig 8.36 PGE concentration vs Cu for the Grenada suite

8.9.3.2 Comparison of S-Saturation in Izu-Bonin and Grenada

Comparison of Izu-Bonin boninites measured in this study with boninites from the Bonin-Mariana arc system previously analysed (Hamlyn *et al.*, 1985) shows that boninites analysed previously contain significantly more Pd, but have comparable Cu concentrations to the boninites measured during this study. It is impossible to judge the quality of the existing PGE data on boninites as replicate analyses and detection limits were not presented (Hamlyn *et al.*, 1985). Thus, in the light of this study (Chapter 3) where data acquired by non-I.D. fire-assay was found to be unreliable, it is proposed that the Pd-values previously reported for boninites (Hamlyn *et al.*, 1985) may be too high.

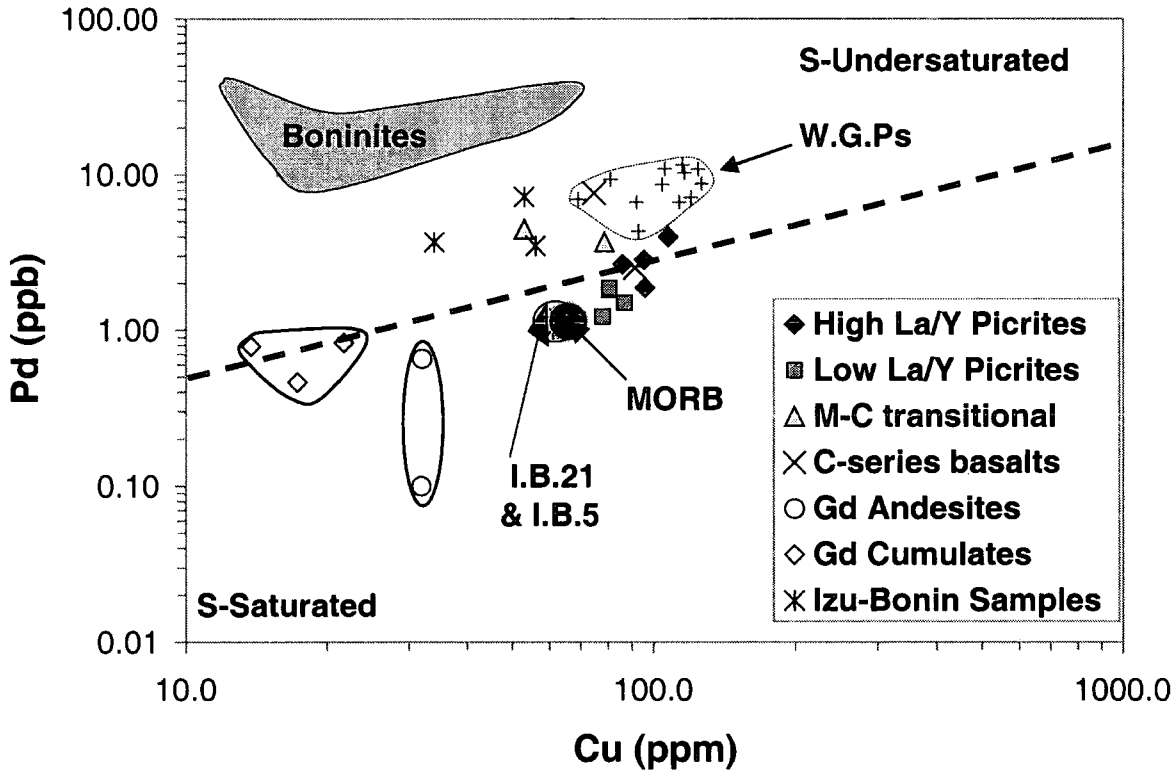

Fig 8.37 Pd vs Cu as a measure of S-saturation (after Brooks *et al.*, 1999); boninite field from Hamlyn *et al.*, 1985. WGPs = West Greenland picrites. N.B. The S-saturation line is empirical (Brooks *et al.*, 1999) and is thus not conclusive proof of S-saturation.

The S-undersaturated nature of boninites has been attributed to their derivation from sources which have been previously depleted by extraction of a MORB-like component. Primary MORB liquids are S-saturated (Fig 8.37) and thus an immiscible sulfide component is retained in the mantle residue. This results in concentration of the PGEs and depletion of the base metals (lower K_d sulfide-liquid) in the residual mantle sulfide fraction. Thus, remelting of this refractory source produces S-deficient, PGE-enriched magmas (Hamlyn *et al.,* 1985).

Three of the Izu-Bonin samples (namely one of the HCBs, the ICB and the ICBrzA) plot within the S-undersaturated field as expected. The other HCB and the rhyolite however, plot below the S-saturation line (Fig 8.37). This is because of their low Pd-content compared to the other Izu-Bonin samples. The reason for the differential behaviour within the HCB group cannot easily be explained. However the S-saturation of the rhyolite may be explained as fractionation, even of an initially undersaturated magma, tends to drive a melt towards S-saturation (Keays, 1995).

There is a great similarity in the position of the M-C picrite and the boninites on Fig 8.37, implying derivation of the M-C picrite from a similar residual source to that of the boninites. The other Grenada picrites generally have higher Cu and lower Pd contents, suggesting that they were derived from a less depleted source than the boninites and M-C picrite.

The S-saturation status of the Grenada magmas varies according to series (Fig 8.37). The high La/Y M-series picrites straddle the S-saturation line, whereas the low La/Y picrites plot below the S-saturation line. The M-C series plot above the S-saturation line. The C-series basalts also show variable behaviour: one sample is S-undersaturated and overlaps with the WGP field, the other plots on the S-saturation line. The andesites of Grenada are quite strongly S-saturated, probably due to assimilation of crust. Separation of an immiscible sulfide phase from these rocks explains the very low concentrations of PGEs measured within the evolved lavas.

It is contrary to expectation that the C-series should be less S-saturated than the M-series since they are more evolved and fractionation usually drives melts towards S-saturation, not vice versa (Keays, 1995). One possible explanation for this is that following removal of immiscible sulphides during C-series fractionation, the magma then becomes S-undersaturated again. This may remain so until further

fractionation (or assimilation of crust) in higher magma-chambers pushes the melt towards S-saturation (i.e. andesites) and precipitation of sulfides again.

The mantle below Grenada is of N-MORB source character, though enriched in LILEs and LREEs from the subducting slab (Thirlwall *et al.,* 1996). The primitive Grenada lavas are however, less S-saturated than typical MORB. It would be expected that the Grenada lavas and MORB should have possessed similar S-saturation patterns as they are both thought to be generated by low to moderate degrees of partial melting of mildly depleted, to undepleted mantle (Hamlyn *et al.,* 1985).

One explanation for this observation is that the mantle-wedge below Grenada is depleted relative to MORB-source with regard to S. Only minor degrees of prior melting are required to deplete the mantle in sulfide as S is highly incompatible (Hertogen *et al.,* 1980). There is some evidence that the M-C series might be derived from a depleted boninite-source like mantle. Thus, the rest of the mantle wedge may also have undergone a minor degree of melt extraction. This is not confirmed by comparison with lithophile elements however (e.g. Nb).

Magmas derived from S-depleted mantle sources (e.g. boninite source; Hamlyn *et al.,* 1985) are often enriched in PGEs. The mildly S-undersaturated Grenada lavas (except the M-C picrite which has high Re, Os and Ir) however, have lower PGE concentrations than the boninites (Fig 8.34). This may be due to the complex multi-stage fractionation history of the Grenada suite and removal of the PGEs from magmas in high-level magma chambers.

8.10 Comparison of Subduction Zone PGE-Signatures with those from Other Tectonic Environments

8.10.1 Inter-Element Comparisons

Direct comparison between environments is not straight-forward since the PGE signatures of the subduction-related rocks (unlike the other high MgO rocks) have been altered by such processes as multi-stage fractionation.

The subduction-related rocks plot within discrete fields on a Re-Os diagram although in general (apart from the M-series picrites) they plot within the same field as OIB (Fig 8.38). The Grenada M-series picrites have equivalent Os-content but lower Re than OIB. This reiterates the point that Re may have been withheld in the M-series source. The M-C series of Grenada plots towards the higher MgO rocks and partially overlap the field defined by the harzburgitic xenoliths from the Cascades and Ichinomegata mantle wedges. This is additional evidence that the M-C series picrite may have been derived from re-melting of a residual source. The Re-Os signatures of the evolved Grenada and Izu-Bonin samples (i.e. rhyolite and C-series basalts) confirm that fractionation increases Re contents, but decreases Os.

On the Ni/Cu vs Pd/Ir plot the Grenada suite separates into two discrete groups: the M and M-C samples and the C-series basalts (Fig 8.39). The Grenada picrites and the boninites plot in or near the field defined by high MgO basalts. Therefore, PGE and chalcophile fractionation within the two primitive subduction suites analysed is not that pronounced.

The C-series basalts are displaced to lower Ni/Cu and slightly higher Pd/Ir than the other Grenada samples and plot near the CFB field. This is further evidence that the C-series basalts are more strongly fractionated than the M-series picrites and M-C group. The C-series has higher Pd/Ir than MORB, but, similar Ni/Cu ratios to MORB suggesting derivation from a source with similar chalcophile element abundances. This may imply that fractionation of the PGEs in hydrous subduction-related melts, or in crustal magma chambers, is more pronounced than in MORB.

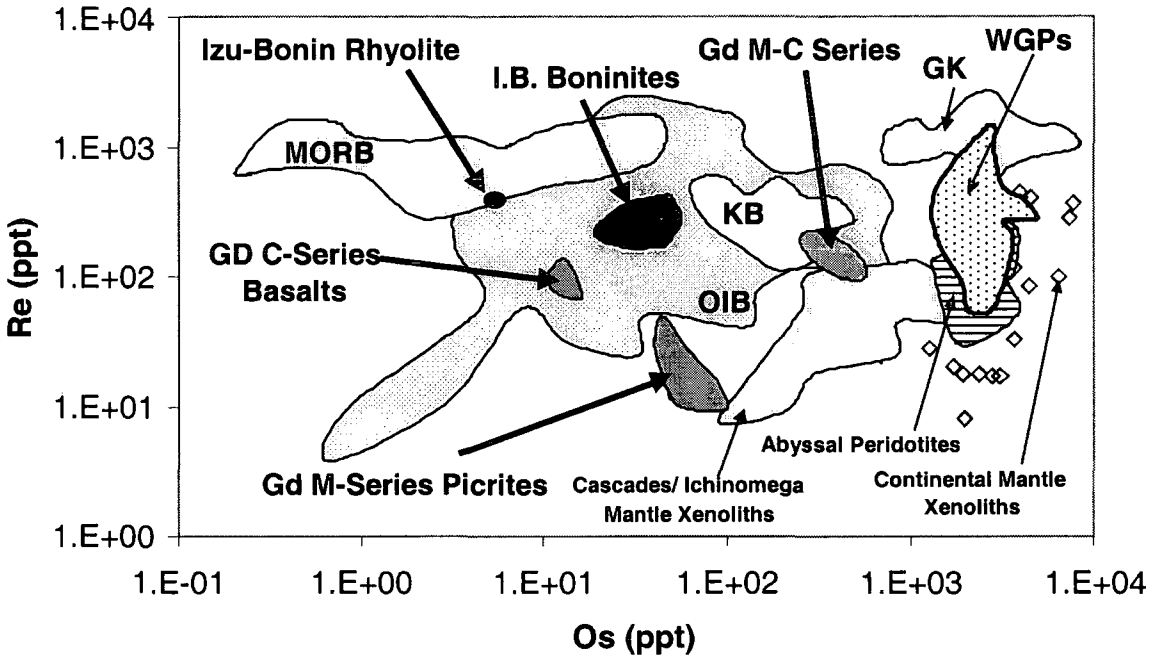

Fig 8.38 Re vs Os discriminant diagram for subduction zone samples compared to other tectonic environments (GK = Gorgona komatiites, Brugmann *et al.*, 1987; KB = Keewanawan basalts, Shirey, 1997; WGP = West Greenland picrites)

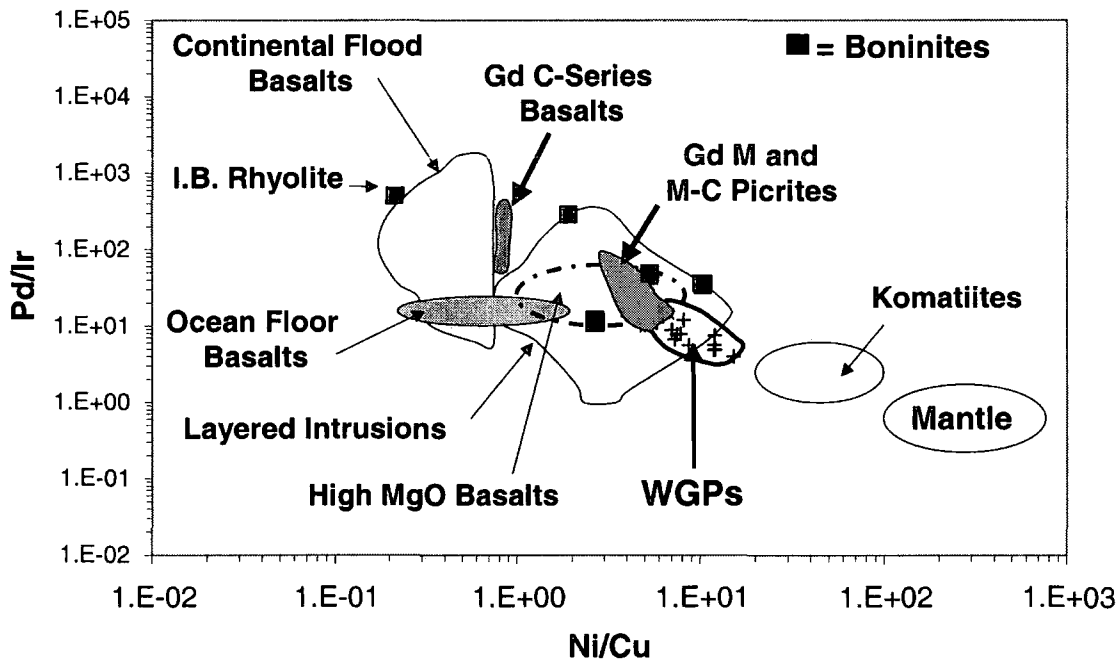

Fig 8.39 Tectonic discriminant diagram based on Ni/Cu vs Pd/Ir ratios (after Vogel *et al.*,1999; fields from Vogel *et al.*,1999. Mantle= fertile, ocean floor basalts = MORB) showing the relative global position of the primitive Grenada and Izu-Bonin suite.

The M-series picrites and M-C transitional series form a coherent field that partially overlaps the WGP field. The M-C transitional picrite most closely resembles the WGPs. Variations in both Ni/Cu and Pd/Ir ratios are predominantly governed by extent of fractionation and partial melting. The position of the Grenada picrites relative to the WGPs, komatiites and primitive mantle, along a negative-sloped line may represent a melting trend. The higher Pd/Ir, lower Ni/Cu ratios of the Grenada lavas compared to the WGPs could be achieved through lower degrees of partial melting or increased amounts of fractionation within the Grenada suite relative to the WGPs. The boninites form a slightly more dispersed group, with the most fractionated samples plotting to higher Pd/Ir and lower Ni/Cu. Thus, although cases can be made for subtle variations in PGE (and chalcophile) behaviour due to subduction zone influence; for primitive magmas PGE fractionation in the two suites analysed appears to be dominantly controlled by melting and fractionation.

8.10.2 Extended PGE Plots for Different Environments

8.10.2.1 Subduction-related Rocks vs MORB

Extended PGE plots for the subduction rocks (Fig 8.40a) illustrate that the Izu-Bonin boninites and the Grenada picrites contain less of the base metal Cu than does MORB. The mantle sources of both Grenada and Izu-Bonin therefore may have been depleted by a previous melting event in which base metals were selectively removed, while the PGEs remained in the residual mantle sulfide. Similarity in source region of Grenada and Izu-Bonin is strongly suggested by the comparable PGE patterns (Fig 8.40a).

Re-depletion within the Grenada M-series picrites relative to the boninites (and MORB) may arise as the picrites are generated at depths where garnet is stable, the boninites conversely are generated at much shallower depths where garnet is not stable. Thus, it is proposed that Re may be retained within garnet in the Grenada M-series source, but not within the boninite source. Re does not behave in a simple compatible or incompatible manner during melting and is more enriched in MORB than might be predicted (Shirey and Walker, 1998). This is because Re's distribution

is controlled by different phases (e.g. garnet and sulfide; Shirey and Walker, 1998). Thus, in the more residual mantle sources (e.g. the M-C series and the boninites), Re may be contained within sulfides, readily accessed during re-melting, so producing Re-enriched magmas.

There is a high degree of overlap between the boninites, Grenada picrites and MORB in terms of their PGEs. Pt concentration in the subduction-related rocks is sometimes higher than in MORB. This may be either because Pt has been enriched by a subduction (fluid?) component, or, because the subduction-related magmas are less S-saturated so allowing more efficient removal of PGEs from the mantle source.

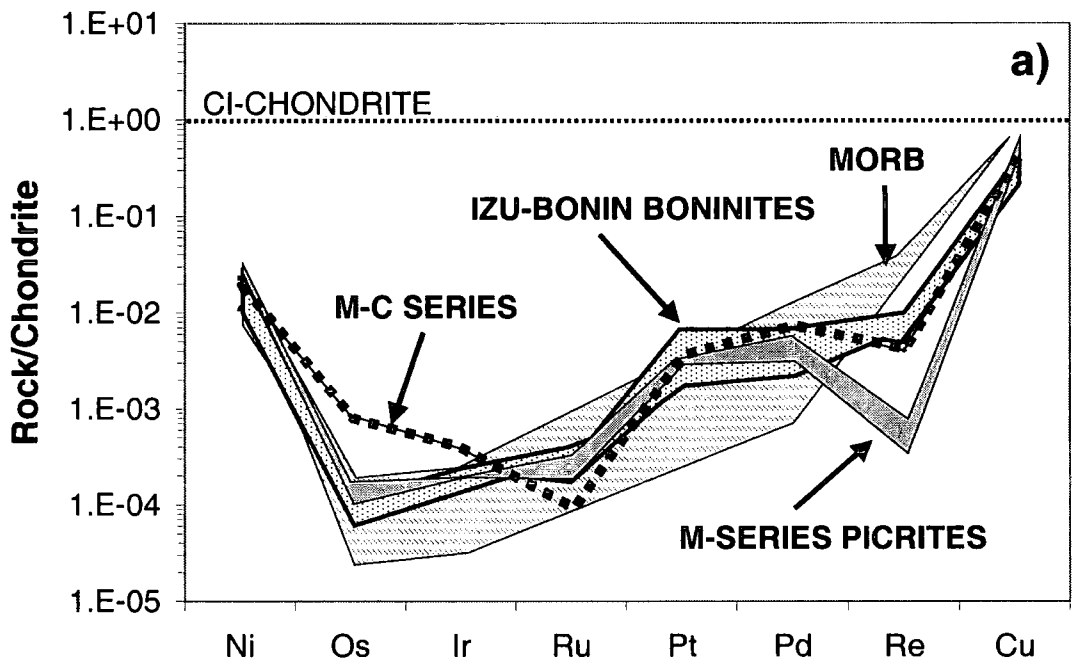

Fig 8.40a Comparison of subduction rocks and MORB (MORB data from Ravizza and Pyle, 1997)

8.10.2.2 Subduction-related Rocks vs OIB and High MgO Rocks

There is significant overlap between the PGE concentrations in primitive subduction related rocks and OIB (although the OIB-range is quite large) except for Os and Re, which are depleted in the M-series picrites relative to OIB. Higher degrees of melting or lower degrees of fractionation in OIB compared to the Grenada samples probably explain the Os trend.

Relative to the subduction-related rocks, OIB and the high MgO rocks (i.e. WGPs and komatiites) are enriched in Cu (Fig 8.40b-d). This requires derivation of the high MgO rocks and OIB from a more fertile reservoir. The high MgO rocks are uniformly enriched in the PGEs relative to the subduction rocks (except for Pd) probably due to a combination of higher degrees of melting and less fractionation within the high MgO rocks. The M-C picrite, kimberlites, WGPs and PUM have very similar Pd-contents.

The coherence in Pd-signatures can be most easily explained with the hypothesis that during mantle melting in S-undersaturated systems (i.e. subduction zones, high degree melts), all PGEs are quantitatively removed from their source. Thus, primary subduction-related melts may have the same PGE-concentrations as higher MgO rocks. However, IPGEs are rapidly impoverished in subduction-related magmas during early fractionation. Pd conversely, being more incompatible, could be retained in S-undersaturated subduction-related lavas or higher MgO lavas, in source-like proportions. This explains why the WGPs and PUM have similar Pd concentrations to some subduction-related samples.

In terms of Os, Ir and Ru concentrations, the subduction-related rocks are lower in concentration than both the high MgO rocks and PUM. This indicates that either the IPGEs are fractionated from the subduction lavas before eruption, or that they remain behind within the mantle residues after melting. Pt and Pd concentration ranges for the subduction rocks also overlap the range of cratonic kimberlites. Since the subduction-related primitive rocks are not greatly enriched in any of the PGEs compared to kimberlite, this might be considered evidence that the PGEs are not selectively mobilised during melting in the subduction environment compared to other tectonic environments.

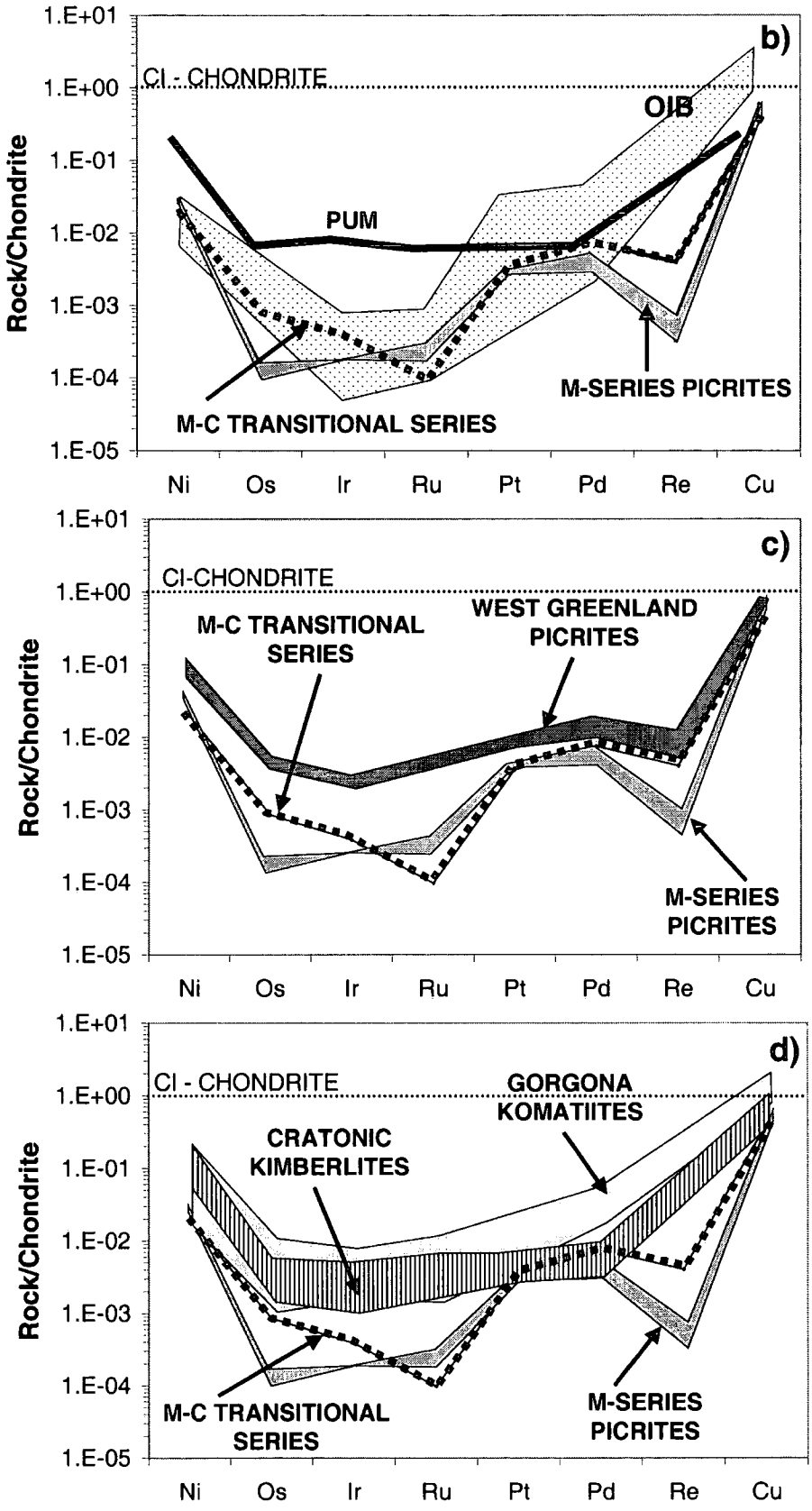

Fig 8.40b-d Comparison of extended PGE patterns of subduction-related rocks and rocks from other tectonic environments (komatiite data: Brügmann *et al.*, 1987; kimberlite data: McDonald *et al.*, 1995; PUM data: Morgan *et al.*, 1981; OIB data: Fryer and Greenough, 1992)

8.11 Economic Potential of Intra-Oceanic Arcs with Regard to PGEs

The world's major economic PGE-deposits are generally linked to eruption of voluminous, S-undersaturated picritic or komatiitic magmas (Keays, 1995). The S-saturation status of a magma has an enormous-bearing on its ore-forming potential. A S-saturated magma either leaves its sulfides (+PGEs) behind within the mantle residue (i.e. MORB) or segregation of sulfide and PGEs occurs enroute to the surface (Keays, 1995). During eruption of S-undersaturated magma however, the PGEs and other chalcophile elements are incompatible and may become enriched in the liquid residua to the point where it is of significant economic potential once S-saturation is finally reached (Hamlyn *et al.*, 1985).

It is believed that mixing of a S-undersaturated boninitic-type magma with another S-saturated magma was responsible for formation of the Merensky Reef of the Bushveld layered intrusion, the world's largest economic PGE-deposit (Keays, 1995). Thus, S-deficient boninitic magmas may be essential to the formation of platiniferous horizons in layered intrusions. The erupted lavas of Grenada are obviously not of any significant economic potential because of their low PGE concentrations. However, the similarity with boninites in terms of their S-undersaturated nature, may be worth some consideration. If the S-undersaturated Grenada magmas do initially pond at deep crustal levels (suggested by the fact that even the picrites have undergone some olivine fractionation) and there is a high throughput of magma, then residual melts within these chambers may become highly enriched in PGEs. S-saturation within such chambers, once active vulcanism ceases and fractionation proceeds, could produce significant economic deposits. Thus, the discovery that some arc picrites are S-undersaturated implies that at least some magma-chambers within arc-crust might be of economic potential, although none have been identified to date.

8.12 Summary of Key Points in Chapter 8

8.12.1 Modification of PGE Signatures in Subduction Systems

Radiogenic Os isotope signatures in Grenada lavas cannot be easily explained by late-stage crustal contamination and are thus taken as evidence that radiogenic Os is contributed to the mantle wedge from the subducting slab. PGE concentrations in the mantle are unlikely to be significantly affected by the low amounts of bulk sediment input from the subducting slab estimated from isotopic constraints. The enhanced isotopic signatures are perceived to be derived from enriched slab-derived fluids, rather than bulk sediment addition. Some correlation of increased Os, Pt, Pd and Re concentrations within primitive lavas derived from melting of mantle with increased slab-fluid input (i.e. the high La/Y picrites) implies that these elements may be selectively mobilised under fluid-rich mantle conditions.

The Izu-Bonin boninites, although thought to be derived from a more depleted source than the Grenada picrites, have very similar PGE patterns and concentrations. Thus, from the two arcs studied, it appears that subduction-related primitive lavas may have common PGE characteristics. Similarity between PGE distribution in subduction-related and other high MgO rocks suggests that while the subduction-environment may cause subtle changes in PGE geochemistry and Os-isotopes, the dominant controls on PGE abundance and ratios are degree of partial melting and fractionation.

8.12.2 Controls on PGE Fractionation in Subduction Systems

It is difficult to assess which mineral phases are controlling PGE fractionation as the sample set is limited and conflicting patterns occur within the same sample group. Rather than being compatible with particular mineral phases, it is likely that the PGEs segregate from the melt with whatever minerals are nucleating in the magma-chamber at a given time (e.g. Peck *et al.*, 1992). In addition, certain elements (particularly Ru) seem to show changes in their compatibility as fractionation of the magma proceeds. This is probably related to changes in O_2/H_2O conditions in the

magma, which in turn cause variation in the oxidation-state and thus compatibility of certain PGEs.

A summary of the phases with which the PGEs show some correlation (Table 8.14 and 8.15) illustrate that subtle differences in PGE-mineral associations occur between Izu-Bonin and Grenada. The most marked difference is that Re and Pd might be mildly compatible with magnetite in Izu-Bonin, but show no such relationship in the Grenada suite.

	Phases with which PGEs co-crystallise, or are compatible
Os	Strong Olivine control, co-crystallises with Cr?
Ir	Olivine, Magnetite, Amphibole ?, co-crystallises with Cr?
Ru	Mildly Olivine controlled - Becomes incompatible during late stage fractionation.
Pt	Mildly Olivine controlled. Compatible with a cumulate phase - CPX/Plag ?/Amphibole?
Pd	Compatible with a late-stage cumulate phase? – **NOT** sulfides or magnetite.
Re	Behaves incompatibly, no obvious relationships to other mineral phases.

Table 8.14 Mineral phases which the PGEs co-crystallise, or are compatible, during fractionation of the Grenada suite

	Phases with which PGEs co-crystallise, or are compatible
Os	Strong olivine control.
Ir	Olivine, Magnetite.
Ru	Incompatible during andesite form^{n}. Compatible during rhyolite form^{n} – Magnetite controlled?
Pt	Olivine, Cr.
Pd	Compatible with Magnetite? – during late stage fractionation only.
Re	Compatible with Magnetite? – during late stage fractionation only.

Table 8.15 Mineral phases which the PGEs co-crystallise, or are compatible, during fractionation of the Izu-Bonin suite

There does not appear to be a strong sulfide control on PGE fractionation within the subduction-related lavas, probably because they are often S-undersaturated. The fact that S-undersaturated primitive lavas occur on Grenada despite relatively low degrees of partial melting, implies that the Grenadian mantle-wedge must have been depleted in S at an earlier stage.

The PG-inter element ratios become modified during magmatic fractionation. Ir/Os decreases on Grenada, but increases on Izu-Bonin with increasing fractionation. Thus, Ir and Os clearly show different compatibilities with different crystallising phases. Hence, caution must be exercised in using Os abundance to infer Ir concentrations in geological samples and vice versa. In both Izu-Bonin and Grenada lava suites, Re/Os and Pd/Ir increases, but Pt/Pd decreases with increasing fractionation.

8.12.3 PGEs within the Sub-arc Mantle Wedge

Re/Os ratios within different subduction-related lava series show more variation than any other ratios. This is thought to be due to preferential retention of Re within different mantle phases in sub-arc mantle wedges. Low Re-concentrations in the Grenada M-series picrites are attributed to retention of Re within garnet during low degree melting episodes. Much higher Re-concentrations (and higher Re/Os) within the boninites and Grenada M-C series are attributed to the fact that Re is hosted within mantle sulfides (rather than garnet), and thus more easily released into the melt during low degree partial melting of these more residual sources.

In terms of their PGE-signatures, the Grenada M-C series magmas are **not** transitional between the Grenada M and C-series magmas. The precious metal and S-saturation characteristics of the M-C picrites of Grenada indicate that they are derived from a more residual source than the M-series picrites. Thus, the PGEs provide unique information which the lithophile elements do not, since lithophile elements can be readily re-fertilised in the mantle-wedge. This might imply that some heterogeneous "blocks" of mantle do occur within subduction zone mantle-wedges and lends credence to the theory of Parkinson *et al.* (1998[a]) that subduction zones may act as graveyards for discrete blocks of ancient-depleted oceanic lithosphere.

9: Conclusions

9.1 Advances in Analytical Procedures for PGE Measurement

The primary goal of this study was to provide a low-blank, routine chemical separation method for the high precision analysis of as many PGEs as possible by ICP-MS, with the possibility of Re-Os isotope analysis of the same sample aliquot by either ICP-MS or N-TIMS. Development of such a method was essential to facilitate analysis of PGE signatures within low PGE abundance volcanic rocks, the second objective of this study.

Following evaluation of isotope dilution Ni-S fire assay for analysis of low abundance geological samples, it was concluded that the use of isotope dilution in conjunction with Ni-S fire assay enables the acquisition of reproducible data for relatively high abundance samples (>1ppb). However, due to the large inherent blanks connected with the Ni-S assay technique (predominantly from the Ni-reagents used), it appears unsuitable for use in measurement of rocks which contain sub-ppb levels of PGEs.

Thus, a new technique employing Carius tube digestion, solvent extraction and anion-exchange chromatography was investigated and developed. Unlike Ni-S fire assay this method permits the routine and precise determination of Re, Os, Ir, Ru, Pt and Pd in geological samples with very low (<<1ppb) abundances of PGEs.

The anion exchange chromatography technique developed compares very favourably with other methods of PGE pre-concentration. The method was evaluated by replicate dissolution of a standard komatiite WITS-1, together with unknowns. For WITS-1, concentrations of Os, Ir and Ru reproduce well, within a factor of two of that expected based on sampling theory. Potential heterogeneity for Pt, Pd and Re is identified at the 1g sampling level used that may be related to alteration. Replicate analyses of picritic basalts in the 1 to 10ppb range show average 2σ reproducibilities of better than 5% for Re, Os, Ir, Pt and Pd, with Ru being better than 10%. Analytical reproducibility is dependent on PGE levels and rock type.

The method allows confidence to be placed in inter-element PGE fractionations in rocks with <<1ppb of a given PGE. As shown by Shirey and Walker (1994) and McDonald (1998), heterogeneity of PGEs will vary greatly in different rock types.

Ordinary Carius tubes are mostly limited to sample sizes of c.5g (Shirey and Walker, 1994) and so the technique will be subject to greater sampling errors than fusion techniques capable of digesting much larger sample sizes. However, the procedure developed offers the opportunity to obtain both Re-Os isotopic measurements and PGE analysis (except Rh) on very low abundance rocks that may not be amenable to other methods of analysis.

Using the developed technique, rocks from two distinct tectonic environments have been characterised for PGEs.

9.2 Constraints on PGE Behaviour from the West Greenland Picrite Study

A suite of picritic lavas (MgO >16%) from West Greenland, generated by the ancestral Iceland plume were analysed for PGEs. The relatively high PGE abundances in these rocks ensure good data quality. In addition, they provide an excellent example of picritic lavas generated in a tectonically simple environment with which to compare the picritic lavas from subduction zones, a much more tectonically and geochemically complex setting. The key points regarding PGE behaviour in this suite of rocks are summarised below:

- The WGPs show good evidence for incorporation of a radiogenic Os-component in their source region. This may reflect either a recycled oceanic crustal component (>500Ma, Pearson pers. comm.) or incorporation of minor amounts of outer core material. This component has affected the Os-isotopic signature of the picrites, but has not noticeably affected overall PGE concentrations.
- Os-isotopic and REE data shows that the influence of MORB-source mantle decreases, stratigraphically upwards through the lava succession.

- The WGPs have relatively flat chondrite normalised PGE patterns, similar to those of other high MgO rock types (e.g. komatiite). This confirms their derivation via high degrees of melting of a fertile source and that they have undergone only very limited fractionation.
- Re is depleted within the WGPs compared to other high MgO rocks. Plots of Re-Yb and HREE-depletion relative to MORB indicate that Re may have been retained within garnet in the source region of the WGPs
- Correlation between Ir and Os, Mg No. and Ni implies that Os and Ir co-crystallised with early cumulus phases such as olivine. It is not possible to constrain whether the IPGEs were compatible with olivine or whether they are contained as inclusions (alloys?) within cumulus phases.
- Os/Ir ratios are much higher (ca 1.9) than in other magmatic rocks. This means that they do not behave in a strictly analogous manner during mantle melting/fractionation and as such, Ir concentrations should not be used to infer Os concentrations in geological samples and vice versa.
- Strong correlations between the other PGEs and crystallising silicate phases do not occur. Thus, the behaviour of Ru and the PPGEs is decoupled from Os and Ir behaviour.
- Pd behaves in the most incompatible manner during fractionation and behaves in a very different manner to all of the other PGEs, including Pt.
- Pt abundance in the picritic lavas is sensitive to subtle variations in melt fraction (inferred by correlation with La/Sm) but Ir, Os, Ru and Pd are not. This implies that the PPGEs and IPGEs may be hosted by different mantle phases. A model (after Ballhaus, 1995) is preferred whereby following dissolution of sulfides during partial melting, Ru-Ir-Os alloys are stabilised within the melt and may be precipitated along with cumulate phases, while Pt remains within the silicate melt.
- Progressive decrease in Pd/Ir ratios with degree of melting in high MgO-rocks indicates that this is the controlling factor in dictating PGE signatures. This rapidly becomes masked however by fractionation processes as rocks become more evolved.

- Pd-Cu systematics suggest that the WGPs were S-undersaturated at the time of eruption. As there is no evidence of source depletion, this implies degrees of partial melting in excess of 25%. Hence, there does not appear to be any sulfide-control on distribution of PGEs within the picritic lavas even for Pd, the most chalcophile of the PGEs.
- Eruption of voluminous S-undersaturated high MgO lavas in West Greenland raises the possibility that economically viable PGE-deposits could be present.

9.3 Constraints on PGE Behaviour in Subduction Zone Systems

Rocks generated above subduction zones were analysed and a suite of rocks from the island of Grenada (intra-oceanic arc without any back-arc spreading) were compared with a suite of rocks from the Izu-Bonin forearc (intra-oceanic arc with back arc-spreading). Major element chemistries of these arcs vary from mildly alkaline (Grenada), to boninitic (Izu-Bonin) due to the difference in tectonic setting. In addition, picritic lavas are unusually abundant on Grenada and thus provide a unique opportunity to study relatively "unfractionated" subduction zone PGE-signatures. The key points regarding PGE behaviour in this tectonic environment are summarised below:

- Identification of phases with which the PGEs are 'compatible' during fractionation is, strictly speaking, not possible as the PGEs probably just co-crystallise with other phases. They may either nucleate around silicate phenocrysts (e.g. Peck *et al.*, 1992) or in turn be enclosed within silicate phases (e.g. Edwards, 1990). Thus, phases with which the PGEs are 'associated' include: Olivine (Os, Ir and Pt in both the Izu-Bonin and Grenada suites). Magnetite (Ir only in Grenada suite; Ir, Pd, Re and possibly Ru in Izu-Bonin suite). Cr-rich phases (Os and Ir in Grenada suite; Pt in Izu-Bonin suite). Other silicates (particularly Ir, Pt and Pd with amphibole, and possibly Pt with cpx in Grenada suite).

- The behaviour of Ru changes during magma fractionation. In both the Grenada and Izu-Bonin suites, Ru exhibits moderate compatibility with early crystallising phases but then becomes increasingly less compatible, such that high Ru concentrations are observed within andesitic compositions. It is suggested that this may be related to change in oxidation state of Ru as fO_2 of the magma increases during fractionation.
- There does not appear to be a strong sulfide control on PGE fractionation in either the Izu-Bonin or Grenada suites.
- Ir/Os ratios change as fractionation proceeds, increasing in Izu-Bonin but decreasing on Grenada. As in Greenland, this demonstrates that Os and Ir do not behave analogously. Furthermore, PGE partition coefficients for crystallising phases must be directly affected by conditions such as fS_2 and fO_2 which vary between different magma chambers in different arcs.
- Re/Os, Pd/Ir and Pd/Pt increase with fractionation illustrating the mildly incompatible behaviour of both Pd and Re compared to the other PGEs.
- Similarity in shape of PGE patterns (except for Re) between Grenada M-series picrites, Izu-Bonin boninites and other high MgO rock types, implies that PGE signatures are dictated by degree of melting (Fig 9.1). Generation above a subduction zone, does not therefore have a significant impact on the PGE distribution in mantle melts compared to other tectonic environments.
- Subtle differences in subduction zone conditions between Izu-Bonin and Grenada, such as variation in sediment input, do not appear to have influenced the PGE signatures in the two island arcs studied.
- In both Grenada and Izu-Bonin suites, overall PGE-concentrations decrease (apart from Re) and PGE patterns become steeper as fractionation proceeds. This highlights the importance of high-level magma chamber processes in generating PGE signatures of evolved geological samples.

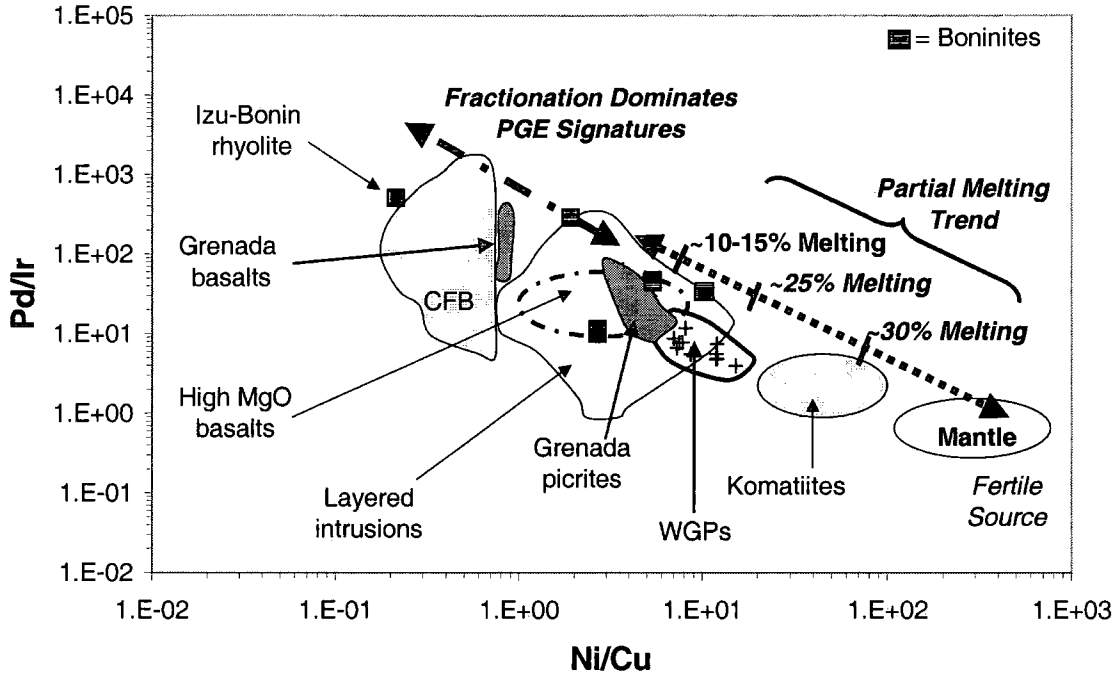

Fig 9.1 Pd/Ir vs Ni/Cu diagram to illustrate the dependence of PGE signatures on degree of partial melting and extent of fractionation (after Vogel *et al.*, 1999). Note that subduction-derived rocks plot on a continuum from the higher MgO rocks – implying that melt generation above a subduction zone, does not cause any significant difference in PGE-behaviour.

- Re enrichment within the boninites relative to the Grenada picrites is attributed to retention of Re within garnet in the Grenada source. The boninites are generated at much shallower depths where garnet is not stable. Thus, Re is probably hosted by sulfide within the boninite source region.
- There is some evidence that Pt, Pd and Os may be mobilised through subduction-derived fluid input.
- Within the Grenada suite there are two distinct sub-groups of primitive lavas with regard to PGE signatures (M and M-C series). The M-C group contains significantly higher Os, Ir and Re concentrations. This cannot be explained through differences in fractionation histories. Thus, it is proposed that the M-C picrites were derived from a more residual source in which Os and Ir were concentrated by a previous melt-extraction event.

- This provides some support for the 'graveyard theory' (Parkinson *et al.*, 1998[a]) where mantle wedges above subduction zones 'trap' blocks of depleted oceanic lithosphere.
- Os-isotopic studies of the Grenada lavas indicate that they have highly radiogenic Os signatures. These cannot be explained purely by high-level crustal contamination. Thus, the elevated $^{187}Os/^{188}Os$ ratios are strongly suggestive of radiogenic Os-input from the subducting slab. Since the amount of bulk sediment mixing into the mantle wedge is minor (~2%) and overall Os-concentrations are low in Grenada picrites, the radiogenic component is probably fluid derived from dehydration of ancient sediments.
- The Izu-Bonin suite is more S-undersaturated than the Grenada suite. This is consistent with derivation from a more depleted source region. Some of the primitive Grenada lavas are mildly S-undersaturated however, which implies that the source region of the Grenada lavas has also suffered some depletion. Fractionation within both suites increases S-saturation
- By analogy with boninitic magmas which are thought to have been involved in generation of some of the world's major layered intrusion PGE deposits, Grenada magmas may also have had the potential to produce economic concentrations of PGEs. If such deposits occur, they are probably at deep crustal levels where magmas ponded and fractionated.
- It is considered that PGE patterns and abundances are not an effective way in which to trace sediment recycling in subduction zones as the signatures seen in resultant lavas are too greatly influenced by fractionation processes. Os-isotopic studies, conversely are a much better method by which to fingerprint slab-derived input to a subduction system.

9.4 Major Differences in PGE Signatures Between Rocks Derived from a Plume Source (West Greenland Picrites) and from Subduction Sources (Grenada and Izu-Bonin)

As previously mentioned there is overall similarity in shape of PGE patterns between the different tectonic environments implying that degree of melting is probably the controlling factor in determining PGE signatures. It has been previously suggested (Brandon *et al.*, 1996) that particular PGEs (namely Os) may have been selectively mobilised in subduction environments relative to the other PGEs. Comparison of subduction and non-subduction related rocks however, reveals that this effect is not obvious.

Some subtle differences do occur in PGE behaviour between the different tectonic environments and these are summarised below:

- Overall PGE concentrations are lower in the subduction-related picrites than the plume-related picrites. This is probably due to a combination of higher degrees of melting and less fractionation in the plume-related lavas.
- The PGEs are associated with a wider range of crystallising phases in the subduction-related lavas. In the plume-related picrites olivine (or associated phases) seems to exert the only control on PGE fractionation. In the subduction-related lavas however, there is evidence for PGE crystallisation with phases such as magnetite and amphibole, as well as olivine.
- There is much better correlation between the PGEs (particularly Os and Ir) within the plume-related rocks. It is proposed that this is due to the simplicity of the fractionation history (and volatile evolution?) of this suite compared to the arc lavas. Fractionation causes progressive variation in Os/Ir ratios in the arc suites.
- The plume-related picrites are generally more S-undersaturated than the subduction-related lavas. This is probably due to greater degrees of partial melting in the plume source (i.e. >25% vs 10-15%).

References

Albarède F, (1995), Introduction to Geochemical Modelling, Cambridge University Press.

Allègre CJ and Turcotte DL, (1986), Implications of a Two Component Marble-Cake Mantle, *Nature,* **323:** 123-127.

Alves S, Schiano P and Allègre CJ, (1999), Re-Os Isotopic Investigation of Java Subduction Zone Lavas, *E.P.S.L.,* **168:** 65-77.

Amosse J, Allibert M, Fischer W and Piboule M, (1990), Experimental Study of the Solubility of Platinum and Iridium in Basic Silicate Melts - Implications for the Differentiation of PGE's during Magmatic Processes, *Chem. Geol.*, **81**: 45-53.

Anbar AD, Wasserburg GJ, Papanastassiou DA and Andersson PS, (1996), Ir in Natural Waters, *Science,* **273**: 1524-1528.

Anbar AD, Papanastassiou DA and Wasserburg GJ, (1997), Determination of Ir in Natural Waters by Clean Chemical Extraction and Negative Thermal Ionisation Mass Spectrometry, *Anal. Chem.*, **69**: 2444-2450.

Arculus RJ, (1973), The Alkali Basalt, Andesite Association of Grenada, Lesser Antilles, Ph.D. thesis, University of Durham, England.

Arculus RJ, (1976), Geology and Geochemistry of the Alkali Basalt-Andesite Association of Grenada, Lesser Antilles Arc, *Geol. Soc. Am. Bull.* **87:** 612-624.

Arculus RJ, (1978), Mineralogy and Petrology of Grenada, Lesser Antilles Island Arc, *Contrib. Min Pet.,* **65:** 413-424.

Ballhaus C, (1995), Is the Upper Mantle Metal-Saturated ? , *E.P.S.L,* **132**: 75 – 86.

Ballhaus C and Sylvester P, (1997), Spatial PGE Distribution in Magmatic Sulfides – Implications for PGE Behaviour During Mantle Melting, p.14, *from Conference Abstracts of the "Origin and Fractionation of HSE in the Earth's Mantle".*

Barnes SJ, Naldrett AJ and Gorton MP, (1985), The Origin of the Fractionation of the PGEs in Terrestrial Magmas, *Chem. Geol.*, **53**: 303-323.

Barnes SJ and Picard CP, (1993), The Behaviour of PGEs During Partial Melting, Crystal Fractionation and Sulfide Segregation: An Example from the Cape Smith Fold Belt, Northern Quebec, *Geochim. Cosmochim. Acta*, **57:** 79-87.

Barnes S J, Achterbergh E and Makovicky E, (1997), Partitioning of Ni, Cu and PGE among Monosulfide Solid Solution, Sulfide Liquid and Metal Alloys, p.15-17, *from Conference Abstracts of the "Origin and Fractionation of HSE in the Earth's Mantle".*

Barovich KM, Beard BL, Cappel JB, Johnson CM, Kyser TK and Morgan BE, (1995), A Chemical Method for Hf Separation from High-Ti Whole Rock and Zr samples, *Chem. Geol.*, **121**: 303-308.

Bezmen NI, Asif M, Brugmann GE, Romanenko IM and Naldrett AJ, (1994), Distribution of Pd, Ir, Os and Au Between Sulfide and Silicate melts, *Geochim. Cosmochim. Acta*, **58**: 1251-1260.

Bezmen NI, Asif M and Naldrett AJ, (1997), Solubility of Pd and Pt in Silicate Melt in the Presence of H_2-H_2O Fluid: Implication for Core and Mantle Abundances, p.20, *from Conference Abstracts of the "Origin and Fractionation of HSE in the Earth's Mantle".*

Borisov A and Palme H, (1997), Experimental Investigation of Noble Metal Solubilities in Silicate Melts: New Results and Geochemical Implications, p.23, *from Conference Abstracts of the "Origin and Fractionation of HSE in the Earth's Mantle".*

Boudreau AE and McCallum IS, (1992), Concentration of PGE by Magmatic Fluids in Layered Intrusions, *Econ. Geol.*, **87**: 1830-1848.

Bowles JFW, Gize AP and Cowden A, (1994), The Mobility of the PGEs in the Soils of the Freetown Peninsula, Sierra Leone, *Can. Mineral.* **32**: 957-967.

Brandon AD, Creaser RA, Shirey SB and Carlson RW, (1996), Os Recycling in Subduction Zones, *Science,* **272:** 861-825.

Brandon AD, Walker RJ, Morgan JW, Norman MD and Prichard HM, (1998), Coupled ^{186}Os and ^{187}Os Evidence for Core-Mantle Interaction, *Science,* **280:**1570-1573.

Brod JA, (1999), Petrology and Geochemistry of the Tapira Alkaline Complex, Minas Gerais State, Brazil. PhD thesis; Durham University.

Brooks CK, Keays RR, Lambert DD, Frick LR and Nielsen TFD, (1999), Re-Os Isotope Geochemistry of Tertiary Picritic and Basaltic Magmatism of East Greenland: Constratints on Plume-Lithosphere Interactions and the Genesis of the Platinova Reef, Skaergard Intrusion, *Lithos.*, **47:** (1-2) 107-126.

Brügmann GE, Arndt NT, Hofmann AW and Tobschall HJ, (1987), Noble Metal Abundances in Komatiite Suites from Alexo, Ontario, and Gorgona Island, Columbia, *Geochim. Cosmochim. Acta,* **51:** 2159-2169.

Buchanan DL, (1988), PGE Exploration, *Developments in Economic Geology*, **26**, Elsevier, p.3-5.

Burnham OM (1995), The Geochemistry of Re-Os in Ultramafic Rocks from the Pyrenees and Massif Central France. Ph.D. Thesis, *Unpub.*

Capobianco CJ and Drake MJ, (1990), Partitioning Of Ru, Rh and Pd Between Spinel and Silicate Melt, *Geochim. Cosmochim. Acta*, **54**: 869-874.

Capobianco CJ, Drake MJ and Hervig RL, (1994), Experiments on Ru, Rh and Pd Compatibility in Fe-Oxides Crystallising from Silicate Melt, *Chem. Geol.*, **113**: 23-43.

Chou CL, Shaw DM and Crocket JH, (1983), Siderophile Trace Elements in the Earth's Oceanic Crust and Upper Mantle, *In*, Proceedings of the Thirteenth Lunar and Planetary Science Conference, Part 2, J. *Geophys. Res.*, **88**: A507-A518.

Cohen AS, and Waters FG, (1996), Separation of Osmium from Geological Materials by Solvent Extraction for Analysis by Thermal Ionisation Mass Spectrometry. *Anal. Chim. Acta,* **332**: 269-275.

Colodner DC, Boyle EA and Edmond JM, (1993), Determination of Rhenium and Platinum in Natural Waters and Sediments and Iridium in Sediments by Flow Injection Isotope Dilution Inductively Coupled Plasma Mass #Spectrometry. *Anal. Chemistry*, **65:** 1419-1425.

Cousins CA, (1973), Notes on the Geochemistry of the Platinum Group Elements, *Trans. Geol. Soc. S. Afr.*, **76**: 77-81.

Crocket JH, Keays RR and Hsieh S, (1968), Determination of some Precious Metals by Neutron Activation Analysis. *J. Radioanal. Chem.*, **1:** 487.

Crocket JH, Macdougall JD and Harriss RC, (1973), Au, Pd and Ir in Marine Sediments, *Geochim. Cosmochim. Acta,* **37**: 2547-2556.

Crocket JH, (1979), Platinum-Group Elements in Mafic and Ultramafic Rocks: A Survey, *Can. Mineral.*, **17**: 391-402.

Crocket JH, (1981), Geochemistry of the PGEs, in Platinum-Group Elements: Mineralogy, Geology and Recovery, Cabri LJ (ed), C. I. M. Special Volume **23**; 47-64.

Crocket JH, Officer CB, Wezel FC and Johnson GD, (1988), Distribution of Noble Metals Across the Cretaceous / Tertiary Boundary at Gubbio, Italy: Ir Variation as a Constraint on the Duration and Nature of Cretaceous / Tertiary Boundary Events, *Geology*, **16**: 77-80.

Crocket JH, Fleet ME and Stone W, (1992), Experimental Partitioning of Os, Ir and Au between Basalt Melt and Sulfide Liquid at 1300°C, *Aust. J. Earth Sci.*, **39:** 427-432.

Crocket JH, Fleet ME and Stone WE, (1997), Implications of Composition for Experimental Partitioning of PGE-Au Between Sulfide Liquid and Basalt Melt: The Significance of Ni Content, p.31, *from Conference Abstracts of the "Origin and Fractionation of HSE in the Earth's Mantle".*

Date AR, Davis AE and Cheung YY, (1987), The Potential of Fire-Assay and ICP-MS for the Determination of PGE's in Geological Materials, *in* Geo-Platinum'87, Prichard, Potts, Bowles and Cribb (eds), 43-44.

Davidson JP, (1986), Isotopic and Trace Element Constraints on the Petrogenesis of Subduction-Related Lavas from Martinique, Lesser Antilles, *J. Geophys. Res.*, **91:** 5943-5962.

Davidson JP, (1987), Crustal Contamination Versus Subduction Zone Enrichment: Examples from the Lesser Antilles and Implications for Mantle Source Compositions of Island Arc Volcanic Rocks, *Geochim. Cosmochim. Acta,* **51:** 2185-2198.

Davidson JP and Harmon RS, (1989), Oxygen Isotope Constraints on the Petrogenesis of Volcanic Arc Magmas from Martinique, Lesser Antilles, *E.P.S.L.,* **95:** 255-270.

Edwards SJ, (1990), Harzburgites and Refractory Melts in the Lewis Hills Massif, Bay of Islands Ophiolite Complex: The Base-Metals and Precious-Metals Story, *Can. Mineral.*, **28**: 537-552.

Ely JC, Neal CR, O'Neill JA, and Jain JC, (1999), Quantifying Platinum Group Elements (PGEs) and Gold in geological samples using Cation Exchange Pre-treatment and Ultrasonic Nebulisation Inductively Coupled Plasma-mass spectrometry (USN-ICP-MS). *Chem. Geol.* **157:** 219-234.

Enzweiller J, Potts PJ and Jarvis KE, (1995), Determination of Pt, Pd, Ru and Ir in Geological Samples by Isotope Dilution Inductively Coupled Plasma Mass Spectrometry Using a Sodium Peroxide Fusion and Tellurium Coprecipitation, *Analyst*, **120**: 1391-1396.

Evans NJ, Gregoire DC, Goodfellow WD, McInnes BI, Miles N and Veizer J, (1993), Ru/Ir ratios at the Cretaceous-Tertiary boundary: implications for PGE source and fractionation within the ejecta cloud. *Geochim. Cosmochim. Acta,* **57**: 3149-3158.

Falkner KK and Edmond JM, (1990), Au in Seawater, *E.P.S.L.*, **98**: 208-221.

Faure G, (1986), Principles of Isotope Geology, John Wiley and Sons Inc.

Fitton JG, Saunders AD, Norry MJ, Hardarson BS and Taylor RN, (1997), Thermal and Chemical Structure of the Iceland Plume, *E.P.S.L.,* **153:** 197-208.

Fleet ME, Stone WE and Crocket JH, (1991), Partitioning of Pd, Ir and Pt between Sulfide Liquid and Basalt Melt: Effects of Melt Composition, Concentration, and Oxygen Fugacity, *Geochim. Cosmochim. Acta*, **55**: 2545-2554.

Fleet ME and Wu TW, (1993), Volatile Transport of PGE in Sulfide-Chloride Assemblages at 1000°C, *Geochim. Cosmochim. Acta*, **57**: 3519-3531.

Fleet ME, Crocket JH and Stone WE, (1996), Partitioning of PGEs and Au between Sulfide Liquid and Basalt Melt, *Geochim. Cosmochim. Acta*, **13**: 2397-2412.

Fleet ME, (1997), Laboratory Partitioning of PGE-Au in the (Fe,Ni)-Sulfide-Alloy-Silicate System, p.33, *from Conference Abstracts of the "Origin and Fractionation of HSE in the Earth's Mantle"*.

Fryer BJ and Greenough JD, (1992), Evidence for Mantle Heterogeneity from PGE Abundances in Indian Ocean Basalts, *Can. J. Earth Sci.*, **29:** 2329-2340.

Gijbels R and Zels J, (1977), The analytical problem of determining ruthenium in silicate rocks, *J. Radioanal. Chem.*, **35**: 115-125.

Gordon CL, Schlecht WG and Wichers E, (1944), Use of Sealed Tubes for the Preparation of Acid solutions of Samples for Analysis or for Small-scale Refining: Pressures of Acids Heated above 100°C, *J. of the National Bureau of Standards*, **33:** 457-470.

Graham DW, Larsen LM, Hanan BB, Storey M, Pedersen AK and Lupton JE, (1998), He Isotope Composition of the Early Iceland Mantle Plume Inferred from the Tertiary Picrites of West Greenland, *E.P.S.L.*, **160:** 241-255.

Gregoire DC, (1988), Determination of Platinum, Palladium, Ruthenium and Iridium in Geological Materials by ICP-MS with Sample Introduction by Electrothermal Vaporization. *J. Anal. At. Spectrom.*, **3:** 309-314.

Gregoire DC, (1990), Sample introduction techniques for the determination of osmium isotope ratios by inductively coupled plasma mass spectrometry. *Anal. Chem.*, **62:** 141-146.

Groves DI and Keays RR, (1979), Mobilisation of Ore-Forming Elements During Alteration of Duniyes Mt. Keith - Betheno, Western Australia, *Can. Mineral.*, **17:** 373-389.

Gueddari K, Piboule M, and Amosse J, (1996), Differentiation of platinum-group elements (PGE) and of gold during partial melting of peridotites in the lherzolitic massifs of the Betico-Rifean range (Ronda and Beni Bousera). *Chem. Geol.*, **134:** 181-197.

Hall GEM and Pelchat JC, (1994), Analysis of Geological Materials for Au, Pt and Pd at Low ppb Levels by Fire Assay-ICP Mass Spectrometry, *Chem. Geol.*, **115**: 61-72.

Hamlyn PR, Keays RR, Warrington EC, Crawford AJ and Waldron HM, (1985), Precious Metals in Magnesian Low-Ti Lavas: Implications for Metallogenesis

and Sulfur Saturation in Primary Magmas, *Geochim. Cosmochim. Acta*, **49:** 1797-1811.

Hart SR and Ravizza GE, (1996), Os Partitioning Between Phases in Lherzolite and Basalt, *In*; Earth Processes: Reading the Isotopic Code, Geophysical Monograph 95, AGU, 123-134.

Haughton DR, Roeder PL and Skinner BJ, (1974), Solubility of sulfur in Mafic Magmas, *Econ. Geol.* **69**: 451-467.

Hauri E and Hart SR, (1993), Re-Os isotope systematics in HIMU and EMII ocean island basalts. *Earth Planet. Sci. Lett.*, **114:** 253-271.

Hauri E and Hart SR, (1997), Re Abundances and Systematics in Oceanic Basalts, *Chem. Geol.*, **139:** 185-205.

Heath E, MacDonald R, Belkin H, Hawkesworth CJ and Sigurdsson H, (1998[a]), Magmagenesis at Soufriere Volcano, St Vincent, Lesser Antilles Arc, *J.Pet.*, **39:** 1721-1764.

Heath E, Turner SP, MacDonald R, Hawkesworth CJ and Van Calsteren P, (1998[b]), Long Magma Residence times at an Island Arc Volcano (Soufriere, St. Vincent) in the Lesser Antilles: Evidence from ^{238}U-^{230Th} Isochron Dating, *E.P.S.L.*, **160:** 49-63.

Hertogen J, Janssens MJ and Palme H, (1980), Trace Elements in Ocean Ridge Basalt Glasses: Implications for Fractionations During Mantle Evolution and Petrogenesis, *Geochim. Cosmochim. Acta,* **44:** 2125-2143.

Heumann KG, (1988), Isotope dilution mass spectrometry. *In* F. Adams, Ed. Inorganic Mass Spectrometry, p. 301-376. John Wiley, New York.

Hodge V, Stallard M, Koide M and Goldberg ED, (1986), Determination of Pt and Ir in Marine Waters, Sediments, and Organisms, *Anal. Chem*, **58**: 616-620.

Hoffman EL, Naldrett AJ, Van Loon JC, Hancock RGV and Mason A, (1978), The determination of all the platinum group elements and gold in rocks and ore by neutron activation analysis after preconcentration by a nickel sulfide fire-assay technique of large samples. *Anal. Chim. Acta*, **102**: 157-166.

Holm PM, Gill RCO, Pedersen AK, Larsen JG, Hald N, Nielsen TFD and Thirlwall MF, (1993), The Tertiary Picrites of West Greenland: Contributions from Icelandic and Other Sources, *E.P.S.L.*, **115:** 227-244.

Jacinto GS and Van de Berg CMG, (1989), Different Behaviour of Pt in the Indian and Pacific Oceans, *Nature*, **338**: 332-334.

Jackson SE, Fryer BJ, Gosse W, Healey DC, Longerich HP and Strong DF, (1990), Determination of the Precious Metals in Geological Materials by ICP-

MS with Nickel Sulfide Fire Assay Collection and Tellerium Coprecipitation, *Chem. Geol.*, **83:** 119-132.

Jagoutz E, Palme H, Baddenhausen H, Blum K, Cendales M, Dreibus G, Spettel B, Lorenz B and Wanke H, (1979), The Abundances of Major, Minor and Trace Elements in the Earth's Mantle as Derived from Primitive Ultramafic Nodules, *Proc. Lunar Plan. Sci. Conf.*, 2031-2050.

Jarvis I, Totland MM and Jarvis KE, (1997a), Assessment of Dowex 1- X8-based Anion-exchange Procedures for the Separation and Determination of Ru, Rh, Pd, Ir, Pt and Au in Geological Samples by Inductively Coupled Plasma Mass Spectrometry, *Analyst,* **122**: 19-26.

Jarvis I, Totland M.M. and Jarvis K.E., (1997b), Determination of the Platinum Group Elements in Geological Materials by ICP-MS using Microwave Digestion, Alkali Fusion and Cation-exchange Chromatography, *Chem. Geol.*, **143**: 27-42.

Jochum KP, (1996), Rhodium and other PGEs in Carbonaceous Chondrites, *Geochim. Cosmochim. Acta,* **60:** 3353-3357.

Jones JH and Drake MJ (1986), Geochemical Constraints on Core Formation in the Earth, *Nature,* **322:** 221-228.

Juvonen R, Kallio E and Lakona T, (1994), Determination of Precious Metals in Rocks by Inductively Coupled Plasma Mass Spectrometry using Nickel Sulphide Concentration. Comparison with other Pre-treatment Methods. *Analyst,* **119:** 617-621.

Kane JS, Beary ES, Murphy KE and Paulsen PJ, (1995), Impact of Inductively Coupled Plasma Mass Spectrometry on Certification Programmes for Geochemical Reference Materials, *Analyst,* **120:** 1505-1511.

Keays RR and Davison RM, (1976), Pd, Ir and Au in the Ores and Host Rocks of Nickel Sulfide Deposits in Western Australia, *Econ. Geol.*, **71**: 1214-1228.

Keays RR, Ross JR and Woolrich P, (1981), Precious Metals in Volcanic Peridotite Associated Ni-Sulfide Deposits in Western Australia, *Econ. Geol.*, **76**: 1645-1674.

Keays RR, (1995), The Role of Komatiitic and Picritic Magmatism and S-Saturation in the Formation of Ore-Deposits, *Lithos,* **34:** 1-18.

Kleeman A, (1967), Sampling error in the Chemical Analysis of Rocks. *J. of the Geol. Soc. of Australia,* **14(I):** 43-47.

Korkisch J and Klakl H, (1968), Anion-exchange behaviour of the platinum metals and gold in hydrochloric acid-organic solvent media. *Talanta*, **15:** 339-346.

Korkisch J, (1989), Handbook of ion exchange resins: Their application to analytical inorganic chemistry. CRC Press.

Kucha H, (1982), Platinum Group Metals in the Zechstein Copper Deposits, Poland, *Econ. Geol.*, **77:** 1578-1591.

Leblanc M, Gervilla F and Jedwab J, (1989), Noble Metals Segregation and Fractionation in Magmatic Ores from Ronda and Beni Bousera Lherzolite Massifs, *Mineral. Petrol.*, **41**.

Leblanc M, (1991), PGEs and Au in Ophiolitic Complexes: Distribution and Fractionation from Mantle to Oceanic Floor, *in* Ophiolite Genesis and Evolution of the Oceanic Lithosphere, TJ Peters *et al* (Eds), 231-260.

Lee DS, (1983), Pd and Ni in North-East Pacific Waters, *Nature*, **305**: 47-48.

Lightfoot PC, Hawkesworth CJ, Olshefsky K, Green T, Doherty W and Keays RR, (1997), Geochemistry of Tertiary Tholeiites and Picrites from Qeqertarssuaq (Disko Island) and Nuussuaq, West Greenland with Implications for the Mineral Potential of Comagmatic Intrusions, *Contrib. Min. Pet.*, **128:** 139-163.

Loon JCV and Barefoot RR, (1991), Determination of the precious metals. P.276. John Wiley, Chichester.

Lydon JW, (1987), The Potential for Hydrothermal Platinum Deposits, *in* Geo-Platinum '87, Prichard HM, Potts PJ, Bowles JFW and Cribb SJ. (Eds), 111-112.

Martin-Kaye P, (1969), A Summary of the Geology of the Lesser Antilles, *in Overseas Geol. and Min. Res.*, **10:** 172-206.

Martin CE, (1990), Re-Os Isotope Geochemistry of the Mantle, PhD thesis, Unpublished Yale University.

Martin CE, Carlson RW, Shirey SB, Frey FA and Chen CY, (1994), Os Isotopic Variation in Basalts from Haleakala Volcano, Maui, Hawaii: A Record of Magmatic Processes in Oceanic Mantle and Crust, *E.P.S.L.*, **128:** 287-301.

Mathez EA and Peach CL, (1987), The Geochemistry of the PGE's in Mafic and Ultramafic Rocks, *In,* Geo-Platinum '87, Prichard HM, Potts PJ, Bowles JFW and Cribb SJ. (Eds): 33-40.

Mathez EA and Peach CL, (1997), Fractionation and Behaviour of the PGE's as Inferred from Experiments in Sulfide-bearing Systems and Analysis of Rocks, p.51, *from Conference Abstracts of the "Origin and Fractionation of HSE in the Earth's Mantle".*

McDonald I, Hart RJ and Tredoux M, (1994), Determination of PGE's in South African Kimberlites by Ni-Sulfide Fire Assay and Neutron Activation Analysis, *Anal. Chim. Acta.*, **289**: 237-247.

McDonald I, De Wit MJ, Smith CB, Bizzi LA and Viljoen KS, (1995), The Geochemistry of the Platinum Group Elements in Brazilian and South African Kimberlites, *Geochim. Cosmochim. Acta,* **59:** 2883-2903.

McDonald I, (1998), The need for a common framework for collection and interpretation of data in Platinum-Group Element Geochemistry. *Geostandards Newsletter,* **22**: 85-91.

McDonough WF and Sun SS, (1995), The composition of the Earth. *Chem. Geol.,* **120:** 223-253.

Meadows JWT and Matlack GM, (1962), Radiochemical Determination of ruthenium by solvent extraction and preparation of carrier-free ruthenium activity, *Anal. Chem.,* **34:** 89-91.

Minster J.F. and Allegre C.J., (1982), The isotopic composition of zirconium in terrestrial and extraterrestrial samples: implicatoins for extinct ^{92}Nb, *Geochim. et Cosmochim. Acta,* **46:** 565-573.

Mitchell RH and Keays RR, (1981), Abundance and Distribution of Au, Pd and Ir in some Spinel and Garnet Lherzolites - Implications for the Nature and Origin of Precious Metal-rich Intergranular Components in the Upper Mantle, *Geochim. Cosmochim. Acta,* **45**: 2425-2445.

Morgan JW, Wandless GA, Petrie RK and Irving AJ, (1981), Composition of the Earth's Upper Mantle - Siderophile Elements in Ultramafic Nodules, *Tectonophysics,* **75**:.47-67.

Morgan JW, (1986), Ultramafic Xenoliths: Clues to Earth's Late Accretionary History, *J. Geophys. Res.*, **91**: 12375-12387.

Morgan JW, Golightly DW and Dorrzapf AF, (1991), Methods for the separation of rhenium, osmium and molybdenum applicable to isotope geochemistry. *Talanta,* **38:** 259-265.

Mountain BW and Wood SA, (1987), Solubility and Transport of PGE in Hydrothermal Solutions: Thermodynamic and Physical Chemical Constraints, 57-82.

Murton BJ, Petae DW, Arculus RJ, Pearce JA and Van der Laan SR, (1992) Trace-Element Geochemistry of Volcanic Rocks from Site 786: The Izu-Bonin Forearc, *Proc. of the ODP. Scien. Results,* **125:** 211-235.

Naldrett AJ, Hoffman EL, Green AH, Chou CL and Naldrett SR, (1979), The composition of Ni-Sulfide ores, with Particular Reference to their Content of PGE and Au, *Can. Mineral.* **17**: 403-415.

Naldrett AJ and Barnes SJ, (1986), The Behaviour of PGE's During Fractional Crystallisation and Partial Melting with Special Reference to the Composition of Magmatic Sulfide Ores, *Fortschr. Miner.* **64**: 113-133.

Naldrett AJ and Duke JM, (1980), Pt Metals in Magmatic Sulfide Ores; The Occurrence of hese Metals is Discussed in Relation to the Formation and Importance of these Ores, *Science*, **208:** 1417-1424.

Naldrett AJ, (1997), The Composition of Fe-Ni-Cu-S Ores as a Consequence of the Equilibration of Sulfide Liquid with Silicate Magma and Subsequent Fractional Crystallisation, p. 59, *from Conference Abstracts of the "Origin and Fractionation of HSE in the Earth's Mantle".*

O'Neill H, (1997), Partitioning of the Highly Siderophile Elements in Some Geologically Relevant Materials at High Temperaures: A Reductionist Approach, p.60-62, *from Conference Abstracts of the "Origin and Fractionation of HSE in the Earth's Mantle".*

Parkinson IJ, Hall GEM and Pearce JA, (1992), Pd, Pt and Au Distribution in Serpentinite Seamounts in the Mariana and Izu-Bonin Forearcs: Evidence from Leg 125 Fluids and Serpentinites, *Proceedings of the O.D.P.*, Scientific Results, **125**: 507-518.

Parkinson IJ, Hawkesworth CJ and Cohen AS, (1998[a]), Ancient Mantle in a Modern Arc: Osmium Isotopes in Izu-Bonin-Mariana Forearc Peridotites, *Science,* **281:** 2011-2013.

Parkinson IJ, Hawkesworth CJ and Cohen AS, (1998[b]), Ancient Mantle in Modern Arc Systems: Os Isotopes in Subduction Zone Peridotites, *AGU Abstracts No.V41D-11*, p. F1012.

Parry SJ, (1980), Simultaneous Determination of the Noble Metals in Geological Samples by Radiochemical Neutron Activation Analysis, *Analyst,* **105:** 1157-1162.

Pattou L, Lorand JP and M Gros, (1996), Non-chondritic platinum-group element ratios in the Earth's mantle. *Nature,* **379:** 712-715.

Peach CL, Mathez EA and Keays RR, (1990), Sulfide Melt-Silicate Melt Distribution Coefficients for the Noble Metals and Other Chalcophile Metals as Deduced from MORB; Implications for Partial Melting, *Geochim. Cosmochim. Acta,* **54:** 3379-89.

Peach CL, Mathez EA, Keays RR and Reeves SJ, (1994), Experimentally Determined Sulfide Melt-Silicate Melt Partition Coefficients for Ir and Pd, *Chem. Geol.*, **117:** 361-377.

Peach CL and Mathez EA, (1996), Constraints on the Formation of PGE Deposits in Igneous Rocks, *Econ. Geol.*, p 439-450.

Pearce JAP, (1982), Trace Element Characteristics of Lavas from Destructive Plate Boundaries, *In* Andesites, *Ed.* R.S.Thorpe, p 526-544.

Pearce JA, Van der Laan SR, Arculus RJ, Murton BJ, Ishii T, Peate DW and Parkinson IJ, (1992[a]), Boninite and Harzburgite from Leg 125 (Bonin-Mariana Forearc): A Case Study of Magma Genesis During the Initial Stages of Subduction, *Proc. of the ODP. Scien. Results,* **125:** 623-659.

Pearce JA, Thirlwall MF, Ingram G, Murton BJ, Arculus RJ and Van der Laan SR, (1992[b]), Isotopic Evidence for the Origin of Boninites and Related Rocks Drilled in the Izu-Bonin (Ogasawara) Forearc, Leg 125, *Proc. of the ODP. Scien. Results,* **125:** 237-261.

Pearce JA and Parkinson IJ, (1993), Trace Element Models for Mantle Melting: Application to Volcanic Arc Petrogenesis, *from* Prichard, Alabaster, Harris and Neary (eds.) 'Magmatic Processes and Plate Tectonics', *Geol. Soc. Special Publications*, **76**: 273-294.

Pearce JA and Peate DW, (1995), Tectonic Implications of the Composition of Volcanic Arc Magmas, *Annu. Rev. E.P.S.,* **23:** 251-285.

Pearce JA, Baker PE, Harvey PK and Luff IW, (1995), Geochemical Evidence for Subduction Fluxes, Mantle Melting and Fractional Crystallisation Beneath the South Sandwich Island Arc, *J. Pet.,* **36:** 1073-1109.

Pearson DG, Shirey SB, Carlson RW, Boyd FR, Pokhilenko NP and Shimizu N, (1995), Re-Os, Sm-Nd, and Rb-Sr Isotope Evidence for thick Archaean Lithospheric Mantle Beneath the Siberian Craton Modified by Multistage Metasomatism, *Geochim. Cosmochim. Acta,* **59:** 959-977.

Pearson DG, Shirey SB and Carlson RW, (1998), Sulfide Inclusions in Diamonds from the Koffiefontein Kimberlite, S Africa: Constraints on Diamond Ages and Mantle Re-Os Systematics, *E.P.S.L.,* **160:** 311-326.

Pearson DG, Ottley CJ and Woodland SJ, (1999), Precise measurement of Os by direct injection ICP-MS. *In* J.G. Holland, and S.C. Tanner, Eds. Developments in ICP-MS. Royal Society of Chemistry.

Pearson DG and Woodland SJ, (2000), Solvent extraction/anion exchange separation and analysis of PGE's (Os, Ir, Pt, Pd, Ru) and Re-Os isotopes in geological samples by isotope dilution ICP-MS. *Chem. Geol.,* **165:** No.1-2, p87-107.

Pearson DG, Larsen L, Walker RJ, Woodland SJ, (1999), The Deep Sources of Plumes: Re-Os, Pt-Os Isotopic and Platinum Group Element Systematics of High He^3 /He^4 West Greenland Picrites, In: *9th Annual Goldschmidt Conf. Proc.*, p223.

Peate DW and Pearce JA, (1998), Causes and Spatial Compositional Variations in Mariana Arc Lavas: Trace Element Evidence, in *The Island Arc*, 7: 479-495.

Peck DC, Keays RR and Ford RJ, (1992), Direct Crystallisation of Refractory PGE Alloys from Boninitic Magmas: Evidence from Western Tasmania, *Aust. J. of Earth. Sci.*, **39:** 373-387.

Petrie RK and Morgan JW, (1982), Anion-exchange separation of Pt and Pd using perchloric and hydrochloric acid solutions, *J. Radioanal. Chem.*, **74**: No. 1, 15-23.

Plessen HG and Erzinger J, (1997), Distribution of PGE and Au in Magmatic rocks of different Tectonic Setting, p. 66-67, *from Conference Abstracts of the "Origin and Fractionation of HSE in the Earth's Mantle".*

Plimer IR and Williams PA, (1987), New Mechanisms for the Mobilisation of the PGE's in the Supergene Zone, *in* Geo-Platinum '87, Prichard HM, Potts PJ, Bowles JFW and Cribb SJ. (Eds), 83-92.

Potts PJ, (1987), A Handbook of Silicate Rock Analysis, Blackie and Sons Limited.

Powell M, (1978), Crystallisation Conditions of Low-Pressure Cumulate Nodules from the Lesser Antilles Island Arc, *E.P.S.L.*, **39:** 162-172.

Prichard HM and Lord RA, (1990), Pt and Pd in the Troodos Ophiolite Complex, Cyprus, *Can. Mineral.*, **28**: 607-617.

Prichard Hm and Lord RA, (1993), An Overview of the PGE Concentrations in the Shetland Ophiolite Complex, *from* Prichard, Alabaster, Harris and Neary (eds.) 'Magmatic Processes and Plate Tectonics', *Geol. Soc. Special Publications*, **76**: 273-294.

Prichard HM, Ixer RA, Lord RA, Maynard J and Williams N, (1994), Assemblages of Platinum Group Minerals and Sulfides in Silicate Lithologies and Chromite-Rich Rocks Within the Shetland Ophiolite, *Can. Mineral.* **32** : 271-294.

Prichard HM and Lord RA, (1994), Evidence for Differential Mobility of PGE in the Secondary Environment in Shetland Ophiolite Complex, *Trans. Instn. Min. Metall.*, **103**: B79-B86.

Prichard HM, Lord RA and Neary R, (1996), A Model to Explain the Occurrence of Pt and Pd Rich Ophiolite Complexes, *J. Geol. Soc. Lond.*

Ravizza G and Pyle D, (1997), PGE and Os isotopic analyses of single sample aliquots with NiS fire assay preconcentration, *Chem. Geol.*, **141**; 251-268.

Ragland PC, (1989), Basic Analytical Petrology, *Oxford University Press.*

Rehkämper M and Halliday AN, (1997), Development and application of new ion-exchange techniques for the separation of the platinum group and other siderophile elements from geological samples, *Talanta*, **44:** 663-672.

Rehkämper M, Halliday AN, Barfod D, Fitton JG and Dawson BJ (1997), PGE Abundance Patterns in Different Mantle Environments, *Science,* **278:** 1595-1598.

Rehkämper M, Halliday AN and Wentz RF, (1998), Low-blank digestion of geological samples for platinum group element analysis using a modified carius tube design, *Fresenius J. Anal. Chem.*, **361**; 217-219.

Reisberg L and Lorand JP, (1995), Longevity of Sub-Continental Mantle Lithosphere from Os-Isotope Systematics in Orogenic Peridotite Massifs, *Nature*, **376:** 159-162.

Righter K and Hauri EK, (1998), Compatibility of Re in Garnet During Mantle Melting and Magma Genesis, *Science,* **280:** 1737-1741.

Righter K, Chesley JT, Geist D and Ruiz J, (1998), Behaviour of Re During Magma Fractioantion: An Example from Volcán Alcedo, Galapágos, *J. Pet.*, **39:** 785-795.

Robért RVD, van Wyck E and Palmer R, (1971), Concentration of the Noble Metals by a Fire Assay Technique using Nickel Sulfide as the Collector, *Natl. Inst. Metall., Johannesburg, Rep.* No. **1371**, 1-15.

Rollinson H, (1993), Using Geochemical Data: Evaluation, Presentation, Interpretation, Longman Scientific and Technical.

Ross JR and Keays RR, (1979), Precious Metals in Volcanic-type Nickel Sulfide deposits in Western Australia, I Relationship with the Composition of the Ores and their Host rocks, *Can. Mineral.* **17**: 417-435.

Roy-Barman M and Allègre CJ, (1995), $^{187}Os/^{186}Os$ in Oceanic Island Basalts: Tracing Oceanic Crust Recycling in the Mantle, *E.P.S.L.,* **129:** 145-161.

Sattari P, Brenan JM, Horn I and McDonough WF, (1998), The Relative Significance of Sulfide Liquid and Chromite on Re and PGE Fractionation During Melting and Solidification, *from Abstracts of 1998 National GSA, Toronto.*

Shazali I, Van't Dack L and Gijbels R, (1987), Preconcentration of Precious Metals by Tellurium Sulfide Fire-assay Followed by Instrumental Neutron Activation Analysis, *In* Geo-Platinum '87, *eds* Prichard *et al*, p 29-43.

Shimizu N and Arculus RJ, (1975), Rare Earth Element Concentrations in a Suite of Basanitoids and Alkali Olivine Basalts from Grenada, Lesser Antilles, *Contrib. Mineral. Petrol.*, **50:** 231-240.

Shirey SB and Walker RJ, (1994), Carius tube digestions for Re-Os chemistry: An old technique applied to new problems. *EOS,* **75:** 355-356.

Shirey SB and Walker RJ, (1995), Carius Tube Digestion for Low-Blank Rhenium Osmium Analysis, *Anal. Chem.*, **67**: 2136-2141.

Shirey SB (1997), Re-Os Isotopic Compositions of Midcontinent Rift System Picrites: Implications for Plume-Lithosphere Interaction and Enriched Mantle Sources, *Can. J. Earth Sci.*, **34:** 489-503.

Shirey SB and Walker RJ, (1998), The Re-Os Isotope System in Cosmochemistry and High-Temperature Geochemistry, *Annu. Rev. E.P.S.*, **26:** 423-500.

Sigurdsson H, Tomblin JF, Broen GM, Holland JG and Arculus RJ, (1973), Strongly Undersaturated Magmas in the Lesser Antilles Island Arc, *E.P.S.L.*, **18:** 285-295.

Snow JE and Reisberg L, (1995), Os Isotope Systematics of the MORB Mantle: Results from Altered Abyssal Peridotites, *E.P.S.L,* **133:** 411-421.

Snow JE and Schmidt G, (1998), Constraints on Earth Accretion Deduced from Noble Metals in the Oceanic Mantle, *Nature,* **391:** 166-169.

Stone W, Crocket JH and Fleet ME, (1990), Partitioning of Pd, Ir, Pt and Au between Sulfide Liquid and Basalt Melt at 1200°C, *Geochim. Cosmochim. Acta,* **54:** 2341-2344.

Sun SS and McDonough WF, (1989), Chemical and Isotopic Systematics of Oceanic Basalts: Implications for Mantle Composition and Processes, *from Saunders AD & Norry MJ (eds), Magmatism in the Ocean Basins. Geol. Soc. Spec. Pub.*, **42:** 313-345.

Sun SS, (1982), Chemical Composition and Origin of the Earth's Upper mantle, *Geochim. Cosmochim. Acta,* **46**: 179-192.

Sun M, Jain JS, Zhou MF and Kerrich R, (1993), A Procedural Modification for Enhanced Recovery of Precious Metals (Au, PGE) Following Nickel Sulfide Fire Assay and Te-coprecipitation. Application for Analysis of Geological Samples by ICP-MS. *Can. J. Appl. Spectrosc.*, **38:** 103-108.

Surasiti C and Sandell EB, (1960), Determination of submicrogram quantities of ruthenium by catalysis of the cerium (IV) - arsenic (III) reaction, *Anal. Chim. Acta.*, **22:** 261-269.

Sylvester PJ, Campbell IH, Saunders AD and Babbs TL, (1998), Behaviour of Re, Au and the PGE's during Mantle Melting: The View from Ontong Java, *Volcanic & Magmatic Studies Group, Conf. Abstract,* p45.

Thirlwall MF and Graham AM, (1984), Evolution of High-Ca, High-Sr C-series Basalts from Grenada, Lesser Antilles: The Effects of Intra-crustal Contamination, *J.Geol. Soc. London,* **141:** 427-445.

Thirlwall MF, Smith TE, Graham AM, Theodorou N, Hollings P, Davidson JP and Arculus RJ, (1994), High Field Strength Element Anomalies in Arc Lavas: Source or Process?, *J. Pet.,* **35:** part 3, 819-838.

Thirlwall MF, Graham AM, Arculus RJ, Harmon RS and Macpherson CG, (1996), Resolution of the Effects of Crustal Assimilation, Sediment Subduction and Fluid Transport in Island Arc Magmas: Pb-Sr-Nd-O Isotope Geochemistry of Grenada, Lesser Antilles, *Geochim. Cosmochim. Acta,* **60:** 4785-4810.

Thompson RN, Morrison MA, Dickin AP and Hendry GL, (1983), Continental Flood Basalts... Arachnids Rule OK? *in, Continental Basalts and Mantle Xenoliths,* C.J. Hawkesworth and M.J. Norry (eds), p. 158-185.

Turner SP, Hawkesworth CJ, Van Calsteren V, Heath E, Macdonald R and Black S, (1996), U-Series Isotopes and Destructive Plate Margin Magmagenesis in the Lesser Antilles, *E.P.S.L.,* **142:** 191-207.

Tredoux M, De Wit MJ, Hart RJ, Lindsay NM, Verhagen B and Sellschop JPF, (1989), Chemostratigraphy Across the Cretaceous-Tertiary Boundary and a Critical Assessment of the Ir Anomaly, *J. Geology*, **97:** 585-605.

Tredoux M and McDonald I, (1996), Komatiite WITS-1, low concentration nobel metal standard for the analysis of non-mineralised samples. *Geostandards Newsletter,* **20:** 267-276.

Van Heuzen AA, Hoekstra T andVan Wingerden B, (1989), Precision and Accuracy Attainable with Isotope Dilution Analysis Applied to Inductively Coulped Plasma Mass Spectrometry : Theory and Experiments, *J. of Anal. At. Spectrometry*, **4:** 483-489.

Vogel DC and Keays RR, (1997), The Petrogenesis and PGE Geochemistry of the Newer Volcanic Province, Victoria, Australia, *Chem. Geol.,* **136:** 181-204.

Vogel DC, Keays RR, James RS and Reeves SJ, (1999), The geochemistry and Petrogenesis of the Agnew Intrusion, Canada: A Product of S-undersaturated, High-Al and Low Ti Tholeiitic Magmas, *J. Pet.,* **40:** 423-450.

Walker RJ, Morgan JW, Hanski EJ and Smolkin VF, (1997), Re-Os Systematics of Early Proterozoic Ferropicrites, Pechenga Complex, Northwestern Russia: Evidence for Ancient ^{187}Os-Enriched Plumes, *Geochim. Cosmochim. Acta*, **61:** 3145-3160.

Walker RJ, Storey M, Kerr AC and Tarney J, (1998), Implications of ^{187}Os Isotopic Heterogeneities in a Mantle Plume: Evidence from Gorgona Island and Curaçao, *Geochim. Cosmochim. Acta*, **63:** 713-728.

Watkinson DH and Jones PC, (1996), Platinum-Group Minerals in Fluid Inclusions from the Marathon Deposit, Coldwell Complex Canada, *Mineralogy and Petrology,* **57:** 91-96.

White WM, Dupré B and Vidal P, (1985), Isotope and Trace Element Geochemistry of Sediments from the Barbados Ridge- Demerara Plain Region, Atlantic Ocean, *Geochim. Cosmochim. Acta*, **49:** 1875-1886.

White WM and Dupré B, (1986), Sediment Subduction and Magma Genesis in the Lesser Antilles: Isotopic and Trace Element Constraints, *J. Geophys. Res.*, **91:** 5927-5941.

Widom E and Shirey SB, (1996), Os Isotope Systematics in the Azores: Implications for Mantle Plume Sources, *Earth and Planetary Science Letters.*, **142:** 451-465.

Wilson M, (1989), Igneous Petrogenesis: A Global Tectonic Approach, Chapman and Hall.

Wood SA, (1987) Thermodynamic Calculations of the Volatility of the PGEs: The PGE Content of Fluids at Magmatic Temperatures, *Geochim. Cosmochim. Acta*, **51:** 3041-3050.

Woodland SJ and Pearson DG, (1999), Platinum Group Element Analysis of Geological Samples using Isotope Dilution: A comparison between Ni-S Fire Assay and Anion Exchange Chromatography Preconcentration Techniques. *In* J.G. Holland, and S.C. Tanner, Eds. Developments in ICP-MS. Royal Society of Chemistry.

Xie Q and Kerrich R, (1995), Application of Isotope Dilution for Precise Measurement of Zr and Hf in Low Abundance Samples and International Reference Materials by ICP-MS: Implications for Zr (Hf) / REE Fractionations in Kimberlites, *Chem. Geol.*, **123**: 17-27.

Yi YV and Masuda A., (1996), Simultaneous determination of Ru, Pd, Ir and Pt at Ultratrace Levels by Isotope Dilution Inductively Coupled Plasma Mass Spectrometry in Geological Samples, *Anal. Chem.*, **68**; 1444-1450.

Zereini F, Skerstupp B and Urban H, (1994), Comparison Between the Use of Sodium and Lithium Tetraborate in Platinum-Group Element Determination by Nickel Sulfide Fire-Assay, *Geostandards Newsletter*, **18**: 105-109.

Zoller NH, Parrington JR and Phelan Kotra JM, (1983), Ir Enrichment in Airborne Particles from Kilauea Volcano, *Science*, **22**: 1118-1121.

APPENDIX I: Trace and Major Element Data - Sample Preparation, Analysis and Results

AI.1 Sample Crushing

Hand specimens were initially cut with a steel-bladed, rotary saw, such that fresh specimens were selected. Surfaces with saw-marks were thoroughly scrubbed and washed in MQ. Subsequently the samples were reduced to rock-chips with a stainless steel, Fritsch Pulverisette jaw crusher. These chips were then ground to a fine powder in a Fritsch Pulverisette agate ball-mill which was thoroughly cleaned between each sample, by grinding with silica sand. Tungsten carbide mills were deliberately avoided to ensure that there was no contamination of the PGE-signatures in the low-abundance samples.

AI.2 Major Element Analysis by XRF

AI.2.1 Loss on Ignition

All rock powders are dried overnight in an oven (~100°C), to drive off any surface moisture. Then ~2g of dry powder is weighed into a ceramic crucible, this in turn is placed into a furnace for 2 hours at a temperature of 900°C in order to remove the water of crystallisation. The 'ignited' powders are then quickly reweighed to determine the loss on ignition.

AI.2.2 XRF Fusion Discs

The major elements were analysed by means of XRF fusion discs, these were prepared in the following manner:

Both the ignited powders and lithium tetraborate fusion flux are dried prior to use. The flux and sample powders are then combined in a ratio of 0.45g sample: 2.25g flux ± 0.001g, in an agate mill to ensure thorough mixing. This charge is then fused in a platinum crucible at a temperature of 1050°C for 20 minutes. The charge is

poured into a graphite mould whilst molten and pressed with an aluminium plunger to produce the final disc.

The fusion discs were analysed at the University of Durham with a Phillips PW1400 X-ray fluorescence Spectrometer fitted with a Pwa500/10 automatic sample changer. A Rh tube was used as the source of X-rays. Calibration and correction factors were calculated using Phillips X40 software. The operating conditions were 80Kv and 35mA for all the major elements.

AI.3 Analysis of Trace Elements by ICP-MS

AI.3.1 Sample Preparation

- Sample powders are dried overnight in an oven at ~105°C
- Screw-top Teflon vials are cleaned by refluxing with Analar HNO_3 for 24 hours then rinsing with MQ before use
- Weigh 0.1 ± 0.001g into the Teflon vial
- Digest on a hotplate (~150°C) for 48hrs using HF (4mls) and HNO_3 (1ml)
- After digestion, evaporate to a moist residue
- Redissolve sample in HNO_3 (1mls), evaporate, then repeat this step
- Add 2.5mls of HNO_3 then dilute to ~10mls with MQ
- Spike with internal standard (-1.25mls; typically contains 2ppm Bi and Rh)
- Sample is now further diluted (to 50mls) with MQ
- 1ml of this solution is further diluted by addition of 10mls of MQ before ICP-MS analysis- final dilution factor is 1/5000

AI.3.2 Analytical Procedure

The dissolved samples were analysed for a range of elements (Table A1.1) at the University of Durham using a Perkin-Elmer Sciex Elan 6000 ICP-MS, equipped

with a cross-flow nebuliser and an auto-sampler set to a sample uptake rate of 1ml/min. The plasma was operated at 1100 to 1300 W. Analytical results were processed using software supplied by Sciex. Instrumental performance is monitored using a daily check solution from which oxide production and machine sensitivity can be assessed and optimised.

Data quality is ensured by:

- Analysing procedural blanks to ensure samples were not contaminated during preparation
- Using internal standards which compensate for any sample loss during dilution and fluctuation in machine sensitivity during an analytical session
- Analysing a range of international samples with different levels of trace-elements, against which the unknown samples are calibrated. Standards used include AGV-1, BCR-1, W-2 and X-108.
- A wash-out time of 3 minutes (3.5% HNO_3) is allowed between each sample to eliminate any inter-sample, instrumental memory effects

AI.4 Summary of Different Nebuliser Types used in Conjunction with ICP-MS during this Study.

Scott-Type Double Pass Nebuliser (Cross flow) – supplied as standard with the Perkin Elmer ICP-MS. Sample is pumped through a capillary tube to a glass nebuliser which feeds sample liquid, aspirated with Ar gas, into a voluminous double-pass spray chamber (Fig A1). Here any large sample droplets condense and are removed from the system. The fine monodispersed aerosol which remains is carried into the ICP-MS by the Ar sweep gas. This system has a large dead volume, utilises a lot of sample and is prone to memory effects from certain elements.

Direct Injection Nebuliser (DIN) – (Trade name Microneb 2000). Made by CETAC Technologies. This nebuliser is designed to produce an extremely fine aerosol of sample, generated by interaction of the sample liquid with a high velocity gas stream (Fig A2). It is unique because the sample is delivered through a narrow, thin-walled,

highly inert capillary tube. The fine sample mist produced by the high velocity gas stream eliminates the need for a spray chamber, thus the sample is injected directly into the ICP-MS. This minimises wash-out time between samples, memory effect and dead volume. Since sample liquids have to pass through a long narrow capillary (Teflon) an injection valve is coupled with a high pressure pump to deliver the sample to the nebuliser.

Micro-concentric Nebuliser (MCN) – (Trade name: Aridus). Also made by Cetac Technologies. This desolvating system utilises a low-flow Teflon^{R} nebulizer, with a normal flow rate of approximately 60 μL/min, thus the Aridus can determine all required elements with less than 1 mL of sample. This system is unique as once the sample is aspirated (with Ar) it passes through a chamber comprising a semi-permeable membrane, water vapour contained within the sample passes out through this membrane and is carried away by Ar sweep gas (Fig A3). Thus, the sample that enters the ICP-MS is desolvated and so less prone to polyatomic isobaric interferences. Long wash-out times for certain elements however suggest that they may stick to the membrane.

AI.5 Full trace and Major Element Data Tables for Samples Quantified for their PGE-Contents During this Project

Samples from Grenada and West Greenland were analysed for trace elements by ICP-MS at Durham (using the technique in AI.3). The major and trace element data for the Izu-Bonin samples was taken from Pearce *et al.* (1992) as insufficient sample powder was available to permit trace element analysis. Likewise, the Greenland samples were provided as powders by Lotte Larsen and the GGU and had already been analysed for major elements. Element data tables for each of the regions studied are now presented (p vi).

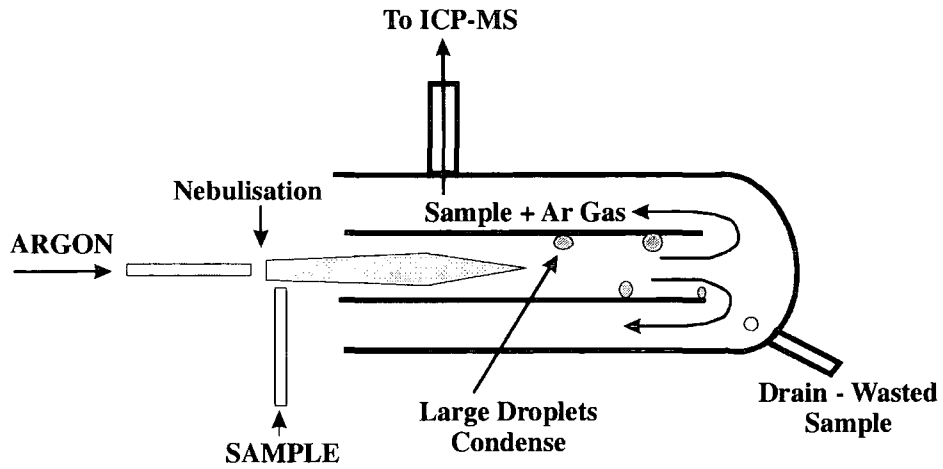

Fig A1: Scott-type Double Pass Spray Chamber (after C. Ottley pers.comm.)

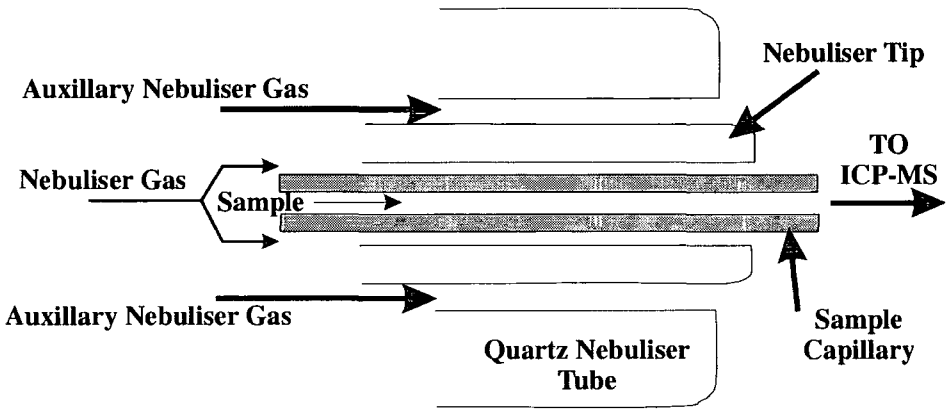

Fig A2: Direct Injection Nebuliser (DIN) from CETAC Technologies Product Information

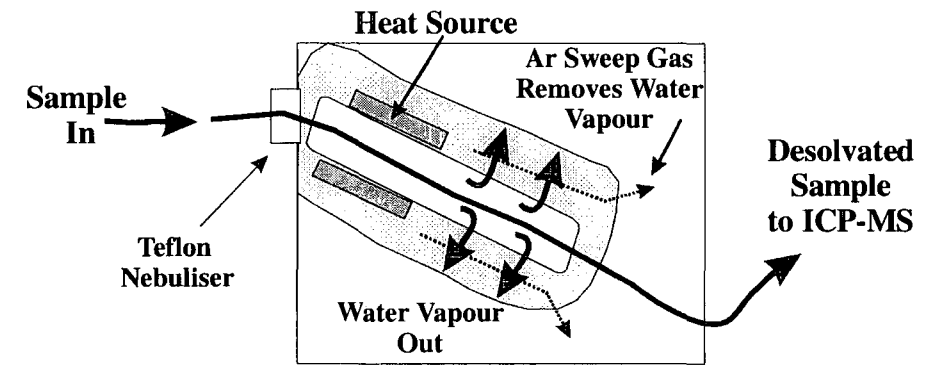

Fig A3: Simple Schematic Drawing of A microconcentric Nebuliser (MCN)

Sample	GD5	GD18	GD21	*Thirlwalls*	AMG 6078	AMG 6103	AMG 6157
Series	M-C series	C-series	C-series	*Samples*	M-series	M-series	M-C series
Rock type	Basalt	Basalt	Basalt		Picrite	Picrite	Picrite
Centre	MMM	MGF	MGF		MMM	SEM	MGF
Latitude	11° 6'	7° 1'	7 °7'		6° 1'	6° 8'	7° 0'
Longitude	45° 6'	43° 8'	45° 0'		45° 1'	40° 4'	44° 7'
SiO_2	47.24	48.55	46.98		45.88	45.10	47.36
Al_2O_3	15.18	17.59	16.38		12.49	12.53	13.43
Fe_2O_3	10.62	10.11	10.49		10.38	10.45	10.04
MgO	10.49	5.8	7.15		14.47	15.28	12.79
CaO	11.72	12.45	14.81		12.21	12.30	11.63
Na_2O	2.42	2.64	1.97		1.88	1.93	2.07
K2O	0.49	1.346	0.981		1.10	0.54	0.75
TiO_2	0.987	1.204	1.004		1.13	0.92	0.88
MnO	0.173	0.164	0.172		0.17	0.18	0.18
P_2O_5	0.13	0.31	0.19		0.30	0.23	0.15
TOTAL	99.44	100.16	100.13		100.02	99.45	99.27
Ti	5431.5	7281.5	6117.3		6606.5	3219.3	4472.3
V	261.9	309.3	323.6		285.0	257.0	262.0
Cr	804.2	148.2	121.4		967.0	908.0	956.0
Mn	1308.9	1270.2	1240.8		8782.8	7117.7	6792.4
Co	46.8	37.6	41.6				
Ni	243.6	75.0	63.9		379.0	404.0	359.0
Cu	78.7	91.4	74.7		96.0	86.0	53.0
Zn	67.2	80.5	69.5		74.0	72.0	74.0
Ga	14.1	19.0	17.3		14.0	14.0	14.0
Rb	12.7	17.0	16.9		24.9	10.6	10.9
Sr	333.5	699.7	1216.3		529.2	679.0	576.0
Y	18.4	29.1	21.0		19.4	17.4	17.9
Zr	55.2	124.1	76.5		99.2	66.4	63.0
Nb	4.6	16.3	4.3		20.1	6.7	5.1
Cs	0.8	1.0	0.8				
Ba	140.0	386.8	276.7		368.0	268.0	210.0
La	8.2	21.6	16.7		20.8	18.0	10.2
Ce	17.2	42.0	37.1		41.2	35.9	23.0
Pr	2.4	5.5	5.0				
Nd	11.0	24.1	22.1		21.3	18.4	14.3
Sm	2.9	5.1	4.7		4.5	4.0	3.5
Eu	0.9	1.6	1.5		1.4	1.2	1.1
Gd	3.2	5.0	4.2		4.2	3.8	3.6
Tb	0.5	0.7	0.6				
Dy	3.2	4.1	3.4		3.4	3.2	3.1
Ho	0.6	0.8	0.7				
Er	1.7	2.2	1.7		1.8	1.7	1.8
Tm	0.3	0.4	0.3				
Yb	1.6	2.1	1.6		1.5	1.5	1.6
Lu	0.3	0.3	0.2			0.2	0.2
Hf	1.5	2.8	2.0				
Ta	0.3	0.8	0.2				
Pb	2.0	3.0	2.0		4.2	2.2	1.7
Th	2.2	6.2	4.5		7.0	5.5	3.0
U	0.9	2.7	2.6		2.0	2.0	1.9

Table AI.1 Geochemistry of Grenada basalts (errors on data as in Table AI.). Data for Thirlwall's samples in Thirlwall *et al.* (1996). Oxides as wt%, ICP-MS data in ppm.

Sample	GD8	GD10	GD11	GD12	GD 14	GD16	GD 25	Gd 17
Series	M-series	M-series	M-series	M-series	M-series	M-series		
Rock type	Picrite	Picrite	Picrite	Picrite	Picrite	Picrite	Andesite	Andesite
Centre	MMM	MMM	MMM	MGF	MMM	MMM	SMM	MGF
Latitude	3° 7'	3° 7'	3° 7'	5° 8'	4° 5'	5° 3'	3° 8'	6° 95'
Longitude	45° 1'	45° 1'	45° 1'	45° 2'	43° 9'	43° 1'	45° 5'	45° 3'
SiO_2	46.35	46.50	46.68	45.36	46.03	44.89	64.44	58.61
Al_2O_3	14.36	14.34	14.59	13.26	14.72	14.26	18.43	17.24
Fe_2O_3	10.24	10.30	10.17	10.35	10.37	9.90	4.68	6.65
MgO	13.86	14.15	14.06	13.66	14.41	13.55	0.35	2.95
CaO	10.94	10.88	10.80	12.51	10.85	12.70	4.12	7.43
Na_2O	1.93	1.90	1.92	1.78	2.12	2.39	4.95	4.22
K2O	0.36	0.39	0.40	1.03	0.40	0.68	2.04	1.94
TiO_2	0.86	0.85	0.86	1.15	0.88	0.91	0.42	0.69
MnO	0.17	0.17	0.17	0.17	0.16	0.18	0.04	0.11
P_2O_5	0.11	0.10	0.11	0.29	0.11	0.36	0.18	0.24
TOTAL	99.17	99.58	99.75	99.56	100.05	99.81	99.66	100.06
Ti	5351.7	5245.0	5292.4	7021.3	5515.4	5701.3	2493.0	4329.6
V	267.2	268.4	258.8	286.9	262.2	271.0	98.1	183.9
Cr	973.7	943.1	888.3	914.9	1144.6	643.2	9.5	29.7
Mn	1256.2	1243.1	1244.6	1198.2	1258.6	1552.9	290.4	861.2
Co	58.7	59.5	58.8	58.1	59.6	56.4	7.5	19.8
Ni	420.9	435.2	429.1	389.6	432.1	378.9	10.8	21.7
Cu	77.9	80.4	80.5	94.5	86.7	107.6	31.9	32.1
Zn	67.9	66.0	65.2	70.0	69.4	71.2	102.5	35.4
Ga	14.5	14.2	14.5	14.8	14.8	15.9	20.5	19.6
Rb	5.8	7.9	8.8	24.5	7.9	22.2	109.1	45.5
Sr	255.7	254.7	244.1	513.0	251.8	752.9	995.1	946.3
Y	18.6	18.3	19.5	18.5	18.5	20.7	18.0	26.0
Zr	53.4	53.3	55.2	101.2	54.6	124.2	82.1	173.7
Nb	4.1	4.2	4.5	21.5	4.3	11.2	19.9	13.2
Cs	0.1	0.2	0.3	1.0	0.1	1.4	1.0	0.5
Ba	94.5	101.3	91.9	335.0	105.5	389.6	812.9	638.8
La	5.6	5.5	5.9	19.3	5.3	32.0	50.2	40.5
Ce	12.8	12.5	12.8	38.1	12.2	61.6	80.3	66.4
Pr	1.8	1.8	1.9	4.7	1.8	7.3	8.7	8.8
Nd	8.6	8.5	8.9	19.6	8.3	28.5	30.3	34.5
Sm	2.3	2.3	2.3	4.1	2.3	5.2	5.0	6.3
Eu	0.8	0.8	0.8	1.3	0.8	1.5	1.4	1.8
Gd	2.6	2.7	2.8	3.7	2.7	4.3	3.6	5.1
Tb	0.5	0.4	0.5	0.6	0.5	0.6	0.6	0.7
Dy	2.7	2.8	2.9	3.0	2.7	3.3	2.9	4.0
Ho	0.6	0.6	0.6	0.6	0.6	0.6	0.5	0.8
Er	1.6	1.5	1.6	1.5	1.6	1.6	1.4	2.0
Tm	0.3	0.3	0.3	0.2	0.3	0.3	0.2	0.3
Yb	1.5	1.5	1.7	1.3	1.5	1.5	1.5	2.0
Lu	0.3	0.2	0.3	0.2	0.2	0.2	0.2	0.3
Hf	1.4	1.4	1.4	2.3	1.4	2.7	2.0	3.6
Ta	0.2	0.2	0.3	1.1	0.2	0.5	1.2	0.8
Pb	1.5	1.6	1.6	3.4	1.4	6.4	18.4	1.4
Th	1.2	1.2	1.2	5.9	1.1	13.0	24.3	15.4
U	0.4	0.4	0.5	2.1	0.5	4.67	9.6	6.7

Table AI.2 Geochemistry of Grenada picrites and andesites (errors on data as in Table AI.) Oxides as wt%, ICP-MS data in ppm

Sample	GD1	GD2	GD3		Standard
Series				Detection	Error
Rock type	Cumulates	Cumulates	Cumulates	Limit	%
Centre	MMM	MMM	MMM		
Latitude	11° 6'	11° 6'	11° 6'		
Longitude	45° 6'	45° 6'	45° 6'		
SiO_2	42.34	42.08	44.11		0.2
Al_2O_3	13.15	18.10	23.36		0.17
Fe_2O_3	11.68	13.54	9.23		0.08
MgO	14.87	7.62	4.20		0.11
CaO	13.39	15.77	15.91		0.09
Na_2O	2.48	1.29	1.67		0.03
K2O	0.42	0.14	0.18		0.01
TiO_2	1.65	1.15	0.71		0.01
MnO	0.15	0.16	0.11		0.005
P_2O_5	0.03	0.02	0.06		0.01
TOTAL	100.15	99.86	99.52		
					RSD (%)
Ti	9994.3	7150.8	3627.0	0.929	3.12
V	442.7	449.5	236.9	1.963	2.6
Cr	781.4	39.4	6.6	9.075	4.46
Mn	1111.4	1158.7	683.1		4.78
Co	64.0	47.7	24.9	0.042	5.62
Ni	293.8	58.6	31.7	1.047	5.69
Cu	21.8	13.7	17.3	0.072	5.5
Zn	58.4	65.3	38.6		6.43
Ga	12.5	19.1	19.5	0.031	3.49
Rb	2.1	0.7	2.9	0.018	2.32
Sr	236.4	601.3	1416.9	0.047	2.39
Y	21.7	16.7	9.2	0.005	0.78
Zr	33.2	27.1	25.7	0.043	0.72
Nb	3.3	2.1	1.4	0.01	0.75
Cs	0.01	0.01	0.2		2.39
Ba	77.0	40.3	73.2	0.135	2.27
La	2.5	2.7	5.1	0.003	3.18
Ce	7.8	7.7	10.6	0.005	2.96
Pr	1.5	1.4	1.5	0.002	2.68
Nd	8.6	8.3	7.0	0.007	2.78
Sm	3.0	2.6	1.7	0.007	1.89
Eu	1.1	0.9	0.7	0.002	1.68
Gd	3.8	3.0	1.7	0.007	2.65
Tb	0.6	0.5	0.3	0.002	1.61
Dy	3.5	2.7	1.4	0.004	0.92
Ho	0.7	0.5	0.3	0.001	1.28
Er	1.8	1.4	0.8	0.002	1.62
Tm	0.3	0.2	0.1	0.001	0.75
Yb	1.5	1.2	0.7	0.002	0.82
Lu	0.2	0.2	0.1	0.001	1.8
Hf	1.2	0.9	0.7	0.005	0.84
Ta	0.2	0.1	0.1	0.005	2.04
Pb	0.1	0.2	0.6		1.59
Th	0.2	0.2	1.1	0.001	2.85
U	0.1	0.04	0.6	0.001	2.96

Table AI .3 Geochemistry of Grenada cumulates
Standard errors and RSDs after Brod (1999). XRF error: expressed as the standard error in the regression of observed results on recommended values for international standards. ICP-MS error: RSD of repeated standard analysis throughout the analytical run.

GGU name	660400 444	660400 492	660332 771	660408001.233	66u332788	66u332828
Name: this study	Gp1	*Gp2*	Gp3	Gp4	Gp5	Gp6
Member	Anaanaa	Anaanaa	Naujang.	Anaanaa	Ordling.	Ordling.
SiO_2	46.80	46.04	45.56	47.44	44.51	45.22
TiO_2	1.03	1.03	1.01	0.78	1.06	1.02
Al_2O_3	10.62	10.94	10.85	11.77	8.00	9.44
Fe_2O_3	1.51	1.42	1.47	1.42	1.50	1.56
FeO	10.06	9.49	9.78	9.50	9.99	10.41
MnO	0.18	0.18	0.19	0.17	0.17	0.17
MgO	20.09	19.30	19.31	18.76	26.31	22.54
CaO	8.18	10.18	10.45	8.75	7.12	8.50
Na_2O	1.31	1.30	1.26	1.25	0.89	1.03
K_2O	0.14	0.05	0.05	0.05	0.35	0.04
Ti	6138.9	6228.8	6150.9	4502.3	6444.6	6210.8
V	247.6	253.4	260.5	240.6	206.8	234.7
Cr	1265.2	1012.1	1018.7	1383.8	1704.4	956.3
Mn	1386.4	1394.1	1378.6	1239.2	1355.4	1401.9
Co	88.5	87.3	87.3	81.3	104.0	99.7
Ni	826.7	869.2	858.4	734.6	1408.1	1104.2
Cu	69.0	116.3	105.7	126.4	92.8	91.9
Zn	76.7	73.9	77.3	74.0	81.1	87.0
Ga	12.6	13.4	12.6	12.0	9.7	12.9
Rb	2.6	0.5	0.6	0.8	11.9	1.6
Sr	105.4	119.3	109.8	69.0	171.6	118.3
Y	18.3	18.5	18.1	16.2	13.6	16.1
Zr	61.5	54.2	53.6	39.88	62.1	54.1
Nb	2.9	1.7	1.9	1.4	5.7	2.0
Cs	0.1		0.01	0.02	0.03	0.02
Ba	34.2	6.2	7.0	14.3	62.0	8.4
La	4.0	2.1	2.3	2.1	4.8	2.4
Ce	10.4	6.5	6.9	5.7	12.2	7.2
Pr	1.6	1.2	1.2	0.9	1.9	1.3
Nd	8.2	6.5	6.8	5.0	8.9	6.9
Sm	2.4	2.2	2.2	1.6	2.4	2.2
Eu	0.9	0.8	0.8	0.6	0.8	0.8
Gd	3.0	2.9	2.9	2.2	2.7	2.7
Tb	0.5	0.5	0.5	0.4	0.4	0.5
Dy	3.1	3.1	3.1	2.6	2.4	2.8
Ho	0.7	0.6	0.6	0.6	0.5	0.6
Er	1.8	1.8	1.8	1.6	1.3	1.5
Tm	0.27	0.27	0.3	0.3	0.2	0.2
Yb	1.6	1.6	1.6	1.5	1.1	1.3
Lu	0.3	0.3	0.3	0.2	0.2	0.2
Hf	1.7	1.5	1.5	1.1	1.6	1.5
Ta	0.2	0.2	0.2	0.1	0.4	0.2
Pb	1.1	0.4	0.3	0.6	0.6	0.5
Th	0.7	0.1	0.2	0.3	0.4	0.1
U	0.1	0.04	0.05	0.08	0.1	0.04

Table AI.4 Data for West Greenland picrites – trace element by ICP-MS. Major element data from Larsen pers.comm. Oxides in wt%, trace elements in ppm.

GGU name	66u362149	66u113333	66u138228	66u 264217	66u 113210	66u 400457
Name: this study	Gp7	Gp8	Gp9	Gp10	Gp11	Gp12
Member	Naujang.	Ordling.	Ordling.	Naujang.	Naujang.	Anaanaa
SiO_2	45.21	46.26	45.74	45.55	45.99	45.66
TiO_2	0.87	1.21	1.27	0.94	0.94	0.95
Al_2O_3	9.55	10.34	11.07	10.62	10.90	10.28
Fe_2O_3	1.47	1.46	1.57	1.45	1.41	1.46
FeO	9.83	9.76	10.44	9.67	9.42	9.75
MnO	0.18	0.18	0.19	0.18	0.19	0.18
MgO	23.72	20.60	17.32	21.19	20.87	21.72
CaO	8.07	8.70	10.74	9.06	8.86	8.71
Na_2O	0.99	1.27	1.47	1.26	1.26	1.16
K_2O	0.03	0.09	0.08	0.01	0.08	0.07
Ti	5443.5	6690.4	7337.9	5509.4	5413.5	5581.4
V	223.1	257.0	282.5	243.9	250.1	231.3
Cr	1225.8	1473.3	1022.2	1115.7	1673.0	1375.8
Mn	1494.8	1378.6	1425.1	1394.1	1386.4	1394.1
Co	99.4	85.9	82.9	84.4	85.1	87.8
Ni	1244.8	981.3	841.6	900.0	901.4	961.1
Cu	104.3	113.5	120.2	115.3	124.4	81.0
Zn	79.1	86.1	87.1	76.6	72.1	74.1
Ga	10.9	13.6	22.3	12.1	12.3	11.5
Rb	0.5	0.6	1.1	0.3	1.6	2.4
Sr	92.9	152.5	153.3	87.2	79.6	103.9
Y	15.4	16.9	18.6	17.7	18.5	16.6
Zr	48.0	56.5	66.2	43.4	44.0	47.8
Nb	2.5	2.6	4.1	1.3	1.4	1.4
Cs	0.01	0.00	0.02	0.00	0.1	0.01
Ba	7.3	15.0	14.3	6.5	11.6	31.6
La	2.4	2.7	3.9	1.7	1.8	1.8
Ce	6.9	7.9	10.6	5.3	5.4	5.7
Pr	1.2	1.4	1.7	1.0	1.0	1.0
Nd	6.1	7.4	9.0	5.6	5.5	5.8
Sm	1.9	2.3	2.7	2.0	2.0	2.0
Eu	0.7	0.9	1.0	0.7	0.7	0.7
Gd	2.5	2.9	3.2	2.6	2.7	2.6
Tb	0.4	0.5	0.5	0.5	0.5	0.5
Dy	2.6	3.0	3.2	2.9	3.1	2.8
Ho	0.5	0.6	0.6	0.6	0.7	0.6
Er	1.5	1.6	1.7	1.7	1.8	1.6
Tm	0.23	0.25	0.26	0.26	0.29	0.25
Yb	1.3	1.5	1.5	1.6	1.7	1.5
Lu	0.2	0.2	0.2	0.2	0.3	0.2
Hf	1.3	1.6	1.8	1.3	1.3	1.4
Ta	0.2	0.4	0.3	0.1	0.1	0.1
Pb	0.3	0.4	0.4	0.3	0.4	0.3
Th	0.2	0.2	0.3	0.1	0.1	0.1
U	0.1	0.1	0.1	0.03	0.04	0.03

Table AI.5 Data for West Greenland picrites – trace element by ICP-MS. Major element data from Larsen pers.comm. Oxides in wt%, trace elements in ppm.

	I.B.1	I.B.21	I.B.40	I.B.5	I.B.67
	ICBrzA	Rhyolite	HCB	HCB	ICB
SiO_2	61.72	71.12	52.04	52.32	53.00
Al_2O_3	12.80	14.23	13.30	15.00	12.46
Fe_2O_3	7.30	3.92	8.74	8.90	7.54
MgO	8.06	0.92	10.20	7.99	13.08
CaO	6.16	2.76	12.70	11.34	6.70
Na_2O	2.97	4.19	2.23	2.56	2.76
TiO_2	0.20	0.26	0.29	0.37	0.25
K_2O	0.65	2.46	0.32	1.30	0.21
MnO	0.12	0.09	0.16	0.11	0.14
P_2O_5	0.03	0.07	0.02	0.1	0.04
TOTAL	100.02	100.02	100	99.99	98.74
V	171	19	187	237	202
Cr	99	3	961	333	786
Co	29	8	47	40.7	38.5
Ni	101	13	349	170	296
Cu	53	61	34	63	56
Zn	171	19	187	237	202
Rb	13.0	30.0	7.0	6.0	3.1
Sr	165.0	128.0	131.0	147.0	136.0
Y	5.6	12.0	8.0	13.0	6.5
Zr	38.6	79.0	23.0	34.0	27.0
Nb	0.59	1.1	0.4	0.4	0.4
Cs	0.16	0.7	0.3	0.	
Ba	38.6	68.0	25.0	18.0	7.6
La	1.7	3.9	1.3	2.1	1.2
Ce	3.9	9.4	3.0	4.2	2.6
Pr	0.6	1.3	0.6	0.7	0.4
Nd	2.8	6.1	2.8	4.0	2.0
Sm	0.6	1.5	0.7	1.0	0.6
Eu	0.2	0.4	0.3	0.4	0.2
Gd	1.0	2.0	1.2	1.6	0.8
Tb	0.1	0.3	0.2	0.3	0.2
Dy	0.9	1.9	1.3	1.7	1
Ho	0.2	0.4	0.3	0.4	0.2
Er	0.6	1.3	0.8	1.1	0.7
Tm	0.1	0.2	0.2	0.2	0.1
Yb	0.7	1.4	0.9	1.2	0.8
Lu	0.1	0.2	0.1	0.2	0.1
Hf	1.2	2.4	0.7	1.0	0.7
Ta	0.04	0.1	0.02	0.02	0.03
Pb	1.9	3.5	0.9	1.3	0.7
Th	0.4	0.8	0.1	0.2	0.2
U	0.2	0.4	0.1	0.2	0.1

Table AI.6 Trace and Major Element Chemistry for Izu-Bonin Samples (from Pearce *et al.*, 1992). Oxides in wt%, trace elements in ppm.

APPENDIX II: Full PGE Data for All Samples and Replicates Analysed

To ensure high data quality samples were analysed at least in duplicate where sufficient powder was available.

AII.1 Spike Calculation Methods

The method used to calculate the amount of spike needed for isotope dilution studies (and spike calibrations) is outlined below:

Method for Spike Addition Calculations:

E.g. For calculation of a spike-standard calibration

Conc. of Ir Std = 10ppm = 10000ng = 3730ng ^{191}Ir + 6270ng ^{193}Ir

Aiming for a Spike/Normal ratio of ~ 2.38

Therefore need: 2.38 x 6270 = 14922.6ng of ^{191}Ir

As 3730 ng of ^{191}Ir is already contributed from the standard, need:

14922.6 - 3730 = 11192.6ng of ^{191}Ir from the spike

Conc. of Ir Spk = 11.2ppm = 11200ng of ^{191}Ir

Therefore need: 11192.6/11200 = ~ 0.999ml of spk : 1ml of std

E.g. For calculation of Spike needed for WITS-1

Ir Conc. in WITS-1 = 1.7ppb , for a 10g sample = 17ng Ir, = 11.3ng ^{193}Ir

Need 2.38 x 11.3 = 26.89 ng of ^{191}Ir

In a 10g sample of WITS-1 already have 5.66ng of ^{191}Ir

Therefore need: 21.23 ng of ^{191}Ir from spike.

As concentration of spike is 13.5ppb need 21.23/13.5 = ~ 1.6ml of spike

E.g. For calculation of Amount of spike needed for making mixed spikes

Ir conc. in 1g of Picrite = 1.2ng/g = 1.2 x 0.627 = 0.7524 ng ^{193}Ir

191/193 ratio of 2.38 ∴ need 0.7524 x 2.38 = 1.79ng ^{191}Ir

Already have 1.2 x 0.373 = 0.448ng from sample,

∴ need 1.79 - 0.448 = 1.34 ng from spike

Vol. of spk needed ∴ = 1.34/1459 (ppb, spk conc.) = 0.0092ml

BUT want to add 0.1ml of spike to samples for ease of measurement:

∴ 0.1/0.0092 = 108.88 (the dilution factor necessary for the spike)

i.e. 1 ml of spike : 107.88mls of diluant

Or, as spike is to be made up to 250mls

2.32mls of spike : 250mls of diluant

This calculation is repeated for all of the other elements to be included in the spike. The total volume of spikes is then added up and the remainder of the 250mls of spike is made up by diluant (i.e. 4N UPA HCl).

All data was obtained using Carius tube digestion, and anion exchange preconcentration followed by ICP-MS analysis. A cross-flow nebuliser was used for obtaining the bulk of the data, except for Os where the direct injection nebuliser was used to minimise memory effects.

AII.2 Grenada PGE Data

SAMPLE	Rock Type		Re	Os	Ir	Ru	Pt	Pd
Gd17 A	Andesites		0.362	0.017	0.003	0.092	1.914	0.638
Gd 17 B	(Basic)		0.357	0.019	0.005		1.879	0.673
		Average	**0.360**	**0.018**	**0.004**	**0.092**	**1.896**	**0.655**
		*2*stdev*	*0.01*	*0.003*	*0.002*		*0.05*	*0.05*
		*2*stdev (%)*	*2.00*	*18.65*	*53.70*		*2.60*	*7.55*
Gd 25 A	(High SiO_2)		0.056	0.016	0.000		1.217	0.135
Gd 25 C			0.055	0.018	0.001	0.173	1.097	0.065
		Average	**0.056**	**0.017**	**0.000**	**0.173**	**1.157**	**0.100**
		*2*stdev*	*0.001*	*0.004*	*0.001*		*0.17*	*0.10*
		*2*stdev (%)*	*2.03*	*20.98*	*212.13*		*14.66*	*99.93*
Gd 1 A	Cumulates		0.057	0.050	0.229	0.202	9.097	3.026
Gd 1 B			0.028	0.064	0.170	0.191	4.806	0.578
GD 1C	(Amphibole		0.013	0.139	0.499	0.198	3.388	0.924
GD 1D	-rich)		0.030	0.044	0.155	0.116	2.863	0.975
		Average	**0.032**	**0.074**	**0.263**	**0.177**	**5.038**	**1.376**
		*2*stdev*	*0.04*	*0.09*	*0.32*	*0.08*	*5.65*	*2.23*
		*2*stdev (%)*	*113.28*	*118.29*	*122.00*	*46.13*	*112.24*	*162.00*
GD 2A	(Plagioclase		0.014	0.012	0.073	0.025	5.140	0.804
GD 2B	-bearing)		0.017	0.009	0.042	0.019	3.178	0.765
		Average	**0.015**	**0.011**	**0.058**	**0.022**	**4.159**	**0.785**
		2*stdev	0.003	0.004	0.04	0.01	2.77	0.06
		*2*stdev (%)*	20.20	40.41	78.21	36.89	66.72	7.12
GD3A	(Plagioclase		0.082	0.009	0.016	0.017	6.762	0.496
GD 3B	-bearing)		0.088	0.008	0.013	0.032	4.788	0.427
		Average	**0.085**	**0.008**	**0.014**	**0.025**	**5.775**	**0.462**
		*2*stdev*	*0.01*	*0.002*	*0.003*	*0.02*	*2.79*	*0.10*
		*2*stdev (%)*	*10.81*	*28.45*	*23.57*	*83.12*	*48.33*	*21.07*

Table AII.1 PGE concentrations (ppb) of Grenada andesites and cumulates– Reproducibility of replicates shown as 2*stdev

SAMPLE	Rock Type		Re	Os	Ir	Ru	Pt	Pd
Gd 8A	**M-series**		0.014	0.070	0.062		2.062	1.297
Gd 8B	**Low La/Y**			0.089	0.048	0.326	1.742	1.113
Gd8 C	**Picrites**		0.006	0.101	0.055	0.074	1.837	1.275
		Average	**0.010**	**0.087**	**0.055**	**0.200**	**1.880**	**1.228**
		*2*stdev*	*0.01*	*0.03*	*0.01*	*0.36*	*0.33*	*0.20*
		*2*stdev (%)*	*116.46*	*35.52*	*25.56*	*178.73*	*17.46*	*16.36*
Gd 10 A	**Low La/Y**			0.117	0.056	0.213	2.401	1.626
Gd 10 B	**Picrites**		0.012	0.083	0.070	0.209	2.318	1.792
Gd 10 C			0.016	0.054	0.107		2.891	2.051
		Average	**0.014**	**0.085**	**0.078**	**0.211**	**2.537**	**1.823**
		*2*stdev*	*0.01*	*0.06*	*0.05*	*0.01*	*0.62*	*0.43*
		*2*stdev (%)*	*38.39*	*73.98*	*68.94*	*3.28*	*24.41*	*23.48*
Gd 11 A	**Low La/Y**		0.011	0.054	0.052	0.266	2.198	2.280
Gd 11 B	**Picrites**		0.013	0.083	0.060	0.200	2.157	1.453
		Average	**0.012**	**0.069**	**0.056**	**0.233**	**2.177**	**1.867**
		*2*stdev*	*0.00*	*0.04*	*0.01*	*0.09*	*0.06*	*1.17*
		*2*stdev (%)*	*19.95*	*60.02*	*21.02*	*40.44*	*2.66*	*62.61*
Gd 14 A	**Low La/Y**		0.018	0.078	0.148	0.290	3.858	2.166
Gd 14 B	**Picrites**		0.012	0.073	0.166	0.219	3.349	1.151
GD14 C			0.000	0.082	0.037	0.064	2.956	1.193
		Average	**0.010**	**0.078**	**0.117**	**0.191**	**3.388**	**1.503**
		*2*stdev*	*0.02*	*0.01*	*0.14*	*0.23*	*0.91*	*1.15*
		*2*stdev (%)*	*176.98*	*11.79*	*118.88*	*121.10*	*26.71*	*76.43*
Gd 12 A	**M-series**		0.033	0.043	0.098		3.968	2.852
Gd 12 B	**High La/Y**		0.032	0.041	0.082	0.154	3.483	2.820
	Picrites	**Average**	**0.033**	**0.042**	**0.090**	**0.154**	**3.725**	**2.836**
		*2*stdev*	*0.001*	*0.003*	*0.02*		*0.68*	*0.04*
		*2*stdev (%)*	*4.35*	*8.10*	*24.88*		*18.38*	*1.58*
Gd 16 A	**High La/Y**		0.012	0.063	0.068	0.171	3.117	4.015
Gd 16 B	**Picrites**		0.013	0.038	0.048		3.746	3.961
		Average	**0.013**	**0.051**	**0.058**	**0.171**	**3.431**	**3.988**
		*2*stdev*	*0.001*	*0.03*	*0.03*		*0.89*	*0.08*
		*2*stdev (%)*	*9.05*	*68.41*	*48.72*		*25.93*	*1.91*
Thirlwall								
AMG 6078	**High La/Y**		2.596	0.075	0.127	0.070	3.907	1.873
AMG 6103	**Picrites**		0.039	0.045	0.058	0.062	3.805	2.655
	M-C series							
Gd 5	Basalt		0.124	0.537	0.054	0.069	1.839	3.699
AMG 6157	**Picrite**		0.195	0.302	0.316	0.065	5.081	4.471
	C-series							
Gd 18	Basalt		0.088	0.014	0.037	0.046	1.512	2.518
Gd 21	Basalt		0.102	0.012	0.024	0.038	3.146	7.596

Table AII.2 PGE Concentrations of Grenada M-series picrites, M-C series and C-series basalts
Reproducibility of replicates shown as 2*stdev

AII.3 West Greenland Picrite PGE Data

Sample		Re	Os	Ir	Ru	Pt	Pd
GGU 400 444	G.P.1	0.26	1.91	0.93	2.63	7.48	6.97
GGU400 492	G.P.2	1.14	2.53	1.33	3.26	10.69	10.30
GGU 332 771	G.P.3	0.42	1.55	0.93	3.00	9.59	10.95
GGU 408 001.233	G.P.4	0.24	1.50	0.80	2.99	9.52	8.74
GGU 332788	**G.P.5a**	**0.18**	**2.03**	**1.08**	**3.14**	**6.27**	**4.20**
GGU 332788	**G.P.5b**	**0.18**		**1.11**	**2.95**	**6.01**	**4.48**
GGU 332828	G.P.6	0.37	2.68	1.36	3.20	9.41	6.68
GGU 362149	**G.P.7a**	**0.29**	**2.90**	**1.58**	**3.91**	**9.95**	**8.57**
GGU 362149	**G.P.7b**	**0.29**	**2.72**	**1.49**	**3.66**	**9.91**	**8.74**
GGU 113333	G.P.8	0.06	2.26	1.19	3.30	9.54	6.66
GGU 138228	G.P.9	0.33	1.52	0.81	2.55	8.76	7.14
GGU 264217	**G.P.10a**	**0.48**	**2.78**	**1.48**	**4.26**	**11.42**	**11.58**
GGU 264217	**G.P.10b**	**0.46**	**2.79**	**1.46**	**4.28**	**11.44**	**11.50**
GGU 113210	G.P.11	0.21	3.12	1.64	4.41	13.00	10.90
GGU 400457	G.P.12	0.36	3.88	1.94	3.61	11.16	9.35

Table AII.3 Full PGE data (ppb) for West Greenland picrites

		Re	Os	Ir	Ru	Pt	Pd
GGU 332788	G.P.5a	0.18	2.03	1.08	3.14	6.27	4.20
GGU 332788	G.P.5b	0.18		1.11	2.95	6.01	4.48
	Average	**0.18**	**2.03**	**1.09**	**3.05**	**6.14**	**4.34**
	*2*stdev (%)*	*0.79*		*3.66*	*8.74*	*5.98*	*8.97*
GGU 362149	G.P.7a	0.29	2.90	1.58	3.91	9.95	8.57
GGU 362149	G.P.7b	0.29	2.72	1.49	3.66	9.91	8.74
	Average	**0.29**	**2.81**	**1.53**	**3.79**	**9.93**	**8.65**
	*2*stdev (%)*	*4.09*	*9.20*	*8.20*	*9.30*	*0.62*	*2.82*
GGU 264217	G.P.10a	0.48	2.78	1.48	4.26	11.42	11.58
GGU 264217	G.P.10b	0.46	2.79	1.46	4.28	11.44	11.50
	Average	**0.47**	**2.79**	**1.47**	**4.27**	**11.43**	**11.54**
	*2*stdev (%)*	*6.18*	*0.81*	*2.05*	*0.81*	*0.18*	*0.99*

Table AII.4 Reproducibility of West Greenland picrites replicates shown as 2*stdev of the average - Note reproducibility better than 10% for all PGEs

AII.4 Izu-Bonin PGE Data

Name	Rock Type	Re	Os	Ir	Ru	Pt	Pd
I.B. 1	ICBrzA	0.247	0.023	0.025	0.242	3.312	7.219
I.B.5	HCB	0.264	0.031	0.104	0.123	1.887	1.187
I.B. 21	R	0.419	0.005	0.002	0.020	0.175	1.016
I.B.40	HCB	0.344	0.049	0.107	0.250	1.536	3.682
I.B. 67A	ICB	0.195	0.043	0.080	0.153	5.765	3.533
I.B. 67B	ICB	0.200	0.024	0.074	0.196	6.268	3.444
I.B.67	**Average**	**0.198**	**0.033**	**0.077**	**0.175**	**6.017**	**3.489**
	*2*stdev (%)*	*3.72*	*82.99*	*11.98*	*34.50*	*11.81*	*3.60*

Table AII.5 PGE data (ppb) for Izu-Bonin Samples – Reproducibility achieved for a typical boninite is expressed as % 2*stdev of the average (I.B. 67) – replicates could not be run for all samples due to shortage of ODP rock powders

APPENDIX III: Papers and Abstracts Published

1) Papers

a) Woodland SJ and Pearson DG, (1999), PGE Analysis of Geological Samples using Isotope Dilution: A Comparison of Fire Assay and Anion-Exchange Chromatography, Preconcentration Techniques, *In* J.G. Holland, and SC. Tanner, Eds. Developments in ICP-MS. Royal Society of Chemistry.

b) Pearson DG and Woodland SJ, (2000), Solvent Extraction/Anion Exchange Separation and Determination of PGEs (Os, Ir, Pt, Pd, Ru) and Re-Os Isotopes in Geological Samples by Isotope Dilution ICP-MS, *Chem. Geol.*, **165:** No.1-2, p87-107.

c) Pearson DG, Ottley C and Woodland SJ, (1999), Precise measurement of Os by direct injection ICP-MS. *In* J.G. Holland, and SC. Tanner, Eds. Developments in ICP-MS. Royal Society of Chemistry.

2) Abstracts

a) Woodland SJ, Pearson DG, Pearce JP and Thirlwall MF, (1999), PGEs in Subduction Zone Magmas: Anion Exchange Preconcentration ICP-MS Analysis of Lesser Antilles and Izu-Bonin Magmas, *in Conf. Proc. of the 9th Annual Goldschmidt Conference.*

b) Pearson GP and Woodland SJ, (1999), Isotope Dilution IC-MS Analyses of Re-Os Isotopes and PGEs via Solvent Extraction and Anion-Exchange Pre-concentration and a Desolvating Nebuliser, *in Conf. Proc. of the 9th Annual Goldschmidt Conference.*

c) Pearson DG, Larsen LM, Walker RJ, Woodland SJ, Pederson AK, Carlson RW and Shirey SB, (1999), Searching for Deep Sources in Flood Basalts: Re-Os – Pt-Os Isotope and PGE Systematics of West Greenland, *in Conf. Proc. of the 9th Annual Goldschmidt Conference.*

PLATINUM GROUP ELEMENT ANALYSIS OF GEOLOGICAL SAMPLES USING ISOTOPE DILUTION : A COMPARISON OF FIRE ASSAY AND ANION-EXCHANGE CHROMATOGRAPHY, PRECONCENTRATION TECHNIQUES

S. J. Woodland and D. G. Pearson

Dept. of Geological Sciences,
University of Durham,
South Road,
Durham. DH1 3LE

1 INTRODUCTION

The platinum group element series provide a unique tool for deducing the history of Earth accretion and subsequent geological processes. Furthermore, the existence of two geochronologically useful decay systems; i.e. $^{187}Re \rightarrow {}^{187}Os$ & $^{190}Pt \rightarrow {}^{186}Os$ within the series, greatly enhance the value of this geochemical group to earth sciences. Recent improvements in analytical equipment (e.g. advances in ICP-MS and N-TIMS), have lowered theoretical detection limits for such elements facilitating quantification of the PGE s in low abundance (i.e. sub ppb level) geological samples. In reality however, achievement of these detection limits with regard to actual rock samples, has been greatly hampered by the absence of a suitable low blank, preconcentration technique.

During this study, traditional preconcentration methods have been critically assessed and a new low blank, isotope dilution method has been developed that allows analysis of Re, Os, Ir, Ru, Pt and Pd from the same sample aliquot by ICP-MS.

2 Ni-S FIRE ASSAY

The most commonly used method of preconcentrating PGE s from geological samples, is via a Ni-S fire assay [1,2]. The advantage of this method is that it enables the use of large sample sizes (20g or more), thereby increasing the amount of PGE s available for analysis and minimising the effects of sample heterogeneity which are an inherent problem with PGE analysis. Recently however, it has been widely noted [3,4] that the success of this technique is highly dependent on experience of the analyst and quality of the reagents available. Experience of using the technique within this study; clearly illustrated that losses of PGE s can occur at many stages of the procedure, particularly during dissolution of the Ni-S button, (see Fig 1), precluding collection of high quality, reproducible data. In addition, Os-concentration could not be quantified due to loss of volatile OsO_4 during the fusion process and subsequent bead dissolution.

In order to address the issue of sporadic loss of PGE s during the fire assay, isotope dilution (I.D.) was implemented as part of the procedure. An isotopically enriched mixed

equilibrium during the fusion process and thus any later sample losses can be tolerated and corrected for.

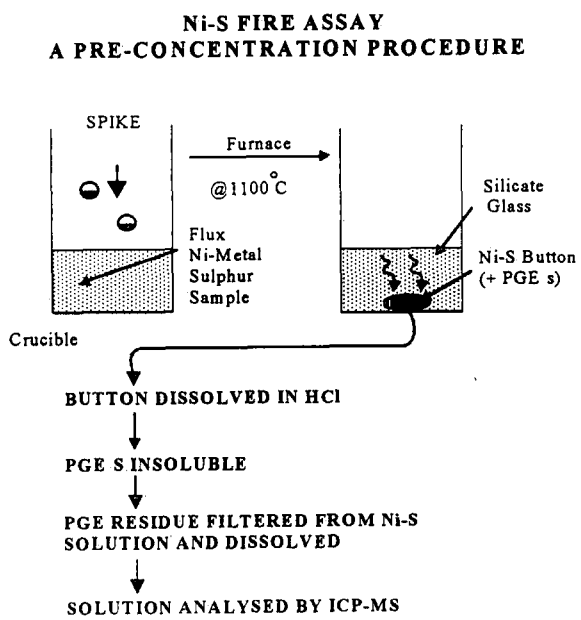

Figure 1 *Ni-S Fire Assay – Experimental Procedure*

2.1 Experimental Procedure for Ni-S Fire Assay

In the above procedure, the reagents used to fuse a 20g rock sample are:

i)Sodium carbonate (12g) and borax (24g), as a flux.

ii)Sulphur (5g) and Ni-powder (8g), as the collector [2]

These reagents are thoroughly mixed with the sample and placed into a porcelain crucible. The mixed PGE spike is then added to the sample and reagents, covered over and allowed to dry, before the crucible is placed in a pre-heated furnace for 1 hour, 30 minutes. After this time the crucibles are removed from the furnace to promote rapid cooling. Once the bead has been removed from the cold silicate slag, it is broken into small chips and dissolved in 12N HCl at 350°C. This procedure typically takes 2-4 hours and must be carefully monitored. During bead dissolution H_2S is evolved, this maintains a reducing environment, which prevents dissolution of the PGE s. Once the bead dissolution is complete however and H_2S production ceases, the solution must be quickly filtered before the PGE s also start to dissolve. Finally, the insoluble PGE residue and filter paper are dissolved in aqua regia before being diluted to a suitable concentration for ICP-MS analysis

The use of I.D. greatly improves the efficiency of the Ni-S fire assay procedure. The main improvement is the ability to obtain reproducible PGE data, as any PGE losses are compensated for. Replicate analyses of standard rock reference materials (e.g. WPR-1 & WITS-1) have yielded reproducibilities with 2-sigma errors of less than 10% for all PGE s (see Table 1). In addition, the use of I.D. enables the total procedural blank to be correctly estimated and thus blank corrections can be applied to data obtained. One major drawback of Ni-S fire assay however, is its limitation in quantification of Re. Previous studies[8] have demonstrated that Re is not quantitatively partitioned into the Ni-S bead. Also, isotopic homogeneity is not achieved for Re which is distributed between the Ni-S bead and silicate glass; thus compromising analytical accuracy. In addition, the inherently high Re blanks associated with Ni-S fire assay are a further complication.

	Ir (ppb)	Os (ppb)	Pt (ppb)	Pd (ppb)
WPR-1 ;1	18.736	21.654	362.417	263.014
WPR-1 ;2	18.047	21.822	378.434	281.274
WPR-1 ;3	18.794	20.922	364.865	276.981
average	18.526	21.466	368.572	273.756
2xstdev	0.831	0.957	17.256	19.095
2 sigma error as %	**4.486**	**4.459**	**4.682**	**6.975**

Table 1 *Replicate analyses for standard rock WPR-1*

2.3 Fire Assay and Low Abundance Samples

Despite the achievement of good, reproducible data for standard rock types, it was decided that Ni-S fire assay is not a technique suited to analyses of very low PGE abundance samples (i.e. sub-ppb). This is predominantly due to high and variable, reagent blank levels (see Table 2) which can adversely affect detection limits for PGE s preconcentrated in this manner.

	Ir (ppb)	Pt (ppb)	Pd (ppb)	Os (ppb)
SEDIMENT	0.014 – 0.126	0.65 – 3.52	0.7 – 7.75	0.15 – 0.46
ANDESITE	<0.23	---	~15	---
MORB	0.02	0.50	1.22	0.017
"CLEAN" Ni	0.25	1.53	6.6	---
"DIRTY" Ni	134.71	1186.79	12.36	295.72

Table 2 *Blank Levels Obtained in Ni-reagents, Compared to Common Geological Samples* [3].

of Ni from the fusion procedure into the solution analysed for PGE s. This can lead to severe Ni-Ar interferences during ICP-MS analysis [3]. Furthermore, the inability to analyse Re precludes the collection of geochronologically useful Re-Os isotope measurements on the same sample split. Finally, the fire assay pre-concentration technique concentrates all the PGE s to be analysed in one solution. This means the level of pre-concentration is limited by the need to measure many isotopic ratios on many masses in the same solution.

3 CARIUS TUBE-ANION EXCHANGE CHROMATOGRAPHY PRECONCENTRATION METHOD

3.1 Methodology

Due to difficulties in applying Ni-S fire assay to low abundance samples, an alternative low-blank preconcentration procedure was investigated. A Carius tube digestion procedure was adopted, as this has been demonstrated as a highly effective method of attacking and dissolving PGE phases held within a silicate matrix [5]. Furthermore, Carius tubes are known to promote sample-spike equilibration (for Re and Os) and also to facilitate low blanks. Special precautions must be instated when using Carius tube procedures due to their potentially dangerous nature. For example, the Carius tubes are enclosed within steel safety jackets, which have the ability to vent gas should a tube explode, whilst in the furnace. Furthermore, all Carius tubes are chilled (to less than -10°C) in order to reduce internal pressure prior to opening.

Following the Carius tube digestion, Os is separated from the matrix via a solvent extraction procedure [9] (see Fig. 2). Anion exchange chromatography is then utilised in order to separate all of the other PGE s from their matrix [6,7]. Prior to loading on a column containing 1ml of acid-cleaned AG1-X8 resin, the aqueous PGE solution is chlorinated in order to oxidise Ir^{3+} to Ir^{4+}, as Ir has greatest affinity for the anion exchange resin in its higher oxidation state. Before elution of the PGE s, Hf and Zr, which form major interfering oxide ions, are removed from the column using a mixed HF/HCl and a dilute HNO_3 wash. Ir and Pt are then eluted as separate fractions following reduction of Ir (to Ir^{3+}) using sulphurous acid. Pd maybe eluted together with Ru and Re (all in 12N HNO_3), or separately, depending on the desired sensitivity/availability of solution.

Yields of 60%, or greater (~95% for Re), are obtained for each of the PGE s within their respective fractions. The use of I.D. means that 100% yields are not required, as isotope ratios of spike-equilibrated samples are measured, rather than actual concentrations. In addition, segregation of each of the PGE s into separate fractions, effectively enhances detection limits by reducing the number of masses which must be measured during analysis. Thus, the samples can be analysed as low volume, very concentrated solutions; permitting detection limits of < 5ppt for each of the PGE s.

3.2 Advantages of Carius-Tube, Chromatography Method over Ni-S Fire Assay

Total procedural blanks for the Carius tube method are extremely low e.g.

Ir ~ 1pg/g	Pd ~ 10pg/g	Ru < 10pg/g
Os ~ 5pg/g	Pt ~ 25pg/g	Re < 10pg/g

This is because the only blank contribution comes from the acids used and the Carius tubes. Seastar SPA/UPA acids are routinely used throughout the procedure. Care must be taken to boil the Carius tubes in aqua regia prior to use as these are the main source of the Pt blank, which can reach up to 200pg/g without thorough cleaning. The blanks obtained by Carius tube digestion are highly reproducible and still however, often an order of magnitude better than those achieved using Ni-S fire assay. In addition, Ru can be quantified via carius tube digestion, as there is no excess Ni in the system to cause large Ni-Ar interference problems unlike with Ni-S fire assay. Lastly, the ability to obtain Os and Re data on the same sample allows geochronological work to be carried out.

3.3 Disadvantage of Carius-Tube Chromatography Method

The only drawback associated with this technique is the limitation of the sample size to 1-2g. In PGE geochemistry it is considered advantageous to analyse as large a sample size as possible to counteract a phenomenon called the "nugget" effect. This effect occurs within geological samples, as the PGE s are often contained within discrete metal-sulphide nuggets. Thus, the apparent PGE concentration of any given sample can vary considerably depending on the homogeneity, or heterogeneity, of distribution of these nuggets. Study of both standard and 'real' rock samples however, has illustrated that considering sampling theory (see Pearson *et al*, this vol. for more explanation), the data obtained using only 1g samples are as reproducible as could be expected. Most other techniques commonly used in PGE geochemistry, yield 2 sigma reproducibility errors, of >40%. In the case of the Carius tube, chromatography method described here however, the reproducibility for all PGE s (except Pt) is considerably better than 40% (see Table 3).

	Mean Conc.	2 Sigma Errors	No. of Replicate Analyses
Ir	1.498 ppb	18 %	18
Os	1.071 ppb	7 %	17
Ru	4.877 ppb	7 %	10
Re	0.064 ppb	28 %	16
Pd	5.745 ppb	35 %	10
Pt	7.140 ppb	65 %	17

Table 3 *Replicates of the Standard rock WITS-1 obtained by Carius tube–Anion Exchange Chromatography*

N.B. The variability in Pt data is believed to be an artefact of Pt-heterogeneity within this standard rock type and has also been noted when using different analytical techniques.

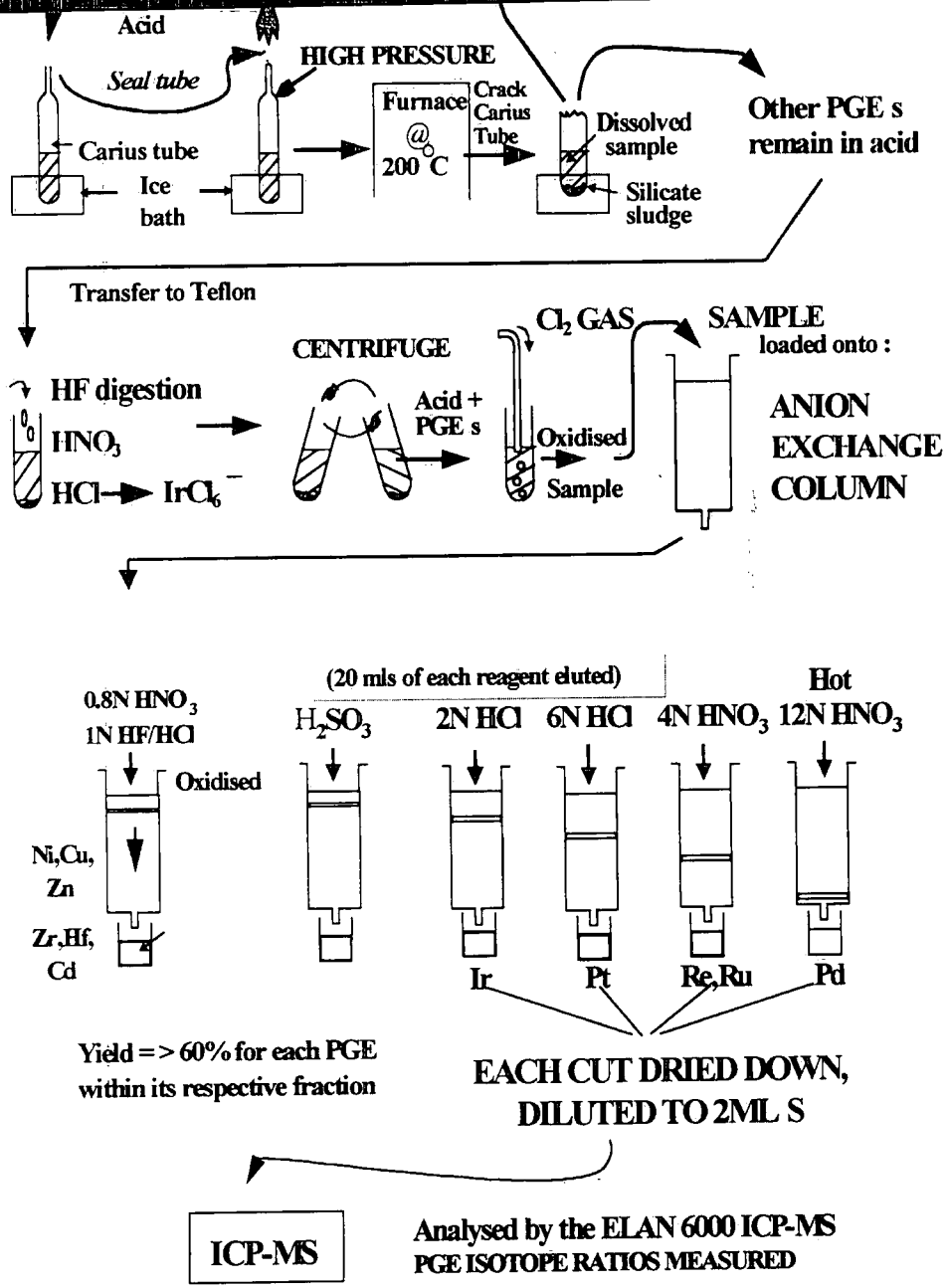

Figure 2 *Carius Tube - Anion Chromatography Preconcentration Method*

PGE analysis is carried out using an Elan 6000 ICP-MS. Os is analysed using a CETAC direct injection nebuliser which is essentially memory free compared to conventional x-flow/Meinhardt nebulisers, or microconcentric nebulisers (See Pearson *et al*, this vol.). High precision, high sensitivity Os isotopic analysis can also be carried out using N-TIMS with a further micro-distillation purification step [9].

Suitable sensitivity can be obtained for all of the other PGE s using a x-flow nebuliser, with Scott-type, double pass spray chamber; although some problems (documented below) are encountered in its use.

4.1 Isobaric Interferences

Oxide production on the Elan 6000 + x-flow nebuliser runs at ~2.5% for the elements of interest in this study. This can lead to relatively high ZrO^+/Zr^+ and HfO^+/Hf^+ production which sometimes necessitates corrections on isotopes of Ir, Pt and Pd; e.g.

$ZrO\ (^{92}Zr + ^{16}O)$ on ^{108}Pd
$HfO\ (^{177}Hf + ^{16}O)$ on ^{193}Ir
$HfO\ (^{178}Hf + ^{16}O)$ on ^{194}Pt

Isobaric interferences can be identified as present by plotting sample data on a spike-sample mixing line (see Fig 3), this necessitates measurement of three different isotopes of any given element, this approach cannot therefore be used for bi-isotopic elements such as Ir and Re.

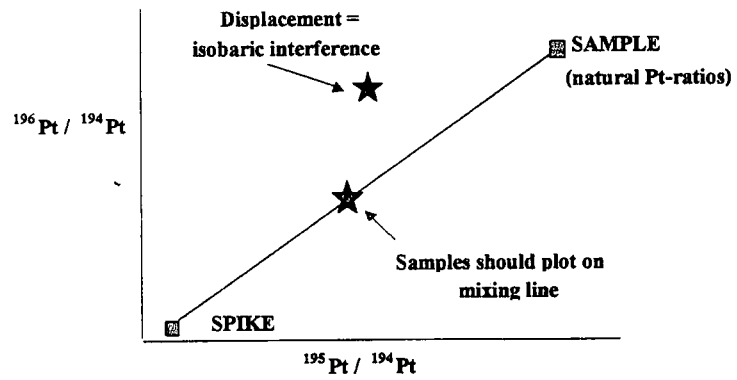

Figure 3 *Effect of Isobaric Interferences on Sample Data (ratios are mass bias corrected).*

This is an instrumental transmission effect, which tends to bias in favour of the heavier isotopes of an element for most quadrupole ICP-MS designs. The resultant mass bias, consequently causes a shift in the isotope ratios measured for standard solutions, away from the expected, natural ratios. Fortunately however, the mass bias effect remains relatively constant (see Fig 4) and can easily be corrected for. Some typical mass bias correction factors are illustrated in Table 4. Although the correction factors are relatively small, all data are corrected to produce the best quality results possible.

	$Ir^{193/191}$	$Ru^{101/99}$	$Re^{187/185}$	$Pt^{196/194}$	$Pd^{105/106}$	$Os^{192/190}$
MBCF	0.983	0.963	0.982	0.987	1.029	0.978
2 sigma errors (%)	0.833	0.399	1.084	1.338	0.495	0.226

Table 4 *Typical Mass Bias Correction Factors for the PGE s using a Cross-Flow Nebuliser (errors based on > 20 separate analyses)*

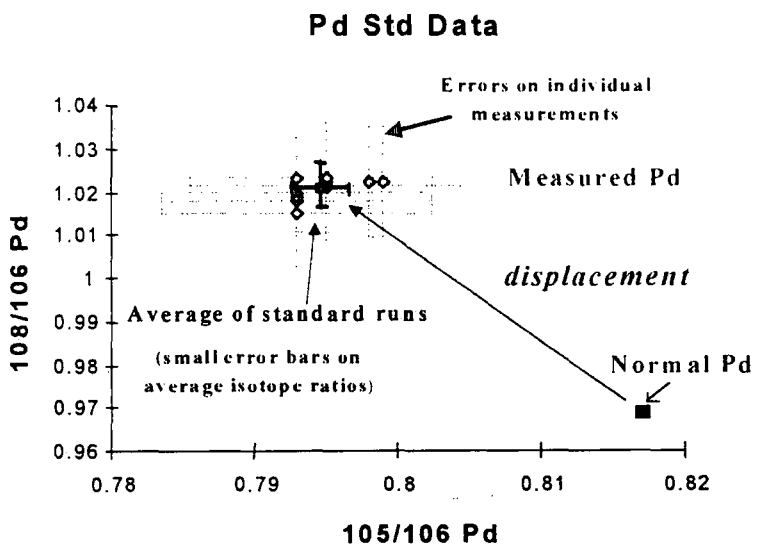

Figure 4 *Effect of Mass Fractionation on Standard Solution Isotope Ratios (2 sigma error bars shown)*

4.3 Ru Isobaric Interferences

Using x-flow nebulisation on the Elan 6000, it was found that isotopic ratios for Ru (^{101}Ru / ^{99}Ru is measured in our I.D. scheme), were increasingly displaced from that expected by an interference, as the concentration of Ru standard solutions decreased (see Fig 5). The source of this interference proved to be from use of Ni-cones, which contributed a substantial Ni-Ar interference. Thus, in order to measure accurate Ru isotopic ratios on dilute solutions (<0.1ppb), Pt cones are used. Pt cones have proved suitable for measurement of all the other PGE s as they do not appear to contribute to PGE-background in the ICP-MS due to the inertness of Pt-metal.

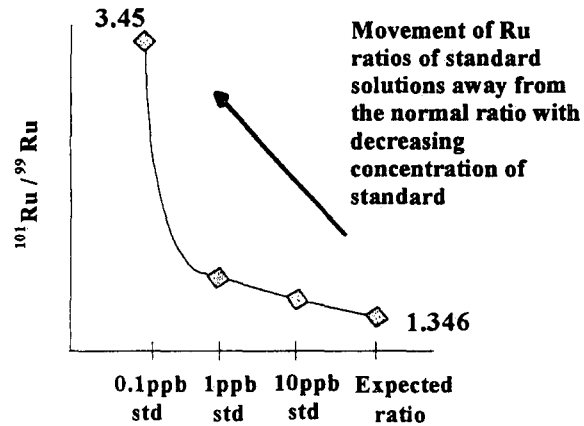

Figure 5 *Effect of Ni-Ar Interference on Ru-isotope Measurements*

5 COMPARISON OF DIFFERENT NEBULISER TYPES

During analysis of the PGE s, 3 main types of nebuliser have been used. The conventional x-flow type nebuliser has proved suitable for quantification of all the PGE s (except Os due to memory effects). The problems of isobaric and Ni-Ar interferences considered above, must be addressed but can generally be overcome. Detection limits using the x-flow are limited by the need to dilute samples to ~2ML s for analysis (sample uptake rate is ~ 1ML/min). In contrast to the cross-flow nebuliser however, the CETAC MCN-6000 nebuliser uses significantly lower sample consumption (50 – 100 µL/min). This promotes greater sensitivity and gains in signal intensity of between 2 to 3 times, for all PGE s (except Os). In addition the dry plasma resulting from the desolvating action of the MCN-6000 serves to minimise oxide production (<0.03% oxides) and seems to eliminate the Ni-Ar interference resulting from use of Ni-cones.

over its competitors, as it does not display any memory effect for Os (see Pearson *et al*, this vol.). Like the MCN-6000, the DIN is capable of very low volume analyses, thus improving sensitivity. The DIN however, has several major problems with regard to PGE chemistry. Firstly, oxide production is high (~ 6 - 12% in optimal nebulisation mode), which leads to substantial isobaric interferences, also the DIN shows some memory effect for Re and Pt. Finally, it was also found that the DIN was difficult to optimise, resulting in a drop in sensitivity and production of very erratic isotope data on standard solutions. Despite this it is considered the nebuliser of choice for measurement of Os.

6 CONCLUSIONS

i) A new Carius-tube anion exchange chromatography procedure has been developed, which is well suited to analysing all of the PGE s (and Re), at sub-ppb level in geological samples.
ii) The total procedural blanks are far superior to existing preconcentration methods, such as Ni-S fire assay. This greatly improves detection limits for PGE geochemistry to ~10ppt (or less), for all elements (except Pt, which is 50ppt or less).
iii) The data achieved using this method are exceptionally reproducible given the low abundances (and often heterogeneous distribution) of PGE s present and the small sample size used (1-2g of rock powder).
iv) Use of a conventional x-flow nebuliser with the Elan 6000 (and Pt-cones), yields acceptable results for analysis of Ir, Re, Pt, Pd and Ru. The CETAC MCN-6000 increases sensitivity for all the PGE's and therefore may be most suitable for measurement of ultra-low abundance PGE samples. The CETAC DIN is far superior to other nebulisers for measurement of Os and is used exclusively for this purpose.

References

1. S. E. Jackson, B. J. Fryer, W. Gosse, D. C. Healey, H. P. Longerich and D. F. Strong, *Chem. Geol.* , 1990, **83**, 119.
2. I. McDonald, R. J. Hart and M. Tredoux, *Anal. Chim. Acta*, 1994, **289**, 237.
3. G.Ravizza and D. Pyle, *Chem. Geol,* 1997, **141**, 251.
4. I. Jarvis, M. M. Totland and K. E. Jarvis, *Analyst,* 1997, **122,** 19.
5. S.B. Shirey and R.J.Walker, *Anal. Chem.* , 1995, **34**, 2136.
6. R. K. Petrie and J. W. Morgan, *J. Radioanal. Chem.*, 1982, **74**, No. 1, 15.
7. M. Rehkamper and A. N. Halliday, *Talanta,* 1997, **44,** 663.
8 Martin C. (1991), PhD thesis, Yale, (Unpublished).
9 A. S. Cohen & F. G. Waters, *Anal. Chim. Acta*, 1996, **332**, 269.

Solvent extraction/anion exchange separation and determination of PGEs (Os, Ir, Pt, Pd, Ru) and Re-Os isotopes in geological samples by isotope dilution ICP-MS

D.G. Pearson & S.J. Woodland

Department of Geological Sciences, Durham University, South Rd, Durham, DH1 3 LE, UK.

Submitted to Chemical Geology 17/12/98
Revised 29/6/99

Keywords: *Platinum Group Elements, Re-Os isotopes, ICP-MS, Isotope Dilution*

ppt level to confidently identify inter-element PGE fractionations. The analytical method works well for a wide variety of rocks types.

1. Introduction

The platinum group elements, Rh, Ru, Pd, Pt, Ir, Os (PGEs) have attracted considerable interest in geological sciences both because of their economic interest and their use as petrogenetic tracers. Recent technological advances have also allowed a proliferation of studies utilising both the ^{187}Re-^{187}Os and ^{190}Pt-^{186}Os isotope decay schemes in Earth and planetary sciences (Shirey and Walker, 1998 and references therein). A multitude of analytical techniques have been employed to determine PGE abundances in geological samples, accompanied by an equally varied spectrum of chemical separation and pre-concentration techniques, a comprehensive review of which is beyond the scope of this paper. Recent developments in ICP-MS instrumentation realistically allow the prospect of ppt detection limits for all PGEs. Negative ion thermal mass spectrometry has also been shown to be capable of ppt level determination of Os and Ir, together with Re (Creaser et al., 1991; Völkening et al., 1991; Walzck and Heumann, 1993). Due to the varying ease with which different PGEs lend themselves to chemical separation from matrices, the limiting factor in the application of instrumental techniques to geological samples is the ability to separate PGEs at the ppt level while maintaining the low blank levels required to match instrumental detection limits. In addition, no general method has hitherto been available that allows determination of Re-Os isotopic compositions and other PGEs on the same sample aliquot. Such a method would take advantage of the geochronological opportunities offered by the Re-Os and Pt-Os decay systems and allow investigation of correlations between Os isotope variations and inter-element PGE fractionations.

The goal of the present study was to provide a low-blank, routine chemical separation method for the high precision analysis of as many PGEs as possible by ICP-MS, with

addition of some "carrier" phase such as quartz, it is not clear that blank measurements always give an accurate reflection blank contributions when samples are analysed. In addition to these points, the method does not quantitatively separate Re for analysis. When fusions are spiked for isotope dilution, isotopic equilibrium between glass and bead is not achieved (Martin, 1990) and high Re blanks are endemic in the flux materials. Therefore, Re is usually determined on a separate sample aliquot, raising problems if the sample is heterogeneous. The isolation of Os from other PGEs for isotopic analysis by either ICP-MS or N-TIMS can probably only be achieved by aliquoting the concentrate at some stage, usually after filtering the bead dissolution residue (e.g. Ravizza and Pyle, 1997), but this reduces overall sensitivity in very low level samples. On dissolution of the filter paper to solubilise the PGEs, Os is largely converted into the oxidised form. Oxidised forms of Os, particularly OsO_4, have enhanced ionisation compared to reduced forms (Gregoire, 1990) but also tend to produce much greater memory effects in ICP introduction systems. Furthermore, determination of Os in solution with Pt, where Pt is often at much higher concentrations, can cause significant interference of $^{190}Pt^+$ on $^{190}Os^+$, reducing precision (Ravizza and Pyle, 1997).

Low level Ru analysis by Ni-S fire assay has proved troublesome in some instances (Ravizza and Pyle, 1997), possibly due to carry over of Ni on the filter paper following bead dissolution, leading to a multitude of possible ^{x}Ni-$^{y}Ar^+$ type interferences. Thus, while the Ni-S fire assay technique has many advantages in dealing with large samples and is well suited to many applications in geochemistry e.g. Ravizza and Pyle (1997), it is not suitable for projects requiring either accurate geochronology or the routine analysis of very low level (<<1ppb) materials for a variety of PGEs solely by ICP-MS.

2.2. Acid dissolution or combined acid dissolution/ sodium peroxide fusion techniques

regia attack at between 220 and 240 °C. Silicates are not completely digested by this method but its effectiveness in quantitatively extracting Os from silicate rocks has been well documented (Cohen and Waters, 1996; Shirey and Walker, 1995) and is confirmed in this study. In addition, Rehkämper and Halliday (1997) have recently demonstrated the efficiency of Carius tube attack in quantifying Ru, Pt, Ir and Pt in geological samples.

The Carius tube digestion technique offers considerable versatility in being able to digest a wide range of materials including organic substances. We have found that chromite samples are readily dissolved in concentrated sulfuric acid at 300 °C for 3 days, or in chromic acid. Although chromites can be dissolved by alkaline fusion for PGE analysis (Cocherie, 1986), the high Re blank of this method makes it inherently unsuitable for geochronological studies due to the commonly very low Re contents of chromites. The low Re blank attainable with Carius tube digestion, using double distilled sulfuric acid, allows analysis of most chromite/spinel samples.

The usual aqua regia attack for Carius tube Re-Os analysis (Shirey and Walker, 1995) creates volatile Os tetraoxide but this is quantitatively retained by the impervious sealed glass vessel. Also, because tubes are not re-used, sample cross contamination, which can be a problem with oxidised Os solution in Teflon, is negligible. The technique requires that samples are very well ground before digestion so that the aqua regia may effectively attack any PGE hosts included within silicates. Some samples may require re-grinding to ensure best results.

One potential drawback of the Carius tube dissolution technique, specific to PGE determinations, is that it is commonly only performed on fairly small sample aliquots, up to c. 5g, depending on sample type. Considering the likely heterogeneous distribution of PGEs in powdered rocks (commonly referred to as "the nugget effect") this may present problems with some rocks that are likely to be naturally highly

Addition of a single mixed spike is desirable to minimise weighing errors. Spike isotopes are selected to avoid major isobaric interferences. The enriched isotopes chosen for our spikes were: ^{99}Ru, ^{106}Pd, ^{185}Re, ^{190}Os, ^{191}Ir and ^{194}Pt. The choice of ^{99}Ru minimises potential Ni-Ar interferents (Table 1). Ravizza and Pyle (1997) have noted that Pt spikes enriched in ^{198}Pt can suffer from ^{198}Hg interferences and should be avoided.

4.1. Spike optimisation

To obtain optimal error propagation for isotope dilution measurements we follow the principles outlined by Heumann (1988) and van Heuzen et al., (1989). When measuring Os isotopes for tracing and geochronological purposes it is desirable to minimise the effects of the spike on the measured isotopic ratios, i.e., ^{187}Os/^{186}Os by not overspiking samples. Natural rocks present some spiking problems in that the relative distribution of PGEs within them can vary over large concentration ranges. For instance, Pt/Ir for basalts can be ~600 but as low as 1-2 in peridotites. As such, no single mixed PGE spike solution will suite all rocks. To address this problem a number of different mixed PGE spikes were prepared so that spiking could be optimised for rocks of varying PGE distribution patterns. We routinely use 3 different spikes; a "peridotite" spike to match samples with a relatively flat PGE distribution pattern but low Re, a "picrite" spike to match samples with moderate Pt/Ir and a "basalt" spike for rocks with much more fractionated Pt/Ir. Spike concentrations are adjusted so that approximately 0.1 mL of spike is added to each sample. This minimises the amount of extra liquid being added to the Carius tubes while still giving acceptable weighing errors.

5. Chemical separation procedures for PGEs

allowed to warm to room temperature and then shaken for 2 minutes and allowed to stand under a heat lamp for 1 hour. On cooling, the Os-bearing HBr was pipetted from the organic phase and dried. This residue is taken up in 1 mL of 3.5% HNO_3 for ICP-MS analysis, or further purified for N-TIMS analysis following Cohen and Waters (1996) and Roy Barman et al. (1995).

From previously published data on the organometallic chemistry of Ru and Os, it would be expected that Ru, if in its highest oxidation state, should be co-extracted with Os into the carbon tetrachloride solution, allowing back extraction into the aqueous phase (Surasiti and Sandell, 1960, Meadows, 1962). Analysis of both organic and aqueous phases during the course of this study failed to show significant amounts of Ru in either phase, whereas large proportions of it remained in the aqua regia fraction following solvent extraction. This is because Ru is insufficiently oxidised during normal aqua-regia attack and hence little RuO_4 is generated, possibly due to the formation of stable nitrosyl complexes (Cotton and Wilkinson, 1988). In an attempt to oxidise Ru to a state where it could be solvent extracted we tried bubbling samples with chlorine gas for 30 minutes and then leaving them for several hours in sealed vessels before extracting Ru with CCl_4. Even after this step Ru yields into the organic solvent were very poor (<<10%) and hence we abandoned trying to solvent extract Ru as part of the separation scheme.

5.2. Chromatographic separation of Ir, Pt, Pd, Ru & Re

5.2.1. Cation chromatography

PGEs tend to form anionic complexes in most mineral acid solutions. Hence, in dilute acid media such as 1N hydrochloric acid, chloro-complexed PGE anionic complexes are not adsorbed on to cation resin and pass straight through cation columns, whereas in dilute acid most other metals should be quantitatively adsorbed. PGE yields through cation columns may be very high (>95%) (Jarvis et al., 1997a), especially if mixed

combinations of eluants, some employing insitu-reduction to aid removal of Ir from the resin, are possible for the separation of Ir, Pt, Pd and Ru from other metals. Rehkämper and Halliday (1997) have presented a scheme for separation of PGEs and Re from anion resin for ICP-MS analysis using mixed acid elutions, but their method does not include the ability to obtain Os. Here we present an anion-exchange separation technique that follows on from solvent extraction of Os.

Stable PGE anionic chloro-complexes in mineral acid solutions are strongly retained by anion exchange resins (Crocket et al., 1968; Korkisch, 1989; Korkisch and Klakl, 1968; Petrie and Morgan, 1982). The controlling factor for the adsorption of most elements appears to be valance state and the possible formation of stable ion pairs between the chloro-complexes and quaternary ammonium groups of the resin (Korkisch, 1989). In particular, reduction of strongly held $IrCl_6^{2-}$ to the weakly retained $IrCl_5^{2-}$ and $IrCl_4^-$ (or $IrCl_4[H_2O]_2^-$) species by the resin itself, is a particular problem that has necessitated the use of oxidants co-loaded onto the column to maintain the oxidation state (Crocket et al., 1968; Yi and Masuda, 1996). A powerful oxidant is required to elevate Ir to the IV+ oxidation state. The use of cerium ammonium nitrate for ICP-MS analysis is not favoured due to problems with isobaric interference of $^{140}Ce^{35}Cl^{16}O^+$ and $^{140}Ce^{37}Cl^{16}O^+$ on $^{191}Ir^+$ and $^{193}Ir^+$ respectively that have been observed by Yi and Masuda (1996). Calcium hypochlorite ($CaOCl_2$) has been preferred by some workers (Yi and Masuda, 1996) however, this reagent introduces both extra matrix to the sample and a source of possible contamination in that it is difficult to obtain at ultra-high purity.

Rehkämper and Halliday (1997) have used bromine-water as an oxidant. Colodner et al (1993) bubbled the sample with chlorine gas prior to sample loading, to ensure complete conversion of Ir into the +4 oxidation state. Anbar et al. (1997) have also used Cl-oxidation of samples to ensure Ir retention on anion resin, followed by reductive elution using sulfurous acid. The attractiveness of this method both in terms of

water, 6N HCl, water, 8N HNO_3, followed by rinsing in water and a final rinse in 6N HCl. This procedure gives resin blanks for all elements of < 1pg/g (Re, Ir, Ru), to 2 pg (Pt and Pd). When followed by cleaning in warm 12N HNO_3 prior to sample loading, blanks on all elements are reduced to sub-pg levels.

5.5. Working anion exchange separation scheme

Figure 2 schematically illustrates the column separation procedure. A more detailed account of the procedure can be obtained from the authors on request. Following Carius tube digestion and extraction of Os by solvent extraction (see above), the sample is treated with conc. HNO_3 to destroy residual organics and then HF/HNO_3 to de-silicify the matrix and further breakdown any partially digested material. The sample is then converted to chloride form, taken up in 10 mLs of 0.5 M HCl and chlorinated by bubbling with chlorine gas for 15 minutes before being left to equilibrate for 12 hours to allow time for full oxidation. We use an in-line teflon micro-filter plus a 0.3 litre H_2O "scrubber" for our chlorination line. Disposable pipette tips are used to bubble chlorine into the sample.

1 mL of Biorad® AG1-X8 100-200# anion exchange resin was loaded into standard Biorad® polypropylene columns with 2 mLs resin capacity and a 10 mLs reservoir. Columns were pre-cleaned by soaking in 6N HCl. Once loaded, the resin was cleaned with 20 mLs of warm (c. 80°C) 12N HNO_3, then washed with water and converted back to the chloride form. 30 mLs of chlorinated water are then eluted to create a non-reducing environment for the sample, to minimise any reduction of Ir^{4+} in solution.

After sample loading, 5 mLs of 0.8M HNO_3 are added to elute transition metals such as Zn (Rehkämper and Halliday, 1997) followed by 8 mLs of 1M HF/HCl. The mixed HF/HCl elution is adopted from Hf isotope chemistry methodology (Barovich et al., 1995) and designed to remove as much Zr and Hf as possible before elution of PGEs.

minimised, hence increasing sensitivity. As indicated above, more rapid separation can be affected by combining groups of appropriate elements providing this does not compromise levels of Hf-Zr elution.

6. Mass spectrometry

6.1. Nebulisation

A Perkin Elmer Sciex Elan 6000 quadrupole ICP-MS was used throughout this study. Most of the data was obtained using 2 types of nebuliser. For Re, Ru, Pt, Ir and Pd a standard cross-flow nebuliser was used with an up-take rate of c. 1 mL per minute. This nebuliser has low memory for such elements. Oxide generation levels for elements that present isobaric interferences are on the order of 0.8 to c. 2.5 % as metal-oxide to metal ratio (Table 2).

The Os fraction can be analysed either by N-TIMS after further micro-distillation (Cohen and Waters, 1996), or by ICP-MS. In the latter case it is necessary to address the frequent severe memory problems that plague many analyses. We experienced irregular, often severe memory effects with the Elan cross-flow nebuliser. To counteract these problems a CETAC Technologies direct injection nebuliser (DIN) was used. The all-Teflon nature of the sample uptake pathway and low dead-volume results in negligible memory for samples in the concentration range used in this study. In addition, for samples processed by the method described above, the reduced oxidation state of the Os (IV) following back extraction and reduction with HBr, is also conducive to low memory. Experimentation with various nebulisers (cross-flow, micro-concentric, desolvating micro-concentric and DIN) showed that for low-memory Os measurement by ICP-MS the DIN is the nebuliser of choice (Pearson et al., 1999).

Experimentation with a CETAC Technologies MCN-6000 and Aridus desolvating micro-concentric nebulisers showed great promise for Ir, Pd, Pt, Re and Ru analyses

Higher atomic masses show concomitantly lower mass bias with values for Re, Os, Ir and Pt all being less than 1.5% AMU^{-1} (Fig. 3). Mass bias using the DIN is not notably different in magnitude to that obtained using the cross-flow nebuliser (Pearson et al., 1999). The mean Os mass bias factor (0.83 +/- 0.22 % AMU^{-1}) using the DIN is indistinguishable from Ir using the cross-flow nebuliser (0.71 +/- 0.26 % AMU^{-1}), within the assigned uncertainties. One feature of note in the nature of the mass bias shown by the higher atomic mass elements, is that those that are reasonably close in mass such as Ir and Re can show slightly different degrees of mass bias on our instrument, e.g. typically 0.65 to 0.93 % AMU^{-1} for Ir versus 0.72 to 1.38 % AMU^{-1} for Re (Fig. 3). In addition, it is surprising that the mean, long-term mass bias for Pt (1.08 +/- 0.37 % AMU^{-1}) is slightly higher than for Re, Os or Ir. Although the variation is not large and within overall uncertainty, specific analytical sessions can show significantly different behaviour between Ir and Re. For this reason we do not use Re standards to mass-bias correct Ir samples and do not employ internal spiking of samples with non-PGE elements of similar mass to estimate mass bias. Another reason for not utilising the internal spiking method for high atomic mass PGEs is the lack of suitable element solutions that are likely to be PGE free. Overall, the high level of reproducibility of mass-bias in a single analytical session means that the error from this correction in the isotope dilution calculation scheme is trivial.

6.3. Standard analytical procedure

Before sample analysis, PGE standard solutions in the 0.1 to 10 ppb range are run to establish mass-bias correction factors. Following this, Hf, Mo, Zr and Y solutions are run to monitor levels of oxide production. These correction factors are then up-dated in the software before running samples so that all isobaric interferences can be corrected on-line. Under normal running conditions, using a desolvating nebuliser, oxide generation levels are trivial (<0.03%). Standard solutions are interspersed with

6.4. *Interferences*

Isotope dilution schemes can be established for all the elements analysed here so as to minimise direct isobaric interferences. Table 1 lists most of the potentially important isobaric interferences on PGE masses measured in our procedures and shows those which we correct for. One advantage of separating PGEs, especially Os, into different analytical fractions is that inter-PGE isobaric interferences are greatly reduced. The overlap of ^{187}Os on ^{187}Re is avoided due to all the Os being removed in the solvent extraction step. Any residual Os in the aqueous phase will be largely lost in subsequent dry-downs. Hence, if Os is routinely analysed by N-TIMS, or by DIN there is negligible instrument memory. Similarly, ^{190}Pt and ^{192}Pt interferences on ^{190}Os and ^{192}Os were corrected for but levels of Pt in the Os solvent extraction fraction are trivial. Interference corrections for Hg on Pt isotopes and Cd on Pd isotopes are routinely made. Levels of Cd and Hg appearing in relevant PGE column elution fractions are minimal and combined with the low natural abundances of the interfering isotopes means that corrections for these isobars are insignificant. Interfering Ni^x-Ar^{y+}species were encountered in the Ru mass range when using Ni sampling and skimmer cones on our instrument and these were minimised using Pt cones. The use of Pt cones does not significantly contribute to our Pt background signal. Interestingly, the dry plasma produced by the desolvating nebulisers acted to minimise Ni^x-Ar^{y+} species.

Using the Elan cross-flow nebuliser we found that the most important isobaric interferences were due to metal-oxide species. The most significant observed oxide interference species are Zr, Hf and Y, with Mo also being present (Table 2). Oxide generation levels for these elements, at least in standard solutions, is quite constant during a single analytical session, but can vary on a longer term basis (Table 2). The stability of oxide generation levels within a measurement session lasting 6 hours or more, allows oxide generation to be effectively quantified in most column eluants. This

is demonstrated by a comparison of a column elution of a picritic basalt sample run on the cross-flow nebuliser and a CETAC MCN-6000 desolvating nebuliser, the latter having minimal levels of oxide generation (Table 2). Using the cross-flow nebuliser the $^{105}Pd/^{106}Pd$ value uncorrected for $^{90}Zr^{16}O$ interference is considerably higher than the value obtained when ZrO is corrected for. The oxide corrected value is within error of the $^{105}Pd/^{106}Pd$ value obtained for the same solution run with the desolvating nebuliser operating at very low oxide production levels (0.02%). The effectiveness of oxide corrections and the possible presence of oxide and other intereferences can be evaluated for Pt and Pd by use of spike-sample mixing line plots of the type used by Ravizza and Pyle (1997). An additional check is the correspondence of I.D. concentration calculations produced using different pairs of isotopes of the same element, e.g., for $^{195}Pt/^{194}Pt$ and $^{196}Pt/^{194}Pt$. All samples analysed using the procedure described above plot on, or within error of, spike-sample mixing lines when oxides and mass-bias are properly corrected for. We obtain excellent correspondence (often within 0.5 %) beteween Pt and Pd concentrations calculated using different isotope pairs. The good agreement shows that interferences on a variety of different masses are being effectively corrected for.

7. Measurement precision

Repeat isotopic analyses of the same solution within the same analytical session usually agree to better than 0.5% RSD producing minimal errors in the final ID concentration calculation. For very small sample signals, <1000 cps, repeat analyses of solutions agree to better than 5% i.e., close to counting statistics. Experiments with unspiked samples showed that efficient removal of matrix elements by the column separation procedure ensured very similar mass-bias effects for sample analytes compared to standard solutions.

samples during the day to monitor sensitivity and mass-bias drift, which is usually negligible. Dried column cuts containing PGE fractions are taken up in 3.5% HNO_3 2 to 3 hours before analysis and transferred to micro-centrifuge tubes for analysis. Volumes depend on which elements are being analysed in a particular column cut and which nebuliser is being used. For cross-flow nebulisation with up-take rates of c. 1 mL/minute, 1.5 mLs of solution is typically used. For micro-concentric nebulisers fitted to desolvating systems 0.2 to 0.4 mL is sufficient, depending on the number of masses to be measured.

As noted above, significant amounts of Ir elute in the Pt column fraction. In addition, for certain rock types, Ru shows irregular behaviour. For this reason we routinely scan for one of the Ru isotopes within the Ir and Pt column cut. If significant amounts of Ru appear in this, or the Re column cut then these cuts can be re-run to measure Ru isotopes.

RF power is commonly 1300W for cross-flow nebulisation but can be lower using the desolvating nebuliser. Ion-lens settings are optimised for the mass-range concerned. We generally analyse samples in batches of element types, with re-optimisation of the instrument between different element batches, to ensure best sensitivity. Peak dwell times are normally 30 to 50 mS. 30 mass sweeps are performed to produce one isotopic ratio and this is repeated 30 times. Following calculation of isotopic ratios, all further data reduction is performed off-line via spread-sheets. Direct elemental and oxide isobaric interferences are corrected for on-line. Oxide generation levels are monitored using pure element solutions prior to analysis. Oxide corrections are trivial when using the desolvating nebuliser.

Ratios measured for the isotope dilution schemes are: $^{101}Ru/^{99}Ru$; $^{105}Pd/^{105}Pd$; $^{187}Re/^{185}Re$; $^{192}Os/^{190}Os$; $^{193}Ir/^{191}Ir$; $^{195}Pt/^{194}Pt$. In addition, we routinely measure the ^{196}Pt, ^{189}Os, ^{108}Pd and ^{101}Ru isotopes as a check on data quality.

8. Results

8.1. Blanks and procedural detection limits

A feature of significant note is the low variation in Carius tube blanks reported compared to those of other techniques (Fig. 1). This facilitates more accurate quantitation of very low abundance samples, provided that they are homogenous on the scale of sampling. Procedural blanks are largely reagent dependent. Os blanks over the period of this study ranged from <1 pg to 7 pg, depending on specific batches of reagents. Ir blanks are generally close to, or below 1 pg, Ru and Re are <10 pg while Pd is close to 10 pg (Fig. 1). During the course of experiments we found considerable (up to 200 pg) amounts of Pt in improperly cleaned borosilicate glass Carius tubes. Such levels have also been reported by Rehkämper et al. (1998) who resorted to using quartz-lined Carius tubes to reduce Pt blank levels to <10 pg (Fig. 1). We have found that rigorous boiling of Carius tubes in aqua regia for 3 hours improves blank levels to between 10 - 25 pg which is adequate for most of our purposes. In addition to being significantly more expensive than borosilicate glass Carius tubes, those made of quartz, or with quartz liners are much more liable to failure. Carius tubes made from the same batch of borosilicate glass and cleaned in the same manner give consistent blanks. We estimate procedural detection limits (3* std deviation) of c. 3 pg/g for Os and Ir, 5 pg/g for Re, Ru and Pd and 15 pg/g for Pt. These levels are adequate for most silicate magmatic rocks and sediments and are considerably better, by several orders of magnitude, than most sodium peroxide or Ni-S fusion procedures, with the exception of those reported by Ravizza and Pyle (1997).

8.2. Accuracy and precision

Before examining the results obtained by our PGE analytical method it is useful to outline possible factors affecting the accuracy and reproducibility of PGE analytical data. McDonald (1998) has recently stressed the importance of performing replicate analyses of samples and

standards in assessing PGE data, particularly the significance of inter-element fractionations. In terms of analytical standards, few suitable non-ore ICP-MS standards have been sufficiently characterised to effectively evaluate accuracy in the 1 to 5 ppb range and below. Analysis of "established" ore and mineralised standards using conventional (Jackson et al., 1990) and new PGE analytical techniques (Rehkämper and Halliday, 1997; Yi and Masuda, 1996) show significant discrepancies between "accepted" values and those actually obtained. In other studies where low abundance PGE standards have been analysed, relatively poor reproducibility, or lack of adequate documentation of reproducibility mean that, in many instances, it is difficult to know whether the source of the discrepancy is a poorly constrained "accepted" value, problems with homogeneity of the reference material, problems with the experimental technique, or combinations of all three. Because of the relatively small number of laboratories carrying out routine PGE analysis, and the diversity of analytical techniques that these laboratories employ, reference material rocks tend not to be as well characterised for PGEs compared to other elements commonly used in geochemistry. As such, evaluation of a technique solely by comparison with "reference material" rocks is not necessarily the optimal method of evaluating a given analytical technique.

Most published analytical methods for PGEs quote reproducibilities expressed as 1 sigma relative standard deviations (or coefficient of variation). For evaluation of data at higher confidence levels we express the reproducibility of previously published data, as well as our own, as 2 times the relative standard deviation (2* RSD). For most established PGE analytical techniques applied to common geological materials, reproducibility is on the order of between 20 to > 100% 2*RSD's (McDonald, 1998), i.e., considerably worse than other element groups commonly analysed in geochemistry. Factors contributing to these problems have been discussed by McDonald (1998). Here we will concentrate specifically on the issue of powder homogeneity, a particularly troublesome aspect of PGE analytical chemistry.

In rock powders where the elements of interest are largely contained within a few heterogeneously distributed grains, such as PGEs contained predominantly in trace phases, it is

possible to use sampling theory (Kleeman, 1967) to gain some estimate of the theoretical best possible reproducibility of element abundance measurements (Fig. 4). Within silicate rocks, PGEs are often concentrated within PGE minerals, or within Fe-Cu-Ni sulfides. The high concentrations of PGE in these phases compared to the silicate matrix, together with their scarcity, means that sampling of such "nuggets" becomes more difficult with decreasing size of sample aliquot (van Loon and Barefoot, 1991; McDonald, 1998; Fig. 4). For rock powders crushed to -120 mesh size, where PGEs are wholly contained in "nuggets" that are c. 0.05 vol. % abundant, it is unlikely that abundance measurements can be made that are reproducible to better than 5-6 % (2 sigma RSD) when sampling at the 1 g level. Powders crushed to finer grain size (-200 mesh) are potentially more homogenous and so 1 g aliquots may give reproducibilities of the order of 2 to 3 % (Fig. 4). Larger sample aliquots clearly give improved theoretical sampling statistics and this has been demonstrated for diminishing sample aliquots of standards analysed by Ni-S fire assay (McDonald, 1998).

Two caveats should be borne in mind when considering the simple theoretical approach summarised in Fig. 4. One is that PGEs may be distributed between a variety of phases and this would improve sampling probabilities. On the other hand, it is unlikely that many rocks even approach being perfectly homogenised during preparation and this will act to make matters worse, hence the theoretical calculations appear to offer only a guide to likely best attainable results for given sample sizes.

8.3. Reference material komatiite WITS-1.

We selected the komatiite WITS-1, a reference material recently characterised for PGEs (Tredoux and McDonald, 1996), to evaluate our analytical technique, plus repeat analyses of unknown samples. This standard was selected because its PGE abundance range is within that of the unknowns that we routinely measure and because although not in widespread use, it is one of the best documented of PGE reference materials. Our data are for 1g sample aliquots. Sampling statistics affecting this sampling size can be estimated from Fig. 4. Taking the data

for WITS-1 presented in Table 3, there are 2 apparent groups of elements, those that reproduce well, better than 15% (2 sigma RSD), i.e., Ir, Os and Ru, and those that show worse reproducibilties, of around 20% for Re, Pt and 42% for Pd. Os and Ru reproduce exceptionally well for PGE analyses (7.5 and 8.8% 2 sigma RSD), being close to a factor of 2 within the scatter expected purely on the basis of sample heterogeneties (Table 3; Fig. 4). The mean Ru, Ir and Os concentrations are within error of the mean values suggested for WITS-1 by McDonald (1998), Table 3; our value for Ru being closer to the value of 5.1 ppb originally suggested by Tredoux and McDonald (1996). Our value for Os obtained by DIN-ICP-MS agrees very well with that obtained using the same chemical separation techniques and N-TIMS analysis (Table 2) and we suggest that the mean of both data sets, i.e. 1.08 +/- 0.05, is more likely to be the real value than that given on the basis of preliminary data by Tredoux and McDonald (1996) and McDonald (1998). No previous data has been published for Re on WITS-1 and we put our value forward as an initial value, noting the relatively poor reproducibility. This variability in WITS-1, together with the fact that the $^{187}Os/^{188}Os$ ratio is unsupported by its Re concentration (Pearson, unpublished), suggests the likelihood of post-crystallisation Re loss, possibly during the silicification and greenschist metamorphism identified by Tredoux and McDonald (1996).

Our mean values for Pt and Pd are both lower than those given by McDonald (1998). The mean value for Pd is within 2 sigma error limits of the accepted value. We note that Tredoux and McDonald (1996) originally identified two populations of data in their initial characterisation of this rock, one with substantially lower Pd (4.2 +/- 2.4 ppb, 2 sigma) than the "preferred" value. This may suggest that WITS-1 is in some way heterogeneous with respect to Pd, and that our smaller sampling size is much more sensitive to this than the fire-assay methods used by Tredoux and McDonald (1996). Alternatively, WITS-1 may contain mineral phases rich in Pd that our digestion technique cannot consistently access. Similar reasoning and possibilities might be used to explain the discrepancy between our much lower mean value for Pt of 6.3 +/- 1.2 ppb and the value of 11.8 +/- 3.6 ppb given by McDonald (1998). Details of blank variations are not provided in the compilation of reference data for

WITS-1 and so it is difficult to evaluate whether higher Pt values for the values quoted by Treadoux and McDonald (1996) could be affected by elevated analytical blanks. Our lower value for Pt is within the range of mean values quoted for the different laboratories using in the characterisation of WITS-1 by Treadoux and McDonald (1996).

The possibility for disturbance of some of the more mobile PGEs, enhancing heterogeneity, should be considered in the light of the above comments concerning Re. Currently we favour powder heterogeneity as the most likely cause of the discrepancy between our value for Pt and the mean quoted by Treadoux and McDonald (1996). The good reproducibility of Pt shown by unknowns, including the spinel peridotite GP13, gives us confidence that our method works for Pt in a wide variety of rock types and leads us to believe that the Pt discrepancy between our values and those reported by Tredoux and McDonald (1996) for WITS-1 is not an artifact of our analytical method. Having noted the difference in mean concentration values for WITS-1, we are more encouraged by the fact that the Pt/Pd and Ir/Os ratios calculated for both sets of mean values in Table 3, obtained by very different techniques on quite different sampling aliquot sizes, agree within error.

8.4. Unknowns

The reproducibility of our method for Re and the PGEs was also assessed by analysis of unknown samples. We selected a variety of rocks, ranging from a spinel lherzolite to volcanic rocks, with widely ranging PGE concentrations, so that we could evaluate reproducibility as a function of concentration (Fig. 5). Five replicates of the spinel lherzolite, GP13, from the Beni Bousera peridotite massif, were analysed. PGE analyses of the volcanic rocks are only duplicated and hence reproducibility has not been as thoroughly evaluated as for WITS-1.

In contrast to the relatively poor reproducibility of Pt in WITS-1, 5 replicates of the spinel lherzolite GP13 gave a 2 sigma RSD of 13% for Pt and a mean value of 6.86 ppb; comparable to typical orogenic spinel lherzolites analysed by other methods (Gueddari et al., 1996; Pattou

et al., 1996; mean Pt = 6.5 +/- 0.9 ppb). This level of reproducibility, and the similarity of the Pt value for GP13 to that expected for this type of rock, indicates to us that our technique gives accurate and precise Pt data. Some heterogeneity appears to be present in GP13 but it is of a more systematic nature than that shown by WITS-1 in that the highest Pt values for GP13 are also accompanied by higher Os and Ir values in the same sample digestion (GP13D). Overall Os and Ir reproducibility are affected by the GP13D replicate, which gave systematically higher values than the other dissolutions and slightly different PGE ratios (Table 4). It is possible that some of the variation seen in this sample originates from incomplete digestion of spinels during the Carius tube attack. Excluding this replicate (on an arbitrary basis) reduces the RSD values for GP13 by a factor of 2 for most PGEs. Even including the GP13D replicate the level of reproducibility for all PGEs analysed compares very favourably with other analytical techniques.

The first group of picrites, GP 5, 7 and 10 (Table 4), all have PGE concentrations above 1 ppb and Re concentrations between 0.18 and 0.48 ppb. Bearing in mind the limitations of duplicate analyses, replicates for 3 different picrite samples show similar levels of reproducibility for all PGEs, including Re. Two sigma RSDs are better than 5% for all elements, except Ru at 8.4%, and reproducibilties are better than 6% for Re/Os and Pt/Pd ratios. Os/Ir shows excellent replication (1.6%). Replicate pairs are extremely coherent on chondrite-normalised PGE plots (Fig. 5). Average reproducibility for this suite is within a factor of 2 of that expected for sampling of 1 g powder aliquots containing sparsely distributed PGE-rich nuggets (Fig. 4). Sub-% replication of some elements in certain samples probably indicates that these PGEs are more evenly distributed between mineral phases than the level assumed in the simple sample theory calculations that produced Fig. 4 . The implication of this data is that Carius tubes are highly effective at accessing PGEs contained with minerals in this type of volcanic rock.

The second "unknown" sample group is a suite of 2 picrites and 2 andesites from the Lesser Antilles arc (sample pre-fix Gd). They have Pt and Pd levels from 4 to < 1 ppb and Ru, Ir and Os are all substantially less than 1 ppb, with Ir in andesite GP17 being <5 ppt, i.e., close to

detection limits. Even at such low Ir levels, the data reproduce very well compared to reproducibilities reported for similar rocks by Ravizza and Pyle (1997) and their chondrite normalised PGE patterns are very similar. Even when both Os and Ir are at sub 20 ppt levels, the sense of their relative Os/Ir fractionation shows good replication. Reproducibility of inter-element PGE ratios is clearly not as good as in the GP picrite suite but in general reproduce well (Table 4) compared to data for samples with similar concentrations analysed by other methods. Extensive comparisons are not possible because of a scarcity of published data at this concentration level and a common lack of documented analytical replicates (see McDonald, 1998, for more discussion of the latter point). The decrease in analytical precision for Re and PGEs compared to the GP picrite suite is mostly attributable to lower concentrations. This effect of decreasing concentrations on analytical reproducibility is well illustrated by Re which has a 2 sigma RSD of under 2% for Gd17 (c. 0.35 ppb Re) compared to a value of 20 % for Gd 11 (close to 10 ppt Re).

For rocks with very low levels of some PGEs. e.g., andesite Gd 25, precision for some elements shows a corresponding decline with poor reproducibility for Ir, which is below likely detection limits (Table 4, Fig. 5). Pd also shows relatively poor replication, however, even at these low levels, the general sense of inter-element PGE fractionations are consistent. Re in most of our unknowns replicates very well , even at the 10 ppt level (Table 4, Fig. 5) and in general, better than in WITS-1, lending credence to suspicion that alteration has accentuated heterogeneity for some elements in this rock.

9. Conclusions

Using combined solvent-extraction and anion-exchange pre-concentration techniques coupled with isotope dilution, it is possible to separate Re, Os, Ir, Ru, Pt and Pd from the same sample digestion, allowing Re-Os isotopic analysis and PGE determination on the same sample aliquot. From the above experiments we conclude that our PGE analytical technique compares very favourably with existing analytical methods for the volcanic rocks we have analysed and

allows routine precise analysis of rocks with very low (<<1 ppb) abundances of PGEs on standard quadrupole plasma mass spectrometers. The enhanced sensitivity of magnetic-sector multi-collector plasma mass spectrometers should increase sensitivity further if blanks can be concomitantly decreased. Ultimate precision and accuracy are strongly influenced by potential sample heterogeneity for small sample sizes (Fig. 4).

Analytical reproducibility is dependent on PGE levels and rock type. The method allows confidence to be place in inter-element PGE fractionations in rocks with << 1ppb of a given PGE. As shown by Shirey and Walker (1995) and McDonald (1998), heterogeneity of PGEs will vary greatly in different rock types. Ordinary Carius tubes are mostly limited to sample sizes of c. 5 g (Shirey and Walker, 1994) and so the technique will be subject to greater sampling errors than fusion techniques capable of digesting much larger sample sizes. However, the procedure that we have developed offers the opportunity to obtain both Re-Os isotopic measurements and PGE analysis (except Rh) on very low abundance rocks that may not be amenable to other methods of analysis.

Acknowledgments

We gratefully acknowledge the extensive help given by Chris Ottley with the mass spectrometry procedures during the course of this study. Much helpful guidance on PGE chemistry was initially provided by John Morgan. Iain McDonald supplied ready advice on many aspects of PGE analytical chemistry and standards. Gordon Irvine is thanked for assistance with aspects of the latter parts of chemistry development and for supplying replicate analyses of GP13. We are grateful to NERC for studentship funding (SJW) during this study. The manuscript was improved by comments from Anthony Cohen and an anonymous reviewer.

References

Anbar, A.D., Papanastassiou, D.A., Wasserburg, G.J., 1997. Determination of iridium in natural waters by clean chemical extraction and negative thermal ionisation mass spectrometry. Anal. Chem., 69, 2444-2450.

Barovich, K.A., Beard, B.L., Cappel, J.B., Johnson, C.M., Kyser, T.K., Morgan, B.E., 1995. A chemical method for hafnium separation from high-Ti whole-rock and zircon samples. Chem. Geol., 121, 303-308.

Cocherie, A., 1986. Determination of the noble metals in chromites and other geological materials by radiochemical neutron activation analysis. J. Radioanal. Chem., 113, 133-143.

Cohen, A.S., Waters, F.G., 1996. Separation of osmium from geological materials by solvent extraction for analysis by thermal ionisation mass spectrometry. Anal. Chim. Acta, 332, 269-275.

Colodner, D.C., Boyle, E.A., Edmond, J.M., 1993. Determination of rhenium and platinum in natural waters and sediments and iridium in sediments by flow injection isotope dilution inductively coupled plasma mass spectrometry. Analytical Chemistry, 65, 1419-1425.

Cotton, F.A., Wilkinson, G., 1988. Advanced Inorganic Chemistry. 1455 p. Wiley, New York.

Creaser, R.A., Papanastasio, D.A., Wasserburg, G.J., 1991. Negative thermal ion mass spectrometry of osmium, rhenium and iridium. Geochim. Cosmochim. Acta., 55, 397-401.

Crocket, J.H., Keays, R.R., Hsieh, S., 1968. Determination of some precious metals by neutron activation analysis. J. Radioanal. Chem., 1, 487.

Ely, J.C., Neal, C.R., O.Neill, J.A., Jain, J.C., 1999. Quantifying Platinum Group Elements (PGEs) and Gold in geological samples using cation exchange pretreatment and ultrasonic nebulisation inductively coupled plasma-mass spectrometry (USN-ICP-MS). Chem. Geol. 157, 219-234.

Enzweiler, J., Potts, P.J., Jarvis, K.E., 1995. Determination of platinum, palladium, ruthenium and iridium in geological samples by isotope dilution inductively coupled plasma

mass spectrometry using a sodium peroxide fusion and tellurium co-precipitation. Analyst, 120, 1391-1396.

Evans, N.J., Gregoire, D.C., Goodfellow, W.D., McInnes, B.I., Miles, N., Veizer, J.. 1993. Ru/Ir ratios at the Cretaceous-Tertiary boundary: implications for PGE source and fractionation within the ejecta cloud. Geochim. Cosmochim. Acta, 57, 3149-3158.

Gregoire, D.C., 1988. Determination of platinum, palladium, ruthenium and iridium in geological materials by ICP-MS with sample introduction by electrothermal vaporization. J. Anal. At. Spectrom., 3, 309-314.

Gregoire, D.C., 1990. Sample introduction techniques for the determination of osmium isotope ratios by inductively coupled plasma mass spectrometry. Anal. Chem,, 62(141-146).

Gueddari, K., Piboule, M., Amosse, J., 1996. Differentiation of platinum-group elements (PGE) and of gold during partial melting of peridotites in the lherzolitic massifs of the Betico-Rifean range (Ronda and Beni Bousera). Chem. Geol., 134, 181-197.

Hall, G.E.M., Pelchat, J.C., 1994. Analysis of geological materials for gold, platinum and palladium at low ppb levels by fire-assay ICP mass spectrometry. Chem. Geol., 115, 61-72.

Hauri, E., Hart, S.R., 1993. Re-Os isotope systematics in HIMU and EMII ocean island basalts. Earth Planet. Sci. Lett., 114, 253-271.

Heumann, K.G., 1988. Isotope dilution mass spectrometry. In F. Adams, Ed. Inorganic Mass Spectrometry, p. 301-376. John Wiley, New York.

Heuzen, A.A.v., Hoekstra, T., Wingerden, B.v., 1989. Precision and accuracy attainable with isotope dilution analysis applied to inductively coupled plasma mass spectrometry: theory and experiments. J. Anal. Tom. Spectrom., 4, 483-489.

Hoffman, E.L., Naldrett, A.J., Van Loon, J.C., Hancock, R.G.V., Mason, A., 1978. The determination of all the platinum group elements and gold in rocks and ore by neutron activation analysis after preconcentration by a nickel sulfide fire-assay technique of large samples. Anal. Chim. Acta, 102, 157-166.

Hulbert, L.J., Gregoire, D.C., 1993. Re-Os isotope systematics of the Rankin Inlet Ni ores; an example of the application of ICP-MS to investigate Ni-Cu PGE mineralisation, and the potential use of Os isotopes in mineral exploration. Can. Miner. 31, 861-876.

Jackson, S.E., Fryer, B.J., Gosse, W., Healey, D.C., Longerich, H.P., Strong, D.F., 1990. Determination of the precious metals in geological materials by inductively coupled plasma-mass spectrometry (ICP-MS) with nickel sulphide fire-assay collection and tellurium co-precipitation. Chem. Geol., 83, 119-132.

Jarvis, I., Totaled, M., Jarvis, K., 1997a. Assessment of Dowel 1-X8-based anion-exchange resin procedures for the separation and determination of ruthenium, rhodium, palladium, iridium, platinum and gold in geological samples by inductively coupled plasma mass spectrometry. Analyst, 122, 19-26.

Jarvis, I., Totland, M., Jarvis, K., 1997b. Determination of the platinum-group elements in geological materials by ICP-MS using microwave digestion, alkali fusion and cation exchange chromatography. Chem. Geol., 143, 27-42.

Juvonen, R., Kallio, E., Lakona, T., 1994. Determination of precious metals in rocks by inductively coupled plasma mass spectrometry using nickel sulphide concentration. Comparison with other pre-treatment methods. Analyst, 119, 617-621.

Kleeman, A., 1967. Sampling error in the chemical analysis of rocks. Journal of the Geological Society of Australia, 14(I), 43-47.

Korkisch, J., 1989. Handbook of ion exchange resins: Their application to analytical inorganic chemistry. CRC Press.

Korkisch, J., Klakl, H., 1968. Anion-exchange behaviour of the platinum metals and gold in hydrochloric acid-organic solvent media. Talanta, 15, 339-346.

Martin, C.E., 1990. Rhenium-Osmium Isotope Geochemistry of the Mantle, p. 170. Yale University.

McDonald, I., 1998. The need for a common framework for collection and interpretation of data in Platinum-Group Element Geochemistry. Geostandards Newsletter, 22, 85-91.

McDonald, I., Hart, R.J., Tredoux, M., 1994. The analysis of the platinum group elements in South African and kimberlites by nickel sulphide fire assay and neutron activation analysis. Anal. Chim. Acta., 289, 237-247.

McDonough, W.F., Sun, S.S., 1995. The composition of the Earth. Chem. Geol., 120, 223-253.

Meadows, J.W.T., Marlack, G.M., 1962. Radiomchemical determination of ruthenium by solvent extraction and preparation of carrier free ruthenium activity. Anal. Chim., 34, 89-91.

Morgan, J.W., 1965. The simultaneous determination of rhenium and osmium in rocks by neutron activation analysis. Anal. Chem. Acta, 32, 8-16.

Morgan, J.W., Golightly, D.W., Dorrzapf, A.F., 1991. Methods for the separation of rhenium, osmium and molybdenum applicable to isotope geochemistry. Talanta, 38, 259-265.

Parry, S.J., 1980. Simultaneous determination of the noble metals in geological samples by radiochemical neutron activation analysis. Analyst, 105, 1157-1162.

Pattou, L., Lorand, J.P., Gros, M., 1996. Non-chondritic platinum-group element ratios in the Earth's mantle. Nature, 379, 712-715.

Pearson, D.G., Ottley, C.J., Woodland, S.J., 1999. Precise measurement of Os by direct injection ICP-MS. In Holland, J.G., Tanner, S.C., (Eds). Plasma source mass spectrometry: New developments and applications. Royal Society of Chemistry special publication no 234, 267-276.

Petrie, R.K., Morgan, J.W., 1982. Anion-exchange separation of Pt and Pd using perchloric and hydrochloric acid solutions. J. Radioanal. Chem., 74, 15-23.

Ravizza, G., Pyle, D., 1997. PGE and Os isotopic analyses of single sample aliquots with NiS fire assay preconcentration. Chem. Geol, 141, 251-268.

Rehkämper, M., Halliday, A.N., 1997. Development and application of new ion-exchange techniques for the separation of the platinum group and other siderophile elements from geological samples. Talanta, 44, 663-672.

Rehkämper, M., Halliday, A.N., Wentz, R.F., 1998. Low-blank digestion of geological samples for platinum-group element analysis using a modified Carius tube design. Fresnius. J. Anal. Chem., 361, 217-219.

Roy-Barman, M., Allegre, C.J., 1995. 187Os/186Os in oceanic island basalts: tracing oceanic crust recycling in the mantle. Earth Planet. Sci. Lett., 129, 145-161.

Shirey, S.B., Walker, R.J., 1995. Carius tube digestions for low-blank rhenium-osmium chemistry analysis. Anal. Chem. 67, 2136-2141.

Shirey, S.B., Walker, R.J., 1998. The Re-Os isotope system in cosmochemistry and high-temperature geochemistry. Ann. Rev. Earth Planet. Sci. 26, 423-500.

Sun, M., Jain, J.S., Zhou, M.F., Kerrich, R., 1993. A procedural modification for enhanced recovery of precious metals (Au, PGE) following nickel sulphide fire assay and Te-coprecipitation. Application for analysis of geological samples by ICP-MS. Can. J. Appl. Spectrosc., 38, 103-108.

Surasiti, C., Sandell, E.B., 1960. Determination of submicrogram quantities of ruthenium by catalysis of the Cerium (IV)-arsenic (III) reaction. Anal. Chim. Acta, 22, 261-269.

Tredoux, M., McDonald, I., 1996. Komatiite WITS-1, low concentration nobel metal standard for the analysis of non-mineralised samples. Geostandards Newsletter, 20, 267-276.

van Loon, J.C., Barefoot, R.R., 1991. Determination of the precious metals. 276 p. John Wiley, Chichester.

Völkening, J., Walczyk, T., Heumann, K.G., 1991. Osmium isotope ratio determinations by negative thermal ionization mass spectrometry. International Journal of Mass Spectrometry and Ion Processes, 105, 147-159.

Walzck, T., Heumann, K.G., 1993. Iridium isotope measurements by negative thermal ionisation mass spectrometry and atomic weight of iridium. Int. J. Mass. Spec. Ion Proc., 123, 139-147.

Woodland, S. J., Pearson, D.G., 1999. Analysis of PGEs by ICP-MS: A comparison between fire-assay and carius-tube anion-preconcentration methods, In: Holland, J. G., Tanner, S. D. (eds) Plasma Source Mass Spectrometry - New Developments and Applications. Roy. Soc. Chem. Special Publication No. 234, 267-276.

Yi, Y.V., Masuda, A., 1996. Simultaneous determination of ruthenium, palladium, iridium and platinum at ultratrace levels by isotope dilution inductively coupled plasma mass spectrometry in geological samples. Anal. Chem., 68, 1444-1450.

Figure Captions

Fig. 1. Comparison of total procedural PGE blanks in pg/g for Ni-S fire assay, sodium peroxide fusion/acid dissolution and Carius tube digestions. Only methods that obtain multiple PGEs are illustrated. Dots show individual blanks for a range of studies. Data for Ni-S fire assay from Jackson et al. (1990), Juvonen et al. (1994), Parry (1980), Patou et al. (1996) Ravizza and Pyle (1997), Sun et al. (1993) and Woodland and Pearson (1999). Sodium peroxide/acid dissolution data from Enzweiler et al. (1995), Evans et al. (1993) Gueddari et al. (1996), Yi and Masuda (1996). Carius tube data from this study plus lower points for Pt and Pd from Rehkamper et al (1998).

Fig. 2. Flow chart describing PGE chemical separation procedure. Brackets labeled 1 and 2 indicate that these fractions may be combined together to elute Ir with Pt in fraction 1 and Ru, Re and Pd in fraction 2.

Fig. 3. Mass bias per atomic mass unit for measured PGE isotope ratios. Each data point represents between 5 and 12 separate analyses of standard solutions in the 0.1 to 10 ng/g concentration range. Error bars are 2 standard deviations of the mean standard value for each session. Dashed line indicates the overall mean for the plotted values.

Fig. 4. Sampling error for a single mineral phase (relative deviation at the 95% confidence level) in a powdered rock versus the abundance of the mineral in the rock (volume %) as a function of sample size. Solid lines are for samples powdered to -120 mesh size, dashed lines are for samples powdered to -200 mesh size. The calculation assumes that 1g of sample powdered to -120 mesh size (< 0.167 mm) contains 10^6 grains with density about 2.7 of a *uniform size*. For rocks/minerals of greater density a greater sample weight will be required to attain a given minimum sampling error. PGEs in silicate rocks are often hosted in mineral phases e.g., sulfides, that are less than 0.1 % abundant. If all the PGEs are contained within a

single phase then the sampling error provides a theoretical best possible measurement error for those elements. See Kleeman (1967) for details of calculations.

Fig. 5. Chondrite normalised plots of PGE abundances in replicate analyses of "unknowns" from Table 4. Normalising factors from McDonough and Sun (1995).

Table 1
Observed interferences in the PGE mass spectrum for geological samples processed by Ni-S fire assay and acid dissolution and analysed in a variety of acid media.

Interference	PGE isotope	Interference	PGE isotope
Direct		**Chlorides**	
^{100}Mo (9.63%)	^{100}Ru*	$^{62}Ni^{37}Cl$	^{99}Ru
^{106}Cd (1.25%)	^{106}Pd*	$^{64}Ni^{35}Cl$	^{99}Ru
^{108}Cd (0.89%)	^{108}Pd*	$^{64}Ni^{37}Cl$	^{101}Ru
^{187}Os (@)	^{187}Re*	$^{65}Cu^{35}Cl$	^{100}Ru
^{196}Hg (0.15%)	^{196}Pt*	$^{64}Zn^{35}Cl$	^{99}Ru
		$^{64}Zn^{37}Cl$	^{101}Ru
Oxides		$^{66}Zn^{35}Cl$	^{101}Ru
$^{89}Y^{16}O$	^{105}Pd*		
$^{90}Zr^{16}O$	^{106}Pd*	**Argides**	
$^{92}Zr^{16}O$	^{108}Pd*	$^{60}Ni^{40}Ar$	^{100}Ru
$^{90}Mo^{16}O$	^{106}Pd*	$^{61}Ni^{40}Ar$	^{101}Ru
$^{171}Yb^{16}O$	^{187}Re	$^{61}Ni^{38}Ar$	^{99}Ru
$^{176}Yb^{16}O$	^{192}Os	$^{61}Ni^{40}Ar$	^{101}Ru
$^{175}Lu^{16}O$	^{191}Ir	$^{62}Ni^{38}Ar$	^{100}Ru
$^{176}Lu^{16}O$	^{192}Os	$^{63}Cu^{36}Ar$	^{99}Ru
$^{176}Hf^{16}O$	^{192}Os	$^{65}Cu^{36}Ar$	^{101}Ru
$^{177}Hf^{16}O$	^{193}Ir*	$^{65}Cu^{40}Ar$	^{105}Pd
$^{178}Hf^{16}O$	^{194}Pt*	$^{66}Zn^{40}Ar$	^{106}Pd
$^{179}Hf^{16}O$	^{195}Pt*	$^{68}Zn^{40}Ar$	^{108}Pd
$^{180}Hf^{16}O$	^{196}Pt*		

Numerous trivial REE chlorides and oxides not listed. Those corrected for during our measurement procedure, where samples are run in 3.5% HNO_3, are marked with an asterisk. @ ^{187}Os is variable in nature; the correction is always trivial and we use an abundance of 1.6% for young rocks. Use of a desolvating nebuliser reduces all oxides to trivial levels. Solvent extraction minimises ^{190}Os-^{190}Pt and ^{187}Os-^{187}Re isobaric interferences to insignificant levels.

Table 2: Levels of oxide ion generation in the Elan 6000 cross-flow nebuliser with double-pass spray chamber, compared with typical values for a desolvating micro-concentric nebuliser.

	89Y16O/89Y	90Zr16O/90Zr %	92Mo16O/92Mo	177Hf16O/177Hf	178Hf16O/178Hf
Cross-flow nebuliser	0.933	1.66	0.13	1.95	2.08
	0.947	1.63	0.13	1.98	2.14
	0.946	1.60	0.16	2.00	2.10
	0.959	1.63	0.18	1.95	2.10
		1.65		1.99	2.05
		1.65		1.97	2.00
Mean	0.946	1.637	0.150	1.973	2.078
2*SD	0.021	0.043	0.049	0.040	0.097
Cetac Aridus desolvating nebuliser	0.011	0.011	<0.01	0.013	0.013

	90Zr CPS	105Pd/106Pd	[+/-]	Pd conc. ppb
GP-1: X-flow. No oxide correction	51,046	0.0768	0.002	6.98
GP-1: X-flow. Oxide corrected		0.0741	0.002	6.68
GP-1: MCN 6000 (<0.02% ZrO/Zr)	165000	0.07468	0.0014	6.74

Oxide generation calculated from analyses of single element standard solutions. Data are for a typical analytical session. Boxed area shows results of analysing the same sample column elution for Pd isotopes (105Pd/106Pd), after mass-bias correction, in the presence of Zr (given as counts per second) with both cross-flow and Cetac MCN-6000 desolvating nebuliser.
Errors are 2 standard deviations and the resulting Pd concentration calculated from each ratio is given in ppb.

Table 4. Replicate analyses of "unknowns"

Sample	Rock type	Os ppb	Ir ppb	Ru ppb	Pt ppb	Pd ppb	Re ppb	Re/Os	Os/Ir	Pt/Pd	Pt/Ir
GP 13A	Spinel	3.73	3.22	7.04	6.70	5.92	0.325	0.087	1.16	1.1	2.1
GP 13B	peridotite	3.67	3.23	6.72	6.38	5.36	0.335	0.091	1.14	1.2	2.0
GP 13C		3.85	3.41	6.95	7.46	5.43			1.13	1.4	2.2
GP 13D		4.15	4.09	7.34	7.28	5.27			1.02	1.4	1.8
GP 13E		3.72	3.28	6.71	6.65	5.85			1.13	1.1	2.0
RSD 2 sigma		10.2	21.4	7.4	13.3	10.7	4.3	6.2	10.1	20.1	14.9
GP 5 A	Picrite	2.03	1.08	3.14	6.27	4.20	0.180	0.0887	1.88	1.5	5.8
GP 5 B		2.01	1.11	2.95	6.01	4.48	0.179	0.0891	1.82	1.3	5.4
RSD 2 sigma		1.4	3.7	8.8	6.0	9.1	0.79	0.63	4.6	15.1	10.1
GP 7 A	Picrite	2.9	1.58	3.91	9.95	8.57	0.295	0.102	1.84	1.2	6.3
GP 7 B		2.72	1.49	3.66	9.9	8.74	0.286	0.105	1.83	1.1	6.6
RSD 2 sigma		9.10	8.30	9.30	0.71	2.80	4.40	4.70	0.77	3.50	6.6
GP 10 A	Picrite	2.78	1.48	4.26	11.42	11.58	0.482	0.173	1.88	1.0	7.7
GP 10 B		2.79	1.46	4.48	11.44	11.5	0.461	0.165	1.91	1.0	7.8
RSD 2 sigma		0.51	1.90	7.10	0.25	0.98	6.30	6.80	2.40	1.20	1.8
Gd 11 A	Picrite	0.0542	0.0517	0.266	2.20	2.28	0.0112	0.207	1.05	1.0	42.6
Gd 11 B		0.0834	0.0600	0.200	2.16	1.45	0.0129	0.155	1.39	1.5	36.0
RSD 2 sigma		60.0	21.00	40.1	2.60	62.9	20.0	40.7	39.6	60.5	23.7
Gd 12 A	Picrite	0.0431	0.0977		3.970	2.85	0.033	0.766	0.441	1.4	40.6
Gd 12 B		0.0407	0.0819	0.154	3.48	2.82	0.032	0.786	0.497	1.2	42.5
RSD 2 sigma		8.10	24.9		18.6	1.50	4.40	3.80	16.8	17.1	6.5
Gd 17 A	Andesite	0.0170	0.0032	0.092	1.91	0.638	0.362	21.3	5.31	3.0	596.9
Gd 17 B		0.0194	0.0047		1.88	0.673	0.357	18.4	4.13	2.8	400.0
RSD 2 sigma		18.6	53.7		2.20	7.60	2.00	20.6	35.5	9.80	56.0
Gd 25 A	Andesite	0.0156	0.0001*		1.22	0.135	0.0562	3.60		9.0	
Gd 25 B		0.0181	0.0007*	0.1726	1.10	0.0647	0.0554	3.06		17.0	
RSD 2 sigma		21.0	212		14.6	100	2.00	23.0		86.5	

* signifies below detection limits. GP13 is a spinel lherzolite from the Beni Bousera peridotite massif, N. Morocco. Gp series are picrites. Gd series are picrites and andesites from the Lesser Antilles. Ir in Gd 25 is below detection limits.

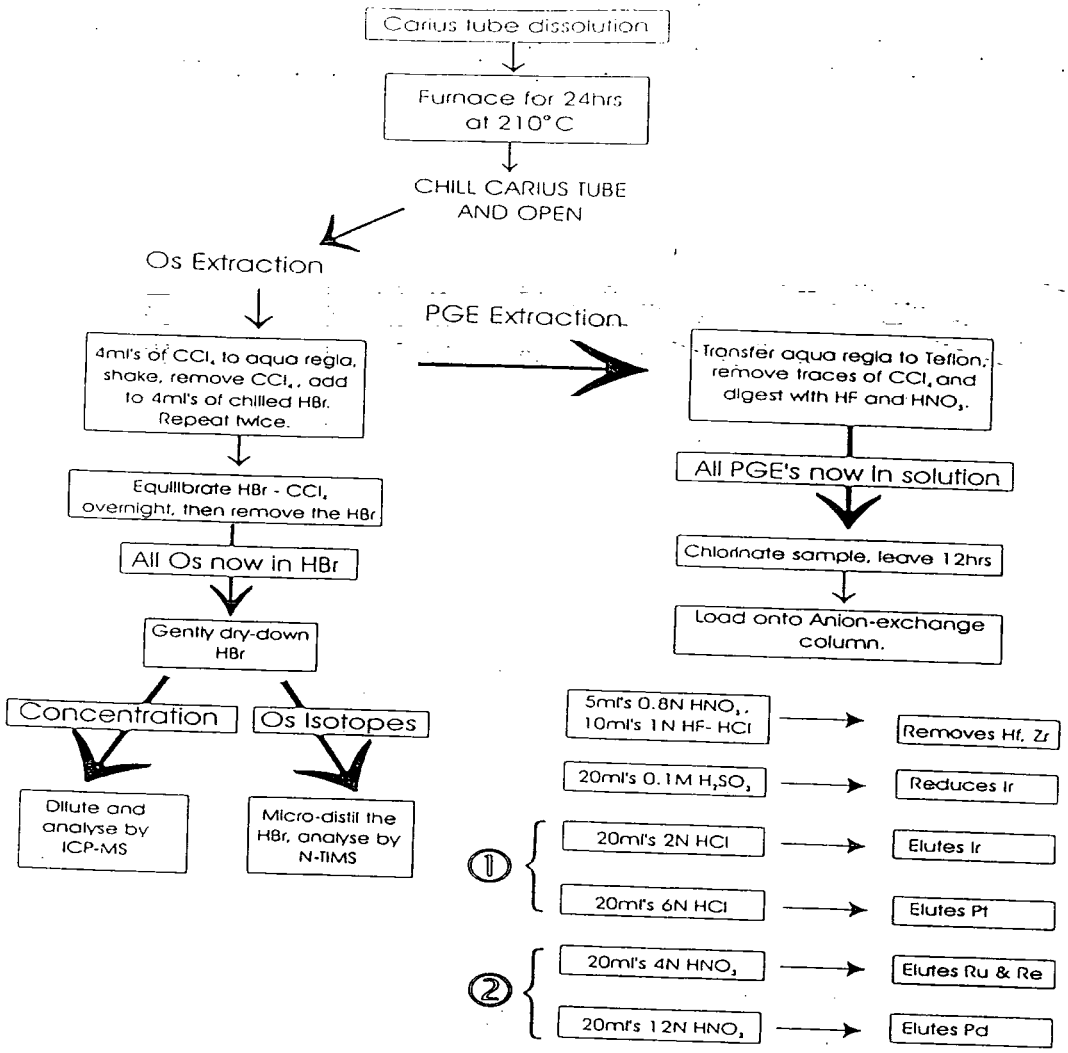
Carius tube dissolution
Furnace for 24hrs at 210°C
CHILL CARIUS TUBE AND OPEN
Os Extraction
4ml's of CCl_4 to aqua regia, shake, remove CCl_4, add to 4ml's of chilled HBr. Repeat twice.
Equilibrate HBr - CCl_4 overnight, then remove the HBr
All Os now in HBr
Gently dry-down HBr
Concentration
Os Isotopes
Dilute and analyse by ICP-MS
Micro-distil the HBr, analyse by N-TIMS
PGE Extraction
Transfer aqua regia to Teflon, remove traces of CCl_4 and digest with HF and HNO_3.
All PGE's now in solution
Chlorinate sample, leave 12hrs
Load onto Anion-exchange column.
5ml's 0.8N HNO_3, 10ml's 1N HF- HCl
Removes Hf, Zr
20ml's 0.1M H_2SO_3
Reduces Ir
1
20ml's 2N HCl
Elutes Ir
20ml's 6N HCl
Elutes Pt
2
20ml's 4N HNO_3
Elutes Ru & Re
20ml's 12N HNO_3
Elutes Pd

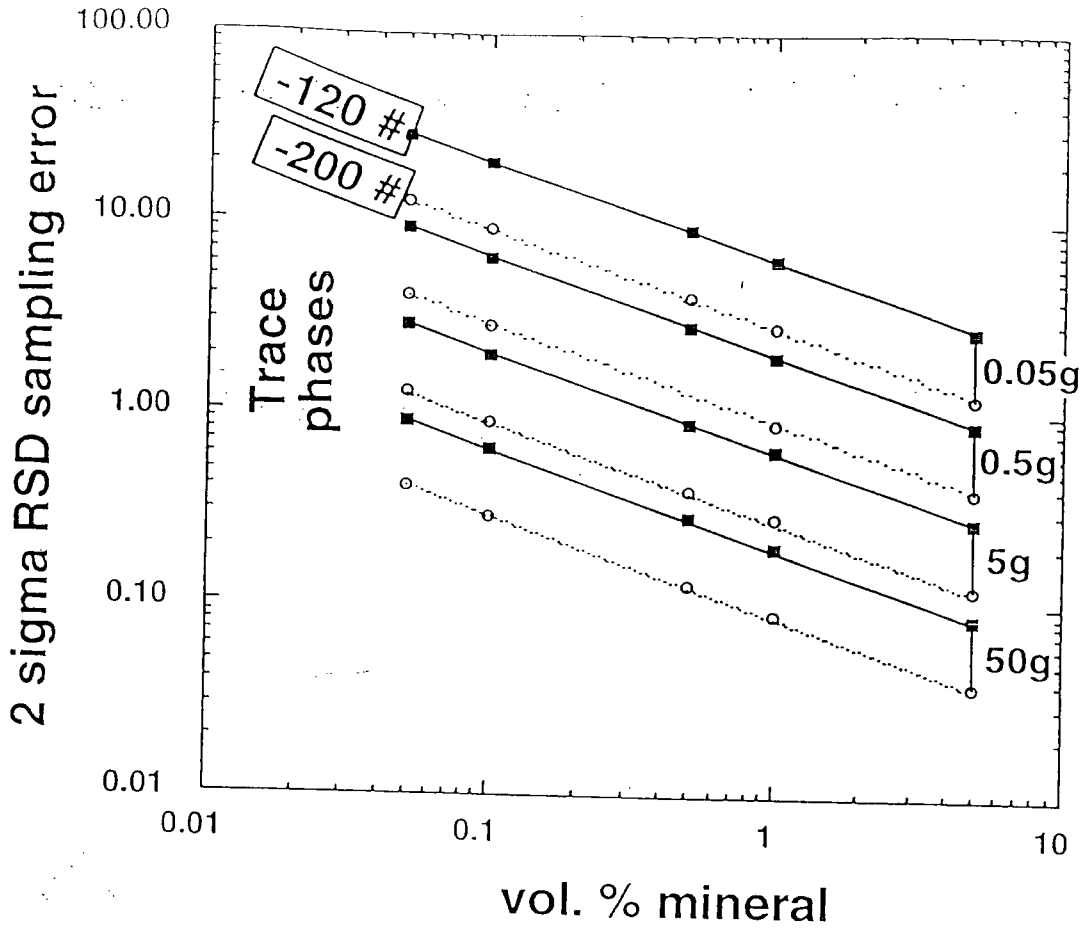
100.00
10.00
1.00
0.10
0.01
2 sigma RSD sampling error
-120 #
-200 #
Trace phases
0.05g
0.5g
5g
50g
0.01
0.1
1
10
vol. % mineral

Fig. 4

single phase then the sampling error provides a theoretical best possible measurement error for those elements. See Kleeman (1967) for details of calculations.

Fig. 5. Chondrite normalised plots of PGE abundances in replicate analyses of "unknowns" from Table 4. Normalising factors from McDonough and Sun (1995).

PRECISE MEASUREMENT OF OSMIUM BY DIRECT INJECTION NEBULISATION ICP-MS

D. G. Pearson, C. J. Ottley and S. J. Woodland

Department of Geological Sciences,
Durham University,
South Rd,
Durham,
DH1 3LE,
UK.

1 INTRODUCTION

The desire for precise and accurate analyses of Os in environmental, geological and planetary sciences comes from a combination of it being one of the Platinum Group elements, which are very useful geochemical tracers, and the use of the ^{187}Re-^{187}Os and ^{190}Pt-^{186}Os isotope systems in geochronology and reservoir tracing[1, 2]. Os can be ionised as negative oxide ions (OsO_3^-) for highly precise isotopic analysis by negative thermal ionisation mass spectrometry;[3, 4] however, this technique is relatively specialised and time consuming. Significant interest exists in analysing Os concentrations, using quadrupole ICP-MS and Os isotopic ratios using the new generation magnetic sector ICP-MS instruments currently available. Such developments have been hampered by analytical problems related to chemical separation techniques and instrument memory. In this contribution we summarise these problems and offer a method of precise, accurate analysis of geological materials to ppt levels using ICP-MS.

2 ANALYTICAL PROBLEMS

Accurate quantitative analysis of Os by ICP-MS in most matrices has proven fraught with difficulty for over a decade. These difficulties are due to a combination of chemical peculiarities that do not lend themselves well to "conventional" analytical chemical procedures and pose significant problems for modern analytical instrumentation. Most problems are a consequence of the difficulty in obtaining solutions where all the Os is in the same oxidation state (or at least the same oxidation state as a given standard solution) and the severe memory effects of Os in commonly used nebulisation systems in ICP s. For ICP-MS, these memory effects compromise the ability to analyse both Os and Re due to the direct isobaric interference of ^{187}Os on ^{187}Re.

For ICP-AES, difficulties arise in standard-sample cross calibration due to large differences in sensitivity, of between 10 to >100 times, between Os in its lower oxidation states (IV and VI) compared to its most oxidised form (VII)[5, 6]. Similar behaviour has

Table 2

Table 2: Levels of oxide ion generation in the Elan 6000 cross-flow nebuliser with double-pass spray chamber, compared with typical values for a desolvating micro-concentric nebuliser.

	89Y16O/89Y	90Zr16O/90Zr %	92Mo16O/92Mo	177Hf16O/177Hf	178Hf16O/178Hf
Cross-flow nebuliser	0.933	1.66	0.13	1.95	2.08
	0.947	1.63	0.13	1.98	2.14
	0.946	1.60	0.16	2.00	2.10
	0.959	1.63	0.18	1.95	2.10
		1.65		1.99	2.05
		1.65		1.97	2.00
Mean	0.946	1.637	0.150	1.973	2.078
2*SD	0.021	0.043	0.049	0.040	0.097
Cetac Aridus desolvating nebuliser	0.011	0.011	<0.01	0.013	0.013

	90Zr CPS	105Pd/106Pd	[+/-]	Pd conc. ppb
GP-1: X-flow. No oxide correction	51,046	0.0768	0.002	6.98
GP-1: X-flow. Oxide corrected		0.0741	0.002	6.68
GP-1: MCN 6000 (<0.02% ZrO/Zr)	165000	0.07468	0.0014	6.74

Oxide generation calculated from analyses of single element standard solutions. Data are for a typical analytical session. Boxed area shows results of analysing the same sample column elution for Pd isotopes (105Pd/106Pd), after mass-bias correction, in the presence of Zr (given as counts per second) with both cross-flow and Cetac MCN-6000 desolvating nebuliser. Errors are 2 standard deviations and the resulting Pd concentration calculated from each ratio is given in ppb.

been observed for ICP-MS in terms of the relative ionisation efficiencies of reduced versus oxidised Os and has lead to analytical procedures that involve directly distilling Os into the mass spectrometer as OsO_4 vapour[6, 7]. Although large sensitivity increases are to be gained by analysing highly oxidised Os, a major draw back is that Os in this form has the most severe memory effects in the instrument, although memory can also be severe even in reduced solutions. Oxidised forms of Os, particularly OsO_4, are highly reactive, being rapidly adsorbed onto plastic surfaces and even diffusing into Teflon when under pressure[8]. Furthermore, oxidised Os is very volatile (OsO_4 B.P. ~ 110 °C) such that samples prepared in this form must be kept at relatively low temperatures and must be analysed rapidly after preparation to avoid loss of sample. OsO_4 will also photo-reduce if stored, leading to mixed oxidation state solutions that are difficult to analyse.

Large errors can occur in analytical procedures for Os where signal intensities are measured, if the digestion procedure for samples does not render Os in exactly the same oxidation state as that in the standard solution used for instrument calibration[5]. To combat this non-linearity problem and the potential loss of Os from samples due to volatilisation during the digestion stages of any analytical procedure involving oxidants, isotope dilution can be employed. Isotope dilution involves the addition of a known amount of an isotopically enriched spike solution to the sample, usually during the digestion stage if the sample is a solid. Once the spike has been equilibrated with the sample, losses can be tolerated as the ratio of spike to normal isotopes is measured to then calculate the sample concentration. In addition, chemical equivalence between standard solutions and sample is not necessary because isotopic ratios are being analysed, not absolute signal intensities. Solving signal non-linearity problems then leaves the issue of significant instrumental Os memory observed when running samples. Here we evaluate the performance of direct injection nebulisation using a very low dead-volume nebuliser for samples of differing oxidation states compared to a standard cross-flow nebuliser. We find that Carius Tube digestion of isotopically spiked samples followed by solvent extraction of the Os and analysis by direct injection ICP-MS produces reproducibilities for 1g aliquots of a standard rock that are close to the theoretical limits expected from sampling theory.

3 SOLUTIONS: ANALYTICAL CHEMISTRY

Although oxidised Os appears to ionise more efficiently from acid solutions than reduced Os, the high sensitivity of modern plasma mass spectrometers means that, at least for concentration measurements by isotope dilution, obtaining sufficient signal for precise measurement is not a major obstacle. Because of this we chose to adopt a chemical extraction method that ensures that all the recovered Os is in reduced form prior to analysis. This provides two significant advantages; firstly that the extracted Os is stable over long time periods (at least several months) so that immediate analysis is not necessary, and secondly; that sample memory and hence potential cross-contamination in reagent vials and instrumentation is reduced.

Samples are loaded into chilled Carius Tubes followed by an appropriate amount of spike, in this case we use a ^{190}Os spike to minimise disturbance of the natural $^{187}Os/^{188}Os$ ratio that can be used as a reservoir tracer. Error propagation calculations indicate optimal spiking when the spike-sample mixture has a $^{190}Os/^{192}Os$ ratio of close to 2.5. We follow a previously published procedure [9] and emphasise the precautions to be observed when handling and opening sealed Carius Tubes. Most samples are digested in inverse aqua-regia, i.e., approx. 3 parts HNO_3 : 1 part HCl. If samples are organic-rich, care must be taken to use excess HNO_3 to ensure oxidation of Os in the digestion step as this promotes equilibration between the sample and the spike[9]. The Carius Tubes are sealed with a blow-torch and enclosed within thick-walled steel cases with a non-sealing cap, before being placed in an oven at 230 °C. For very organic-rich or carbonate rich materials, significant CO_2 may be evolved leading to elevated pressures in the Carius Tubes. In these cases the oven temperature is reduced to below 200 °C. Decarbonating very carbonate-rich samples is recommended before sealing into Carius Tubes. Following digestion, Os is extracted by partitioning into a non-polar solvent, in this case CCl_4, following the procedures described by Cohen and Waters[10], except that we repeat the extraction 3 times and combine the 3 extracts. Using inverse aqua-regia is essential in ensuring a high yield. We found that using the classical aqua-regia mixture produced erratic, much lower yields than the "inverse" aqua-regia, a feature also observed for the extraction of Ru using similar procedures [11]. After organic extraction, the Os is back-extracted in 9N HBr. When warmed in a sealed vessel the Os is converted to the IV oxidation state and into the $OsBr_6^{2-}$ species. This can be safely stored prior to analysis, ready to be taken up in dilute HNO_3 or HCl.

Procedural blanks are entirely reagent dependant and vary from <1 pg to 7 pg depending on the batches of reagents used. Under the most favourable conditions the detection limits are ca. 1 pg.

4 MASS SPECTROMETRY

4.1 Instrumentation and measurement protocol

A Perkin Elmer Sciex Elan 6000 ICP-MS was used for this study. Operating conditions were routine, with RF power being 1200 watts. The auto-lens function was used for "routine" samples. Mass calibration can be optimised using Re. For cross-flow operation we also found it useful to perform mass bias estimations using either Re or Ir although Ir was most often used, the $^{191}Ir/^{193}Ir$ ratio being closer to the mass range of the two Os isotopes measured, i.e., $^{190}Os/^{192}Os$. Instrumental mass bias was found to vary between 0.7 and 1.2 % per AMU in this mass range and is similar for both the cross-flow nebuliser and the direct injection nebuliser (DIN; Fig. 1).

30 sweeps of the mass range were measured to produce 1 isotopic ratio which was repeated at least 30 times, at 20 mS peak dwell times to give a single sample measurement. Where enough sample remained, this measurement was repeated 2 or 3 times. Relative standard deviations for 1 ppb solutions with normal isotopic ratios ($^{190}Os/^{192}Os$ in natural samples = 0.6438[1]) were ca. 0.5% (2 σ) for each measurement. However, repeated measurements of samples and standard solutions suggests that true precision is as good as 0.2% or better.

The Os-specific nature of the solvent extraction means that isobaric interferences on the Os mass spectra are insignificant but Pt is routinely corrected for on masses 190 and 192. Backgrounds are measured for solutions before analysis of a sample using exactly the same measurement routine as for samples. These on-peak backgrounds are then subtracted from the signal intensities to yield background corrected intensities that are then ratioed. For

Table 3
Replicate analyses of reference material komatiite WITS-1.

	Re ppb	Os ppb	Ir ppb	Ru ppb	Pt ppb	Pd ppb	Re/Os	Ir/Os	Pt/Pd
Accepted	-	1.4	1.5	5.5	11.8	7.6	-	1.1	1.6
range	-					4.1 - 7.6			
2*RSD (%)		11	26.4	25.4	30.4	23.6			
This study									
ICP-MS									
Mean conc.	0.063	1.09	1.44	5.29	6.26	5.59	0.059	1.3	1.4
std. dev. (1s)	0.007	0.04	0.09	0.23	0.61	1.18	0.005	0.1	0.1
2*RSD	20.8	7.5	13	8.8	19.5	42.1	18.4	17.7	16.8
n=	17	9*	18	11#	11#	19			
N-TIMS									
Mean conc.		1.07							
std. dev. (1s)		0.05							
2*RSD (%)		4.9							
n=		9*							
Combined		1.08							
(N-TIMS & ICP)		0.05							
		4.2							

Accepted values are from Tredoux and McDonald (1996), standard deviation is quoted at the 1-sigma level but relative standard deviations (RSD) are quoted at the 2-sigma (95%) confidence level. Results for Os run by both DIN-ICP-MS and N-TIMS are also shown. Different numbers of determinations reflects progressive development of the spike solution. * half samples analysed by N-TIMS, half by ICP-MS. # Only values with 99Ru and 194Pt spike used

[illegible] samples analysed using the DIN background counts are <1% on either mass 190 or 192.

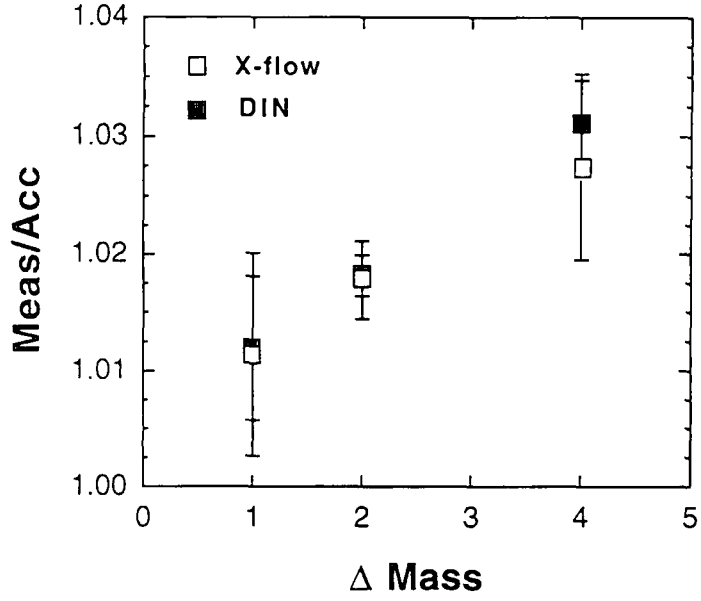

Figure 1 *Mass fractionation for Os isotopes measured by cross-flow nebulisation and DIN relative to an accepted value for $^{192}Os/^{188}Os$ of 3.08271.*

4.2 Cross-flow nebulisation

The cross-flow nebuliser used was the standard model supplied by Sciex which has a Scott-type double pass spray chamber. A typical profile for Os washout is given in Fig. 2, where the sample is introduced in dilute (3%) HNO_3 and washed out with the same solution.

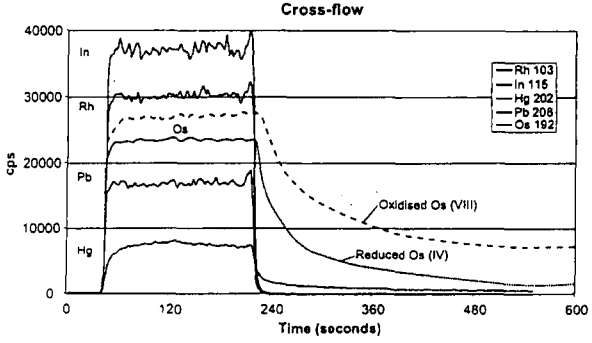

Figure 2 *Cross-flow nebuliser washout profiles for 10 ppb standard solution of Rh, In, Hg and Pb compared to solutions containing Os in either reduced, or oxidised states, note greater sensitivity for Os in VIII oxidation state.*

As has been noted previously by numerous workers, samples show varying washout characteristics, this is probably related to the proportion of Os in the VIII oxidation state, which may vary from sample to sample. The example shown in Fig. 2 compares washout for a standard solution, where Os is probably as $OsCl_6^{2-}$ (IV oxidation state), with that for an organic polymer sample dissolved in concentrated hot HNO_3 and diluted to volume, which contains a high proportion of Os in the VIII oxidation state. The memory for the solution containing oxidised Os appears much worse in this case. We did not quantitatively determine how much of the "enhanced" memory shown by the oxidised solution reflected similar levels of residual Os but greatly enhanced ionisation. Oxidised Os, particularly as OsO_4 is very surface active and is known to cause more severe sample vessel cross-contamination problems than reduced Os. Oxidised Os should stick to the walls of peristaltic tubing, to the spray chamber walls and may even stick to Teflon where large surface areas are involved. Our experiments found most of the Os to be residing in the spray chamber. It is probable that the oxidised solution shown in Fig. 2 shows a component of both increased memory and increased ionisation efficiency. Whatever the relative effects, it is clear that very large proportions of the Os in solution remain in the nebuliser/instrument after an analysis. Sample concentrations of over 50 ppb Os prove particularly difficult to washout, requiring many hours running time to achieve <100 CPS at mass 192, or mass 190 when the samples are spiked.

Our experience has shown that samples containing partially oxidised Os at the 1 ppb level or less, introduced in dilute HNO_3 appear to "wash out" to fairly constant levels, on the order of 500 CPS, in perhaps 10 to 15 minutes. However, in many cases this does not equate to all the Os being washed out of the instrument. If hydrogen peroxide is subsequently introduced, which is particularly effective at re-mobilising any Os adhering in either the oxidised, or reduced form, trapped Os is re-released (Fig. 3).

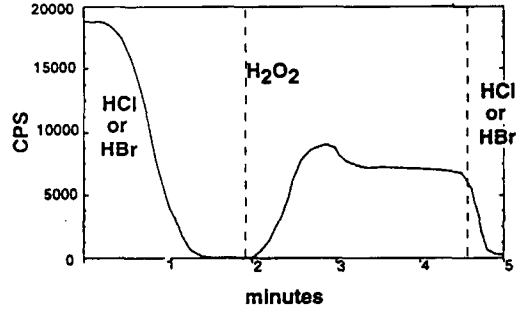

Figure 3 *Schematic diagram illustrating cross-flow nebulisation of a 10 ppb partially oxidised Os solution allowed to wash out with 3% HNO_3 followed by introduction of 30% H_2O_2 solution.*

It may be argued that this residual Os would be unlikely to be re-mobilised if all solutions being eluted through the instrument are kept in a reduced form; however, this is a dangerous strategy as 10's of ng of Os can rapidly accumulate in the instrument with no control on when this Os will be released/remobilised.

Table 4. Replicate analyses of "unknowns"

Sample	Rock type	Os ppb	Ir ppb	Ru ppb	Pt ppb	Pd ppb	Re ppb	Re/Os	Os/Ir	Pt/Pd	Pt/Ir
GP 13A	Spinel	3.73	3.22	7.04	6.70	5.92	0.325	0.087	1.16	1.1	2.1
GP 13B	peridotite	3.67	3.23	6.72	6.38	5.36	0.335	0.091	1.14	1.2	2.0
GP 13C		3.85	3.41	6.95	7.46	5.43			1.13	1.4	2.2
GP 13D		4.15	4.09	7.34	7.28	5.27			1.02	1.4	1.8
GP 13E		3.72	3.28	6.71	6.65	5.85			1.13	1.1	2.0
RSD 2 sigma		10.2	21.4	7.4	13.3	10.7	4.3	6.2	10.1	20.1	14.9
GP 5 A	Picrite	2.03	1.08	3.14	6.27	4.20	0.180	0.0887	1.88	1.5	5.8
GP 5 B		2.01	1.11	2.95	6.01	4.48	0.179	0.0891	1.82	1.3	5.4
RSD 2 sigma		1.4	3.7	8.8	6.0	9.1	0.79	0.63	4.6	15.1	10.1
GP 7 A	Picrite	2.9	1.58	3.91	9.95	8.57	0.295	0.102	1.84	1.2	6.3
GP 7 B		2.72	1.49	3.66	9.9	8.74	0.286	0.105	1.83	1.1	6.6
RSD 2 sigma		9.10	8.30	9.30	0.71	2.80	4.40	4.70	0.77	3.50	6.6
GP 10 A	Picrite	2.78	1.48	4.26	11.42	11.58	0.482	0.173	1.88	1.0	7.7
GP 10 B		2.79	1.46	4.48	11.44	11.5	0.461	0.165	1.91	1.0	7.8
RSD 2 sigma		0.51	1.90	7.10	0.25	0.98	6.30	6.80	2.40	1.20	1.8
Gd 11 A	Picrite	0.0542	0.0517	0.266	2.20	2.28	0.0112	0.207	1.05	1.0	42.6
Gd 11 B		0.0834	0.0600	0.200	2.16	1.45	0.0129	0.155	1.39	1.5	36.0
RSD 2 sigma		60.0	21.00	40.1	2.60	62.9	20.0	40.7	39.6	60.5	23.7
Gd 12 A	Picrite	0.0431	0.0977		3.970	2.85	0.033	0.766	0.441	1.4	40.6
Gd 12 B		0.0407	0.0819	0.154	3.48	2.82	0.032	0.786	0.497	1.2	42.5
RSD 2 sigma		8.10	24.9		18.6	1.50	4.40	3.80	16.8	17.1	6.5
Gd 17 A	Andesite	0.0170	0.0032	0.092	1.91	0.638	0.362	21.3	5.31	3.0	596.9
Gd 17 B		0.0194	0.0047		1.88	0.673	0.357	18.4	4.13	2.8	400.0
RSD 2 sigma		18.6	53.7		2.20	7.60	2.00	20.6	35.5	9.80	56.0
Gd 25 A	Andesite	0.0156	0.0001*		1.22	0.135	0.0562	3.60		9.0	
Gd 25 B		0.0181	0.0007*	0.1726	1.10	0.0647	0.0554	3.06		17.0	
RSD 2 sigma		21.0	212		14.6	100	2.00	23.0		86.5	

* signifies below detection limits. GP13 is a spinel lherzolite from the Beni Bousera peridotite massif, N. Morocco. Gp series are picrites. Gd series are picrites and andesites from the Lesser Antilles. Ir in Gd 25 is below detection limits.

A small number of experiments were performed using a CETAC Technologies MCN-6000 microconcentric desolvating nebuliser coupled to a VG P-54 magnetic sector ICP-MS at the Department of Terrestrial Magnetism, Carnegie Institute of Washington (courtesy of Dr R.W. Carlson). Standard solutions only were analysed on this instrument. Solutions ranging from 10 to 200 ppb were analysed to obtain sufficient signal to make high-precision isotopic measurements using Faraday collectors. At uptake rates of ca. 50 µL per minute, with the Os as $OsCl_6^{2-}$, signals for ^{192}Os ranged up to 1.6 volts and decreased within 2 to 3 minutes to < 1mV. Once the Os signal had apparently died away, a solution of 30% H_2O_2 was washed through the nebuliser producing a ^{192}Os signal approaching 1/3 of the original signal when the sample was being nebulised. This signal was very stable and persistent. If H_2O_2 was replaced with 2N HBr or HCl, the signal died away to <1mV again but returned as soon as the H_2O_2 was re-introduced into the system. Large fractions of the Os entering the nebuliser appeared to be removed onto the desolvating membrane surface. Clearly such attributes are not conducive to memory-free measurement of Os.

4.4 Direct injection nebulisation

For these experiments we used a CETAC Technologies direct injection nebuliser (DIN) with gas displacement pump. The low dead volume of the DIN combined with the all-Teflon nature of almost every component in the sample introduction pathway makes it attractive for use in Os analysis. In Fig. 4 a mass scan for ^{192}Os is shown for a 7.4 ppb solution prepared from an organic sample using hot, concentrated HNO_3, and thus containing a substantial amount of oxidised Os. Peak dwell times are decreased to 5 mS to accurately define the shapes of the profile leading to some apparent signal instability. This sample was run following several others in the same concentration range, within 3 minutes of the previous sample. The profile shows that switching to analyse the carrier solution immediately from a sample does not leave any post-nebuliser instrument contamination. There is a very sharp signal drop off to less than 10% of the former signal in under 5 seconds and this decays to less than 1% of the signal in under 3 minutes. During this time period the sample loop can be washed out independently.

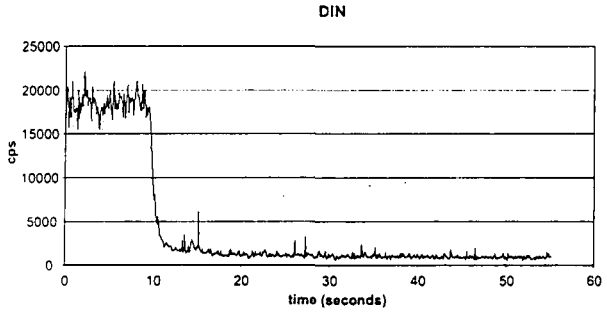

Figure 4 *DIN instrument memory: Signal is monitoring ^{192}Os at 5mS dwell time. Step at 10 seconds illustrates valve switching during nebulisation of a ca. 7 ppb partially oxidised Os solution.*

Sample loop memory is illustrated in Fig. 5, which shows the effect of letting a half full 1 mL sample loop wash out with 3% HNO_3. Signal is reduced to background levels in 5 minutes, or more rapidly if all the Os in the sample loop is used in the analysis. The washout profile in Fig. 5 is for a sample with partially oxidised Os. Our normal sample running protocol using isotope dilution and cross-flow nebulisation for samples in this concentration range, where background signals are required to have decayed to at least <1% of signal, would probably not allow another sample to be run that day. With the DIN however the interval between consecutive analyses would be 5 minutes. Experiments involving rinsing with H_2O_2 indicated that minimal Os was being harboured in the DIN system once the on-peak background had decayed to <<1% of the signal. For samples containing reduced Os, memory is even less significant, allowing samples in the 50 to 100 ppb range to be run. In practice we find that for most geological samples in the 0.1 to 3 ppb range, background signals of between 10 to 30 CPS are achieved within 3 to 5 minutes, enabling high samples throughput without fear of cross-contamination. To ensure thorough washout we routinely switch the inlet valve 2 to 3 times during the washout time to rinse out the very small amount of dead space in the valve volume.

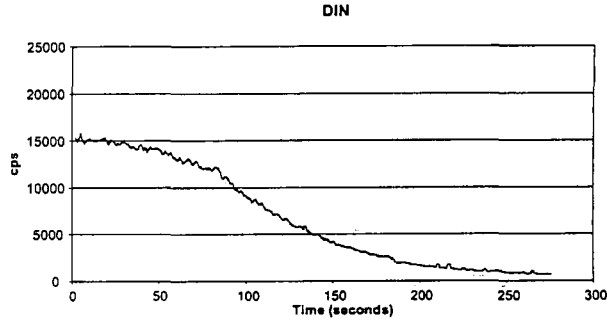

Figure 5 *Washout of a full 1 mL sample loop containing ca. 5 ppb partially oxidised Os solution, the rinsing solution is 3% HNO_3.*

5 SAMPLE REPRODUCIBILITY

Using DIN is clearly the method of choice for analysing Os by ICP-MS. If the same sample is measured at different times of the day, in a given sample batch, isotope ratios can be reproduced to better than 1% providing that instrumental mass-bias has remained constant. This indicates that memory effects are not a significant issue for Os in geological samples in the 0.1 to 10 ppb concentration range using DIN. One test of how well the isotope dilution methodology and DIN technique works is by simple calibration of the spike. This can be reproduced to the 1% (2 σ) level using Carius tube equilibration. However, the ultimate test of how well the analytical protocol works is by analysing real samples.

There are no internationally established geological standards for Os. We have chosen to use a komatiite standard, WITS-1[12] that has ca. 1 ppb Os. Although no certification of this value has been obtained its Os content appears to be very close to 1.1 ppb from isotope dilution measurements using N-TIMS conducted in 2 different laboratories (D.G. Pearson,

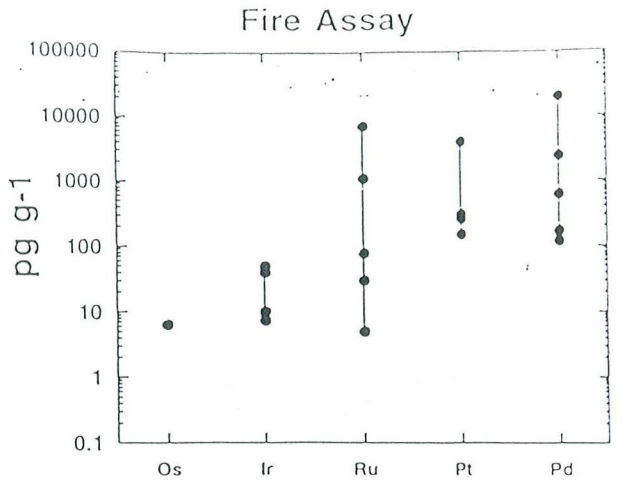
Fire Assay
100000
10000
1000
100
10
1
0.1
pg g-1
Os
Ir
Ru
Pt
Pd

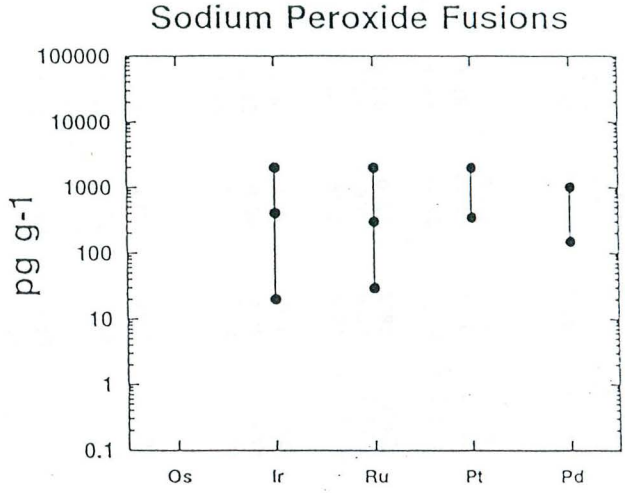
Sodium Peroxide Fusions
100000
10000
1000
100
10
1
0.1
pg g-1
Os
Ir
Ru
Pt
Pd

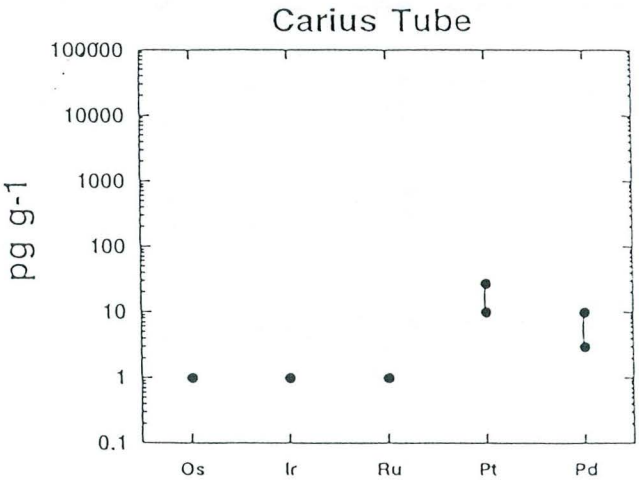
Carius Tube
100000
10000
1000
100
10
1
0.1
pg g-1
Os
Ir
Ru
Pt
Pd

un-published data, S. Shirey, unpublished data). 14 replicates of this sample measured using the DIN give a mean Os concentration of 1.1 ± 0.077 ppb (2 σ SD), or about 7 % overall reproducibility. This level of reproducibility is considerably better than that reported for Os using non-ID fire assay procedures[13]. In addition, our method offers considerably better detection limits due to lower, more consistent blanks. Consideration of simple sampling theory indicates that for the 1 g powder aliquots of standard rock analysed in this study, it is unlikely that reproducibility of concentrations would ever be better than ca. 2 to 3 % (Fig. 6). The reason for this is that in most geological samples, Os is almost entirely contained in sulfide or metal crystals that have a very low abundance in the rock, 0.1 to <0.05 vol. % and are usually heterogeneously distributed in the rock. This is know as the "nugget" effect. Perfectly homogenised powders crushed to -200 # size can only be reproducibly sampled at the 1 g level to between 2 to 3 % given these abundances of sulfide. Hence, if better reproducibility is desired it can often be achieved by increasing sample size, if the nugget effect is a major control on reproducibility. The Carius Tube technique described here can be adapted to digest samples up to ca. 5 g. Above this sample mass special Carius Tube designs have to be used and it may be more practical to use fire-assay techniques.

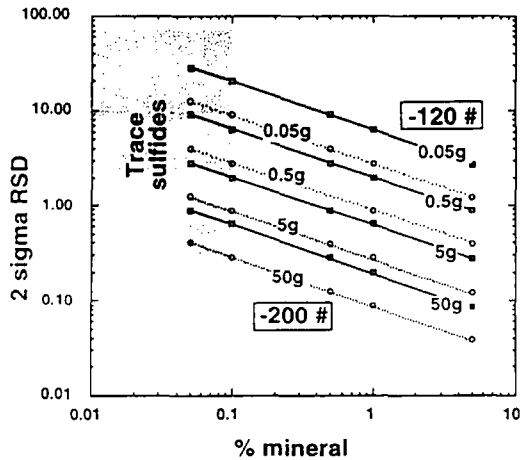

Figure 6 *Theoretical sample reproducibility for an element totally contained with a single mineral in a rock powder (at the 2 sigma level RSD) versus the abundance of that in volume %. Calculations based on theory presented by Kleeman[14]. Solid lines show results for a powder crushed to -120 mesh size, dashed lines show results for powder crushed to -200 mesh size. The likely abundance of Os-bearing sulfides in silicate rocks in shown.*

The negligible effect of Os instrument memory on Re measurements can be gauged from routine analysis of samples and standards in the 50 ppt to 5 ppt range where values are very comparable to those obtained by N-TIMS.

6 SUMMARY

We describe a versatile low-blank chemistry technique suitable for the digestion of Os in a variety of geological samples. The technique is capable of yielding Os blanks of 0.1 ppt or less, and is applicable to samples ranging in size from 0.1 g to 5 g. Total procedural blanks are dominated by the blank of the reagents used in the Carius Tube digestion. Total procedural blanks are reproducible to ± 0.05 ppt (2 σ SD). Os is purified from the digestion solution by solvent extraction and microdistillation. Os is analysed by negative thermal ionisation mass spectrometry (N-TIMS) using the Ba(OH)$_2$ activator technique. Typical analytical precision is 0.2 % (2 σ SD) for 10 ng Os samples. Os instrument memory is a function of their memory for Os. The CETAC Technologies direct injection nebuliser (DIN) has by far the lowest sample-to-sample memory, even for samples containing oxidised Os that present severe memory problems for conventional and desolvating nebulisers. DIN washout times, to levels where on-peak backgrounds are <<1% for all isotopes (190 commonly being highest for spiked samples), for solutions in the 0.1 to 10 ppb range, are on the order of 5 minutes. The technique described above can be used to make accurate, precise measurements of Os in geological samples at levels approaching those expected from sampling theory.

References

1. S.B. Shirey and R.J. Walker, *Ann. Rev. Earth & Planetary Scienes* , 1998, **26,** 423.
2. R.J. Walker, J.W. Morgan, E.S. Beary, M.I. Smoliar, G.K. Czamanske and M.F. Horan *Geochim. Cosmochim. Acta* , 1997, **61**, 4799-4808.
3. R.A. Creaser, D.A. Papanastasio and G.J. Wasserburg*Geochim. Cosmochim. Acta*, 1991, **55**, 397-401.
4. J. Volkening, T. Walczyk and K.G. Heumann *International Journal of Mass Spectrometry and Ion Processes* , 1991, **105,** 147-159.
5. J.W. Morgan, D.W. Golightly and A.F. Dorrzapf, *Talanta*, 1991, **38,** 259-265.
6. G.P. Russ J.M. Bazan and A.R. Date, *Anal. Chem.* 1987, **59**, 984-989.
7. S.B. Beneteau and J.M. Richardson, *Atomic Spectroscopy* , 1992, **13,** 118-122.
8. J.M. Luck and C.J. Allegre, *Earth and Planetary Science* Letters, 1982, **61,** 291-296.
9. S.B. Shirey and R.J. Walker, *Analytical Chemistry*, 1995, **75,** 355-356.
10. A.S. Cohen and F.G. Waters, *Anal. Chim. Acta* , 1996, **332,** 269-275.
11. J.W.T. Meadows and G.M. Marlack, *Anal. Chim*, 1962, **34**, 89-91.
12. M. Treadoux and I. McDonald *Geostandards Newsletter* , 1996, **20,** 267-276.
13. S.E. Jackson, B.J. Fryer, W. Gosse, D.C. Healey, H.P. Longrich and D.F. Strong*Chem. Geol.* 1990, **83,** 119-132.
14. A.W. Kleeman, *J. Geol. Soc. Aust.*, 1967, **14,** 43-47.

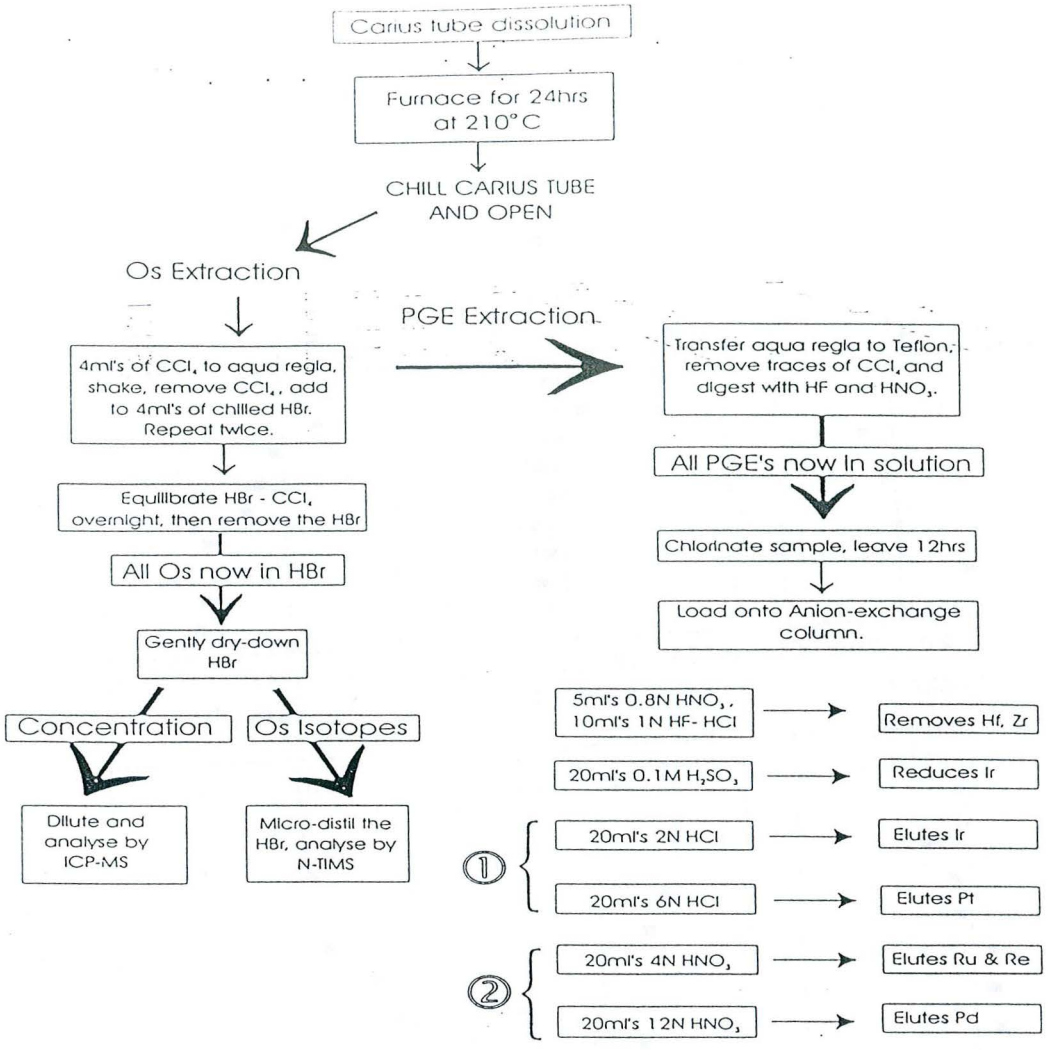
Carius tube dissolution
Furnace for 24hrs at 210°C
CHILL CARIUS TUBE AND OPEN
Os Extraction
PGE Extraction
4ml's of CCl_4 to aqua regia, shake, remove CCl_4, add to 4ml's of chilled HBr. Repeat twice.
Equilibrate HBr - CCl_4 overnight, then remove the HBr
All Os now in HBr
Gently dry-down HBr
Concentration
Os Isotopes
Dilute and analyse by ICP-MS
Micro-distil the HBr, analyse by N-TIMS
Transfer aqua regia to Teflon, remove traces of CCl_4 and digest with HF and HNO_3.
All PGE's now in solution
Chlorinate sample, leave 12hrs
Load onto Anion-exchange column.
5ml's 0.8N HNO_3, 10ml's 1N HF- HCl
Removes Hf, Zr
20ml's 0.1M H_2SO_3
Reduces Ir
1
20ml's 2N HCl
Elutes Ir
20ml's 6N HCl
Elutes Pt
2
20ml's 4N HNO_3
Elutes Ru & Re
20ml's 12N HNO_3
Elutes Pd

PLATINUM GROUP ELEMENTS IN SUBDUCTION ZONE MAGMAS: ANION EXCHANGE PRECONCENTRATION ICP-MS ANALYSES OF LESSER ANTILLES AND IZU-BONIN MAGMAS.

S. J. Woodland,[1] D. G. Pearson,[1] J. A. Pearce[1] and M. F. Thirlwall,[2]. [1]Dept. of Geological Sciences, University of Durham, South Road, Durham, DH1 3LE, UK. E-mail: S.J.Woodland@durham.ac.uk, [2]Dept. of Geology, Royal Holloway University of London, Egham, Surrey TW20 OEX, UK.

Introduction: Platinum group (PGE) data has been obtained on a suite of lavas and associated cumulates from the island of Grenada, Lesser Antilles. The analyzed suite ranges from highly magnesian picrites, to andesites in composition and represents the first complete evaluation of PGE (Os, Ir, Ru, Pt, Pd and Re) abundances in an intra-oceanic arc. In addition, boninitic samples from the Izu-Bonin forearc region (ODP Leg 125, Site 786B) have been investigated as a comparison of relative PGE abundances in these two contrasting subduction environments.

Analytical Procedure: Initial trials with isotope dilution Ni-S fire assay, proved it inadequate for analysis of the sub-ppb PGE concentrations typical of arc volcanics [1]. Samples were thus prepared using a Carius tube digestion technique, coupled with solvent extraction of Os and anion-chromatography preconcentration of the other PGE's [2]. Isotope dilution is utilized to ensure high data quality. Analysis is carried out using an Elan 6000 ICP-MS. In conjunction with the ICP-MS, use of a CETAC Direct Injection Nebuliser permits memory-free Os analysis, whilst the desolvating action of a CETAC ARIDUS achieves interference-free PGE analyses. This low-blank technique allows evaluation of low abundance samples, as blanks are typically <5ppt for Os, Ir and Re, <10ppt for Ru and Pd, and <25ppt for Pt [2].

PGE Signatures of Grenada Suite: PGE patterns are positive (except for Re-depletion) and become steeper as fractionation proceeds e.g. picrite Pd/Ir=25, andesite Pd/Ir=216. Os and Ir are <200ppt (picrites) and <20ppt (andesites). Pt and Pd are <4ppb (picrites) and <2ppb (Pt) and <1ppb (Pd), in andesites. Thus, overall abundances for all PGE's (excluding Re) decrease as fractionation proceeds. The PGE's do not appear do behave as a coherent group during arc-lava fractionation and are variably affected by fractionation of different mineral phases. The M-C series of Grenada [3] have anomalous (high Re, Os, Pd) PGE signatures compared to other Grenada samples.

PGE Signatures of Izu-Bonin Suite: The analyzed andesite, contains slightly lower Os (23ppt) and Ir (25ppt), but higher Ru (242ppt), Pt (3312ppt) and Pd (7219ppt) than the boninites. This implies mildly incompatible behaviour for Ru, Pt and Pd during initial fractionation, but compatible behaviour for Os and Ir. Fractionation of andesite to rhyolite, results in significant decrease in all PGE concentrations, except Re (419ppt), possibly due to initiation of magnetite fractionation [4].

Comparison of Izu-Bonin Boninite and Grenada Picrite PGE Signatures: There is remarkable similarity between PGE abundance and shape of the PGE-patterns, of the primitive rocks from both regions (Fig 1). The Grenadian picrites however are slightly enriched in Os, and significantly depleted in Re (M-series [3]), relative to the boninites.

Implications for PGE Behaviour in Subduction Zones: On the basis of comparison between Izu-Bonin and Grenada, it is suggested that intra-oceanic, subduction-related volcanic rocks, may have universally similar PGE-patterns. Thus, it appears that the PGE's are relatively unaffected by variations in subduction conditions, such as degree of melting and differential fluid/sediment input to their mantle sources. Higher Os concentrations in the more-hydrous Grenada magmas, compared to the boninites, lends support to the theory that Os may be mobilized by Cl-rich aqueous fluids [5]. Recognition of variable Re-depletion and enrichment within Grenada picrites, supports independent Os-isotopic evidence [6], that ancient-depleted mantle may exist beneath Grenada. A "marble-cake" mantle model of isolated fertile and depleted mantle regions is preferred to explain the occurrence of elevated Re concentrations within one particular volcanic center and lava series (M-C) on Grenada.

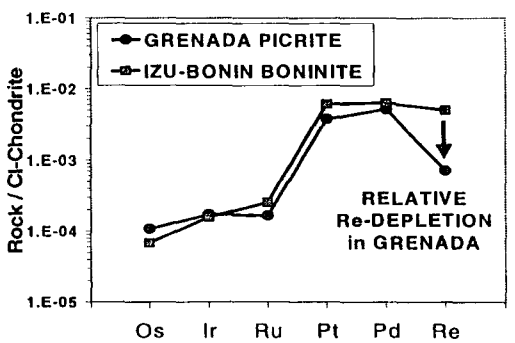

References: [1] Woodland S. J. and Pearson D. G. (1999) *Developments in ICP-MS*, [2] Pearson D. G. and Woodland S. J. (1999) *Chem. Geol. (in press)* [3] Thirlwall M. F. et al. (1996) *Geochim. Cosmochim. Acta., 60*, 4785-4810. [4] Murton et al. (1992) *Proc. ODP, 125*, 211-235. [5] Brandon A. D. et al. (1996) *Nature, 272*, 861-864. [6] Parkinson I. J. et al. (1998) *AGU Abstract-V41D-11*, F1012.

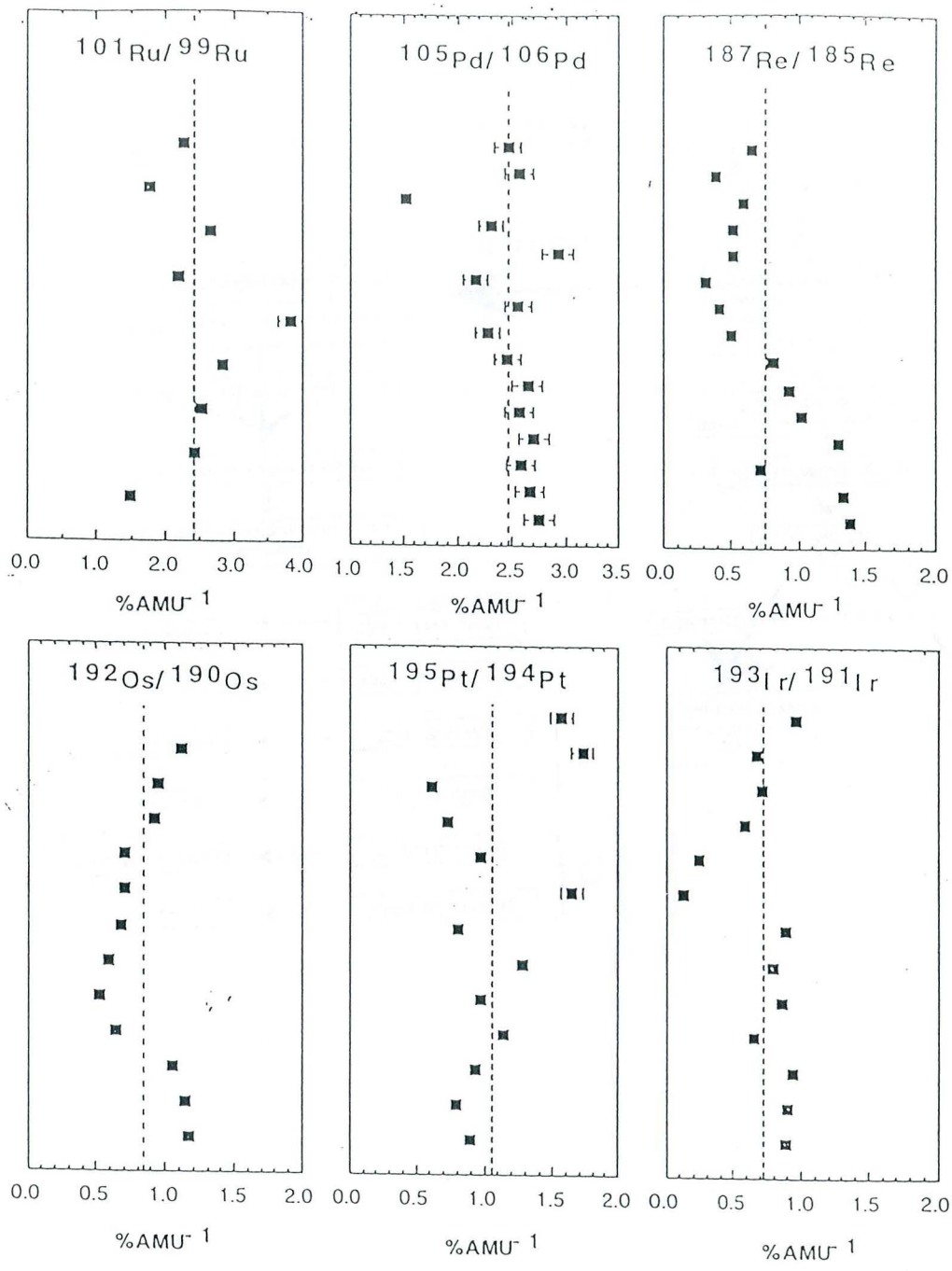
101Ru/99Ru
105Pd/106Pd
187Re/185Re
192Os/190Os
195Pt/194Pt
193Ir/191Ir
%AMU-1

FIG 3

The deep sources of plumes: Re-Os - Pt-Os isotope and PGE systematics of high $^3He/^4He$ West Greenland picrites .

D.G. Pearson[1], L-M. Larsen[2], R.J. Walker[3], S.J. Woodland[1], A. K. Pederson[2] R.W. Carlson[4], and S.B. Shirey[4], [1]Dept. Geological Sciences, Durham University, South Road, Durham, DH1 3LE, UK, [2]Danish Lithosphere Center, Oster Volgade 10, DK-1350 Copenhagen K, Denmark. [3]Department of Geology, University of Maryland, College Park, MD 20742, USA, [4]Department of Terrestrial Magnetism, Carnegie Institution of Washington, 5241 Broad Branch Road, NW Washington, DC 20015, USA.

Introduction: Combined Re-Os and Pt-Os isotope systematics in mantle derived rocks offer considerable promise in being able to discern possible interactions between the Earth's core and mantle source regions of plume-derived magmas [1,2]. The recent discovery of very high $^3He/^4He$ ratios in picrites of the Vaigat Formation, W. Greenland [3] indicates their derivation from a mantle plume sampling a deep, incompletely degassed reservoir such as the lower mantle or core-mantle boundary. We have applied the Re-Os and Pt-Os isotope systems, plus PGE analyses to investigate possible source components in a suite of Vaigat picrites.

Geology: The Vaigat Formation is the earliest of the Tertiary volcanic rocks erupted in W. Greenland, on Disko Island and the Nuussuaq Peninsula. The succession is divided into 3 separate members, the Anaanaa Member (60.5 Ma [4]) overlain by the Naujanguit and then Ordlingassoq members. All 3 members contain an unusually high proportion of picrites [5] with inferred parental magma MgO contents of >19 wt%, indicating very high potential temperatures (1540-1600 C) and large degrees of melting. Sr-Nd-Pb isotope studies suggest that the influence of a MORB-like mantle component decreased with time going from the lower Naujanguit to the Ordlingassoq member [5,6]. The later members contain the clearest signature of the ancestral Iceland Plume. Nd isotope compositions for picrites of the later Ordlingassoq Member are generally enriched relative to N. Atlantic MORB (ε_{Ndi} 7.5 to 9.0). Ordlingassoq and Naujanguit samples have $^3He/^4He$ value ranging up to 30 while one Anaanaa sample has a value of 17.6 [3] Isotope and trace element data indicate minimal levels of crustal contamination [5; L. Larsen, unpublished].

Results: *PGE's.* Abundances of PGE's were determined by isotope dilution ICP-MS using a low-blank Carius Tube digestion technique followed by solvent extraction and anion-exchange separation [7]. Oxide intereferences are minimised using a CETAC ARIDUS desolvating nebuliser.

Picrites from all 3 members of the Vaigat Formation have relatively unfractionated PGE patterns (Pd/Ir ~ 5.8 – 8.0), and high levels of I-PGE's (0.81 – 1.94 ppb Ir) consistent with their derivation as large melt fractions. Ordlingassoq samples generally have slightly lower levels of PGE's, most noticeably P-PGE's, with lower average Pd/Ir and higher Pt/Pd than the lower members of the Vaigat Formation. P-PGE's show good inverse correlations with La/Sm

Re-Os isotope systematics. Re/Os values are low (most < 0.25). γ_{Osi} values for the Anaanaa and Naujanguit Members are close to chondritic (-0.3 to 0.7) and define a correlation on an isochron diagram that is within error of eruption age. Ordlingassoq samples have higher γ_{Osi} values (1.7 to 3.9) and define a steeper correlation on an isochron diagram with a more radiogenic initial $^{187}Os/^{188}Os$. There is no correlation between $^{187}Os/^{188}Os$ and $^3He/^4He$ based on the limited no of He analyses. No systematic trends are apparent in these rocks to indicate that crustal contamination has a significant effect on Os isotope compositions. High Os contents (1.5 to 3.8 ppb) mean that over 10% of Archean crust would be required to generate the most radiogenic $^{187}Os/^{188}Os$ values. For the Ordlingassoq samples, their steep correlation on the Re-Os isochron diagram could be interpreted as mixing with a high Re/Os, radiogenic Os component in the plume source.

Pt-Os isotope systematics. Variations in $^{186}Os/^{188}Os$ for high Os rocks such as the Vaigat picrites are extremely insensitive to contamination by crust. 4 picrites have been analysed for $^{186}Os/^{188}Os$ at UMD. 3 Ordlingassoq samples have chondritic to supra-chondritic $^{186}Os/^{188}Os$ that lie on the lower part of the trend defined by Hawaiian picrites analysed by Brandon et al [1]. The most straightforward interpretation of this data, combined with the Re-Os isotope mixing correlation is that it reveals incorporation of a small component (<<1%) with time-integrated high Re/Os and Pt/Os such as the outer core. This interpretation would be consistent with the very high $^3He/^4He$ ratios in these rocks. One Naujanguit sample with relatively unradiogenic $^{187}Os/^{188}Os$ (γ_{Osi} 0.2) shows enrichment in ^{186}Os relative to chondrites. This observation is more difficult to explain with a 2 component mixing model. The sample also has very high $^3He/^4He$ (R/R_A ~30). If ^{186}Os enrichment does track the deep-plume signature in these magmas then Pt-Os systematics appear more sensitive than trace element discriminants which indicate that the Naujanguit Member is dominated by a MORB-like source.

Conclusions: Trace element and Sr-Nd isotope data for Members of the Vaigat formation suggest a progressively increasing contribution from the Iceland plume source. This model is supported by the distinctly more radiogenic $^{187}Os/^{188}Os$ values of samples from the youngest, Ordlingassoq Member. High $^3He/^4He$ in all members suggests the ubiquitous presence of deeply derived plume material throughout the suite. Preliminary $^{186}Os/^{188}Os$ measurements show supra-chondritic values for samples from both the Ordlingassoq and Naujanguit Members which may record input from the outer core into the source of the Iceland Plume but detailed Re-Os and Pt-Os isotope systematics may be complex..

References: [1] Walker R. J. et al. (1997) *GCA., 32,* A74. [2] Brandon, A.D., et al (1998) *Science,* 1344–1345. [3] Graham, D.W. et al. (1998) *EPSL, 160,* 241–2554. [4] Storey, M., et al, (1998) *EPSL, 160,* 569–586.[5] Larsen, L.M. and Pedersen, A.K., (1996) *J. Conf. Abst.* 1, 349. [6] Holm, P.M., et al, (1993) *EPSL,* 115, 227-44. [7] Pearson, D.G. and Woodland, S.J., in revision, *Chem. Geol.*

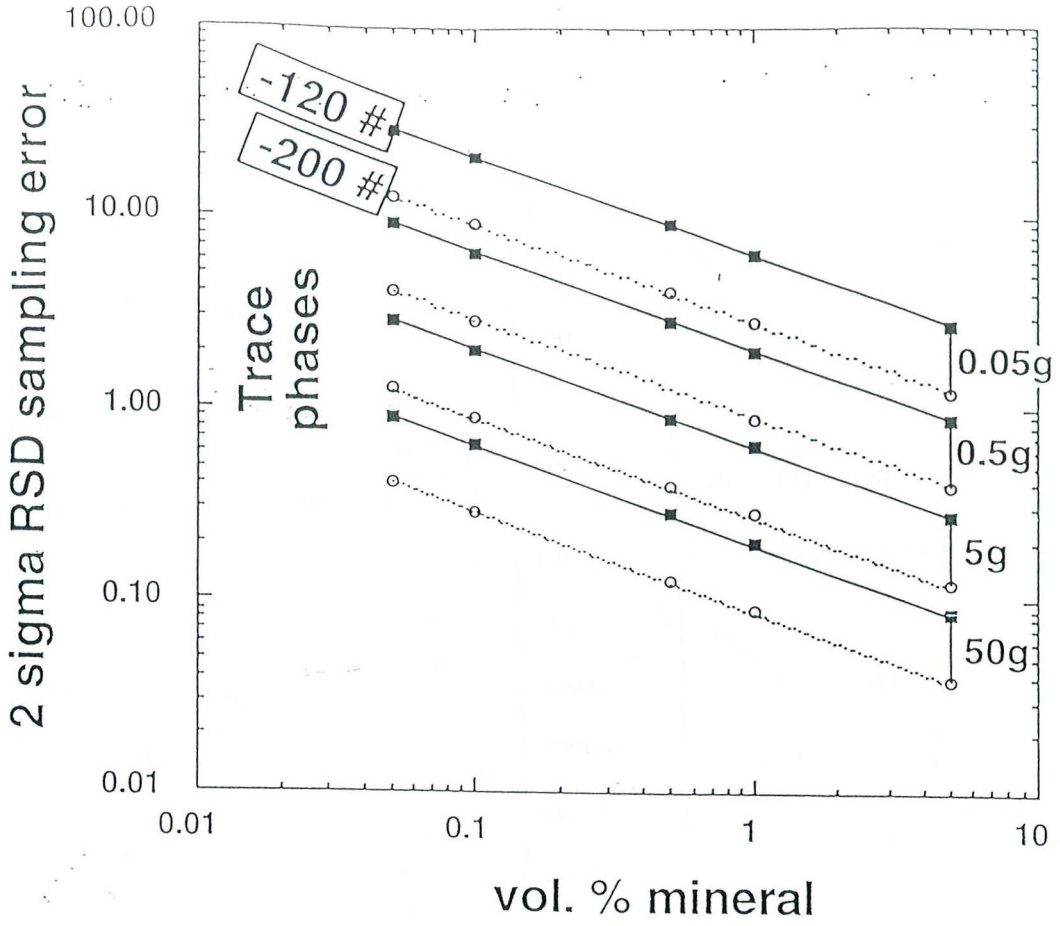
100.00
10.00
1.00
0.10
0.01
2 sigma RSD sampling error
-120 #
-200 #
Trace phases
0.05g
0.5g
5g
50g
0.01
0.1
1
10
vol. % mineral

Fig. 4

ISOTOPE DILUTION ICP-MS ANALYSES OF RE-OS ISOTOPES AND PGE'S VIA SOLVENT-EXTRACTION AND ANION-EXCHANGE PRE-CONCENTRATION AND A DESOLVATING NEBULISER.

D.G. Pearson[1] and S.J. Woodland[1] Dept. Geological Sciences, Durham University, South Road, Durham, DH1 3LE, UK, (d.g.pearson@durham.ac.uk)

Introduction: The recent increase in interest in PGE's and their isotopes for tracing terrestrial fractionation events and possible core-mantle interaction, combined with the wide-spread use of ICP-MS instrumentation, has lead a drive to improve analytical techniques for these elements. Most available PGE analytical techniques for geological samples are not amenable to the analysis of both Re and Os (for isotopes if desired) and other PGE's from the same sample digestion. In addition, many of these techniques suffer from very variable total procedural blanks that are highly reagent dependent, and great effort has to be made to obtain pure reagents. Here we report a low-blank, isotope dilution Carius Tube digestion technique that allows solvent-extraction separation of Os, followed by anion-exchange separation of Ir, Pt, Ru, Re and Pd from the same sample dissolution and analysis by ICP-MS [1].

Chemistry: Samples are spiked with ^{106}Pd, ^{99}Ru, ^{185}Re, ^{190}Os, ^{191}Ir and ^{194}Pt. Following Carius Tube digestion [2]. Os is separated by a triple solvent extraction method, using CCl_4 and HBr, based on Cohen and Waters [3]. The residual aqua regia is dried, treated with Hf-HNO_3, taken up in 1N HCl and chlorinated to oxidise Ir^{3+} to Ir^{4+}. This solution is loaded onto 1 mL of fresh AG1-X8 resin in chloride-form, pre-treated with chlorine water, to maintain an oxidising environment and prevent reduction of Ir IV to Ir III. A mixed 1N HF/HCl wash plus 0.8N HNO_3 is performed to remove excess Hf and Zr which form interfering oxide ions and suppress ionisation. Ir is reduced with sulfurous acid and eluted with 2N HCl. Pt is then eluted with 6N HCl. Re and Ru are eluted with 4N HNO_3. Pd is eluted with warm (80 °C) 12N HNO_3. Re, Ru and Pd can be eluted together as can Ir and Pt if desired. Solutions are dried and diluted to volume to run. Yields are ~ 70% except Ru which is variable.

Blanks: Total procedural blanks are typically <5 pg for Os, Ir and Re, <10 pg for Ru and Pd and <25 pg for Pt. In common with Rehkamper et al [4] we found considerable Pt in poorly cleaned borosilicate glass Carius Tubes. This was reduced to 30 pg or below by rigourous boiling in aqua regia. Such blanks are adequate for most geological samples and apart from Pt, scale with sample size.

Analysis: Solutions containing different PGE fractions were determined by quadrupole ICP-MS on a Perkin Elmer Elan 6000. Oxide intereferences are minimised using a CETAC Aridus desolvating nebuliser. Os concentrations are analysed by ICP-MS using a CETAC direct injection nebuliser which provides a low memory sample introduction system. Os can also be analysed for isotope ratios and concentration by N-TIMS. Mass bias and oxide corrections are made using standard solutions.

Results: The komatiite standard WITS-1 [5] initially was used to assess accuracy and precision. This standard has PGE concentrations within the range of many standard silicate rocks. 18 replicates were run as separate digestions for full PGE analyses. 9 Os samples run by N-TIMS gave 1.09 +/- 0.08 (2SD) ppb, while 9 samples run by DIN-ICP-MS gave 1.07 +/- 0.1 ppb. Os, Ir and Ru reproducibility is 7.5 to 13 % (2* RSD), and close to "accepted" values [5]. More mobile elements such as Re, Pt and Pd appear much less reproducible (20-40% 2*RSD). Although our reproducibility is comparable to other methods using this standard (better for Os, Ir & Ru) it is somewhat worse than expected and we suspect possible heterogeneity for the more mobile PGE's within the sample. Replicates on a suite of W. Greenland Picrites from the Vaigat Formation [6] show much better reproducibility than WITS-1, despite being of similar major element chemistry and PGE concentration range. The following reproducibility was obtained (2* RSD): Os 2.5%; Ir 4%; Ru 5%; Pt 4%; Pd 3%; Re 6%. A suite of volcanic rocks from Grenada, Lesser Antilles arc [7] show progressively poorer reproducibility as PGE abundances decline to <100 ppt, however, the sense of the relative PGE fractionations is consistent for all replicates. It is evident that different geological samples show different levels of sample heterogeneity for PGE's and replicate analyses of particular sample types, rather than standard rocks, are probably the best way to assess reproducibility of data for a particular sample suite.

Summary: Our technique allows accurate and precise measurement of Re, Os, Ir, Ru, Pt and Pd by ICP-MS, with the option of running Os by N-TIMS. Blanks are mostly controlled by reagents and so are easy to regulate. Results for a variety of samples allow confidence to be placed in the reproducibility of inter-element PGE abundances for geological samples in the ppb range, in order to search for evidence of primordial Earth PGE fractionation events.

References: [1] D.G. Pearson and S.J. Woodland (in press) *Chem. Geol.* [2] S.B. Shirey and R.J. Walker (1995) *Anal. Chem.* 67, 2136. [3] Cohen and Waters (1996) *A. Chim. Acta* 332, 269. [4] M. Rehkamper aet al. (1998) *Fress. J. A. Chem.* 361, 217. [5] M. Treadoux and I. McDonald, (1996) *Geost. News Lett.* 20, 267. [6] D.G. Pearson et al, *this volume*. [7] S.J. Woodland et al, *this vol.*

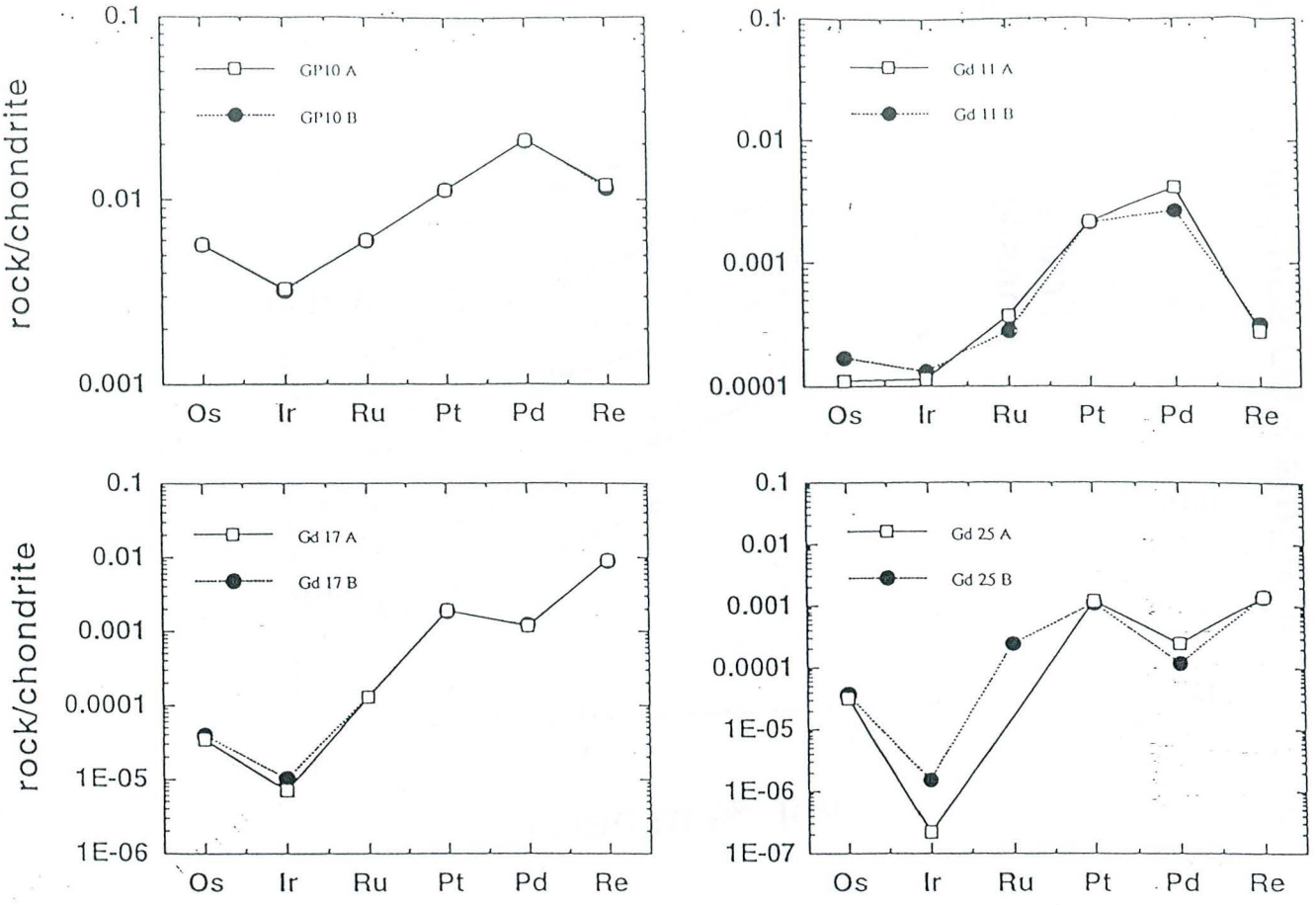
rock/chondrite
0.1
0.01
0.001
GP10 A
GP10 B
Os
Ir
Ru
Pt
Pd
Re
0.1
0.01
0.001
0.0001
Gd 11 A
Gd 11 B
Os
Ir
Ru
Pt
Pd
Re
rock/chondrite
0.1
0.01
0.001
0.0001
1E-05
1E-06
Gd 17 A
Gd 17 B
Os
Ir
Ru
Pt
Pd
Re
0.1
0.01
0.001
0.0001
1E-05
1E-06
1E-07
Gd 25 A
Gd 25 B
Os
Ir
Ru
Pt
Pd
Re

FIG 5

been observed for ICP-MS in terms of the relative ionisation efficiencies of reduced versus oxidised Os and has lead to analytical procedures that involve directly distilling Os into the mass spectrometer as OsO_4 vapour[6, 7]. Although large sensitivity increases are to be gained by analysing highly oxidised Os, a major draw back is that Os in this form has the most severe memory effects in the instrument, although memory can also be severe even in reduced solutions. Oxidised forms of Os, particularly OsO_4, are highly reactive, being rapidly adsorbed onto plastic surfaces and even diffusing into Teflon when under pressure[8]. Furthermore, oxidised Os is very volatile (OsO_4 B.P. ~ 110 °C) such that samples prepared in this form must be kept at relatively low temperatures and must be analysed rapidly after preparation to avoid loss of sample. OsO_4 will also photo-reduce if stored, leading to mixed oxidation state solutions that are difficult to analyse.

Large errors can occur in analytical procedures for Os where signal intensities are measured, if the digestion procedure for samples does not render Os in exactly the same oxidation state as that in the standard solution used for instrument calibration[5]. To combat this non-linearity problem and the potential loss of Os from samples due to volatilisation during the digestion stages of any analytical procedure involving oxidants, isotope dilution can be employed. Isotope dilution involves the addition of a known amount of an isotopically enriched spike solution to the sample, usually during the digestion stage if the sample is a solid. Once the spike has been equilibrated with the sample, losses can be tolerated as the ratio of spike to normal isotopes is measured to then calculate the sample concentration. In addition, chemical equivalence between standard solutions and sample is not necessary because isotopic ratios are being analysed, not absolute signal intensities. Solving signal non-linearity problems then leaves the issue of significant instrumental Os memory observed when running samples. Here we evaluate the performance of direct injection nebulisation using a very low dead-volume nebuliser for samples of differing oxidation states compared to a standard cross-flow nebuliser. We find that Carius Tube digestion of isotopically spiked samples followed by solvent extraction of the Os and analysis by direct injection ICP-MS produces reproducibilities for 1g aliquots of a standard rock that are close to the theoretical limits expected from sampling theory.

3 SOLUTIONS: ANALYTICAL CHEMISTRY

Although oxidised Os appears to ionise more efficiently from acid solutions than reduced Os, the high sensitivity of modern plasma mass spectrometers means that, at least for concentration measurements by isotope dilution, obtaining sufficient signal for precise measurement is not a major obstacle. Because of this we chose to adopt a chemical extraction method that ensures that all the recovered Os is in reduced form prior to analysis. This provides two significant advantages; firstly that the extracted Os is stable over long time periods (at least several months) so that immediate analysis is not necessary, and secondly; that sample memory and hence potential cross-contamination in reagent vials and instrumentation is reduced.

Samples are loaded into chilled Carius Tubes followed by an appropriate amount of spike, in this case we use a ^{190}Os spike to minimise disturbance of the natural $^{187}Os/^{188}Os$ ratio that can be used as a reservoir tracer. Error propagation calculations indicate optimal spiking when the spike-sample mixture has a $^{190}Os/^{192}Os$ ratio of close to 2.5. We follow a previously published procedure [9] and emphasise the precautions to be observed when handling and opening sealed Carius Tubes. Most samples are digested in inverse aqua-regia, i.e., approx. 3 parts HNO_3 : 1 part HCl. If samples are organic-rich, care must be taken to use excess HNO_3 to ensure oxidation of Os in the digestion step as this promotes equilibration between the sample and the spike[9]. The Carius Tubes are sealed with a blow-torch and enclosed within thick-walled steel cases with a non-sealing cap, before being placed in an oven at 230 °C. For very organic-rich or carbonate rich materials, significant CO_2 may be evolved leading to elevated pressures in the Carius Tubes. In these cases the oven temperature is reduced to below 200 °C. Decarbonating very carbonate-rich samples is recommended before sealing into Carius Tubes. Following digestion, Os is extracted by partitioning into a non-polar solvent, in this case CCl_4, following the procedures described by Cohen and Waters[10], except that we repeat the extraction 3 times and combine the 3 extracts. Using inverse aqua-regia is essential in ensuring a high yield. We found that using the classical aqua-regia mixture produced erratic, much lower yields than the "inverse" aqua-regia, a feature also observed for the extraction of Ru using similar procedures [11]. After organic extraction, the Os is back-extracted in 9N HBr. When warmed in a sealed vessel the Os is converted to the IV oxidation state and into the $OsBr_6^{2-}$ species. This can be safely stored prior to analysis, ready to be taken up in dilute HNO_3 or HCl.

Procedural blanks are entirely reagent dependant and vary from <1 pg to 7 pg depending on the batches of reagents used. Under the most favourable conditions the detection limits are ca. 1 pg.

4 MASS SPECTROMETRY

4.1 Instrumentation and measurement protocol

A Perkin Elmer Sciex Elan 6000 ICP-MS was used for this study. Operating conditions were routine, with RF power being 1200 watts. The auto-lens function was used for "routine" samples. Mass calibration can be optimised using Re. For cross-flow operation we also found it useful to perform mass bias estimations using either Re or Ir although Ir was most often used, the $^{191}Ir/^{193}Ir$ ratio being closer to the mass range of the two Os isotopes measured, i.e., $^{190}Os/^{192}Os$. Instrumental mass bias was found to vary between 0.7 and 1.2 % per AMU in this mass range and is similar for both the cross-flow nebuliser and the direct injection nebuliser (DIN; Fig. 1).

30 sweeps of the mass range were measured to produce 1 isotopic ratio which was repeated at least 30 times, at 20 mS peak dwell times to give a single sample measurement. Where enough sample remained, this measurement was repeated 2 or 3 times. Relative standard deviations for 1 ppb solutions with normal isotopic ratios ($^{190}Os/^{192}Os$ in natural samples = 0.6438[1]) were ca. 0.5% (2 σ) for each measurement. However, repeated measurements of samples and standard solutions suggests that true precision is as good as 0.2% or better.

The Os-specific nature of the solvent extraction means that isobaric interferences on the Os mass spectra are insignificant but Pt is routinely corrected for on masses 190 and 192. Backgrounds are measured for solutions before analysis of a sample using exactly the same measurement routine as for samples. These on-peak backgrounds are then subtracted from the signal intensities to yield background corrected intensities that are then ratioed. For

most samples analysed using the DIN background counts are <1% on either mass 190 or 192.

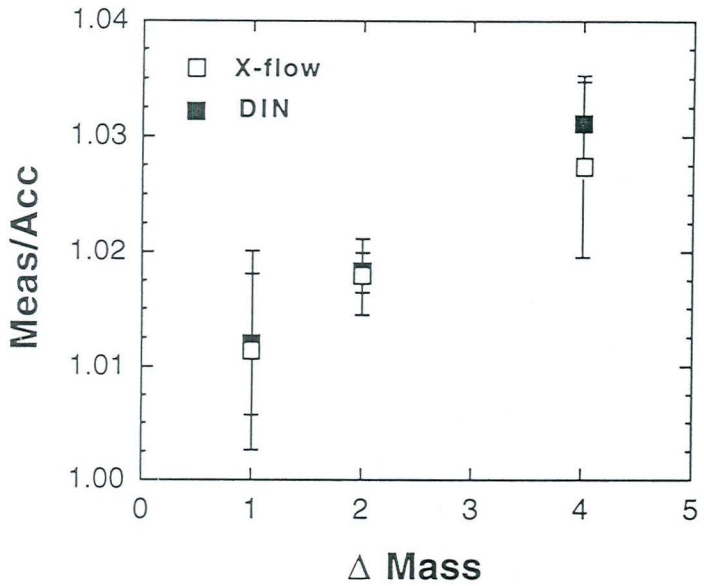

Figure 1 *Mass fractionation for Os isotopes measured by cross-flow nebulisation and DIN relative to an accepted value for $^{192}Os/^{188}Os$ of 3.08271.*

4.2 Cross-flow nebulisation

The cross-flow nebuliser used was the standard model supplied by Sciex which has a Scott-type double pass spray chamber. A typical profile for Os washout is given in Fig. 2, where the sample is introduced in dilute (3%) HNO_3 and washed out with the same solution.

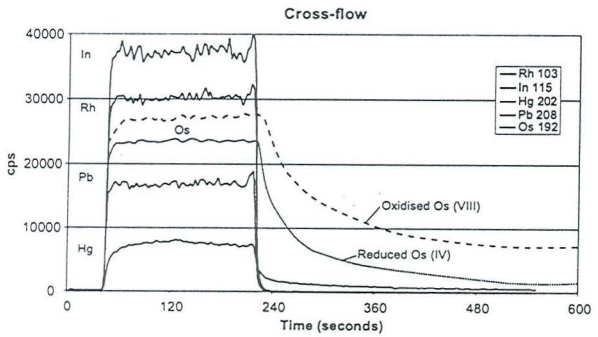

Figure 2 *Cross-flow nebuliser washout profiles for 10 ppb standard solution of Rh, In, Hg and Pb compared to solutions containing Os in either reduced, or oxidised states, note greater sensitivity for Os in VIII oxidation state.*

As has been noted previously by numerous workers, samples show varying washout characteristics, this is probably related to the proportion of Os in the VIII oxidation state, which may vary from sample to sample. The example shown in Fig. 2 compares washout for a standard solution, where Os is probably as $OsCl_6^{2-}$ (IV oxidation state), with that for an organic polymer sample dissolved in concentrated hot HNO_3 and diluted to volume, which contains a high proportion of Os in the VIII oxidation state. The memory for the solution containing oxidised Os appears much worse in this case. We did not quantitatively determine how much of the "enhanced" memory shown by the oxidised solution reflected similar levels of residual Os but greatly enhanced ionisation. Oxidised Os, particularly as OsO_4 is very surface active and is known to cause more severe sample vessel cross-contamination problems than reduced Os. Oxidised Os should stick to the walls of peristaltic tubing, to the spray chamber walls and may even stick to Teflon where large surface areas are involved. Our experiments found most of the Os to be residing in the spray chamber. It is probable that the oxidised solution shown in Fig. 2 shows a component of both increased memory and increased ionisation efficiency. Whatever the relative effects, it is clear that very large proportions of the Os in solution remain in the nebuliser/instrument after an analysis. Sample concentrations of over 50 ppb Os prove particularly difficult to washout, requiring many hours running time to achieve <100 CPS at mass 192, or mass 190 when the samples are spiked.

Our experience has shown that samples containing partially oxidised Os at the 1 ppb level or less, introduced in dilute HNO_3 appear to "wash out" to fairly constant levels, on the order of 500 CPS, in perhaps 10 to 15 minutes. However, in many cases this does not equate to all the Os being washed out of the instrument. If hydrogen peroxide is subsequently introduced, which is particularly effective at re-mobilising any Os adhering in either the oxidised, or reduced form, trapped Os is re-released (Fig. 3).

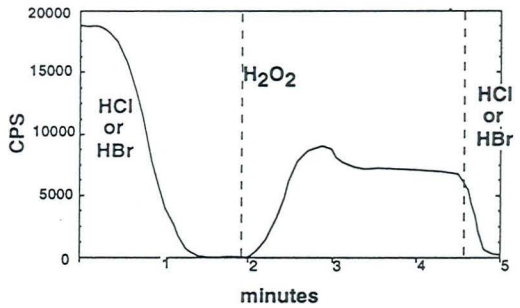

Figure 3 *Schematic diagram illustrating cross-flow nebulisation of a 10 ppb partially oxidised Os solution allowed to wash out with 3% HNO_3 followed by introduction of 30% H_2O_2 solution.*

It may be argued that this residual Os would be unlikely to be re-mobilised if all solutions being eluted through the instrument are kept in a reduced form; however, this is a dangerous strategy as 10's of ng of Os can rapidly accumulate in the instrument with no control on when this Os will be released/remobilised.

due to low sample uptake rates (c. 45-70 µL per minute depending on optimisation) and very low oxide production levels (see Table 2). Severe memory problems were encountered for Os but not for other PGEs, where washout times were on the order of 3 to 5 minutes. Both the Cetac MCN6000 and Aridus nebulisers generally produced increased signal sizes on the Elan 6000 compared to the cross-flow nebuliser. In addition, their low up-take rate allows much greater levels of pre-concentration because column fractions can be taken up in much smaller volumes of solution prior to analysis. In general, for analysing Re, Pt, Pd, Ru and Ir a desolvating nebuliser is clearly optimal in that it minimises oxide interferences and provides significant signal enhancement.

6.2. Instrumental mass-bias and precision

Mass bias was estimated by analysis of standard solutions throughout the data collection session. 0.1 to 10 ppb standard solutions were generally used, this concentration range being close to the sample concentrations in most instances and providing sufficient signal for accurate isotope ratio measurement. No significant differences in mass bias were found for standards in this concentration range, although within-run errors and overall reproducibility showed a corresponding decline in quality for the smaller signals obtained from dilute solutions .

Fig. 3 summarises mass bias effects for the ratios measured. As expected, lower atomic mass elements show the largest mass bias, those for Pd and Ru being on the order of 2.5% per atomic mass unit (AMU^{-1}). Although slightly variable between different analytical sessions, the exact value of this mass bias is very reproducible throughout each session, with typical 2 sigma RSDs of 0.2 to 0.3 %. The variability in mass bias for Ru (2.44 +/- 0.67 % AMU^{-1}) is twice that of Pd (2.47 +/- 0.33 % AMU^{-1}, Fig. 3) probably due to a combination of increased error from small signals (natural abundances of ^{101}Ru and ^{99}Ru are lower than for ^{105}Pd and ^{106}Pd) and the increased possibility of interferences (Table 1).